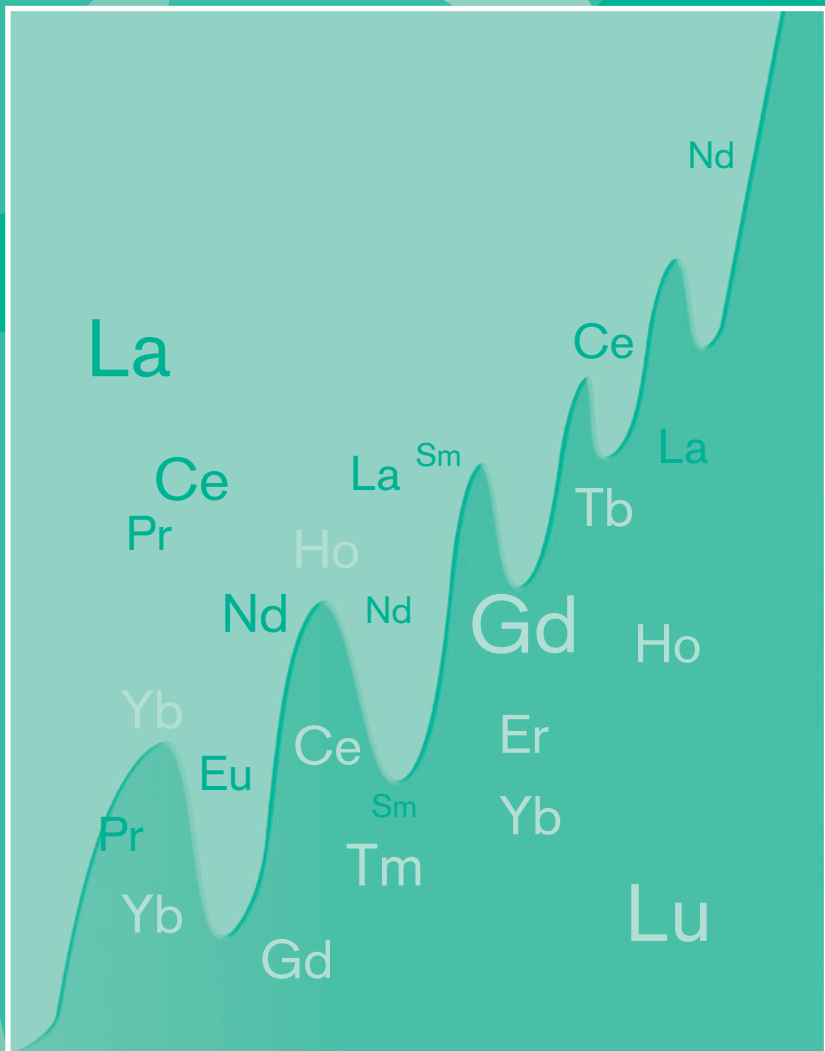


Rare Earth Elements in Ultramafic and Mafic Rocks and their Minerals

Minor and Accessory Minerals

F.P. Lesnov



Rare Earth Elements in Ultramafic and Mafic Rocks and their Minerals

This page intentionally left blank

Rare Earth Elements in Ultramafic and Mafic Rocks and their Minerals

Minor and accessory minerals

F.P. Lesnov

Institute of Geology and Mineralogy, Novosibirsk, Russia

Scientific editor

G.N. Anoshin

Member of Russian Academy of Natural Sciences, Russia



CRC Press

Taylor & Francis Group

Boca Raton London New York Leiden

CRC Press is an imprint of the
Taylor & Francis Group, an **informa** business

A BALKEMA BOOK

CRC Press
Taylor & Francis Group
6000 Broken Sound Parkway NW, Suite 300
Boca Raton, FL 33487-2742

© 2012 by Taylor & Francis Group, LLC
CRC Press is an imprint of Taylor & Francis Group, an Informa business

No claim to original U.S. Government works
Version Date: 20120306

International Standard Book Number-13: 978-0-203-11967-9 (eBook - PDF)

This book contains information obtained from authentic and highly regarded sources. Reasonable efforts have been made to publish reliable data and information, but the author and publisher cannot assume responsibility for the validity of all materials or the consequences of their use. The authors and publishers have attempted to trace the copyright holders of all material reproduced in this publication and apologize to copyright holders if permission to publish in this form has not been obtained. If any copyright material has not been acknowledged please write and let us know so we may rectify in any future reprint.

Except as permitted under U.S. Copyright Law, no part of this book may be reprinted, reproduced, transmitted, or utilized in any form by any electronic, mechanical, or other means, now known or hereafter invented, including photocopying, microfilming, and recording, or in any information storage or retrieval system, without written permission from the publishers.

For permission to photocopy or use material electronically from this work, please access www.copyright.com (<http://www.copyright.com/>) or contact the Copyright Clearance Center, Inc. (CCC), 222 Rosewood Drive, Danvers, MA 01923, 978-750-8400. CCC is a not-for-profit organization that provides licenses and registration for a variety of users. For organizations that have been granted a photocopy license by the CCC, a separate system of payment has been arranged.

Trademark Notice: Product or corporate names may be trademarks or registered trademarks, and are used only for identification and explanation without intent to infringe.

Visit the Taylor & Francis Web site at
<http://www.taylorandfrancis.com>

and the CRC Press Web site at
<http://www.crcpress.com>

Dedicated to my wife, Emma, of blessed memory

This page intentionally left blank

Contents

<i>Preface</i>	ix
1 Garnets	1
1.1 Brief survey of modern studies into the geochemistry of rare earth elements in garnets	2
1.2 General regularity of REE distribution in garnets of the most common of their parageneses	7
1.3 On the nature of sinusoidal chondrite-normalized REE patterns of garnets	60
1.4 Coefficients of REE distribution between garnets and coexisting melts	64
1.5 Coefficients of REE distribution between garnets and coexisting clinopyroxenes and other minerals	71
1.6 Some crystal-chemical aspects of the REE isomorphism in garnets	85
2 Chrome-spinels	89
3 Ilmenites	101
3.1 REE composition of ilmenites	101
3.2 Coefficients of REE distribution between ilmenite and coexisting phases	122
4 Zircons	127
4.1 Key regularities of REE distribution in zircons from some types of magmatic and metamorphic rocks	128
4.2 Coefficients of REE distribution between zircons and coexisting phases	166
4.3 On the isomorphism of REE in zircons and conditions of their crystallization	170

5 Apatites	173
5.1 The REE composition of apatites	173
5.2 The coefficients of REE distribution between apatite and melts as well as coexisting perovskites	185
5.3 On isomorphism of REE in apatites	188
6 Titanites	191
7 Perovskites	197
8 Micas	207
9 Some general regularities of REE distribution in the minor and accessory minerals of ultramafic, mafic and some other rocks	217
10 Geochemical relationship between REE and PGE in mafic and ultramafic rocks and their petrogenetic significance	223
10.1 Mafic-ultramafic massifs in Tuva (Russia)	224
10.2 Naransky massif (West Mongolia)	244
10.3 Kokpektinsky massif (South Urals, Kazakhstan)	249
10.4 Ultramafic xenoliths in alkaline basalts from Eifel and Vogelsberg provinces (Germany)	254
10.5 Luobusa massif (Southern Tibet, China)	259
10.6 Iti and Kallidromon massifs (Greece)	259
10.7 Komatiite-basalt complex of North-West Vietnam	259
10.8 Komatiite-basalt complexes of Gorgona Island (Colombia), Alexo (Ontario, Canada), Onverwacht, Barberton, Perseverance (Africa) and Kambalda (West Australia) provinces	265
10.9 Bushveld massif (South Africa)	265
10.10 Muskox massif (Canada)	267
10.11 Galmoenan massif (Koryak highland, Russia)	270
<i>Conclusion</i>	281
<i>References</i>	283

Preface

When discussing different, empirically established, regularities, it is important to comprehend the degree of their completeness but to avoid categorical judgment.

Yu.N. Avsyuk

In the first book of the monograph “Rare Earth Elements in Ultramafic and Mafic rocks and their minerals. Main types of rocks. Rock-forming minerals” [Lesnov, 2010] we summarized the available data on the geochemistry of Rare Earth Elements (REE) in the main types of ultramafic and mafic rocks as well as in their rock-forming minerals. This book summarizes analytical data accumulated in the world literature and other materials about the regularities of the REE distribution in minerals contained in ultramafic and mafic rocks as accessory phases. These minerals are tentatively divided into two groups. The first includes garnets, zircons, apatites and perovskites, which can accumulate increased amounts of REE in their structure. The second consists of minerals whose structure can accumulate only limited contents of these trace elements. These are chrome-spinels, ilmenites, and micas. These minerals, in respect of REE geochemistry, are studied to a varying degree because of the different levels of accumulations of these elements, different degrees of occurrence in rocks, tiny sizes of their grains and other reasons. The overwhelming majority of presently available data on REE geochemistry in accessory minerals from ultramafic and mafic rocks have only been published in the last 15 years. The studies became possible due to the development and introduction of new highly sensible microprobe analyses allowing the detection of REE and many other trace elements in mineral grains in thin sections. The greatest number of these analyses were performed for garnets and zircons, fewer for apatites, and the fewest for chrome-spinels, ilmenites, micas, and perovskites. In general, the regularities of REE distribution in these minerals from ultramafic and mafic rocks are less studied compared to the rock-forming minerals from ultramafic and mafic rocks. Among the analytical methods, which were used to study the REE composition of accessory minerals, the most efficient was the mass-spectrometry with inductively coupled plasma (ICP-MS). In addition to the materials on the geochemistry of REE in accessory and minor minerals from ultramafic, mafic and some other types of magmatic rocks, in a separate chapter of this book we generalize scarce data on the geochemical bonds between the REE and Platinum Group Elements (PGE) in

the rocks of ultramafic and mafic composition. These groups of chemical elements with contrasting physical and chemical properties, as assumed, must differ significantly both in the character of fractionation during generation and crystallization of magmatic melts. Owing to this, the complex data on the distribution of REE and PGE in rocks can, probably, be used further as additional geochemical indicators of such processes.

Chapter I

Garnets

Garnets occur in more than 30 natural mineral parageneses forming the rocks of magmatic, metamorphic and metasomatic origin, which suggests their crystallization in a wide range of physicochemical parameters. By the ratio of main components (Ca, Mg, Al, Fe, Cr, Mn), garnets are divided into two major groups: almandine (pyrope, almandine, and spessartite) and andradite (grossular, andradite, and uvarovite). Pyropes are contained mainly in high-temperature peridotites and eclogites from deep xenoliths carried by kimberlite and alkaline-basaltic melts. In high-temperature and mesobaric metamorphic complexes (eclogites, granulites, gneisses, and schist), as well as in metasomatic rocks (skarns) garnets are represented by the varieties of almandine-grossular-pyrope series. When systematizing garnets by chemical compositions and parageneses in which they occur, normally different binary diagrams are used, including the diagrams in CaO–Cr₂O₃ coordinates [Sobolev, 1964; Sobolev *et al.*, 1973].

According to the data available, the crystalline structure of garnets can accumulate considerable amounts of different trace elements, including REE. The latter are, in most cases, intensely fractionated, which results in the significant predominance of heavy elements. In geochemical analyses of garnets from ultramafic and mafic deep xenoliths in kimberlites and alkali basalts and for the interpretation of their results, researchers often use the numerical modeling techniques with due regard for data on REE.

The first findings of REE in garnets were performed when studying single garnet samples from eclogites of Japan and New Zealand [Haskin & Frey, 1966]. Data was soon obtained which showed that the values of REE distribution coefficients in the garnet-bearing rock and garnet-clinopyroxene systems increase from light to heavy. Based on these data, an assumption was made that garnets accumulate mainly heavy elements [Masuda, 1967]. The keen interest to the problems of geochemistry of REE in garnets, especially those from deep xenoliths, contributed to the accumulation of numerous new analytical data on the REE composition of this mineral. In recent years, local (microprobe) methods of their analyses are used more frequently than others. The published analyses were dominated by those of garnets from peridotite and eclogite deep xenoliths as well as from microinclusions in diamonds. By far: fewer data are available on garnets from eclogite rocks, occurring in metamorphic complexes, and from some gabbroid rocks, effusive, and skarns. Analyses of REE in garnets were performed using many analytical methods (percentages of their quantity in the database in brackets): INAA (13%), RNAA (5%), IDMS (6%), SIMS (20%), IPMA (45%), and LA ICP-MS (12%). The above-mentioned methods have

different thresholds of detectability of elements, locality, and determination accuracy. For example, determination accuracy of REE was ~30% for RNAA, and from 3–15% [Hauri *et al.*, 1994] to 10–20% for IPMA [Shimizu *et al.*, 1997a, b]. The inaccuracy of determinations in the analyses performed using the SIMS technique on Cameca IMS-4f was ~1% in case the content of individual REE content was 10 ppm, 10–15% for 1–0.1 ppm and about 50% for 0.01–0.005 ppm [Harte & Kirkley, 1997]. The inaccuracies of determinations by the LA ICP-MS technique, depending on the element, varied in the range of 20–30% (from data of the Analytical Center laboratory, IGM SB RAS, Novosibirsk). Not always the content of all REE was determined in the garnets. The most abundant data are available on Ce, Nd, Sm, Eu, Dy, Er, Yb, scarcer are for La, Gd, Ho, Tm and Lu, and still scarcer are for Pr. The analyses show that garnets are characterized by considerable variations in the total contents of REE and differ in the ratios of light, medium, and heavy elements.

The calculations performed using the database (about 300 analyses) showed that for the light (except Ce) and medium REE the differences between the maximum and minimum contents amount to two-three orders of magnitude, whereas for Yb, Lu and Ce they may increase to four orders. The average content of elements for these samples in all types of garnets increases in the following series (ppm): 0.8-Eu; 1.1-La; 1.5-Pr; 2.6-Tb; 2.8-Nd; 3.3-Tm; 3.6-Ce; 4.1-Er; 6.5-Lu; 8.3-Gd; 55-Sm; 315-Dy; 387-Ho; 554-Yb. The total REE content decreases from the varieties of garnets enriched in Ca and Fe occurring in gabbroids, metamorphic, and metasomatic rocks to low-Ca and high-Mg pyropes from ultramafic rocks contained in xenoliths from kimberlites and alkali basalts. The chondrite-normalized concentrations of light REE in the garnets of all types vary in the range of 0.1–1.0, and those of HREE, in the range of 10–800. The preferred accumulation of HREE in garnet structure is responsible for the observed steep positive slope of their REE pattern and low values of the $(La/Yb)_n$ parameter.

In the publications dealing with the REE distribution in garnets the most frequently discussed problems are: 1) comparative evaluation of the levels of REE accumulation in the samples of different chemical compositions and different paragenetic types; 2) systematization of garnets on the basis of distribution parameters of chondrite-normalized contents of REE; 3) physicochemical processes causing various anomalies in the distribution of REE in a mineral; 4) estimation of the distribution coefficients of REE between garnets and coexisting phases, including melts of different compositions (in natural and experimental systems); 5) calculation of the REE composition of model parental melts, using the distribution coefficients of REE; 6) crystallochemical properties of garnets and the related problems of REE isomorphism.

I.1 BRIEF SURVEY OF MODERN STUDIES INTO THE GEOCHEMISTRY OF RARE EARTH ELEMENTS IN GARNETS

Research on the geochemistry of REE in garnets started in the late 1960s by Haskin, Frey and Masuda and other researches, has been especially intensive for the past twenty years. Let us discuss the most significant results, beginning from the work concerned with the problems of the chemistry of garnets and some other minerals from eclogites [Caporuscio & Smith, 1990]. On the basis of representative data obtained

by the INAA technique, the authors studied geochemical properties of garnets and clinopyroxenes from eclogites forming xenoliths from kimberlites of Bobbejaan and Roberts Victor diamond deposits (South Africa). The contents of REE in these garnets vary considerably depending on the variations in the contents of major components. In particular, with increasing contents of Fe and Ca, the REE patterns of the mineral become gentler relative to heavy elements. All the garnets from this collection are depleted in LREE and enriched in HREE, the values of $(\text{La/Yb})_n$ parameter change in the range of 0.027–0.700. It was also shown that the REE distribution values in the clinopyroxene-garnet system increase with the enrichment of minerals in Mg, and in Ca-enriched samples the values of these coefficients are low. Based on the established regularities in the variation of K_d (clinopyroxene/garnet), the authors conclude that REE in studied minerals have an equilibrium distribution. The distribution of major and trace elements both in garnets and clinopyroxenes corresponds to their equilibrium at 3–5 GPa and temperature of 950–1150°C. Making reference to the previous research efforts, Caporuscio and Smith suggested that in garnets REE isomorphously replace bivalent cations Ca, Mg, and Fe, which occur in an octahedral coordination.

The REE distribution in zonal garnets from the contacting-metamorphosed rocks of the Kwoiek Area (British Columbia, Canada) was studied using the IPMA technique [Hickmott & Shimizu, 1990]. The obtained data gives evidence that the contents of MREE and HREE, as well as Y, decrease from the inner zones of garnet grains toward the outer zones. Unlike other elements, the content of Dy remains nearly the same within the inner zones of grains, but it decreases toward their peripheral zones.

The same analytical method was used in the detailed studies of the REE distribution in two types of garnets and coexisting clinopyroxenes from gabbros of the Ivrea Verbano complex (Italy) [Mazzucchelli *et al.*, 1992]. The first type of garnets are large porphyroblastic segregations and the second occur in reactional rims developed on the borders of mineral grains. The REE patterns of garnets from porphyroblastic segregations are positively sloping lines with negative Eu anomalies of low intensity. The patterns of garnets from reactional rims at times display positive Eu anomalies. In the mineral from porphyroblastic segregations the values of $(\text{Yb/Nd})_n$ parameter equal 12–36, whereas in garnets from reactional rims the parameter is normally <6. In the garnets from porphyroblastic segregations the K_d (clinopyroxene/garnet) gradually increases with increasing atomic number of REE, and in the mineral from reactional rims this regularity is not so distinct. The authors report significantly wider variations of K_d (clinopyroxene/garnet) values for Ce compared to other REE.

The REE distribution in pyropes from megacrystals in peridotite xenoliths occurring in kimberlites from the Udachnaya pipe (Yakutia, Russia) was studied in details by Pokhilenko *et al.* [1993]. They showed that most of the described pyropes have a sinusoidal shape of REE spectra, due to the more or less intense enrichment in LREE compared to HREE. Following Shimizu & Richardson [1987], the authors draw a conclusion that garnet-bearing peridotites from studied xenoliths underwent deep-level metasomatism under the influence of fluids which were genetically related to carbonatite melt.

The study of the REE distribution between garnets and coexisting melts, conducted by Beattie [1993] evidences that the values of K_d (garnet/melt) somehow depend on the concentration of these trace elements in the system. He believes that the studied magmatic system in relation to REE does not obey the Henry's rule, the same as the earlier established distribution of Ni in the "olivine-melt" system.

The observations of Pearson and coauthors [Pearson *et al.*, 1993] evidence that, according to the distribution of REE between the coexisting garnets and clinopyroxenes, pyroxenites of the Beni Bousera massif (Morocco) have much in common with the parageneses of these minerals from garnet-bearing pyroxenites of the Lherz massif (France), where the garnet is considered to be the secondarily formed phase. At the same time, the presence of garnets with cubo-octahedral faceting in the Beni Bousera massif, which form inclusions in graphitized diamond, suggests that these are a high-temperature phase in this case. On the basis of data obtained the authors suggest that the experimentally established coefficients of REE distribution in the crystal-liquid system do not exactly correspond to the mantle rocks, as the chemical composition of the latter was significantly changed under subsolidus conditions.

The study of the REE distribution in high-Ca garnets from metasomatic granites of the ore zone in the Broken Hill deposit (Australia), using the SIMS procedure, showed that they are significantly enriched in LREE compared to low-Ca garnets [Schwandt *et al.*, 1993]. It was also revealed that the rims of garnet grains compared to the center are normally enriched in HREE. The REE patterns of garnets from ore body often display positive Eu anomalies, whereas garnet from the rocks occurring at a distance from the zone of ore mineralization is depleted in Eu. The authors suggest that HREE are concentrated directly in the structure of garnets, while considerable amounts of LREE occur in the intragrain material which also contains chlorites, chlortoids and some other phases enriched in titanium.

Analyses of REE in orthopyroxenes from high-temperature pyroxenites of the Zabargad ultramafic massif (Red Sea) [Vannucci *et al.*, 1993] evidence that this mineral contains unusually high concentrations of heavy elements. The authors believe that this feature of orthopyroxenes results from the fact that they formed during decompression reactions by the replacement of earlier garnets, which proceeded at $T > 1000^{\circ}\text{C}$ and $P \approx 20\text{--}30$ kbar.

The estimates of K_d (REE) for the garnet–melt and garnet–clinopyroxene systems were obtained in the physical experiments with high-aluminous basalts [Hauri *et al.*, 1994]. The estimates of K_d (garnet/melt) for La and Lu were close to the values published earlier, whereas the values of K_d for medium REE were higher. The plots of variations in K_d , based on these data, have a nearly ‘flat’ shape relative to heavy elements. The authors attribute the discrepancy in K_d values to some features of the chemical compositions of studied garnets.

Experimental works of Johnson [1998] show that the values of K_d (garnet/melt) successively increase from La (0.002) to Lu (8–9), and changes in temperature have a less significant influence on the variations in the values of K_d (garnet/melt) for REE than on the values of K_d (Ti).

The problem of the occurrence of sinusoidal patterns of REE distribution in garnets from high-temperature rocks in connection with metasomatic processes was discussed in the work of Hoal and coauthors [Hoal *et al.*, 1994]. They think that this phenomenon is related to the effect of lagging of heavy elements compared to light elements during the metasomatic rearrangement of REE in the mineral structure, which is, in turn, associated with the different diffusion rates of these groups of elements. Most likely, the sinusoidal REE patterns of garnets reflect the state of incomplete equilibrium of elements during the metasomatic process, which could remain in the high-temperature varieties of this mineral. It is also worth noting that the REE

patterns of garnets from deep xenoliths, occurring in off-cratonic and intra-cratonic regions, are characterized by both sinusoidal REE patterns and REE patterns typical of this mineral. The calculations of Hoal and coauthors show that the REE compositions of model metasomatized melts are similar to the REE compositions of kimberlites and lamproites, but not to those kimberlites in which these garnet-bearing xenoliths occur.

Experimental study of the influence of carbonatite metasomatism on the variations in the ratios of LREE and HREE in garnets and other minerals from peridotites [Sweeney *et al.*, 1995] evidences that at $P = 18\text{--}46$ kbar the K_d (garnet/carbonatite melt) value for Lu varies in the range of 11.6–17.7, whereas in the process with participation of silicate melt the K_d values are considerably lower (7).

New data on the distribution of REE between coexisting garnets and clinopyroxenes were obtained when studying eclogite xenoliths from the Roberts Victor (using SIMS method) [Harte, Kirkley, 1997]. It was shown that the values of K_d (clinopyroxene/garnet) for REE, the same as for Sr and Y, decrease with increasing $\text{Ca}/(\text{R}^{2+})$ value in these minerals, decreasing by three orders of magnitude for light REE. Study of garnets and clinopyroxenes from eclogite xenoliths of some deposits in South Africa and Siberia shows that the observed significant variations in the values of K_d (clinopyroxene/garnet) for REE are the function of Ca contents in these minerals.

Data on the distribution of REE in garnets in the studies of Iherzolite xenoliths occurring in kimberlites from Camsell Lake Field (Canada) were obtained by Pokhilenko *et al.* [1998]. These garnets have a high content of Cr (to 17 wt%) and they display sinusoidal patterns of REE distribution normally observed in subcalcium pyropes from garnet-bearing harzburgite-dunite parageneses.

Blundy *et al.* [1998] paid attention to the fact that the values of K_d (garnet/melt) are typically >1 and successively increase from light to heavy elements, beginning from Gd and from Eu as well, which allows the above REE to be regarded as quite compatible with garnet structure. Study of the geochemistry of garnets from eclogite xenoliths occurring in the Mbuji-Mayi province (Congo) showed that diffusion of light REE from phosphates (apatite, whitlockite) in contacting garnet grains as well as clinopyroxenes, results in their increased contents in these minerals [Demaiffe *et al.*, 1998].

The survey of major problems of REE geochemistry in garnets was presented by Jacob and coauthors [Jacob & Foley, 1998; Jacob & Mattey, 1998; Jacob *et al.*, 1998]. On examples of garnets from diamondiferous eclogite xenoliths (Udachnaya pipe), layered diamondiferous and non-diamondiferous kyanite eclogite xenoliths (Roberts Victor pipe) and subcalcium garnets from peridotite xenoliths (Somerset Island and Saskatchewan province) (Canada) they studied the relationships between the REE composition of garnets and their total chemical composition and the content of other trace elements, as well as the probable formation conditions of subcalcium garnets during metasomatic transformations of spinel harzburgites in the diamond stability field.

The detailed investigation of REE geochemistry in garnet inclusions in diamonds contained in some kimberlite pipes of Siberia [Pearson & Milledge, 1998] showed that the marginal zones of garnets are nonuniformly enriched in La и Ba, whereas in the central zones these elements are distributed uniformly. In another work [Pearson *et al.*, 1998] the problems of the systematization of garnets from kimberlites and lamproites on the basis of their REE compositions were discussed. It was shown that in

6 Rare earth elements in ultramafic and mafic rocks and their minerals

most cases these garnets are depleted in HREE and are enriched in MREE, as a result of which their REE patterns have a sinusoidal shape.

The conditions of the origin of sinusoidal REE patterns in garnets were also discussed on the example of samples from ultramafic complexes in kimberlites from the Roberts Victor pipe and from inclusions of diamonds from the Akwitia province (Ghana) [Stachel *et al.*, 1998]. The authors conclude that, being the derivatives of one and the same spinel-harzburgite protolith, garnets from lherzolites imprinted the event of its enrichment in REE, which did not involve garnets occurring in harzburgites. Burgess & Harte [1999] discuss the relationship between the REE composition of garnets and the shape of their patterns, on the one hand, and their total chemical composition and crystallization temperatures, on the other.

On the basis of experimental data obtained at $P = 2.4\text{--}2.8 \text{ GPa}$ the features of REE distribution between the garnet containing 24% grossular component and coexisting melts were studied [Salters & Longhi, 1999]. These authors established that the crystallochemical dependence of the $K_d(\text{garnet}/\text{melt})$ for light REE is rather weak and that the main factors of REE distribution are pressure and temperature. It was reported that the influence of garnet composition on the REE distribution in them increases with an increase in their atomic numbers. The dominating factor controlling the distribution of HREE in garnets is the content of grossular component.

It is reasonable to refer here to the work of Bocchio *et al.* [2000] in which they describe the specific features of the crystallochemistry of REE in garnets and clinopyroxenes from eclogites and other metamorphic rocks of the Soazza province (Switzerland) and, in particular, substantiate the notion on the dependence of REE distribution in these minerals and geochemistry of their crystallochemical structure on the sizes of ionic radii of replacing and replaced ions and the balance of their charges. Some more recently published works discuss the geochemistry of REE distribution in garnets forming microinclusions in garnets [Harris *et al.*, 2004; Promprated *et al.*, 2004; Stachel *et al.*, 2004] and those occurring in skarns [Gaspar *et al.*, 2008].

Lehtonen [2005] published data on REE distribution in pyrope garnets from the Kaavi-Kuopio kimberlites (Finland). Garnets from lherzolite parageneses are depleted in LREE compared to MREE and HREE. The enrichment of garnets in MREE and HREE is related to the metasomatism resulting in the increase in Ti content in this mineral. The detected contents of REE in garnets from kimberlites of this region are evidence of several events of enrichment and depletion of mantle material.

In the example of garnets from eclogites of the Soazza province (Switzerland) Baumgartner & Skora [2006] modeled the diffusion processes of REE during the crystal growth of this mineral. The authors made a conclusion that the growth of garnets occurs over 10 million years. The content of Lu is distributed nonuniformly, which is related to the specific diffusion of this rare-earth element, depending on temperature and pressure parameters.

The study of garnets from peridotites in xenoliths in kimberlites and volcanic rocks from the Mengyin and Shanwang provinces (North China craton) showed that this mineral is characterized by different total chemical compositions and geochemical properties depending on the composition and location of rocks [Zheng *et al.*, 2006]. Garnets from Mengyin province have a total of REE 10–12 ppm, and $(\text{La/Yb})_n = 0.06\text{--}0.07$; they show depleted LREE and flat HREE patterns from Sm to Lu. The garnets from Shanwang province contain 25–58 ppm of ΣREE and $(\text{La/Yb})_n = 0.02\text{--}0.17$;

the REE pattern is weakly convex upward and has a negative Ce anomaly. Khazan & Ariasova [2007] studied the REE composition of garnets and coexisting clinopyroxenes from xenoliths carried out by kimberlites of the Kaapvaal province (Southern Africa) and Somerset Island province (Arctic Canada). They established considerable variations in REE composition of clinopyroxenes and, to a lesser degree, garnets from pressure at 2–6 GPa. The authors think that the spatial fractionation of REE was the result of their nonequilibrium differentiation between melt and restite, which was accompanied by the episodes of scaled melting of the mantle. According to the model proposed in the work, the spatial fractionation of REE could result from moderately high (10–20%) melting of preliminarily depleted peridotite. This episode of melting preceded the episode of a higher-degree melting that led to the ‘wash-out’ of a considerable part of clinopyroxene and garnet from the mantle. The considerable differences between clinopyroxenes and garnets from the upper mantle in the character of variations in REE composition depending on the pressure are explained by the difference in the activation energy of REE diffusion: 400–500 kJ/mole in clinopyroxene and less than 300 kJ/mole in garnet. In their other work the authors emphasize once again that the character of dependence of REE contents in garnets and clinopyroxenes from xenoliths carried out by kimberlites on the pressure, regularly changes in the series from La to Lu. The observed regularity is explained by the nonequilibrium differentiation of these trace elements between the melt and polymimetic restite owing to the high degree of partial melting of mantle substrate and further segregation of generated magmas [Ariasova & Khazan, 2007]. In the work of Spera *et al.* [2007] a compilation of solid-fluid and melt-fluid distribution coefficients for about 30 trace elements, including REE, among coexisting garnet, clinopyroxene, plagioclase and some other minerals is provided. Study of the geochemistry of olivine-bearing rocks with garnets and omphacite from high-temperature granulites of the Kandalaksha massif (Kola Peninsula, Russia) showed positive Eu anomalies, which are not typical of most garnet-bearing formations [Skublov & Terekhov, 2009]. This led the authors to assume that garnets from these metamorphic rocks are also characterized by positive Eu anomalies, which is observed quite rarely. Li *et al.* [2010] studied the REE composition of hydrogrossular from rodingites, included in ultramafic rocks of the Changawuzi ophiolite in southwestern Tien Shan (China). The hydrogrossular formed during rodingitization and does not display strong enrichment of HREE. The crystals show very low total REE, with overall flat HREE patterns, a positive increase in LREE with increasing atomic number and pronounced positive Eu anomaly. This unusual Eu anomaly in garnet may reflect the special origin of Ca-rich garnet during Ca metasomatism.

1.2 GENERAL REGULARITY OF REE DISTRIBUTION IN GARNETS OF THE MOST COMMON OF THEIR PARAGENESSES

Features of geochemistry of REE in garnets are considered depending on those petrographic types of rocks they participate in. The most common types of garnet-bearing rocks are the following: 1) high-pressure peridotites, mainly harzburgites and lherzolites from xenoliths in kimberlites, and 2) lherzolites and pyroxenites from xenoliths

in alkaline basalts, and 3) inclusions in diamonds, and 4) eclogites from xenoliths in kimberlites and alkaline basalts, and 5) eclogites from high-pressure metamorphic complexes, and 6) some types of gabbros, and 7) some varieties of effusive rocks, and 8) skarns, and 9) gneisses, schist and other metamorphic mesobaric rocks.

High-pressure garnet peridotites, mainly harzburgites and lherzolites. Garnets from these ultramafic rocks are studied in detail, particularly regarding the REE distribution in samples from diamondiferous and non-diamondiferous deep-seated xenoliths presented in kimberlites (Table 1.1, Figure 1.1). By chemical composition they are predominantly high-chromium ($>5\% \text{ Cr}_2\text{O}_3$) and subcalcium pyropes. The observations indicate significant heterogeneity of the REE distribution in them, including their total compositions and the levels of accumulation of certain elements, the degree of fractionation of REE and configuration of the patterns. Based on the total sample of analysis of garnets from these rocks, compiled from our database, we found that the total REE content in them is from the first grams per ton to 35 ppm.

In the garnets from harzburgite xenoliths presented in the Roberts Victor kimberlite pipe, the total REE concentrations vary in the range of 1.5–18.6 ppm, while for garnets from lherzolite xenoliths – 0.8–10.9 ppm. In the minerals from harzburgites we can observe wider fluctuations in concentrations for medium and heavy REE, while in the minerals from lherzolites – for light elements. Some samples of garnets from harzburgites show depletion in heavy elements, starting with Sm and ending with Yb that is why their patterns have a sinusoidal configuration (see Figure 1.1, 1), they show smooth peaks in Pr area, as well as smooth minima in the range between Gd and Er. Almost all analyzed garnets from lherzolite xenoliths of Roberts Victor pipe are depleted by LREE, and in the medium and heavy elements area their patterns have a flattened shape (see Figure 1.1, 2). Evidence of heterogeneity of REE distribution in garnets from xenoliths of this pipe is wide variations in $(\text{La/Yb})_n$ values – from 0.01 to 14.2. According to the studies, REE composition of garnets from diamondiferous peridotite xenoliths of Roberts Victor pipe corresponds to the composition of REE in this mineral from the primitive mantle. It is assumed that garnets from lherzolite parageneses characterize the event of its enrichment in LREE, whereas the samples of garnets from harzburgite parageneses have not been subjected to such enrichment [Stachel *et al.*, 1998; Nixon *et al.*, 1987].

Having examined the representative collection of samples of garnets from peridotite xenoliths of Udachnaya kimberlite pipe (Yakutia), Pokhilenko *et al.* [1993] and Shimizu *et al.* [1997a] determined that the total REE content in them varies in a very wide range (0.7–39.8 ppm). A significant part of the studied garnets had sinusoidal REE pattern (see Figure 1.1, 13, 15). Such patterns are often observed in garnets from peridotite xenoliths of Yubileynaya pipe (see Figure 1.1, 16). Apart from the garnets with sinusoidal patterns in the xenoliths from Udachnaya pipe, there were identified certain varieties, significantly depleted by LREE and at the same time enriched in heavy elements. These garnets are characterized by more simple in form, positively inclined patterns, flattened in the heavy REE (see Figure 1.1, 14). An overwhelming majority of the garnets from xenoliths of Udachnaya pipe is characterized by very low values of $(\text{La/Yb})_n = 0.01–0.20$, rarer are the samples with $(\text{La/Yb})_n = 2.1–9.4$. By the configuration of garnet patterns of Udachnaya pipe are comparable with some samples from peridotite xenoliths of South African kimberlite from Jagersfontein, Kimberley, Lourensen, Premier (see Figure 1.1, 4, 5, 7, 8) and some other manifestations (see Figure 1.1 9–12). Relatively simple in form,

Table 1.1 REE compositions of garnets from harzburgites, lherzolites and peridotites from xenoliths in kimberlites of some provinces and pipes (ppm).

Roberts Victor pipe, Ghana											
	[Stachel et al., 1998], SIMS										
	RV168	RV162	RV167	RV174	RV175	RV177	RV179	BD1174	BD1195	RV160	RV161
Element	<i>Harzburgites</i>										<i>Lherzolite</i>
La	0,190	0,210	0,080	1,920	0,330	0,810	0,400	0,080	0,240	0,070	0,050
Ce	1,500	0,760	0,800	7,930	3,060	5,360	3,950	0,840	2,070	0,960	0,780
Pr	0,390	0,100	0,270	1,210	0,490	0,910	0,600	0,320	0,430	0,230	0,360
Nd	2,270	0,310	2,190	4,930	2,060	4,320	1,870	3,490	1,460	0,970	1,920
Sm	0,510	0,020	0,660	0,750	0,260	0,770	0,120	2,890	0,060	0,110	0,390
Eu	0,130	0,010	0,220	0,200	0,050	0,170	0,030	1,060	0,010	0,020	0,090
Gd	0,490	0,010	0,710	0,670	0,090	0,480	0,200	3,120	0,040	0,040	0,510
Tb	0,120	N.d.	0,140	0,090	0,010	0,070	0,010	0,320	0,010	N.d.	0,100
Dy	0,820	0,010	0,940	0,350	0,050	0,280	0,050	1,490	0,020	0,010	0,740
Ho	0,230	N.d.	0,190	0,070	0,010	0,070	0,010	0,150	N.d.	N.d.	0,200
Er	0,730	N.d.	0,720	0,200	0,040	0,220	0,040	0,310	0,020	0,010	0,710
Tm	N.d.	N.d.	N.d.	N.d.	N.d.	N.d.	N.d.	N.d.	N.d.	N.d.	N.d.
Yb	1,060	0,010	0,910	0,210	0,090	0,340	0,040	0,310	0,130	0,050	1,130
Lu	0,170	0,010	0,170	0,040	0,030	0,080	0,020	0,060	0,040	0,030	0,210
Total	8,61	1,45	8,00	18,57	6,57	13,9	7,34	14,4	4,53	2,50	7,19
(La/Yb) _n	0,12	14,2	0,06	6,17	2,47	1,61	6,75	0,17	1,25	0,94	0,03

(Continued)

Table I.I (Continued).

Roberts Victor pipe, Ghana						Bultfontein pipe, South Africa		Jagersfontein pipe, South Africa		Endekuil pipe, South Africa	
[Stachel et al., 1998], SIMS						[Shimizu, 1975], IDMS		[Hoal et al., 1994], IPMA			
	RV166	RV169	RV170	RV176	BD1173	BD1196	BUL6	JJG352	JAG9006A	JAG84595	EDKI
Element	Lherzolites										
La	0,060	0,010	0,130	1,200	N.d.	0,020	N.d.	N.d.	0,062	0,017	N.d.
Ce	0,670	0,090	0,700	5,530	0,050	0,150	0,957	0,763	0,460	0,286	0,282
Pr	0,240	0,040	0,180	0,390	0,020	0,060	N.d.	N.d.	N.d.	N.d.	N.d.
Nd	2,140	0,330	1,350	2,080	0,200	0,760	3,000	3,960	1,493	2,480	1,005
Sm	0,750	0,360	0,570	0,470	0,090	0,710	1,570	1,870	1,252	2,780	0,869
Eu	0,210	0,110	0,220	0,120	0,030	0,350	0,842	0,679	0,500	1,350	0,380
Gd	1,130	0,420	0,860	0,450	0,070	1,500	2,520	2,050	N.d.	N.d.	N.d.
Tb	0,160	0,120	0,130	0,040	0,020	0,250	N.d.	N.d.	N.d.	N.d.	N.d.
Dy	1,160	0,860	1,150	0,290	0,080	1,810	1,690	1,470	2,583	3,420	3,439
Ho	0,260	0,210	0,270	0,040	0,020	0,350	N.d.	N.d.	N.d.	N.d.	N.d.
Er	0,820	0,760	1,020	0,110	0,070	1,010	0,604	0,688	2,050	1,890	2,373
Tm	N.d.	N.d.	N.d.	N.d.	N.d.	N.d.	N.d.	N.d.	N.d.	N.d.	N.d.
Yb	0,760	1,060	1,190	0,110	0,120	0,860	0,572	0,757	2,132	2,670	2,405
Lu	0,160	0,130	0,180	0,020	0,020	0,180	N.d.	N.d.	N.d.	N.d.	N.d.
Total	8,52	4,50	7,95	10,9	0,79	8,01	11,8	12,2	10,5	14,9	10,8
(La/Yb) _n	0,05	0,01	0,07	7,36	N.d.	0,02	N.d.	N.d.	0,02	N.d.	N.d.

(Continued)

Table I.1 (Continued).

	Kimberley province, South Africa		Lesotho province, South Africa		Lourensia prov., South Africa		Premier pipe, South Africa		Rietfontein pipe, South Africa		Sanddrift
	[Hoal et al., 1994], IPMA										
	AJE25	AJE1181	PHN1611	PHN2302	L24	L14	PREM9006	RVD408	RIET5	RIET2	SDD591
Element	Peridotites										
La	0,047	0,072	N.d.	N.d.	0,045	N.d.	0,054	0,059	N.d.	N.d.	0,040
Ce	0,451	0,715	0,983	3,850	0,211	0,989	0,535	0,615	0,211	0,527	0,864
Pr	N.d.	N.d.	N.d.	N.d.	N.d.	N.d.	N.d.	N.d.	N.d.	N.d.	N.d.
Nd	2,190	4,872	1,770	3,590	0,476	3,390	2,237	2,130	1,300	2,580	3,160
Sm	2,020	4,025	1,220	1,940	0,594	3,380	2,351	1,250	2,040	3,190	2,138
Eu	0,949	1,165	0,570	0,831	0,374	1,380	0,998	0,341	1,140	1,180	0,823
Gd	N.d.	N.d.	N.d.	N.d.	N.d.	N.d.	N.d.	N.d.	N.d.	N.d.	N.d.
Tb	N.d.	N.d.	N.d.	N.d.	N.d.	N.d.	N.d.	N.d.	N.d.	N.d.	N.d.
Dy	5,840	0,709	3,040	1,420	4,170	3,930	5,921	0,652	5,950	1,730	3,414
Ho	N.d.	N.d.	N.d.	N.d.	N.d.	N.d.	N.d.	N.d.	N.d.	N.d.	N.d.
Er	4,590	0,562	1,970	0,356	3,550	1,850	3,752	0,404	3,500	0,752	2,037
Tm	N.d.	N.d.	N.d.	N.d.	N.d.	N.d.	N.d.	N.d.	N.d.	N.d.	N.d.
Yb	6,330	0,632	1,880	0,355	3,770	2,070	4,890	0,469	4,180	1,200	1,545
Lu	N.d.	N.d.	N.d.	N.d.	N.d.	N.d.	N.d.	N.d.	N.d.	N.d.	N.d.
Total	22,4	12,8	11,4	12,3	13,2	17,0	20,7	5,92	18,3	11,2	14,0
(La/Yb) _n	0,01	0,08	N.d.	N.d.	0,01	N.d.	0,01	0,08	N.d.	N.d.	0,02

(Continued)

Table I.I (Continued).

	<i>Liqhobong province</i>	<i>Thaba Putsoa province</i>		<i>Mothae pipe</i>	<i>Udachnaya pipe, Yakutia, Russia</i>						
[Shimizu, 1975]											
	PHN2302	PHN1566	PHN1611	PHN1925	379/86	667/86	394/86	404	404k	465/86	450/89
Element											
<i>Lherzolites</i>											
La	N.d.	N.d.	N.d.	N.d.	6,940	1,260	0,340	0,400	0,450	0,650	1,840
Ce	3,850	1,540	0,983	N.d.	18,890	8,440	3,410	2,400	2,710	5,660	7,310
Pr	N.d.	N.d.	N.d.	N.d.	N.d.	N.d.	N.d.	N.d.	N.d.	N.d.	N.d.
Nd	3,590	3,100	1,770	1,330	4,920	7,400	2,920	2,610	2,530	2,850	5,240
Sm	1,940	2,140	1,220	0,912	0,990	2,990	0,740	0,760	0,760	0,140	1,220
Eu	0,831	1,040	0,570	0,483	0,130	0,650	0,150	0,270	0,240	0,080	0,250
Gd	2,440	3,820	2,280	2,110	N.d.	N.d.	N.d.	N.d.	N.d.	N.d.	N.d.
Tb	N.d.	N.d.	N.d.	N.d.	N.d.	N.d.	N.d.	N.d.	N.d.	N.d.	N.d.
Dy	1,420	5,040	3,040	3,360	0,360	0,510	0,090	0,390	0,440	0,140	0,560
Ho	N.d.	N.d.	N.d.	N.d.	N.d.	N.d.	N.d.	N.d.	N.d.	N.d.	N.d.
Er	0,356	3,290	1,970	2,360	0,400	0,310	0,120	0,230	0,210	0,190	0,230
Tm	N.d.	N.d.	N.d.	N.d.	N.d.	N.d.	N.d.	N.d.	N.d.	N.d.	N.d.
Yb	0,355	2,960	1,880	2,450	0,500	0,410	0,180	0,260	0,240	0,770	0,400
Lu	N.d.	N.d.	N.d.	N.d.	N.d.	N.d.	N.d.	N.d.	N.d.	N.d.	N.d.
Total	14,8	22,9	13,7	13,0	33,1	22,0	7,95	7,32	7,58	10,5	17,1
(La/Yb) _n	N.d.	N.d.	N.d.	N.d.	9,37	2,07	1,27	1,04	1,27	0,57	3,10

(Continued)

Table I.I (Continued).

<i>Udachnaya pipe, Yakutia, Russia</i>											
Element	[Pokhilenko et al., 1993], IPMA					[Shimizu et al., 1997a], IPMA					
	25I/86	25I/86k	514/86	177/89	44I/86	52/76	80/92	239/89	51/92	74/89c	74/89r
<i>Peridotites</i>											
La	1,090	0,630	0,040	0,300	0,010	0,184	0,190	0,239	0,083	0,091	0,055
Ce	2,620	1,700	0,120	2,440	1,370	1,785	1,450	2,050	0,739	0,606	0,662
Pr	N.d.	N.d.	N.d.	N.d.	N.d.	N.d.	N.d.	N.d.	N.d.	N.d.	N.d.
Nd	0,600	0,410	0,500	2,010	4,170	5,030	3,110	4,410	2,300	1,410	1,590
Sm	0,150	0,170	1,000	0,560	8,690	2,930	2,460	2,920	1,250	0,591	1,170
Eu	0,020	0,070	0,600	0,060	9,910	1,220	0,986	1,060	0,529	0,323	0,564
Gd	N.d.	N.d.	N.d.	N.d.	N.d.	N.d.	N.d.	N.d.	N.d.	N.d.	N.d.
Tb	N.d.	N.d.	N.d.	N.d.	N.d.	N.d.	N.d.	N.d.	N.d.	N.d.	N.d.
Dy	0,050	0,050	3,950	0,250	6,310	2,620	4,480	1,650	3,220	1,660	2,520
Ho	N.d.	N.d.	N.d.	N.d.	N.d.	N.d.	N.d.	N.d.	N.d.	N.d.	N.d.
Er	0,090	0,080	2,680	0,390	3,990	1,110	2,090	0,777	1,880	0,923	1,140
Tm	N.d.	N.d.	N.d.	N.d.	N.d.	N.d.	N.d.	N.d.	N.d.	N.d.	N.d.
Yb	0,420	0,280	2,550	1,050	4,420	1,140	2,150	0,961	2,120	0,980	1,440
Lu	N.d.	N.d.	N.d.	N.d.	N.d.	N.d.	N.d.	N.d.	N.d.	N.d.	N.d.
Total	5,04	3,39	11,4	7,06	38,9	16,0	16,9	14,1	12,1	6,58	9,14
(La/Yb) _n	1,75	1,52	0,01	0,19	N.d.	0,11	0,06	0,17	0,03	0,06	0,03

(Continued)

Table I.I (Continued).

<i>Udachnaya pipe, Yakutia, Russia</i>											
	[Shimizu et al., 1997a], IPMA										
	74/89r	424/89	121/91	246/89c	246/89r	76/92	70/92	267/89c	267/89r	228/89	115/89
Element	<i>Peridotites</i>										
La	0,055	0,150	0,133	0,038	0,186	0,179	0,192	0,121	0,083	0,101	0,050
Ce	0,662	1,290	1,180	0,558	1,220	1,770	1,660	0,592	0,327	0,875	0,525
Pr	N.d.	N.d.	N.d.	N.d.	N.d.	N.d.	N.d.	N.d.	N.d.	N.d.	N.d.
Nd	1,590	3,080	1,770	0,570	1,560	0,827	2,840	1,480	1,560	1,570	1,810
Sm	1,170	1,460	0,516	0,235	1,360	0,089	0,616	0,962	1,350	0,867	1,050
Eu	0,564	0,540	0,117	0,080	0,620	0,027	0,193	0,397	0,691	0,363	0,399
Gd	N.d.	N.d.	N.d.	N.d.	N.d.	N.d.	N.d.	N.d.	N.d.	N.d.	N.d.
Tb	N.d.	N.d.	N.d.	N.d.	N.d.	N.d.	N.d.	N.d.	N.d.	N.d.	N.d.
Dy	2,520	1,190	0,227	0,280	2,890	0,034	0,368	2,160	3,560	1,280	1,010
Ho	N.d.	N.d.	N.d.	N.d.	N.d.	N.d.	N.d.	N.d.	N.d.	N.d.	N.d.
Er	1,140	0,530	0,193	0,580	2,060	0,093	0,269	1,930	2,780	0,596	0,675
Tm	N.d.	N.d.	N.d.	N.d.	N.d.	N.d.	N.d.	N.d.	N.d.	N.d.	N.d.
Yb	1,440	0,640	0,272	0,623	2,460	0,196	0,297	2,130	2,810	0,742	0,826
Lu	N.d.	N.d.	N.d.	N.d.	N.d.	N.d.	N.d.	N.d.	N.d.	N.d.	N.d.
Total	9,14	8,88	4,41	2,96	12,4	3,22	6,44	9,77	13,2	6,39	6,35
(La/Yb) _n	0,03	0,16	0,33	0,04	0,05	0,62	0,44	0,04	0,02	0,09	0,04

(Continued)

Table I.I (Continued).

<i>Udachnaya pipe, Yakutia, Russia</i>										
	[Shimizu et al., 1997a], IPMA									
	107/89	61/91	285/89	274/89c	274/89r	417/89	100/91	293/89	25/91	306/89
<i>Element</i>	<i>Peridotites</i>									
La	0,332	0,172	0,085	0,083	0,073	0,030	0,115	0,061	0,062	0,066
Ce	1,720	1,310	0,150	0,021	0,230	0,060	0,054	0,127	0,682	0,375
Pr	N.d.	N.d.	N.d.	N.d.	N.d.	N.d.	N.d.	N.d.	N.d.	N.d.
Nd	3,180	2,120	0,141	0,135	0,192	0,290	0,123	0,033	0,637	0,216
Sm	2,210	0,920	0,049	0,057	0,107	0,430	0,072	0,014	0,085	0,161
Eu	0,690	0,291	0,016	0,016	0,037	0,290	0,023	0,007	0,023	0,065
Gd	N.d.	N.d.	N.d.	N.d.	N.d.	N.d.	N.d.	N.d.	N.d.	N.d.
Tb	N.d.	N.d.	N.d.	N.d.	N.d.	N.d.	N.d.	N.d.	N.d.	N.d.
Dy	1,660	1,090	0,069	0,047	0,085	2,560	0,115	0,037	0,170	0,369
Ho	N.d.	N.d.	N.d.	N.d.	N.d.	N.d.	N.d.	N.d.	N.d.	N.d.
Er	0,778	0,871	0,121	0,063	0,053	1,880	0,206	0,027	0,475	0,322
Tm	N.d.	N.d.	N.d.	N.d.	N.d.	N.d.	N.d.	N.d.	N.d.	N.d.
Yb	0,965	0,855	0,250	0,247	0,237	2,030	0,803	0,197	1,310	0,568
Lu	N.d.	N.d.	N.d.	N.d.	N.d.	N.d.	N.d.	N.d.	N.d.	N.d.
Total	11,54	7,63	0,88	0,67	1,01	7,57	1,51	0,50	3,44	2,14
(La/Yb) _n	0,23	0,14	0,23	0,23	0,21	0,01	0,10	0,21	0,03	0,08

(Continued)

Table I.I (Continued).

Yubileynaya pipe, Yakutia, Russia					Lekkerfontein		Monastery pipe, South Africa			
	[Aschepkov et al., 2004], LA ICP-MS				[Jones, 1987], RNAA					
	Asch-1	Asch-2	Asch-3	Asch-4	Asch-5	RAJ L26	263IA	263IB	263IC	263ID
Element	Peridotites					Megacrystals in kimberlites				
La	0,150	0,050	0,030	0,020	0,160	0,040	N.d.	N.d.	N.d.	N.d.
sCe	0,610	0,140	0,100	0,110	0,290	0,260	0,510	0,450	0,410	0,380
Pr	0,130	0,030	0,020	0,020	0,080	N.d.	N.d.	N.d.	N.d.	N.d.
Nd	1,000	0,410	0,230	0,270	0,470	0,990	1,960	1,660	1,660	1,540
Sm	0,370	0,270	0,200	0,160	0,510	0,890	1,750	1,420	1,500	1,400
Eu	0,100	0,100	0,070	0,070	0,270	0,480	0,910	0,740	0,780	0,740
Gd	0,250	0,440	0,300	0,210	1,140	1,850	3,680	3,400	3,680	3,400
Tb	0,010	0,070	0,050	0,040	0,200	N.d.	N.d.	N.d.	N.d.	N.d.
Dy	0,080	0,420	0,310	0,150	1,120	N.d.	7,060	6,710	7,100	5,900
Ho	0,010	0,100	0,060	0,020	0,180	N.d.	N.d.	N.d.	N.d.	N.d.
Er	0,040	0,290	0,150	0,050	0,350	2,930	5,850	4,530	5,160	4,720
Tm	0,010	0,050	0,020	N.d.	0,040	N.d.	N.d.	N.d.	N.d.	N.d.
Yb	0,070	0,250	0,170	0,060	0,260	2,830	5,410	4,540	4,890	4,680
Lu	0,010	0,050	0,030	0,020	0,040	N.d.	N.d.	N.d.	N.d.	N.d.
Total	2,84	2,67	1,74	1,20	5,11	10,27	27,13	23,45	25,18	22,76
(La/Yb) _n	1,45	0,13	0,12	0,22	0,42	N.d.	N.d.	N.d.	N.d.	N.d.

(Continued)

Table I.1 (Continued).

	Monastery pipe, South Africa		Premier pipe, South Africa		Frank Smith pipe,	Saskatchewan province, Canada			Hartebeest- fontein	
	[Jones, 1987], RNAA	[Irving, Frey, 1978]	[Jones, 1987], RNAA			[Fedorowich et al., 1995], LA ICP-MS			[Hoal et al., 1994], IPMA	
	263IE	M-I	RAP10	RAP11	FS-I	KM1P	KM2P	KM3P	KM4P	HBF27
Element	Megacrysts in kimberlites									Peridotite
La	N.d.	0,049	0,070	0,330	0,300	0,030	0,030	0,550	0,020	0,037
Ce	0,420	N.d.	0,410	1,050	0,800	0,370	0,350	8,300	0,150	0,353
Pr	N.d.	N.d.	N.d.	N.d.	0,190	0,180	0,160	2,800	0,070	N.d.
Nd	1,630	N.d.	1,240	2,030	1,900	2,000	2,600	18,000	0,700	0,924
Sm	1,470	1,670	0,970	1,540	1,600	0,900	1,360	3,400	0,640	0,781
Eu	0,770	0,800	0,490	0,800	0,800	0,220	0,450	0,560	0,270	0,228
Gd	3,680	5,100	2,170	3,450	3,800	0,700	1,000	0,840	0,800	N.d.
Tb	N.d.	0,800	N.d.	N.d.	0,750	0,110	0,100	0,050	0,140	N.d.
Dy	6,600	N.d.	4,010	4,570	6,200	0,800	0,510	0,170	1,040	0,983
Ho	N.d.	1,470	N.d.	N.d.	0,140	0,230	0,150	0,020	0,220	N.d.
Er	4,900	N.d.	2,800	6,570	4,400	0,800	0,750	0,050	0,740	0,883
Tm	N.d.	N.d.	N.d.	N.d.	0,630	0,150	0,140	0,010	0,110	N.d.
Yb	4,940	5,000	2,900	4,950	4,300	1,190	1,200	0,130	0,900	1,099
Lu	N.d.	0,840	0,470	0,780	0,630	0,200	0,250	0,030	0,130	N.d.
Total	24,41	15,73	15,53	26,07	26,44	7,88	9,05	34,91	5,93	5,29
(La/Yb) _n	N.d.	0,01	0,02	0,04	0,05	0,02	0,02	2,86	0,01	0,02

Note: Here and further: N.d. – no data. After the references are listed the analytical methods for determination of REE (abbreviations see [Lesnov, 2010, Table I.1]).

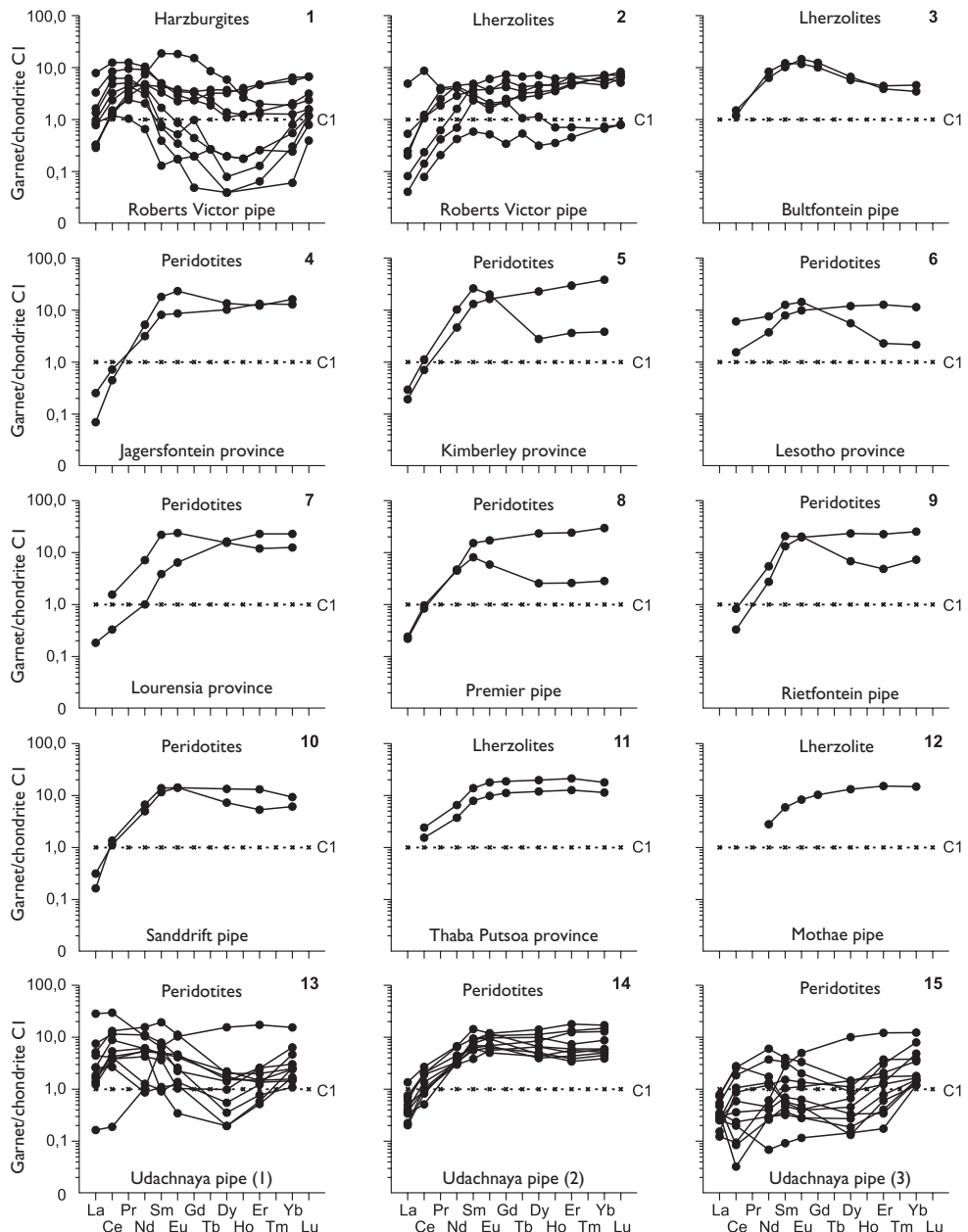


Figure 1.1 (Continued).

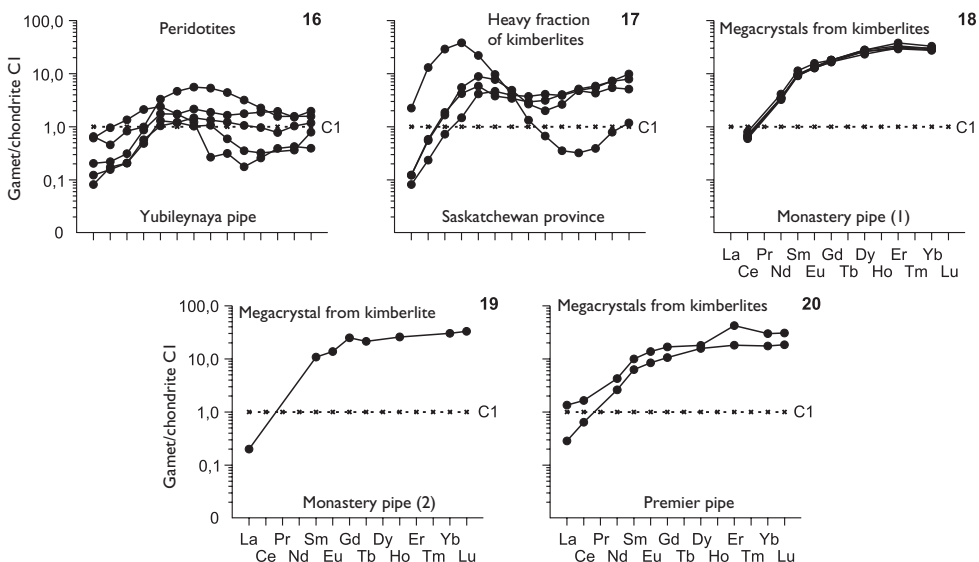


Figure 1.1 Chondrite-normalized REE patterns for garnets from peridotites in xenoliths, as well as megacrystals from kimberlites (data Table 1.1). Here and further, the valuation was carried out on the chondrite CI according (data [Evensen et al., 1978]).

positively inclined REE distribution patterns were observed in garnets of megacrystals in kimberlites of Monastery (see Figure 1.1, 18, 19) and Premier pipes (see Figure 1.1, 20). All of these garnets are characterized by a fairly intense fractionation of REE, the level of accumulation of LREE in them is 0.2–2.0 t.ch. (t.ch. – times of chondrite by [Evensen et al., 1978]), and of heavy elements – 20–40 t.ch.

According to Pokhilenko et al. [1993] subcalcium chrome pyropes from peridotite xenoliths from Udachnaya pipe had undergone mantle metasomatism under the influence of fluids that allegedly had geochemical characteristics of the carbonatite melt. Probably, as a result of this process, pyrope garnets were enriched to varying degrees in LREE and simultaneously depleted in Ti.

Garnet lherzolites and pyroxenites from xenoliths in alkali basalts. Features of the REE compositions of garnets are considered on the example of individual samples from xenoliths of Vitim province (Russia), and in samples of lherzolite not the full range of REE was determined at that (Table 1.2, Figure 1.2). In the garnets from pyroxenites the fractionation of REE is more intensive, they are significantly depleted by LREE ($\text{La} \approx 0.1$ t.ch.) and are enriched with heavy ones ($\text{Lu} \approx 100$ t.ch.), the parameter (La/Yb) in them is extremely low (~0.001–0.006).

Inclusions in diamonds. The adoption of microprobe methods of analysis of REE, including the method of LA ICP-MS, into geochemical studies of minerals allowed us to obtain much more reliable data on the composition of those REE garnets that are present in diamond crystals in the form of monomineral or polymimetic microinclusions. The prevailing elements of these microinclusions are subcalcium and high-chrome pyropes, which in association with clinopyroxene, orthopyroxene and olivine form a peridotite parageneses. Garnets of other compositions are usually found in

Table 1.2 Rare earth elements compositions of garnets from lherzolites and pyroxenites xenoliths in alkali basalts of Vitim province (ppm).

[Ionov et al., 1993]										[Litsov, 1998], SIMS			
	313-1	313-3	313-37	313-4	313-5	313-54	313-6	313-8	313-113G	V-231	V-102	V-437	
Element	Lherzolites										Pyroxenites		
La	N.d.	N.d.	N.d.	N.d.	N.d.	N.d.	N.d.	N.d.	N.d.	0,010	0,020	0,020	
Ce	N.d.	N.d.	N.d.	N.d.	N.d.	N.d.	N.d.	N.d.	N.d.	0,090	0,060	0,140	
Pr	N.d.	N.d.	N.d.	N.d.	N.d.	N.d.	N.d.	N.d.	N.d.	N.d.	N.d.	N.d.	
Nd	N.d.	N.d.	N.d.	N.d.	N.d.	N.d.	N.d.	N.d.	N.d.	0,630	0,590	0,700	
Sm	0,560	0,550	0,475	0,720	0,580	0,590	0,550	0,630	0,660	0,650	0,790	0,570	
Eu	0,375	0,416	0,470	N.d.	0,420	0,395	H. д.	0,440	0,463	0,340	0,460	0,310	
Gd	N.d.	N.d.	N.d.	N.d.	N.d.	N.d.	N.d.	N.d.	2,950	N.d.	N.d.	N.d.	
Tb	0,710	0,550	0,700	0,750	0,540	0,530	0,620	0,560	0,720	N.d.	N.d.	N.d.	
Dy	N.d.	N.d.	N.d.	N.d.	N.d.	N.d.	N.d.	N.d.	N.d.	4,280	9,580	2,910	
Ho	1,37	1,19	1,64	1,64	1,70	1,16	1,01	1,45	1,80	N.d.	N.d.	N.d.	
Er	N.d.	N.d.	N.d.	N.d.	N.d.	N.d.	N.d.	N.d.	N.d.	3,42	10,61	2,08	
Tm	N.d.	N.d.	N.d.	N.d.	N.d.	N.d.	N.d.	N.d.	N.d.	N.d.	N.d.	N.d.	
Yb	4,78	3,79	7,45	5,45	4,73	3,49	2,99	5,65	8,75	4,27	15,42	2,38	
Lu	0,710	0,650	1,09	0,830	0,770	0,510	0,462	0,990	1,42	N.d.	N.d.	N.d.	
Total	N.d.	N.d.	N.d.	N.d.	N.d.	N.d.	N.d.	N.d.	N.d.	13,7	37,5	9,11	
(La/Yb) _n	N.d.	N.d.	N.d.	N.d.	N.d.	N.d.	N.d.	N.d.	N.d.	0,002	0,001	0,006	

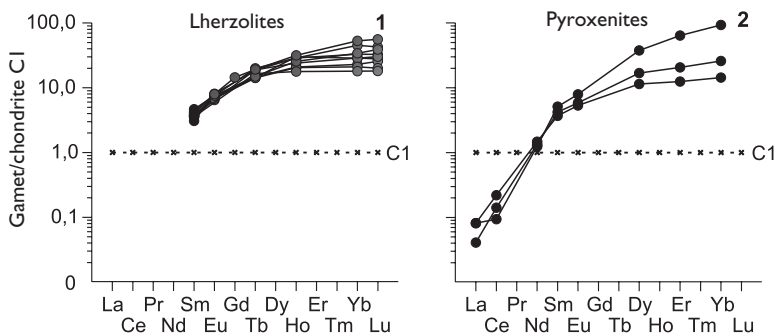


Figure 1.2 Chondrite-normalized REE patterns for garnets from lherzolites and pyroxenites in xenoliths from alkaline basalts of Vitim province (data Table 1.2).

association only with clinopyroxene (eclogite parageneses), characterized by low content of Cr and Mg and high contents of Ca and Al.

Let us consider the peculiarities of REE distribution in garnets from diamond microinclusions on the example of samples from Udachnaya, Mir and Aykhal kimberlite pipes (Yakutia province) [Shimizu *et al.*, 1997a], as well as pipes with placer manifestations confined to them, that are present in several provinces of South Africa and Canada (Table 1.3, Figure 1.3).

In general, the garnets that are present in diamond microinclusions from peridotite xenoliths are usually divided into two paragenetic types that, to a certain extent, differ in Ca content: harzburgite and lherzolite. In harzburgite parageneses samples the content of CaO varies in the range of ~0.6–6 wt%, which is considerably less than in the garnets from the microinclusions of lherzolite parageneses (5–8.6 wt%) [Stachel *et al.*, 2004]. Nevertheless, both types of garnets are almost identical by a total level of REE accumulation, as well as by the configuration of REE pattern, that both have sinusoidal shape. Compared with the garnets from the microinclusions in diamonds that belong to the peridotite parageneses, the samples of microinclusions of eclogite parageneses have rare-earth pattern of a simpler form. Most often it is a slightly convex upward line with an overall steep positive slope (Figure 1.4).

Within the available sample analyses of garnets from microinclusions in diamond, the total REE concentrations vary in the range of 1.2–78 ppm. At an average grade of ~9.6 ppm, the value of the $(La/Yb)_n$ parameter varies from 0.008 to 11.5. For particular samples of analysis of garnets from diamond microinclusions, the total REE concentrations vary within the following ranges by different pipes: 1) xenoliths of megacrystalline peridotites of Udachnaya pipe – 3–39 ppm; 2) xenoliths of peridotites of Aykhal pipe – 1.5–1.9 ppm; 3) xenoliths of peridotites of Mir pipe – ~5 ppm; 4) xenoliths of peridotites in Yubileynaya pipe – 1.2–5.1 ppm.

Heterogeneity of the REE composition of garnets from diamond inclusions, represented in each of kimberlite pipes, manifests in variations of not only the total content of elements, but also of the configuration of the pattern. For example, in the garnets from Udachnaya and Mir pipes the peak of the patterns is in the Sm area, while in other cases – in the Nd area (Figure 1.3, 1–4). Such differences in the pattern were also

Table 1.3 REE compositions of garnets from microinclusions in diamonds from kimberlites of some provinces, pipes and placers (peridotitic and eclogitic parageneses) (ppm).

Udachnaya pipe, Yakutia, Russia											
	[Shimizu et al., 1997b], IPMA										
	I33/9-1	I33/9-3	I33/9-7	56K	I36/9	I18/29-1	I18/29-6	I35/9-21	I35/9-22	I35/9-23	I35/9-3
Element	Peridotite parageneses										
La	0,028	0,016	0,063	0,185	0,362	0,086	0,221	0,154	0,343	0,094	0,082
Ce	0,254	0,230	0,358	1,700	3,890	2,470	2,930	0,784	1,450	0,957	0,848
Pr	N.d.	N.d.	N.d.	N.d.	N.d.	N.d.	N.d.	N.d.	N.d.	N.d.	N.d.
Nd	0,617	0,841	0,992	2,01	3,72	3,78	3,63	2,40	2,150	2,10	2,35
Sm	1,02	1,24	1,17	0,386	0,590	0,605	0,511	0,553	0,531	0,610	0,716
Eu	0,234	0,275	0,260	0,138	0,183	0,162	0,209	0,176	0,156	0,140	0,182
Gd	N.d.	N.d.	N.d.	N.d.	N.d.	N.d.	N.d.	N.d.	N.d.	N.d.	N.d.
Tb	N.d.	N.d.	N.d.	N.d.	N.d.	N.d.	N.d.	N.d.	N.d.	N.d.	N.d.
Dy	0,270	0,311	0,273	0,110	0,192	0,275	0,249	0,292	0,290	0,390	0,246
Ho	N.d.	N.d.	N.d.	N.d.	N.d.	N.d.	N.d.	N.d.	N.d.	N.d.	N.d.
Er	0,085	0,181	0,170	0,109	0,141	0,207	0,165	0,181	0,196	0,162	0,196
Tm	N.d.	N.d.	N.d.	N.d.	N.d.	N.d.	N.d.	N.d.	N.d.	N.d.	N.d.
Yb	0,210	0,134	0,273	0,318	0,292	0,368	0,416	0,290	0,117	0,155	0,303
Lu	N.d.	N.d.	N.d.	N.d.	N.d.	N.d.	N.d.	N.d.	N.d.	N.d.	N.d.
Total	2,72	3,23	3,56	4,96	9,37	7,95	8,33	4,83	5,23	4,61	4,92
(La/Yb) _n	0,09	0,08	0,16	0,39	0,84	0,16	0,36	0,36	1,98	0,41	0,18

(Continued)

Table 1.3 (Continued).

<i>Mir pipe, Yakutia, Russia</i>											
	[Shimizu et al., 1997b], IPMA										
	717-1	717-5	51-10	51-11	51-12	92/9-26	92/9-27	92/9-28	92/9-29	92/9-30	92/9-31
Element	<i>Peridotite parageneses</i>										
La	0,337	0,643	0,269	0,335	0,302	0,156	0,233	0,056	0,034	0,187	0,208
Ce	3,72	4,67	1,53	1,41	1,38	1,80	1,58	1,59	0,151	0,644	0,603
Pr	N.d.	N.d.	N.d.	N.d.	N.d.	N.d.	N.d.	N.d.	N.d.	N.d.	N.d.
Nd	2,60	3,18	2,06	2,08	2,36	4,79	5,55	4,86	0,972	2,45	1,46
Sm	0,793	0,560	0,538	0,327	0,262	2,68	2,74	2,80	1,32	2,10	1,20
Eu	0,167	0,266	0,077	0,055	0,033	0,846	0,948	0,931	0,644	0,769	0,529
Gd	N.d.	N.d.	N.d.	N.d.	N.d.	N.d.	N.d.	N.d.	N.d.	N.d.	N.d.
Tb	N.d.	N.d.	N.d.	N.d.	N.d.	N.d.	N.d.	N.d.	N.d.	N.d.	N.d.
Dy	0,410	0,314	0,128	0,169	0,112	1,59	1,98	2,19	1,40	1,74	1,46
Ho	N.d.	N.d.	N.d.	N.d.	N.d.	N.d.	N.d.	N.d.	N.d.	N.d.	N.d.
Er	0,219	0,146	0,135	0,140	0,208	0,649	0,607	0,937	0,557	0,451	0,507
Tm	N.d.	N.d.	N.d.	N.d.	N.d.	N.d.	N.d.	N.d.	N.d.	N.d.	N.d.
Yb	0,278	0,284	0,260	0,397	0,295	0,601	0,756	0,887	0,652	0,609	0,554
Lu	N.d.	N.d.	N.d.	N.d.	N.d.	N.d.	N.d.	N.d.	N.d.	N.d.	N.d.
Total	8,52	10,1	5,00	4,91	4,95	13,1	14,39	14,25	5,73	8,95	6,52
(La/Yb) _n	0,82	1,53	0,70	0,57	0,69	0,18	0,21	0,04	0,04	0,21	0,25

(Continued)

Table I.3 (Continued).

<i>Mir pipe, Yakutia, Russia</i>											
	[Shimizu et al., 1997b], IPMA										
Element	129/15H1	129/15H2	129/15L1	129/15L2	49-13-1	49-13-3	49-14-1	49-14-D	49-14-2	49-14-4	49-15
<i>Peridotite parageneses</i>											
La	1,56	0,819	0,028	0,098	0,514	0,434	0,549	0,405	0,239	0,319	0,216
Ce	3,86	2,94	0,788	0,828	2,26	2,01	2,22	1,67	1,77	1,75	1,60
Pr	N.d.	N.d.	N.d.	N.d.	N.d.	N.d.	N.d.	N.d.	N.d.	N.d.	N.d.
Nd	2,06	1,54	1,55	1,64	2,57	2,49	2,96	2,58	2,64	2,95	2,72
Sm	0,680	0,383	0,230	0,543	0,900	0,826	0,679	0,417	0,362	0,455	0,377
Eu	0,555	0,216	0,064	0,127	0,132	0,079	0,338	0,488	0,085	0,125	0,136
Gd	N.d.	N.d.	N.d.	N.d.	N.d.	N.d.	N.d.	N.d.	N.d.	N.d.	N.d.
Tb	N.d.	N.d.	N.d.	N.d.	N.d.	N.d.	N.d.	N.d.	N.d.	N.d.	N.d.
Dy	0,309	0,116	0,247	0,272	0,327	0,329	0,280	0,238	0,181	0,265	0,232
Ho	N.d.	N.d.	N.d.	N.d.	N.d.	N.d.	N.d.	N.d.	N.d.	N.d.	N.d.
Er	0,391	0,378	0,285	0,217	0,293	0,292	0,202	0,236	0,249	0,219	0,208
Tm	N.d.	N.d.	N.d.	N.d.	N.d.	N.d.	N.d.	N.d.	N.d.	N.d.	N.d.
Yb	0,296	0,122	0,363	0,426	0,366	0,527	0,452	0,412	0,301	0,308	0,443
Lu	N.d.	N.d.	N.d.	N.d.	N.d.	N.d.	N.d.	N.d.	N.d.	N.d.	N.d.
Total	9,71	6,51	3,56	4,15	7,36	6,99	7,68	6,45	5,83	6,39	5,93
(La/Yb) _n	3,56	4,53	0,05	0,16	0,95	0,56	0,82	0,66	0,54	0,70	0,33

(Continued)

Table I.3 (Continued).

<i>Aykhal pipe, Yakutia, Russia</i>										
	[Shimizu et al., 1997b], IPMA									
	49-17-1	49-17-3	49-17-5	267-2	267-8	267-10	217-1	217-2	217-5	189
<i>Element</i>	<i>Peridotite parageneses</i>									
La	0.284	0.518	0.209	0.131	0.133	0.115	0.258	0.013	0.042	0.082
Ce	1.88	2.34	1.66	0.598	0.517	0.539	0.429	0.028	0.064	0.969
Pr	N.d.	N.d.	N.d.	N.d.	N.d.	N.d.	N.d.	N.d.	N.d.	N.d.
Nd	2.77	2.85	2.52	0.203	0.375	0.226	0.424	0.166	0.165	2.46
Sm	0.371	0.862	0.486	0.098	0.265	0.102	0.945	0.711	0.761	0.761
Eu	0.101	0.093	0.070	0.024	0.075	0.040	0.392	0.353	0.445	0.186
Gd	N.d.	N.d.	N.d.	N.d.	N.d.	N.d.	N.d.	N.d.	N.d.	N.d.
Tb	N.d.	N.d.	N.d.	N.d.	N.d.	N.d.	N.d.	N.d.	N.d.	N.d.
Dy	0.222	0.268	0.195	0.087	0.080	0.068	0.750	0.627	0.704	0.187
Ho	N.d.	N.d.	N.d.	N.d.	N.d.	N.d.	N.d.	N.d.	N.d.	N.d.
Er	0.220	0.283	0.233	0.082	0.143	0.089	0.268	0.263	0.205	0.116
Tm	N.d.	N.d.	N.d.	N.d.	N.d.	N.d.	N.d.	N.d.	N.d.	N.d.
Yb	0.304	0.566	0.345	0.232	0.316	0.277	0.406	0.476	0.349	0.439
Lu	N.d.	N.d.	N.d.	N.d.	N.d.	N.d.	N.d.	N.d.	N.d.	N.d.
Total	6.15	7.78	5.72	1.46	1.90	1.46	3.87	2.64	2.74	5.20
(La/Yb) _n	0.63	0.62	0.41	0.38	0.28	0.28	0.43	0.02	0.08	0.13

(Continued)

Table 1.3 (Continued).

	Venetia province, South Africa								Slave craton, Canada	
	[Stachel et al., 2004], SIMS								[Pomprated et al., 2004]	
Element	V-64a	V-87b	V-95	V-112a	V-167b	V-169a	V-195a	V-197ab	3-3/00-1	3-3/00-2
<i>Peridotite parageneses</i>										
La	0,440	0,450	0,010	0,740	0,340	0,200	0,230	0,060	0,150	0,160
Ce	5,33	4,05	0,160	21,6	2,34	1,60	2,48	0,760	0,640	0,560
Pr	1,17	1,28	0,080	7,88	0,570	0,380	0,820	0,240	0,140	0,140
Nd	6,12	11,3	0,890	39,5	3,570	3,87	8,01	1,89	0,810	1,01
Sm	0,730	4,89	0,550	3,42	0,890	2,61	4,66	0,360	0,260	0,250
Eu	0,110	1,71	0,220	0,720	0,280	0,850	1,83	0,100	0,069	0,075
Gd	0,400	3,60	0,880	2,71	0,740	2,07	6,35	0,230	0,160	0,220
Tb	0,010	0,320	0,100	0,210	0,150	0,200	0,960	0,040	0,032	0,024
Dy	0,050	0,870	0,550	1,16	0,750	0,980	5,83	0,360	0,140	0,140
Ho	0,010	0,150	0,080	0,120	0,170	0,150	1,13	0,090	0,019	0,034
Er	0,040	0,350	0,170	0,200	0,570	0,650	2,96	0,390	0,065	0,078
Tm	N.d.	N.d.	N.d.	N.d.	N.d.	N.d.	N.d.	N.d.	0,009	0,018
Yb	0,090	0,560	0,180	0,080	0,900	0,800	2,24	0,680	0,120	0,200
Lu	0,040	0,090	0,060	0,010	0,130	0,150	0,280	0,150	0,025	0,050
Total	14,5	29,6	3,93	78,4	11,4	14,5	37,8	5,35	1,91	2,96
(La/Yb) _n	3,30	0,54	0,04	6,24	0,25	0,17	0,07	0,06	0,84	0,54

(Continued)

Table 1.3 (Continued).

Slave craton, Canada								Namibia province		
[Promprated et al., 2004]								[Harris et al., 2004], SIMS		
Element	3-3/00-3	31-3/00-35	31-3/00-36	5-6/00-112	5-6/00-113	6/00-114	5-6/00-115	5-6/00-116	Nam-24	Nam-46
La	0,120	1,03	1,36	0,031	N.d.	0,014	N.d.	N.d.	0,110	0,140
Ce	0,590	8,66	9,36	0,150	0,170	0,089	0,093	0,086	0,550	2,24
Pr	0,160	2,20	2,22	0,051	0,039	0,028	0,037	0,023	0,210	0,730
Nd	0,970	11,3	12,0	0,420	0,300	0,230	0,330	0,230	1,14	5,06
Sm	0,240	1,81	2,19	0,330	0,210	0,180	0,230	0,170	0,250	1,23
Eu	0,095	0,430	0,450	0,150	0,095	0,089	0,070	0,098	0,080	0,310
Gd	0,210	1,22	1,46	0,730	0,480	0,570	0,550	0,440	0,370	0,990
Tb	0,041	0,160	0,170	0,200	0,130	0,160	0,150	0,130	0,070	0,200
Dy	0,170	0,770	0,830	1,95	1,58	1,40	1,38	1,38	0,380	0,900
Ho	0,026	0,150	0,130	0,530	0,410	0,440	0,360	0,380	0,100	0,140
Er	0,120	0,330	0,390	2,05	1,79	1,69	1,56	1,55	0,360	0,280
Tm	0,022	0,060	0,066	0,370	0,360	0,310	0,270	0,280	N.d.	N.d.
Yb	0,170	0,440	0,480	2,67	2,39	2,13	2,43	2,11	0,480	0,230
Lu	0,039	0,084	0,100	0,560	0,440	0,450	0,490	0,380	0,120	0,020
Total	2,97	28,6	31,2	10,2	N.d.	7,78	N.d.	N.d.	4,22	12,5
(La/Yb) _n	0,48	1,58	1,91	0,01	N.d.	N.d.	N.d.	N.d.	0,15	0,41

(Continued)

Table I.3 (Continued).

	Namibia province									
	[Harris et al., 2004], SIMS									
	Nam-65	Nam-31	Nam-108	Nam-94	Nam-113	Nam-55	Nam-16	Nam-29	Nam-50	Nam-101
Element	Peridotite parageneses									
La	0,050	0,970	1,37	0,070	0,010	0,440	1,20	0,030	0,120	0,140
Ce	1,11	1,26	2,59	0,160	0,030	2,84	5,90	0,370	1,91	1,97
Pr	0,370	0,130	0,270	0,080	0,020	0,420	0,770	0,130	0,740	0,460
Nd	2,05	0,220	0,910	0,070	0,340	1,16	2,80	1,69	4,97	2,08
Sm	1,430	0,020	0,120	0,060	0,140	0,150	1,20	0,140	0,370	0,220
Eu	0,230	0,020	0,030	0,010	0,060	0,060	0,150	0,400	0,070	0,070
Gd	0,800	0,020	0,100	0,370	0,140	0,360	0,780	0,020	0,050	0,140
Tb	0,130	0,010	0,020	0,010	0,030	0,030	0,060	0,010	N.d.	0,010
Dy	0,600	0,030	0,070	0,070	0,070	0,240	0,270	N.d.	0,190	0,120
Ho	0,160	N.d.	0,020	0,020	0,020	0,010	0,020	N.d.	0,010	0,010
Er	0,420	0,040	0,040	0,190	0,090	0,050	0,120	0,010	0,050	0,020
Tm	N.d.	N.d.	N.d.	N.d.	N.d.	N.d.	N.d.	N.d.	N.d.	N.d.
Yb	0,290	0,190	N.d.	N.d.	0,300	0,090	N.d.	0,140	0,170	0,070
Lu	0,050	0,050	0,040	0,130	0,120	0,070	0,080	0,030	0,070	0,090
Total	6,43	2,96	N.d.	N.d.	1,37	5,92	N.d.	N.d.	N.d.	5,40
(La/Yb) _n	0,12	3,45	N.d.	N.d.	0,02	3,30	N.d.	0,14	0,48	1,35

(Continued)

Table 1.3 (Continued).

Namibia province										
	[Harris et al., 2004], SIMS					[Stachel et al., 2004], SIMS				
Element	Nam-110	Nam-71	Nam-118	Nam-33	Nam-92	Nam-13	Nam-35	Nam-38	Nam-47	Nam-5
<i>Peridotite parageneses</i>					<i>Eclogite parageneses</i>					
La	0,180	0,680	0,130	0,080	0,070	0,020	0,100	0,060	N.d.	0,100
Ce	2,01	5,03	2,41	0,580	0,480	0,380	1,050	0,150	0,030	1,98
Pr	0,880	0,980	0,940	0,150	0,090	0,150	0,430	0,040	0,020	0,910
Nd	5,12	4,91	5,88	0,990	1,10	1,55	4,17	0,470	0,140	9,30
Sm	0,240	1,08	1,98	1,29	0,790	1,62	2,80	0,640	0,230	5,22
Eu	0,070	0,180	0,580	0,530	0,070	0,94	1,33	0,440	0,100	1,48
Gd	0,090	0,650	1,59	1,75	0,460	4,92	5,25	2,04	0,500	7,32
Tb	0,020	0,070	0,150	0,080	0,030	1,22	1,16	0,640	0,140	1,31
Dy	0,120	0,240	0,370	0,310	0,220	8,49	8,50	5,27	1,56	8,10
Ho	0,010	0,030	0,030	0,050	0,050	1,93	1,90	1,28	0,450	1,67
Er	0,010	0,050	0,090	0,040	0,120	5,40	6,14	4,20	1,89	5,01
Tm	N.d.	N.d.	N.d.	N.d.	N.d.	N.d.	N.d.	N.d.	N.d.	N.d.
Yb	0,070	0,040	0,160	0,100	0,080	5,39	7,44	5,11	2,91	4,75
Lu	0,010	0,010	0,020	0,030	0,030	0,650	1,11	0,820	0,460	0,680
Total	8,83	14,0	14,3	5,98	3,59	32,7	41,4	21,2	N.d.	47,8
(La/Yb) _n	1,74	11,47	0,55	0,54	0,59	0,003	0,009	0,008	N.d.	0,014

(Continued)

Table I.3 (Continued).

Namibia province									
	[Stachel et al., 2004], SIMS								
	Nam-59	Nam-63	Nam-68	Nam-74	Nam-80	Nam-86	Nam-89	Nam-202	Nam-203
Element	Eclogite parageneses								
La	0,050	0,030	0,160	0,280	N.d.	0,030	0,030	0,010	0,010
Ce	0,430	0,160	0,850	2,78	N.d.	0,380	0,300	0,020	0,160
Pr	0,130	0,070	0,260	0,770	0,170	0,150	0,100	N.d.	0,110
Nd	1,50	1,17	3,15	6,80	0,980	2,23	0,750	0,080	2,30
Sm	1,76	1,19	2,92	4,31	0,540	1,79	0,590	0,300	2,20
Eu	0,920	0,470	1,47	1,34	0,350	1,04	0,420	0,210	1,10
Gd	2,62	2,52	4,13	8,56	1,57	4,04	1,12	3,000	4,40
Tb	0,550	0,700	0,720	1,91	0,250	0,770	0,320	1,50	0,880
Dy	3,62	6,030	3,98	12,8	1,40	1,15	2,52	12,0	6,90
Ho	0,860	1,38	0,850	2,72	0,290	1,03	0,520	2,00	1,50
Er	2,30	4,45	2,45	2,39	0,380	2,41	1,70	4,50	4,40
Tm	N.d.	N.d.	N.d.	N.d.	N.d.	N.d.	N.d.	N.d.	N.d.
Yb	2,88	5,98	2,12	10,0	0,390	1,93	2,09	N.d.	N.d.
Lu	0,380	0,860	0,300	1,47	0,080	0,300	0,360	0,520	0,800
Total	18,0	25,0	23,4	56,1	N.d.	17,3	10,8	N.d.	24,8
(La/Yb) _n	0,012	0,003	0,051	0,019	N.d.	0,010	0,010	N.d.	N.d.

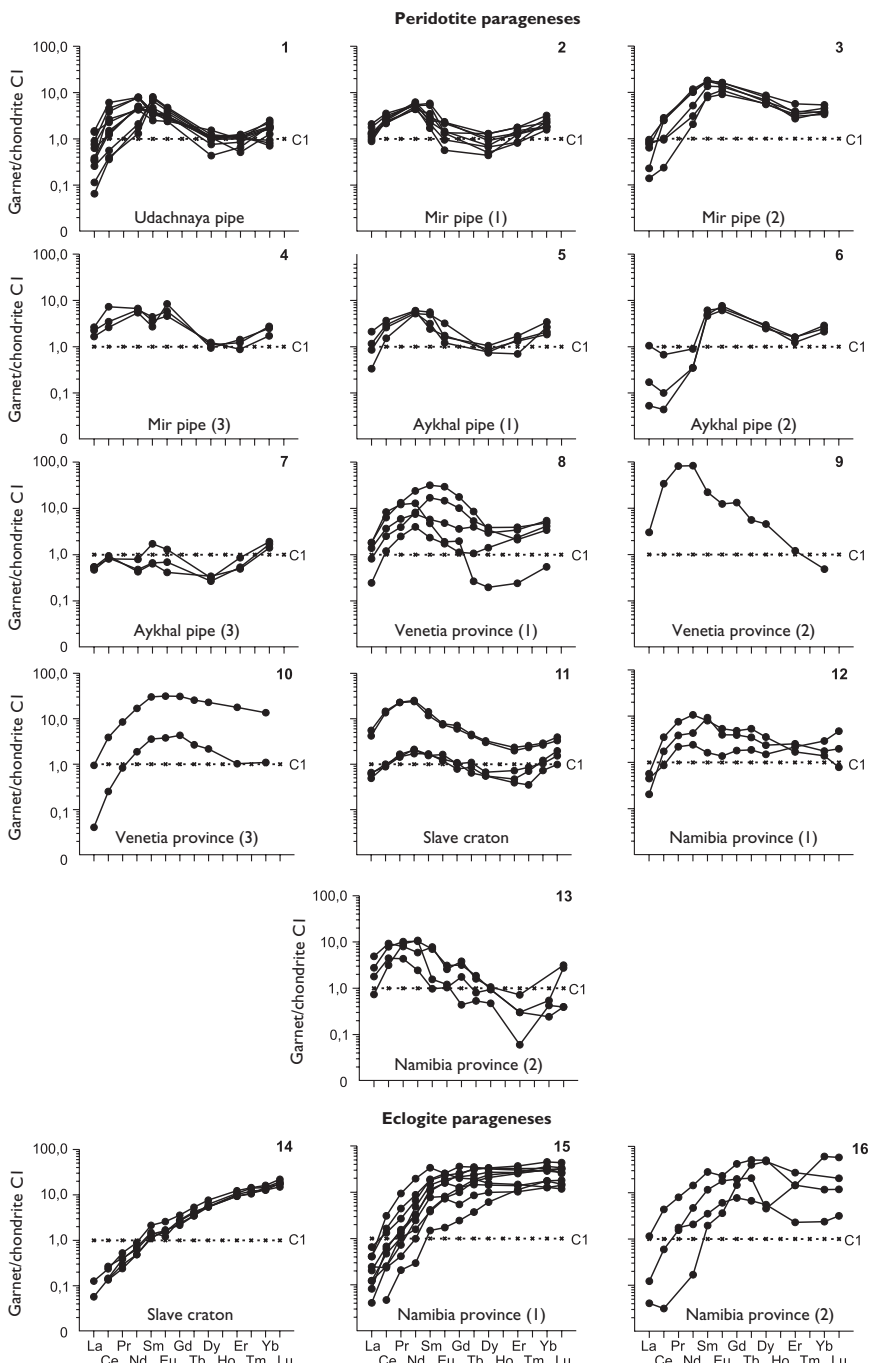


Figure 1.3 Chondrite-normalized REE patterns for garnets from microinclusions in diamonds (peridotite and eclogite parageneses) from xenoliths in kimberlites, as well as products of their disintegration (data Table 1.3).

observed for the garnets from xenoliths from Aykhal pipe (Yakutia province, Russia), Venetia, and Namibia provinces (South Africa), as well as Slave craton (Canada) (Figure 1.3, 5–13). All of these garnets in one way or another differ in the $(La/Sm)_n$ parameter values, by using these values we divided the garnets from diamond micro-inclusions of Udachnaya pipe into two groups: for the first, $(La/Sm)_n = 0.008\text{--}0.097$ and for the second – $0.220\text{--}0.407$. The garnets from microinclusions in the diamonds of Mir pipe are divided into three groups with different $(La/Sm)_n$ values: $0.013\text{--}0.109$, $0.268\text{--}0.726$ and $1.346\text{--}1.444$, respectively. Similar differences in REE composition were observed in garnets from some other kimberlite manifestations and provinces.

As emphasized above, the garnets from the microinclusions in diamonds of eclogite parageneses differ significantly in the REE composition from those that are present in peridotite parageneses. Within the whole operational sample of analysis of these garnets, the total REE compositions varies in the range of $6.4\text{--}56$ ppm with an average of 22.6 ppm; $(La/Yb)_n$ values are ranging from 0.003 to 0.050 with an average value of 0.015 . Their REE patterns often have a steep positive slope, which is most clearly observed in samples from the Slave craton (Canada) and Namibia province. However, it should be noted that in contrast to the pattern of garnets from the Slave craton, which have a close to straight shape of line (Figure 1.3, 14), the patterns of the samples from Namibia province are characterized by a subhorizontal location in the area of heavy elements (Figure 1.3, 15), more rarely they have a negative slope due to the relative depletion of a mineral by heavy elements (Figure 1.3, 16).

Eclogites from xenoliths. The REE composition of garnets from eclogite xenoliths is characterized by the example of samples from Roberts Victor, Bobbejaan and Koidu pipes (Table 1.4). Garnets of this type contain a relatively low amount of pyrope mineral and have a high content of grossular mineral. The total REE contents in garnets from eclogites of Roberts Victor pipe vary in the range of $3\text{--}13$ ppm. The exception is sp. HRV-175, for which the total REE is as high as 35 ppm which is mainly due to the anomalous enrichment with medium elements. In the garnets from Bobbejaan and Koidu pipes the total REE contents are comparable to those for samples from Roberts Victor pipe – $3.3\text{--}18.1$ ppm, the only exception is the sp. KEC 86–19 for which the total REE is 52 ppm due to enrichment with medium and heavy elements. Chondrite-normalized HREE contents in all garnets from eclogites parageneses are much higher than that of light elements, the values of $(La/Yb)_n$ range from 0.001 to 0.47 (Figure 1.5). This pattern is most clearly expressed in samples from xenoliths of Roberts Victor and Koidu pipes. By their configuration of REE pattern the garnets from Roberts Victor pipe are divided into two types: 1) garnets that are moderately depleted by LREE and, accordingly, have a flattened form of the patterns in the area of medium and heavy elements, and 2) garnets intensively depleted by LREE, particularly by cerium. In one of the samples the garnet is anomalously enriched with Eu. To add more, some garnets from eclogites, provided in the xenoliths from kimberlites of Udachnaya pipe, are characterized by a zonal distribution of REE, which becomes apparent in a gradual increase of the content of light elements moving from the central zone of garnet grains to the marginal, as well as in the depletion by HREE in the same direction.

Eclogites of high-pressure metamorphic complexes. Eclogites of this type are spread in tectonically exhumed high-pressure metamorphic formations among the ancient folded structures. Some features of the REE distribution in garnets of these areas are

Table 1.4 REE compositions of garnets from eclogites from xenoliths in kimberlites of some provinces and pipes (ppm).

Roberts Victor pipe, South Africa									
	[Harte, Kirkley, 1997], SIMS								
	HRV-145	HRV-247	HRV-173	HRV-110	HRV-30-7	HRV-243	HRV-30-1	HRV-30-6	HRV-244
Element	Eclogites								
La	0,030	0,060	0,040	0,010	0,140	0,030	0,270	0,040	0,010
Ce	0,230	0,570	0,250	0,080	0,450	0,250	0,660	0,210	0,010
Pr	N.d.	N.d.	N.d.	N.d.	N.d.	N.d.	N.d.	N.d.	N.d.
Nd	1,79	1,96	0,870	0,280	1,25	0,790	1,18	0,890	0,140
Sm	0,840	1,22	0,450	0,330	1,00	0,420	0,800	0,810	0,280
Eu	0,390	0,580	0,230	0,220	0,480	0,240	0,390	0,390	0,220
Gd	N.d.	N.d.	N.d.	N.d.	N.d.	N.d.	N.d.	N.d.	N.d.
Tb	0,200	0,340	0,420	0,140	0,440	0,220	0,360	0,330	0,290
Dy	1,44	2,33	3,820	1,170	3,10	2,010	2,63	2,39	2,29
Ho	0,260	0,480	0,980	0,300	0,710	0,560	0,610	0,600	0,540
Er	0,830	1,22	3,10	1,01	2,35	1,93	1,86	1,78	1,79
Tm	N.d.	N.d.	N.d.	N.d.	N.d.	N.d.	N.d.	N.d.	N.d.
Yb	N.d.	N.d.	N.d.	N.d.	N.d.	N.d.	N.d.	N.d.	N.d.
Lu	0,110	0,130	0,440	0,300	0,350	0,450	0,290	0,290	0,330
Total	6,12	8,89	10,6	3,84	10,3	6,90	9,05	7,73	5,90
(La/Yb) _n	0,03	0,06	0,04	0,01	0,14	0,03	0,27	0,04	0,01

(Continued)

Table 1.4 (Continued).

Element	Roberts Victor pipe, South Africa				Bobbejaan pipe, South Africa				
	[Harte, Kirkley, 1997], SIMS				[Caporuscio, Smith, 1990], INAA				
	HRV-67	HRV-175	HRV-277	HRV-98	SBB-2H	SBB-3H	SBB-7P	SBB-25	SBB-34
<i>Eglogites</i>									
La	0,010	0,020	0,230	0,020	0,224	0,107	0,576	0,563	0,320
Ce	0,020	0,020	1,40	0,260	0,644	0,381	2,050	1,26	0,895
Pr	N.d.	N.d.	N.d.	N.d.	N.d.	N.d.	N.d.	N.d.	N.d.
Nd	0,080	0,240	4,04	0,660	0,397	0,642	4,85	0,653	0,395
Sm	0,200	0,960	2,62	0,510	0,179	0,215	1,88	0,580	0,461
Eu	0,170	0,700	1,43	0,200	0,148	0,206	0,843	0,266	0,269
Gd	N.d.	N.d.	N.d.	N.d.	N.d.	N.d.	N.d.	N.d.	N.d.
Tb	0,190	1,42	0,340	0,090	0,090	0,291	0,418	0,233	0,299
Dy	1,87	13,0	1,49	0,570	1,01	0,136	0,906	1,56	1,95
Ho	0,460	3,50	0,290	0,100	N.d.	N.d.	N.d.	N.d.	N.d.
Er	1,60	13,1	0,800	0,360	N.d.	N.d.	N.d.	N.d.	N.d.
Tm	N.d.	N.d.	N.d.	N.d.	N.d.	N.d.	N.d.	N.d.	N.d.
Yb	N.d.	N.d.	N.d.	N.d.	0,552	2,710	0,824	1,80	4,88
Lu	0,330	2,53	0,110	0,080	0,071	0,429	0,128	0,272	0,804
Total	4,93	35,4	12,8	2,85	N.d.	N.d.	N.d.	N.d.	N.d.
(La/Yb) _n	0,01	0,02	0,23	0,02	0,27	0,03	0,47	0,21	0,04

(Continued)

Table 1.4 (Continued).

	<i>Bobbejaan pipe, South Africa</i>			<i>Koidu province, Sierra Leone</i>						
	[Caporuscio, Smith, 1990], INAA			[Barth et al., 2002], LA ICP-MS						
	SBB-37	SBB-39	SBB-61	KEC 80-B1	KEC 81-2	KEC 86-15	KEC 86-19	KEC 86-58	KEC 86-73B	KEC 86-107
Element	Eclogites									
La	0,398	0,082	0,995	0,030	0,015	0,030	0,030	0,100	0,200	0,031
Ce	0,827	0,360	1,85	0,037	0,120	0,034	0,160	0,080	0,090	0,200
Pr	N.d.	N.d.	N.d.	0,050	N.d.	0,020	N.d.	N.d.	N.d.	0,060
Nd	0,905	0,301	1,81	0,300	0,500	0,230	0,830	0,350	0,520	0,640
Sm	0,854	0,409	1,42	0,610	0,720	0,360	0,970	0,490	0,700	0,600
Eu	0,456	0,190	0,708	0,390	0,400	0,280	0,530	0,220	0,330	0,340
Gd	N.d.	N.d.	N.d.	2,20	2,070	1,47	3,000	1,430	1,600	1,70
Tb	0,521	0,275	0,461	0,550	N.d.	0,370	N.d.	N.d.	N.d.	0,450
Dy	3,73	0,266	2,24	4,75	3,69	3,140	11,3	3,75	3,91	3,60
Ho	N.d.	N.d.	N.d.	1,11	0,870	0,760	N.d.	N.d.	N.d.	0,850
Er	N.d.	N.d.	N.d.	3,56	2,78	2,35	14,0	3,40	2,96	3,83
Tm	N.d.	N.d.	N.d.	0,510	N.d.	0,340	N.d.	N.d.	N.d.	0,390
Yb	6,55	3,07	1,66	3,47	2,73	2,11	17,9	3,78	3,19	2,70
Lu	1,02	0,493	0,239	0,580	0,450	0,330	2,93	0,630	0,470	0,430
Total	N.d.	N.d.	N.d.	18,2	N.d.	11,8	N.d.	N.d.	N.d.	15,8
(La/Yb) _n	0,04	0,02	0,40	0,006	0,004	0,010	0,001	0,018	0,042	0,008

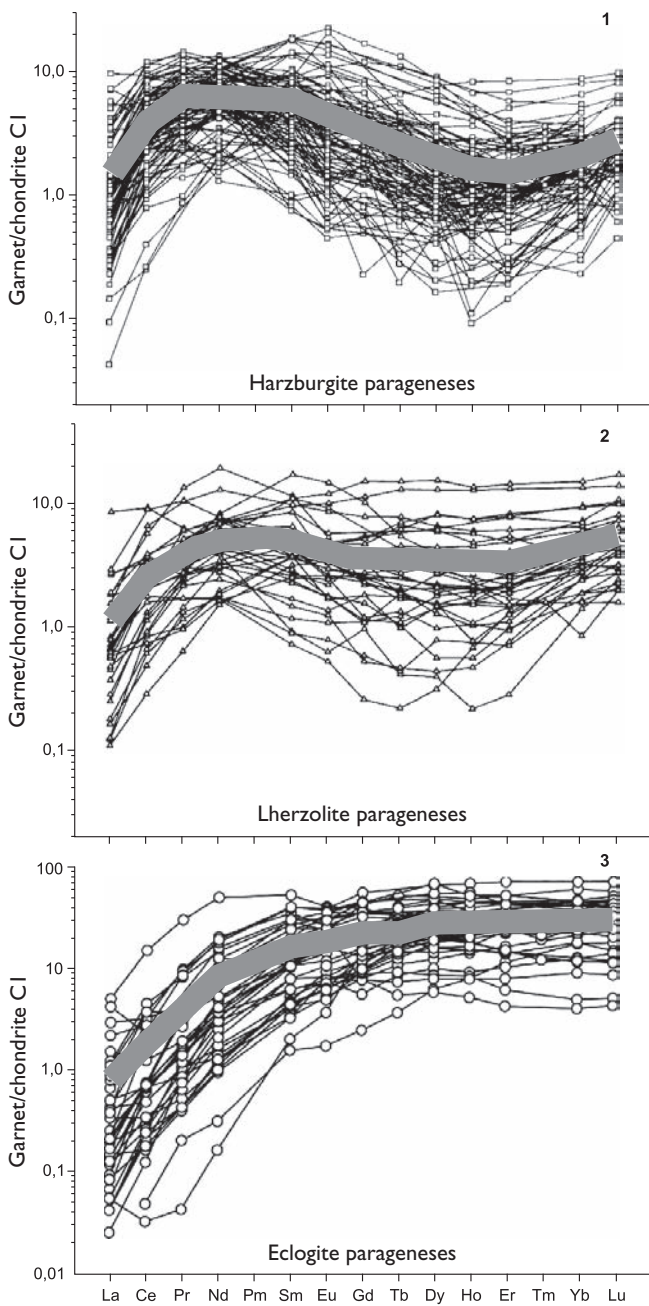


Figure 1.4 Chondrite-normalized REE patterns for garnets from inclusions in diamonds from harzburgite, lherzolite, and eclogite parageneses. Grey specks – patterns for average REE composition of garnets from inclusions in diamonds (data [Stachel *et al.*, 2004]).

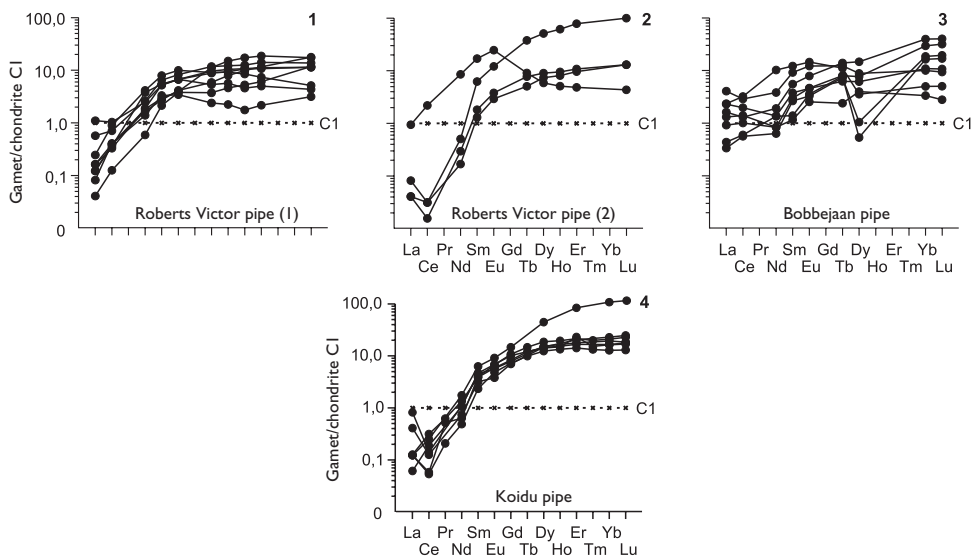


Figure 1.5 Chondrite-normalized REE patterns for garnets from eclogite xenoliths from kimberlites (data Table 1.4).

considered by the example of the samples from Norway, Switzerland, Kazakhstan and Kyrgyzstan metamorphic complexes (Table 1.5). Garnets from eclogites presented in Norwegian metamorphic complexes are notable for a much lower total REE content (6.5–18.2 ppm) compared with the samples from Soazza complex (Switzerland) (34–148 ppm). Garnets from eclogites represented in Kazakhstan (22–44 ppm) and Kyrgyzstan (16.4–31.6 ppm) metamorphic complexes occupy an intermediate position on this basis. The samples of Soazza complex demonstrate the most intense fractionation of REE, which is due to its depletion by LREE and enrichment with heavy elements, as it is shown on the configuration of REE pattern (Figure 1.6). Due to the relative enrichment with LREE, patterns of garnets from Kazakhstan complexes (Kumdy-Kol', Sulu Tube, Chiglinka, Kulet), as well as from Atbashi complex in South Tien Shan (Kyrgyzstan) [Shatsky, 1990], have a more gentle positive slope. In some patterns we can observe negative Eu anomalies (Sulu Tube complex), or Nd and Sm anomalies (Norwegian complexes). Let us consider in detail the collected data on the geochemistry of REE in garnets from eclogites of Atbashi metamorphic complex. Eclogites from Atbashi metamorphic complex are denuded in a series of small tectonic blocks in the valley of Kembel' river, draining the western spurs of Atbashi ridge. Their first structural-geological description was given by Bakirov [1964], and then a detailed petrographic, petrochemical, mineralogical and geochemical study of eclogites was carried out from this, as well as from some other eclogite-bearing complexes of Tien Shan [Shatsky, 1990]. Recently, the additional data on the chemical composition of garnets, omphacites and glaucophanes from eclogites of Atbashi complex as well as estimates of *PT*-parameters of their formation have been published [Lesnov *et al.*, 2004b]; by LA ICP-MS method we determined REE contents in these garnets and coexisting minerals [Lesnov *et al.*, 2005a].

Table 1.5 REE compositions of garnets from eclogites in some high pressure metamorphic provinces and complexes (ppm).

	Norway					Soazza complex, Switzerland		
	[Griffin, Brueckner, 1985], NAA					[Bocchio et al., 2000], ICP-MS		
	N-16	IB-I	Ah-6	Ar-8 (ID)	Ar-8	78-M-12	75-M-47	75-M-48
Element	<i>Eclogites</i>							
La	1,30	0,400	0,900	N.d.	1,00	N.d.	N.d.	N.d.
Ce	3,60	3,50	2,30	0,106	2,80	0,030	N.d.	0,010
Pr	N.d.	N.d.	N.d.	N.d.	N.d.	N.d.	N.d.	N.d.
Nd	1,00	0,800	0,800	0,683	1,20	0,660	0,130	0,100
Sm	1,40	0,100	0,500	0,820	1,10	2,890	0,840	0,970
Eu	1,10	0,070	0,250	0,397	0,530	1,760	0,780	1,06
Gd	N.d.	N.d.	N.d.	N.d.	N.d.	8,030	5,85	7,39
Tb	1,40	0,140	0,260	N.d.	0,490	N.d.	N.d.	N.d.
Dy	N.d.	N.d.	N.d.	3,39	N.d.	17,001	1,6	19,3
Ho	N.d.	N.d.	N.d.	N.d.	N.d.	N.d.	N.d.	N.d.
Er	N.d.	N.d.	N.d.	2,47	N.d.	11,40	7,45	8,23
Tm	N.d.	N.d.	N.d.	N.d.	N.d.	N.d.	N.d.	N.d.
Yb	7,20	7,50	1,30	2,70	3,30	11,70	7,48	5,62
Lu	1,20	1,40	0,230	N.d.	0,600	N.d.	N.d.	N.d.
Total	N.d.	N.d.	N.d.	10,6	N.d.	53,5	34,1	42,7
(La/Yb) _n	0,12	0,04	0,47	N.d.	0,21	N.d.	N.d.	N.d.

(Continued)

Table 1.5 (Continued).

Complexes							
	Soazza	Kumdy Kol'	Sulu Tube		Chiglinka	Kulet	Atbashi
	Switzerland	Kazakhstan					Kirgystan
[Bocchio et al., 2000], ICP-MS	[Shatsky, 1990], INAA						
78-M-6	KK 8203	ST 81-5	ST 84-6	T 84-3	KU 84-27	AT 83-22	AT 83-28
Element	Eclogites						
La	N.d.	2,50	2,90	2,48	4,10	2,00	4,200
Ce	0,010	6,20	5,33	5,60	9,60	7,90	N.d.
Pr	N.d.	N.d.	N.d.	N.d.	N.d.	N.d.	N.d.
Nd	0,100	4,80	N.d.	9,35	N.d.	N.d.	N.d.
Sm	1,04	1,75	1,98	0,920	3,20	2,75	1,89
Eu	1,89	0,800	0,670	0,180	N.d.	0,810	1,25
Gd	21,8	N.d.	N.d.	N.d.	N.d.	N.d.	N.d.
Tb	N.d.	0,860	0,640	0,400	1,80	1,32	0,780
Dy	68,3	N.d.	N.d.	N.d.	N.d.	N.d.	N.d.
Ho	N.d.	N.d.	N.d.	N.d.	N.d.	N.d.	N.d.
Er	30,5	N.d.	N.d.	N.d.	N.d.	N.d.	N.d.
Tm	N.d.	1,00	N.d.	N.d.	N.d.	N.d.	N.d.
Yb	24,2	7,40	21,8	22,5	7,00	6,23	19,6
Lu	N.d.	1,10	3,11	2,66	1,94	0,710	N.d.
Total	148	26,4	36,4	44,1	N.d.	N.d.	N.d.
$(La/Yb)_n$	N.d.	0,23	0,09	0,07	0,40	0,22	0,14
							0,07

(Continued)

Table 1.5 (Continued).

<i>Atbashi complex, Kyrgyzstan</i>								
	[Shatsky, 1990], INAA	[Lesnov et al., 2005a], LA ICP-MS						
Element	AT 83-4	L-12-1 (r)	L-12-2 (c)	L-12-3 (r)	L-12-4 (c)	L-13-9 (r)	L-13-10 (c)	L-13-11 (r)
<i>Eclogites</i>								
La	2,63	3,55	3,61	4,67	4,63	3,70	4,19	4,33
Ce	8,52	6,00	6,20	8,00	7,76	6,73	7,80	8,00
Pr	N.d.	0,676	0,681	0,900	0,879	0,722	0,853	0,856
Nd	N.d.	2,63	2,62	3,47	3,45	2,62	3,00	3,200
Sm	1,88	0,502	0,488	0,661	0,662	0,488	0,617	0,653
Eu	0,690	0,118	0,112	0,146	0,154	0,102	0,127	0,137
Gd	N.d.	0,682	0,535	0,705	0,693	0,453	0,518	0,541
Tb	1,12	0,176	0,163	0,167	0,161	0,070	0,091	0,084
Dy	N.d.	1,68	2,270	1,84	2,25	0,511	0,743	0,594
Ho	N.d.	0,381	0,813	0,471	0,855	0,120	0,184	0,126
Er	N.d.	1,10	3,18	1,50	3,76	0,378	0,612	0,386
Tm	N.d.	0,144	0,491	0,215	0,616	0,055	0,098	0,054
Yb	11,1	0,995	3,90	1,57	4,95	0,391	0,756	0,395
Lu	N.d.	0,147	0,586	0,229	0,731	0,059	0,099	0,059
Total	N.d.	18,8	25,7	24,5	31,6	16,4	19,7	19,4
(La/Yb) _n	0,16	2,41	0,62	2,01	0,63	6,39	3,74	7,40

Note: The analyses from L-12-1(r) to L -13-11(r) carried out by LA ICP-MS method on mass-spectrometry "Element" with UV Laser Prob (laser Nd:YAG = 266 nm) (firm Finnigan MAT, Germany) in the Analytical Center IGM SB RAS (analyst A. Kuchkin). Errors of determination of individual elements - 20–30%; (r) – rim, (c) – core.

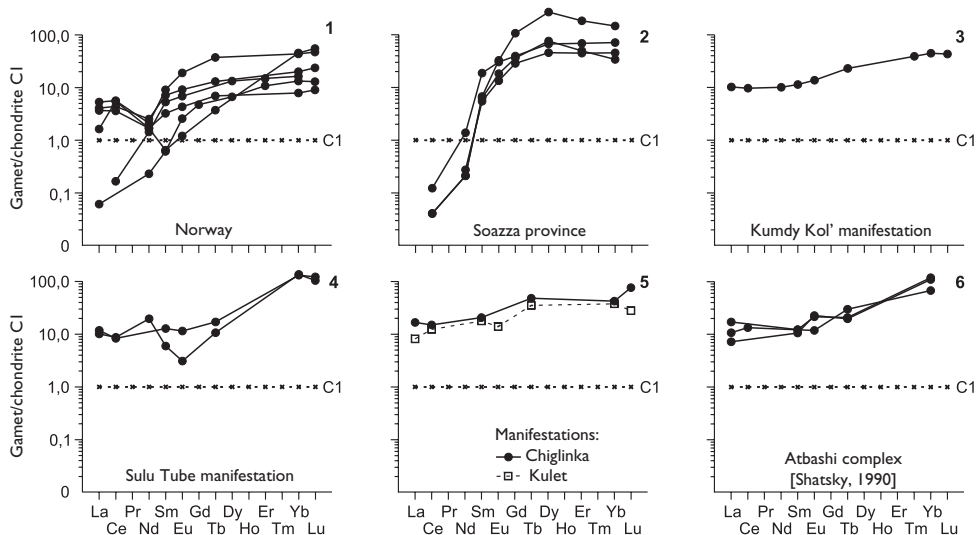


Figure 1.6 Chondrite-normalized REE patterns for garnets from eclogites from high-pressure metamorphic complexes (data Table 1.5).

By their chemical composition the eclogites of Atbashi complex are close to the basalts containing SiO_2 in the range of 44.4–52.8 wt% and some – to trachybasalts and trachyandesit-basalts (Table 1.6), in some portion of the samples Na_2O substantially prevails over K_2O , which implies the resemblance of their protoliths to oceanic basalts. In the diagram with following coordinates $(\text{Na}_2\text{O} + \text{K}_2\text{O}) - \text{FeO} - \text{MgO}$ the figurative points of the vast majority of eclogites of Atbashi complex are concentrated in the area of basalts of calc-alkaline series, although some get to the area of basalts of tholeiitic series. In the diagram with the coordinates of $\text{MnO} - \text{TiO}_2 - \text{P}_2\text{O}_5$ the compositions of these eclogites are also located mainly in the area of tholeiites of island arcs. Thus, it is not possible to unambiguously determine chemical composition of the protoliths of eclogites from this complex by the content of major components.

We have studied in detail two representative samples of eclogites from metamorphic Atbashi complex – L-12 and L-13. The first is formed by numerous relatively large (3–4 mm) idiomorphic crystals – porphyroblasts of garnet, immersed in the matrix that consists of the dominant small prismatic segregations of clinopyroxene. In the inner zones of garnet crystals there are numerous microscopic inclusions of clinopyroxene and more rare – plagioclase in the form of albite. Garnet porphyroblasts have a distinct optical zoning, which is due to the presence of narrow peripheral zones surrounding the wider inner zones of the grains. In the direction from the inner zones of the crystals to the periphery the Mg content is increasing, while the contents of Ca, Fe and Mn are reducing (Table 1.7). Inner zones of garnet grains have a mineral composition of (%): almandine (65–66), grossular (23–24), pyrope (9), spessartine (2). In the peripheral areas there are less almandine (60%) and grossular (21–22%), but more pyrope (17%) and spessartine (1%) minerals. Thus, the garnets from the

Table 1.6 Chemical compositions of eclogites from Atbashi metamorphic complex, Kyrgyzstan (wt%).

Component	[Lesnov et al., 2004b]		[Sakiev, 2002]							
	L-12	L-13	CI-96	CI-98	CI-113c	C73-125c	C73-129a	C73-124x	C73-128b	C73-128e
SiO ₂	47,69	44,40	50,30	47,87	48,28	46,96	48,82	45,57	47,96	49,20
TiO ₂	1,66	1,75	1,10	0,85	0,68	1,20	1,00	0,20	0,90	0,75
Al ₂ O ₃	10,54	13,98	12,25	14,33	13,00	14,57	13,45	8,62	15,88	10,60
Fe ₂ O ₃	12,82	16,86	8,87	6,12	6,44	13,32	10,60	12,89	10,89	9,06
MnO	0,19	0,26	0,14	0,12	0,17	0,18	0,18	0,20	0,18	0,23
MgO	7,93	7,10	7,99	3,35	7,47	6,05	7,25	9,97	7,76	11,62
CaO	13,32	9,17	11,78	13,97	14,02	12,15	11,87	13,90	10,61	6,19
Na ₂ O	4,64	2,97	3,65	3,88	3,29	3,30	4,30	2,54	3,59	3,96
K ₂ O	0,11	0,14	0,20	0,20	0,30	0,50	0,12	0,21	0,50	0,68
P ₂ O ₅	0,04	0,02	0,14	0,17	0,20	0,11	0,07	0,04	0,14	0,13
LOI	0,32	0,91	2,99	4,64	5,40	0,67	1,42	5,46	1,02	6,75
Total	99,26	97,56	99,41	95,50	99,25	99,01	99,08	99,60	99,43	99,17

(Continued)

Table 1.6 (Continued).

	S73-130e	Sh83-41	Sh83-4	Sh83-24	Sh83-14	Sh83-21	Sh83-8	Sh83-12	Sh83-16	Average
Component	[Sakiev, 2002]	[Shatsky, 1990]								n = 19
SiO ₂	44,90	49,26	49,69	49,72	48,30	45,53	48,75	52,80	52,24	48,33
TiO ₂	0,70	0,71	0,70	1,17	1,33	2,02	0,94	0,46	0,53	0,98
Al ₂ O ₃	15,50	13,60	13,41	14,22	15,20	12,44	16,01	11,00	12,68	13,23
Fe ₂ O ₃	10,02	11,05	11,17	11,61	10,49	14,78	9,23	6,22	9,24	10,61
MnO	0,14	0,17	0,17	0,20	0,22	0,29	0,17	0,18	0,17	0,19
MgO	7,05	7,23	7,33	5,80	7,08	9,88	7,10	9,49	5,86	7,54
CaO	11,73	11,34	11,29	8,21	12,17	6,17	10,46	11,53	10,82	11,09
Na ₂ O	3,20	2,64	2,56	5,40	2,16	2,70	2,80	5,46	6,04	3,64
K ₂ O	1,16	0,77	0,86	1,01	0,24	0,87	0,77	0,12	0,25	0,47
P ₂ O ₅	0,08	0,14	0,14	0,09	0,13	0,09	0,05	0,03	0,08	0,10
LOI	3,43	1,92	1,49	1,37	0,99	2,54	2,18	2,21	0,53	2,43
Total	97,91	98,83	98,81	98,80	98,31	97,31	98,46	99,50	98,44	98,61

Note: The analyses of samples L-12 and L-13 were done by the X-ray-fluorescence method in the Analytical Centre of UIGGM SB of USSR AS (analyst A.D. Kireev).

Table 1.7 Chemical compositions of garnets from eclogites from Atbashi metamorphic complex, Kirgystan (wt%).

Component	Number of samples							
	L-12				L-13			
Number of analyses								
	L-12-4 (c)	L-12-5 (c)	L-12-6 (r)	L-12-14	L-13-22 (c)	L-13-23 (r)	L-13-24	L-13-32
SiO ₂	36,31	37,18	37,96	37,61	38,00	38,41	38,81	39,24
TiO ₂	0,126	0,073	0,048	0,049	0,064	0,022	1,06	0,02
Al ₂ O ₃	19,75	20,31	20,77	20,58	20,55	21,25	21,19	21,67
Cr ₂ O ₃	0,018	0,026	0,034	0,02	0,059	0,133	0,042	0,054
FeO	30,84	30,45	28,51	28,85	26,17	23,88	23,65	24,68
MnO	1,02	0,851	0,417	0,726	0,412	0,454	0,453	0,488
MgO	2,17	2,2	4,38	3,85	4,35	6,32	6,59	6,56
CaO	7,74	8,25	7,53	7,82	9,54	8,82	8,34	8,81
Na ₂ O	0,035	0,038	0,043	0,027	0,042	0,014	0,03	0,029
K ₂ O	N.d.	0,001	0,006	N.d.	N.d.	N.d.	0,004	N.d.
Total	98,01	99,38	99,70	99,53	99,19	99,30	100,17	101,55

Note: The analyses carried out done by the X-ray microprobe method on apparatus "Camebax-Micro" (analyst O. Khmel'nikova) in Analytical Centre of UIGGM SB of USSR AS (Novosibirsk). (c) – core, (r) – rim.

sp. L-12 are characterized by a progressive chemical zoning. The presented microscopic inclusions of clinopyroxene by their composition correspond to omphacites containing 31–33% of jadeite minal. Isolated small segregations of glaucophane were found, they are concentrated on the border between porphyroblastic garnet crystals and smaller omphacite segregations.

The matrix of the eclogite from the sp. L-13 is composed of deformed and partially recrystallized grains of omphacite. The matrix contains a number of relatively large and usually idiomorphic crystals-porphyroblasts of an optically zoned garnet. Inner zones of the crystals contain numerous microscopic inclusions of epidote and omphacite, and in marginal zones single xenomorphic selections of rutile were detected. In the central zones of garnet crystals in the intergranular space of rocks there are small isolated selections of epidote. Inner zones of garnet crystals have a following minal composition (%): almandine (55) grossular (27); pyrope (17), spessartine (1). The marginal zones, in comparison with the inner zones, contain smaller amounts of almandine (49–51%) and grossular (23–24%) minals, but higher amounts of pyrope minal (25%). These data indicate the presence of progressive chemical zoning in garnets from this sample of eclogites. In the omphacite presented in this sample, of eclogite, the content of jadeite minal was 23–32%. Among the deformed grains of omphacite we detected some isolated small segregations of actinolite enriched with sodium, which have a diamond-shaped cross section.

These data on the REE composition of the considered samples of eclogites (Table 1.8) showed that the sp. L-12 is characterized by a low total REE content (~41 ppm) compared to sp. L-13 (~66 ppm) (Figure 1.7, 1). In both cases, there is a slightly fractionated REE ($(\text{La}/\text{Yb})_n \approx 0.6\text{--}1.0$), and the patterns have europium minima of minor intensity – $(\text{Eu}/\text{Eu}^*) \approx 0.7\text{--}0.8$. Regarding the content of LREE, the two samples are intermediate between N-MORB and E-MORB basalts, while the content of heavy elements in them is slightly higher.

According to our studies, the eclogites from Atbashi complex by their geochemical characteristics are comparable with the samples, previously described by Shatsky [1990], although the overall level of REE accumulation in our data turned out to be slightly higher.

The REE composition of garnets from eclogites of Atbashi complex have been characterized by the example of several crystals with a distinct optical zoning being observed (Table 1.5.). Garnets from L-12 and L-13 samples are quite similar in their REE composition (Figure 1.8). Firstly, in the REE pattern patterns of middle and peripheral zones of their crystals there are negative Eu anomalies, uncommon for garnets: $(\text{Eu}/\text{Eu}^*)_n = 0.62\text{--}0.69$ (such an anomaly was also observed in one of the garnets from eclogites of Sulu Tube complex, Figure 1.6, 4). Secondly, the content of light elements in the middle and peripheral zones of garnet crystals is almost identical, and the values of $(\text{La}/\text{Sm})_n$ change in a very narrow range (4.2–4.8). Thirdly, the crystals have a distinct geochemical zonation caused by the fact that the concentration of heavy REE in the peripheral areas is much lower than in the inner zones. And lastly, in the internal zones of studied garnet crystals the values of $(\text{Gd}/\text{Yb})_n$ are much lower than in the peripheral areas: for sp. L-12 they are 0.11 and 0.36–0.55; for sp. L-12 are 0.55 and 0.94–1.12. From the inner zones of the crystals, out to their periphery, the Sc content is reducing: in sp. L-12 from 14.7–16.5 to 8.3–11.5 ppm, for sp. L-12

Table 1.8 REE composition of eclogites from Atbashi metamorphic complex, Kyrgyzstan (ppm).

Element	L-12	L-13
La	3,75	8,26
Ce	6,49	15,84
Pr	1,25	2,14
Nd	6,72	9,10
Sm	2,03	2,45
Eu	0,63	0,80
Gd	3,36	4,13
Tb	0,70	0,99
Dy	5,55	7,65
Ho	1,33	1,84
Er	3,91	5,51
Tm	0,63	0,92
Yb	4,14	5,74
Lu	0,63	0,84
Total	41,1	66,2
La/Yb_n	0,61	0,97
$(\text{Eu/Eu}^*)_n$	0,73	0,76

Note: The analyses carried out by the ICP-MS method on mass-spectrometer "Element" (firm Finnigan MAT, Germany) in the Analytical Centre of UIGGM SB of USSRAS (analysts S. Palesskii & I. Nikolaeva). Relative standard deviation – less 10%.

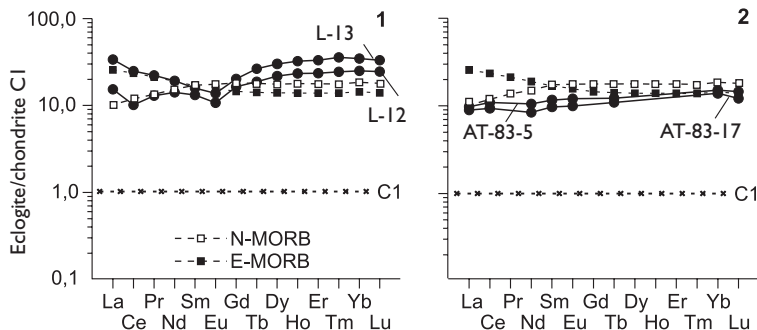


Figure 1.7 Chondrite-normalized REE patterns for eclogites from Atbashi metamorphic complex (Kyrgyzstan). 1 – data Table 1.8; 2 – data by [Shatsky, 1990]. N-MORB and E-MORB – patterns for normal and enriched basalts of mid-ocean ridges (MORB) according to (data [Sun & McDonough, 1989]).

from 4.0 to 3.6 ppm. Rather distinct zonation, which is typical for the distribution of most other incompatible trace elements, has not been identified in the studied garnets. Different zones of garnet crystals have approximately the same values of Zr/Hf (39.8–44.5) and Nb/Ta (30.0–34.4) in both eclogite samples.

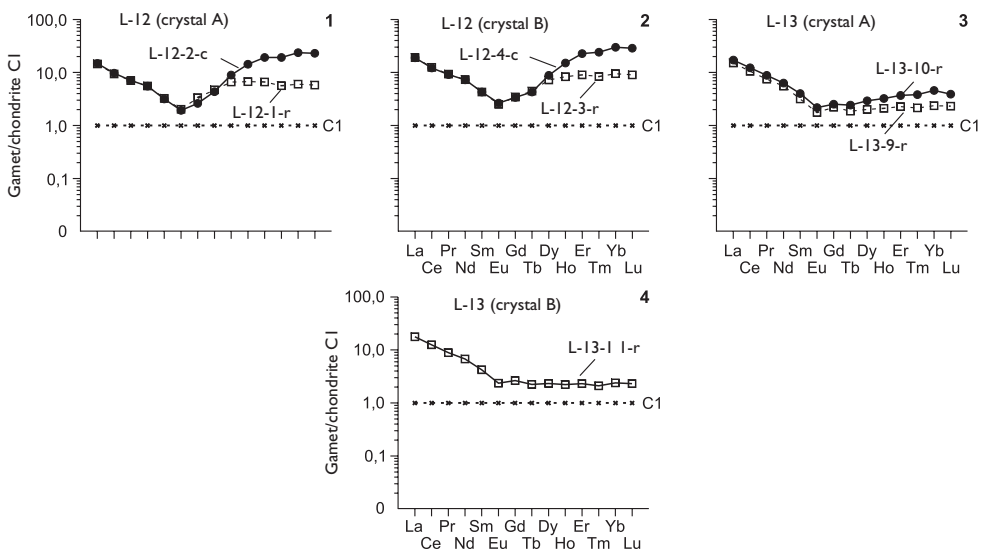


Figure 1.8 Chondrite-normalized REE patterns for garnets from eclogites from Atbashi metamorphic complex (Kyrgyzstan) (data Table 1.5).

On the basis of results of analyses of the chemical composition of garnets from eclogites of the Atbashi complex as well as coexisting omphacites, we estimated the *PT*-parameters of metamorphism of their protoliths [Lesnov *et al.*, 2004b]. Judging by them, during the formation of the peripheral zones of garnet crystals and coexisting omphacites of sp. L-12 the pressure reached ~23 kbar and the temperature (according to different geothermometers) varied in the range ~720–760°C. The formation of internal and middle zones of garnet crystals occurred at a higher pressure (~23.8 kbar) and a lower temperature (~570–620°C). Therefore, during the formation of the eclogite represented in the sp. L-12 the growth of garnet crystals from the inner to the peripheral areas was carried out under the conditions of increasing temperature and decreasing pressure, i.e. on progressive stage of metamorphism. Similar calculations were made for sp. L-13 and they showed that the marginal zones of the garnet grains were formed at a pressure of 22.7 kbar and temperature (according to different geothermometers) of 840–880°C. The calculations carried out by using the data on the composition of omphacite grains that are present in the inner zones of garnet crystals in the form of micro-inclusions, indicate a higher pressure (~23.7 kbar) and a lower temperature (from 690 to 740°C).

Thus, the garnets from eclogites of the samples from Atbashi complex have a progressive chemical zoning, which becomes apparent in the enrichment with Mg and depletion by Ca of the peripheral zones of their crystals. They were formed in the progressive stage of metamorphism of protolith under conditions of increasing temperature. Towards the periphery of garnet crystals the heavy REE content is consistently decreasing, whereas the contents of light elements remain approximately at the same level as in the internal zones of the crystals. This kind of zonal distribution

of REE was observed in garnets from metamorphic rocks formed under conditions of granulite and amphibolite facies [Skublov & Drugova, 2004]. The observed depletion of the marginal zones of garnet crystals from metamorphic rocks by HREE corresponds to the depletion by Ca, divalent ions of which are known to be preferred for heterovalency isomorphous substitution of ions of heavy REE, as they have a slightly smaller ionic radii compared with light elements.

Gabbros. It is known that the garnets are relatively rarely found in gabbro content. Their REE composition is characterized by the example of samples from specific varieties of rocks presented in Ivrea-Verbano mafic-ultramafic complex [Mazzucchelli *et al.*, 1992]. The amount of almandine mineral in these garnets varies in the range of 47.3–52.2%, of grossular mineral – 15.7–19.4%, while the content of Cr is 16–278 ppm. By the morphology of grains two groups of varieties were formed: 1) garnets that are a part of reaction rims at the grain boundaries of olivine or clinopyroxene, on the one hand, and plagioclase grains, on the other 2) porphyric grains that were probably formed as a liquidus phase. In the garnets from the rims the total REE content was 13.9–47.5 ppm, which is slightly smaller than their contents in the mineral from porphyric segregations (43.1–80.6 ppm) (Table 1.9). Both types of garnets are depleted by LREE and enriched with HREE, and their REE patterns have a steep positive slope (Figure 1.9). In contrast to the patterns of garnets from porphyric segregations that sometimes have low-intensity negative Eu anomalies, the patterns of garnet from reaction rims are often complicated by intense positive anomalies of this element. According to Mazzucchelli *et al.*, garnet-bearing gabbros from Ivrea Verbano complex were formed under the conditions of granulite facie in the lower crust.

Effusive rocks. The REE composition of garnets from volcanic rocks is characterized by the example of a small collection of samples with different chemical compositions, which are presented in the form of relatively large phenocrysts or megacrystals in alkali olivine basalts (pyrope), hawaiites (almandine), nepheline basanites (pyrope), andesites (almandine), dacites (almandine), rhyodacites (almandine) and rhyolites (almandine) (Table. 1.9, Figure 1.9). Most of them are characterized by high total REE content (167–653 ppm); the highest values are in the mineral from rhyolites. A partial exception is the garnet from basanite with a total REE content ~17 ppm. The REE patterns of garnets from effusive rocks of mafic composition have the form of almost straight lines with a steep positive slope: $(\text{La/Yb})_{\text{n}} \approx 0.002–0.015$. The REE patterns of garnets from dacites, rhyodacites and rhyolites are complicated by intense negative Eu anomalies, which is probably due to the preferential occurrence of Eu in plagioclase that is prevailing in these effusions.

Skarns. The REE composition of garnets from skarns was studied in samples of Broken Hill lead-zinc-silver deposit (Australia) [Shwandt *et al.*, 1993], as well as from Ocna de Fier province (Romania) [Nicolescu *et al.*, 1998]. In the ore bodies of Broken Hill deposit as a part of fine-medium-grained granatites the garnets make up 80–95% of their volume, excelling with very low MgO content (0.14–2.8 wt%). Given the distribution of MnO, the spessartine (18.3–28.4 wt%) and the almandine (2.4 wt%) are singled out among them. Within the individual grains of these garnets, the REE distribution is uneven: in the inner areas the total content varies in the range of 12.4–48.3 ppm, and in the peripheral areas it is slightly higher (12.5–54.5 ppm) which is associated with a significant accumulation of heavy REE (Table 1.10, Figure 1.10, 1–4). On this basis the garnets from skarns differ from garnets from eclogites and

Table 1.9 REE compositions of garnets from gabbros, and volcanogenic rocks from some provinces, complexes and manifestations (ppm).

Ivrea Verbania complex, Italy											
	[Mazzucchelli et al., 1992], IPMA										
	MPI(c)	MPI(c*)	MP3(p)	MP5(p)	MO95(c)	MP6(c)	MP9(c)	MZ145(c)	MP12(p)	MP13(p)	MP18(p)
Element	Gabbros										
La	N.d.	N.d.	N.d.	N.d.	N.d.	N.d.	N.d.	N.d.	N.d.	N.d.	
Ce	0,180	0,720	0,410	0,570	1,460	0,500	0,940	0,180	0,120	0,090	
Pr	N.d.	N.d.	N.d.	N.d.	N.d.	N.d.	N.d.	N.d.	N.d.	N.d.	
Nd	0,730	1,160	2,060	1,820	2,320	2,660	7,250	1,440	1,360	2,870	
Sm	2,340	1,780	3,600	2,700	2,320	2,630	5,810	1,090	3,720	5,590	
Eu	1,870	1,050	1,670	1,320	3,010	4,510	6,140	2,410	1,560	1,890	
Gd	N.d.	N.d.	N.d.	8,230	N.d.	N.d.	N.d.	N.d.	N.d.	N.d.	
Tb	N.d.	N.d.	N.d.	N.d.	N.d.	N.d.	N.d.	N.d.	N.d.	N.d.	
Dy	12,42	15,09	17,37	15,20	8,480	8,880	11,78	3,120	16,31	22,04	
Ho	N.d.	N.d.	N.d.	N.d.	N.d.	N.d.	N.d.	N.d.	N.d.	N.d.	
Er	8,210	12,55	9,360	11,10	4,820	5,280	7,890	2,770	9,790	14,12	
Tm	N.d.	N.d.	N.d.	N.d.	N.d.	N.d.	N.d.	N.d.	N.d.	N.d.	
Yb	10,34	15,13	8,640	10,93	4,360	4,310	8,290	2,890	10,44	15,01	
Lu	N.d.	N.d.	N.d.	N.d.	N.d.	N.d.	N.d.	N.d.	N.d.	N.d.	
Total	36,1	47,5	43,1	51,9	26,8	28,8	48,1	13,9	43,3	61,6	
(Ce/Yb) _n	0,005	0,012	0,012	0,013	0,087	0,030	0,029	0,016	0,003	0,002	

(Continued)

Table 1.9 (Continued).

Provinces										
	West Sangilen, Tuva, Russia	Mt. Nijo, Japan	Binge Point, Australia	Dutsen Dushowo, Nigeria	Merenga, Nigeria	Breziny, Chekhoslo- vakia	Tumut, Australia	Mt. Coburn, USA	Black Spur, Australia	
Egorova, 2005, LA ICP-MS	[Irving, Frey, 1978], INAA									
EKB2	N5g	MN-7	BBP-5	DD-2	M-3	B-6	T-8	CM-10	BS-9	
Element	Gabbro- norite	Gabbro	Dacite	Hawaiite	Basanite	Oliv. Basalt	Andesite	Rhyodacite	Rhyolites	
La	N.d.	0,01	8,100	0,630	0,034	N.d.	2,210	13,20	42,60	13,70
Ce	0,05	0,12	27,80	2,900	N.d.	N.d.	N.d.	40,00	172,0	83,00
Pr	0,03	0,08	N.d.	N.d.	N.d.	N.d.	N.d.	N.d.	N.d.	N.d.
Nd	0,61	2,12	17,40	N.d.	N.d.	N.d.	N.d.	63,00	12,00	
Sm	0,86	2,73	25,10	3,390	1,050	0,860	5,350	5,340	17,70	7,500
Eu	0,48	1,15	1,550	1,780	0,600	0,780	1,890	0,232	0,550	0,313
Gd	2,42	11,55	65,00	11,70	N.d.	N.d.	19,60	35,00	62,00	45,00
Tb	0,54	3,23	11,60	3,800	0,830	1,120	4,400	7,700	17,90	14,30
Dy	5,44	38,67	N.d.	N.d.	N.d.	N.d.	N.d.	N.d.	N.d.	N.d.
Ho	1,28	10,07	24,20	13,00	1,870	1,910	14,30	24,30	55,20	43,10
Er	4,32	35,45	N.d.	N.d.	N.d.	N.d.	N.d.	N.d.	N.d.	N.d.
Tm	0,74	6,22	N.d.	N.d.	N.d.	N.d.	N.d.	N.d.	N.d.	N.d.
Yb	4,96	41,51	54,50	97,00	10,30	9,000	101,0	82,00	194,0	197,0
Lu	0,86	6,40	7,800	18,30	1,970	1,800	18,00	12,60	28,50	27,00
Total	29,6	153	243	153	N.d.	N.d.	N.d.	220	653	443
(La/Yb) _n	N.d.	0,002	N.d.	0,004	0,002	N.d.	N.d.	0,109	0,148	0,047

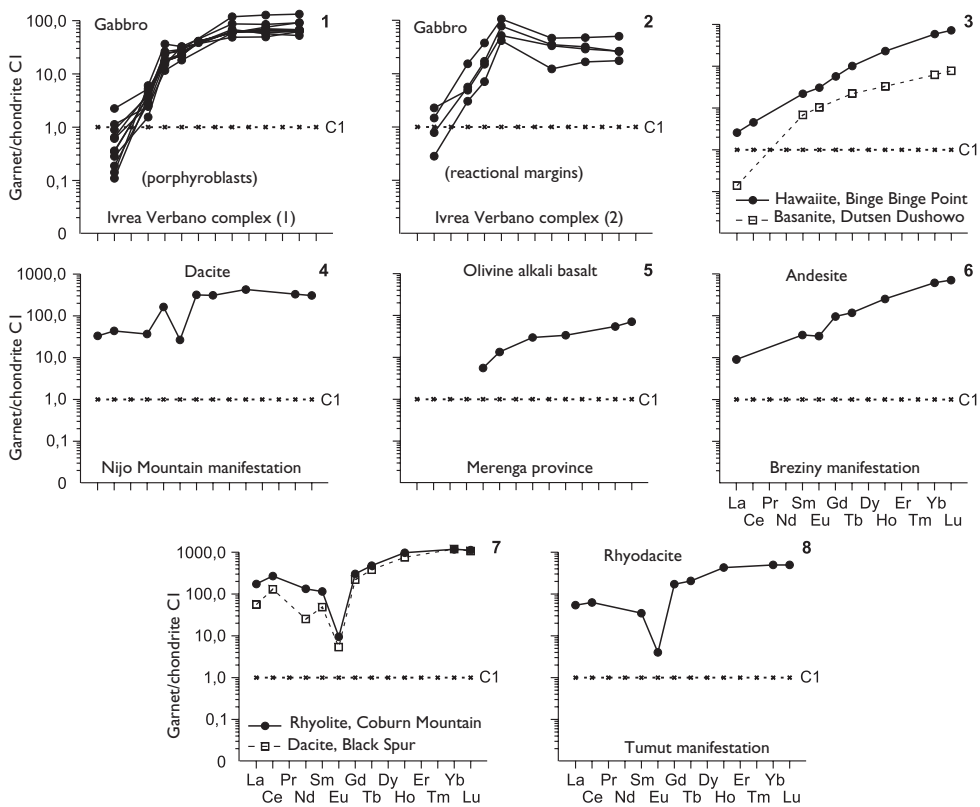


Figure 1.9 Chondrite-normalized REE patterns for garnets from gabbros and effusive rocks (data Table 1.9).

other rocks of metamorphic complexes, in which the peripheral zones of grains are depleted by HREE. Garnets from skarns are characterized by intense fractionation of REE: $(\text{La}/\text{Yb})_n = 0.002\text{--}0.033$. According to the conclusion of researchers, REE composition of garnets from skarns of Broken Hill deposit is inherited from the composition of protolite, which was enriched with REE well in advance of the appearance of metamorphic garnet in it, i.e. it is not associated with later hydrothermal processes [Shwandt *et al.*, 1993].

Garnets from skarns of Ocna de Fier province (Romania) are present in the form of andradite (sample NM33b) and grandite (sample NM34). The total REE content in them is much lower (6.8–7.5 ppm) than in samples from Broken Hill deposit. Because of the anomalous enrichment of these garnets with LREE their patterns have a negative slope: $(\text{La}/\text{Yb})_n = 11\text{--}16$ (Figure 1.10, 5, 6).

REE composition of garnets from skarns of Crown Jewel gold deposit (Washington State, USA) [Gaspar *et al.*, 2008] was studied in more details. They are represented by varieties of grossular-andradite series with fairly wide variations in the contents of grossular and andradite minerals. Among them there are both anisotropic and isotropic versions. All of these garnets are depleted in large-ionic lithophytic elements,

Table 1.10 REE compositions of garnets from skarns from some provinces (ppm).

	Broken Hill deposit, Australia								Ocna de Fier province, Romania	
	[Schwandt et al., 1993], SIMS								[Nicolescu et al., 1998], SIMS	
Element	G-1cor	G-1rim	G-3cor	G-3rim	G-4cor	G-4rim	G-5cor	G-5rim	MM33b	NM34
<i>Skarns (garnetites)</i>								<i>Skarns</i>		
La	0,32	0,27	N.d.	0,03	N.d.	N.d.	0,03	N.d.	2,81	1,79
Ce	3,83	3,48	0,31	0,23	0,03	0,20	0,19	N.d.	1,74	1,84
Pr	N.d.	N.d.	N.d.	N.d.	N.d.	N.d.	N.d.	N.d.	0,380	0,410
Nd	10,99	11,14	1,69	2,34	0,70	0,46	1,16	1,15	1,39	1,57
Sm	6,79	7,55	2,85	4,62	2,71	2,37	1,69	1,13	0,31	0,29
Eu	5,21	5,41	1,21	1,75	0,59	0,90	1,94	1,90	0,07	0,08
Gd	N.d.	N.d.	N.d.	N.d.	N.d.	N.d.	N.d.	N.d.	0,31	0,26
Tb	N.d.	N.d.	N.d.	N.d.	N.d.	N.d.	N.d.	N.d.	N.d.	N.d.
Dy	8,82	9,88	11,93	20,12	9,17	13,13	2,93	3,49	0,25	0,26
Ho	N.d.	N.d.	N.d.	N.d.	N.d.	N.d.	N.d.	N.d.	N.d.	N.d.
Er	5,45	8,17	7,03	11,68	5,33	8,02	2,04	2,34	0,11	0,14
Tm	N.d.	N.d.	N.d.	N.d.	N.d.	N.d.	N.d.	N.d.	N.d.	N.d.
Yb	6,63	8,55	7,74	12,58	5,63	8,28	2,38	2,51	0,12	0,11
Lu	N.d.	N.d.	N.d.	N.d.	N.d.	N.d.	N.d.	N.d.	N.d.	N.d.
Total	N.d.	N.d.	N.d.	N.d.	N.d.	N.d.	N.d.	N.d.	N.d.	N.d.
(La/Yb) _n	0,03	0,02	N.d.	0,002	N.d.	N.d.	0,009	N.d.	15,8	11,0

(Continued)

Table 1.10 (Continued).

Crown Jewel province, USA														
	[Gaspar et al., 2008], LA ICP-MS													
	195-300a	195-300b	195-341-5	197-235	201-123*	204-428a**	204-428b*	207-135a	207-135b**	207-152a	207-152b	209-78**	209-78	211-139
Element	Skarns													
La	0,27	0,37	0,82	<0,1	0,20	1,00	<0,1	<0,1	0,27	<0,1	<0,1	<0,1	0,37	0,19
Ce	2,55	4,15	9,45	<0,1	0,65	1,06	0,21	<0,1	0,70	0,18	<0,1	<0,1	1,54	0,21
Pr	1,03	1,64	2,62	<0,1	0,28	0,09	0,15	<0,1	0,17	0,16	<0,1	0,10	0,36	<0,1
Nd	9,44	12,86	13,71	1,10	2,00	0,13	2,12	<0,1	1,04	2,29	<0,1	0,96	2,00	0,16
Sm	3,39	3,44	2,76	1,77	0,87	<0,1	2,50	<0,1	0,24	2,03	<0,1	0,95	0,19	<0,1
Eu	2,66	4,46	2,94	1,39	2,57	0,11	2,32	0,09	3,29	0,37	<0,1	1,31	2,01	<0,1
Gd	3,38	3,58	2,53	5,64	1,18	<0,1	4,54	0,14	0,16	4,51	<0,1	2,16	<0,1	<0,1
Tb	0,51	0,49	0,32	1,25	0,17	<0,1	0,78	<0,1	0,04	0,81	<0,1	0,42	<0,1	<0,1
Dy	3,41	3,01	1,51	10,42	1,01	<0,1	4,91	0,17	0,31	6,17	<0,1	3,83	<0,1	0,16
Ho	0,74	0,57	0,22	2,45	0,24	<0,1	0,91	<0,1	<0,1	1,48	<0,1	1,15	<0,1	<0,1
Er	2,09	1,49	0,62	7,53	0,67	<0,1	2,28	0,12	0,18	4,19	<0,1	4,94	<0,1	0,16
Tm	0,32	0,20	0,07	1,18	<0,10	<0,1	0,26	<0,1	<0,1	0,51	<0,1	0,96	<0,1	<0,1
Yb	2,54	1,47	0,57	9,84	0,37	<0,1	1,67	0,10	0,13	<0,1	<0,1	7,83	<0,1	0,18
Lu	0,37	0,21	0,90	1,46	<0,1	<0,1	0,22	<0,1	<0,1	0,34	<0,1	1,23	<0,1	<0,1
Total	32,7	37,94	39,04	N.d.	N.d.	N.d.	N.d.	N.d.	N.d.	N.d.	N.d.	N.d.	N.d.	N.d.
(La/Yb) _n	0,07	0,17	0,97	<0,002	0,36	N.d.	N.d.	N.d.	1,40	N.d.	N.d.	N.d.	N.d.	0,71
(Eu/Eu*) _n	2,38	3,86	3,34	1,23	7,75	N.d.	2,08	N.d.	48,43	0,36	N.d.	2,70	N.d.	N.d.

Note: Sample 195-300a – feebly anisotropic, Gr (41,3%), And (56,4%); sample 195-300b – feebly anisotropic, Gr (47,7%), And (48,4%); sample 195-341-5 – feebly anisotropic, (Gr 36,2%), And (61,0%); sample 201-123 – isotropic, core of grain, Gr (16,2%), And (80,5%); sample 204-4286 – anisotropic, core of grain, Gr (45,9%), And (47,8%); sample 207-152a – anisotropic, Gr (38,2%), And (58,9%); sample 197-135 – anisotropic, Gr (56,6%), And (35,3%); sample 209-78a – anisotropic, rim of grain, (Gr 43,2%), And (53,9%). Gr - grossular minal, And - andradite minal. (*) - analyses carried out in the core of grains. (**) - analyses carried out in the rim of grains.

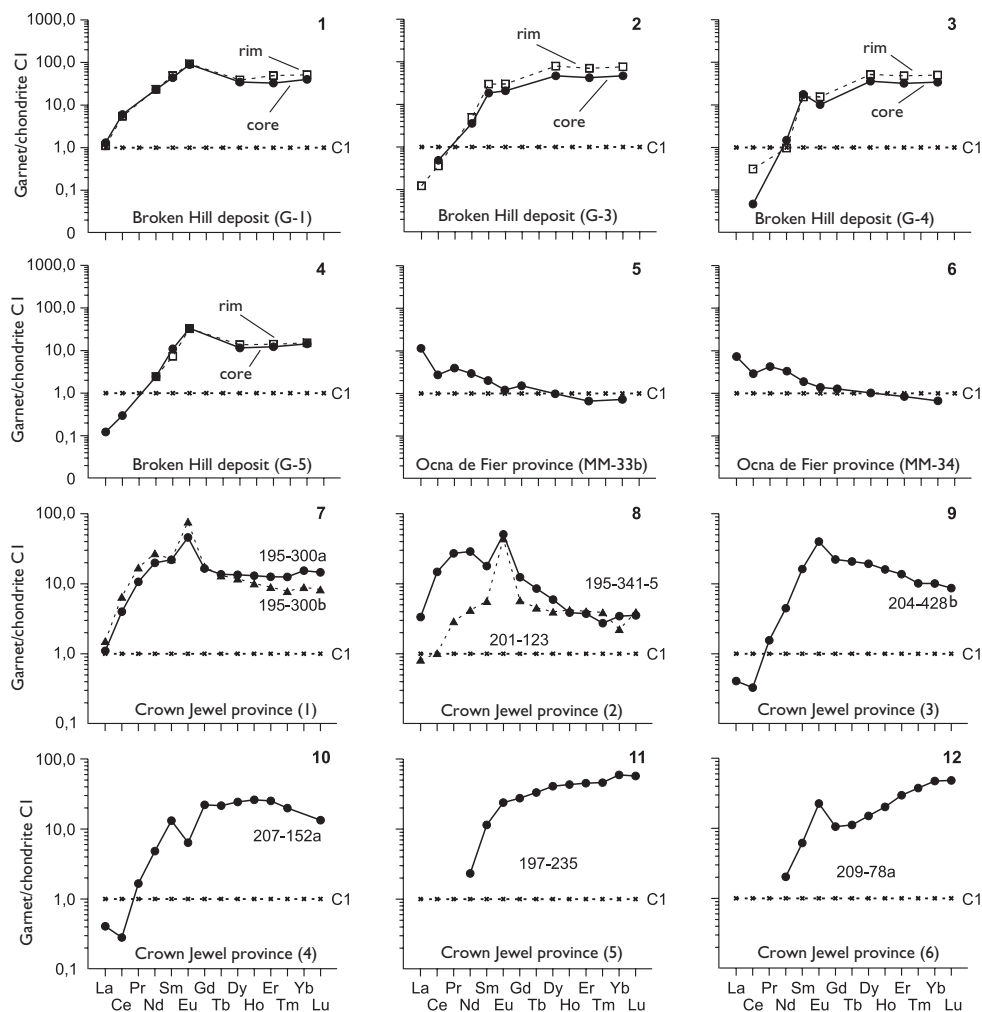


Figure 1.10 Chondrite-normalized REE patterns for garnets from skarns (data Table 1.10).

as well as Ta, Hf and Th. The total REE contents in them vary in a very wide range, in certain samples some of the elements are contained within the limit of detection. The values of La/Yb_{n} (0.001–18) and $(\text{Eu/Eu}^*)_{\text{n}}$ (0.3–47) also have a very wide range (Table 1.10). There is a positive correlation between total REE content and the content of Al, moreover the varieties of garnets enriched with Al, are also enriched in Y, Zr and Sc. REE patterns of most of the garnets indicates their enrichment with HREE relative to LREE, as well as a slight excess of Eu (Figure 1.10). Garnet varieties, containing more than 90% of andradite mineral, are characterized by a lower overall level of REE accumulation, relative enrichment with LREE, as well as more significant

excess of Eu. In addition, the named researchers examined some aspects of crystallochemistry of garnets from the Crown Jewel deposit and possible mechanisms of isomorphous entry of REE to their structure.

Gneises, schists and other metamorphic rocks. Data on REE composition of almandine from this group of rocks from Belomorsky, Ladoga, Laplandsky, Keiv and Nurundukan metamorphic complexes widely spread in different Russian regions, are presented (Table 1.11). They are poor in MgO (0.58–11.20 wt%) and CaO (1–16 wt%), but enriched with FeO and Al₂O₃. A progressive (increase of MgO content towards the periphery of the grains) and regressive (decrease of MgO content towards the periphery of the grains) zoning was observed in them.

The most representative analytical data on the geochemistry of REE was obtained for the garnets from the gneisses of Belomorsky metamorphic complex. Along with the zonal distribution of macro-components in garnets from metamorphic rocks a zonal distribution of REE is observed. The total REE content in garnets varies in a wide range (6.6–340 ppm), which is mainly due to the uneven distribution of heavy elements. Marginal zones of garnet crystals are sometimes depleted by HREE compared to the inner zones, while there is an opposite tendency in the distribution of light elements (Figure 1.11, 3, 4). In all of these garnets the REE are significantly fractionated: (La/Yb)_n = 0.0001–0.009 (Figure 1.11, 1, 2); their REE patterns often show negative Eu anomalies of low intensity. A similar distribution of REE was ascertained in garnets from rocks of Laplandsky and Nurundukansky complexes. In the rocks of the Ladoga and Keiv complexes (Figure 1.11, 8, 10) the peripheral zones of garnet crystals were found depleted not only by heavy but also by light elements (Figure 1.11, 5, 9). Moreover, there are significant fluctuations of the heavy and light REE contents in the peripheral zones of grains of described garnets, though the content of the medium elements doesn't change significantly. Based on the data presented, Skublov & Drugova [2004] came to a conclusion that the decrease of HREE content and increase of LREE content in the marginal zones of garnet crystals are due to higher temperatures in the later stages of their growth. In addition, the garnets from metamorphic rocks of the granulite facie from Skorian [Pride & Muecke, 1981] and Eifel [Loock *et al.*, 1990] provinces have flat positively inclined REE pattern, often complicated by positive Eu anomalies of low-intensity.

Our analyses, included in the compiled databank, yielded estimates of the average content of REE in garnets from rocks of various composition and genesis (Table 1.12, Figure 1.12). According to the research, the average REE contents vary from very low, typical to samples of garnets from peridotite xenoliths of Aykhal pipe (2.36 ppm), to very high (314 ppm), ascertained in the samples of dacites volcanogenic complex (Japan). The vast majority of these values are in some way superior to the content of REE in C1 chondrite. In the garnets from peridotite xenoliths of Aykhal pipe, from pyroxenite xenoliths in basalts of Vitim plateau, from eclogites in xenoliths of Roberts Victor pipe, from Soazza metamorphic complex, as well as from skarns of Broken Hill deposit, the average content of light REE is smaller than in C1 chondrite. To add, distribution patterns of the average REE contents in garnets from peridotite xenoliths of diamondiferous kimberlites of Roberts Victor, Udachnaya, Aykhal and Mir pipes have a sinusoidal configuration.

Table 1.11 REE compositions of garnets from gneisses and schist from some metamorphic complexes (ppm).

Belomorsky complex, Russia									
	[Skublov, Drugova, 2004], SIMS								
	315a(c)	315a(r)	916a(c)	916a(r)	973(c)	973(r)	972a(c)	972a(r)	19(c)
<i>Element</i>	<i>Gneisses</i>								
La	0,029	0,047	0,031	0,088	0,010	0,018	0,008	0,017	0,009
Ce	0,079	0,094	0,073	0,125	0,023	0,065	0,033	0,043	0,027
Pr	N.d.	N.d.	N.d.	N.d.	N.d.	N.d.	N.d.	N.d.	N.d.
Nd	0,265	0,083	0,189	0,175	0,167	0,220	0,220	0,167	0,091
Sm	0,719	1,033	1,598	1,556	1,078	1,513	1,261	1,252	0,850
Eu	0,161	1,155	0,244	0,205	0,216	0,336	0,498	0,358	0,198
Gd	N.d.	N.d.	N.d.	N.d.	N.d.	N.d.	N.d.	N.d.	N.d.
Tb	N.d.	N.d.	N.d.	N.d.	N.d.	N.d.	N.d.	N.d.	N.d.
Dy	28,45	15,14	24,09	16,22	79,51	34,51	12,76	19,83	26,49
Ho	N.d.	N.d.	N.d.	N.d.	N.d.	N.d.	N.d.	N.d.	N.d.
Er	27,63	9,490	21,40	6,710	130,6	33,53	9,020	10,44	15,99
Tm	N.d.	N.d.	N.d.	N.d.	N.d.	N.d.	N.d.	N.d.	N.d.
Yb	29,46	9,840	23,51	6,010	127,6	30,74	7,480	10,29	12,18
Lu	N.d.	N.d.	N.d.	N.d.	N.d.	N.d.	N.d.	N.d.	N.d.
Total	86,8	36,9	71,1	31,1	339	101	31,3	42,4	55,8
(Ce/Yb) _n	0,001	0,003	0,001	0,010	0,0001	0,0004	0,001	0,001	0,0005

(Continued)

Table 1.11 (Continued).

Belomorsky complex, Russia										
	[Skublov, Drugova, 2004], SIMS									
	19(r)	91g(c)	91g(r)	309g(c)	309g(r)	14b(c)	14b(r)	28b(c)	28g(r)	82g(c)
<i>Element</i>	<i>Gneisses</i>									
La	0,043	0,018	0,008	0,005	0,105	0,010	0,020	0,003	0,008	0,009
Ce	0,144	0,039	0,055	0,025	2,402	0,033	0,042	0,036	0,021	0,028
Pr	N.d.	N.d.	N.d.	N.d.	N.d.	N.d.	N.d.	N.d.	N.d.	N.d.
Nd	0,120	0,273	0,264	0,023	1,102	0,032	0,042	0,089	0,092	0,071
Sm	0,404	1,494	0,971	1,514	4,244	0,048	0,021	0,822	0,592	0,147
Eu	0,125	0,436	0,245	0,257	0,998	0,033	0,025	0,372	0,716	0,120
Gd	N.d.	N.d.	N.d.	N.d.	N.d.	N.d.	N.d.	N.d.	N.d.	N.d.
Tb	N.d.	N.d.	N.d.	N.d.	N.d.	N.d.	N.d.	N.d.	N.d.	N.d.
Dy	45,57	14,51	19,56	19,62	25,34	1,970	1,060	26,60	28,80	8,280
Ho	N.d.	N.d.	N.d.	N.d.	N.d.	N.d.	N.d.	N.d.	N.d.	N.d.
Er	43,22	6,970	11,63	12,63	8,480	2,870	2,230	16,13	14,61	8,800
Tm	N.d.	N.d.	N.d.	N.d.	N.d.	N.d.	N.d.	N.d.	N.d.	N.d.
Yb	37,23	6,070	10,10	9,160	8,180	4,790	3,120	15,62	11,53	10,31
Lu	N.d.	N.d.	N.d.	N.d.	N.d.	N.d.	N.d.	N.d.	N.d.	N.d.
Total	127	29,8	42,8	43,2	50,9	9,79	6,56	59,7	56,4	27,8
(Ce/Yb) _n	0,001	0,002	0,001	0,0004	0,009	0,001	0,004	0,0001	0,0005	0,001

(Continued)

Table 1.11 (Continued).

	<i>Belomorsky complex, Russia</i>		<i>Ladoga complex, Russia</i>			<i>Laplandia complex, Russia</i>				
	82d(r)	193z(c)	779-l(c)	779-l(r)	245d(c)	245d(r)	249(c)	249(r)	620g(c)	620g(r)
Element	Gneisses		Garnet-biotite gneisses			Garnet-hypersthene gneisses				
La	0,021	0,005	0,022	0,005	0,016	0,044	0,029	0,040	0,014	0,010
Ce	0,032	0,053	0,062	0,012	1,129	0,253	0,229	0,219	0,060	0,137
Pr	N.d.	N.d.	N.d.	N.d.	N.d.	N.d.	N.d.	N.d.	N.d.	N.d.
Nd	0,027	0,091	0,116	0,091	1,680	2,858	1,600	3,219	4,775	4,158
Sm	0,089	1,054	0,722	0,728	4,360	6,997	5,243	7,686	8,713	7,985
Eu	0,057	1,080	0,500	0,645	0,151	0,285	0,450	0,767	1,120	1,251
Gd	N.d.	N.d.	N.d.	N.d.	N.d.	N.d.	N.d.	N.d.	N.d.	N.d.
Tb	N.d.	N.d.	N.d.	N.d.	N.d.	N.d.	N.d.	N.d.	N.d.	N.d.
Dy	6,050	3,840	79,91	26,46	15,02	22,87	52,47	25,63	58,68	34,48
Ho	N.d.	N.d.	N.d.	N.d.	N.d.	N.d.	N.d.	N.d.	N.d.	N.d.
Er	7,970	2,000	67,12	13,91	10,57	11,84	11,02	18,35	55,38	29,97
Tm	N.d.	N.d.	N.d.	N.d.	N.d.	N.d.	N.d.	N.d.	N.d.	N.d.
Yb	9,670	2,220	62,8	11,09	9,370	12,89	8,470	19,52	57,58	32,55
Lu	N.d.	N.d.	N.d.	N.d.	N.d.	N.d.	N.d.	N.d.	N.d.	N.d.
Total	23,9	10,3	211	52,9	42,3	58,0	79,5	75,4	186	111
(Ce/Yb) _n	0,001	0,002	0,0002	0,0003	0,001	0,002	0,002	0,001	0,0002	0,0002

(Continued)

Table 1.11 (Continued).

	<i>Laplandia complex, Russia</i>		<i>Nurundukansky complex, Russia</i>					<i>Keiv complex, Russia</i>		
	[Skublov, Drugova, 2004], SIMS									
	45o(c)	45o(r)	133(c)	133(r)	538(c)	538(r)	271/10(c)	271/10(r)	349/5(c)	349/5(r)
Element	Garnet-hypersthenes' gneisses		Mafitic orthoschists						Garnet-biotitic gneisses	
La	0,109	0,013	0,143	0,147	N.d.	0,006	0,180	0,358	0,033	0,035
Ce	0,263	0,084	0,610	0,842	0,008	0,007	0,454	0,967	0,087	0,047
Pr	N.d.	N.d.	N.d.	N.d.	N.d.	N.d.	N.d.	N.d.	N.d.	N.d.
Nd	0,884	1,593	0,149	0,224	0,172	N.d.	0,194	0,302	0,315	0,283
Sm	5,076	6,027	0,064	0,078	0,660	0,064	0,040	0,097	2,060	2,363
Eu	0,312	0,302	0,025	0,032	0,579	0,050	0,143	0,103	9,735	9,442
Gd	N.d.	N.d.	N.d.	N.d.	N.d.	N.d.	N.d.	N.d.	N.d.	N.d.
Tb	N.d.	N.d.	N.d.	N.d.	N.d.	N.d.	N.d.	N.d.	N.d.	N.d.
Dy	60,69	68,31	1,840	2,000	5,770	3,460	1,840	2,420	53,26	24,38
Ho	N.d.	N.d.	N.d.	N.d.	N.d.	N.d.	N.d.	N.d.	N.d.	N.d.
Er	41,91	47,56	6,090	2,310	3,820	2,790	2,670	2,360	55,79	11,60
Tm	N.d.	N.d.	N.d.	N.d.	N.d.	N.d.	N.d.	N.d.	N.d.	N.d.
Yb	35,48	41,58	11,90	3,450	4,140	2,590	3,930	3,030	56,91	8,650
Lu	N.d.	N.d.	N.d.	N.d.	N.d.	N.d.	N.d.	N.d.	N.d.	N.d.
Total	145	165	20,8	9,08	15,2	8,97	9,45	9,64	178	56,8
(Ce/Yb) _n	0,002	0,0002	0,008	0,029	N.d.	0,002	0,031	0,080	0,0004	0,003

Note: (c) – core of grain, (r) – rim of grain.

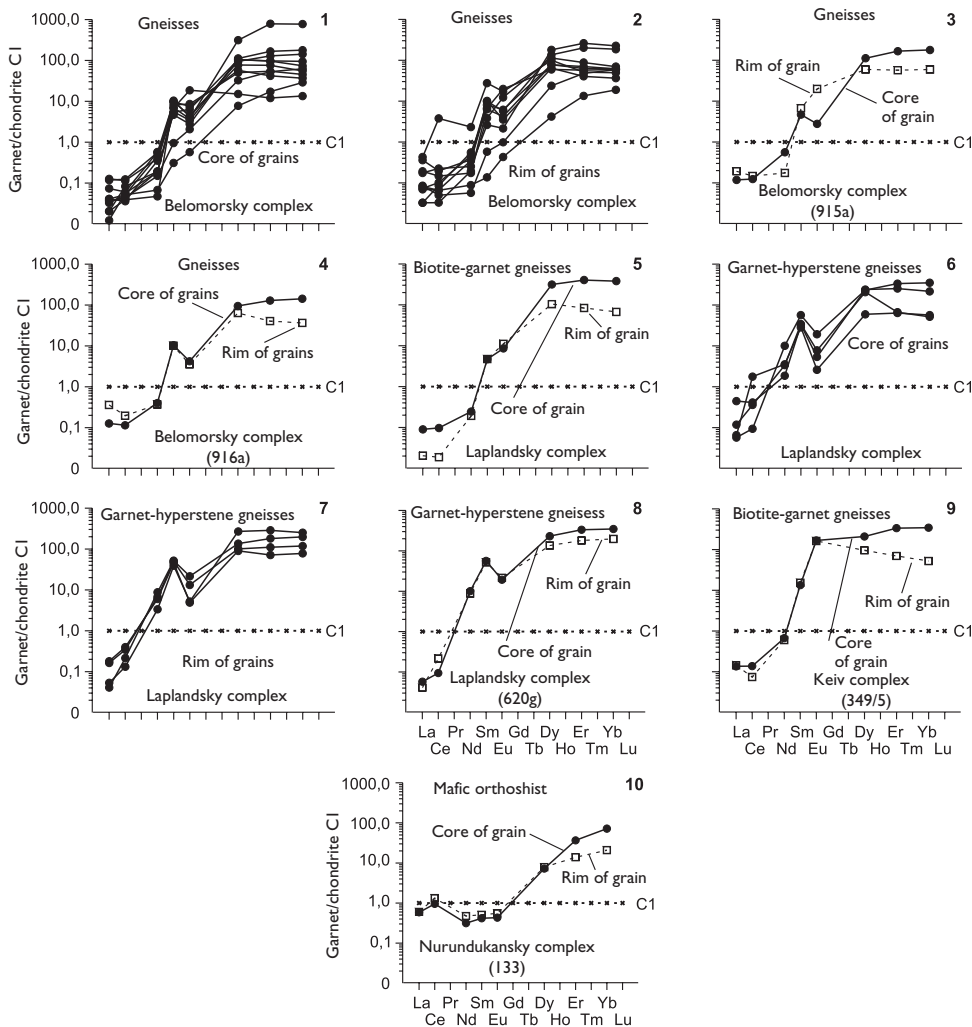


Figure 1.11 Chondrite-normalized REE patterns for garnets from metamorphic rocks (data Table 1.11).

1.3 ON THE NATURE OF SINUSOIDAL CHONDRITE-NORMALIZED REE PATTERNS OF GARNETS

Studies on the patterns of REE distribution in garnets, which are in the parageneses with diamonds in kimberlites and the xenoliths of mantle peridotite contained in them, in recent years received increasing attention. These garnets by their chemical composition correspond with pyropes and usually have specific sinusoidal REE patterns, which have been described for the first time by Shimizu & Richardson [1987]. The most important feature of these garnets is an anomalous enrichment in LREE with a relative depletion by medium and heavy elements, and this is due to the unusual sinusoidal shape of the patterns. Pyropes with similar REE patterns at different times were

Table 1.12 Average REE compositions of garnets from some parageneses from some provinces and complexes (ppm).

	Provinces (complexes, pipes)													
Element	1 (10)	2 (7)	3 (10)	4 (9)	5 (10)	6 (6)	7 (8)	8 (3)	9 (13)	10 (8)	11 (4)	12 (11)	13 (2)	14 (2)
La	0,433	0,245	N.d.	1,51	0,149	0,115	0,495	0,017	0,070	0,408	N.d.	N.d.	N.d.	N.d.
Ce	2,72	1,14	N.d.	5,90	1,43	0,363	1,92	0,097	0,339	1,03	0,010	0,476	23,9	0,170
Pr	0,495	0,184	N.d.	N.d.	N.d.	N.d.	N.d.	N.d.	N.d.	N.d.	N.d.	N.d.	N.d.	N.d.
Nd	2,39	1,26	N.d.	3,28	2,15	0,260	2,11	0,640	1,09	1,24	0,100	2,31	16,2	1,12
Sm	0,615	0,477	0,617	0,880	0,482	0,480	0,400	0,670	0,803	0,750	1,01	3,24	20,1	2,78
Eu	0,190	0,161	0,436	0,207	0,139	0,222	0,197	0,370	0,434	0,386	1,48	2,46	1,49	0,900
Gd	0,585	0,706	2,67	N.d.	N.d.	N.d.	N.d.	N.d.	N.d.	N.d.	14,6	8,23	59,3	N.d.
Tb	0,096	0,117	0,640	N.d.	N.d.	N.d.	N.d.	N.d.	0,368	0,324	N.d.	N.d.	11,6	N.d.
Dy	0,402	0,870	N.d.	0,288	0,255	0,386	0,188	5,59	2,93	1,48	43,8	14,6	122	10,6
Ho	0,104	0,193	1,39	N.d.	N.d.	N.d.	N.d.	N.d.	0,722	N.d.	N.d.	N.d.	24,2	N.d.
Er	0,254	0,643	N.d.	0,207	0,219	0,175	0,253	5,37	2,44	N.d.	19,4	9,73	77,9	6,18
Tm	N.d.	N.d.	N.d.	N.d.	N.d.	N.d.	N.d.	N.d.	N.d.	N.d.	N.d.	N.d.	N.d.	N.d.
Yb	0,315	0,747	4,92	0,384	0,298	0,343	0,306	7,36	N.d.	2,76	14,9	10,2	62,4	6,69
Lu	0,065	0,129	0,784	N.d.	N.d.	N.d.	N.d.	N.d.	0,442	0,432	N.d.	N.d.	8,95	N.d.
Total	8,59	6,83	N.d.	12,7	5,13	2,34	5,87	20,1	9,64	N.d.	N.d.	N.d.	N.d.	N.d.
$(\text{La}/\text{Yb})_n$	3,37	1,26	N.d.	2,44	0,49	0,25	1,41	0,003	N.d.	0,186	N.d.	N.d.	0,100	N.d.

Note: 1 – pipe Roberts Victor (Ghana), garnet harzburgites from xenoliths in kimberlites [Stachel et al., 1998]; 2 – pipe Roberts Victor (South Africa), garnet lherzolites from xenoliths in kimberlites [Stachel et al., 1998]; 3 – Vitim province (Transbaikalia, Russia), garnet lherzolites from xenoliths in alkaline basalts [Ionov et al., 1993]; 4 – pipe Udachnaya (Yakutia, Russia), garnet peridotites from xenoliths in kimberlites [Pokhilenko et al., 1993]; 5 – pipe Udachnaya (Yakutia, Russia), garnet peridotites from xenoliths in kimberlites [Shimizu et al., 1997a]; 6 – pipe Aykhal (Yakutia, Russia), garnet peridotites from xenoliths in kimberlites [Shimizu et al., 1997a]; 7 – pipe Mir (Yakutia, Russia), garnet peridotites from xenoliths in kimberlites [Shimizu et al., 1997a]; 8 – Vitim province (Transbaikalia, Russia), garnet pyroxenites from basalts [Litasov, 1998]; 9 – pipe Roberts Victor (South Africa), eclogites from xenoliths in kimberlites of [Harte, Kirkley, 1997]; 10 – pipe Bobbejaan (South Africa), eclogites from xenoliths in kimberlites [Caporuscio, Smith, 1990]; 11 – Soazza metamorphic complex (Switzerland), eclogites [Boccio et al., 2000]; 12 – Ivrea Verbanio complex (Italy), garnet gabbros [Mazzucchelli et al., 1992]; 13 – volcanic complex (Japan), dacites [Schnetzler, Philpotts, 1970]; 14 – Broken Hill complex (Australia), skarn (garnetite) [Schwandt et al., 1993].

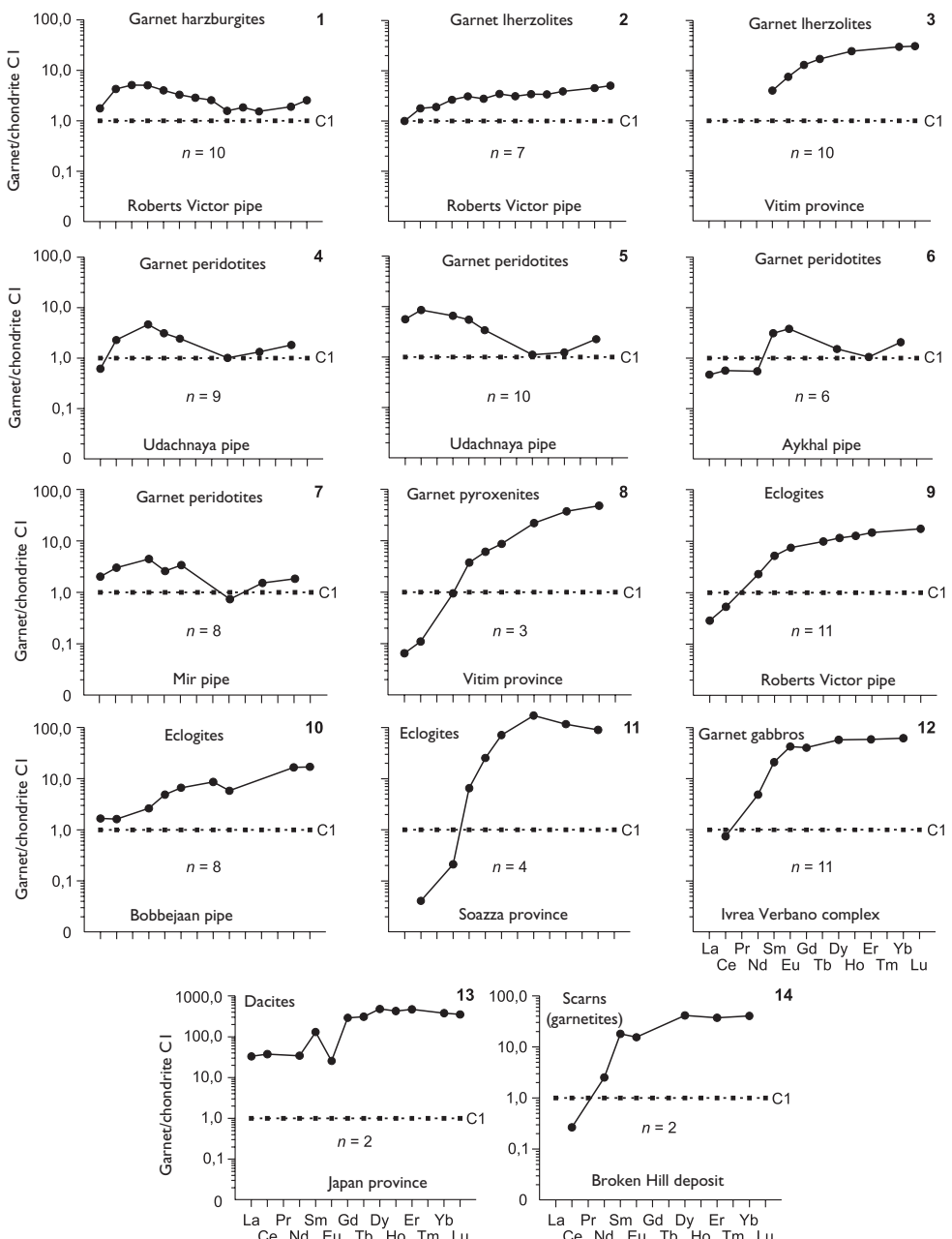


Figure 1.12 Chondrite-normalized REE patterns for average composition of garnets from some rock types (data Table 1.12).

found in the diamond fields from Liqhobong, Lesotho, Jagersfontein and Premier (South Africa) provinces [Nixon *et al.*, 1987; Hoal *et al.*, 1994; Shimizu *et al.*, 1994; Pearson *et al.*, 1998], in xenoliths of megacrystalline peridotites from Udachnaya, Mir, Aykhal pipes and others (Yakutia) [Pokhilenko *et al.*, 1993; Pearson *et al.*, 1993; Hoal *et al.*, 1994; Shimizu & Sobolev, 1995; Shimizu *et al.*, 1997a, b; Pearson & Milledge, 1998], in xenoliths of harzburgites and lherzolites from Roberts Victor pipe (South Africa) [Stachel *et al.*, 1998], in xenoliths of eclogites from Mbaji-Mayi deposit (Congo) [Demaiffe *et al.*, 1998], in xenocrysts of kimberlites from Camsell Lake (Canada) [Pokhilenko *et al.*, 1998]. As mentioned above, the sinusoidal REE patterns have been also ascertained in many garnets, which are micro-inclusions in diamond crystals. However, there are examples when sinusoidal patterns, which are typical for inner zones of garnet crystals from micro-inclusions in diamonds, moving towards the peripheral zones were replaced by those more common for garnet patterns of simple form with a steep positive slope [Shimizu *et al.*, 1997b]. Apart from sinusoidal shape of patterns in the garnets associating with diamonds, other kinds of anomalous patterns were found: in particular, arched up or with an almost flat shape in the range between Sm and Lu.

The nature of sinusoidal shape of the REE patterns of garnets is still a subject of debate. Originally it was assumed that the origin of such patterns in garnets was caused by metasomatic change of mantle substrate that preceded the formation of garnets and diamonds in peridotite parageneses [Shimizu, Richardson, 1987]. Later it was suggested that peridotites, containing garnets with a sinusoidal REE distribution, right after its formation have undergone a metasomatic recycling under the influence of deep-seated melts that were geochemically similar to carbonatite and that this process was a really time-consuming one [Pokhilenko *et al.*, 1993]. It is the proximity of the REE compositions of garnets from micro-inclusions in diamond crystals and their varieties, which are parts of peridotite xenoliths from Roberts Victor and Akwatiya pipes, that allowed to assume that the garnets from harzburgites and lherzolites, presented in the xenoliths, were formed from protolith, which had previously been depleted during partial melting in stability field of spinel [Stachel *et al.*, 1998]. There is also a hypothesis that subcalcium pyropes from deep-seated xenoliths were formed during the metasomatic transformation of spinel harzburgites in the stability field of diamond, and the process involved carbon-bearing fluids or melts [Jacob *et al.*, 1998]. It was also assumed that zoning in the distribution of REE and other impurities in subcalcium garnets, associating with diamonds, could be due to the continuous growth of grains on the background of the changes in PT-conditions of crystallization [Shimizu *et al.*, 1994]. It was taken into account that the inner zones of garnet grains, apparently, were originally crystallized under nonequilibrium conditions, which have been replaced by the equilibrium conditions till the moment of crystallization of the peripheral zones, and it was considered that the growth of zonal garnet crystals and associating diamonds occurred shortly before they got into the kimberlite matrix. According to Shimizu *et al.* [1997b], a similar mechanism of formation of garnet can explain the transformation from the sinusoidal patterns of REE distribution to ordinary patterns as we move from the inner zones of garnet crystals towards the peripheral.

Apparently, for a more accurate study of the proposed mechanisms of arising for sinusoidal patterns of REE distribution in garnets, associating with diamonds,

additional research is needed. However, it is already obvious that this multistage and different, by *PT*-parameters, history of garnet crystals growth was the most important reason that even within a single manifestation the garnet samples of identical petrographic composition of the mantle xenoliths often differ on the basis of the REE pattern configuration. The examples of such geochemical heterogeneity can be the garnets from diamondiferous Roberts Victor, Udachnaya, Aykhal and Mir kimberlite pipes. It is important to mention that the sinusoidal REE pattern, identified in the garnets containing more than 12 wt% Cr₂O₃ and having a higher content of knorringite mineral (more than 30%), are currently supposed to be the most important search criteria for assessing the potential diamond-bearing of kimberlite provinces [Pokhilenko *et al.*, 1998].

It is well known that on the periphery of garnet segregations presented in the form of xenocrystals in kimberlites those were often observed kelyphitic rims of complex structure, the formation of which is usually associated with exposure of kimberlite melts and fluids. Special studies showed that this kind of rims by their REE composition are close to the garnet crystals surrounded by them and differ significantly from their host kimberlites. These observations suggest that the formation of kelyphitic rims around the garnet crystals is not causally associated with exposure of the kimberlite melts which have passed them to the surface, but is caused by some earlier abyssal metasomatic processes [Spetsius & Griffin, 1998].

1.4 COEFFICIENTS OF REE DISTRIBUTION BETWEEN GARNETS AND COEXISTING MELTS

Researchers studying the geochemistry of garnets are constantly paying attention to the regularity of distribution of REE and other trace elements between this mineral and coexisting melts, and solid phases [Lesnov, 2001]. In order to obtain estimates of K_d(garnet/melt) there are usually both natural and experimental systems involving ultramafic, basaltic, andesitic, dacitic, rhyodacitic and rhyolitic melts used. To date, the biggest number of K_d estimates is obtained for Sm, Yb, Lu and Ce, very little data for Gd, Tb, Ho and almost no data for Pr and Tm (Table 1.13). The diagrams of change of K_d(garnet/melt) estimates are shown in Figure 1.13.

Among the first there were obtained the estimates of K_d(garnet/melt) upon the analysis of REE in garnet phenocrystals and containing them poorly crystallized matrix of dacites from volcanic complexes in Japan [Schnetzler & Philpotts, 1970]. In this case, the values of K_d(garnet/dacitic melt) for La, Ce and Nd range between 0,3 and 0,4, then, increasing for Sm, have a distinct minimum for Eu, after which the curve gets a steeper positive slope with increasing K_d values in the series from Gd (10.5) to Yb (26.0) and Lu (24.6) (Figure 1.13, 6). Over time, the results of experimental studies were mainly used to determine the values of K_d(garnet/melt) [Shimizu & Kushiro, 1975; Irving & Frey, 1978]. The effect of such parameters as the chemical composition of the garnets, the total REE content in the system, the silica content in the melts, as well as temperature and pressure during crystallization, is usually taken into account during these studies [Mysen, 1978; Beattie, 1993; Wim van Westrenen *et al.*, 1999]. The data obtained by these experiments confirmed earlier observations that indicated that the majority of the diagrams of K_d(garnet/melt) values have a steep

Table I.13 The coefficients of REE distribution between garnets and coexisting ultramafic, basaltic, hawaiitic, basanitic, andesitic, dacitic, rhyodacitic, and rhyolitic melts (experimental data).

Element	Ultramafic melt										[Ionue et al., 2000]				
	[Salters, Longhi, 1999]														
	M6943	M6946	M6954	M12952	O8952	O8953	O8951	O12953	O12951	BK7973	950608	950517	950613	SB2501	SB2778
La	N.d.	N.d.	N.d.	N.d.	N.d.	N.d.	N.d.	N.d.	N.d.	N.d.	0,080	0,020	0,020	0,050	0,030
Ce	0,018	0,013	0,015	0,049	0,012	0,037	0,012	0,016	0,015	0,014	N.d.	N.d.	N.d.	N.d.	N.d.
Nd	0,059	0,011	0,069	0,155	0,091	0,148	0,082	0,063	0,063	0,066	N.d.	N.d.	N.d.	N.d.	N.d.
Sm	0,220	0,318	0,286	0,520	0,337	0,490	0,290	0,232	0,232	0,237	0,080	0,060	0,130	0,050	0,040
Gd	N.d.	N.d.	N.d.	N.d.	N.d.	N.d.	N.d.	N.d.	N.d.	N.d.	0,390	0,160	0,230	0,120	0,030
Er	2,54	3,13	2,97	4,22	3,58	5,04	3,51	2,70	4,14	2,58	N.d.	N.d.	N.d.	N.d.	N.d.
Yb	4,02	5,17	4,55	6,07	6,07	8,47	6,07	4,75	7,03	5,06	2,36	1,77	1,73	0,800	0,320
Lu	5,01	6,44	5,76	11,2	7,68	9,46	7,60	5,65	8,45	6,82	N.d.	N.d.	N.d.	N.d.	N.d.
K _p (Yb)/ K _p (Ce)	223	398	303	124	506	229	506	297	469	361	N.d.	N.d.	N.d.	N.d.	N.d.

(Continued)

Table I.13 (Continued)

<i>Basaltic melt</i>															
	[Nicholls, Harris, 1980]										[Shimizu, 1975]	[Mysen, 1978]	[Harrison, 1981]	[Irving, Frey, 1978]	
Element	N-4883	N-4890	N-4934	N-4935	N-4863	N-4867	N-4869	N-4872	N-4861	SK-75	Mys-1	Mys-2	Harr-1	Harr-2	Kakan-1
Ce	N.d.	N.d.	N.d.	N.d.	N.d.	N.d.	N.d.	N.d.	N.d.	0,020	0,071	0,077	0,009	0,009	0,007
Nd	N.d.	N.d.	N.d.	N.d.	N.d.	N.d.	N.d.	N.d.	N.d.	0,090	N.d.	N.d.	N.d.	N.d.	0,026
Sm	N.d.	N.d.	1,00	N.d.	N.d.	0,700	N.d.	N.d.	N.d.	0,220	2,71	3,52	0,293	0,321	0,131
Eu	N.d.	N.d.	N.d.	N.d.	N.d.	N.d.	N.d.	N.d.	N.d.	0,320	N.d.	N.d.	N.d.	N.d.	0,187
Gd	N.d.	N.d.	N.d.	N.d.	N.d.	N.d.	N.d.	N.d.	N.d.	0,500	N.d.	N.d.	N.d.	N.d.	0,680
Dy	N.d.	N.d.	N.d.	N.d.	N.d.	N.d.	N.d.	N.d.	N.d.	1,10	N.d.	N.d.	N.d.	N.d.	1,94
Ho	N.d.	3,90	N.d.	N.d.	N.d.	N.d.	3,50	N.d.	3,300	N.d.	N.d.	N.d.	N.d.	N.d.	N.d.
Er	N.d.	N.d.	N.d.	N.d.	N.d.	N.d.	N.d.	N.d.	N.d.	2,00	N.d.	N.d.	N.d.	N.d.	4,70
Tm	N.d.	N.d.	N.d.	N.d.	N.d.	N.d.	N.d.	N.d.	N.d.	N.d.	9,55	9,55	1,27	1,31	N.d.
Yb	8,70	N.d.	N.d.	8,00	5,90	N.d.	N.d.	5,60	N.d.	N.d.	N.d.	N.d.	N.d.	N.d.	8,00
K _p (Yb)/ K _p (Ce)	N.d.	N.d.	N.d.	N.d.	N.d.	N.d.	N.d.	N.d.	N.d.	N.d.	N.d.	N.d.	N.d.	N.d.	1443

(Continued)

Table 1.13 (Continued).

Element	Basaltic melt						Hawaiitic melt	Basanitic melt	Andesitic melt						
	[Johnson, 1998]			[Cox, 1982]	[Shimizu, 1980]	[Hauri et al., 1994]	[Shimizu, 1980]	Binge Point, Austral.	Dutsen Dushawo Nigeria						
	Joh-I	Cox-I	EH3033	EH3036	I430°	EH3054	BBP-5	DD-2	N-4082	N-4079	N-4083	N-4091	N-4253	N-4252	N-4513
La	0,002	N.d.	0,236	0,188	0,0164	0,121	0,026	0,001	N.d.	N.d.	N.d.	N.d.	N.d.	N.d.	N.d.
Ce	0,005	0,020	0,223	0,193	0,065	0,144	0,051	N.d.	N.d.	N.d.	N.d.	N.d.	N.d.	N.d.	N.d.
Nd	0,052	N.d.	0,286	0,257	0,363	0,232	N.d.	N.d.	N.d.	N.d.	N.d.	N.d.	N.d.	N.d.	N.d.
Sm	0,250	0,220	0,635	0,566	1,100	0,541	0,600	0,101	2,00	1,70	1,10	1,00	0,700	1,00	1,30
Eu	0,400	0,320	0,845	0,719	2,02	0,623	1,000	0,185	N.d.	N.d.	N.d.	N.d.	N.d.	N.d.	N.d.
Gd	N.d.	N.d.	1,43	1,27	N.d.	1,190	2,10	N.d.	N.d.	N.d.	N.d.	N.d.	N.d.	N.d.	N.d.
Tb	N.d.	N.d.	N.d.	N.d.	N.d.	N.d.	4,10	0,540	N.d.	N.d.	N.d.	N.d.	N.d.	N.d.	N.d.
Dy	2,200	N.d.	3,23	2,89	4,13	2,56	N.d.	N.d.	25,0	16,6	13,4	13,9	9,50	N.d.	N.d.
Ho	N.d.	N.d.	N.d.	N.d.	N.d.	N.d.	13,2	2,11	N.d.	N.d.	N.d.	N.d.	N.d.	N.d.	N.d.
Er	3,60	N.d.	5,21	5,30	3,95	4,24	N.d.	N.d.	N.d.	N.d.	N.d.	N.d.	N.d.	N.d.	N.d.
Yb	6,60	4,00	6,48	7,90	3,88	5,73	35,6	6,40	44,6	34,9	37,6	37,0	23,0	20,0	N.d.
Lu	7,10	N.d.	6,64	8,53	3,79	6,30	41,0	8,50	N.d.	N.d.	N.d.	N.d.	N.d.	N.d.	N.d.
K _p (Yb)/ K _p (Ce)	1320	200	29,1	40,9	59,7	39,8	698	N.d.	N.d.	N.d.	N.d.	N.d.	N.d.	N.d.	N.d.

(Continued)

Table I.13 (Continued).

Element	Andesitic melt							Dacitic melt		Rhyodacitic	Rhyolitic melt	
								Mt. Nijo, Japan	Tumut	Black Spur, Australia	Mt. Koburn, USA	
	[Nicholls, Harris, 1980]									[Irving, Frey, 1978]		
Element	N-5292	N-5301	N-5322	N-4697	N-4693	N-4694	N-4192	MN-7	GSFC2	T-8	BS-9	CM-10
La	N.d.	N.d.	N.d.	N.d.	N.d.	N.d.	N.d.	0,370	N.d.	0,370	0,278	0,540
Ce	N.d.	N.d.	N.d.	N.d.	N.d.	N.d.	N.d.	0,530	0,348	0,510	0,790	0,930
Nd	N.d.	N.d.	N.d.	N.d.	N.d.	N.d.	N.d.	0,810	0,525	N.d.	0,270	0730
Sm	1,30	0,900	0,600	0,800	N.d.	N.d.	0,600	5,50	2,66	0,760	0,840	1,04
Eu	N.d.	N.d.	N.d.	N.d.	N.d.	N.d.	N.d.	1,37	1,50	0,214	0,167	0,310
Gd	N.d.	N.d.	N.d.	N.d.	N.d.	N.d.	N.d.	13,6	10,5	5,30	5,30	3,70
Tb	N.d.	N.d.	N.d.	N.d.	N.d.	N.d.	N.d.	19,6	N.d.	8,90	11,9	7,20
Dy	N.d.	N.d.	N.d.	N.d.	N.d.	N.d.	N.d.	N.d.	28,6	N.d.	N.d.	N.d.
Ho	N.d.	N.d.	N.d.	N.d.	5,500	N.d.	N.d.	31,1	N.d.	18,4	34,5	28,2
Er	N.d.	N.d.	N.d.	N.d.	N.d.	N.d.	N.d.	N.d.	42,8	N.d.	N.d.	N.d.
Tm	N.d.	N.d.	N.d.	N.d.	N.d.	N.d.	N.d.	N.d.	N.d.	N.d.	N.d.	N.d.
Yb	N.d.	N.d.	10,6	N.d.	N.d.	10,0	11,7	26,0	39,9	26,0	67,0	54,0
Lu	N.d.	N.d.	N.d.	N.d.	N.d.	N.d.	N.d.	23,5	29,6	24,6	64,0	47,0
K _p (Yb)/ K _p (Ce)	N.d.	N.d.	N.d.	N.d.	N.d.	N.d.	N.d.	49,0	115	51,0	84,8	58,1

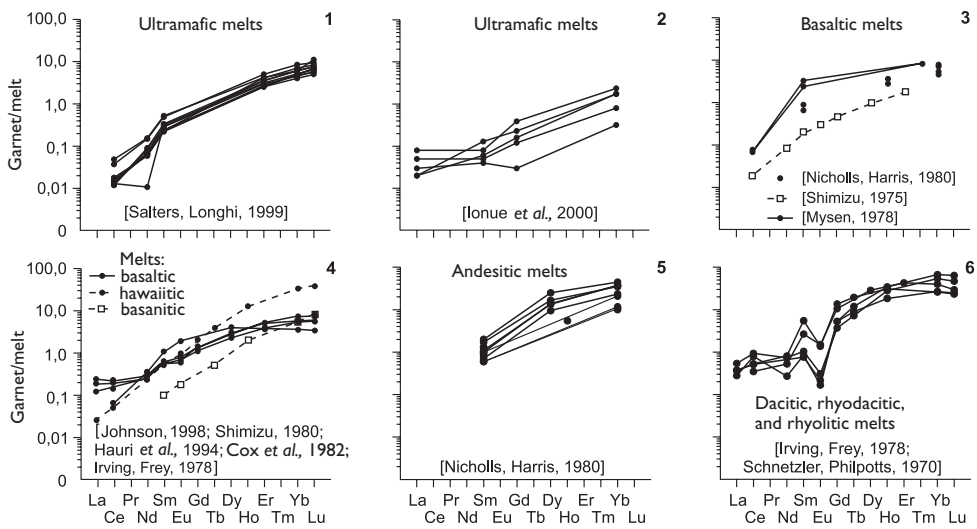


Figure 1.13 The graphs of coefficients of REE distribution between garnets and melts (experimental data) (data Table I.13).

positive slope, but sometimes they are complicated by anomalies for several elements. There was also a trend found in increasing of K_d values for all REE while changing of the chemical composition of melts from high-Mg ultramafic to basaltic and high-Si, and this tendency is more significant for K_d values for HREE. The function of values of K_d on the temperature and pressure of crystallization of the mineral was studied in the experiments in garnet-ultramafic melt system [Salters & Longhi, 1999; Inoue et al., 2000]. In particular, it was shown that with decreasing pressure in the range of 20–5.5 GPa the values of K_d (garnet/ultramafic melt) vary in the following ranges: La (0.03–0.08); Sm (0.04–0.208); Gd (0.03–0.39); Yb (0.32–2.36). In another experiment it was determined that during the crystallization of garnet at 1420°C the value of K_d (garnet/andesitic melt) for Yb is 12, and at a temperature of 940°C – about 44 [Nicholls & Harris, 1980]. Moreover, according to the results of these experiments, in almost all the cases the values of K_d (garnet/melt) for the LREE are less than 1, while for the elements from Sm to Lu, they are usually >1 .

Judging by the shape and slope of diagrams of change in the values of K_d (garnet/melt) for the ultramafic and mafic melts, these values are close to a straight and inverse logarithmic function on the ionic radii of the REE. In contrast to the diagrams of changes of K_d (garnet/melt) for the ultramafic and mafic melts, such graphics for high-Si melts are usually complicated by the minimum for Eu. In this case, the available data give grounds to conclude that during the crystallization of garnet from a melt of any composition their residual fractions have been intensively depleted by HREE and, conversely, enriched with LREE. Based on the fact that K_d (garnet/melt) for the heavy REE with smaller ionic radii tend to have values >1 , and for light elements with large ionic radii – <1 , it can be assumed that LREE in the garnet structure represented incompatible elements, and the heavy REE possessed the properties of fully compatible trace elements [Blundy et al., 1998].

The $K_d(Yb)/K_d(Ce)$ parameter values, calculated from the experimental studies on the distribution of REE between coexisting garnets and melts of different composition, describing the fractionation intensity of these impurities during the crystallization of garnet, vary within very wide limits (Table 1.13). Thus, for ultramafic melts the range of variation of this parameter is 120–500, for basaltic melts it is much wider – 30–1320, and for melts of dacite, rhyodacite and rhyolite composition, by contrast, it is much narrower – 25–64.

Available data on $K_d(\text{garnet}/\text{melt})$ values are often used in solving inverse problems, i.e. determining the REE compositions of model parental melts, from which garnets were crystallized. Similar calculations were performed using the average REE compositions of garnets from the ultramafic xenoliths from Roberts Victor, Udachnaya, Aykhal and Mir kimberlite pipes, and have shown that the REE compositions of the model parental melts for ultramafites of these xenoliths were very similar, both by the overall level of REE accumulation and by the relations between individual elements; the greatest similarity is observed for the contents of Sm (Figure 1.14, a, b). Assuming that the calculated model REE composition is close enough to the real one, we can conclude that the REE in these melts were rapidly fractionated. Level of accumulation of elements in them repeatedly decreased from La (30–100 t.ch.) to Lu (0.02–0.2 t.ch.). Such calculations of REE distribution in the model melts, which are crystallized into garnets presented in ultramafic xenoliths from basalts of Vitim province, suggest that the REE in the parental melt of these ultramafites were relatively low fractionated (Figure 1.14, b, 2). Unlike all the previous ones, REE compositions of model melts for the garnets from eclogites presented in the xenoliths from kimberlites of Bobbejaan pipe, in gabbros from Ivrea Verbano complex, as well as from basanites of Dutsen Dushowo, are characterized by a certain Eu excess (Figure 1.14 c).

Let us emphasize once again that the estimates of REE distribution coefficients between garnets and coexisting melts of different composition are an important geochemical characteristic of both the garnet and those of magmatic systems, in which

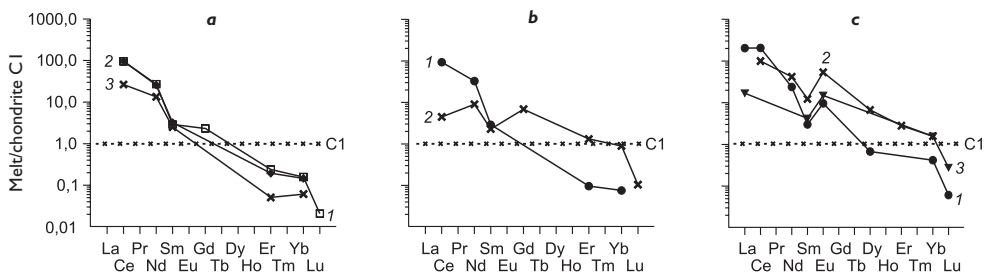


Figure 1.14 Chondrite-normalized REE patterns for model melts from which presumably crystallized garnets, presented in various types of ultramafic and mafic rocks. *a* – ultramafic rocks from xenoliths in kimberlite pipes: (1) Roberts Victor ($n = 23$), (2) Udachnaya ($n = 50$) and (3) Aykhal ($n = 8$); *b* – (1) ultramafic rocks from xenoliths in Mir kimberlite pipe ($n = 25$), (2) ultramafic rocks from xenoliths in alkaline basalts of Vitim province ($n = 18$); *c* – (1) eclogites from xenoliths in Bobbejaan kimberlite pipe ($n = 8$); (2) gabbros from Ivrea Verbano complex ($n = 15$), (3) phenocrysts from basanites of Dutsen Dushowo complex ($n = 1$). In the calculations were used the average values of $K_d(\text{garnet}/\text{ultramafic melt})$, as well as $K_d(\text{garnet}/\text{basaltic melt})$ "Kakan-I" (see Table 1.13).

they crystallized. As shown, the values of K_d (garnet/melt) for all REE and for parental melts of different compositions are consistently increasing from light to heavy elements, thus, their graphs tend to have a positive slope. It was also found that the values of K_d (garnet/melt) for all REE increase from ultramafic to basaltic, andesite, dacite and rhyolite melts. At the same time, the values of K_d of REE increase with decreasing temperature and pressure of the crystallization of mineral. Considering the fact that the values of K_d (garnet/melt) for LREE are usually less than 1, while for medium and especially heavy elements they are always barely greater than 1, we can assume that, unlike the incompatible LREE, medium and heavy elements found in garnet structure had properties of quite compatible trace elements. In the graphs of change of K_d (garnet/melt) for melts with high SiO_2 content of, Eu minimums are commonly observed, contrasting to its absence on graphs of ultramafic and mafic melts. Model parental melts for garnets from ultramafic xenoliths of Roberts Victor, Udachnaya, Aykhal and Mir kimberlite pipes are similar in many respects, both by the content of REE and by the nature of their distribution.

1.5 COEFFICIENTS OF REE DISTRIBUTION BETWEEN GARNETS AND COEXISTING CLINOPYROXENES AND OTHER MINERALS

Since parageneses of garnets and clinopyroxenes is widely represented in the rocks of different composition and genesis, the data on the REE distribution coefficients between these coexisting minerals is also of great interest. Estimates of K_d (garnet/clinopyroxene) reveal some important trends in the behavior of trace elements during crystallization of these minerals from melts, including the involvement of fluids. Representative estimates of K_d (garnet/clinopyroxene) for clinopyroxene-bearing harzburgites, lherzolites and eclogites, as well as for some other garnet-bearing rocks are systematized in Table 1.14. You can see that the largest amount of data was obtained for peridotites from xenoliths from Udachnaya-Vostochnaya kimberlite pipe, as well as for eclogites from xenoliths of Roberts Victor and Bobbejaan pipes, while for the peridotites, lherzolites, clinopyroxenites and eclogites from other manifestations there are only single estimates of K_d values. Due to the fact that the garnets almost always accumulate in its structure mainly HREE, while clinopyroxenes – medium and light elements, the values of K_d (garnet/clinopyroxene) for LREE in most cases do not exceed 1, for medium elements they are close to 1, and for heavy REE are almost always greater than 1, only in some cases reaching 50–100.

Parageneses of garnets and clinopyroxenes from xenoliths of Udachnaya-Vostochnaya and Roberts Victor pipes is characterized by approximately the same ranging of K_d (garnet/clinopyroxene) for most REE, excluding the values for La and Ce from eclogites of Roberts Victor pipe (Figure 1.15, 11, 12), as well as from several other pipes. Graphs of change of K_d for a significant part of these samples are close to each other and have a similar configuration. Many of them are positively inclined and almost straight lines, which reflect the inverse relationship between the logarithms of the values of K_d (garnet/clinopyroxene) and ionic radii of REE. A significant part of parageneses of these minerals in peridotites has a less steep slope of these lines. Accordingly, the value of the $K_d(\text{Yb})/K_d(\text{Ce})$ parameters in them is about 100 or

Table I.14 The coefficients of REE distribution between coexisting garnets and clinopyroxenes from different provinces and parageneses.

Udachnaya-Vostochnaya pipe (Yakutia, Russia)										
	[Shimizu et al., 1997a]									
	52/76	80/92	239/89	51/82	74/89	424/89	121/91	246/89	76/92	70/92
<i>Element</i>	<i>Garnet peridotites</i>									
La	0,077	0,069	0,094	0,029	0,036	0,077	0,047	0,011	0,174	0,074
Ce	N.d.	0,153	0,237	0,072	0,070	0,189	0,125	0,049	0,493	0,186
Pr	N.d.	N.d.	N.d.	N.d.	N.d.	N.d.	N.d.	N.d.	N.d.	N.d.
Nd	0,889	0,433	0,770	0,309	0,308	0,629	0,238	0,078	2,46	0,486
Sm	2,15	1,34	2,41	0,625	0,518	1,80	0,272	0,146	1,12	0,411
Eu	3,03	1,89	3,81	0,883	1,08	2,25	0,257	0,135	3,29	0,404
Gd	N.d.	N.d.	N.d.	N.d.	N.d.	N.d.	N.d.	N.d.	N.d.	N.d.
Tb	N.d.	N.d.	N.d.	N.d.	N.d.	N.d.	N.d.	N.d.	N.d.	N.d.
Dy	4,08	5,26	4,61	3,79	3,24	5,95	0,359	0,275	0,662	0,529
Ho	N.d.	N.d.	N.d.	N.d.	N.d.	N.d.	N.d.	N.d.	N.d.	N.d.
Er	3,00	8,97	6,70	5,01	5,16	8,83	0,583	1,66	1,96	0,810
Tm	N.d.	N.d.	N.d.	N.d.	N.d.	N.d.	N.d.	N.d.	N.d.	N.d.
Yb	5,70	7,52	9,69	8,98	5,10	9,14	1,48	2,59	6,36	1,35
Lu	N.d.	N.d.	N.d.	N.d.	N.d.	N.d.	N.d.	N.d.	N.d.	N.d.
Kd(Yb)/ Kd(Ce)	N.d.	49,05	40,88	124	72,9	48,3	11,8	52,8	12,9	7,26

(Continued)

Table 1.14 (Continued)

										Thaba Putsoa Province
	Udachnaya-Vostochnaya pipe (Yakutia, Russia)									[Shimizu et al., 1997a]
	267/89	228/89	115/89	107/89	61/91	417/89	100/91	25/91	306/89	[Shimizu, 1975]
Element	Garnet peridotites									Lherzolite
La	0,045	0,037	0,028	0,181	0,091	0,009	8,33	0,004	0,057	N.d.
Ce	0,068	0,090	0,082	0,343	0,187	0,008	2,09	0,017	1,23	0,144
Pr	N.d.	N.d.	N.d.	N.d.	N.d.	N.d.	N.d.	N.d.	N.d.	N.d.
Nd	0,218	0,244	0,340	1,03	0,311	0,053	3,79	0,181	1,577	0,380
Sm	0,609	0,476	0,921	3,26	0,503	0,312	N.d.	0,748	1,41	1,03
Eu	1,02	0,685	0,849	3,86	0,626	0,537	1,32	0,863	0,892	1,43
Gd	N.d.	N.d.	N.d.	N.d.	N.d.	N.d.	N.d.	N.d.	N.d.	2,11
Tb	N.d.	N.d.	N.d.	N.d.	N.d.	N.d.	N.d.	N.d.	N.d.	N.d.
Dy	2,40	1,66	1,53	7,83	1,56	3,37	3,12	2,73	3,85	4,78
Ho	N.d.	N.d.	N.d.	N.d.	N.d.	N.d.	N.d.	N.d.	N.d.	N.d.
Er	3,76	1,99	2,50	6,59	3,06	6,48	4,98	5,41	2,73	9,52
Tm	N.d.	N.d.	N.d.	N.d.	N.d.	N.d.	N.d.	N.d.	N.d.	N.d.
Yb	7,55	2,58	4,35	15,5	3,75	9,23	19,2	14,9	6,10	15,9
Lu	N.d.	N.d.	N.d.	N.d.	N.d.	N.d.	N.d.	N.d.	N.d.	N.d.
Kd(Yb)/ Kd(Ce)	1121	28,5	53,2	44,6	20,0	1204	9,2	853	5,0	111

(Continued)

Table 1.14 (Continued).

	<i>Thaba</i> <i>Putsoa</i> province	<i>Bultfontein</i> pipe	<i>Motha</i> province	<i>Liqhobong</i> province	<i>Vitim province (Russia)</i>					
	[Shimizu, 1975]					[Ionov et al., 1993]				
	1925	G352	BUL 6	1566	2302	313-1	313-3	313-4	313-5	313-6
<i>Element</i>										
La	N.d.	N.d.	N.d.	N.d.	N.d.	N.d.	N.d.	N.d.	N.d.	N.d.
Ce	N.d.	0,041	0,045	0,256	0,158	N.d.	N.d.	N.d.	N.d.	N.d.
Pr	N.d.	N.d.	N.d.	N.d.	N.d.	N.d.	N.d.	N.d.	N.d.	N.d.
Nd	0,215	N.d.	N.d.	0,525	0,236	N.d.	N.d.	N.d.	N.d.	N.d.
Sm	0,604	0,182	0,139	1,31	0,524	0,373	0,340	0,326	0,324	0,325
Eu	0,906	0,703	0,295	1,71	0,784	0,721	0,743	N.d.	0,689	N.d.
Gd	1,25	N.d.	N.d.	2,33	1,29	N.d.	N.d.	N.d.	N.d.	N.d.
Tb	N.d.	1,21	0,573	N.d.	N.d.	2,73	2,25	2,44	2,19	2,37
Dy	3,59	2,20	0,926	4,76	2,61	N.d.	N.d.	N.d.	N.d.	N.d.
Ho	N.d.	N.d.	N.d.	N.d.	N.d.	N.d.	N.d.	N.d.	N.d.	N.d.
Er	6,47	3,20	2,44	8,44	4,96	N.d.	N.d.	N.d.	N.d.	N.d.
Tm	N.d.	N.d.	N.d.	N.d.	N.d.	N.d.	N.d.	N.d.	N.d.	N.d.
Yb	12,6	N.d.	N.d.	11,6	15,0	N.d.	N.d.	28,7	26,3	N.d.
Lu	N.d.	N.d.	N.d.	N.d.	N.d.	N.d.	N.d.	34,6	28,5	9,63
Kd(Yb)/ Kd(Ce)	N.d.	7,6	6,0	45,3	94,9	N.d.	N.d.	N.d.	N.d.	N.d.

(Continued)

Table 1.14 (Continued).

Vitim province (Russia)					Wesselton province (South Africa)					
	[Ionov et al., 1993]				[Van Achterbergh et al., 1998]					
Element	313-8	313-37	313-54	313-113G	314-580	959	960	965	966	968
<i>Garnet lherzolites</i>					<i>Garnet peridotites</i>					
La	N.d.	N.d.	N.d.	N.d.	N.d.	0,008	0,007	0,003	0,022	0,013
Ce	N.d.	N.d.	N.d.	N.d.	N.d.	0,009	0,008	0,006	0,034	0,030
Pr	N.d.	N.d.	N.d.	N.d.	N.d.	0,032	0,016	0,022	0,078	0,081
Nd	N.d.	N.d.	N.d.	N.d.	N.d.	0,064	0,052	0,047	0,191	0,172
Sm	0,330	0,371	0,362	0,361	0,409	0,344	0,319	0,273	0,832	0,722
Eu	0,733	1,04	0,693	0,759	0,750	0,486	0,643	0,597	1,000	0,955
Gd	N.d.	N.d.	N.d.	1,67	0,99	1,01	0,952	1,39	1,42	1,63
Tb	2,14	2,19	2,21	2,47	1,94	N.d.	N.d.	N.d.	N.d.	N.d.
Dy	N.d.	N.d.	N.d.	N.d.	N.d.	3,51	4,21	6,11	4,57	2,48
Ho	N.d.	N.d.	N.d.	N.d.	N.d.	6,50	6,72	10,2	N.d.	1,16
Er	N.d.	N.d.	N.d.	N.d.	N.d.	6,70	8,56	14,5	N.d.	1,71
Tm	N.d.	N.d.	N.d.	N.d.	N.d.	N.d.	N.d.	N.d.	N.d.	N.d.
Yb	29,7	N.d.	21,2	N.d.	N.d.	N.d.	9,80	N.d.	N.d.	N.d.
Lu	N.d.	45,4	15,0	71,0	6,85	3,47	4,87	N.d.	N.d.	3,33
Kd(Yb)/ Kd(Ce)	N.d.	N.d.	N.d.	N.d.	N.d.	N.d.	1225	N.d.	N.d.	N.d.

(Continued)

Table I.14 (Continued).

Massifs				Roberts Victor pipe (South Africa)						
Beni Bousera (Morocco)		Lherz (Italy)	Freychinene (France)							
[Pearson, 1993]		[Bodinier et al., 1987]			[Caporuscio, Smith, 1990]		[Philpotts et al., 1972]			
	GP87	GP147		70-291	70-385	70-357	SRV-4	XM-37		
<i>Garnet clinopyroxenites</i>					<i>Eclogites</i>					
La	0,042	0,733	0,620	N.d.	0,500	0,040	0,113	N.d.	N.d.	N.d.
Ce	0,028	0,153	0,333	N.d.	0,444	0,153	0,318	0,340	0,214	0,078
Pr	N.d.	N.d.	N.d.	N.d.	N.d.	N.d.	N.d.	N.d.	N.d.	N.d.
Nd	0,111	0,124	N.d.	N.d.	N.d.	0,536	1,268	0,258	0,261	0,169
Sm	0,613	0,537	0,481	0,190	0,306	2,07	4,49	0,652	0,782	0,474
Eu	1,16	0,881	N.d.	0,387	0,706	4,04	7,29	1,03	1,31	0,863
Gd	1,80	1,23	N.d.	N.d.	N.d.	N.d.	N.d.	1,82	2,07	1,47
Tb	N.d.	N.d.	4,65	0,740	1,81	10,8	18,1	N.d.	N.d.	N.d.
Dy	N.d.	N.d.	N.d.	N.d.	N.d.	2,42	15,9	5,69	5,75	4,97
Ho	N.d.	N.d.	N.d.	N.d.	N.d.	N.d.	N.d.	N.d.	N.d.	N.d.
Er	20,8	12,3	N.d.	N.d.	N.d.	N.d.	N.d.	13,4	12,6	10,6
Tm	N.d.	N.d.	N.d.	N.d.	N.d.	N.d.	N.d.	N.d.	N.d.	N.d.
Yb	50,0	17,6	38,4	2,59	25,1	86,3	80,0	29,0	21,4	21,1
Lu	N.d.	N.d.	77,5	2,95	32,4	66,8	147	29,7	26,7	27,3
Kd(Yb)/ Kd(Ce)	1808	115	115	N.d.	56,4	564	252	85,4	99,7	271

(Continued)

Table I.14 (Continued).

<i>Roberts Victor pipe (South Africa)</i>										
	<i>[Harte, Kirkley, 1997]</i>									
	145	247	173	110	30-7	312	243	177-5	177-4	30-1
<i>Element</i>	<i>Eclogites</i>									
La	0,003	0,016	0,007	0,007	0,318	N.d.	0,004	0,016	0,217	0,466
Ce	0,006	0,053	0,013	0,015	0,238	N.d.	0,011	0,033	0,155	0,265
Pr	N.d.	N.d.	N.d.	N.d.	N.d.	N.d.	N.d.	N.d.	N.d.	N.d.
Nd	0,057	0,272	0,093	0,047	0,587	0,026	0,064	0,141	0,222	0,431
Sm	0,275	1,21	0,346	0,317	1,961	0,172	0,247	0,568	0,634	1,36
Eu	0,557	1,93	0,697	0,550	3,00	0,311	0,436	1,00	1,13	2,29
Gd	N.d.	N.d.	N.d.	N.d.	N.d.	N.d.	N.d.	N.d.	N.d.	N.d.
Tb	1,176	6,80	2,10	1,27	7,33	1,26	1,47	2,36	2,92	6,00
Dy	1,78	11,1	3,24	2,60	13,5	2,17	2,96	4,56	4,80	12,0
Ho	2,89	12,0	6,13	3,75	23,7	3,96	6,22	7,44	9,00	15,3
Er	3,46	15,3	8,86	5,94	29,4	6,97	12,1	11,5	13,6	18,6
Tm	N.d.	N.d.	N.d.	N.d.	N.d.	N.d.	N.d.	N.d.	N.d.	N.d.
Yb	N.d.	N.d.	N.d.	N.d.	N.d.	N.d.	N.d.	N.d.	N.d.	N.d.
Lu	2,20	13,0	14,7	15,0	17,5	18,7	22,5	24,0	27,0	29,0
Kd(Yb)/ Kd(Ce)	N.d.	N.d.	N.d.	N.d.	N.d.	N.d.	N.d.	N.d.	N.d.	N.d.

(Continued)

Table I.14 (Continued).

	Roberts Victor pipe (South Africa)									
	[Harte, Kirkley, 1997]									
	30-6	244	67	4	G6	175	RV-6	277	313	98
Element	Eclogites									
La	0,077	1,000	0,500	0,024	0,500	2,000	0,009	0,885	0,040	0,008
Ce	0,095	0,200	0,500	0,027	1,00	0,667	0,032	2,22	0,094	0,013
Pr	N.d.	N.d.	N.d.	N.d.	N.d.	N.d.	N.d.	N.d.	N.d.	N.d.
Nd	0,405	0,304	0,667	0,140	1,08	0,800	0,127	8,60	0,451	0,108
Sm	1,72	0,824	2,22	0,447	2,73	2,13	0,583	21,8	1,82	0,381
Eu	3,00	1,38	2,83	0,839	4,43	3,89	0,771	47,7	3,14	0,556
Gd	N.d.	N.d.	N.d.	N.d.	N.d.	N.d.	N.d.	N.d.	N.d.	N.d.
Tb	8,25	5,80	19,0	2,23	14,5	14,2	2,93	N.d.	11,0	0,563
Dy	12,9	7,63	20,8	4,19	22,4	22,0	5,34	149	13,4	0,814
Ho	20,0	10,8	23,0	7,46	31,4	38,9	9,40	N.d.	40,0	2,50
Er	29,7	14,9	53,3	11,4	52,5	62,1	17,5	80,0	30,5	2,12
Tm	N.d.	N.d.	N.d.	N.d.	N.d.	N.d.	N.d.	N.d.	N.d.	N.d.
Yb	N.d.	N.d.	N.d.	N.d.	N.d.	N.d.	N.d.	N.d.	N.d.	N.d.
Lu	29,0	33,0	33,0	39,5	40,7	84,3	86,7	N.d.	N.d.	N.d.
Kd(Yb)/ Kd(Ce)	N.d.	N.d.	N.d.	N.d.	N.d.	N.d.	N.d.	N.d.	N.d.	N.d.

(Continued)

Table I.14 (Continued).

Kakanui volcano		<i>Bobbejaan pipe (South Africa)</i>								
[Philpotts et al., 1972]		[Caporuscio, Smith, 1990]								
	21	SBB-2H	SBB-3H	SBB-7P	SBB-25	SBB-34	SBB-37	SBB-39	SBB-61	RV-1
Element	Eclogites									
La	N.d.	0,268	0,032	0,072	0,273	0,222	0,041	0,073	0,469	0,683
Ce	0,03	0,424	0,055	0,078	0,202	0,171	0,024	0,088	0,314	1,34
Pr	N.d.	N.d.	N.d.	N.d.	N.d.	N.d.	N.d.	N.d.	N.d.	N.d.
Nd	0,10	0,679	0,274	0,262	0,129	0,082	0,036	0,084	0,436	4,26
Sm	0,41	4,07	0,471	0,451	0,475	0,401	0,170	0,444	1,78	15,9
Eu	0,74	4,93	0,888	0,883	0,715	0,721	0,317	0,714	3,05	18,0
Gd	1,22	N.d.	N.d.	N.d.	N.d.	N.d.	N.d.	N.d.	N.d.	N.d.
Tb	N.d.	3,46	1,25	2,60	2,68	2,18	1,14	2,99	6,99	25,2
Dy	4,05	4,34	0,290	0,563	2,13	2,95	1,10	0,334	3,75	3,62
Ho	N.d.	N.d.	N.d.	N.d.	N.d.	N.d.	N.d.	N.d.	N.d.	N.d.
Er	90,3	N.d.	N.d.	N.d.	N.d.	N.d.	N.d.	N.d.	N.d.	N.d.
Tm	N.d.	N.d.	N.d.	N.d.	N.d.	N.d.	N.d.	N.d.	N.d.	N.d.
Yb	14,7	29,0	29,5	23,5	19,4	18,8	18,3	20,2	57,2	59,6
Lu	N.d.	23,7	39,0	21,3	27,2	23,7	29,1	27,4	47,8	34,3
Kd(Yb)/ Kd(Ce)	480	68,4	536	302	95,8	110	762	230	182	44,5

(Continued)

Table 1.14 (Continued).

Element	Soazza province (Switzerland) [Bocchio et al., 2000]			Atbashi complex (Kyrgyzstan) [data F. Lesnov]				Ivrea Verbania complex (Italy) [Mazzucchelli et al., 1992]		
	M-12	M-6	M-48	AT2-5	AT4-5	AT2-7	AT4-7	MP1c	MP1r	MP3
<i>Eclogites</i>		<i>Garnet gabbros</i>								
La	N.d.	N.d.	N.d.	0,793	1,018	0,778	0,998	N.d.	N.d.	N.d.
Ce	0,015	0,029	0,091	0,779	0,975	0,775	0,970	0,013	0,057	0,024
Pr	N.d.	N.d.	N.d.	0,777	1,00	0,749	0,967	N.d.	N.d.	N.d.
Nd	0,128	0,081	0,417	0,777	1,024	0,740	0,975	0,042	0,075	0,063
Sm	1,12	0,825	1,94	0,775	1,05	0,684	0,928	0,345	0,286	0,357
Eu	2,59	4,12	5,59	0,848	1,17	0,644	0,885	0,667	0,417	0,769
Gd	5,00	15,4	15,2	0,964	1,249	0,802	1,04	N.d.	N.d.	N.d.
Tb	N.d.	N.d.	N.d.	2,06	2,04	1,753	1,731	N.d.	N.d.	N.d.
Dy	27,0	200	111	4,19	4,15	4,20	4,17	1,00	1,67	5,00
Ho	N.d.	N.d.	N.d.	6,35	6,68	7,60	7,99	N.d.	N.d.	N.d.
Er	76,9	333	143	7,91	9,35	9,35	11,1	1,14	3,70	16,7
Tm	N.d.	N.d.	N.d.	7,79	9,78	10,5	13,1	N.d.	N.d.	N.d.
Yb	125	200	111	7,91	10,0	10,5	13,3	1,43	5,00	33,3
Lu	N.d.	N.d.	N.d.	8,25	10,3	10,9	13,5	N.d.	N.d.	N.d.
Kd(Yb)/ Kd(Ce)	8389	6803	1222	10,2	10,3	13,5	13,7	107	88,5	1372

(Continued)

Table I.14 (Continued).

<i>Ivrea Verbania complex (Italy)</i>								
	[Mazzucchelli et al., 1992]							
	MP5	MO95	MP6	MP9	MZ145	MP12	MP13	MP18
<i>Element</i>	<i>Garnet gabbros</i>							
La	N.d.	N.d.	N.d.	N.d.	N.d.	N.d.	N.d.	N.d.
Ce	0,017	0,036	0,011	0,014	0,006	0,009	0,003	0,003
Pr	N.d.	N.d.	N.d.	N.d.	N.d.	N.d.	N.d.	N.d.
Nd	0,047	0,072	0,091	0,122	0,125	0,058	0,061	0,048
Sm	0,250	0,357	0,625	0,556	1,00	0,412	0,412	0,333
Eu	0,526	0,714	0,769	0,909	1,00	0,833	0,833	0,667
Gd	N.d.	N.d.	N.d.	N.d.	N.d.	N.d.	N.d.	N.d.
Tb	N.d.	N.d.	N.d.	N.d.	N.d.	N.d.	N.d.	N.d.
Dy	5,00	5,00	10,0	10,0	10,0	5,00	10,0	10,0
Ho	N.d.	N.d.	N.d.	N.d.	N.d.	N.d.	N.d.	N.d.
Er	14,3	7,69	25,0	16,7	33,3	16,7	25,0	20,0
Tm	N.d.	N.d.	N.d.	N.d.	N.d.	N.d.	N.d.	N.d.
Yb	50,0	9,09	50,0	25,0	100	50,0	50,0	50,0
Lu	N.d.	N.d.	N.d.	N.d.	N.d.	N.d.	N.d.	N.d.
Kd(Yb)/ Kd(Ce)	2890	254	4386	1838	15625	5882	19231	16667

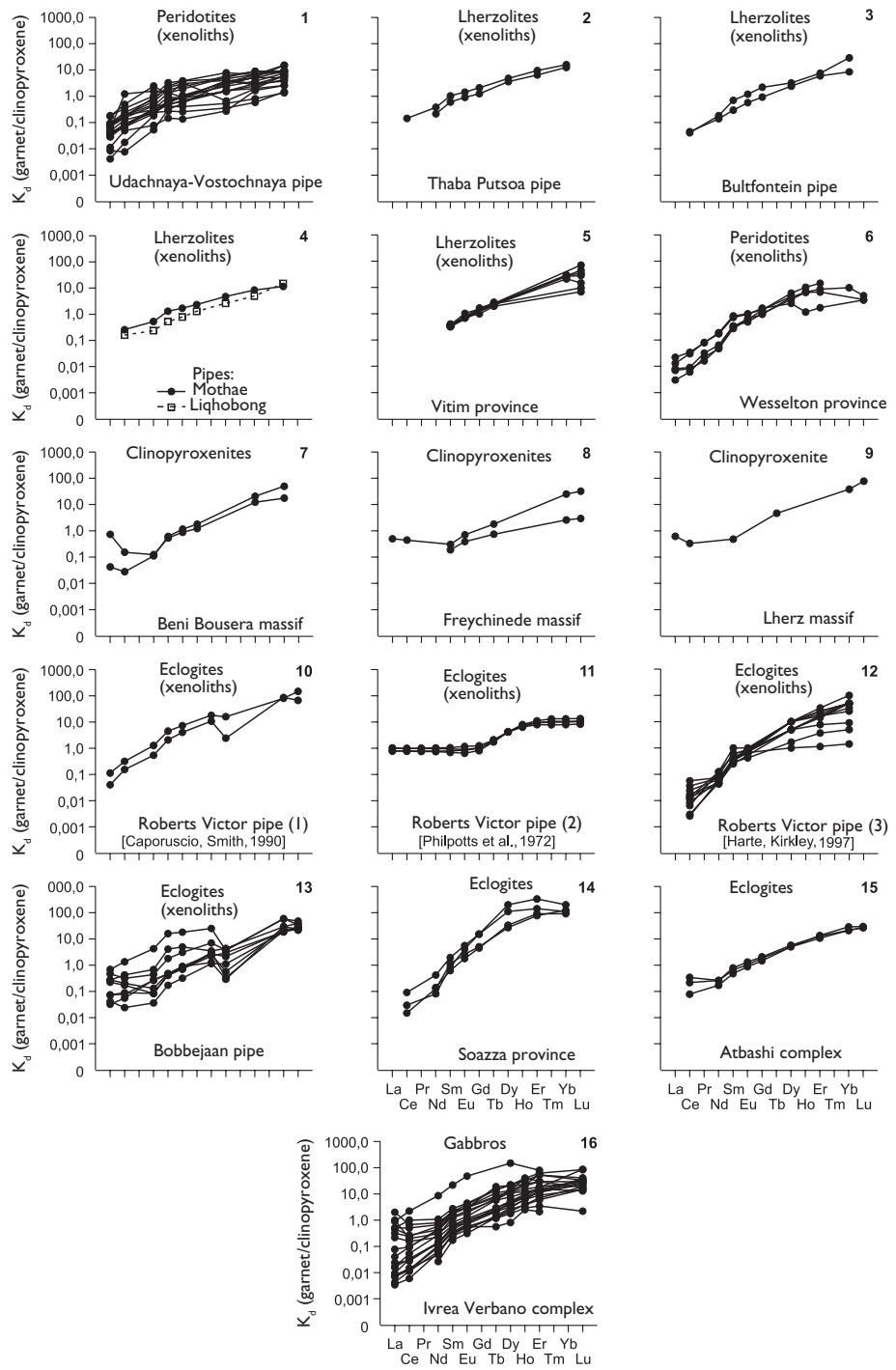


Figure 1.15 The graphs of coefficients of REE distribution between garnets and coexisting clinopyroxenes from different types of rocks (data Table 1.14).

slightly more, while for the same parageneses of eclogites the values of this parameter reach 1000, and in garnet-bearing gabbros, represented in Ivrea Verbano complex, their values reach up to several thousand. The lowest values of the $K_d(Yb)/K_d(Ce)$ parameters are ascertained for the garnet-clinopyroxene parageneses of the eclogites from Atbashi metamorphic complex (Table. 1.14). What is more, the distinguisher for the graphs of change of the values of $K_d(\text{garnet}/\text{clinopyroxene})$ for all of eclogites from Bobbejaan pipe, as well as for the graphs for some eclogites from Roberts Victor pipe, is the minimum for Dy observed in them (Figure 1.15, 10, 13).

The given data show that the $K_d(\text{garnet}/\text{clinopyroxene})$ values are to certain in some degree correlated with the composition and genesis of garnet-clinopyroxene rocks. In particular, it was ascertained that for diamondiferous eclogites those values of K_d that are close to unity are typically observed for Sm or Eu, while for non-diamondiferous eclogites such K_d values are frequently observed for Gd [Spetsius *et al.*, 1998]. There was also revealed a dependence between the values of $K_d(\text{garnet}/\text{clinopyroxene})$, on the one hand, and the contents of Mg and Ca in the parental melts of garnet-bearing rocks, on the other [Caporuscio & Smith, 1990].

According to the results of physical experiments, during the crystallization of basaltic melts, generated in the process of partial melting of garnet lherzolite at $P = 35$ kbar and $T = 1580\text{--}1635^\circ\text{C}$, the $K_d(\text{garnet}/\text{clinopyroxene})$ values for Ce, Sm and Tm were increasing with the reduction of the temperature in the system and, correspondingly, with the decrease in the degree of partial melting of lherzolite (Table 1.15). Apparently, such dependence of K_d is not really connected with partial change in the ratio of concentrations of these elements in garnets and clinopyroxenes, crystallized from basaltic melts, but associated with the change in the overall concentration of REE in the parental basaltic liquids that arises due to different degrees of partial melting of garnet lherzolite.

As mentioned above, various types of garnet-clinopyroxene rocks differ in the intensity of REE fractionation between coexisting garnets and clinopyroxenes. Taking this into account, such parameters as $K_d(Yb)/K_d(Ce)$, $K_d(Yb)/K_d(La)$, $K_d(Lu)/K_d(Ce)$ and some others can be used as geochemical indicators for classification of rocks of this kind of composition. For example, it was found that fractionation of REE between garnet and clinopyroxene in eclogites from Soazza metamorphic complex, as well as from Roberts Victor kimberlite pipe, is more intensive in comparison with these minerals, which were synthesized by physical experiments with basaltic systems.

Contiguous location, as well as conformality of the graphs of changing $K_d(\text{garnet}/\text{clinopyroxene})$ values in the garnet-clinopyroxene rocks from the same manifestation give grounds to conclude that such rocks were formed in a geochemical equilibrium of garnets and clinopyroxenes, which haven't been unbalanced by later processes. On the contrary, in cases, when the graphs of these K_d values are significantly fragmented and have different configurations, a geochemical equilibrium between garnet and clinopyroxene was not achieved initially, or it has been unbalanced as a result of a later redistribution of the elements. In particular, a considerable spread of values of $K_d(\text{garnet}/\text{clinopyroxene})$ for LREE, which is observed in the graphs for the eclogites from Roberts Victor kimberlite pipe, might indicate that in this case the geochemical equilibrium between garnet and clinopyroxene might have been partially unbalanced by later processes. These statements might be illustrated by the example of REE distribution between zonal garnet crystals and coexisting omphacite crystals from eclogites

Table 1.15 The coefficients of Ce, Sm, and Tm distribution between garnets and coexisting clinopyroxenes from basalts (experimental data).

Element	Degree of melting of garnet lherzolite, %	REE compositions, ppm			K_d garnet/clinopyroxene
		Melt	Garnet	Clinopyroxene	
Ce	2,29	55,169	0,477	11,337	0,042
	8,00	19,649	0,173	4,705	0,037
Sm	2,29	16,148	4,732	4,036	1,172
	8,00	11,538	3,704	3,569	1,038
Tm	2,29	1,370	1,794	0,296	6,061
	8,00	1,281	1,625	0,286	5,623

Note: The coefficients were calculated according to the results of analyses of products of crystallization of basaltic melts, received by experiments at partial melting of garnet lherzolite [Harrison, 1981].

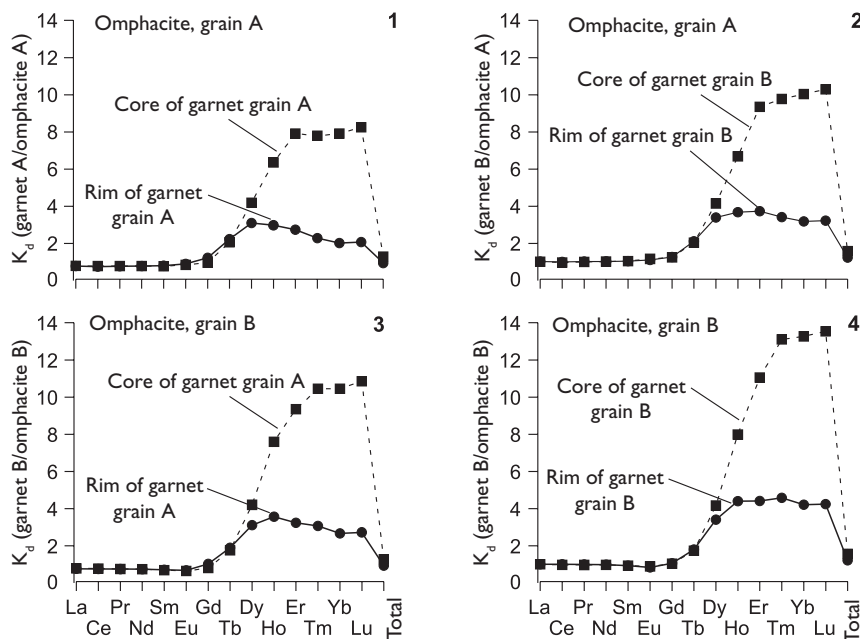


Figure 1.16 The graphs of coefficients of REE distribution between coexisting zonal garnets and clinopyroxenes (omphacites) from eclogites from Atbashi metamorphic complex, sample L-12 (data [Lesnov et al., 2005a]).

of Atbashi metamorphic complex (Figure 1.16). For example, graphics of K_d (garnet/clinopyroxene) for internal and external zones of garnet crystals in LREE area up to Gd have the shape of straight horizontal lines, matching on by location, but in heavy elements area they differ significantly, both in the position and the shape. We can assume that at the stage of formation of marginal zones of the garnet crystals their

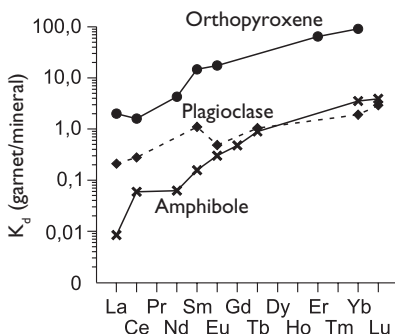


Figure 1.17 The graphs of coefficients of REE the distribution between garnets and coexisting orthopyroxenes from garnet lherzolites, and coexisting amphiboles and plagioclases from the granulites.

initial geochemical balance, which was achieved during the formation of inner zones of these crystals, has been upset, and therefore garnets turned out to be much poorer in HREE [Lesnov *et al.*, 2005a].

Despite the fact that data on the REE distribution between garnets and coexisting orthopyroxenes, plagioclases and amphiboles currently are of very limited amount, they show that due to preferential accumulation of HREE in garnets, the graphs of change of K_d (garnet/orthopyroxene), K_d (garnet/amphibole) and K_d (garnet/plagioclase) mainly have a positive slope, and the values of K_d (garnet/orthopyroxene) for all the elements are usually greater than 1, the values of K_d (garnet/amphibole) and K_d (garnet/plagioclase) for most of the REE do not reach 1, and exceed 1 only for Yb and Lu (Figure 1.17).

1.6 SOME CRYSTAL-CHEMICAL ASPECTS OF THE REE ISOMORPHISM IN GARNETS

The available data on this issue indicate that the crystal structure of garnets, regardless of their chemical composition and genesis, is able to accumulate a higher amount of REE, mainly of heavy elements. Parameters of their distribution in this mineral contain very important, but not meaningful enough genetic information. In addition, the forms of REE presence in garnets structure and the mechanisms that caused their isomorphic occurrence to this structure, haven't been sufficiently explored as of today. Nevertheless, already at this stage of study of this question we can assume with a sufficient confidence that one of the determinants of preferential accumulation of isomorphous admixture of HREE in the crystal structure of garnets are intrinsic properties of the structure, which is characterized by a relatively small size of a unit cell. Another important factor that plays an essential role in this isomorphism is apparently some of the properties of trivalent ions of HREE, namely the smaller size of their ionic radii compared with the trivalent ions of LREE. In this regard, the opinion that the crystal structure of garnets is the 'perfect place to find heavy lanthanides' is quite legitimate [Pride & Muecke, 1981].

As evidenced by the above presented data on the REE distribution in the zoned garnets, the REE composition of real crystals is largely caused by their common chemical composition. The level of HREE accumulation in garnets increases regularly with increasing of Ca content in them and of some other components in the direction from the core of the crystals to the peripheral zone [Shimizu *et al.*, 1997b]. According to other sources, variations in the level of REE accumulation in the garnet structure are connected not only with changes in their chemical composition, but also with concomitant changes in the geometry of the unit cell of mineral structure, as well as with the size of ionic radii and charge balance of some other elements involved in the process of heterovalent isomorphous substitution in garnets [Bocchio *et al.*, 2000].

It is commonly believed that Ca^{2+} ions due to their crystal-chemical properties, especially the size of ionic radius, are the most likely contenders for the isomorphic substitution of trivalent REE ions in the structural points of lattice of calcium-bearing silicate minerals [Piatenko & Ugriumova, 1988]. Data obtained while studying the properties of synthetic garnets are the evidence that this assertion is reasonable [Wim van Westrenen *et al.*, 1999]. This work particularly shows that with decreasing of the pyrope mineral content from 84 to 9% in synthetic garnets the values of $K_d(\text{garnet}/\text{melt})$ for La are increasing from 0,004 to 0,2, i.e., by 50 times. These data allowed the authors to assume that the values of $K_d(\text{garnet}/\text{melt})$ for all REE have an inverse relationship with the magnitude of $\text{Mg}/(\text{Mg}+\text{Ca})$ parameter.

While doing statistic calculations based on overall database to determine REE in garnets of the various manifestations, different composition, and genesis, we managed to determine a positive correlation between the Eu concentrations in garnet, on the one hand, and the content of network-forming elements such as Ca, Al, Fe, Mn, on the other hand. A positive correlation was also observed between pairs of components such as Yb-FeO and Sm-FeO (Figure 1.18). In addition, between the contents of Sm, on the one hand, and the contents of Si and Mg – on the other hand, there was found a negative correlation. However, as believed by some researchers, we should not oversimplify the relationship between the general chemical composition of garnets and their REE compounds, because there are cases when with sufficiently large variations in REE content the overall chemical composition of garnets is almost the same [Shimizu *et al.*, 1997b].

The possible options for coordinating the positions of REE in the structure of this mineral were discussed in several works on the crystallochemistry of garnets. In particular, it was shown that the HREE, as well as Li, Na, Sc and Y, can be localized in the structure of garnets in the eightfold coordination [Hickmott & Shimizu, 1990]. Another study ascertains that in the structure of synthetic yttrium garnets the trivalent La, Nd, Dy and Yb substituting Y^{3+} ions are in eightfold coordination [Cherniak, 1998]. In addition, while studying the crystal-chemical properties of synthetic pyropes and grossulars, it was found that Yb^{3+} ions in them, being located in the dodecahedral position, substitute the divalent Ca and Mg ions [Quartieri *et al.*, 1999].

While considering some aspects of the isomorphism of REE in grossular-andradite garnets, M. Gaspar *et al.* [2008] proceed from the chemical formula of garnets, which they recorded as follows: $X_3\text{Y}_2\text{Z}_3\text{O}_{12}$. According to them, the X position is occupied by divalent cations Ca, Mg, Mn or Fe^{2+} ; Y position – by trivalent cations (Fe^{3+} , Al or Cr), and Z position is mostly occupied by Si ions. Based on these assumptions, Gaspar *et al.* suggested that an isomorphic occurrence of REE into the garnet

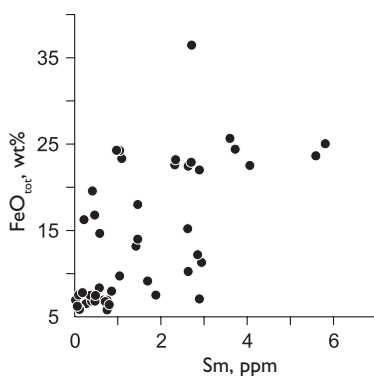
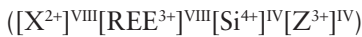


Figure 1.18 The graphs of correlation between contents of Sm and FeO_{tot} in garnets of some paragenetic types (data of different authors).

structure of grossular-andradite series is realized in accordance with the YAG-type mechanism, which has previously been justified in the study of synthetic yttrium-aluminum garnets:



According to this formula, Eu²⁺ ions can substitute the cations which are on X²⁺ position. According to the results of their research, these authors concluded that in garnets of grossular-andradite series the heavy REE predominantly accumulate in those of their species, where grossular mineral is dominating, in turn, light REE predominantly accumulate in those varieties of garnets, in which andradite mineral is dominating.

Identified at this stage of research garnet differences in the level of REE accumulation, as well as in the quantitative relationship between light and heavy elements, are presumably based on the end result of complex heterovalent isomorphous substitution, in which the number of network-forming elements could be involved, mainly Ca, Fe, Mg and Al cations. The intensity of the substitution of these cations by REE ions was increasing with the decrease in the pyrope mineral content in the real garnet crystals, as well as with lowering the temperature of mineral crystallization. Preferential accumulation of HREE in the garnet structure, most likely due to the relatively smaller sizes of the radii of their trivalent ions compared with ions of LREE, which in turn contributed to a better compatibility of these REE with the crystal structure of this mineral. However, in garnets with a high content of andradite component the isomorphism of LREE could play a more significant role.

Numerous varieties of natural parageneses that include garnets, indicate the great variety of PT – conditions, under which this mineral is able to crystallize. The study of patterns of REE distribution in garnets is one of the important trends in the geochemistry of magmatic, metamorphic and metasomatic rocks they belong to. Currently,

many paragenetic types of garnets haven't been studied with regard to regularities of REE distribution. The REE composition of high-Mg garnets, and presented in peridotite and eclogite from xenoliths in kimberlites, including those which are in the form of microinclusions in diamonds was studied in more detail than the garnets from gabbros, metamorphic and metasomatic rocks.

The overall level of REE accumulation in garnets increases in a row from high-Mg (subcalcium) and high-Cr pyropes of ultramafic rocks to high-Ca and high-Fe garnets from eclogites, some gabbros, metamorphic and metasomatic formations. The overwhelming majority of the studied garnets of different composition are characterized by a relative enrichment with HREE compared with the MREE and especially LREE. The garnets, the REE patterns of which have a steep positive slope and, consequently, very low La/Yb_n values are particularly prevalent. Specific sinusoidal shape of the patterns of REE distribution is typical for almost exclusively pyrope garnets from diamond-bearing ultramafic parageneses, presented in mantle xenoliths, including those that are directly in the form of inclusions in diamond crystals. Some researchers suggest that the REE patterns with such configuration are typical to those garnets, which are present in rocks subjected to deep-seated metasomatism under the influence of carbonatite melts and associated fluids. In the patterns of garnets from high-Si magmatic and metamorphic rocks negative Eu anomalies are sometimes observed.

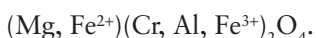
In general the coefficients of REE distribution between coexisting garnets and melts are increasing in the series from light to heavy elements and from magnesian to ferriferous melts, as well as with lowering temperature of mineral crystallization. In this case, K_d for LREE are usually less than 1, while for medium and especially for heavy elements K_d are usually greater than 1. It is therefore assumed that in the structure of garnets the HREE possessed properties of quite compatible trace elements. REE distribution coefficients between coexisting garnets and clinopyroxenes, as well as its graphs might be used as criteria for the geochemical classification of garnet-clinopyroxene rocks of different composition and genesis. Configuration and position of the curves of change in values of K_d(garnet/clinopyroxene) might be used as criteria for the intensity of REE fractionation between coexisting mineral phases under various conditions of crystallization. Close location, as well as the similarity of the configuration of these curves within a collection of rock samples from the same manifestation are an indication that these garnets and clinopyroxenes are in the state of geochemical equilibrium, which has not been misbalanced at later events.

Between the level of accumulation of REE in garnets, their general chemical composition and crystallization conditions there were empirically identified some regular dependences, a more detailed, in-depth study of which should become a subject to a further research in this important field of studies. At the present stage of geochemical study of garnets we can assume that the occurrence of REE into their structure was carried out by heterovalent isomorphous substitutions of divalent Ca ions by trivalent REE ions, during which the ions of Fe, Mg, Al, as well as certain other elements could play the role of compensating charge. The preferred occurrence of HREE in the garnet structure was apparently due to slightly smaller radii of their trivalent ions compared with ions of LREE, and this, in turn, created conditions for better compatibility with the crystal structure of garnets.

Chapter 2

Chrome-spinels

As an accessory phase, chrome-spinels are almost always present in the dunites, harzburgites, lherzolites, wehrlites, pyroxenites, olivine and some non-olivine gabbroids constituting the mafic-ultramafic massifs within the folded regions and platforms, as well as presented in abyssal xenoliths of alkali-basalts and kimberlites. As a part of many massifs they form deposits of various scale and schlieren of massive and densely disseminated ores, as well as cross veins, most often localized among the dunites and harzburgites. By their structure and chemical composition their chrome-spinels belong to the multiple oxide groups. A considerable variation of the main components – MgO, FeO, Al₂O₃ and Cr₂O₃ is observed in its content. Chemical formula of the chrome-spinels is usually written as follows:



Cr₂O₃ contents in the accessory chrome-spinels vary in the range 17–62 wt% and average about 55 wt%, which is slightly lower than the average content of component in the facies of the mineral composing ore deposits (~59 wt%). For example, the content of Cr₂O₃ in the chrome-spinels of Naran massif ore deposits (Mongolia) is 53–64 wt% [Lesnov & Simonov, 1989]. Ore chromitites from this massif were divided into two types depending on the composition of the fluid components: 1) with predominantly oxidized fluid, and 2) with predominantly reduced fluids. The content of Cr₂O₃ in chrome-spinels of Ergak massif chromitites (West Sayan, Russia) is 58,8–59,4 wt%, while in the accessory varieties of dunites is 54.9 wt% [Mongush *et al.*, 2004]. Compatible trace elements in the chrome-spinels are Ni, Co, Mn, V, Ti, V and others. Various classifications of chrome-spinels on the basis of their chemical compositions were proposed and discussed by Plaksenko [1989]. The minerals of the ultramafic restitutions, that compose the alpine massifs, mainly contain the facies of chrome-spinels which, according to the ratio between the contents of Cr₂O₃ and Al₂O₃, are forming the series from the most chromous to the most aluminiferous: chromite → alumochromite → chromopicotite → picotite. Most commonly used parameters for the taxonomy of chrome-spinels on the chemical composition are the values like $100 \cdot \text{Cr}_2\text{O}_3 / (\text{Cr}_2\text{O}_3 + \text{Al}_2\text{O}_3)$ and $100 \cdot \text{FeO}_{\text{tot}} / (\text{Mg} + \text{FeO}_{\text{tot}})$. A number of papers dealt with the issues on typomorphism of chrome-spinels based on its chemical composition and physical properties [Makeev *et al.*, 1985; Plaksenko, 1989; Makeev, 1992; Malakhov, 2002].

Chrome-spinels are yet little examined with respect to the distribution of lithophile trace elements, REE included, contained in relatively low concentrations. Application of methods of analysis of REE in the individual grains, in particular, the method of LA ICP-MS, slightly expanded opportunities for studying the features of the impurities' distribution in it. Below is a rare earth element chrome-spinels composition characterized by the example of a limited collection of specimens that are represented as an accessory phase in the spinel and garnet peridotites of some abyssal xenoliths in alkaline basalts and kimberlites, in dunites from Dovyrensky mafic-ultramafic massif (Northern Baikal region, Russia) of the ultramafites from Ergak massif (West Sayan, Russia), a number of kimberlite manifestations of Brazil, as well as the ore chromitites present in harzburgites of Voykar-Syn'insky massif (Polar Urals, Russia).

According to Vakhrusheva *et al.* [2006], chrome-spinels of the Voykar-Syn'insky massif's ore deposits summarily contain REE concentrations in the range from 1.2 to 14.1 ppm (Table 2.1), and their REE patterns have a flatter negative slope: $(La/Yb)_n = 1.2\text{--}3.6$. At the same time, we can observe positive Eu anomalies on the patterns of specimens from the high-chromous deposits, while it is absent on the patterns of the minerals from low-chromous deposits (Figure 2.1, 7, 8). Approximately the same level of REE concentrations is established for accessory chrome-spinels of dunite in Dovyrensky massif, but in this case its fractionation is more intense (Figure 2.1, 6). Lower chondrite-normalized REE contents – from 0.1 to 1.0 t.ch., are recorded in the accessory chrome-spinels from xenoliths of garnet peridotites in kimberlites and alkaline basalts. The REE patterns of these specimens have a complex configuration, which is, perhaps, partly due to analytical errors in the determination of Ce, Nd, Ho and Lu (Figure 2.1, 1–5). Accessory chrome-spinels from peridotite xenoliths of alkaline basalt province Dreiser Weiher (Germany) have a more homogeneous REE composition in comparison with specimens from other manifestations [Stosch & Seck, 1980; Stosch, 1982]. According to the research [Melluso *et al.*, 2008], chrome-spinels from kimberlites and kamaufites of Alto Paranaiba province (Brazil) are characterized by low total REE concentrations, but they contain relatively high amounts of La, Tm and Lu in relation to other elements (Figure 2.1, 9).

The REE composition of chrome-spinels from Ergak ultramafic massif, which is located in Ergak-Targak-Tayga ridge (West Sayan) has been investigated in detail and structurally confined to the junction between Kurtushibinsky and North Sayan ophiolite belts ($94^{\circ}25'30''E$; $53^{\circ}17'40''N$). The massif size of 6×15 km, its bare area is about 85 sq. km. [Lesnov *et al.*, 2008]. It occurs among the Vendian-Cambrian volcanic-terrigenous formations in the form of protrusion bounded by the dislocations with a break in continuity along which the ultramafites are intensely serpentinized and dynamic-metamorphosed. The massif is divided into Lysansky and Maloergaksky blocks by the northeast striking fracture. Harzburgites prevail in its structure, while dunites, lherzolites and olivinites play a subordinate role, and harzburgite and dunite often contain admixture of clinopyroxene. The massif manifested the indigenous bedding of single ore chromitite veins ranging from a few to tens of centimeters, as well as their eluvial lumps sized up to 3.5 m [Krivenko *et al.*, 2004; Mongush *et al.*, 2004].

Accessory chrome-spinels in Ergak massif's ultramafites are idiomorphic, rarely – xenomorphic grains ranging in size from a millimeter to 3 mm, sometimes

Table 2.1 REE compositions of chrome-spinels from peridotites, kimberlites, kamafugites, and chromitites from some provinces and manifestations (ppm).

Element	Dreiser Weiher province (Germany)						Australia		Shavarin Tsaram paleovolcano (Mongolia)		
	[Stosch, Seck, 1980], RNAA			[Stosch, 1982], RNAA			[Eggins et al., 1998], LA ICP-MS		[Lesnov et al., 2009], LA ICP-MS		
	Ia/236	Ib/2	Ib/KI	D-42/I	D-42/2	D-45	402/I	402/2	A-17	A-31	A-42
<i>Spinel Iherzolites</i>											
La	0,008	0,007	0,007	0,0009	0,0002	0,0007	<0,0009	0,006	0,027	N.d.	0,001
Ce	0,016	0,010	0,008	N.d.	N.d.	N.d.	<0,0007	0,014	0,063	N.d.	0,001
Pr	N.d.	N.d.	N.d.	N.d.	N.d.	N.d.	N.d.	N.d.	0,006	N.d.	0,001
Nd	N.d.	0,0186	N.d.	N.d.	N.d.	N.d.	<0,0024	0,008	N.d.	N.d.	N.d.
Sm	0,0012	0,0013	0,001	0,0002	0,0001	0,0001	<0,0019	0,005	0,004	0,003	N.d.
Eu	0,0006	N.d.	0,001	N.d.	N.d.	N.d.	<0,0010	0,012	0,003	N.d.	N.d.
Gd	N.d.	N.d.	N.d.	N.d.	N.d.	N.d.	<0,0023	0,005	N.d.	0,001	N.d.
Tb	N.d.	N.d.	0,0003	N.d.	N.d.	N.d.	N.d.	N.d.	0,001	N.d.	0,001
Dy	N.d.	N.d.	N.d.	N.d.	N.d.	N.d.	<0,0018	0,006	N.d.	0,001	0,001
Ho	N.d.	N.d.	0,0005	N.d.	N.d.	N.d.	N.d.	N.d.	N.d.	0,001	N.d.
Er	N.d.	N.d.	N.d.	N.d.	N.d.	N.d.	<0,0014	N.d.	N.d.	0,004	N.d.
Tm	N.d.	N.d.	N.d.	N.d.	N.d.	N.d.	N.d.	N.d.	N.d.	0,001	0,002
Yb	0,002	0,001	0,002	0,0005	0,0006	0,0008	<0,0016	0,003	0,003	0,005	N.d.
Lu	N.d.	0,0003	0,0003	0,0002	0,0002	0,0002	<0,0003	N.d.	N.d.	0,002	N.d.
Total	N.d.	N.d.	N.d.	N.d.	N.d.	N.d.	N.d.	N.d.	N.d.	N.d.	N.d.
(La/Yb) _n	3,18	3,37	2,18	1,12	0,18	0,63	0,38	1,31	7,37	N.d.	N.d.

(Continued)

Table 2.1 (Continued).

Massifs												
Yubileynaya pipe (Yakutia, Russia) [Aschepkov et al., 2004], LA ICP-MS		Dovyrensky (Russia) [Lesnov, Gora, 1993], RNAA		Voykar-Syn'insky (Urals, Russia) [Vakhrusheva et al., 2006], ICP-MS		Alto Paranaiba province (Brazil) [Melluso et al., 2008]						
Element	Asch-11	Asch-12	L-14	3660*	3730*	3943*	3992	4047	4334	8536	Lim-1	PO-2
Element	Garnet peridotites		Dunite	Chromitites high-Cr		Chromitites high-Al		Kimberlite		Kamafugite		
La	0,024	0,05	5,88	0,193	0,456	1,38	1,31	0,114	0,460	2,09	0,439	0,055
Ce	0,052	0,25	13,2	0,462	1,100	3,27	2,80	0,293	1,15	4,97	0,022	0,037
Pr	0,009	0,01	N.d.	0,070	0,169	0,506	0,442	0,046	0,182	0,689	N.d.	N.d.
Nd	0,035	0,14	2,04	0,360	0,772	2,40	1,92	0,234	0,885	3,11	0,017	N.d.
Sm	0,025	0,07	1,50	0,104	0,232	0,669	0,487	0,067	0,244	0,663	N.d.	N.d.
Eu	0,024	0,02	0,52	0,043	0,110	0,203	1,22	0,110	0,199	0,338	0,014	0,009
Gd	0,081	0,09	1,86	0,126	0,276	0,482	0,624	0,081	0,269	0,524	N.d.	N.d.
Tb	0,010	0,011	0,30	0,020	0,046	0,154	0,094	0,014	0,042	0,090	0,004	N.d.
Dy	0,025	0,07	N.d.	0,124	0,297	0,902	0,535	0,078	0,253	0,575	0,013	0,038
Ho	0,060	0,13	N.d.	0,025	0,067	0,200	0,121	0,017	0,053	0,121	0,003	0,002
Er	0,025	0,02	N.d.	0,072	0,204	0,617	0,386	0,054	0,170	0,372	0,01	0,008
Tm	0,003	0,004	0,13	0,011	0,034	0,100	0,064	0,009	0,029	0,060	0,021	0,012
Yb	0,014	0,02	1,02	0,075	0,249	0,673	0,463	0,063	0,196	0,396	0,018	0,047
Lu	0,004	0,10	0,15	0,012	0,041	0,106	0,075	0,010	0,033	0,061	0,02	N.d.
Total	0,391	0,985	N.d.	1,70	4,05	11,7	10,5	1,19	4,16	14,1	N.d.	N.d.
$(\text{La}/\text{Yb})_n$	1,16	1,69	N.d.	1,74	1,24	1,38	1,91	1,22	1,58	3,56	16,5	0,8

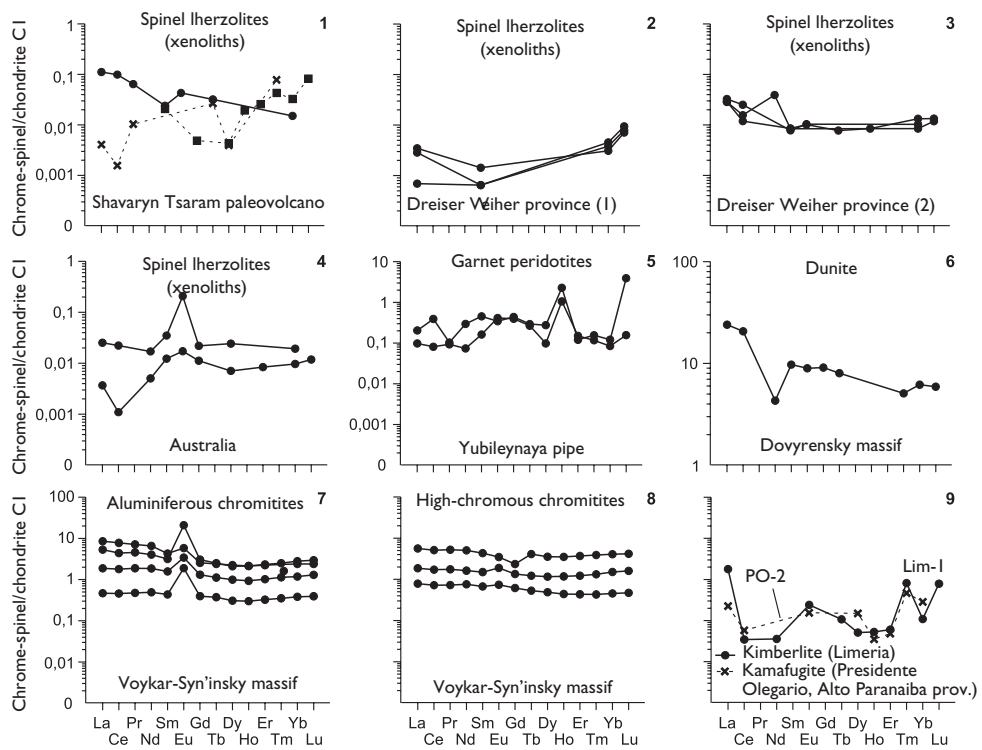


Figure 2.1 Chondrite-normalized REE patterns for accessory chrome-spinels from some ultramafic rocks and from chromitite ores (data Table 2.1).

up to 5 mm. Their content in the rock usually does not exceed 2%. In the narrow outer zones the chrome-spinel grains are often replaced with magnetite. Chrome-spinel grains were studied under the electron microscope that identified in its content xenomorphic, rarely – idiomorphic solid-phase microinclusions (20–200 μm), which are identified as olivine, clinopyroxene and amphibole. Microprobe analysis of 90 individual chrome-spinel grains extracted from artificial heavy concentrates of ultramafic rocks of the massif, showed wide variations in the contents of Cr_2O_3 and Al_2O_3 , and low content of impurities Ti, V, Zn and Ti [Krivenko *et al.*, 2004]. In the minerals from Lysansky block rocks the Cr_2O_3 content was on the average slightly lower than in specimens from Maloergaksky block rocks. Interval values $\text{Cr}^\# = \text{Cr} \cdot 100/(\text{Cr} + \text{Al})$ (formula units) in the total collection of specimens of chrome-spinels of Ergak massif rocks values were 19–83.5 with an average value of 41.5. By the chemical composition, these chrome-spinels refer to chromopictite-alumochromite series.

Earlier, using electron microprobe method on a series of individual grains of the accessory chrome-spinels, we studied in detail the general chemical composition of this mineral from harzburgites of Lysansky block of Ergak massif [Krivenko *et al.*, 2004],

and later we determined REE in some of them. These determinations were performed in the Analytical Center IGM SB RAS (Novosibirsk) by LA ICP-MS method using the ‘Element’ mass spectrometer and laser-top boxes (UV Laser Probe, laser Nd: YAG $\lambda = 266$ nanometer) produced by Finnigan Mat (Germany) [Lesnov *et al.*, 2008a, b]. The size of the laser-scanned polygon within the individual chrome-spinel grains varied between 400–800 square microns. The NIST-610 glass was used as an external standard, and as an internal standard – the contents of Zn and Mn in these chrome-spinel grains according to microprobe method. The results of these tests are provided in Table 2.2.

According to the identifications made, total REE content in the chrome-spinel grains studied from ultramafic Ergak massif vary in a fairly wide range. At the same time, like in other minerals from ultramafic massifs, chondrite-normalized light REE concentration in them was higher than the concentration of medium and in particular heavy items. Their rare earth element patterns have a shape of sinuous lines with a common negative slope (Figure 2.2). Patterns that are based on the average, maximum and minimum contents of elements in the studied specimens, are shown in Figure 2.3. The REE patterns of some chrome-spinel grains show different intensity anomalies of Tm and Er; their presence is confirmed by control assays of the grains from sample 204 (four definitions), and sample 214 (three definitions), previously studied under the electron microscope for the absence of any micro-inclusions.

On the basis of 15 performed tests on chrome-spinels we calculated the coefficients of simple correlation between REE contents, on the one hand, and the contents of major and minor components – on the other. The values of these coefficients, except for a pair of Gd-NiO, were below the limits of statistical significance for this sample ($r_{01} = 0.53$). Nevertheless, the values obtained for the coefficients indicate the presence of trends in an inverse relationship between the contents of REE and the contents of Cr_2O_3 , FeO_{tot} and TiO_2 . In addition, the evidence of a direct relationship between the content of the majority of REE, on the one hand, and the contents of Al_2O_3 , NiO, and MgO, on the other, were found out.

Representative data available on the chemical composition of chrome-spinels from ultramafic Ergak massif, allowed to discuss the possibility of determining the degree of partial melting of mantle source for the formation of these rocks as restites [Lesnov *et al.*, 2008], using the results of physical experiments [Hirose & Kawamoto, 1995]. The works of these researchers presented the results of experiments on partial melting of lherzolite at 1 GPa pressure and temperatures from 1100 to 1350°C in the presence of 0.1–0.9 wt% of H_2O . They found that the value of the chromium indicator of chrome-spinels ($\text{Cr}^{\#}$) formed in the experimental refractory remnants, consistently increased with increasing degree of partial melting of lherzolite (Table 2.3). Based on these data, we have calculated the regression equation:

$$D_{\text{melt}} = 0.426 \cdot \text{Cr}^{\#} + 1.538,$$

where D_{melt} – the degree of partial melting (%), $\text{Cr}^{\#}$ – chromium indicator of chrome-spinels (%). The regression line corresponding to equation is shown in Figure 2.4. In the equation we substitute the values of $\text{Cr}^{\#}$ of chrome-spinels from harzburgite specimens from Ergak massif, which were determined by REE. Thus, we have obtained estimates of the degree of partial melting of the mantle protolith (Table 2.2). According to the

Table 2.2 REE (ppm), major, and minor elements (wt%) compositions of accessory chrome-spinels from harzburgites from Ergak massif (West Sayan, Russia).

Element	Er-204	Er-206	Er-207	Er-208	Er-209	Er-210	Er-211	Er-212	Er-213	Er-214	Er-215	Er-216	Er-217	Er-218	Er-219	Detection limits
La	0,26	4,0	3,4	5,6	0,073	1,95	0,18	1,77	1,33	0,11	0,41	0,19	0,28	1,76	3,4	0,0010
Ce	0,54	12,3	8,2	9,6	0,23	3,6	0,31	1,21	2,2	0,26	1,09	0,56	0,40	3,1	8,0	0,0011
Pr	0,062	1,95	1,08	1,68	0,033	0,54	0,024	0,048	0,17	0,027	0,14	0,097	0,044	0,57	1,38	0,0005
Nd	0,11	5,7	4,9	2,9	0,059	2,0	0,11	0,20	0,67	0,12	0,29	0,81	0,13	1,36	5,0	0,0008
Sm	0,029	1,25	0,54	0,32	0,010	0,43	0,012	0,044	0,13	0,020	0,059	0,19	0,007	0,37	0,59	0,0004
Eu	0,014	0,085	0,10	0,029	0,002	0,064	0,002	0,004	0,039	0,006	0,020	0,005	0,002	0,022	0,19	0,0003
Gd	0,031	0,28	0,37	0,12	0,010	0,084	0,012	0,005	0,023	0,016	0,040	0,003	0,004	0,16	0,11	0,0003
Tb	0,003	0,008	0,012	0,011	0,001	0,007	0,002	0,0006	0,002	0,002	0,002	0,0003	0,0002	0,022	0,013	0,0002
Dy	0,014	0,028	0,067	0,033	0,002	0,034	0,007	0,004	0,016	0,012	0,010	0,004	0,003	0,24	0,031	0,0002
Ho	0,004	0,004	0,022	0,007	0,0002	0,007	0,0004	0,0006	0,002	0,002	0,002	0,001	0,0006	0,055	0,006	0,0002
Er	0,012	0,016	0,056	0,020	0,0004	0,031	0,001	0,002	0,004	0,008	0,005	0,007	0,004	0,25	0,009	0,0002
Tm	0,005	0,003	0,015	0,003	0,00007	0,006	0,0001	0,0004	0,0003	0,001	0,0007	0,001	0,0008	0,041	0,0004	0,0001
Yb	0,009	0,011	0,10	0,014	0,0004	0,042	0,0007	0,003	0,001	0,007	0,004	0,009	0,005	0,33	0,001	0,0002
Lu	0,001	0,002	0,021	0,004	0,0001	0,007	0,0002	0,0004	0,0002	0,0005	0,0004	0,002	0,0005	0,058	0,0002	0,0001
Total REE	1,10	25,6	18,9	20,5	0,42	8,85	0,65	3,29	4,61	0,60	2,07	1,88	0,88	8,35	18,7	—
(La/Yb) _n	18,8	241	22,1	263	119	31,6	180	448	757	11,0	76,7	14,1	39,9	3,6	1968	—
Component																
Cr ₂ O ₃	53,16	21,85	21,24	28,14	47,8	51,90	37,76	36,17	20,37	37,19	22,80	33,83	33,65	23,42	41,62	—
Al ₂ O ₃	14,32	45,02	47,65	40,63	20,48	3,68	31,03	30,99	47,60	30,98	45,86	34,59	34,62	45,88	24,58	—
FeO _{tot}	19,89	13,86	13,96	14,90	20,66	34,22	16,12	17,92	14,43	17,32	14,25	16,95	17,18	14,59	19,63	—
MgO	11,57	17,91	17,63	16,54	11,02	3,12	14,76	13,55	17,71	14,21	17,51	14,88	14,87	17,34	13,16	—
MnO	0,26	0,13	0,15	0,17	0,17	0,82	0,19	0,22	0,13	0,13	0,09	0,13	0,14	0,10	0,18	—
V ₂ O ₅	N.d.	N.d.	N.d.	N.d.	0,22	0,43	N.d.	N.d.	N.d.	0,23	0,19	0,21	0,20	0,17	0,24	—
NiO	0,07	0,22	0,25	0,15	0,06	N.d.	0,13	0,13	0,25	0,09	0,26	0,13	0,15	0,24	0,09	—
TiO ₂	0,10	0,02	0,01	0,06	0,04	0,11	0,04	0,04	0,02	0,09	0,04	0,05	0,03	0,04	0,07	—
ZnO	0,13	0,18	0,19	0,17	0,15	0,25	0,13	0,18	0,19	0,13	0,16	0,20	0,18	0,15	0,16	—
Total	99,50	100,20	101,08	100,79	100,62	97,12	100,16	99,19	100,70	100,37	101,15	100,97	101,01	101,93	99,73	—
Cr [#] , %	71,4	24,1	23,0	31,8	61,1	83,2	45,1	43,8	22,2	44,6	25	39,7	39,4	25,3	53,2	—
D _{melt} , %	32	12	11	15	28	37	21	20	11	21	12	18	18	12	24	—

Note: The analyses were done in the Analytical Center of IGM SB RAS: the analyses of the REE - LA ICP-MS method, analyst S. Palesskii; the analyses of major and minor components – X-ray microprobe “Camebax-Micro”, analyst L. Pospelova. Detection limits for REE were defined resulting from 3σ background intensities of the signal in gas Ar; errors of determination of individual elements – 20–30 %; Cr[#] = Cr · 100/(Cr + Al); D_{melt} % – model estimation of partial melting degree of mantle protolite.

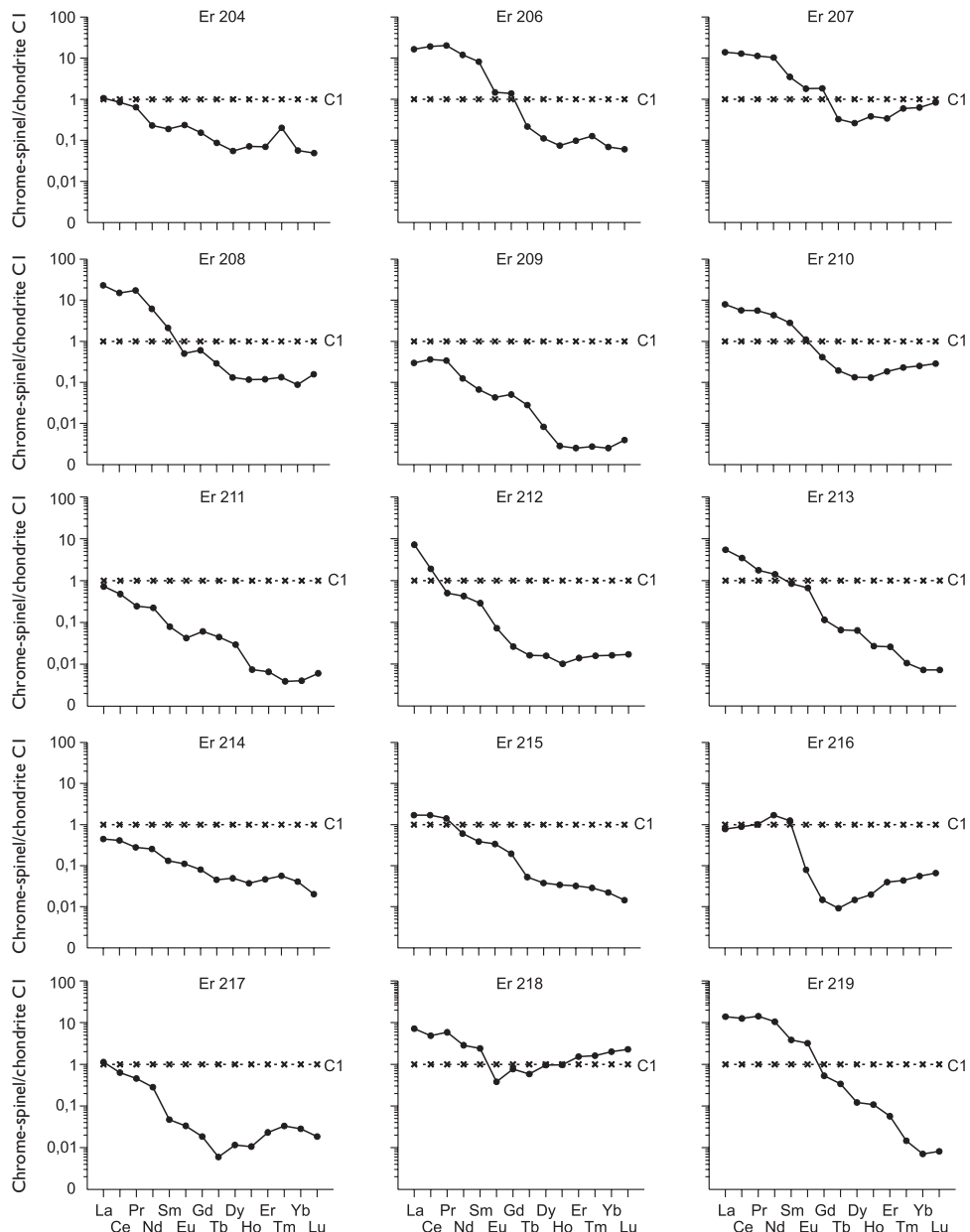


Figure 2.2 Chondrite-normalized REE patterns for accessory chrome-spinels from harzburgites from Ergak massif (West Sayan, Russia) (data Table 2.2).

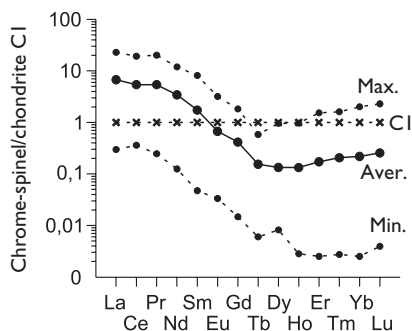


Figure 2.3 Chondrite-normalized REE patterns of average, maximum and minimum contents of elements in the accessory chrome-spinels from harzburgites from Ergak massif (West Sayan, Russia) (data Table 2.2).

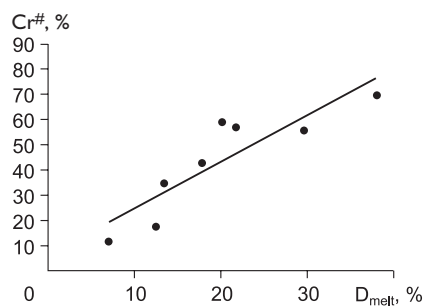


Figure 2.4 The graphs of relationship between Cr# % parameter for accessory chrome-spinels and degree of partial melting of Iherzolite (D_{melt}, %) (data Table 2.3).

Table 2.3 Relationship between Cr# parameter values of accessory chrome-spinels and the degree of partial melting of Iherzolites (D_{melt}) (experimental data [Hirose, Kawamoto, 1995]).

Cr#	D _{melt}
11,5	7,0
17,5	12,4
34,5	13,4
42,6	17,8
55,7	29,6
56,8	21,8
58,8	20,1
69,5	38,0

Note: Cr#, % = Cr · 100/(Cr + Al).

data, during the formation of harzburgite of Ergak massif the degree of partial melting of the mantle protolite should have changed in a fairly wide range – from 12 to 37%. Almost the same range of values of D_{melt} determined in the calculations based on the general sample of 90 chemical analyses of chrome-spinels from ultramafic Ergak massif. In addition, the results of the same physical experiments have been previously used to construct an appropriate scale which allows us to determine the degree of partial melting of mantle source, based on the values of Cr# for the accessory chrome-spinels [Page *et al.*, 2008]. Estimates obtained using the named scale, show that ultramafic rocks from Ergak massif could be formed as restites for a very wide range of variations in the degree of partial melting of the mantle protolite (Figure 2.5, a).

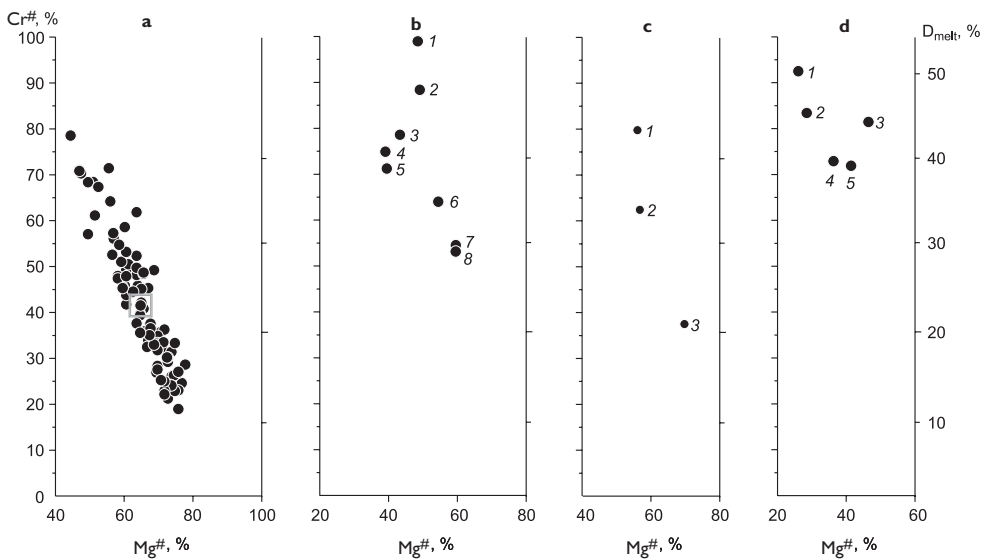


Figure 2.5 The graphs of relationship between $\text{Cr}^{\#} \% = \text{Cr} \cdot 100 / (\text{Cr} + \text{Al}) \%$ and $\text{Mg}^{\#} \% = \text{Mg} \cdot 100 / (\text{Mg} + \text{Fe}^{2+})$ of the accessory chrome-spinels from ultramafic rocks from some ultramafic massifs. a – Ergak massif (West Sayan, Russia) (data [Krivenko et al., 2004]). In the square – average values for the general totality of analysis, b – Idzhimsky massif (West Sayan, Russia) (data [Sibilev, 1980]): 1-5 – dunites, 6 – harzburgite; 7, 8 – lherzolites; c – Kempirsay massif (South Urals, Kazakhstan) (data [Makeev, 1992]): 1 – chrome-spinels from dunites (average of 21 analyses), 2 – alumochrome-spinels and subferrialumochrome-spinels from harzburgites (average of 19 analyses), 3 – chromepicrites and pikotites from lherzolites (average of 34 analyses); d – Ray Iz massif (North Urals, Russia) (data [Makeev, 1992]): 1 – subferrichrome-spinels from dunites (average of 16 analyses), 2 – subferrialumochrome-spinels from dunites (average of 17 analyses), 3 – ferrialumochrome-spinels from dunites (average of 11 analyses), 4 – subferrialumochrome-spinels from dunites (average of 7 analyses), 5 – ferrichrome-spinels from dunites (average of 4 analyses). D_{melt} , % – degree of partial melting of mantle ultramafic protolite during the formation of restites (data [Page et al., 2008]).

Similar calculations of the D_{melt} values were performed using the data on chemical compositions of chrome-spinels from ultramafic rocks of several other mafic-ultramafic massifs. Thus, it was found that for the ultramafic rocks of Idzhimsky massif, that is just like Ergak is a part of the Kurtushibinsky ophiolite belt (West Sayan, Russia), the values of D_{melt} successively reduce from dunite to harzburgite and lherzolite (Figure 2.5, b). The values obtained for D_{melt} from ultramafic rocks of Kempirsay (Kazakhstan) and Ray Iz massifs (Polar Urals, Russia), are shown in Figure 2.5, c and d.

Thus, the described calculation method allows us to obtain approximate estimates of the degree of partial melting of mantle sources during the formation of ultramafic restites using chromium indicator of the accessory chrome-spinels represented in it. If we accept the results of these calculations to be close to the real values of D_{melt} , we can conclude that during the formation of ultramafic restites, that composed fairly large

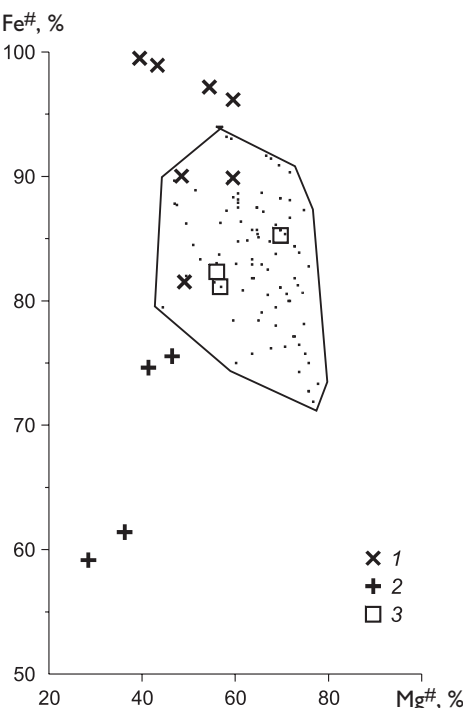


Figure 2.6 The graphs of relationship between parameters $\text{Fe}^{\#} \text{ \%} = \text{Fe}^{2+} \cdot 100 / (\text{Fe}^{2+} + \text{Fe}^{3+})$ and $\text{Mg}^{\#} \text{ \%} = \text{Mg} \cdot 100 / (\text{Mg} + \text{Fe}^{2+})$ in the accessory chrome-spinels from harzburgites. 1 – Idzhimsky massif (West Sayan, Russia) (data [Sibilev, 1980]), 2 – Ray Iz massif (North Urals, Russia) (data [Makeev, 1992]), 3 – Kempirsay massif (South Urals, Kazakhstan). The contour denotes the field of figurative points of chrome-spinels from Ergak massif (West Sayan, Russia) (data [Krivenko et al., 2004]).

protrusion, partial melting of its mantle sources has not been uniform. This conclusion is consistent with the well-known fact, according to which the composition of almost all large ultramafic massifs belonging to the ophiolite associations, usually has a complicated alternation of close proximity of bodies formed with lherzolites, harzburgites and dunites, formation of which is expected to occur at obviously different degrees of partial melting of mantle sources. In addition, according to our estimates, chrome-spinels from ultramafic rocks of Ergak massif on the degree of reduction of iron is comparable with the specimens of chrome-spinels from ultramafic rocks of Kempirsay massif, which is supposed to be one of the largest deposits of chromitites. At the same time, on the degree of reduction of iron, chrome-spinels from rocks of Ergak and Kempirsay massifs occupy an intermediate position between the specimens of the mineral from Idzhimsky massif, in which iron is in a more reduced state, and from Ray Iz massif, in which it is largely oxidized (Figure 2.6).

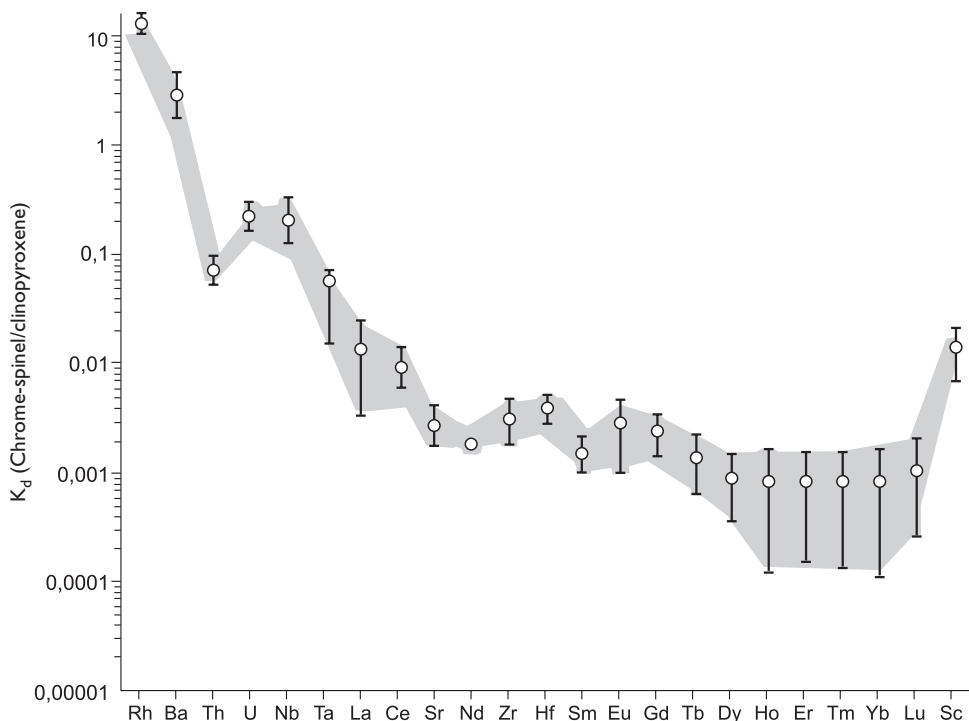


Figure 2.7 The graph of coefficients of the average composition of REE and other trace elements distribution between chrome-spinels and coexisting clinopyroxenes from peridotites and websterites from Ronda massif (Spain). White dots denotes average values of coefficients; top and bottom contour of the gray fields – limits of their standard deviations (data [Garrido & Bodinier, 1999]).

On the example of chrome-spinels from spinel peridotites and websterites of Ronda massif (Spain), the estimates of K_d (chrome-spinel/clinopyroxene) were obtained for REE and some other trace elements [Garrido & Bodinier, 1999]. Judging by the graph from that paper, the average values of K_d consistently reduced in number from La (~0,02) to Ho and then to the rest of the heavy REE (~0.003) (Figure 2.7). Contrasting to the previous work the values for K_d (chrome-spinel/clinopyroxene) are lower and for some elements were obtained from the chrome-spinels from peridotites provided in the xenoliths from alkaline basalts of Dreiser Weiher province: Eu – 0.0007, Sm – 0.0006 [McDonough *et al.*, 1992].

Structural position that REE ions can take up in the crystal lattice of chrome-spinel haven't been elucidated yet. However, on the assumption of the size of the REE ionic radii, which are in eightfold coordination [Shannon, 1976], among the cations, which are included into the structure of the chrome-spinels, as the most likely candidates for the isomorphic substitution of trivalent ions of heavy REE ($^{VIII}\text{Tm}^{3+}$ – 0,994 Å; $^{VIII}\text{Yb}^{3+}$ – 0,985 Å; $^{VIII}\text{Lu}^{3+}$ – 0,977 Å) can be expected to be called ions $^{VIII}\text{Fe}^{2+}$ (0,920 Å) and $^{VIII}\text{Mg}^{2+}$ (0,890 Å).

Ilmenites

Ilmenites as an accessory phase are represented in many varieties of magmatic rocks, including normal and calc-alkaline gabbroids, diorites, pyroxenites, subvolcanic and volcanic mafic rocks of normal and high alkalinity, kimberlites, carbonatites and some schists and other formations. In gabbroids and pyroxenites from some massifs there is a dense impregnation of ilmenites observed, as well as deposits of their massive ores. Due to their mechanical strength the ilmenites are able to accumulate in the products of disintegration of rocks containing them and to form placer manifestations and deposits [Rikhvanov *et al.*, 2001]. By chemical composition the ilmenites are usually divided into three main isomorphous series: $\text{FeTiO}_3\text{--MgTiO}_3$, $\text{FeTiO}_3\text{--MnTiO}_3$ and $\text{FeTiO}_3\text{--Fe}_2\text{O}_3$. The enriched with magnesium facies of ilmenites that are presented mainly in kimberlites and carbonatites belong to picroilmenites [Frantsesson, 1968; Dawson, 1983]. MgO content in them is 4–10 wt%, while in the samples from carbonatites it sometimes reaches 20% [Malakhov, 2002]. In addition to Mg in the form of impurity in ilmenites there are usually Mn, Al, V, Zr, Hf, Zn, REE and other elements. The chemical formula of ilmenites is usually written as follows: $(\text{Fe}^{2+}, \text{Mn}, \text{Mg}) (\text{Ti}, \text{Fe}^{3+})\text{O}_3$.

3.1 REE COMPOSITION OF ILMENITES

Currently the REE composition of ilmenites from many massifs and species composing them is studied only by single samples. More representative data were obtained from the ilmenites from the rocks of mafic-ultramafic Skaergaard massif (Greenland), from a set of kimberlite pipes located on the territory of Yakutia (Russia), Tigray massif (Primorie province, Russia) and some others. Among the investigated ilmenites there are samples of such rocks as gabbro, gabbro-norites, wehrlites, pyroxenites, kimberlites, as well as monzonites, rhyolites, some metamorphic and other species [Paster *et al.*, 1974; Borisenko & Lyapunov, 1980; Nash & Crecraft, 1985; Jones, 1987; Zack & Brumm, 1998; Nowell *et al.*, 1999; Jang & Naslund, 2002; Lesnov *et al.*, 2004a; Golubeva *et al.*, 2007; Aschepkov *et al.*, 2007]. Determination of REE in ilmenites was carried out using methods such as INAA, RNAA, ICP-MS, LA ICP-MS.

According to available data the total REE contents in ilmenites of different types of magmatic rocks vary within the following ranges: kimberlites – 0.02–298 ppm, pyroxenites in xenoliths of alkaline basalts – 0.13–0.66 ppm, websterites – 5.3–17.6 ppm, gabbro-norites and gabbro – 5.1–40 ppm. In ilmenites from metamorphic

schists of Polar Urals REE total content reaches 107 ppm, and in sample of ilmenite from rhyolite – 1700 ppm. In the mineral from the gabbros of Skaergaard massif REE total content varies in the range of 1.94–9.05 ppm (Table 3.1).

In picroilmenites of Frank Smith, Monastery (South Africa) and Mir (Yakutia, Russia) kimberlite pipes there were observed increased chondrite-normalized REE contents of LREE and to a smaller extent Yb and Lu compared with MREE, while the patterns of REE distribution in these samples have a common negative slope (Figure 3.1, 1–4). In turn, the patterns of ilmenites from Yubileynaya kimberlite pipe (Yakutia, Russia) and from the pyroxenites presented in the xenoliths indicate their enrichment with medium and heavy REE. At the same time the patterns of picro-ilmenites of kimberlites from Yubileynaya pipe have a shape close to sinusoidal (Figure 3.1, 5). Unlike previous ones, the ilmenites from pyroxenites presented in the xenoliths from basalts of Bayuda (Sudan) and Kakanui volcano (New Zealand) volcanoes are depleted by LREE relative to HREE, respectively, their patterns have the same positive slope (Figure 3.1, 6, 7). The patterns of some ilmenites have positive or negative Eu anomalies of different intensity (Figure 3.1, 10, 12).

We have investigated the collection of samples of accessory ilmenites from gabbro-norites and websterites composing the Tigrovyy massif (Primorie province, Russia) [Lesnov *et al.*, 2004a] which, as well as Ariadninsky, Kedimiysky, Uonchovsky massifs and the others, is situated in the southern part of Khabarovsk territory, in Sikhote Alin ridge [Shcheka *et al.*, 1973; Shcheka *et al.*, 2003]. Numerous indigenous manifestations of disseminated and massive ilmenite ores and ilmenite placers are connected to all these massifs spatially and genetically. The ilmenite content in the massive ore sometimes reaches 50%. In the accessory ilmenites of Tigrovyy massif the TiO_2 content varies in the range of 47.0–53 wt%, FeO_{tot} – 46–49 wt%, MnO – 0.7–1.6 wt%, and the presence of impurities of MgO and Cr_2O_3 was identified only in some of the cases (Table 3.2). Determination of REE in these ilmenites was carried out by INAA method and in the certain grains was duplicated by ICP-MS method (Table 3.1). According to the method of INAA, the total REE content in ilmenites of Tigrovyy massif varies in the range of 5.81–6.98 ppm, and the differences between ilmenites from websterites and gabbro-norites on this basis have not been identified. All ilmenites in this collection demonstrate a relative enrichment with LREE: $(\text{La/Yb})_{\text{n}} = 3.0\text{--}4.8$, respectively, their patterns have a common negative slope (Figure 3.1, 8, 9). Analyses of those ilmenites from gabbro-norites, which were performed by ICP-MS method, indicated the presence of a substantial surplus of Eu in them (Figure 3.1, 10). According to the data obtained by the mentioned method for the ilmenites from gabbro-norites the values $(\text{Sm/Eu})_{\text{n}} = 0.19\text{--}0.28$, which is slightly less than in its samples from websterites (0.38–0.48). Determination of REE in the three samples of ilmenites made by INAA method and duplicated by ICP-MS showed results comparable both on the basis of the content of certain elements and their total content (Table 3.1). Positive Eu anomalies on the REE pattern of ilmenites from websterite (sp. Sch-095D*, Figure 3.1, 8) and gabbro-norite (analyses Sch-093 g*, 1a, b, c; Figure 3.1, 10) which were identified according to ICP-MS method, also show a slight excess of this element in the samples stated. According to observations made under an optical microscope, the ilmenite grains from these and other samples from the Tigrovyy massif are mostly xenomorphic regarding coexisting crystals of pyroxene and plagioclase, which indicates their belated crystallization relative to these silicate

Table 3.1 REE compositions of ilmenites from kimberlites, peridotites, pyroxenites, troctolites, gabbros and other rocks from some provinces, complexes and pipes (ppm).

	Frank Smith pipe (South Africa)			Monastery pipe (South Africa)			Mir pipe (Russia)	Yubileynaya pipe (Russia)		Alto Paranaiba province (Brazil)	
	[Nowell et al., 1999], INAA			[Jones, 1987], INAA			[Mel'gunov, Lesnov, 2003], INAA	[Aschepkov et al., 2004], LA ICP-MS		[Melluso et al., 2008], LA ICP-MS	
	3241-1	3241-2	MON-1	2626R	2626RI	2633C	VII-34/2	Asch-6	Asch-7	Ind-c-1	Ind-c-2
Element	Kimberlites										
La	0,060	0,160	0,250	0,720	0,660	0,200	1,50	0,030	0,020	0,013	0,013
Ce	0,090	0,340	0,500	0,690	0,350	0,290	2,000	0,044	0,043	0,054	0,028
Pr	0,010	0,030	0,060	N.d.	N.d.	N.d.	N.d.	0,008	0,005	0,005	0,007
Nd	0,080	0,120	0,220	0,330	0,250	0,130	N.d.	0,059	0,041	0,032	N.d.
Sm	0,020	0,020	0,050	0,065	0,061	0,026	0,180	0,06	0,032	0,008	0,02
Eu	0,010	0,010	0,010	N.d.	0,022	0,010	0,050	0,034	0,011	0,007	N.d.
Gd	0,020	0,010	0,040	0,080	0,063	0,030	N.d.	0,073	0,046	N.d.	0,025
Tb	N.d.	N.d.	N.d.	N.d.	N.d.	N.d.	N.d.	0,016	0,005	0,003	N.d.
Dy	0,020	0,020	0,050	0,079	0,062	0,041	N.d.	0,068	0,025	0,031	0,028
Ho	N.d.	N.d.	N.d.	N.d.	N.d.	N.d.	N.d.	0,011	0,003	0,004	0,012
Er	0,010	0,010	0,030	0,045	0,042	0,028	N.d.	0,034	0,006	0,021	0,032
Tm	N.d.	N.d.	N.d.	N.d.	N.d.	N.d.	N.d.	0,004	0,001	0,001	0,005
Yb	0,020	0,020	0,040	0,187	0,064	0,051	0,190	0,017	0,020	0,075	0,048
Lu	N.d.	N.d.	N.d.	N.d.	N.d.	N.d.	0,140	0,005	0,007	0,011	0,03
Total	0,340	0,740	1,25	2,20	1,57	0,806	N.d.	0,463	0,445	0,265	0,248
$(La/Yb)_n$	2,02	5,40	4,22	2,60	6,96	2,65	5,33	0,03	0,02	0,12	0,18

(Continued)

Table 3.1 (Continued).

Bayuda province (Sudan)		Kakanui volcano (New Zealand)			Ukraine		Urals (Russia)		Ukraine		Urals (Russia)		
[Zack, Brumm, 1998], INAA								[Borisenko, Liapunov, 1980]					
	C59	C42	K2b	K4	K7	BL-1	BL-2		BL-3	BL-4	BL-5	BL-6	
Element	Pyroxenites		Peridotite Pl- bearing			Wehrlite	Pyroxenite (4)	Troctolite (2)	Gabbro (13)		Gabbro		
La	<0,02	0,0017	<0,01	0,004	0,009	0,05	0,15	0,14	0,18	0,24	0,80		
Ce	0,0081	0,016	<0,01	0,006	0,010	0,13	0,60	0,37	0,36	0,52	1,85		
Pr	<0,01	0,0033	<0,01	0,006	0,003	N.d.	N.d.	N.d.	N.d.	N.d.	N.d.		
Nd	<0,18	0,068	0,01	0,014	0,034	N.d.	N.d.	N.d.	N.d.	N.d.	N.d.		
Sm	<0,11	<0,05	0,012	0,007	0,002	0,012	0,20	0,18	0,071	0,11	0,59		
Eu	<0,03	0,0065	0,0077	0,002	0,005	0,003	0,084	0,072	0,020	0,039	0,16		
Gd	<0,13	<0,07	<0,10	0,014	0,028	N.d.	N.d.	N.d.	N.d.	N.d.	N.d.		
Tb	<0,05	<0,01	0,0086	0,005	0,007	0,036	0,39	0,055	0,038	0,031	0,083		
Dy	<0,09	<0,04	<0,07	0,022	0,053	N.d.	N.d.	N.d.	N.d.	N.d.	N.d.		
Ho	<0,02	N.d.	<0,01	0,002	0,011	N.d.	N.d.	N.d.	N.d.	N.d.	N.d.		
Er	N.d.	N.d.	N.d.	N.d.	N.d.	N.d.	N.d.	N.d.	N.d.	N.d.	N.d.		
Tm	<0,03	<0,01	0,0065	0,003	0,010	N.d.	N.d.	N.d.	N.d.	N.d.	N.d.		
Yb	<0,14	0,082	<0,04	0,025	0,050	0,56	0,059	0,075	1,49	0,18	0,14		
Lu	<0,03	<0,04	<0,02	0,013	0,006	0,15	0,021	0,019	0,38	0,053	0,028		
Total	0,66	0,38	0,26	0,126	0,228	N.d.	N.d.	N.d.	N.d.	N.d.	N.d.		
$(\text{La}/\text{Yb})_n$	<0,02	0,0017	0,13	0,11	0,12	0,06	1,72	1,26	0,08	0,90	3,86		

(Continued)

Table 3.1 (Continued).

Ukraine		Urals (Russia)		Ukraine		Urals (Russia)	Tigrovyy massif (Sikhote Alin', Primorie, Russia)				
		BL-7	BL-8	BL-9	BL-10	BL-11	BL-12	Gol-I	[Golubeva et al., 2007]	[Lesnov et al., 2004a], INAA	
Element	Gabbro (2)	Gabbro-norite (5)	Gabbro-anorthosite (3)	Gabbro-amphibolite (5)	Monzonite	Rapakivi granite	Schist (3)	Websterites	Sch-085c	Sch-095d	Sch-095D
<i>[Borisenko, Liapunov, 1980], RNAA</i>											
La	0,72	1,85	2,61	0,20	9,43	9,05	19,26	4,30	3,80	0,848	
Ce	1,53	3,52	4,85	0,40	21,6	18,9	36,30	7,20	5,70	1,772	
Pr	N.d.	N.d.	N.d.	N.d.	N.d.	N.d.	N.d.	N.d.	N.d.	0,252	
Nd	N.d.	N.d.	N.d.	N.d.	N.d.	N.d.	N.d.	4,50	3,00	1,037	
Sm	0,18	0,39	0,54	0,05	2,51	2,29	4,93	1,00	0,760	0,266	
Eu	0,024	0,046	0,060	0,005	0,20	0,06	0,730	0,230	0,130	0,144	
Gd	N.d.	N.d.	N.d.	N.d.	N.d.	N.d.	N.d.	N.d.	N.d.	0,271	
Tb	0,030	0,083	0,119	0,014	0,36	0,36	0,700	0,100	0,040	0,036	
Dy	N.d.	N.d.	N.d.	N.d.	N.d.	N.d.	N.d.	N.d.	N.d.	0,226	
Ho	N.d.	N.d.	N.d.	N.d.	N.d.	N.d.	N.d.	N.d.	N.d.	0,037	
Er	N.d.	N.d.	N.d.	N.d.	N.d.	N.d.	N.d.	N.d.	N.d.	0,121	
Tm	N.d.	N.d.	N.d.	N.d.	N.d.	N.d.	N.d.	N.d.	N.d.	0,024	
Yb	1,04	1,18	1,27	0,072	1,02	1,68	1,12	0,260	0,140	0,184	
Lu	0,34	0,34	0,35	0,014	0,24	0,22	0,160	0,036	0,025	0,032	
Total	N.d.	N.d.	N.d.	N.d.	N.d.	N.d.	N.d.	N.d.	N.d.	5,25	
$(\text{La}/\text{Yb})_n$	0,16	0,22	1,39	1,88	6,24	3,64	11,61	11,16	18,32	3,11	

(Continued)

Table 3.1 (Continued).

<i>Tigrovyy massif (Sikhote Alin', Russia)</i>								<i>Twin Peaks</i>	<i>Skaergaard massif</i>	
<i>[Lesnov et al., 2004a], INAA</i>								<i>[Nash, Crecraft, 1985]</i>	<i>[Paster et al., 1974]</i>	
	<i>Sch-084g</i>	<i>Sch-093g</i>	<i>Sch-095c</i>	<i>Sch-096c</i>	<i>Sch-93g (1a)</i>	<i>Sch-093g (1b)</i>	<i>Sch-093g (1c)</i>	<i>Sch-096C</i>	<i>Nash-I</i>	<i>4312</i>
<i>Element</i>	<i>Gabbro-norites</i>								<i>Rhyolites</i>	<i>Gabbro</i>
La	5,30	8,00	5,80	10,0	1,13	1,30	1,29	1,06	423	3,70
Ce	9,60	14,0	9,00	18,0	1,72	2,06	1,93	1,68	900	9,60
Pr	N.d.	N.d.	N.d.	N.d.	0,240	0,260	0,240	0,232	N.d.	N.d.
Nd	5,50	8,00	6,00	9,00	0,800	0,900	0,830	0,782	325	8,40
Sm	0,920	1,30	1,10	2,30	0,160	0,170	0,190	0,193	39,0	2,90
Eu	0,240	0,480	0,300	0,170	0,380	0,400	0,280	0,210	1,38	0,690
Gd	N.d.	N.d.	N.d.	N.d.	0,160	0,210	0,190	0,201	N.d.	2,90
Tb	0,120	0,130	0,100	0,180	0,020	0,020	0,020	0,037	3,80	0,450
Dy	N.d.	N.d.	N.d.	N.d.	0,210	0,240	0,240	0,226	19,5	N.d.
Ho	N.d.	N.d.	N.d.	N.d.	0,050	0,050	0,050	0,048	N.d.	0,440
Er	N.d.	N.d.	N.d.	N.d.	0,140	0,140	14,0	0,157	N.d.	N.d.
Tm	N.d.	N.d.	N.d.	N.d.	N.d.	N.d.	N.d.	0,028	N.d.	N.d.
Yb	0,500	0,280	0,290	0,260	0,160	0,190	0,170	0,217	11,9	1,09
Lu	0,080	0,058	0,056	0,050	0,020	0,020	0,020	0,042	1,66	N.d.
Total	N.d.	N.d.	N.d.	N.d.	5,19	5,96	19,45	5,11	N.d.	N.d.
(La/Yb) _n	7,15	19,29	13,50	25,96	4,77	4,62	5,12	3,29	24,0	3,70

(Continued)

Table 3.1 (Continued).

<i>Skaergaard massif (Greenland)</i>										
[Jang, Naslund, 2002], ICP-MS										
	Sk-783	Sk-782	Sk-776	Sk-795	Sk-797	Sk-813	Sk-815	Sk-778	Sk-50	Sk-51
<i>Element</i>	<i>Gabbros</i>									
La	0,36	0,39	0,23	0,27	0,24	0,38	0,33	0,37	0,27	0,31
Ce	0,79	0,94	0,47	0,59	0,40	0,65	0,50	0,62	0,44	0,47
Pr	0,11	0,12	0,05	0,07	0,05	0,07	0,09	0,09	0,05	0,06
Nd	0,59	0,69	0,21	0,36	0,24	0,36	0,32	0,34	0,31	0,21
Sm	0,16	0,16	0,06	0,11	0,05	0,09	0,07	0,10	0,08	0,09
Eu	0,05	0,05	0,03	0,03	0,03	0,04	0,03	0,04	0,03	0,03
Gd	0,18	0,19	0,08	0,12	0,08	0,11	0,09	0,10	0,12	0,12
Tb	0,04	0,04	0,02	0,03	0,02	0,03	0,02	0,02	0,03	0,02
Dy	0,29	0,27	0,13	0,19	0,16	0,21	0,13	0,15	0,18	0,15
Ho	0,07	0,07	0,04	0,05	0,05	0,06	0,03	0,04	0,04	0,06
Er	0,39	0,35	0,21	0,26	0,26	0,35	0,19	0,21	0,22	0,26
Tm	0,10	0,08	0,05	0,06	0,06	0,07	0,04	0,05	0,05	0,07
Yb	0,82	0,81	0,44	0,51	0,52	0,58	0,37	0,45	0,48	0,46
Lu	0,21	0,20	0,09	0,12	0,11	0,12	0,08	0,10	0,13	0,13
Total	4,16	4,36	2,11	2,77	2,27	3,12	2,29	2,68	2,43	2,44
(La/Yb) _n	0,30	0,32	0,35	0,36	0,31	0,44	0,60	0,55	0,38	0,45
(Eu/Eu*) _n	0,90	0,88	1,32	0,79	1,44	1,23	1,16	1,21	0,93	0,88

(Continued)

Table 3.1 (Continued).

<i>Skaergaard massif (Greenland)</i>										
[Jang, Naslund, 2002], ICP-MS										
	Sk-296	Sk-281	Sk-63	Sk-769	Sk-772	Sk-773	Sk-830	Sk-831	Sk-833	Sk-806
<i>Element</i>	<i>Gabbros</i>									
La	0,27	0,27	0,27	0,28	0,37	0,38	0,40	0,43	0,53	0,31
Ce	0,38	0,40	0,41	0,47	0,58	0,62	0,91	1,02	1,12	0,63
Pr	0,05	0,05	0,06	0,07	0,08	0,09	0,12	0,15	0,17	0,09
Nd	0,23	0,23	0,33	0,33	0,35	0,37	0,68	0,87	0,92	0,59
Sm	0,06	0,06	0,08	0,06	0,09	0,10	0,19	0,22	0,25	0,14
Eu	0,02	0,02	0,04	0,02	0,03	0,03	0,06	0,08	0,09	0,04
Gd	0,08	0,11	0,14	0,09	0,14	0,10	0,22	0,26	0,30	0,17
Tb	0,02	0,02	0,03	0,02	0,03	0,02	0,04	0,04	0,06	0,04
Dy	0,11	0,17	0,12	0,23	0,21	0,21	0,32	0,35	0,43	0,27
Ho	0,04	0,04	0,06	0,04	0,06	0,06	0,07	0,09	0,11	0,07
Er	0,20	0,25	0,43	0,23	0,35	0,35	0,33	0,42	0,53	0,43
Tm	0,04	0,05	0,09	0,06	0,08	0,08	0,08	0,08	0,11	0,10
Yb	0,35	0,45	0,41	0,81	0,58	0,71	0,69	0,69	0,84	0,81
Lu	0,09	0,11	0,18	0,11	0,16	0,16	0,17	0,18	0,20	0,20
Total	1,94	2,23	2,65	2,82	3,11	3,28	4,28	4,88	5,66	3,89
(La/Yb) _n	0,52	0,40	0,44	0,23	0,43	0,36	0,39	0,42	0,43	0,26
(Eu/Eu*) _n	0,88	0,74	1,14	0,83	0,81	0,91	0,90	1,02	1,00	0,79

(Continued)

Table 3.1 (Continued).

<i>Skaergaard massif (Greenland)</i>											
	[Jang, Naslund, 2002], ICP-MS										
	Sk-805	Sk-803	Sk-802	Sk-801	Sk-800	Sk-107	Sk-110	Sk-753	Sk-755	Sk-756	Sk-757
<i>Element</i>	<i>Gabbros</i>										
La	0,32	0,31	0,24	0,23	0,79	0,27	0,30	0,28	0,32	0,27	0,58
Ce	0,70	0,61	0,50	0,55	1,77	0,49	0,68	0,65	0,66	0,75	1,19
Pr	0,10	0,07	0,07	0,06	0,25	0,07	0,08	0,08	0,09	0,09	0,19
Nd	0,54	0,45	0,31	0,28	1,27	0,29	0,45	0,40	0,33	0,48	0,89
Sm	0,14	0,13	0,08	0,07	0,36	0,10	0,12	0,11	0,10	0,12	0,26
Eu	0,04	0,04	0,03	0,03	0,12	0,03	0,05	0,05	0,05	0,05	0,09
Gd	0,16	0,11	0,09	0,10	0,41	0,09	0,12	0,13	0,14	0,16	0,33
Tb	0,03	0,03	0,02	0,02	0,09	0,02	0,03	0,03	0,04	0,04	0,07
Dy	0,27	0,22	0,18	0,20	0,63	0,15	0,20	0,32	0,22	0,28	0,49
Ho	0,11	0,07	0,05	0,07	0,20	0,04	0,09	0,07	0,07	0,08	0,15
Er	0,38	0,30	0,26	0,34	0,96	0,25	0,36	0,35	0,38	0,46	0,76
Tm	0,09	0,07	0,06	0,08	0,22	0,06	0,09	0,08	0,10	0,09	0,17
Yb	0,64	0,53	0,63	0,74	1,59	0,61	0,60	0,56	0,59	0,89	1,29
Lu	0,18	0,14	0,12	0,15	0,39	0,12	0,19	0,19	0,15	0,20	0,33
Total	3,70	3,08	2,64	2,92	9,05	2,59	3,36	3,30	3,24	3,96	6,79
$(La/Yb)_n$	0,34	0,39	0,26	0,21	0,34	0,30	0,34	0,34	0,37	0,20	0,30
$(Eu/Eu^*)_n$	0,81	1,00	1,08	1,10	0,95	0,95	1,26	1,28	1,29	1,10	0,94

(Continued)

Table 3.1 (Continued).

<i>Yakutia (Russia)</i>										
	<i>Aykhal pipe</i>						<i>Komsomol'skaya pipe</i>			
	[Ashcepkov et al., 2007], LA ICP-MS									
	Ay-1	Ay-2	Ay-4	Ay-9	Ay-10	Ay-11	Ay-22	Koms-1	Koms-2	Koms-3
<i>Element</i>	<i>Kimberlites</i>									
La	4,98	4,96	17,69	0,44	0,0027	0,32	0,30	0,087	0,35	0,94
Ce	10,58	7,42	28,99	0,76	0,0083	0,51	0,56	0,053	0,56	2,17
Pr	1,16	0,79	2,95	0,047	0,0006	0,052	0,041	0,011	0,045	0,12
Nd	4,02	3,04	12,21	0,20	0,0024	0,17	0,15	0,05	0,18	0,45
Sm	0,67	0,44	1,79	0,037	0,0008	0,027	0,02	0,032	0,028	0,102
Eu	0,15	0,099	0,40	0,0085	0,0003	0,0066	0,0066	0,002	0,008	0,015
Gd	0,42	0,28	1,16	0,032	0,0013	0,023	0,023	0,004	0,014	0,036
Tb	0,042	0,027	0,11	0,0038	0,0003	0,0021	0,003	0,0004	0,002	0,004
Dy	0,20	0,12	0,50	0,022	0,0014	0,012	0,018	0,004	0,011	0,023
Ho	0,025	0,017	0,068	0,004	0,0004	0,0019	0,0026	0,002	0,003	0,005
Er	0,053	0,036	0,14	0,01	0,0013	0,0071	0,0079	0,005	0,016	0,009
Tm	0,0048	0,0031	0,013	0,0017	0,0001	0,0009	0,0012	0,0008	0,001	0,001
Yb	0,026	0,017	0,070	0,01	0,0011	0,007	0,0066	0,012	0,008	0,012
Lu	0,0031	0,0017	0,007	0,0014	0,0001	0,001	0,0013	0,001	0,002	0,001
Total	22,32	16,86	64,11	1,57	0,02	1,15	1,13	0,26	1,23	3,88
(La/Yb) _n	128,2	178,1	171,5	29,65	1,60	30,62	30,87	4,89	29,78	52,7

(Continued)

Table 3.1 (Continued).

	Yakutia (Russia)										
	Sytykanskaya pipe					Yubileynaya pipe					
	[Aschepkov et al., 2007], LA ICP-MS										
	Syt-01	Syt-06	Syt-07	Syt-09	Syt-10	Syt-11	Syt-12	Syt-13	Yub-1	Yub-2	Yub-3
Element	Kimberlites										
La	4,53	17,59	0,13	0,0085	0,011	0,0012	69,98	67,26	0,037	0,021	0,0026
Ce	9,31	28,98	0,83	0,015	0,023	0,078	74,52	77,86	0,043	0,042	0,0066
Pr	1,28	2,12	0,049	0,0057	0,0018	0,0076	5,70	7,33	0,0080	0,0052	0,0014
Nd	5,72	9,13	0,26	0,057	0,0089	0,049	18,7	26,17	0,062	0,043	0,010
Sm	0,67	1,13	0,072	0,026	0,0065	0,016	2,36	3,24	0,056	0,030	0,017
Eu	0,13	0,29	0,016	0,0073	0,0029	0,0033	0,58	3,95	0,035	0,011	0,012
Gd	0,24	0,61	0,058	0,014	0,024	0,021	1,68	2,32	0,071	0,045	0,022
Tb	0,028	0,091	0,0067	0,0039	0,0039	0,0087	0,19	0,23	0,016	0,0051	0,0031
Dy	0,15	0,39	0,040	0,041	0,029	0,021	0,99	1,00	0,072	0,026	0,016
Ho	0,027	0,049	0,0085	0,013	0,0052	0,0031	0,17	0,13	0,011	0,0031	0,0024
Er	0,078	0,11	0,024	0,012	0,016	0,019	0,41	0,27	0,034	0,0059	0,0030
Tm	0,0090	0,026	0,0027	0,0045	0,0031	0,0080	0,063	0,026	0,0044	0,0009	0,0006
Yb	0,098	0,10	0,032	0,026	0,034	0,022	0,45	0,095	0,017	0,015	0,012
Lu	0,022	0,017	0,0053	0,0073	0,0066	0,0052	0,050	0,016	0,0047	0,0067	0,0042
Total	22,30	60,64	1,53	0,24	0,18	0,27	175,9	189,9	0,47	0,26	0,11
(La/Yb) _n	31,24	114,17	2,74	0,22	0,22	0,37	104,6	476,9	1,43	0,93	0,14

(Continued)

Table 3.1 (Continued).

Yakutia (Russia)												
	Ozernaya pipe						Zarnitsa pipe		Ukrainskaya pipe			
	[Aschepkov et al., 2007], LA ICP-MS											
	Oz-15	Oz-16	Oz-17	Oz-18	Oz-19	Oz-20	Zrn-12	Zrn-13	Ukr-3	Ukr-4	Ukr-5	Ukr-6
Element	Kimberlites											
La	0,17	0,56	17,14	0,051	18,72	0,084	10,10	28,57	1,54	6,93	3,51	8,81
Ce	0,15	0,92	34,84	0,12	31,79	0,19	12,62	63,36	2,26	9,75	6,65	13,52
Pr	0,022	0,12	3,54	0,027	2,72	0,032	1,35	3,75	0,25	1,31	0,75	2,42
Nd	0,22	0,32	14,30	0,29	10,42	0,17	5,15	17,74	0,93	0,48	1,73	7,38
Sm	0,074	0,11	2,51	0,065	0,77	0,088	0,76	4,01	0,094	1,15	0,26	0,86
Eu	0,037	0,028	0,691	0,036	0,093	0,034	0,63	0,49	0,03	0,25	0,12	0,25
Gd	0,13	0,13	1,19	0,13	0,37	0,16	0,51	1,21	0,067	0,64	0,20	0,73
Tb	0,022	0,017	0,19	0,020	0,040	0,015	0,040	0,15	0,0060	0,089	0,014	0,02
Dy	0,11	0,11	0,94	0,097	0,19	0,085	0,24	0,59	0,050	0,33	0,10	0,32
Ho	0,023	0,026	0,20	0,017	0,028	0,020	0,038	0,089	0,0068	0,048	0,020	0,051
Er	0,063	0,10	0,38	0,038	0,096	0,038	0,16	0,29	0,021	0,13	0,049	0,20
Tm	0,0076	0,023	0,051	0,0054	0,021	0,0095	0,022	0,075	0,0059	0,019	0,0074	0,024
Yb	0,057	0,17	0,37	0,038	0,13	0,083	0,073	0,57	0,019	0,063	0,046	0,067
Lu	0,024	0,021	0,031	0,0047	0,042	0,0070	0,0094	0,070	0,0033	0,010	0,0057	0,0090
Total	1,12	2,67	76,38	0,93	65,42	1,02	31,69	120,9	5,69	26,08	13,45	34,72
(La/Yb) _n	2,08	2,22	31,33	0,91	99,72	0,68	93,07	34,12	54,65	74,84	51,16	89,11

(Continued)

Table 3.1 (Continued).

Yakutia (Russia)												
	Festival'naya pipe						Dal'naya pipe				Udachnaya pipe	
Element	[Aschepkov et al., 2007], LA ICP-MS											
	Fest-8	Fest-9	Fest-10	Fest-11	Fest-12	Fest-13	Daln-11	Daln-12	Daln-13	Daln-14	Ud-1402	Ud-1293
Kimberlites												
La	3,13	3,00	0,81	0,038	1,91	0,020	0,023	0,032	0,033	0,075	0,45	0,013
Ce	2,80	4,81	1,63	0,051	3,15	0,059	0,074	0,038	0,066	0,079	0,39	0,040
Pr	0,22	0,80	0,12	0,0069	0,52	0,0098	0,015	0,0056	0,012	0,0085	0,038	0,0050
Nd	0,76	2,33	0,38	0,028	1,17	0,037	0,079	0,041	0,11	0,065	0,16	0,018
Sm	0,15	0,49	0,083	0,026	0,22	0,029	0,032	0,018	0,047	0,030	0,027	0,0050
Eu	0,017	0,12	0,018	0,0001	0,076	0,0083	0,014	0,0083	0,019	0,015	0,010	0,0020
Gd	0,13	0,31	0,031	0,0078	0,16	0,036	0,032	0,029	0,076	0,054	0,033	0,0080
Tb	0,013	0,067	0,0084	0,0006	0,026	0,0022	0,0048	0,0052	0,010	0,0071	0,0070	0,0030
Dy	0,068	0,47	0,044	0,0054	0,13	0,0066	0,027	0,0167	0,025	0,032	0,036	0,024
Ho	0,019	0,085	0,010	0,0006	0,019	0,0019	0,0045	0,0036	0,0064	0,0068	0,0070	0,0040
Er	0,069	0,24	0,015	0,0018	0,052	0,0076	0,012	0,0090	0,017	0,022	0,033	0,017
Tm	0,012	0,036	0,0018	0,0003	0,0072	0,0015	0,0036	0,0016	0,0039	0,0049	0,0030	0,0020
Yb	0,084	0,21	0,029	0,0021	0,048	0,014	0,035	0,012	0,039	0,041	0,024	0,022
Lu	0,011	0,027	0,0035	0,0005	0,0058	0,0045	0,0056	0,0029	0,043	0,017	0,0040	0,0040
Total	7,49	13,0	3,18	0,17	7,49	0,42	0,36	0,22	0,50	0,46	1,22	0,17
(La/Yb) _n	25,06	9,55	18,74	12,07	26,89	9,89	0,44	1,85	0,57	1,26	12,63	0,40

(Continued)

Table 3.1 (Continued).

Yakutia (Russia)												
	Udachnaya pipe					Mir pipe						
	[Aschepkov et al., 2007], LA ICP-MS											
	Ud-1504	Ud-1240	Ud-1506	Ud-1505	Ud-1507	Mir-9	Mir-13d	Mir-23	Mir-26	Mir-29	Mir-13	Mir-13a
Element	Kimberlites											
La	0,12	0,28	0,077	0,0010	0,0040	1,54	42,75	0,53	0,020	0,0020	25,28	23,92
Ce	0,12	0,32	0,016	0,0090	0,017	1,74	68,58	0,46	0,16	0,018	33,20	32,13
Pr	0,012	0,032	0,0020	0,0020	0,0017	0,17	8,08	0,042	0,017	0,0020	3,50	3,45
Nd	0,040	0,18	0,13	0,19	0,0040	0,69	30,52	0,15	0,075	0,010	13,08	13,49
Sm	0,010	0,027	0,0050	0,0040	0,0010	0,093	4,38	0,019	0,024	0,012	1,88	1,85
Eu	0,0040	0,013	0,0020	0,0010	0,0005	0,020	0,99	0,0070	0,011	0,0030	0,38	0,40
Gd	0,015	0,051	0,011	0,0060	0,0030	0,091	2,95	0,024	0,016	0,0090	1,31	1,44
Tb	0,0035	0,010	0,0020	0,0030	0,0010	0,012	0,26	0,0040	0,0020	0,0020	0,14	0,14
Dy	0,036	0,040	0,022	0,022	0,014	0,068	1,12	0,027	0,016	0,031	0,64	0,64
Ho	0,0060	0,0090	0,0040	0,0040	0,0030	0,014	0,15	0,0060	0,0050	0,0060	0,093	0,15
Er	0,019	0,026	0,017	0,012	0,012	0,036	0,037	0,016	0,012	0,019	0,22	0,22
Tm	0,0030	0,0040	0,0030	0,0030	0,0020	0,0060	0,033	0,0040	0,0030	0,0030	0,024	0,024
Yb	0,0022	0,037	0,015	0,019	0,010	0,038	0,18	0,022	0,017	0,025	0,15	0,15
Lu	0,0040	0,0060	0,0030	0,0030	0,0030	0,0090	0,019	0,0040	0,0040	0,0030	0,019	0,019
Total	0,41	1,04	0,19	0,11	0,08	4,53	160,4	1,30	0,38	0,15	79,91	77,98
(La/Yb) _n	3,53	5,14	3,46	0,04	0,27	27,41	154,4	16,17	0,79	0,05	116,9	107,7

(Continued)

Table 3.1 (Continued).

Yakutia (Russia)										
	Internatsional'naya pipe					Nurbinskaya pipe				
	[Aschepkov et al., 2007], LA ICP-MS									
	Int-16	Int-19	Int-21	Int-22	Int-27	Int-28	Nur-1	Nur-2	Nur-3	Nur-4
Element	Kimberlites									
La	0,016	0,0040	0,024	0,27	0,0020	0,010	0,15	0,11	74,17	5,83
Ce	0,034	0,0070	0,032	0,30	0,017	0,014	0,15	0,040	132,7	10,13
Pr	0,0040	0,0035	0,0063	0,024	0,0020	0,0050	0,0034	0,025	16,01	1,05
Nd	0,021	0,024	0,035	0,095	0,021	0,029	0,048	0,0048	59,0	3,68
Sm	0,030	0,035	0,016	0,027	0,0018	0,020	0,0062	0,019	8,00	0,48
Eu	0,012	0,017	0,0084	0,0094	0,0090	0,0060	0,0099	0,0040	1,59	0,11
Gd	0,066	0,086	0,039	0,045	0,020	0,015	0,012	0,0057	3,98	0,35
Tb	0,013	0,015	0,012	0,010	0,013	0,012	0,014	0,0021	0,40	0,031
Dy	0,070	0,083	0,088	0,094	0,082	0,076	0,020	0,0076	1,71	0,18
Ho	0,014	N.d.	0,015	0,016	0,015	0,016	0,010	0,0017	0,22	0,024
Er	0,037	0,031	0,025	0,034	0,029	0,029	0,035	0,0051	0,40	0,069
Tm	0,0049	0,0041	0,0032	0,0041	0,0071	0,0061	0,0093	0,0014	0,037	0,0093
Yb	0,030	0,020	0,018	0,026	0,032	0,034	0,042	0,0067	0,18	0,047
Lu	0,0035	0,0040	0,0030	0,0040	0,0030	0,0040	0,011	0,0024	0,026	0,0082
Total	0,36	0,33	0,32	0,95	0,25	0,28	0,25	0,23	298,5	21,99
(La/Yb) _n	0,36	0,13	0,90	7,01	0,04	0,20	0,25	10,54	284,7	83,10

(Continued)

Table 3.1 (Continued).

Yakutia (Russia)										
	Nurbinskaya pipe		Novinka pipe	Trudovaya pipe						
Element	Nur-5	Nur-7	Nov-1	Tru-02	Tru-03	Tru-04	Tru-07	Tru-08	Tru-11	Tru-12
<i>[Aschepkov et al., 2007], LA ICP-MS</i>										
La	0,13	0,62	0,057	1,17	0,11	0,093	0,41	0,14	25,64	13,07
Ce	0,25	0,88	0,13	2,65	0,23	0,17	0,48	0,15	42,85	39,06
Pr	0,017	0,10	0,017	0,24	0,024	0,016	0,067	0,034	4,58	5,51
Nd	0,045	0,20	0,051	0,59	0,12	0,056	0,20	0,072	15,83	13,95
Sm	0,012	0,036	0,020	0,11	0,012	0,010	0,077	0,011	1,97	1,86
Eu	0,0057	0,013	0,0050	0,027	0,0029	0,0042	0,013	0,0043	0,38	0,33
Gd	0,014	0,027	0,011	0,066	0,0086	0,012	0,038	0,018	1,00	1,18
Tb	0,0017	0,0040	0,0020	0,012	0,0016	0,0019	0,0053	0,0025	0,097	0,090
Dy	0,0060	0,025	0,0080	0,056	0,011	0,0095	0,026	0,011	0,43	0,41
Ho	0,0014	0,0061	0,0020	0,012	0,025	0,0016	0,0063	0,0016	0,055	0,046
Er	0,0038	0,017	0,0045	0,031	0,0060	0,0045	0,018	0,0039	0,088	0,10
Tm	0,0026	0,0022	0,0010	0,0037	0,0009	0,0005	0,0027	0,0006	0,010	0,0087
Yb	0,014	0,011	0,010	0,026	0,013	0,0039	0,018	0,0065	0,063	0,059
Lu	0,0027	0,0006	0,0013	0,0043	0,0029	0,0006	0,0040	0,0011	0,0092	0,0083
Total	0,51	1,95	0,32	4,99	0,54	0,39	1,37	0,46	93,02	75,70
(La/Yb) _n	6,65	38,71	3,85	30,69	5,53	16,35	15,80	14,79	276,7	150,37

(Continued)

Table 3.1 (Continued).

Yakutia (Russia)										
	Trudovaya pipe		Nebaybit pipe					Khardakh pipe		
	[Aschepkov et al., 2007], LA ICP-MS									
	Tru-18	Tru-20	Neb-2	Neb-3	Neb-4	Neb-5	Neb-6	Neb-7	Khd-18	Khd-19
Element	Kimberlites									
La	0,75	0,17	0,076	10,82	0,053	0,026	0,025	0,32	19,90	4,15
Ce	1,94	0,55	0,34	18,53	0,15	0,047	0,082	0,48	37,41	7,33
Pr	0,21	0,090	0,21	2,07	0,10	0,027	0,075	0,068	4,45	0,77
Nd	1,00	0,19	1,22	4,62	0,76	1,11	0,55	0,29	13,66	2,79
Sm	0,12	0,032	0,25	1,250	0,17	0,20	0,17	0,12	2,10	1,01
Eu	0,034	0,011	0,064	0,047	0,017	0,049	0,028	0,041	0,49	0,20
Gd	0,048	0,028	0,011	1,37	0,026	0,10	0,077	0,077	1,71	0,61
Tb	0,0058	0,0019	0,013	0,18	0,0033	0,014	0,012	0,019	0,23	0,11
Dy	0,021	0,0096	0,037	1,17	0,015	0,053	0,065	0,021	0,88	0,77
Ho	0,0054	0,0030	0,0078	0,26	0,0039	0,011	0,015	0,0037	0,13	0,19
Er	0,017	0,012	0,031	0,70	0,0220	0,043	0,027	0,010	0,33	0,65
Tm	0,0021	0,0014	0,0062	0,066	0,0033	0,0063	0,0038	0,0018	0,031	0,14
Yb	0,014	0,0091	0,061	0,67	0,029	0,077	0,018	0,023	0,24	1,23
Lu	0,0021	0,0009	0,0013	0,10	0,0033	0,012	0,0017	0,0066	0,030	0,20
Total	4,16	1,11	2,42	42,28	1,35	0,77	1,14	1,48	80,59	20,15
(La/Yb) _n	36,05	12,78	0,84	10,87	5,53	0,23	0,93	9,43	53,82	2,27

Note: The analyses Sch-0959D, Sch-93 g(1a), Sch-093 g(1b), Sch-093 g(1c), and Sch-096C in addition were done by method ICP-MS; analyses Asch-6, and Asch-7 – by method LA ICP-MS; analyses VII-34/2, 4312, and Nash-1 – by INAA method. In brackets – number of analyses for calculation of average rock compositions. The ilmenites from Yakutian pipes (data [Aschepkov et al., 2007]) were done using megacrysts from heavy mineral separates of kimberlites.

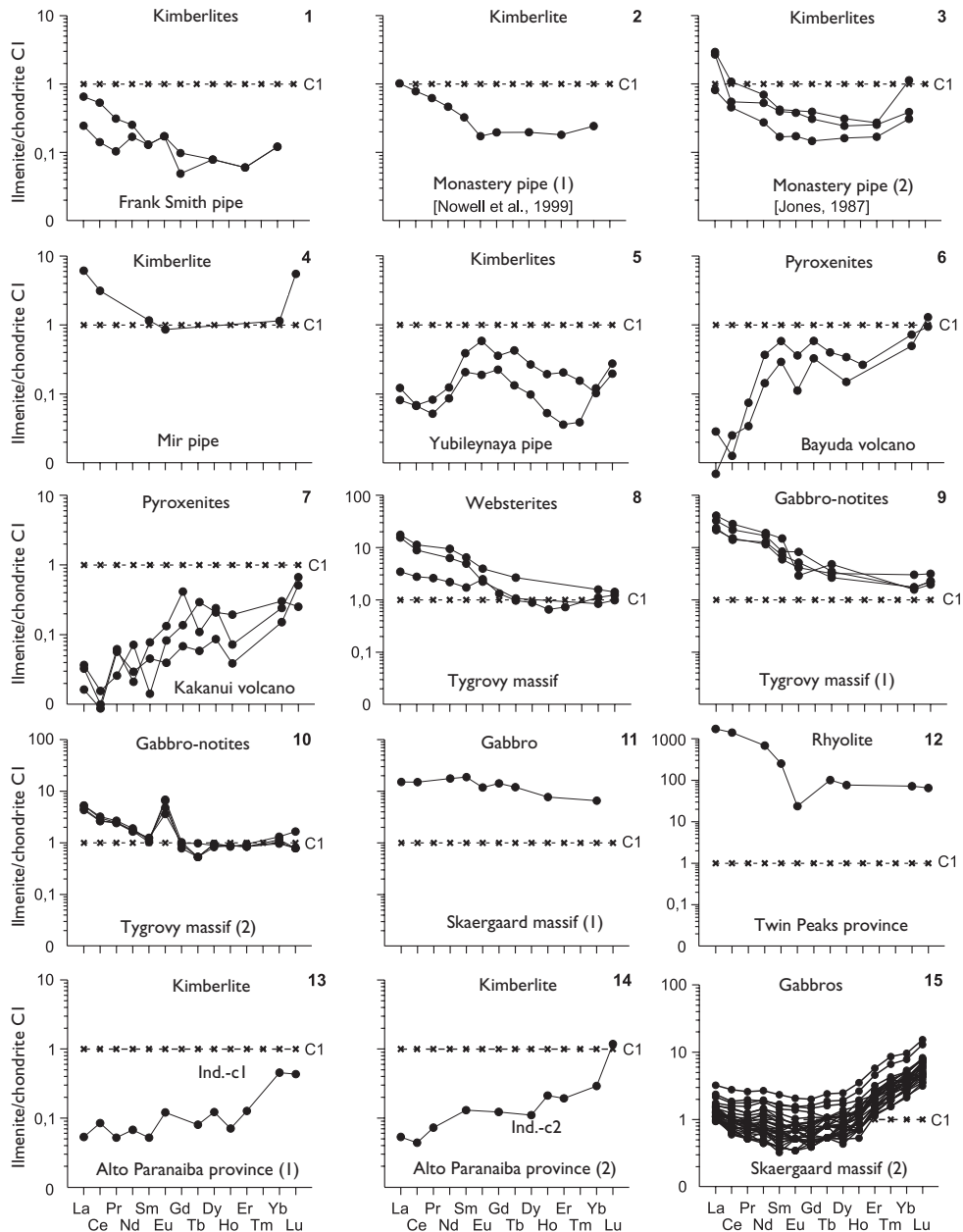


Figure 3.1 Chondrite-normalized REE patterns for ilmenites from some rocks (data Table 3.1).
1–5 – phenocrysts, 6–15 – accessory grains.

Table 3.2 Chemical compositions of ilmenites from gabbro-norites and websterites from Tigrovyy massif (Primorie province, Russia) (wt%).

	Sch-093g	Sch-095c	Sch-096c	Sch-085c	Sch-095d
Component	Gabbro-norites			Websterites	
TiO ₂	52,84	47,80	50,53	48,15	47,09
Al ₂ O ₃	0,04	N.d.	0,01	0,06	0,01
Cr ₂ O ₃	N.d.	N.d.	N.d.	0,23	0,13
FeO _{tot}	46,41	47,45	49,24	49,53	49,05
MgO	N.d.	0,07	N.d.	N.d.	N.d.
MnO	1,06	1,36	0,69	1,60	1,56
CaO	0,01	0,37	N.d.	N.d.	0,01
Na ₂ O	N.d.	0,01	N.d.	N.d.	N.d.
K ₂ O	N.d.	0,04	N.d.	N.d.	N.d.
Total	100,36	97,10	100,47	99,57	97,85

Note: Microprobe analyses were done in the Institute of volcanology and seismology, Far East Branch of RAS, Petropavlovsk Kamchatsky (data V. Rybalko).

phases. It is obvious that in these two silicate phases during the crystallization have focused the vast majority of available Eu in parent melt. Therefore, the residual portion of the latter, which then became the material of crystallization of ilmenite, should be exhausted with respect to Eu, so its excess in this ilmenite was not supposed to take place. Considering the possible causes of the observed positive Eu anomalies in these ilmenites, one would assume that they are caused by the presence of some amounts of micro-inclusions of plagioclase in their grains. However, the phase X-ray analysis of these ilmenites had shown, that the admixture of plagioclase has not been detected. Thus, the reason for the positive Eu anomalies in the patterns of these ilmenites has not been ascertained yet. What is more, a very intense negative Eu anomaly was found on the spectrum of ilmenite from the rhyolite, which is characterized by very high concentrations of REE (Figure 3.1, 12).

According to the analysis of ilmenites of kimberlites from Indaia manifestation (Alto Paranaiba province, Brazil) it was ascertained that the overall level of accumulation of REE in them is significantly lower than in C1 chondrite, while the chondrite-normalized contents of HREE in them is higher than the content of LREE (Figure 3.1, 13, 14).

Judging by the configuration of REE pattern, all the researched ilmenites from gabbros of Skaergaard massif demonstrate a slight enrichment with LREE and a more significant enrichment with HREE compared with the MREE, and many of these patterns show very weak positive or negative Eu anomalies (Figure 3.1, 15).

Aschepkov *et al.* [2007] investigated the REE composition of great collections of ilmenite megacrystals from 50 pipes from six regions of the kimberlite magmatism in Yakutia (Russia). In this work it was shown that ilmenites from the researched kimberlite pipes both as a whole and from each of the pipe are characterized by very wide variations of REE composition, as can be seen both in the total content of elements and the configuration and slope of their distribution (Table 3.1, Figure 3.2). Thus, the total

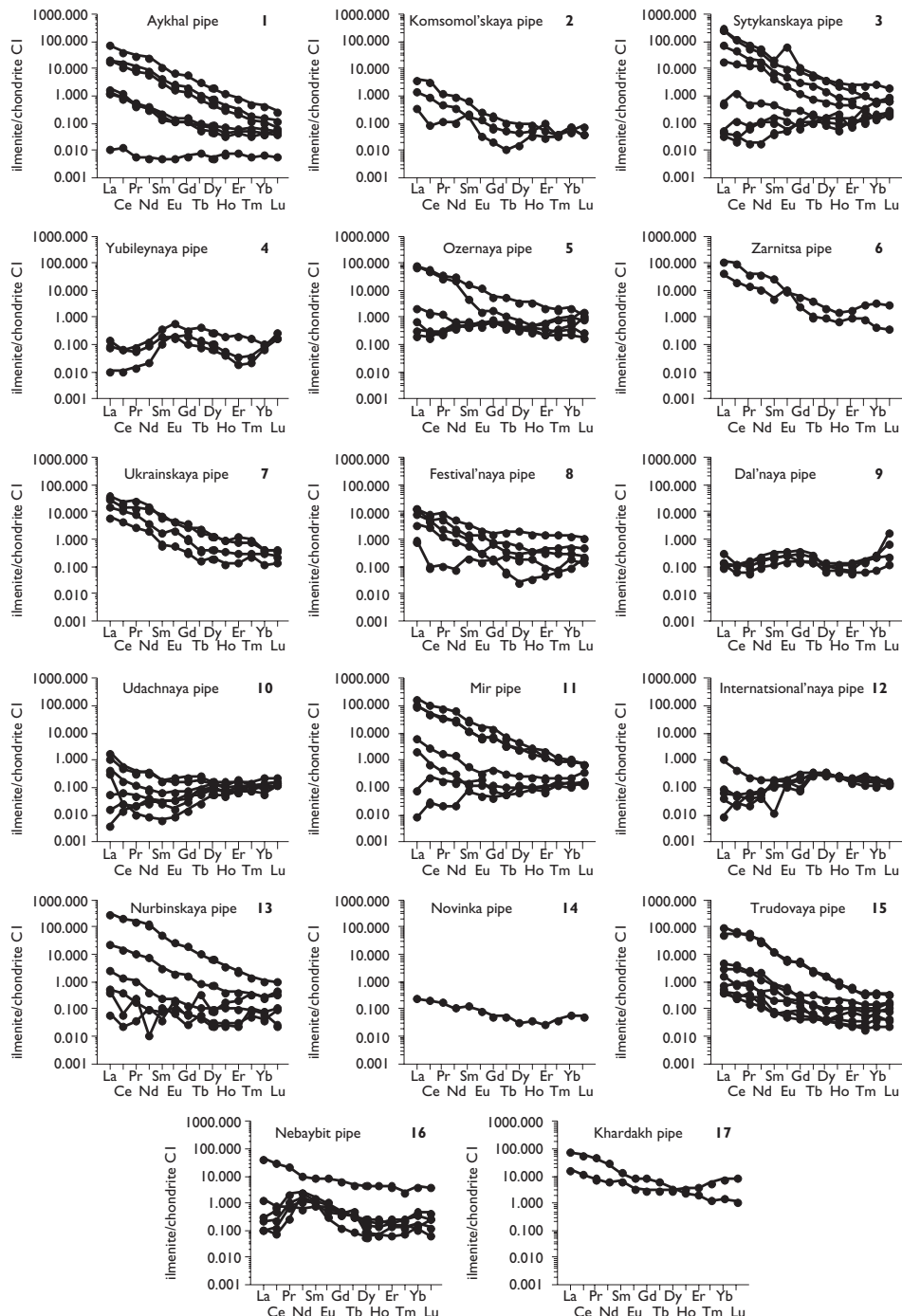


Figure 3.2 Chondrite-normalized REE patterns for ilmenites from heavy fractions of kimberlites from some pipes of Yakutian province (Russia) (data Table 3.1).

REE content within this entire collection of the ilmenite samples ranged from 0.02 to 298 ppm, and values $(\text{La/Yb})_n$ – from 0.04 to 477. The highest average total REE content, as well as the increased values of the parameter $(\text{La/Yb})_n$ define ilmenites from Ozernaya, Zarnitsa, Mir, International'naya and Khardakh pipes. The overwhelming majority of the patterns of ilmenites from this collection have a negative slope. The patterns of ilmenites from Yubileynaya, Dal'naya and Nebaybit pipes have a specific sinusoidal configuration, which is comparable to one that is typical for the patterns of already described garnets from diamond-bearing parageneses. Note that all the analyzed ilmenites from Komsomolskaya, Yubileynaya, Zarnitsa, Ukrainskaya, Dal'naya and Trudovaya kimberlite pipes are almost identical, both in configuration and in slope of REE patterns. Contrasting to them, the patterns of the ilmenites from Aykhal and Udachnaya pipes and especially from Sytykanskaya, Mir and Nurbinskaya pipes are characterized by significant variations in the shape and slope angle, especially in the LREE area. Based on data on concentrations of LREE, the ilmenites from these kimberlite pipes can be divided into two groups: 1) with a moderate amount of LREE, and 2) dramatically increased content of LREE. As we assume, in those samples of ilmenite, which proved to be anomalously enriched with LREE, a significant portion of these elements might be presented not as an isomorphous (structural) impurity, but in the form of unstructured impurity, localized in the microcracks of ilmenite crystals, as well as in solid or fluid microinclusions.

In generalizing the data on representative samples of kimberlites analyses in order to identify the correlations between the contents of petrogenic components and REE, it has been shown that in these rocks between the contents of TiO_2 and FeO , on the one hand, and the HREE, on the other hand, there is a directly proportional dependence [Lesnov, 2002, 2003b; Vasilenko *et al.*, 2003]. Proceeding from the fact that both of these major kimberlite components are mainly concentrated in accessory segregations and phenocrystals of picroilmenite, it was suggested that picroilmenites accumulate mainly the HREE in their structure (Table 3.1). This assumption was later confirmed by the analysis of picroilmenite phenocrystal from Mir kimberlite pipe by using INAA method [Melgunov & Lesnov, 2003]. In addition to the REE in this picroilmenite phenocrystal there have been found elements in form of impurity such as (ppm): Hf (28.8), Ta (351), Sc (45.2), Co (207), Cr (14789) and Zn (176). The ilmenites are known to accumulate rather significant amounts of Zr in their structure. Thus, in some of their samples from alkaline mafic rocks the content of this element reaches 3850 ppm [Pearce, 1990]. The average content of Zr in ilmenites of gabbro from Skaergaard massif is 485 ppm [Jang & Naslund, 2002]. It was also noted that the average content of Zr in the accessory ilmenites consistently decreases in the sequence from mafic rocks to rocks rich in silicon [Bea *et al.*, 2006]. In this regard, it is important to mention that in the grains of accessory ilmenites from anorthosite rocks of Eastern Canada complexes there were discovered rim width from 1 to 100 microns, formed by microsegregations of zircon [Morisset & Scoates, 2008]. Taking into account these observations we can assume that such rims consisting of microsegregations of zircon might be present also around grains of accessory ilmenite and in other rock complexes, and that they were not identified because of their submicroscopic size. Given the fact that the structure of zircon, as it will be shown in the following chapter, is very favorable for the accumulation of REE, especially heavy items, we can assume that the observed uneven enrichment with REE

ascertained in some studied ilmenites is due to the presence around their grain and in their microcracks of very narrow zones, which are composed of submicroscopic segregations of later zircon.

3.2 COEFFICIENTS OF REE DISTRIBUTION BETWEEN ILMENITE AND COEXISTING PHASES

As of today there are limited data on estimation of the K_d (REE) between ilmenites and coexisting phases, including the melts (Table 3.3). Thus, in experiments using ilmenites from garnet pyroxenite it was determined that the values of K_d (ilmenite/melt) successively increase from La (~0.00003) to Yb (0.2) and then slightly decrease towards Lu (0.1) [Zack & Brumm, 1998] (Figure 3.3 and 3.4, 1). A similar trend in the values of these K_d from light to HREE was ascertained in the course of another experiment, but in this case the obtained values were slightly different: from 0.0072 – for La to 0.029 – for Lu [Nielsen *et al.*, 1992] (Figure 3.4, 2). Based on the results of the determination of REE composition of ilmenites from Skaergaard massif (Table 3.1), it was found that the average K_d (ilmenite/melt) decreases in the sequence from La to Sm, and then slightly increases in the sequence from Sm to Lu (Figure 3.4, 3). These data are consistent with available information on the strong positive correlation between contents of HREE and contents of FeO_{tot} and TiO_2 in ilmenites (Lesnov, 2010).

Using experimental data, it was found that the values of K_d (ilmenite/clinopyroxene) for La (~0.00054) and Ce (0.00063) by nearly three orders of magnitude are smaller than those for Tm (0.22), Yb (0.40) and Lu (0.19) (Table 3.3). On this basis we can assume that the contents of HREE in ilmenites might be approximately 20–40% of their amount in the coexisting clinopyroxenes. In this regard, it should be mentioned that according to the data obtained in the study of ilmenites from Skaergaard massif, the values of K_d (ilmenite/gabbro), K_d (ilmenite/clinopyroxene) and K_d (ilmenite/magnetite) obtained for REE were determined as unusually high [Paster *et al.*, 1974] (Figure 3.3, 4–6). Moreover, according to Asavin [1994] the estimates of the values of K_d (ilmenite/melt of basic composition) for Zr are 0.28 and for Nb – 0.8. In addition, according to data obtained from ilmenites from Skaergaard massif it follows that the contents of Ce and Yb in them increase with increasing content of Zr and Nb, as well as with reducing content of V (Figure 3.5). Given the fact that the K_d (ilmenite/melt) for the LREE have lower values compared with the K_d for HREE, it is logically assumed that the latter are more compatible with the structure of this mineral compared with the first one.

* * *

Some regularities in the distribution of REE in ilmenites were considered above relying on the analyses of limited collection of samples from kimberlites, gabbro, pyroxenites, rhyolites and some other rocks, despite the fact that this mineral is a much more widespread one. It was found that the overall level of REE accumulation in most species of ilmenites does not exceed their level in C1 chondrite. Nevertheless, in some samples of this mineral in gabbros from Skaergaard massif the contents of

Table 3.3 The coefficients of REE distribution between ilmenites and coexisting phases.

Element	K_q (ilmenite/melt)			K_d (ilmenite/clinopyroxene)		K_d (ilmenite/gabbro)	K_d (ilmenite/magnetite)
	[Zack, Brumm, 1998]	[Nielsen et al., 1992]	[Jang, Naslund, 2002]	[Zack, Brumm, 1998]		Calculated by data [Paster et al., 1974]	
La	0,000029	0,0072	0,015	0,00054	1,61	0,276	6,85
Ce	0,000054	N.d.	0,012	0,00063	0,417	0,234	6,76
Pr	0,00019	N.d.	N.d.	0,0013	N.d.	N.d.	N.d.
Nd	0,00048	N.d.	0,010	0,0026	0,467	0,255	5,25
Sm	0,00059	0,0091	0,009	0,0020	0,164	0,293	7,25
Eu	0,0011	N.d.	0,010	0,0036	0,377	0,238	4,06
Gd	0,0034	0,0077	0,011	0,0085	0,341	0,242	7,63
Tb	0,006	N.d.	0,018	0,016	0,341	0,273	7,63
Dy	0,009	N.d.	N.d.	0,022	N.d.	N.d.	N.d.
Ho	0,01	0,012	0,035	0,024	0,306	0,270	8,00
Er	N.d.	N.d.	0,067	N.d.	N.d.	N.d.	N.d.
Tm	0,1	N.d.	0,102	0,22	N.d.	N.d.	N.d.
Yb	0,2	N.d.	0,13	0,40	0,352	0,454	9,48
Lu	0,1	0,029	0,19	0,19	N.d.	N.d.	N.d.

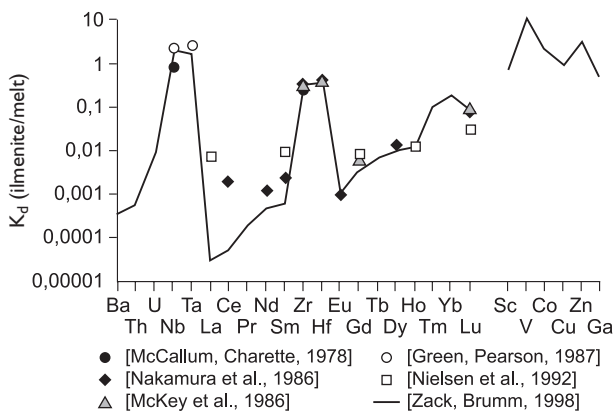


Figure 3.3 The graph of coefficients of REE and other trace elements distribution between ilmenites and melts (data [Zack & Brumm, 1998]).

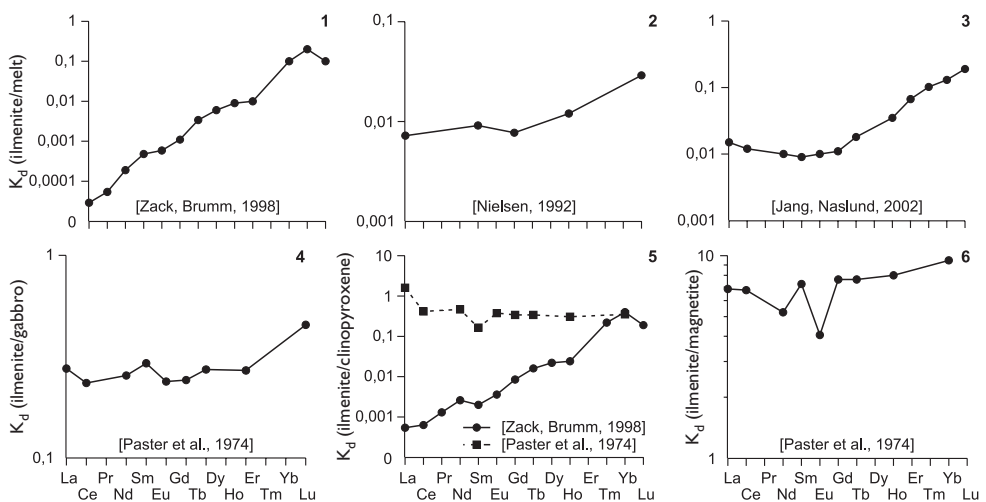


Figure 3.4 The graphs of coefficients of REE distribution between ilmenites and melts, as well as between ilmenites and some coexisting minerals (data Table 3.3).

Lu, Yb and Tm are slightly higher than their content in C1 chondrite. In many studied ilmenites the chondrite-normalized HREE contents exceed the LREE contents. At the same time, abnormally high contents of LREE were ascertained in some ilmenites of kimberlites from Yakutia. In all ilmenites of gabbros and pyroxenites from Tigrovyy massif, as well as in many of their samples from gabbros of Skaergaard massif, a more or less significant Eu excess was observed, whereas, in their certain samples from gabbros of Skaergaard massif, the same for the rhyolites, on the contrary, the deficit

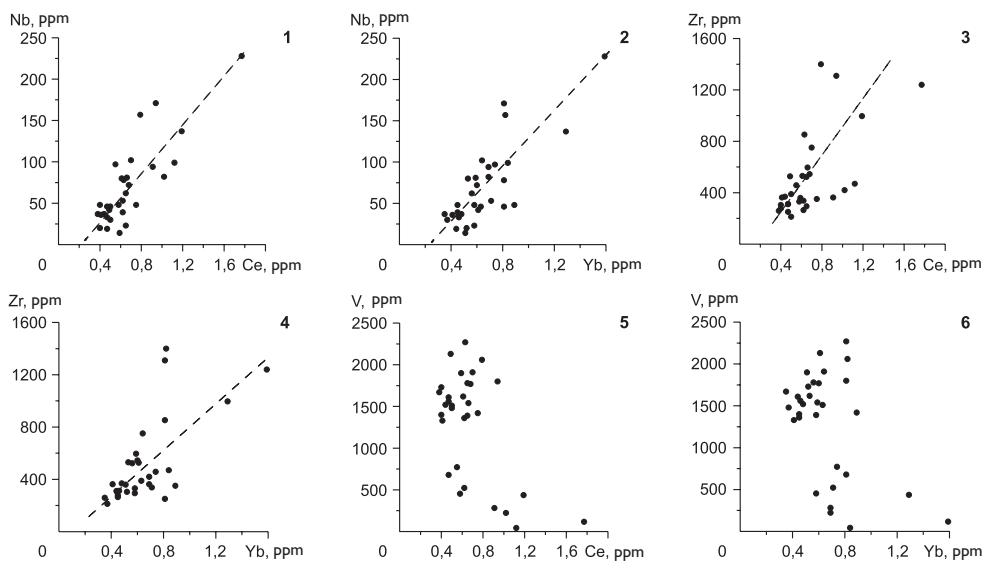


Figure 3.5 The graphs of relationship between contents of REE (Ce, Yb) and other trace elements in ilmenites from gabbros of Skaergaard massif (Greenland) (data [Jang & Naslund, 2002]). Dotted line – estimated trend.

of this element was identified. It is ascertained that all the REE have relatively low values of K_d (ilmenite/melt), which are generally increasing in sequence from LREE to HREE. This suggests that the HREE are more compatible with the ilmenite structure in comparison with LREE. It is assumed that more or less significant anomalous enrichment with LREE or HREE observed in some ilmenites is associated with the presence on the surface of their grains and in the microcracks of submicroscopic segregations of zircon, apatite and some other phases with high content of REE.

This page intentionally left blank

Chapter 4

Zircons

Zircon is one of the most prevailing accessory minerals of magmatic, metamorphic and some metasomatic formations of different composition. Due to its mechanical strength, during the disintegration of indigenous sources the zircons sometimes accumulate in the sedimentary rocks up to the formation of placer deposits. This mineral is presented in high amounts in the granites, diorites, nepheline syenites, lamproites, carbonatites and alkaline metasomatic rocks, more rarely it occurs in the gabbros, eclogites, kimberlites, minettes, lamproites, carbonatites, gneisses, amphibolites and other metamorphic rocks. Main regularities of distribution of REE in zircons from many types of magmatic and metamorphic rocks of different composition and genesis of the series of articles discussed in the book edited by Hancher & Hoskin [Zircon., 2003]. Recently, the zircons were found in ultramafites from some mantle xenoliths in alkali basalts in several provinces of China and Russia [Zheng *et al.*, 2006, Saltykova *et al.*, 2008], in ore chromitites occurring among phlogopite-bearing peridotites of Finero massif (Southern Alps) [Grieco *et al.*, 2001], as well as in dunites and ore chromitites of Voykar-Syn'insky massif (Polar Urals, Russia) [Savel'eva *et al.*, 2006, 2007]. In the latter case, as the authors assume, zircons crystallized from the residual portions of fractionated basic melts that infiltrated into peridotites. Zircons with Archean U-Pb isotopic age have recently been identified in the dunites of the Nizhnetagilsky massif, which is a part of Platinum-bearing belt of the Urals (Russia) [Malich *et al.*, 2009]. Note that in some gabbroid rocks the crystals of accessory ilmenites were identified surrounded by narrow (1–100 microns) rims that consist of microcrystals of zircon. The formation of the latter, as suggested by the researchers, was due to a later infiltration of high-temperature interstitial fluids enriched with Zr [Morisset & Scoates, 2008].

According to its crystal structure and chemical composition the zircons are orthosilicates. Their chemical formula is usually written as follows: ZrSiO_4 . The average SiO_2 content in them is ~33 wt%, ZrO_2 content is ~67 wt%. The main trace elements in zircons might be REE, Hf, Y, Ta, U, Th, Pb, Mo, Fe, Ti, Ca, P, the total amount of them can reach first weight percents. In recent decades, the zircons have been widely used for isotope dating of magmatic and metamorphic rocks using U-Pb-method, which considerably increased interest in a more detailed geochemical study of this mineral, including the study of REE distribution in it. Note that previously we presented a brief review of materials published in recent decades on REE distribution in zircons from rocks of different composition and origin [Lesnov, 2005], as well as on some features of their isomorphism in this mineral [Lesnov, 2011].

4.1 KEY REGULARITIES OF REE DISTRIBUTION IN ZIRCONS FROM SOME TYPES OF MAGMATIC AND METAMORPHIC ROCKS

First of all, it should be noted that to date the regularities of REE distribution in zircons have been studied much better in comparison with other accessory minerals. In particular, a fairly representative data have been published on the distribution of REE in zircons from kimberlites, eclogites, minettes, granitoids, gabbros, and ultramafic rocks, some of the effusive and metamorphic rocks.

Kimberlites. A sufficiently large amount of analytical data on the REE composition of zircons was published on the results of their study in the kimberlites of several provinces in Australia, South Africa and Yakutia (Russia) [Belousova *et al.*, 1998]. This work shows that zircons from kimberlites of these provinces are more or less different both in the general level of REE accumulation and in the concentration of some other trace elements. The authors concluded that the zircons from kimberlites in its geochemical properties are very different from zircons presented in lamproites, carbonatites and some mafic rocks. In general, the zircons from the studied kimberlites are characterized by relatively low total REE content (less than 50 ppm), including heavy elements, and their REE patterns often have a more or less gentle positive slope. A low content of U (6–20 ppm) and Y (6–200 ppm) is observed in these zircons. In addition, Belousova *et al.* drew attention to the fact that the zircons from kimberlites differ from the zircons from most other magmatic rocks crystallized in the earth's crust and the former has higher values of Hf(wt%)/Y(ppm) parameter.

While studying the geochemistry of zircons from kimberlites of Timber Creek province (Northern Australia) it was found that by their REE composition they are very similar to zircons from kimberlites of several other provinces of Australia, as well as provinces in Southern Africa and Yakutia, but differ in slightly reduced overall level of REE accumulation [Berryman *et al.*, 1999]. Thus, the total REE contents in zircons from the Timber Creek province range from 3.4 to 43.6 ppm (with an average of 12 ppm) (Table 4.1), which corresponds to the lower limit of this parameter for zircons from kimberlites in general. Zircons from kimberlites of Timber Creek province are depleted by lanthanum, the average chondrite-normalized content of which is ~0.19 t.ch., while they are moderately enriched with HREE. Thus, the average chondrite-normalized Yb content in them is about 22 t.ch., which causes a relatively low average value of $(La/Yb)_n$ – around 0.02. On REE patterns of almost all of these zircons there are positive Ce anomalies of various intensity. The values of $(Ce/Ce^*)_n$ parameter in them range between 1.2 and 7.6 with an average of 3.1 (Figure 4.1). Finally, it should be noted that the zircons from kimberlites of Timber Creek province mostly have relatively low average contents of U (~8 ppm) and Th (~4 ppm).

The study of zircons from kimberlites of Kampfersdam province (Africa) showed that their crystals are characterized by a zonal distribution of REE: in the kernels the contents of REE are higher compared to the peripheral zones of the crystals, and the chondrite-normalized contents of elements increase manifold in the row from La (2 t.ch.) to Lu (400 t.ch.) [Hamilton *et al.*, 1998]. In the peripheral zones of crystals the REE are less fractionated; respectively, their chondrite-normalized contents vary in a narrow range – from 0.15 t.ch. (La) to 50 t.ch. (Lu). The REE patterns of internal and peripheral zones of zircon crystals from kimberlites of the province, having the form

Table 4.1 REE compositions of zircons from kimberlites, lherzolites, gabbros, gabbro-norites, anorthosites from some provinces (ppm).

Timber Creek province (North Australia)

	[Berryman et al., 1999], LA ICP-MS												
	1-V-t	1-V-b	2-V-t	2-V-b	3-V-t	3-V-b	4-V-t	4-V-b	5-V-t	5-V-b	6-P-t	6-P-b	7-P
Element	Kimberlites												
La	0,020	0,040	0,020	0,030	0,070	0,050	0,030	0,060	0,190	0,030	0,020	0,030	0,060
Ce	0,260	0,920	0,330	0,370	0,270	1,030	0,530	0,370	0,430	0,390	0,370	0,380	0,550
Pr	0,030	0,040	0,020	0,030	0,040	0,100	0,030	0,040	0,030	0,040	0,020	0,030	0,060
Nd	0,170	0,730	0,310	0,410	0,220	0,500	0,750	0,230	0,330	0,220	0,140	0,330	0,790
Sm	0,180	0,730	0,270	0,460	0,420	0,570	0,700	0,530	0,680	0,330	0,700	0,160	0,630
Eu	0,080	0,500	0,140	0,050	0,060	0,150	0,260	0,070	0,120	0,250	0,100	0,200	0,280
Gd	0,180	2,820	0,680	0,970	0,460	0,940	1,22	0,420	1,38	1,12	1,20	1,020	1,500
Tb	N.d.	N.d.	N.d.	N.d.	N.d.	N.d.	N.d.	N.d.	N.d.	N.d.	N.d.	N.d.	N.d.
Dy	0,640	8,46	1,66	1,42	1,01	2,52	3,60	0,960	1,75	1,79	3,89	3,37	3,65
Ho	0,160	2,470	0,460	0,750	0,320	0,630	0,950	0,220	0,570	0,610	0,830	1,10	1,12
Er	0,720	10,18	1,82	2,49	0,990	2,26	4,31	0,510	1,41	1,45	3,58	3,79	3,31
Tm	N.d.	N.d.	N.d.	N.d.	N.d.	N.d.	N.d.	N.d.	N.d.	N.d.	N.d.	N.d.	N.d.
Yb	0,800	13,9	1,76	3,26	2,18	3,26	5,60	0,910	3,19	2,33	4,58	5,04	5,17
Lu	0,120	2,79	0,470	0,570	0,330	0,630	1,050	0,240	0,560	0,530	0,830	0,890	1,01
Total	3,36	43,6	7,94	10,8	6,37	12,6	19,0	4,56	10,6	9,09	16,3	16,3	18,1
$(\text{La/Yb})_n$	0,017	0,002	0,008	0,006	0,022	0,010	0,004	0,045	0,040	0,009	0,003	0,004	0,008
$(\text{Eu/Eu}^*)_n$	1,35	0,93	0,95	0,22	0,42	0,62	0,85	0,44	0,37	1,13	0,33	1,14	0,84
$(\text{Ce/Ce}^*)_n$	2,08	5,00	3,58	2,68	1,21	2,61	3,84	1,76	1,24	2,28	4,02	2,75	1,99

(Continued)

Table 4.1 (Continued).

Timber Creek province (North Australia)													
	[Berryman et al., 1999], LA ICP-MS												
	8-P-t	8-P-b	9-P	10-P-t	10-P-b	11-Y-t	11-Y-b	12-Y-b	13-Y	14-Y-t	14-Y-b	15-Y-t	15-Y-b
Element		Kimberlites											
La	0,020	0,030	0,030	0,030	0,040	0,050	0,170	0,010	0,030	0,020	0,030	0,030	0,040
Ce	0,420	0,710	0,370	0,440	0,570	0,990	0,930	0,940	0,800	1,02	1,030	0,770	0,870
Pr	0,030	0,030	0,060	0,060	0,050	0,050	0,090	0,180	0,020	0,040	0,100	0,040	0,020
Nd	0,160	0,230	0,160	0,170	0,370	0,140	0,400	0,700	0,160	0,530	0,380	0,150	0,150
Sm	0,340	0,530	0,240	0,310	0,880	0,410	0,260	0,670	0,210	0,410	0,810	0,230	0,250
Eu	0,040	0,140	0,220	0,100	0,220	0,090	0,180	0,410	0,090	0,430	0,130	0,150	0,280
Gd	0,770	1,07	1,13	1,090	1,43	1,26	0,350	2,85	0,740	2,78	1,55	1,29	1,20
Tb	N.d.	N.d.	N.d.	N.d.	N.d.	N.d.	N.d.	N.d.	N.d.	N.d.	N.d.	N.d.	N.d.
Dy	1,70	2,42	2,61	2,06	3,50	2,88	1,89	6,43	2,80	4,74	3,73	3,38	3,47
Ho	0,620	0,890	0,800	0,810	0,970	0,930	0,500	1,54	0,630	1,44	0,850	0,770	1,29
Er	2,11	3,66	3,20	2,20	2,87	2,64	1,14	5,07	2,22	5,37	4,36	3,95	4,92
Tm	N.d.	N.d.	N.d.	N.d.	N.d.	N.d.	N.d.	N.d.	N.d.	N.d.	N.d.	N.d.	N.d.
Yb	3,67	4,44	2,97	4,24	4,24	4,15	2,22	6,76	4,23	5,98	4,02	5,35	5,11
Lu	0,540	0,880	0,930	0,670	0,960	0,960	0,400	1,29	0,680	1,31	0,610	1,05	1,13
Total	10,42	15,03	12,72	12,18	16,10	14,55	8,53	26,9	12,6	24,1	17,6	17,2	18,7
(La/Yb) _n	0,004	0,005	0,007	0,005	0,006	0,008	0,052	0,001	0,005	0,002	0,005	0,004	0,005
(Eu/Eu [*]) _n	0,23	0,56	1,07	0,47	0,60	0,35	1,82	0,77	0,62	0,91	0,35	0,66	1,29
(Ce/Ce [*]) _n	3,36	5,14	1,56	1,86	2,62	4,30	1,79	1,55	7,61	6,45	2,79	4,50	7,36

(Continued)

Table 4.1 (Continued).

Timber Creek province (North Australia)													
	[Berryman et al., 1999], LA ICP-MS												
	16-O-t	16-O-b	17-O-t	17-O-b	18-O-t	19-O-t	19-O-b	20-O-t	20-O-b	21-G	22-G	23-G-t	23-G-b
Element	Kimberlites												
La	0,030	0,040	0,020	0,020	0,040	0,030	0,020	0,070	0,050	0,220	0,060	0,030	0,040
Ce	0,270	0,660	0,340	0,350	0,330	0,370	0,340	0,430	0,270	0,160	0,340	0,690	0,250
Pr	0,030	0,020	0,050	0,020	0,020	0,020	0,060	0,040	0,030	0,050	0,020	0,020	0,040
Nd	0,120	0,200	0,310	0,240	0,340	0,140	0,120	0,240	0,220	0,240	0,250	0,310	0,210
Sm	0,470	0,200	0,170	0,170	0,210	0,170	0,150	0,310	0,280	0,310	0,330	0,250	0,260
Eu	0,060	0,190	0,100	0,160	0,050	0,080	0,040	0,160	0,070	0,080	0,080	0,170	0,070
Gd	0,480	0,630	1,02	0,820	0,120	0,640	0,180	0,190	0,170	0,180	0,410	1,160	0,730
Tb	N.d.	N.d.	N.d.	N.d.	N.d.	N.d.	N.d.	N.d.	N.d.	N.d.	N.d.	N.d.	N.d.
Dy	0,790	5,49	3,15	1,55	1,08	1,83	1,19	1,50	0,730	0,620	0,260	2,37	1,51
Ho	0,400	2,00	1,03	0,460	0,220	0,550	0,360	0,260	0,300	0,150	0,140	0,910	0,800
Er	1,64	6,56	3,81	2,08	0,980	2,42	1,28	0,380	0,530	0,560	0,490	3,45	2,20
Tm	N.d.	N.d.	N.d.	N.d.	N.d.	N.d.	N.d.	N.d.	N.d.	N.d.	N.d.	N.d.	N.d.
Yb	2,42	7,18	3,92	3,24	1,60	3,42	2,83	0,320	1,27	0,930	1,21	3,65	2,48
Lu	0,260	1,17	0,990	0,75	0,230	0,480	0,360	0,490	0,250	0,170	0,180	0,590	0,610
Total	6,97	24,3	14,9	9,86	5,22	10,2	6,93	4,39	4,17	3,67	3,77	13,6	9,20
(La/Yb) _n	0,008	0,004	0,003	0,004	0,017	0,006	0,005	0,148	0,027	0,160	0,033	0,006	0,011
(Eu/Eu*) _n	0,38	1,49	0,57	1,08	0,88	0,65	0,74	1,87	0,91	0,95	0,67	0,80	0,46
(Ce/Ce*) _n	1,95	5,59	1,78	3,80	2,79	3,52	1,52	1,93	1,64	0,35	2,36	6,56	1,36

(Continued)

Table 4.1 (Continued).

Tolstik manifestation and Yavrozero district (Kola Peninsula, Russia)													
[Kaulina, 2010], LA ICP-MS													
Element	Gabbros				Gabbro-anorthosites			Gabbro-norites			Anorthosites		
	742-51a	742-51b	742-51c	742-51c	763-1a	763-1b	763-1c	GKR-7a	GKR-7b	GKR-7c	A-3-1	A-3-2	A-3-3
La	0,5	0,2	1,8	0,4	0,2	0,1	0,2	0,1	0,5	0,1	0,1	0,03	0,04
Ce	35	39	40	23	33	34	27	1,4	1,2	1,0	3,0	1,0	2,0
Pr	1,3	0,7	1,0	1,1	0,2	0,2	0,1	0,01	0,02	0,01	0,05	0,04	0,01
Nd	14	9	10	12	2	3	2	0,1	0,1	0,1	0,4	0,3	0,1
Sm	13	12	11	10	4	6	4	0,3	0,3	0,3	0,5	0,5	0,1
Eu	2,7	1,2	1,0	1,7	0,2	0,2	0,1	0,1	0,2	0,1	1,3	1,0	0,1
Gd	70	58	54	43	20	25	15	2	3	2	2	2	0,4
Tb	N.d.	N.d.	N.d.	N.d.	N.d.	N.d.	N.d.	N.d.	N.d.	N.d.	N.d.	N.d.	N.d.
Dy	248	202	200	132	64	75	53	14	18	13	3	3	1
Ho	N.d.	N.d.	N.d.	N.d.	N.d.	N.d.	N.d.	N.d.	N.d.	N.d.	N.d.	N.d.	N.d.
Er	510	425	435	252	121	134	97	38	51	36	2	3	1
Tm	N.d.	N.d.	N.d.	N.d.	N.d.	N.d.	N.d.	N.d.	N.d.	N.d.	N.d.	N.d.	N.d.
Yb	842	741	748	428	203	216	177	96	135	94	3	4	3
Lu	130	121	122	66	32	34	29	18	26	18	0,3	0,4	0,2
Total	1866	1609	1624	971	481	528	404	169	234	165	15	14	8
(Yb/La) _n	2178	6066	575	1381	1262	3384	1466	2546	3836	1988	59	151	113
(Eu/Eu*) _n	0,2	0,1	0,1	0,2	0,1	0,04	0,04	0,4	0,4	0,4	3,5	3,2	1,3
(Ce/Ce*) _n	7	16	7	6	35	48	41	16	11	12	13	6	27

(Continued)

Table 4.1 (Continued).

<i>Tolstik manifestation and Yavrozero district (Kola Peninsula, Russia)</i>											
	<i>[Kaulina, 2010], LA ICP-MS</i>										
Element	A-3-4	A-3-5	A-3-6	A-3-7	A-2-1	A-2-2	A-1	A-3	U-1a	U-1b	U-1c
	<i>Anorthosites</i>										<i>Lherzolites</i>
La	0,03	0,03	0,01	0,02	0,01	0,01	0,003	0,02	0,04	0,01	0,1
Ce	1	1	1	1	10	6	2	9	4	4	5
Pr	0,03	0,01	0,01	0,01	0,1	0,1	0,03	0,3	0,02	0,02	0,04
Nd	0,2	0,1	0,04	0,04	1,3	0,8	0,3	3	0,2	0,1	0,4
Sm	0,3	0,3	0,1	0,1	1,7	0,9	0,7	3	0,3	0,3	0,4
Eu	0,8	0,7	0,2	0,2	0,7	0,4	0,1	1,8	0,1	0,1	0,1
Gd	1	1	0,3	0,4	5	3	2	6	1	1	1
Tb	N.d.	N.d.	N.d.	N.d.	N.d.	N.d.	N.d.	N.d.	N.d.	N.d.	N.d.
Dy	2	3	1	1	16	12	5	8	5	5	6
Ho	N.d.	N.d.	N.d.	N.d.	N.d.	N.d.	N.d.	N.d.	N.d.	N.d.	N.d.
Er	3	3	1	1	34	38	6	6	12	10	13
Tm	N.d.	N.d.	N.d.	N.d.	N.d.	N.d.	N.d.	N.d.	N.d.	N.d.	N.d.
Yb	5	3	1	2,1	82	103	9	4	26	24	30
Lu	0,5	0,4	0,1	0,2	14	19	1	1	5	4	5
Total	14	12	4	6	164	184	26	42	53	48	62
(La/Yb) _n	0,004	0,007	0,006	0,006	0,0006	0,0009	0,003	0,03	0,001	0,0004	0,001
(Eu/Eu*) _n	3,6	3,0	2,8	2,9	0,7	0,6	0,3	1,3	0,3	0,5	0,4
(Ce/Ce*) _n	7	12	10	14	24	13	19	7	39	44	26

(Continued)

Table 4.1 (Continued).

Markov depression (Mid-Atlantic Ridge)													
[Zinger et al., 2010], LA ICP-MS													
	L1153-49						L1097-1						
Element	Grain's number												
	a-1	a-2	b-1	b-2	c-1	c-2	d-2	e-1	e-2	f-2	g-1	h-1	i-1
Gabbros													
La	0,04	0,06	1,11	0,15	0,09	0,03	0,49	0,01	0,01	0,02	0,12	0,02	0,02
Ce	6,71	5,92	9,43	5,82	10,13	30,23	45,92	1,75	3,68	7,97	22,09	21,96	24,83
Pr	0,08	0,27	1,21	0,09	0,25	0,18	0,68	0,04	0,05	0,12	0,12	0,10	0,13
Nd	2,09	5,90	13,18	1,43	4,93	4,66	12,31	0,85	0,98	2,07	2,26	2,34	2,72
Sm	5,80	12,58	14,26	3,96	11,94	15,04	30,79	1,83	2,18	5,15	6,30	6,52	7,37
Eu	1,57	3,76	4,37	1,13	2,75	2,69	5,12	0,52	0,67	0,97	0,60	0,57	0,67
Gd	33,53	72,97	49,31	27,36	73,46	105,74	189,69	9,16	17,08	30,86	41,30	41,81	47,83
Tb	13,96	27,24	15,24	10,71	27,20	39,98	69,63	3,51	7,02	12,39	17,25	17,84	19,98
Dy	150,89	317,13	170,90	138,45	342,27	516,98	823,73	38,81	89,91	148,96	210,30	223,00	244,37
Ho	60,01	125,66	63,88	56,02	136,15	200,29	325,71	13,89	36,68	59,79	85,89	91,14	100,81
Er	296,87	553,91	284,06	260,24	613,79	895,53	1456,14	58,25	156,45	271,97	401,18	429,54	457,55
Tm	68,37	115,11	57,24	59,67	131,88	197,45	305,86	12,89	34,52	62,58	90,58	95,22	103,72
Yb	623,27	977,95	469,84	520,83	1065,79	1638,11	2547,81	117,78	302,58	533,39	777,40	775,96	904,41
Lu	106,38	160,40	101,46	95,82	217,63	312,22	457,53	20,07	48,00	87,15	128,62	128,54	150,44
Total	1370	2379	1255	1182	2638	3959	6271	279	700	1223	1784	1835	2065
(La/Yb) _n	0,00004	0,00004	0,002	0,0002	0,00006	0,00001	0,0001	0,00006	0,00002	0,00003	0,0001	0,00002	0,00001
(Eu/Eu*) _n	0,27	0,30	0,45	0,24	0,22	0,15	0,16	0,32	0,24	0,18	0,09	0,08	0,08
(Ce/Ce*) _n	21,2	6,1	1,7	11,8	10,7	47,6	15,9	12,0	20,6	18,8	39,9	61,5	54,4

(Continued)

Table 4.1 (Continued).

Northern Catena Costiera area (Southern Italy)													
[Liberi et al., 2011], LA ICP-MS													
	M53						M57						
Grain's number													
	Zrn-7	Zrn-10a	Zrn-10b	Zrn-13a	Zrn-14	Zrn-18a	Zrn-35a	Zrn-16a	Zrn-1	Zrn-7	Zrn-8	Zrn-13	Zrn-14
Element	Gabbros												
La	<0,021	<0,020	<0,019	<0,019	N.d.	<0,024	N.d.	<0,023	0,01	N.d.	0,08	0,03	0,01
Ce	0,70	3,48	5,58	2,49	0,84	1,41	2,94	2,85	0,72	0,77	1,86	1,40	1,73
Pr	0,02	0,02	0,04	<0,014	0,02	<0,017	0,06	<0,023	0,07	<0,015	0,09	0,02	<0,016
Nd	0,56	0,49	0,50	0,63	0,11	0,15	0,63	0,47	1,22	<0,094	0,73	0,65	0,50
Sm	0,97	0,75	1,60	0,57	0,21	0,31	1,59	1,17	5,15	0,93	1,69	1,35	1,58
Eu	0,50	0,46	0,51	0,71	0,12	0,36	0,72	0,50	0,31	0,12	0,54	0,08	0,21
Gd	4,47	4,68	8,37	3,47	1,37	2,66	6,42	5,94	25,28	6,54	8,80	9,65	10,30
Tb	1,85	1,87	2,92	1,84	0,77	0,96	2,10	1,79	5,88	2,08	5,36	3,33	3,62
Dy	23,36	24,59	35,69	23,19	11,70	11,16	23,42	19,72	29,62	26,71	64,79	49,70	46,49
Ho	9,39	9,70	13,29	9,65	4,65	4,33	9,26	7,44	4,77	10,08	29,00	20,52	19,16
Er	46,19	51,09	62,20	51,01	25,18	19,92	44,81	34,91	10,42	48,21	149,52	101,52	86,33
Tm	10,08	11,47	15,43	12,67	6,14	4,78	9,66	7,86	1,10	9,66	33,76	23,93	18,55
Yb	103,22	131,73	148,82	144,09	62,13	47,42	104,49	80,56	6,52	96,30	337,01	274,41	188,17
Lu	22,86	30,38	33,80	34,74	16,06	10,25	22,92	19,03	1,12	19,69	76,44	55,16	37,44
Total	224	271	329	285	129	104	229	182	92	221	710	542	414
$(\text{Yb}/\text{Gd})_n$	27,94	34,05	21,51	50,24	54,87	21,57	19,69	16,41	0,31	17,81	46,33	34,40	22,10
$(\text{Eu}/\text{Eu}^*)_n$	0,73	0,75	0,43	1,54	0,67	1,19	0,69	0,58	0,08	0,15	0,43	0,07	0,16

(Continued)

Table 4.1 (Continued).

Northern Catena Costiera area (Southern Italy)										
[Liberi et al., 2011], LA ICP-MS										
	M57	EP78								
Element	Grain's number									
	Zrn-25	Zrn-49	Zrn-4b	Zrn-7b	Zrn-10a	Zrn-11b	Zrn-19	Zrn-24	Zrn-27	Zrn-28a
La	<0,029	0,02	<0,0167	N.d.	<0,0245	0,01	0,01	0,03	0,01	N.d.
Ce	1,26	0,55	4,11	3,95	5,17	3,81	7,72	9,94	10,25	5,64
Pr	N.d.	<0,0161	0,02	0,02	0,03	0,03	0,05	0,08	0,11	0,04
Nd	0,34	0,31	0,51	0,40	0,92	<0,143	1,23	2,76	1,67	0,83
Sm	1,56	0,97	1,12	0,98	1,75	0,76	2,81	4,25	3,67	2,33
Eu	<0,048	0,22	0,65	0,49	1,14	0,37	1,20	1,62	1,98	0,78
Gd	5,23	8,09	5,68	4,19	10,55	4,46	15,46	21,14	18,24	11,75
Tb	1,98	3,48	1,92	1,60	3,81	1,26	5,65	6,09	6,12	3,80
Dy	31,31	48,71	24,42	17,81	38,73	15,85	59,33	71,06	73,02	42,36
Ho	14,17	19,21	7,62	6,16	14,27	5,86	22,84	28,56	25,98	15,12
Er	75,26	97,96	33,65	26,29	64,93	26,39	101,74	129,39	122,72	72,19
Tm	16,87	21,02	7,30	5,67	14,60	5,83	22,36	29,59	25,36	14,67
Yb	203,13	202,72	72,67	53,28	148,90	56,96	230,15	292,13	257,56	152,12
Lu	41,81	44,18	15,76	11,96	31,21	12,39	48,41	63,43	55,12	33,62
Total	393	447	175	133	336	134	519	660	602	355
$(\text{Yb/Gd})_n$	46,99	30,32	15,48	15,38	17,08	15,45	18,01	16,72	17,08	15,66
$(\text{Eu/Eu}^*)_n$	N.d.	0,23	0,79	0,74	0,81	0,62	0,55	0,52	0,73	0,45

(Continued)

Table 4.1 (Continued).

Beriozovsky massif, Sakhalin Island (Russia)															
[data F. Lesnov], LA ICP-MS															
	1606-I										1597				
	Grain's number														
Element	1	2	3	4	5	6	7	8	9	10	1	2	3	4	5-1
Gabbro-pyroxenite											Pyroxenite				
La	0,60	0,31	0,05	0,06	0,02	0,06	0,01	0,05	0,02	0,02	0,06	0,08	0,03	0,09	0,68
Ce	14,98	19,32	7,00	18,07	11,63	7,46	23,38	16,26	8,54	6,94	3,10	28,5	5,5	96,4	24,0
Pr	0,49	0,97	0,29	0,72	0,15	0,18	0,28	0,20	0,12	0,06	0,05	0,80	0,09	0,39	0,45
Nd	3,38	12,53	4,27	9,63	2,42	2,75	3,11	3,44	1,40	1,20	1,30	6,30	1,60	5,00	4,60
Sm	4,97	15,43	6,92	15,09	4,90	4,92	7,43	4,73	3,19	1,49	2,80	12,2	2,30	11,3	5,10
Eu	0,19	1,53	0,47	1,25	0,67	0,31	1,88	1,19	1,09	0,50	0,30	2,53	1,18	2,04	0,52
Gd	18,7	40,2	21,4	47,5	13,0	20,4	26,0	17,4	19,37	5,86	14,1	41,6	11,1	34,0	25,2
Tb	6,37	12,2	6,98	18,1	5,23	7,52	9,18	6,52	8,82	2,38	5,40	15,6	4,30	13,7	8,30
Dy	74	129	77	209	60	96	99	75	121	31	63	181	54	129	107
Ho	24	41	23	71	22	32	32	26	52	13	19	64	19	42	36
Er	115	177	104	349	105	158	158	119	311	72	94	311	98	174	172
Tm	26	35	23	80	24	38	36	29	80	20	21	76	22	36	35
Yb	248	315	210	755	243	351	347	286	975	236	207	762	232	331	340
Lu	33	40	28	103	36	45	46	40	168	40	29	112	34	37	46
Total	570	840	512	1678	527	764	789	625	1749	430	461	1613	486	911	805
$(\text{La/Yb})_n$	0,0016	0,0007	0,0002	0,0001	0,0001	0,0001	0,00003	0,0001	0,00001	0,00005	0,0002	0,0001	0,0001	0,0002	0,0014
$(\text{Eu/Eu}^*)_n$	0,05	0,18	0,11	0,13	0,24	0,08	0,37	0,35	0,32	0,45	0,12	0,31	0,59	0,29	0,11
$(\text{Ce/Ce}^*)_n$	6,25	5,36	6,91	7,33	22,25	11,00	25,03	23,06	21,30	29,90	13,47	10,37	16,77	68,51	10,12
Age, Ma	623	601	1061	1412	626	1366	2121	518	154	716	2048	697	3096	974	2031

(Continued)

Table 4.1 (Continued).

Beriozovsky massif, Sakhalin Island (Russia)																			
[data F. Lesnov], LA ICP-MS																			
1597					1658														
Grain's number																			
Element	Pyroxenite					Gabbro-diorite													
	5-2	6	7	8	9	1	2	3	4	5	6	7	8	9	10				
La	0,10	0,03	0,04	0,05	0,05	0,05	0,02	0,005	0,18	0,05	0,02	0,05	0,09	0,09	0,04				
Ce	12,1	16,0	10,5	7,8	15,2	4,2	6,8	4,3	12,1	4,7	2,9	7,6	7,2	8,2	5,5				
Pr	0,08	0,15	0,14	0,19	0,09	0,05	0,38	0,04	0,15	0,23	0,11	0,06	0,37	0,39	0,25				
Nd	1,90	2,40	1,50	2,70	1,00	2,30	4,00	0,70	2,40	3,50	1,40	1,70	4,50	4,60	3,30				
Sm	1,70	4,10	2,80	5,10	3,60	2,90	6,80	2,10	3,70	5,70	2,80	3,00	7,10	8,60	6,50				
Eu	0,18	0,90	1,00	0,41	0,64	1,28	2,04	0,44	1,16	1,58	0,69	0,84	2,23	2,99	2,02				
Gd	8,10	13,8	8,50	16,8	11,0	11,4	27,5	8,50	21,9	20,2	9,00	17,9	29,4	35,1	27,0				
Tb	3,10	5,10	3,30	6,40	4,20	4,30	10,40	3,80	11,3	8,50	3,60	8,40	11,7	11,5	9,40				
Dy	39	57	37	75	54	59	120	52	170	100	46	117	146	143	113				
Ho	14	20	15	26	21	24	47	24	75	37	18	51	55	54	41				
Er	73	107	77	121	110	141	250	140	410	201	106	301	290	296	221				
Tm	17	27	20	27	26	42	70	40	104	51	30	80	79	80	59				
Yb	188	293	223	273	295	577	798	484	1189	633	367	941	861	1015	718				
Lu	27	46	37	36	39	105	135	83	193	104	62	155	140	162	119				
Total	384	592	437	596	580	974	1478	842	2195	1170	649	1685	1633	1821	1326				
$(\text{La/Yb})_n$	0,0004	0,0001	0,0001	0,0001	0,0001	0,0001	0,00002	0,00001	0,0001	0,0001	0,00003	0,00004	0,0001	0,0001	0,00004				
$(\text{Eu/Eu}^*)_n$	0,12	0,33	0,58	0,12	0,28	0,59	0,39	0,27	0,30	0,40	0,38	0,27	0,40	0,45	0,40				
$(\text{Ce/Ce}^*)_n$	30,5	29,1	19,9	11,1	42,6	17,4	5,4	30,1	16,6	5,6	7,2	28,3	5,4	5,8	6,3				
Age, Ma	2045	2267	647	1683	668	153	156	160	161	163	156	161	160	159	160				

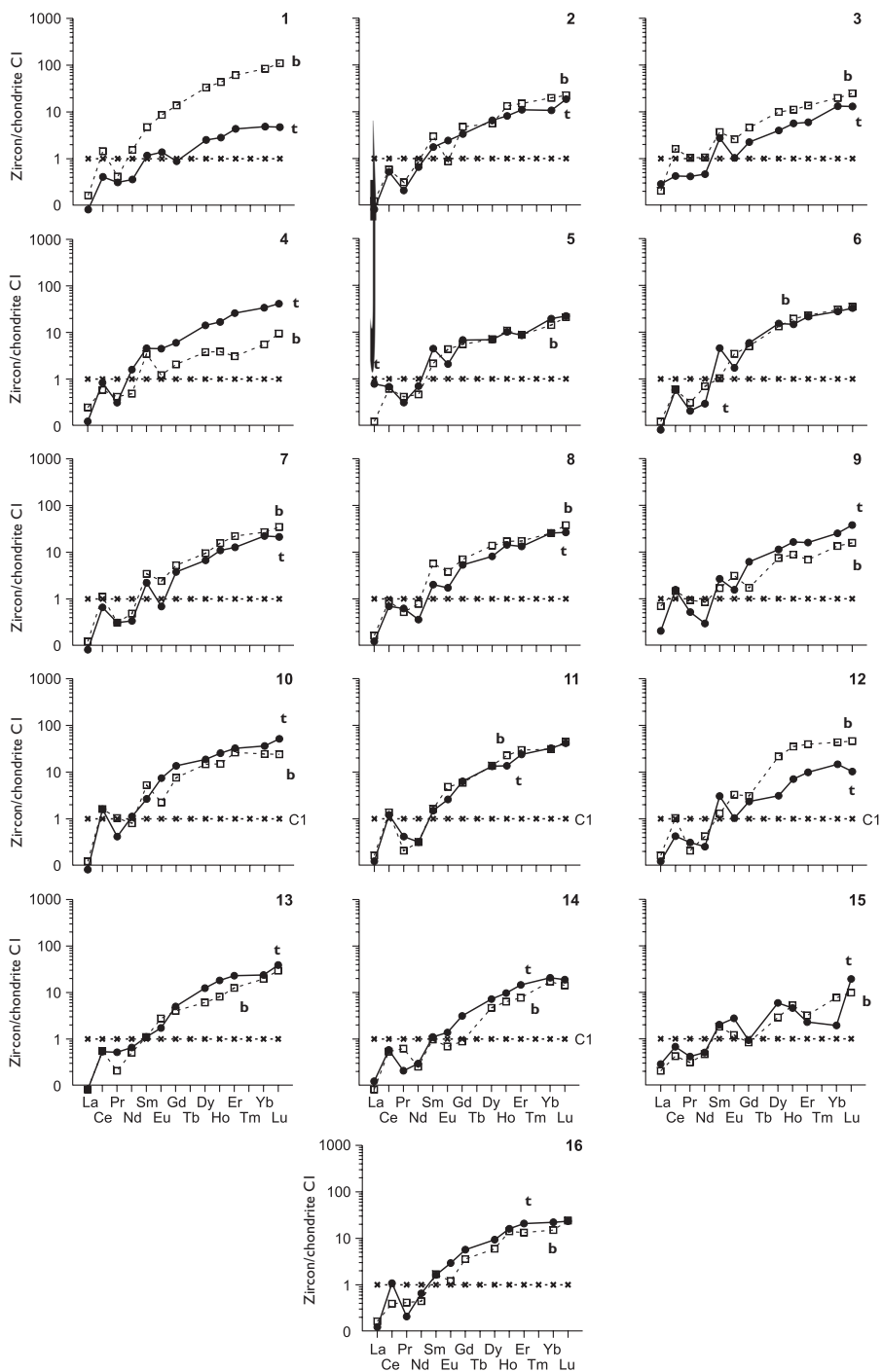


Figure 4.1 Chondrite-normalized REE patterns for zircons from kimberlites from Timber Creek province (North Australia). The letters 't' and 'b' are mean the patterns for inner and outer zones of zircon grains, respectively (data Table 4.1).

of almost straight lines with positive slope, are complicated by intense positive Ce anomalies.

Eclogites. While isotopic dating of eclogites from some metamorphic provinces of Norway by using U-Pb zircon method in the latter there have also been estimated REE contents [Root *et al.*, 2004]. It was ascertained that the total REE content in these zircons vary in the range of 28–54 ppm with the average of 42 ppm (Table 4.2). The zircons from eclogites of Flatraket province (Norway) that were studied in more detail turned out to be almost identical, both in the general level of REE accumulation and the configuration of REE patterns, that in each case are complicated by positive Ce anomalies (Figure 4.2). The average value of the intensity index of these anomalies – $(Ce/Ce^*)_n$ parameter – is 5.6. For the heavy REE the patterns of these zircons have a form of shallow lines, indicating a weak fractionation of these elements. Root *et al.* suggested that the characteristics of REE composition of zircons they studied are caused by the presence in their crystals of syngenetic or later microinclusions of garnet, enriched with pyrope component. The zircons from eclogites of Norwegian province called Verpeneset differ from the mineral of the other provinces by a much more significant enrichment with HREE and less intense positive Ce anomalies.

In the zircons from eclogites of Monte-Rosa complex (Western Alps) the content of LREE, excepting Ce, is below the limits of detection by the analytical method used. In addition, chondrite-normalized contents of Yb and Lu in them exceed 100 t.ch. [Liati & Froitzheim, 2006] (Table 4.2). In order to finish the description of zircons from eclogites, we should add that in their samples from eclogites exposed in Kuru-Vaara manifestation (Kola Peninsula, Russia) [Kaulina, 2010] the total REE contents range from 10 to 176 ppm and the value of $(Ce/Ce^*)_n$ parameter varies in the range of 2.4–3.7. Moreover, their patterns often show intense negative Nd anomalies, which were not observed in the patterns of zircons from eclogites described above.

Minettes. Zircons from these rocks are studied by the example of dikes samples that are cutting the metamorphic complex within Kirovograd block (Ukraine) [Yatsenko *et al.*, 2000]. Note that these minettes have previously been described as lamproites [Belousova *et al.*, 1998]. The minette samples were selected from the core of several holes drilled in order to estimate the prospects for diamond-bearing of these rocks. They usually have a porphyric structure due to the presence of phenocrysts of phlogopite, biotite, hornblende, diopside, rarely – of olivine, which are immersed in the fine- and medium-granular matrix. In the content of the latter there are microcrystals of zircon, common potash feldspar, pseudo-leucite, plagioclase and quartz. The zircons presented in minettes are heterogeneous in size, shape and color of grains. The dominating ones are well-faceted crystals of different habit; the rarely seen are fragments of crystals, as well as grains of irregular shape with evidence of melting with observed fluid microinclusions. The values of Zr/Hf parameter in zircons from this collection vary in a relatively narrow range. Additionally, the contents of most trace elements, including REE, vary widely. At the same time the contents of Y are higher than the contents of U, and the latter are higher than in zircons from kimberlites.

By the general level of REE accumulation the analyzed zircons from minettes of Kirovograd block were divided into four types. The grains of zircons that are prevailing in this collection were assigned to the 1st type and the total REE content in them ranges from 160 to 1400 ppm (Table 4.3). Zircons of this type have almost identical REE patterns by configuration, which usually show positive Ce anomalies of

Table 4.2 REE compositions of zircons from eclogites from some provinces (ppm).

	Flatraket manifestation (Norway)								
	[Root et al., 2004], TIMS								
	1B	1C	1D	1E	1F	2B	2C	2D	3B
<i>Element</i>	<i>Eclogites</i>								
La	0,090	0,090	0,310	0,150	0,050	0,210	0,110	0,030	0,040
Ce	1,31	1,50	1,80	1,62	1,40	1,60	1,38	1,27	1,31
Pr	0,080	0,040	0,110	0,080	0,040	0,140	0,070	0,040	0,080
Nd	0,630	0,610	0,870	0,640	0,530	1,06	0,600	0,480	0,640
Sm	N.d.	N.d.	N.d.	N.d.	N.d.	N.d.	N.d.	N.d.	N.d.
Eu	0,310	0,300	0,370	0,420	0,460	0,380	0,320	0,300	0,370
Gd	2,10	2,60	2,60	2,80	3,30	2,50	2,30	2,20	2,30
Tb	0,420	0,470	0,580	0,610	0,580	0,580	0,530	0,510	0,430
Dy	2,70	3,70	3,90	4,10	4,40	3,60	3,70	3,40	3,20
Ho	0,730	0,880	0,830	0,900	0,930	0,860	0,850	0,850	0,750
Er	2,50	2,90	3,00	3,20	3,00	3,60	3,40	3,00	2,70
Tm	0,420	0,590	0,510	0,500	0,600	0,470	0,560	0,480	0,410
Yb	3,50	4,20	4,30	4,70	4,90	4,60	4,40	4,10	3,40
Lu	0,700	0,900	0,930	0,960	1,040	0,860	0,840	0,760	0,660
Total	15,5	18,8	20,1	20,7	21,2	20,5	19,1	17,4	16,3
$(\text{La/Yb})_n$	0,017	0,014	0,049	0,022	0,007	0,031	0,017	0,005	0,008
$(\text{Eu/Eu}^*)_n$	1,04	0,81	1,00	1,06	0,98	1,07	0,98	0,96	1,13
$(\text{Ce/Ce}^*)_n$	3,43	6,02	2,35	3,52	7,10	2,17	3,69	7,42	4,14

(Continued)

Table 4.2 (Continued).

Element	Flatraket manifestation (Norway)							(Verpeneset (Norw.)		Monte-Rosa (W.Alps)		Kuru-Vaara (Kola Peninsula, Russia)			
	[Root et al., 2004], TIMS							[Liati, Froitzheim, 2006] LA ICP-MS		[Kaulina, 2010] LA ICP-MS					
	3C	3D	3E	3F	3G	4B	4C	PISI-S4	PISI-2	KV05/1a	KV05/1b	KV05/1c	KV05/1d		
Eclogites															
La	0,150	0,070	0,160	N.d.	N.d.	0,040	0,090	N.d.	N.d.	0,04	0,02	0,04	0,11		
Ce	1,54	1,44	1,76	1,63	1,48	0,270	0,460	0,094	0,050	0,21	0,19	0,23	0,65		
Pr	0,020	0,020	0,060	0,020	N.d.	0,030	0,050	N.d.	N.d.	0,01	0,01	0,01	0,03		
Nd	0,740	0,720	0,720	0,510	0,370	0,290	0,260	N.d.	N.d.	0,03	0,02	0,02	0,19		
Sm	N.d.	N.d.	N.d.	N.d.	N.d.	N.d.	N.d.	N.d.	N.d.	0,09	0,06	0,07	1,04		
Eu	0,390	0,410	0,430	0,470	0,410	0,190	0,300	0,061	0,089	0,09	0,04	0,06	0,74		
Gd	2,70	2,400	3,00	3,20	3,10	1,10	1,70	1,09	1,40	0,97	0,61	0,64	10,19		
Tb	0,440	0,480	0,540	0,580	0,710	0,500	0,710	0,669	0,952	N.d.	N.d.	N.d.	N.d.		
Dy	3,30	3,50	3,80	4,10	4,30	5,80	8,30	7,63	11,7	3,84	1,66	4,5	30,77		
Ho	0,760	0,720	0,790	0,86	0,940	1,49	2,40	2,51	3,76	N.d.	N.d.	N.d.	N.d.		
Er	2,40	2,40	2,50	2,60	2,70	5,60	10,50	9,12	16,4	4,41	1,23	2,01	38,24		
Tm	0,500	0,500	0,640	0,480	0,430	1,15	2,41	1,79	3,16	N.d.	N.d.	N.d.	N.d.		
Yb	2,90	3,00	3,10	2,90	3,10	10,0	22,1	18,0	32,7	6,08	2,79	3,87	29,50		
Lu	0,540	0,550	0,570	0,540	0,490	2,25	5,15	3,61	7,03	0,75	0,21	0,29	5,75		
Total	16,4	16,2	18,1	17,9	18,1	28,7	54,4	N.d.	N.d.	26	10	18	176		
$(\text{La/Yb})_n$	0,035	0,016	0,035	N.d.	N.d.	0,003	0,003	N.d.	N.d.	0,005	0,006	0,008	0,003		
$(\text{Eu/Eu}^*)_n$	1,02	1,20	1,01	1,03	0,93	1,22	1,24	N.d.	N.d.	0,06	0,04	0,05	0,005		
$(\text{Ce/Ce}^*)_n$	5,89	9,16	4,33	N.d.	N.d.	1,79	1,63	N.d.	N.d.	2,4	3,7	2,7	2,8		

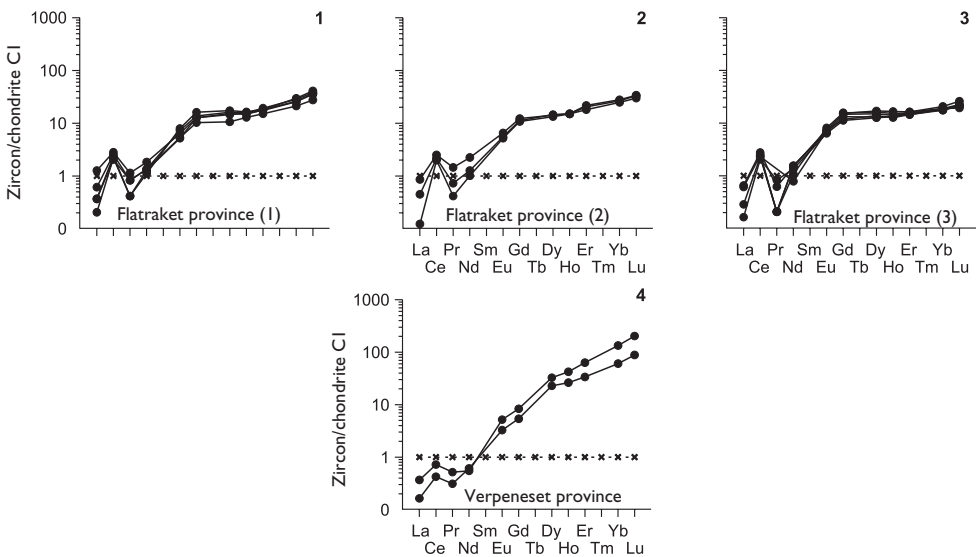


Figure 4.2 Chondrite-normalized REE patterns for zircons from eclogites from some metamorphic provinces in Norway. 1–3 – Flatraket province; 4 – Verpeneset province (data Table 4.2).

moderate intensity and intense negative Eu anomalies (Figure 4.3, 1.3). They are also characterized by very low values for $(\text{La}/\text{Yb})_{\text{n}} = 0,0005\text{--}0,007$. Based on the assumptions that the zircons of this type were crystallized on conditions of equilibrium with the minette parent melt, and that afterwards the trace elements in them have not undergone a substantial redistribution, the calculations on the model REE composition of the minette parent melt were made (Figure 4.4). Results of the calculations showed that this minette parent melt was significantly enriched with LREE, especially with Ce, and at the same time had some Eu deficiency. The estimated model REE composition of minette parent melt gives grounds to consider them as geochemical analogues of lamproites, although in the latter there is usually a less severe Eu deficiency.

The REE composition of the zircon crystals from the considered minettes, which were assigned to the 2nd, 3rd and 4th types, was studied on the example of single grains. It was ascertained that zircons of the 2nd type, being close to zircons of the 1st type by total REE content, differ from them by higher values of $(\text{Ce}/\text{Ce}^*)_{\text{n}}$ parameter (Figure 4.3, 4). Meanwhile, the zircons of 3rd and 4th types show an anomalous enrichment with LREE, while their patterns have no positive Ce anomalies (Figure 4.3, 5, 6). Apart from this, the pattern of zircon, which is referred to the 4th type, has no negative Eu anomaly.

The identified geochemical features of zircons from minettes of Kirovograd block give grounds to consider these zircons to be heterogeneous. Their crystals that are referred to the 1st type are characterized by typical for this mineral significant enrichment with HREE, depletion by LREE, as well as excess content of Ce with Eu deficit. Additionally, the unusual for zircons REE distribution observed in the grains, that are assigned to other three types, melting signs observed in their crystals as well as the presence of fluid microinclusions, lead to the conclusion that these crystals at a late

Table 4.3 REE compositions of zircons from minettes (lamproites) from Kirovograd block, Ukraine (ppm).

	[Yatsenko et al., 2000], LA ICP-MS							
	K-1/29	K-2/30	K-3/17-3	K-4/25-1	K-4/25-2	K-4/25-3	K-6/32-3	K-6/32-4
Element	Type I							
La	0,36	0,56	0,13	0,17	0,20	0,18	0,38	0,44
Ce	6,01	8,17	2,89	2,68	2,26	2,52	3,49	6,14
Pr	0,450	0,420	0,090	0,270	0,120	0,180	0,220	0,790
Nd	3,38	3,69	1,42	3,89	1,84	1,82	3,32	7,32
Sm	4,98	8,35	2,44	7,06	2,49	4,09	4,91	6,64
Eu	0,280	0,600	0,370	0,400	0,440	0,530	0,250	0,960
Gd	23,6	54,6	21,2	25,1	15,1	18,7	18,6	22,6
Tb	N.d.	N.d.	N.d.	N.d.	N.d.	N.d.	N.d.	N.d.
Dy	88,3	226	74,8	77,2	49,1	61,9	38,7	65,4
Ho	33,3	82,6	28,8	26,4	18,2	21,2	10,7	23,3
Er	152	360	126	112	81,0	95,7	34,6	99,8
Tm	N.d.	N.d.	N.d.	N.d.	N.d.	N.d.	N.d.	N.d.
Yb	262	562	186	176	142	157	39,4	159
Lu	55,1	121	42,2	39,3	31,9	34,2	6,55	34,0
Total	630	1428	487	470	344	398	161	426
$(La/Yb)_n$	0,001	0,001	0,0005	0,001	0,001	0,001	0,007	0,002
$(Eu/Eu^{*})_n$	0,07	0,06	0,11	0,08	0,17	0,16	0,07	0,22
$(Ce/Ce^{*})_n$	3,07	3,85	26,3	2,40	3,44	3,04	2,85	1,93

(Continued)

Table 4.3 (Continued).

	K-4/25-5	K-5-1	K-5-2	K-6/32-1	K-6/32-2	K-3/17-2	K-4/25-4	K-3/17-1
Element	Type 1			Type 2			Type 3	Type 4
La	0,29	0,28	0,61	0,06	0,02	2,31	18,7	9,21
Ce	2,79	3,03	5,50	9,26	7,65	8,09	51,4	53,5
Pr	0,150	0,130	0,650	0,240	0,220	1,08	7,38	12,6
Nd	2,50	2,65	6,72	3,08	3,40	7,70	31,8	83,6
Sm	3,45	4,97	9,53	4,29	6,63	6,03	10,0	47,0
Eu	0,470	0,390	0,930	0,290	0,070	0,700	0,460	20,9
Gd	22,1	15,7	62,2	19,8	20,1	28,6	31,3	90,7
Tb	N.d.	N.d.	N.d.	N.d.	N.d.	N.d.	N.d.	N.d.
Dy	76,9	63,4	221	66,3	33,7	79,3	83,6	169
Ho	26,5	23,9	81,0	22,7	5,72	28,3	28,4	50,4
Er	119	100	355	200	13,3	115	116	192
Tm	N.d.	N.d.	N.d.	N.d.	N.d.	N.d.	N.d.	N.d.
Yb	182	165	518	168	8,65	178	178	270
Lu	42,8	37,7	111	38,4	1,23	40,7	39,8	54,7
Total	480	417	1372	532	101	495	597	1053
$(La/Yb)_n$	0,001	0,001	0,001	0,0002	0,002	0,009	0,071	0,023
$(Eu/Eu^*)_n$	0,12	0,12	0,09	0,08	0,02	0,14	0,07	0,96
$(Ce/Ce^*)_n$	3,19	3,81	1,87	10,6	10,2	1,23	1,05	1,00

Note: Type 1: K-1/29 – heads of cherry crystals; K-2/30 – dark-cherry crystals; K-3/17-3 – pink prisms with gas inclusions and flowed surface; K-4/25-1, K-4/25-2, K-4/25-3 – pink prisms with hard inclusions and flowed surface; K-4/25-5 – orange-pink flat prisms; K-5 – 1, K-5-2 – orange prisms; K-6/32 – 3, K-6/32-4 – cream-coloured oval grains. Type 2: K-6/32-1, K-6/32-2 – cream-coloured oval grains. Type 3: K-3/17-2 – pink prisms with gas inclusions and flowed surface, K-4/25-4 – pink flat prisms. Type 4: K-3/17-1 – pink prisms with gas inclusions and flowed surface.

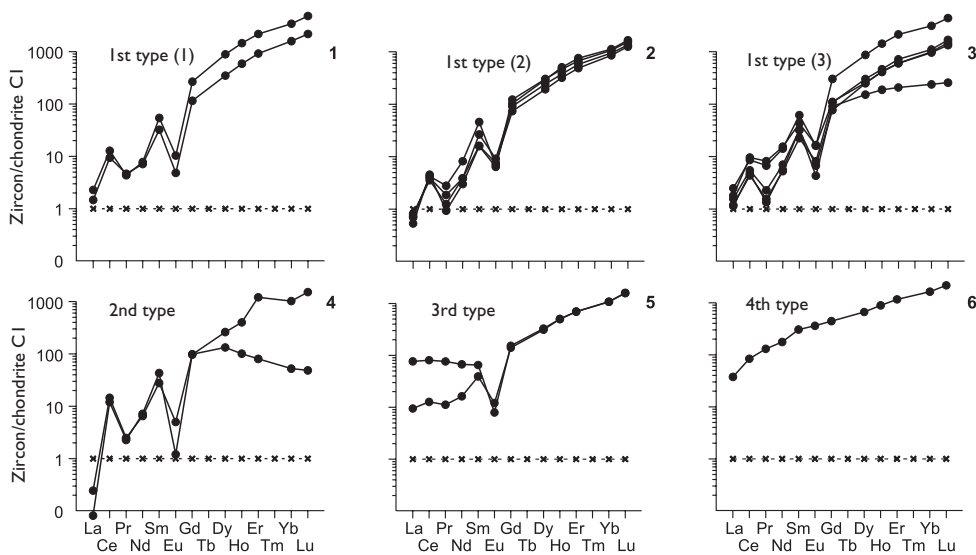


Figure 4.3 Chondrite-normalized REE patterns for zircons from minettes from Kirovograd block (Ukraine) (data Table 4.3.).

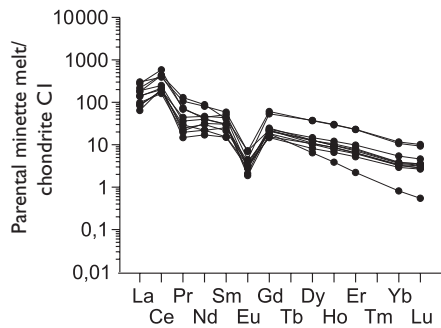


Figure 4.4 Chondrite-normalized REE patterns for model parental melts of minettes from Kirovograd block (Ukraine). REE composition of parental melts were calculated on the basis of their contents in the zircons, assigned to the 1st type (see Table 4.3.), and using the values of K_d (zircon/melt) (data [Hinton & Upton, 1991]).

stage of its crystallization have undergone different intensity effects of the residual portions of the parent melt, resulting in partial redistribution of these trace elements, REE included.

Ultramafic rocks. In these rocks the accessory zircons are much rarer present and in much smaller quantities than in most other varieties of magmatic and metamorphic rocks, so they are still the least studied with respect to the geochemistry of REE and other trace elements. Recent detailed studies include the zircons from peridotites forming massifs in the Northern Tibet [Song *et al.*, 2005] and Sulu provinces (China)

[Zhang *et al.*, 2005], from ultramafic xenoliths in kimberlites of Gibeon province (Southern Namibia) [Liati *et al.*, 2004], as well as from ultramafic xenoliths of some diatremes of Hinyang province (North China) [Zheng *et al.*, 2006a]. According to the research, in the zircons from Hinyang province the total REE contents, except for Tb and Tm, vary in the range from 435 to 1483 ppm (Table 4.4). Also there have been identified the contents of Y (572–1933 ppm), P (202–586 ppm), Pb (1.35–23.5 ppm), Fe (10–2535 ppm) Mn (0.22–5.40 ppm) and HfO_2 (1.2–2.49 wt%). Judging by multielemental patterns, these zircons are characterized by a certain deficit of Fe and Mn. The zircons from ultramafites of Hinyang province by the values of $(\text{La/Yb})_{\text{N}}$ parameter can be divided into two geochemical types – with lower (0.0001–0.0003) and with relatively higher (0.0016–0.0074) values of this parameter. On REE patterns of the first type of zircons the positive Ce anomalies have a higher intensity (Figure 4.5, 1) compared to zircons of the second type (Figure 4.5, 2). It can be assumed that the relative enrichment of the second type of zircon with LREE and specificity of their patterns are due to the presence in the microcracks of their crystals of small amounts of unstructured LREE impurities, brought by epigenetic processes. The configurations of the multielemental patterns of the observed zircons also indicate their anomalous enrichment with uranium and thorium (Figure 4.5, 3). The average value of U/Th parameter in them is 3.3.

Saltykova *et al.* [2008] analyzed the REE composition and identified a U-Pb isotopic age of zircons from garnet-spinel lherzolites, presented in the xenoliths from alkaline basalts of Vitim province (Russia) (Table 4.4). These zircons form elongate colorless prismatic crystals, which quite often contain melt, fluid and solid (apatite, sillimanite, quartz) microinclusions. Some of these crystals contained round or irregularly shaped relict ‘core’, which indicates their zonal structure. It should be noted that on the surface and in microcracks of some crystals there were signs of corrosion, which colored them brownish.

Based on the data collected by isotope dating, the authors divided the collection of zircons from ultramafic xenoliths of Vitim province into four groups. The first group consists of three samples, which are defined as the oldest ones. Two of these zircons with ages of 1694 and 1506 million years show a significant depletion by La. On their patterns there are intense positive Ce anomalies, as well as negative Eu anomalies. The third sample of zircon with the age of 1088 million years showed a significant enrichment with light elements – La, Ce, Pr and Nd. On its spectrum the negative Eu anomaly has a low intensity, and the positive Ce anomaly is completely absent (Figure 4.5, 4). Compared with the first group, the samples from the second, third and fourth groups showed significantly lower values of the isotopic age (277–139 Ma). All of them have patterns complicated by intense positive Ce anomalies, while the intensity of negative Eu anomalies consistently decreases in them from the second group to the fourth group, which has Eu anomaly completely neutralized (Figure 4.5, 5–7). We assume that such a ‘reduction’ of the isotopic ages of zircons and the accompanying changes of their REE composition were caused by later processes of redistribution of impurities and disturbances in the original U-Pb isotopic system in the process of thermal and isotopic-geochemical influence of those fluids that were separated from basaltic melts, subtracting xenoliths of garnet-spinel lherzolites from the upper-mantle level to the surface and seeped into the xenoliths and their minerals by the systems of microcracks. Such an assumption correlates with the presence of fluid microinclusions

Table 4.4 REE compositions of zircons from peridotites and garnet-spinel lherzolites from xenoliths in alkaline basalts from Hinyang province (China) and from Vitim province (Transbaykalia, Russia) (ppm).

Element	[Zheng et al., 2006], LA ICP-MS						
	Y971-4c	Y971-5	Y971-7	Y972-16	Y974-25	Y974-29	Y974-30
<i>Peridotites</i>							
HfO ₂	1,23	1,71	1,61	1,60	1,20	2,49	1,79
La	0,05	0,08	5,48	1,05	0,1	N.d.	0,48
Ce	3,2	13,3	30,7	32,6	17,3	25,8	28,8
Pr	0,03	0,08	2,41	1,0	0,11	0,08	0,24
Nd	0,42	1,38	12,8	7,44	1,57	1,68	1,99
Sm	1,12	3,26	6,27	6,58	2,56	3,09	3,21
Eu	0,09	0,62	0,23	0,92	1,11	0,37	0,41
Gd	7,92	22,1	28	31	17,5	15,7	16,3
Tb	N.d.	N.d.	N.d.	N.d.	N.d.	N.d.	N.d.
Dy	46,8	119	149	152	83,8	68,9	74,4
Ho	18,6	49,6	61,8	61,2	31,7	26,9	28,3
Er	90,4	246	309	293	146	132	132
Tm	N.d.	N.d.	N.d.	N.d.	N.d.	N.d.	N.d.
Yb	226	636	745	661	314	328	299
Lu	40,4	112	132	115	50,4	59,6	53,5
Total	435	1203	1483	1363	666	662	639
(La/Yb) _n	0,0002	0,0001	0,0074	0,0016	0,0003	N.d.	0,0016
(Ce/Ce*) _n	80	166	7,78	31,8	165	645	80
(Eu/Eu*) _n	0,004	0,010	0,003	0,009	0,022	0,008	0,008

(Continued)

Table 4.4 (Continued).

[Saltykova et al., 2008], LA ICP-MS													
	Vt-19.2.1	Vt-16.11.1	Vt-16.11.2	Vt-16.1.1	Vt-16.9.1	Vt-16.3.1	Vt-16.5.1	Vt-19.3.1	Vt-19.2.2	Vt-19.1.1	Vt-16.7.1	Vt-19.4.1	Vt-16.2.2
Element	Garnet-spinel lherzolites												
La	0,02	0,02	8,71	9,74	0,02	0,01	0,01	0,03	0,04	4,07	N.d.	0,02	0,33
Ce	30,35	19,27	29,98	58,82	28,90	49,08	36,50	30,31	28,55	24,70	17,75	11,04	5,21
Pr	0,19	0,33	3,83	2,84	0,15	0,24	0,15	0,33	0,13	3,00	0,03	0,07	0,13
Nd	2,46	5,05	16,80	12,19	2,00	3,64	2,15	4,90	2,24	14,02	0,29	1,01	1,02
Sm	3,76	10,36	11,41	4,02	3,19	6,70	3,35	7,97	4,93	8,52	0,48	2,06	1,54
Eu	0,68	0,06	0,38	0,65	1,03	1,45	1,12	2,06	2,39	2,25	0,29	1,48	0,73
Gd	9,09	38,16	21,14	7,95	9,07	19,56	9,10	24,14	12,44	9,35	1,64	9,41	3,56
Tb	3,07	16,90	8,88	2,93	3,37	7,26	2,93	8,77	3,63	3,15	0,57	2,32	0,95
Dy	34,27	221,39	101,69	37,83	42,98	82,51	33,37	105,44	35,60	26,14	6,64	21,32	8,94
Ho	11,94	85,97	32,63	15,21	17,06	30,25	11,56	38,90	11,60	10,54	2,63	6,80	2,95
Er	48,95	361,53	124,48	68,85	74,35	129,03	46,27	162,78	47,65	44,96	12,69	27,88	13,22
Tm	11,28	75,26	24,55	16,14	16,73	28,70	9,70	36,16	9,48	11,39	3,23	6,32	3,26
Yb	120,85	662,27	216,74	166,67	172,82	284,05	95,77	356,40	101,00	117,32	38,22	63,42	36,05
Lu	19,33	88,65	28,54	25,41	26,90	43,86	14,35	52,68	14,63	19,14	7,22	9,39	6,04
Total	296,3	1585,2	629,7	429,3	398,0	686,3	266,3	830,9	274,3	298,5	91,8	162,5	83,9
(La/Yb) _n	0,00011	0,00002	0,02712	0,03945	0,00008	0,00002	0,00007	0,00006	0,00027	0,02342	N.d.	0,00021	0,00618
(Eu/Eu [*]) _n	0,35	0,01	0,07	0,35	0,55	0,36	0,58	0,42	0,89	0,77	0,90	0,86	0,92
(Ce/Ce [*]) _n	46,4	17,2	1,2	2,7	55,3	60,8	71,7	26,8	59,2	1,6	178,8	42,8	6,1

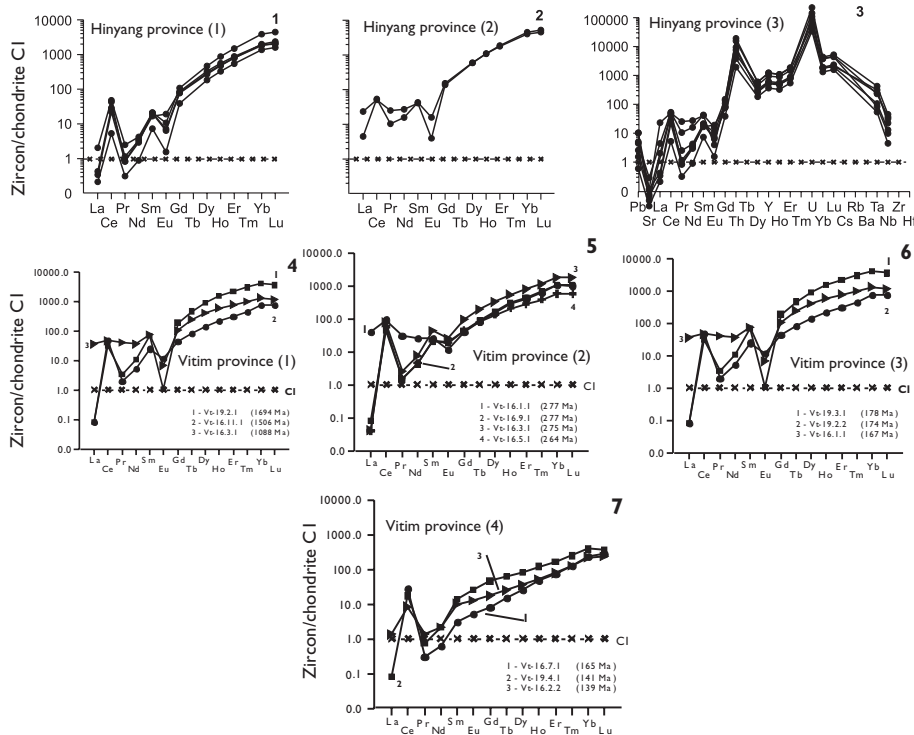


Figure 4.5 1–3 – chondrite-normalized REE patterns and multielemental patterns for zircons from peridotites in xenoliths from Hinyang alkaline basalt province (North China): 1 – zircons in which LREE concentrations were not changed by epigenetic processes; 2 – zircons in which LREE concentrations were changed by epigenetic processes; 3 – multielemental patterns for zircons. 4–7 – chondrite-normalized REE patterns for zircons from peridotite in xenoliths from Vitim alkaline basalt province (Transbaykalia, Russia) with different isotopic age: 4 – 1088–1694 Ma; 5 – 264–277 Ma; 6 – 167–178 Ma; 7 – 139–165 Ma (data Table 4.4).

in some zircons, as well as the appearance of a brownish color, which indicates their relative enrichment with LREE.

Gabbros, diorites, pyroxenites. The REE composition of zircons from these rocks is studied by the example of samples of pegmatite gabbros forming Khayalygsky massif (South-Western Tuva, Russia) [Oydup *et al.*, 2006; Lesnov *et al.*, 2007]. These zircons are represented by idiomorphic short-columnar crystals of 0.2–1 mm in size and of a color from pink to colorless. According to the results of U-Pb isotopic dating the age of these zircons is 447.4 ± 1.3 million years (Late Ordovician). Using the microprobe technique it was determined that the content of ZrO_2 in them is 66.4–66.9 wt%, HfO_2 – 0.85–0.99 wt%. The value of $\text{ZrO}_2/\text{HfO}_2$ vary in the range of 67–78. The total REE content varies in the range of 128–156 ppm, the values of $(\text{La/Yb})_{\text{N}}$ in the range of 0.004–0.012 (Table 4.5). On the REE patterns of the studied zircons there are relatively weak positive Ce anomalies and negative Eu anomalies. At the same time, their multielemental patterns show intense positive anomalies

Table 4.5 Main components (wt%) and trace elements (ppm) compositions of zircons from hornblende gabbros from Khayalygsky massif (West Tuva, Russia).

Element	[Oydup et al., 2011], LA ICP-MS			
	Kha-3	Kha-3a	Kha-7	Kha-7a
SiO ₂	31,92	31,95	32,07	31,95
ZrO ₂	66,93	66,40	66,82	66,51
HfO ₂	0,98	0,85	0,97	0,99
Total	99,83	99,20	99,86	99,45
ZrO ₂ /HfO ₂	68,3	78,1	68,9	67,2
La	—	—	1,1	0,48
Ce	—	—	2,8	2,0
Pr	—	—	0,31	0,17
Nd	—	—	1,6	0,99
Sm	—	—	0,67	0,76
Eu	—	—	0,16	0,22
Gd	—	—	2,2	3,2
Tb	—	—	0,67	0,98
Dy	—	—	8,9	13
Ho	—	—	3,8	5,2
Er	—	—	21	27
Tm	—	—	5,3	6,5
Yb	—	—	65	81
Lu	—	—	14	15,1
Total REE	—	—	128	156
(La/Yb) _n	—	—	0,012	0,004
(Eu/Eu*) _n	—	—	0,37	0,38
(Ce/Ce*) _n	—	—	1,11	1,73
Rb	—	—	1,4	2,8
Sr	—	—	2,4	1,4
Y	—	—	126	161
Zr	—	—	163999	203403
Nb	—	—	0,25	0,60
Cs	—	—	0,95	5,8
Ba	—	—	5,9	3,1
Hf	—	—	3265	3643
Ta	—	—	0,12	0,13
Pb	—	—	423	172
Th	—	—	35	46
U	—	—	118	128

for Zr, Hf, and U, less obvious – for Th and Pb, as well as negative anomalies for Sr, Rb and Nb (Figure 4.6). Note that by the configuration of the multielemental patterns of the zircons from gabbros of Khayalygsky massif are rather similar to those zircons described above, that are from peridotites represented in deep xenoliths of North China provinces (Figure 4.5, 3), although the latter are somewhat richer in Ce, medium and heavy REE, Th, U, Ta and Nb, and poorer in Pb and Sr.

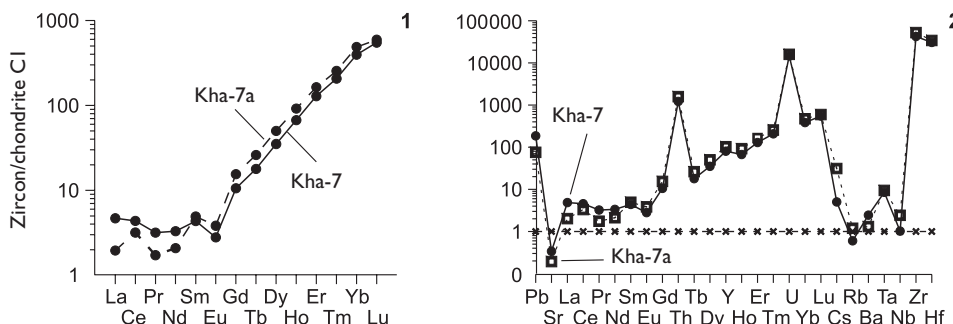


Figure 4.6 Chondrite-normalized REE (1) and multielemental (2) patterns for zircons from hornblende gabbros of Khayalygsky massif (Tuva, Russia) (data Table 4.5).

While isotopic dating of hornblende gabbros of Chernostochinsky and Reftinsky massifs (Urals, Russia) by accessory zircons in individual samples of the latter their, REE composition was determined [Krasnobaev *et al.*, 2004]. In these zircons the chondrite-normalized HREE contents predominate over the contents of LREE, as indicated by the steep positive slope of the REE patterns. The zircons from the rocks of Chernostochinsky massif have higher overall level of REE accumulation (La – 40 t.ch., Lu – 3000 t.ch.) compared with the mineral from rocks of Reftinsky massif (La – 0.6 t.ch., Lu – 1300 t.ch.). Nevertheless, a positive Ce anomaly on patterns of zircon from Chernostochinsky massif has a much lower intensity than this anomaly in the mineral from rocks of Reftinsky massif. In the spectrum of the latter the positive Eu anomaly is of minimal importance, while it is very clearly shown in the spectrum of zircon from Chernostochinsky massif.

Ronkin & Nesbit [1997] studied the REE composition of zircons from certain kinds of rocks that form the Berdyauushsky massif (Urals, Russia), including gabbro. It was ascertained that in the zircons from this gabbro the chondrite-normalized La contents are around 0.015–03 t.ch., which is about the same level as the Pr content. The determined Ce content in these zircons is about 1–8 t.ch., which causes the presence of Ce positive anomalies in their patterns. At the patterns intervals between Pr and Lu they have a form of almost straight positively inclined lines complicated by weak negative Eu anomalies.

Interesting data was obtained during studies on REE composition of zircons from gabbros that underwent brittle-plastic deformation and are dredged in Markov depression (Mid-Atlantic Ridge) [Zinger *et al.*, 2010] (Table 4.1, Figure 4.7). According to the U-Pb isotope dating of zircon grains from the gabbros, it was determined that their age varies from 2.3 to 0.7 million years. The authors of this paper concluded that under the plastic deformation, accompanied by infiltration of the intergranular fluids of unknown nature, the studied zircon crystals have undergone an uneven enrichment with several trace elements, including REE, U, Th, Hf, P and Y. On the example of zircon crystals from particular sample of gabbro it was found that the $^{238}\text{U}/^{206}\text{Pb}$ parameter varies significantly even within individual grains of the mineral. At the same time, the values may differ in order, to some extent correlated with the

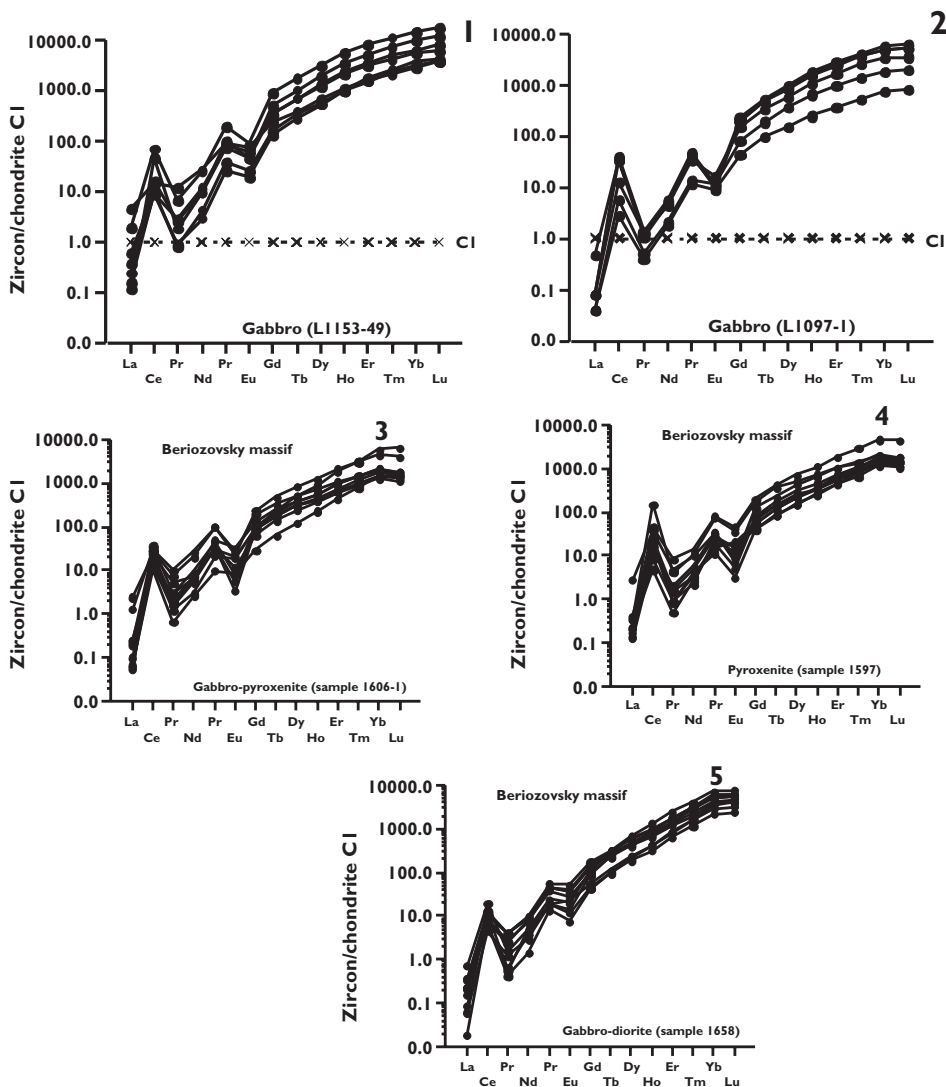


Figure 4.7 Chondrite-normalized REE patterns for zircons: 1, 2 – gabbros from Markov depression (Mid-Atlantic Ridge) (samples L1153-49 and L1097-1) (data [Zinger et al., 2010]); 3–5 – rocks from Beriozovsky massif (Sakhalin Island, Russia (data [F. Lesnov]) (see Table 4.1).

intensity of brittle-plastic deformations experienced by these grains. Thus, in a weakly deformed zircon crystal (f) the values for $^{238}\text{U}/^{206}\text{Pb}$ ranged from 287 to 670. While in a strongly deformed and recrystallized zircon crystal (g) the value of the parameter was in the range of 4363–5473. These data led to the conclusion that redistribution of trace elements, including REE, U, Hf and Th, accompanying the plastic deformations of zircon crystals of the gabbro, had a significant effect on the parameters of U-Pb

isotopic system, which, in turn, affected the reliability of the estimates of isotopic age obtained on the basis of these zircons.

We obtained the first data on REE composition (LA ICP-MS method), as well as on the isotopic age (U-Pb method, SHRIMP II) of zircons from gabbros, gabbro-diorites, gabbro-pyroxenites, pyroxenites and some other rocks that form Beriozovsky mafic-ultramafic massif, which is a part of Eastern-Sakhalin ophiolite association (Sakhalin Island, Russia) (Table 4.1). In the gabbros of this complicated massif there were numerous xenoliths of ultramafites found. Due to the active influence of mafic melts and their fluids on the rocks of earlier ultramafic protrusion, as well as on the surrounding terrigenous-volcanic rocks, along their boundaries there were formed contact-reaction zones composed of heterogeneous in quantitative-mineral composition and often banded hybrid rocks (wehrlites, plagioclase-bearing wehrlites, pyroxenites, gabbro-pyroxenites, gabbro-diorites, diorites and others). These observations led us to the conclusion that the gabbro intrusion have formed later in relation to protrusion of ultramafic restites it was spatially brought together with and that Beriozovsky massif is polygenic [Lesnov *et al.*, 1998; 2011].

Based on the performed isotope studies it was ascertained that zircons from rocks of gabbro intrusion, which is a part of Beriozovsky massif, have an average age of about 158 million years (late Jurassic). However, some grains of zircon from the hybrid pyroxenites and gabbro-pyroxenites have an older age – from about 1000 to about 2500 Ma and more. On this basis we can assume that these older zircons are xenogeny and that they were captured by mafic melt during the process of its interaction with more ancient mantle ultramafic restites.

Table 4.1 shows a representative REE analyses of zircons only from certain types of rocks from Beriozovsky massif. According to the general results of these studies the total REE content of zircons from different rocks of this massif vary over a very wide range – from ~100 to ~17000 ppm. On those REE patterns of zircons from rocks of this massif that show a very steep positive slope, some intense positive Ce anomalies are observed, as well as less intense negative Eu anomalies. In the interval from Yb to Lu the steep slope of these patterns usually becomes less steep (Figure 4.7). The contents of the main components in the zircons from rocks of the massif are (% wt): Zr_2O (63.8–66.3), Hf_2O (0.86–2.15), UO_2 (<0.045–0.29), the parameter Zr_2O/Hf_2O ranges from 29.9 to 76.9.

Metamorphic rocks. During the mineralogical-geochemical and isotopic-geochronological studies of metamorphic and magmatic complexes within the Belomorsky mobile belt, Lapland granulite belt and Tana belt (Russia), among others, there were data obtained on the geochemistry of zircons from gabbros of Cape Tolstik and from granulites [Kaulina, 2010] (Table 4.1, Figure 4.8). Among these zircons two types were distinguished, they differ in morphology and color of the crystals, in the isotopic age, as well as in the distribution of trace elements, including REE. The more rare zircons of the first type, represented by short-prismatic crystals of yellowish-brown color (2443 ± 10 million years age) are characterized by high contents of REE as well as U, Th and Y. The zircons of the second type are much more common and are represented by colorless long-prismatic crystals (2410 ± 3 million years age). The contents of REE and other trace elements are slightly lower than in the zircons of the first type. The intensity of the negative anomalies of Eu and Pr, as well as the positive Ce anomalies in zircons from both types, varies significantly. In general, the intensity

of Ce anomalies in the zircons of the first type is slightly smaller than in the zircons of the second type (Figure 4.7). Zircons of both types are characterized by similar values of the Th/U parameter that ranges from 1.1 to 1.3.

In one of granulite samples Kaulina found a broken chain of small (5–20 mm) zircon grains located on the periphery of a large rutile crystal. It is noted that this type of zircon microsegregations (size ~10 mm), that are located on the periphery of larger ilmenite crystals, have also been found in eclogites-facies rocks of Bergen Arcs province (Norway) [Bingen *et al.*, 2004]. According to Kaulina, such microsegregations of zircon could be formed in the process of infiltration of fluids, which was accompanied by partial or complete pseudomorphic ilmenite substitution for rutile, while the ilmenite was a source of Zr.

During geochemical studies of zircon and coexisting garnets from high-pressure schist and eclogites in metamorphic complexes of Australia (Reynolds Range) and Alps (Sesia-Lanzo Zone, Zermatt Saas Fee ophiolites) it was found that zircons from these rocks are characterized by very wide variations in content of all trace elements, including REE [Rubatto, 2002]. At the same time, the author showed that regardless of the composition of rocks, metamorphosed in eclogite facies, the zircons, represented in them, show low values of Th/U parameter, a slight enrichment with HREE and low intensity of negative Eu anomalies, which distinguishes them from zircons of magmatic rocks. It should be noted that the reduced Eu anomaly in the metamorphic zircon is interpreted as indicating the absence of feldspars. According to Rubatto, the REE composition of zircons from metamorphic rocks studied allows to correlate their formation with certain stages and facies of metamorphism, including eclogite, granulite and greenschist facies.

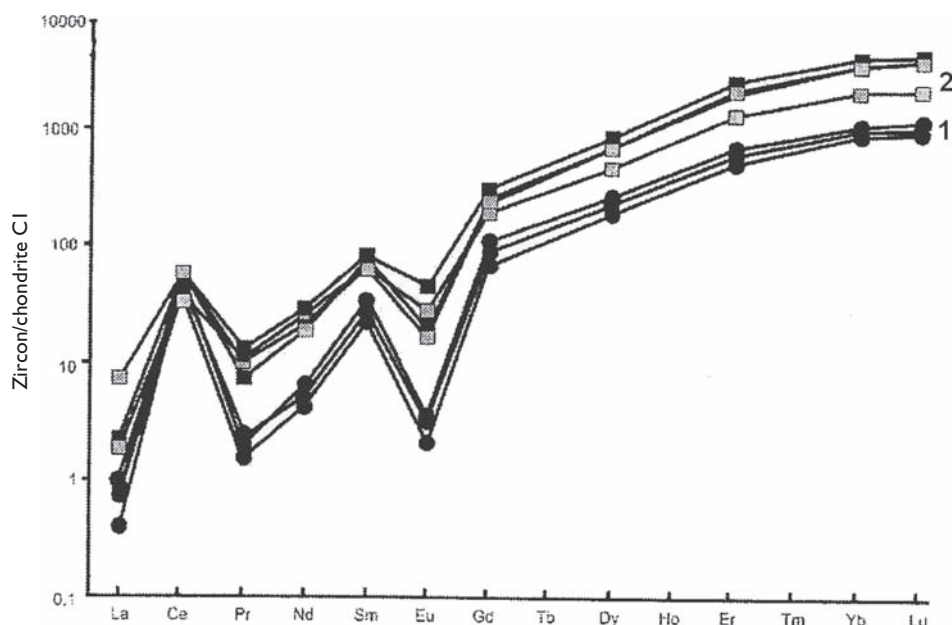


Figure 4.8 Chondrite-normalized REE patterns for zircons from gabbro-anorthosites (1) and gabbros (2) from Tolstik manifestation (Kola Peninsula, Russia) (data [Kaulina, 2010]) (see Table 4.1).

The isotope-geochronological and geochemical studies were recently carried out of the large collections of zircon samples from the Archean and Paleoproterozoic hypersthene gneisses forming Irkutny granulitic-gneiss block of Sharyzhalgaisky ledge in south-western part of the Siberian craton (Russia) [Turkina *et al.*, 2011]. Based on the identified distinguishing features of zircons, including the morphology of their crystals, isotopic age and REE composition, the authors singled out three generations of this mineral. The first, represented in the cores of the crystals with relict growth zoning, is defined as a magmatic generation. The zircons relating there to (age 3.16 billion years) are characterized by relatively high values of $(\text{Lu}/\text{Gd})_{\text{n}}$ parameter (11–36) and very intense positive Ce anomalies. Zircons of the second generation, which is defined as metamorphogenetic (age ~3.04 billion years), are present in the form of multiplanar crystals, shells and nonzonal cores of crystals. These zircons are depleted by REE and are characterized by much lower values of the $(\text{Lu}/\text{Gd})_{\text{n}}$ parameter, than the zircons of the first generation. The third generation of zircon is the latest and also identified as metamorphogenetic one. Zircons of this generation (age ~1.85 billion years) are represented by narrow rims surrounding the crystals of zircon of the earlier generations. They are characterized by medium values of $(\text{Lu}/\text{Gd})_{\text{n}}$ parameter.

Fedotova *et al.* [2008] studied the REE composition of zircons from subalkaline magmatic rocks, syenites and tonalites of the Karelian region and metamorphic rocks of granulite facies of the Ukrainian shield. Zircons from tonalites and syenites, which crystallized in equilibrium with the melt, have positive slopes of distribution patterns of REE chondrite-normalized contents. They are complicated by the maxima of Ce and minima of Eu. Zircons from metamorphic rocks, which crystallized under granulite facies, have the REE patterns dramatically different from the minerals of the syenite and tonalites lower concentrations of HREE, which is due to the competing influence of coexisting garnets.

Origin and REE compositions of zircon in jadeitite from the Nishisonogi metamorphic rocks (Kyushu, Japan) were examined by Mori *et al.* [2011]. The cores of zircon grains are richer in Y, Th, Ti and REE, but the rims are richer in Hf and U. Chondrite-normalized REE patterns of the cores indicate higher $(\text{Sm}/\text{La})_{\text{n}}$ ratios, lower $(\text{Yb}/\text{Gd})_{\text{n}}$ ratios and larger positive Ce anomalies compared with those of the rims.

Granitoids and acid effusive rocks. The REE composition of zircons, presented in high-silicon plutonic and volcanic rocks that differ in composition and conditions of formation, have been studied with various degree of detail (Table 4.6). In addition, the zircons from granite and dacite, that are common in some parts of Japan, were investigated regarding the REE distribution among the first [Nagasawa, 1970]. In this study it was shown that the zircons from Osumi and Takakuma granitoidal massifs have chondrite-normalized contents of the elements increasing in the row from Ce (200–400 t.ch.) to Yb (2000–4000 t.ch.) (Figure 4.9, 2, 3). Moreover, in the zircons from dacites that are forming Torihama and Ito massifs, the level of Ce accumulation turned out to be even higher (Figure 4.9, 4).

Later on, the studies were concentrated on the zircons from tonalities of Quottoon complex (British Columbia, Canada), the content of REE in which, as well as their total amounts, show considerable variation (Table 4.6). Chondrite-normalized contents of the elements in them are dramatically increasing in the row from La (1–20 t.ch.) to Yb (600–6000 t.ch.), while the configuration of REE patterns and intensity of positive Ce anomalies are only marginally affected (Figure 4.9, 1).

A large amount of analytical data was obtained in studies on REE composition of zircons from granitoids of the Boggy Plain pluton (New South Wales, Australia). It is composed of adamellites that are subdivided in two varieties – the internal and external; subordinate granodiorites that are also divided into two types – the internal and external; less common diorites and aplites (Table 4.7). Zircons from all these varieties of granitoids are generally slightly different in chondrite-normalized REE content and form of the patterns of their distribution (Figure 4.10). At the same time the total contents of elements in the mineral slightly decrease in the row from the external adamellites (870 ppm) to the external granodiorites (638 ppm). The patterns of chondrite-normalized REE contents of zircon from rocks of this pluton are characterized by very steep positive slope ($\text{La} = 0.08\text{--}20 \text{ t.ch.}$; $\text{Lu} = 1500\text{--}47000 \text{ t.ch.}$). All of them are complicated by intense positive Ce anomalies, as well as by less intense negative Eu anomalies. A total collection of zircons from the Boggy Plain pluton show that the average value of $(\text{La/Yb})_n$ parameter is 0.0002. The values of $(\text{Ce/Ce}^*)_n$ parameter is somewhat reduced in a row from the external granodiorites samples (234) to the samples of diorite (163). In addition to these, the negative Eu anomalies in these zircons are of approximately equal intensity: the values of $(\text{Eu/Eu}^*)_n = 0.21\text{--}0.25$.

Hoskin & Ireland [2000] published their own summary and literature data on the REE composition of zircons from the many varieties of magmatic and metamorphic rocks, including diorites, plagiogranites, aplites, gabbros, kimberlites, carbonatites,

Table 4.6 REE compositions of zircons from tonalites, granites and dacites from British Columbia province, Canada (ppm).

Element	<i>[Thomas et al., 2002], SIMS</i>							
	#1	#I-I	#B1	#B2	#4	#7	#I-III	#35
<i>Tonalites</i>								
La	1,04	0,91	2,69	4,27	2,90	0,40	1,92	7,89
Ce	70,8	34,4	112	38,8	186	22,1	52,7	67,8
Pr	N.d.	N.d.	N.d.	N.d.	N.d.	N.d.	N.d.	N.d.
Nd	15,7	2,53	14,0	5,84	30,8	1,43	9,14	16,2
Sm	18,0	5,51	19,9	7,91	30,4	4,16	14,6	10,5
Eu	N.d.	N.d.	N.d.	N.d.	N.d.	N.d.	N.d.	N.d.
Gd	N.d.	N.d.	N.d.	N.d.	N.d.	N.d.	N.d.	N.d.
Tb	N.d.	N.d.	N.d.	N.d.	N.d.	N.d.	N.d.	N.d.
Dy	245	66,3	202	107	365	72,4	168	159
Ho	N.d.	N.d.	N.d.	N.d.	N.d.	N.d.	N.d.	N.d.
Er	388	113	291	194	625	137	284	303
Tm	N.d.	N.d.	N.d.	N.d.	N.d.	N.d.	N.d.	N.d.
Yb	670	249	494	348	348	290	439	569
Lu	N.d.	N.d.	N.d.	N.d.	N.d.	N.d.	N.d.	N.d.
Total	1409	472	1136	706	1588	527	969	1133
$(\text{La/Yb})_n$	0,001	0,002	0,004	0,008	0,006	0,001	0,003	0,009
$(\text{Eu/Eu}^*)_n$	N.d.	N.d.	N.d.	N.d.	N.d.	N.d.	N.d.	N.d.
$(\text{Ce/Ce}^*)_n$	52,2	29,0	31,9	6,97	49,2	42,4	21,1	6,59

(Continued)

Table 4.6 (Continued).

Element	British Columbia province (Canada)			Japan				
	[Thomas et al., 2002], SIMS			[Nagasawa, 1970], IPMA				
	#46	#I	#G	9Z	10Z	1Za	1Zb	4Z
Tonalites				Granites			Dacites	
La	0,62	0,41	0,84	N.d.	N.d.	N.d.	N.d.	N.d.
Ce	23,9	27,9	24,0	23,6	15,6	127	312	104
Pr	N.d.	N.d.	N.d.	N.d.	N.d.	N.d.	N.d.	N.d.
Nd	7,91	2,10	1,34	8,90	13,1	36,6	97	34,1
Sm	2,60	3,26	2,06	5,70	20,6	9,7	17	6,5
Eu	N.d.	N.d.	N.d.	0,21	0,56	2,16	1,64	0,74
Gd	N.d.	N.d.	N.d.	N.d.	N.d.	28,9	32,8	N.d.
Tb	N.d.	N.d.	N.d.	N.d.	N.d.	N.d.	N.d.	N.d.
Dy	64,7	82,7	34,1	124	264	130	125	126
Ho	N.d.	N.d.	N.d.	N.d.	N.d.	N.d.	N.d.	N.d.
Er	114	131	55,3	211	418	269	249	249
Tm	N.d.	N.d.	N.d.	N.d.	N.d.	N.d.	N.d.	N.d.
Yb	259	268	145	392	720	598	591	529
Lu	N.d.	N.d.	N.d.	N.d.	154	143	152	105
Total	473	515	263	765	1606	1344	1577	1154
$(La/Yb)_n$	0,002	0,001	0,004	N.d.	N.d.	N.d.	N.d.	N.d.
$(Eu/Eu^*)_n$	N.d.	N.d.	N.d.	N.d.	N.d.	N.d.	N.d.	N.d.
$(Ce/Ce^*)_n$	29,6	52,2	21,9	N.d.	N.d.	N.d.	N.d.	N.d.

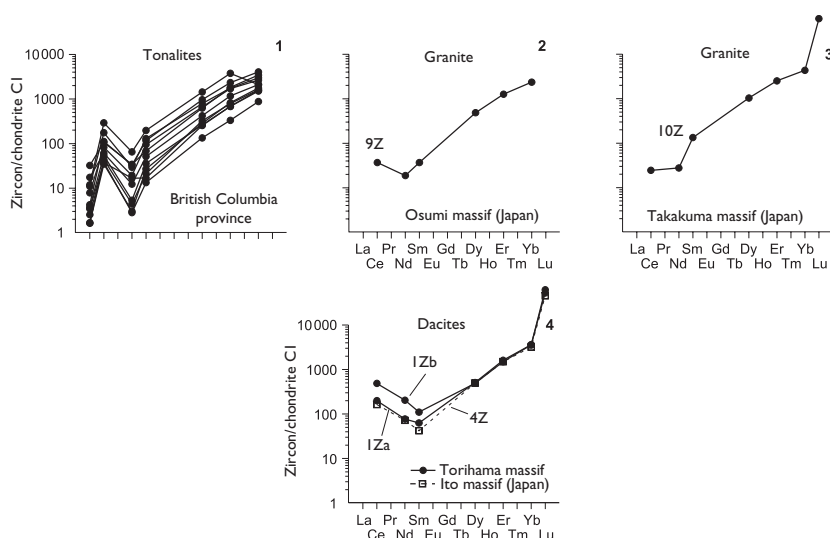


Figure 4.9 Chondrite-normalized REE patterns for zircons from tonalites of British Columbia (1), and from granites and dacites from some massifs of Japan (2–4) (data Table 4.6).

Table 4.7 REE compositions of zircons from diorites, granodiorites, adamellites, and aplites from Boggy Plain massif (New South Wales province, Australia) (ppm).

[Hoskin et al., 2000], SIMS													
	39-a.I	39-b.I	39-c.I	39-d.I	39-e.I	39-f.I	39-g.I	7-b.I	7-c.I	7-d.I	7-e.I	7-f.4	7-g.I
Element	Diorites							Granodiorites (outer)					
La	0,03	0,05	0,03	0,02	0,07	0,03	0,03	0,24	0,02	0,03	0,02	0,02	0,13
Ce	3,6	5,7	4,9	4,4	8,3	6,3	5,2	21	11	17	11	9,4	41
Pr	0,01	0,09	0,04	0,01	0,13	0,08	0,04	19	0,02	0,12	0,02	0,01	0,32
Nd	0,4	2,6	1	0,5	3,8	2,6	1,3	4,9	0,7	3,9	0,7	0,5	9
Sm	0,9	5	2,1	1,2	6	5	2,6	8,3	19	7,3	1,9	1,4	15
Eu	0,2	0,7	0,4	0,3	1	0,8	0,5	1,2	0,4	1	0,3	0,3	2
Gd	6,3	21	12	8,2	30	23	15	44	14	35	13	10	73
Tb	2,1	6,2	3,9	2,4	9,5	6,9	4,6	14	5	11	4,7	3,5	24
Dy	25	67	44	29	108	73	52	152	59	117	56	43	292
Ho	10	26	18	11	46	28	21	59	25	45	24	18	122
Er	51	127	84	55	218	127	102	272	129	211	125	93	580
Tm	11	26	18	12	44	26	21	55	29	43	28	21	117
Yb	122	270	193	125	462	269	231	582	323	455	323	237	1191
Lu	27	59	42	27	100	55	49	121	71	92	71	52	246
Total	260	616	423	276	1037	623	505	1354	686	1038	659	489	2712
(La/Yb) _n	0,00017	0,00012	0,00010	0,00011	0,00010	0,00008	0,00009	0,00028	0,00004	0,00004	0,00004	0,00006	0,00007
(Eu/Eu*) _n	0,19	0,18	0,19	0,22	0,19	0,19	0,19	0,15	0,07	0,16	0,14	0,18	0,15
(Ce/Ce*) _n	180	81	140	293	83	115	149	2,18	550	227	550	627	182

(Continued)

Table 4.7 (Continued).

Boggy Plain massif (New South Wales province, Australia)												
	[Hoskin et al., 2000], SIMS											
	16-a.I	16-b.I	16-c.I	16-d.I	16-e.I	22-a.I	22-b.2	22-b.3	22-c.I	22-d.I	22-e.I	22-f.I
Element	Granodiorites (inner)					Adamellites (outer)						
La	0,07	0,05	0,13	0,05	0,07	0,08	0,04	0,03	0,03	0,04	0,03	0,02
Ce	15	3,5	7	3,7	25	17	20	16	14	18	13	12
Pr	0,14	0,04	0,07	0,03	0,05	0,14	0,1	0,05	0,05	0,07	0,05	0,04
Nd	3,6	1,2	1,8	0,7	1	3,2	2,3	0,7	0,6	1,3	0,9	0,3
Sm	6	3	3,9	2,2	2,2	6	5	1,5	1,5	2,8	2,1	0,7
Eu	0,7	0,2	0,4	0,3	0,5	1,4	1,4	0,5	0,4	0,7	0,6	0,2
Gd	24	19	23	18	15	30	26	6,3	10	15	12	5,2
Tb	7,1	6,5	7,5	7,3	4,9	9,3	8	3	3,3	4,8	4,3	1,6
Dy	64	66	80	90	52	97	81	33	38	51	49	18
Ho	22	25	29	36	20	38	31	13	15	20	20	7
Er	109	131	158	204	135	162	132	60	75	104	94	44
Tm	22	27	32	43	30	32	27	13	16	22	20	10
Yb	218	277	336	449	325	326	278	143	173	237	222	120
Lu	48	61	74	102	76	71	62	33	30	52	52	29
Total	540	620	753	956	687	793	674	323	377	529	490	248
$(\text{La/Yb})_n$	0,00022	0,00012	0,00026	0,00008	0,00015	0,00017	0,00010	0,00014	0,00012	0,00011	0,00009	0,00011
$(\text{Eu/Eu}^*)_n$	0,15	0,06	0,10	0,10	0,20	0,26	0,30	0,42	0,23	0,26	0,29	0,23
$(\text{Ce/Ce}^*)_n$	143	78	70	93	417	155	286	400	350	327	325	400

(Continued)

Table 4.7 (Continued).

<i>Boggy Plain massif (New South Wales province, Australia)</i>												
	[Hoskin et al., 2000], SIMS											
	III-a.2	III-a.3	III-a.5	III-c. I	III-d. I	III-e. I	III-f. I	42-a. I	42-b. I	42-b.2	42-c. I	42-d.2
Element	<i>Adamellites (inner)</i>							<i>Aplites</i>				
La	0,03	0,05	0,04	0,11	0,07	0,07	0,09	0,09	0,06	0,06	0,06	0,23
Ce	15	15	15	15	16	16	14	15	16	19	14	22
Pr	0,05	0,05	0,04	0,02	0,02	0,01	0,04	0,14	0,11	0,16	0,08	0,12
Nd	0,7	1,4	0,6	0,6	1,2	1,3	1,2	0,9	1	1,5	1,3	2
Sm	1,7	2,8	1,5	1,3	2,5	2,6	2,2	2,1	2,2	4,1	2,4	3,2
Eu	0,5	0,8	0,4	0,2	0,4	0,7	0,6	0,6	0,4	0,5	0,5	1,1
Gd	11	18	11	8,9	14	15	14	14	12	31	14	18
Tb	3,8	6,1	3,7	2,7	3,6	3,2	2,8	4,7	4,1	12,9	4,5	6,6
Dy	41	65	41	35	51	50	49	50	41	149	44	71
Ho	16	26	17	15	19	19	19	20	16	63	17	31
Er	83	129	83	50	89	102	87	107	83	346	90	177
Tm	16	27	18	17	20	22	22	21	16	70	18	38
Yb	176	288	184	182	216	241	230	225	174	773	186	452
Lu	39	68	46	44	49	57	57	53	39	177	41	113
Total	404	647	421	372	482	530	499	514	405	1647	433	935
(La/Yb) _n	0,00012	0,00012	0,00015	0,00041	0,00022	0,00020	0,00026	0,00027	0,00023	0,00005	0,00022	0,00034
(Eu/Eu*) _n	0,27	0,26	0,22	0,13	0,16	0,27	0,25	0,25	0,19	0,10	0,20	0,35
(Ce/Ce*) _n	375	300	375	231	356	400	215	130	188	173	200	126

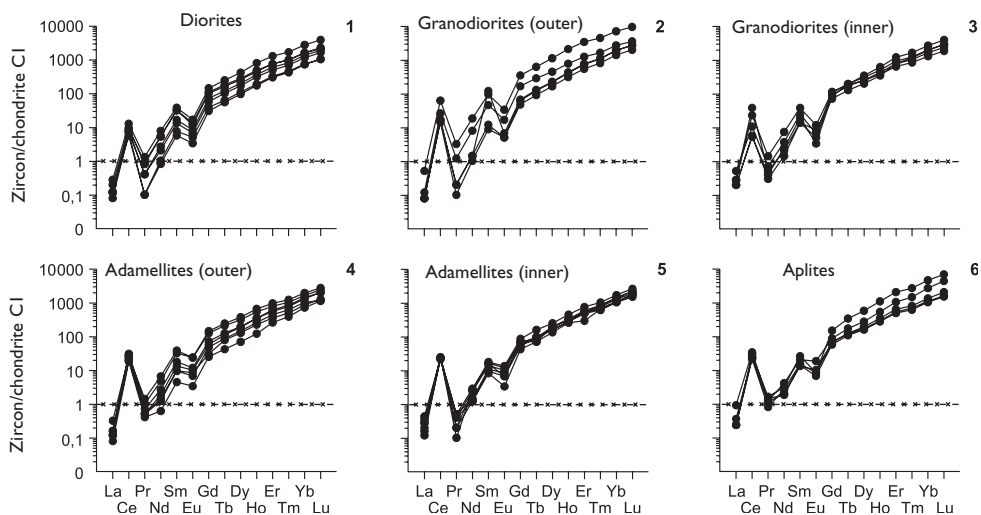


Figure 4.10 Chondrite-normalized REE patterns for zircons from diorites (1), granodiorites (2), adamellites (4, 5), aplites (6) from Boggy Plain massif (New South Wales, Australia) (data Table 4.7).

charnockites and metamorphic rocks from many parts of the world. Before giving any comments on the materials presented it should be noted that in one of authors studied samples of gabbro (weighing about 2 kg), forming Blind massif (Australia), they discovered about 1000 zircon crystals ranging in size from 50 to 250 microns. In the collection of zircon samples, outlined in this article, the chondrite-normalized REE contents are significantly increasing in the row from La (0.1–1.0 t.ch.) to Yb (1000–10000 t.ch.). Their REE patterns in almost all cases are complicated by positive Ce anomalies of various intensities, as well as less intense negative Eu anomalies (Figure 4.11). Moreover, summing up the results of their studies, Hoskin & Ireland emphasized that they didn't manage to detect any significant correlation between the REE composition of zircons and the petrographic types, as well as the genesis of the rocks containing them. These observations led them to conclude that the parameters of REE distribution in zircons shouldn't be used as criteria in determining the sources of ablation of the material during the formation of terrigenous rock mass. An exception was made only for zircons from kimberlites and carbonatites, for which they have identified some specific features, in particular, a significantly reduced overall level of REE accumulation, very gentle slope of REE patterns in the area of heavy elements, as well as the absence of negative Eu anomalies in the patterns of these zircons.

Along with the zircons from the gabbro of Berdyushsky massif (Urals, Russia), the REE composition of which was described above, Ronkin & Nesbit [1997] studied the REE composition of zircons from syenite-diorites, nepheline syenites and rapakivi granites forming this massif. The authors draw attention to a higher level of REE accumulation and more intensive fractionation of elements in zircons from the syenite-diorite compared with the mineral from gabbro. In all of the patterns of zircons from syenite-diorites, nepheline syenites and rapakivi granites of this complex struc-

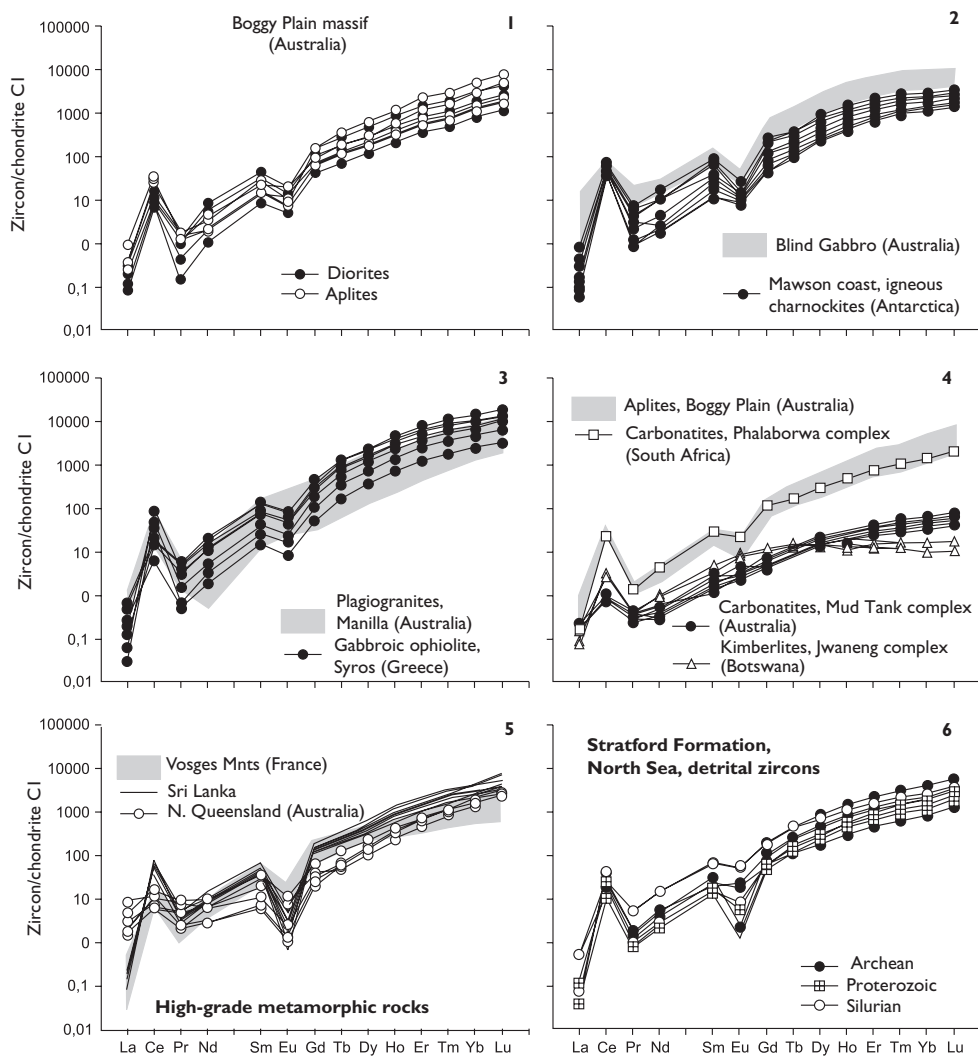


Figure 4.11 Chondrite-normalized REE patterns for zircons from some igneous, metamorphic, and detrital rocks (data [Hoskin & Ireland, 2000]).

tured massif there were observed intense Ce anomalies and negative Eu anomalies. Chondrite-normalized Yb and Lu contents in them ranged from 700 to 8000 t.ch. The REE patterns of zircons from nepheline syenites are different from the others due to sinusoidal configuration caused by a relative enrichment with both heavy and LREE. At the same time, the zircons from rapakivi granites in terms of REE accumulation and patterns configuration are comparable to the zircons from syenite-diorites.

The results of the study of REE composition of zircons from the syenites, nepheline syenites, charnockites and biotite migmatites that are part of a series of magmatic and

Table 4.8 REE compositions of zircons from syenites, charnockites, and biotitic migmatites from magmatic and metamorphic complexes of India (ppm).

India						
	[Murali et al., 1983], RNAA					
	Mur-4	Mur-6	Mur-3	Mur-5	Mur-1	Mur-2
Element	Syenite		Nepheline syenite	Charnokites		
	Mur-4			Mur-3		
Biotite migmatites						
La	2,70	22,0	35,0	0,40	12,0	12,0
Ce	11,0	24,0	50,0	19,0	25,0	25,0
Pr	N.d.	N.d.	N.d.	N.d.	N.d.	N.d.
Nd	N.d.	N.d.	N.d.	N.d.	N.d.	N.d.
Sm	1,50	9,70	10,8	6,40	6,00	6,00
Eu	0,42	2,45	1,00	2,90	0,20	0,20
Gd	N.d.	N.d.	N.d.	N.d.	N.d.	N.d.
Tb	3,50	4,50	6,20	3,00	1,90	1,90
Dy	N.d.	N.d.	N.d.	N.d.	N.d.	N.d.
Ho	N.d.	N.d.	N.d.	N.d.	N.d.	N.d.
Er	N.d.	N.d.	N.d.	N.d.	N.d.	N.d.
Tm	N.d.	N.d.	N.d.	N.d.	N.d.	N.d.
Yb	238	204	250	85,0	36,0	30,0
Lu	47,0	24,0	50,0	10,1	6,20	5,40
Total	304	291	403	127	87,3	80,5
(La/Yb) _n	0,08	0,073	0,094	0,003	0,225	0,270

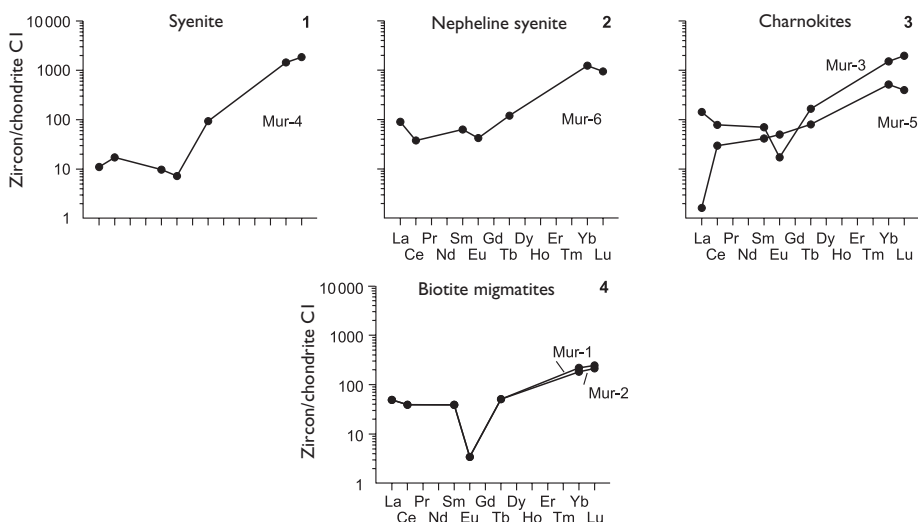


Figure 4.12 Chondrite-normalized REE patterns for zircons from syenites (1), nepheline syenites (2), charnockites (3), and biotite migmatites from some igneous and metamorphic complexes of India (data Table 4.8).

Table 4.9 Average REE compositions of zircons from some placer deposits (ppm).

West Siberia province (Russia)											
[Rikhvanov et al., 2001]											
Placer deposit's number											
Element	1 (4)	2 (3)	3 (13)	4 (17)	5 (32)	6 (4)	7 (17)	8 (10)	9 (4)	10 (32)	11 (2)
La	20,2	4,00	28,0	20,2	57,7	237	20,2	92,50	10,60	57,7	439
Ce	N.d.	N.d.	N.d.	45,5	37,5	68,0	45,5	N.d.	N.d.	37,5	347
Sm	48,5	44,2	39,8	26,7	25,1	45,0	26,7	76,9	62,1	25,1	83,5
Eu	N.d.	N.d.	6,80	5,50	8,90	20,0	5,50	N.d.	7,60	8,90	54,0
Tb	N.d.	N.d.	N.d.	N.d.	11,9	28,0	N.d.	N.d.	N.d.	11,9	49,50
Yb	426	235	330	326	464	365	326	330	240	464	616
Lu	43,6	75,4	84,8	88,2	167	105	88,2	104	74,80	167	256
(La/Yb) _n	0,032	0,011	0,057	0,042	0,084	0,438	0,042	0,189	0,030	0,084	0,481

Note. 1–4 – Tugansky deposit: 1 – Malinovsky section, 2 – North section, 3 – Yuzhno-Alexandrovsky section, 4 – Kuskovo-Shiriaevsky section; 5 – Georgievsky deposit; 6 – Tarsky deposit; 7 – Tugansky deposit (colorless, yellow, and brown zircons); 8 – Georgievsky deposit (colorless, and painted zircons); 9 – Tugansky deposit (brown zircons); 10 – Georgievsky deposit (colorless zircons); 11 – Georgievsky deposit (painted zircons). In brackets – quantity of analyses.

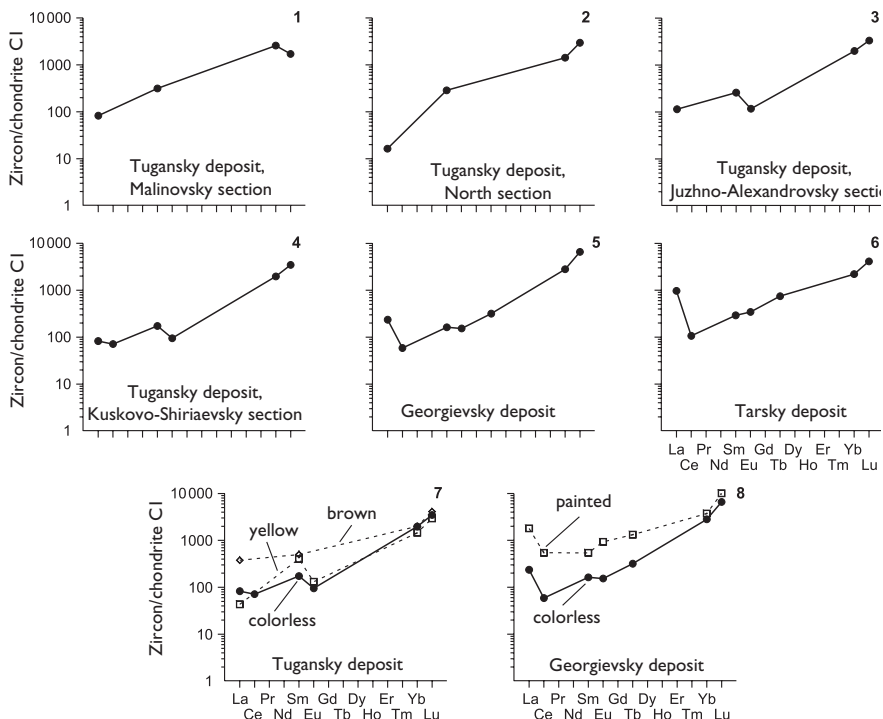


Figure 4.13 Chondrite-normalized REE patterns for zircons from some placer deposits (Western Siberia, Russia) (data Table 4.9).

metamorphic complexes in India were presented in the work of Murali *et al.* [1983]. It was ascertained that the total REE contents in the zircons from these syenites and charnockites are significantly higher than in the mineral from biotite migmatites (Table 4.8). On the REE patterns of all the zircons from this collection there are weak negative Eu anomalies, but an absence of intense positive Ce anomalies (Figure 4.12, 5.6).

Zircons from placer deposits. As already noted, due to their high mechanical strength, zircons are able to accumulate in the terrigenous rock mass and under favorable conditions to form the complex placer deposits. REE composition of zircons from some of the zircon-ilmenite placer deposits in Western Siberia (Russia) is described in the work by Rikhvanov *et al.* [2001] (Table 4.9). Average chondrite-normalized La contents in the zircons from the majority of these deposits are around 100 t.ch., for Yb and for Lu they increased up to 3.000 t.ch. (Figure 4.13, 1–6). The authors showed that for the colorless crystals of zircon the overall REE accumulation is lower compared with its crystals of a yellow, brown or other type of color (Figure 4.13, 7, 8). The data on zircons from some gabbro of the Kola Peninsula (Russia) prove this regularity [Kaulina, 2010]. Finally, we note, that Izokh *et al.* [2010] examined the REE composition of zircon from Dak Nong placer deposit (Vietnam), where they appear as individual crystals and as inclusion in crystals of sapphire. HREE contents in these zircons are much higher than contents of LREE. The levels of accumulation of REE in inner zones of zircon crystals are usually somewhat higher than in the outer zones. Intense Ce positive anomalies and less intense Eu negative anomalies there are on the patterns of REE distribution of these zircons.

4.2 COEFFICIENTS OF REE DISTRIBUTION BETWEEN ZIRCONS AND COEXISTING PHASES

In several works along with the data on the REE composition of zircons there are results of studies on the coefficients of REE distribution between this mineral and melts and coexisting minerals of different composition (Table 4.10, Figure 4.14). Among the first, the data on the values of K_d (zircon/dacite matrix) and K_d (zircon/granite) were published by Nagasawa [1970], according to which the K_d of all REE for these rocks have values >1 , while the values for the light elements were the first units and for heavy elements—366–389 (Figure 4.14, 3). Later, Watson [1980] relying on the results of physical experiments with felsitic melts executed at $T = 800^\circ\text{C}$ and $P = 2$ kbar, determined that the value of K_d (zircon/melt) vary within the following ranges: La (1.4–2.1); Sm (26–40); (Ho >340); Lu (72–126) (Figure 4.14, 7). Data on the REE composition of zircons from syenites and charnockites containing them allowed Murali *et al.* [1983] to calculate the values of K_d for some elements. For a zircon-syenite system they were: La ~ 0.035 and Lu ~ 100 , for zircon-charnockite system: La ~ 3 and Lu ~ 2000 (Figure 4.14, 5, 6). According to the calculations made using the estimations of REE in zircons and the basanite matrix containing them [Irving & Fray, 1984], the following values of K_d (zircon/basanitic melt) were obtained: La ~ 0.09 , Lu-300 (Figure 4.14, 1).

While studying the zircons from amphibole-biotite diorites of Quattoon complex (British Columbia, Canada), the values of K_d (REE) in zircon-dioritic melt system were determined. For this purpose there were used the results of analysis of REE in

Table 4.10 The coefficients of REE distribution between zircons and coexisting different melts.

Melts												
	Basanitic	Alkaline basaltic		Dacitic			Granitic		Felsitic		Sienitic	Charnocitic
	Zircon/matrix			Zircon/rock					Zircon/melt		Zircon/rock	
	[Irving, Frey, 1984]	[Hinton, Upton, 1991]		[Nagasawa, 1970]			[Watson, 1980]		[Murali et al., 1983]			
Element	IrF-I(min)	Hmin-I	Hmax-2	I _{Za}	I _{Zb}	4Z	9Z	10Z	Wat-I	Wat-2	Mur-I	Mur-2
La	0,08	0,033	4,1	N.d.	N.d.	N.d.	N.d.	N.d.	1,4	2,1	0,035	0,3
Ce	0,13	0,4	4	3	7,38	2,29	0,27	0,31	N.d.	N.d.	0,1	0,25
Pr	N.d.	0,082	N.d.	N.d.	N.d.	N.d.	N.d.	N.d.	N.d.	N.d.	N.d.	N.d.
Nd	N.d.	0,176	5	2,43	6,51	1,97	0,26	0,55	N.d.	N.d.	N.d.	N.d.
Sm	0,38	0,891	4,7	3,7	6,5	2,58	0,87	3,24	26	40	0,15	1,0
Eu	1,26	N.d.	4,7	5,22	3,96	1,07	0,18	1,57	N.d.	N.d.	0,5	0,5
Gd	N.d.	3,54	7,9	N.d.	N.d.	N.d.	N.d.	N.d.	N.d.	N.d.	N.d.	N.d.
Tb	N.d.	23,4	24,4	N.d.	N.d.	N.d.	N.d.	N.d.	N.d.	N.d.	4,0	20
Dy	N.d.	26,5	52	53,5	51,5	37,8	25,2	105	N.d.	N.d.	N.d.	N.d.
Ho	N.d.	82	88,5	N.d.	N.d.	N.d.	N.d.	N.d.	340	340	N.d.	N.d.
Er	N.d.	62,9	143	152	141	119	81,5	450	N.d.	N.d.	N.d.	N.d.
Tm	N.d.	282	282	N.d.	N.d.	N.d.	N.d.	N.d.	N.d.	N.d.	N.d.	N.d.
Yb	138	304	304	299	296	242	178	890	N.d.	N.d.	50	500
Lu	172	N.d.	420	366	389	281	N.d.	1230	72	126	100	2000

(Continued)

Table 4.10 (Continued).

													Alkaline basaltic melt	Ionic radii, Å
													[Hinton, Upton, 1991]	[Shannon, 1976]
Element	#I	#I-I	#B-I	#B-2	#4	#7	#I-II	#35	#46	#I	#G	Average	Average (H-I)	
La	0,05	0,04	0,07	0,22	0,03	0,02	0,06	0,26	0,02	0,03	0,05	0,05	0,0083	1,16
Ce ³⁺	2,06	0,83	1,46	0,99	1,4	0,61	0,93	1,26	0,43	1,1	0,75	0,99	0,022	1,143
Pr	N.d.	N.d.	N.d.	N.d.	N.d.	N.d.	0,0635	1,126						
Nd	1,58	0,2	0,5	0,53	0,77	0,11	0,56	0,81	0,35	0,31	0,16	0,5	0,176	1,109
Sm	11,6	2,7	3,56	4,14	5,02	2,49	4,58	3,26	0,75	11,2	1,27	3,56	1,06	1,079
Eu	N.d.	N.d.	N.d.	N.d.	N.d.	N.d.	2,30	1,066						
Gd	N.d.	N.d.	N.d.	N.d.	N.d.	N.d.	5,01	1,033						
Tb	N.d.	N.d.	N.d.	N.d.	N.d.	N.d.	10,9	1,040						
Dy	73,0	20,1	22,5	16,8	19,4	36,6	12,4	52,0	19,3	52,3	26,4	22,5	23,7	1,027
Ho	N.d.	N.d.	N.d.	N.d.	N.d.	N.d.	48,6	1,015						
Er	72,4	29	29,4	21,1	17,9	58,9	13,1	75,0	52,7	60,7	70	52,7	94	1,004
Tm	N.d.	N.d.	N.d.	N.d.	N.d.	N.d.	171	0,994						
Yb	51,5	40,6	35,9	21,9	14,0	66,1	13,0	76,3	82,3	35,1	96,7	40,6	293	0,985
Lu	N.d.	N.d.	N.d.	N.d.	N.d.	N.d.	472	0,977						
Ce ⁴⁺	N.d.	N.d.	N.d.	N.d.	N.d.	N.d.	718	0,970						

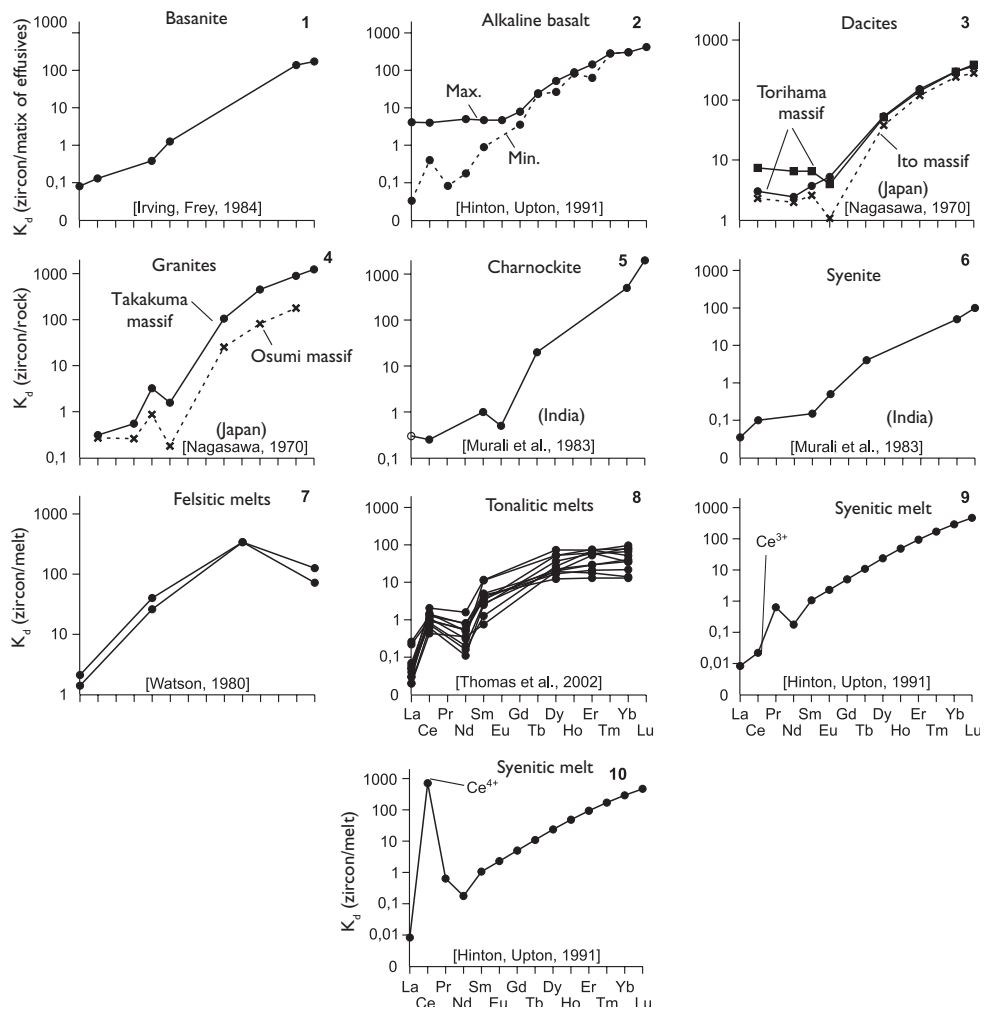


Figure 4.14 The graphs of coefficients of REE distribution between zircons and the bulk matrix of the basanites (1), alkaline basalts (2), dacites (3), between zircons and granites (4), charnockites (5), syenites (6), 7 – between zircons and experimental felsitic melt, 8 – between zircon and tonalitic melts (in microinclusions), 9 – graph is made using K_d for Ce^{3+} , 10 – graph is made using K_d for Ce^{4+} (data Table 4.10).

melt microinclusions contained in these zircons [Thomas *et al.*, 2002]. According to these estimates, the values of K_d for La ranged from 0.02 to 0.26 (average – 0.05); for Ce – from 0.43 to 2.06 (average – 0.99); for Nd the average K_d was 0.5; for all the rest elements the average values of K_d increased consistently: Sm – 3.56, Dy – 22.45, Er – 52.72 (Figure 4.14, 8). The K_d values obtained by J. Thomas *et al.* indicate that under the crystallization of zircons from the diorites of Quattoon complex La, Ce and Nd had the geochemical properties of the incompatible trace elements, while the rest REE had the properties of compatible elements.

Hinton & Upton [1991] determined the values of K_d (zircon/melt) on the basis of the analysis of REE in the individual large crystals of zircon from basanites and syenites. According to them the values of K_d (zircon/syenite melt) are consistently increasing in the row from La (0.0083) to Lu (472), and that these values correlate with a successive decrease in the size of the radii of trivalent ions of these elements – from 1.16 Å for La to 0.977 Å for Lu. However, such a sequence disrupted in case of Ce, the mean value of K_d for which amounted to 718, which is much higher than that for Lu (Figure 4.14, 10). Given these observations, the authors concluded that such an anomaly for Ce is due to the fact that in the zircons they studied this element was in the form of Ce^{4+} ions, which are more favorable for the occurrence in the mineral structure as compared to Ce^{3+} ions, because they have a much smaller radius (0.970 Å) compared with Ce^{3+} ions (1.143 Å). These data suggest that Ce^{4+} ions in the zircon structure would prevail over the Ce^{3+} ions in cases where the zircons were crystallized under high oxygen fugacity.

In conclusion, Rubatto [2002] presented data on the REE distribution between coexisting zircons and garnets, obtained in the study of eclogitic micaschist from Sesia-Lanzo Zone (Alps). According to the research for these rocks the highest values of K_d (zircon/garnet) are typical of Ce (69–90), for all subsequent elements are much lower: Nd (5.7–7.0), Sm (2.1–2.4), Eu (3.2–4.0), Gd (0.94–1.60), Tb (0.93–1.8), Dy (1.3–2.6), Ho (2.0–4.3), Er (3.2–7.1). For the other three elements K_d values are slightly rising: Tm (5.2–11.0), Yb (8.6–17.0), Lu (12.1–23.9).

4.3 ON THE ISOMORPHISM OF REE IN ZIRCONs AND CONDITIONS OF THEIR CRYSTALLIZATION

The level of REE in zircons, as in all other minerals, is largely due to their crystal-chemical properties. According to earlier data of Voytkevich *et al.* [1970], the size of the radius of Zr^{4+} ion as the main net-forming element of zircon is 0.82 Å, which is comparable with the size of the radii of the trivalent ion of heavy REE, especially the Yb^{3+} (0.82 Å) and Lu^{3+} (0.80 Å). Later estimates of the size of the ionic radii of elements were slightly adjusted, resulting in the currently accepted values for Zr^{4+} – 0.84 Å; for Yb^{3+} – 0.985 Å; for Lu^{3+} – 0.977 Å [Shannon, 1976]. It is likely that similar ionic radii of Zr^{4+} and HREE are an important determinant of particularly high values of K_d (zircon/melt) for them, and that these REE are characterized by a high degree of compatibility with the crystal structure of zircons.

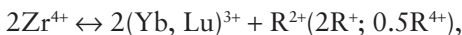
In the study of synthetic zircon by using cathodoluminescence method it has been found that their patterns contain a series of narrow lines in the area of 200–500 nm that were attributed to the REE such as Sm, Eu, Tb, Dy and Er [Cesbron *et al.*, 1993]. In addition, on a laser-fluorescent patterns of zircons from garnet amphibolites of the Cape Kamchatka (Kamchatka, Russia) there were also determined the lines, which were attributed to Er^{3+} ions [Osipenko *et al.*, 2007].

It is assumed that in the structure of zircons there are two basic positions that can potentially be replaced by cations: tetragonal position in which Si^{4+} ions are, and triangular (dodecahedral) position, which contains the Zr^{4+} ions, and the latter is the most favorable for the replacement of heavy REE by ions [Thomas *et al.*, 2002]. However, the relatively high level of compatibility with the zircon crystal structure of

heavy and part of MREE, is obviously not only due to similar size of the radii of their trivalent ions and network-forming ions, but also because of an appropriate balance of their charges. According to the model that has been proposed to solve this problem, an isomorphic substitution of Zr^{4+} ions by trivalent ions of REE and Y is accompanied by the entrance of P^{5+} ions into positions of Si^{4+} ions, which compensates for the balance of charges [Poirrasson *et al.*, 2002]. According to this model, the authors suggested the following scheme of REE isomorphism in zircons, which takes into account the balance of ion charges:



However, while discussing the scheme of REE isomorphism in zircons, some doubts aroused related to the fact that the phosphorus content in natural zircons is generally much lower (202–586 ppm, see above) than the total content of REE^{3+} (in atomic terms). Therefore, in order to maintain a real balance of charges during the isomorphous entrance of REE into the zircon structure, obviously, there should be involved some additional ions as charge compensators [Hinton & Upton, 1991; Hoskin *et al.*, 2000]. In this context a theory emerged, according to which the function of compensating the charge could be carried out by such ions as Mo^{4+} , Li^+ and others, and the heterovalent REE isomorphism in zircons could have the following form [Hanchar *et al.*, 2001]:



where R^{2+} – Ti^{2+} and Fe^{2+} ions, $2R^+$ and $0.5R^{4+}$ – Li^+ and Mo^{4+} ions.

During the reconstruction of the crystallization conditions of natural zircons a considerable attention is usually paid at positive Ce anomalies and negative Eu anomalies observed in many of their REE patterns. It is quite obvious that the appearance of anomalies of these elements, which can change its valence depending on the redox conditions of the environment, may be causally related to their valence state and the corresponding changes in the size of the radii of the ions that are involved in isomorphic substitution, and indirectly connected with the values of K_d (zircon/melt). Therefore, Zr^{4+} ions, the size of the radius of which is 0.84 Å, should be better replaced by Ce^{4+} ions, the size of the radius of which is 0.970 Å, compared with larger Ce^{3+} ions, the size of the radius of which is 1.143 Å. Such differences in the properties of Ce ions that are due to the degree of oxidation of the environment, seem to be the determining factor in a multiple increase of K_d (zircon/melt) values from 0.022 – for Ce^{3+} to 718 – for Ce^{4+} (Table 4.8, Figure 4.12, 9, 10).

The value of Ce^{4+}/Ce^{3+} in the zircons depends on the redox conditions of environment of their crystallization and varies widely. Increasing the degree of medium oxidation will stimulate the transition of certain amounts of Ce^{3+} ions into Ce^{4+} ions, as a result the ratio Ce^{4+}/Ce^{3+} will increase. The intensive positive Ce anomalies observed in the patterns of many zircons from the rocks of different composition and conditions of formation, indicate that in their structure Ce^{4+} ions prevail over Ce^{3+} ions, which may indicate that the crystallization of zircons was under a relatively high degree of medium oxidation. The validity of this conclusion can be proved by the fact that in zircons from lunar rocks that were crystallized in deliberately reducing conditions, Ce

anomalies are not observed [Hinton & Upton, 1991]. Another argument indicating that the crystallization of zircons from many terrestrial magmatic rocks with positive Ce anomalies on their patterns proceeded at a relatively high oxidation degree of crystallizing systems, are negative Eu anomalies, commonly observed in these patterns. The latter indicate the lower values of $\text{Eu}^{2+}/\text{Eu}^{3+}$ ratio, which are indicative of oxidizing conditions of the zircon crystallization.

In conclusion, the results of experiments performed by Cherniak *et al.* [1997] using natural and synthetic zircon crystals; it was found that the rate of REE diffusion in the crystal lattice of this mineral has very low values. These observations have led to the assumption that REE ions might be inactive during the metamorphic transformation of those protoliths, in which the zircons were initially present as accessory phases.

The research results of REE distribution in zircons are different in character, detail and representativeness, as discussed above, which suggests that this mineral, as one of the most common accessory phases of many magmatic, metamorphic and metasomatic rocks, can accumulate in its structure significant amounts of impurities, among which the heavy elements are usually dominating. The overall level of REE accumulation in zircons increases from the rocks of ultramafic and mafic composition to granitoid and alkaline rocks. REE patterns of zircons from magmatic rocks in most cases are complicated by intense positive Ce anomalies and less intense negative Eu anomalies, which, to conclude, is due to crystallization at a relatively high degree of medium oxidation. Crystallization at a relatively high degree of medium oxidation. Unlike the majority of zircons from rocks formed in terrestrial conditions, the mineral samples of lunar rocks formed in initially reducing conditions do not have such Ce anomalies in their patterns. The level of accumulation and distribution of REE in zircon structure is largely determined by the intensity of heterovalent isomorphous substitutions of Zr^{4+} ions by trivalent REE ions with an alleged involvement of ions such as Ti^{2+} , Fe^{2+} , Li^+ , Mo^{4+} and some others, who performed the function of charge compensators.

Chapter 5

Apatites

As an accessory mineral apatite is almost always present in many varieties of magmatic and some metamorphic and metasomatic rocks. In ultramafic rocks the apatites are quite rarely present, more often – in gabbro rocks and very often – in the granitoids and various rocks of heightened alkalinity. Depending on the composition of the anions the apatites are divided into two subgroups: fluorapatites ($\text{Ca}_5[\text{PO}_4]_3\text{F}$) and chlorapatites ($\text{Ca}_5[\text{PO}_4]_3\text{Cl}$), and the latter might contain some amount of F, OH and CO_3 as anions. It is estimated that in fluorapatites the average contents of the following elements are (wt%): CaO (55.5), P_2O_5 (42.3), F (3.8), and in chlorapatites – CaO (53.8), P_2O_5 (41), Cl (6.8). Apatites are able to concentrate in their structure significant amounts of REE, among which the leading role belongs to LREE. In addition to REE there are sometimes Na, Fe, Al and some other elements presented as an impurity [Betekhtin, 1956].

5.1 THE REE COMPOSITION OF APATITES

In general, the regularities of REE distribution in apatites are studied a bit better compared to some other accessory minerals but samples from various petrographic and genetic types of rocks are characterized unevenly by these studies. The total REE content in apatites varies widely and the chondrite-normalized contents of LREE mostly prevail over HREE contents (Table 5.1, Figure 5.1).

Among the first samples of apatite, which were determined to contain some REE, is the sample from gabbro of Skaergaard massif, the total REE content of which was 3000 ppm [Paster *et al.*, 1974]. Chondrite-normalized contents of certain elements in it were (t.ch): La ~1300, Ce ~1550, Nd ~1800, Sm ~1800, Yb ~300. The REE pattern of the apatite was a relatively shallow negative sloping and slightly convex upward line complicated by weak negative Eu anomaly (Figure 5.1, 1). Slightly lower total REE content and a steep negative slope of REE patterns were determined in apatites from hawaiites from the State of Texas (USA) ~2700 ppm and from basanites from the State of Arizona (USA) ~2600 ppm [Irving & Frey, 1984]. The level of La in apatite from hawaiite was 2100 t.ch., from basanite – 2900 t.ch., while the level of Yb accumulation in them was slightly lower (70–120 t.ch.) than in minerals from gabbro of Skaergaard massif. REE patterns of apatites from hawaiites and basanites are almost straight lines with a steep negative slope, on which there are no Eu anomalies,

Table 5.1 REE composition of apatites from some rocks (ppm).

	<i>Skaergaard massif, Greenland province</i>	<i>Aldan prov. (Russia)</i>	<i>Texas State (USA)</i>	<i>Arizona State (USA)</i>	<i>South Dakota State, (USA)</i>				<i>Koksharovskiy massif (Russia)</i>
	[Paster et al., 1974]	[Tabuns, 1996]	[Irving, Frey, 1984]		[Jolliff et al., 1989]				[Oktiabr'sky et al., 2008] LA ICP-MS
	EG4312	Tab-I	188/7	SC73	B2	GIf	B8	B12	Kok-19
Element	Gabbro	Pyroxenite	Hawaiite	Basanite	<i>Granitic pegmatites</i>		<i>Carbonatite</i>		
La	320	290	517	712	N.d.	N.d.	N.d.	N.d.	1127
Ce	990	860	1205	1540	119	57	374	328	2442
Pr	N.d.	N.d.	N.d.	N.d.	N.d.	N.d.	N.d.	N.d.	260
Nd	870	1170	614	N.d.	63	13	157	216	953
Sm	280	210	104	121	15	6,8	27	61	153
Eu	64	N.d.	30,9	34,9	33	3,7	18	29	37,5
Gd	320	165	81,7	N.d.	N.d.	N.d.	N.d.	N.d.	121
Tb	48	N.d.	10,3	14,2	N.d.	N.d.	N.d.	N.d.	16
Dy	N.d.	N.d.	N.d.	N.d.	14	5,6	20	65	75,5
Ho	43	N.d.	N.d.	N.d.	N.d.	N.d.	N.d.	N.d.	11,2
Er	N.d.	N.d.	N.d.	N.d.	12	2,3	17	45	25,8
Tm	N.d.	N.d.	N.d.	N.d.	N.d.	N.d.	N.d.	N.d.	2,42
Yb	52	17	11,3	19,4	10	2,6	18	52	13,5
Lu	N.d.	N.d.	1,52	2,38	N.d.	N.d.	N.d.	N.d.	1,44
Total	2987	2712	2576	2444	266	91	631	796	5239
$(\text{La}/\text{Yb})_n$	4,2	12	31	25	N.d.	N.d.	N.d.	N.d.	56
$(\text{Ce}/\text{Yb})_n$	19	51	107	79	12	22	21	6,3	47

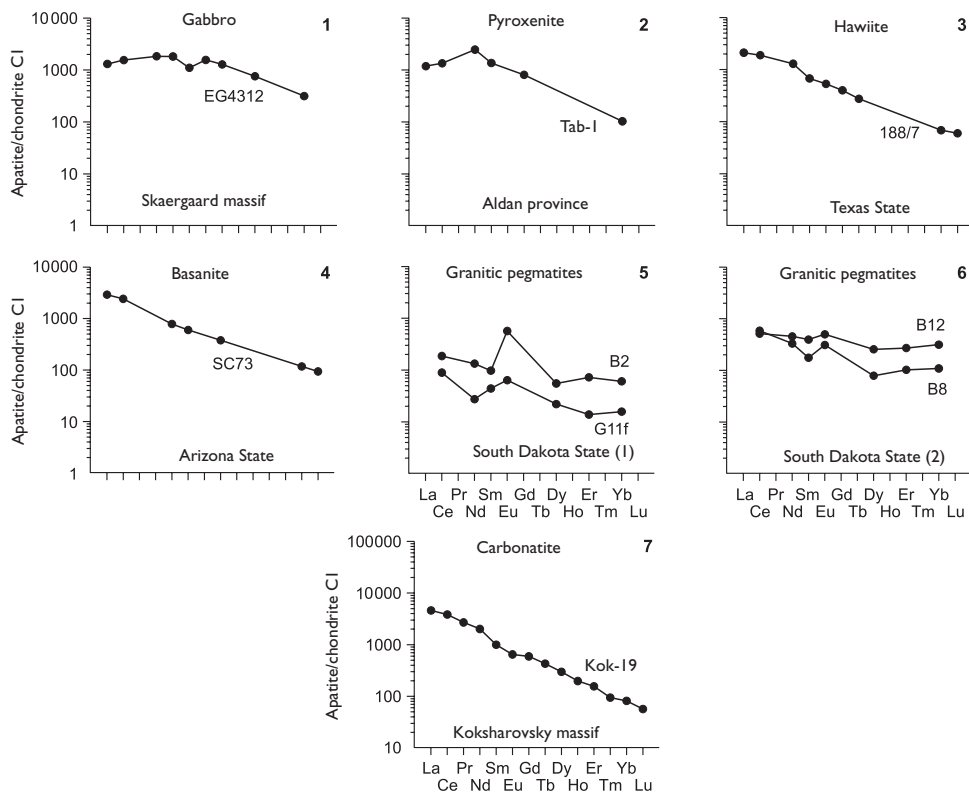


Figure 5.1 Chondrite-normalized REE patterns for apatites from gabbro (1), pyroxenite (2), hawaiite (3), basanite (4), granitic pegmatites (5, 6), and carbonatite (7) (data Table 5.1).

while the value of $(Ce/Yb)_{\text{CI}}$ in the mineral from hawaiite was higher (~107) than in the sample from basanite (~79) (Figure 5.1, 3, 4).

The apatites from granitic pegmatites from the State of South Dakota (USA) were identified to have significantly lower total REE contents in comparison with the mineral from previous objects. In their patterns that have a common shallow negative slope there are positive Eu anomalies of various intensity (Figure 5.1, 5, 6). Apatites from carbonatites of Koksharovsky alkaline ultramafic massif (Primorie province, Russia) have a higher total REE content and their REE patterns are almost rectilinear lines with steep negative slope (Figure 5.1, 7).

Apatites from kimberlites of Benfontein sill (South Africa) show much higher chondrite-normalized La contents in comparison with their samples from kimberlites of Wesselton province, while both have almost rectilinear patterns with a very steep negative slope [Jones & Wyllie, 1984] (Figure 5.2). These authors assumed that significant differences in the level of REE accumulation in apatites of these two kimberlite manifestations are due to the mineralogical-structural differences of rocks containing them. In particular, relatively large and fairly rare apatite grains from kimberlites of Benfontein sill are in parageneses with perovskite, while they are mainly concentrated

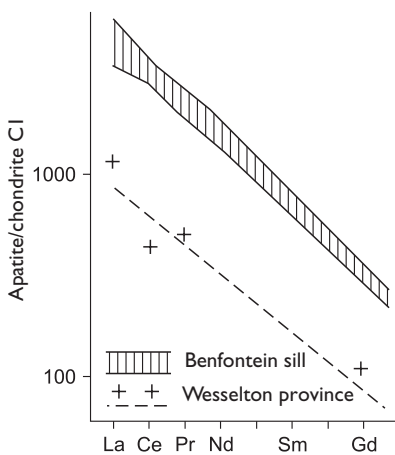


Figure 5.2 Chondrite-normalized REE patterns for apatites from kimberlites from Benfontein sill and from Wesselton province (data [Jones & Wyllie, 1984]). Normalization was performed according to [Nakamura, 1974]).

in the cumulative layers enriched with oxides. Moreover, the apatites from kimberlites of Wesselton province are presented with numerous but smaller segregations and together with associating perovskite grains are evenly distributed in a homogeneous rock matrix enriched with carbonates.

The REE composition of apatites that has been studied in great detail are from Boggy Plain granitoid massif (Australia) and are presented with adamellites (outer and inner), granodiorites (outer and inner), as well as diorites and aplites [Hoskin *et al.*, 2000]. All of these apatites have a high total REE content and their samples from different varieties of granitoids show some differences in REE composition (Table 5.2, Figure 5.3). In particular, the average total REE contents in the mineral increase in the following row of rocks: diorites → granodiorites (outer) → granodiorites (inner) → adamellites (outer) → adamellites (inner) → aplites (Table 5.3, Figure 5.4). All apatites from rocks of this massif have the level of La accumulation several times higher than the level of Lu accumulation. In the mineral from granodiorites forming the inner areas of the massif, the values for $(\text{La}/\text{Yb})_n$ are a much higher (46–65) compared with the mineral from aplites (7–8). All apatites from rocks of Boggy Plain massif have in their patterns some negative Eu anomalies of approximately equal intensity: $(\text{Eu}/\text{Eu}^*)_n = 0.17 - 0.39$. Apatites from granodiorites of the outer zone are different from their samples from other varieties of rocks by the highest average values of $(\text{La}/\text{Yb})_n$ and the most intense negative Eu anomalies. In addition, the apatites from aplites, which are characterized by the highest average total REE content, are also described by the lowest average values of $(\text{La}/\text{Yb})_n$.

The distribution of La, Ce, Nd, Sm and Gd has been studied for the apatites from some samples of metasomatic rocks represented in xenoliths from kimberlites of Matsoku manifestation (Lesotho province, Southern Africa) [Exley & Smith, 1982]. Along with accessory apatite these metasomatic rocks contain phlogopite (amber mica), amphi-

Table 5.2 REE composition of apatites from diorites, granodiorites, adamellites, and aplites from Boggy Plain massif (New South Wales province, Australia) (ppm).

	[Hoskin et al., 2000], SIMS												
	39-1.I	39-2.I	39-4.I	39-5.I	39-6.I	39-7.I	39-8.I	7gd-1.I	7gd-2.I	7gd-2.Ia	7gd-3.Ia	7gd-4.I	7gd-5.I
Element	Diorites							Granodiorites (outer)					
La	729	684	732	702	713	772	680	1215	1393	1534	1414	959	1154
Ce	1627	1676	1733	1672	1510	1611	1645	2304	2267	2462	2711	2003	2149
Pr	213	233	232	230	184	194	229	261	222	243	313	257	258
Nd	920	1046	1004	1016	793	800	1004	1003	754	845	1252	1100	1049
Sm	169	204	191	196	144	144	198	155	110	121	201	200	176
Eu	15,2	15,8	14	15	15	16,2	16	14	12,3	14	14,3	10,2	11,1
Gd	154	188	178	180	138	132	186	131	86	92	172	168	153
Tb	N.d.	N.d.	N.d.	N.d.	N.d.	N.d.	N.d.	N.d.	N.d.	N.d.	N.d.	N.d.	N.d.
Dy	108	128	120	120	96	83	126	79	55	61	111	104	92
Ho	N.d.	N.d.	N.d.	N.d.	N.d.	N.d.	N.d.	N.d.	N.d.	N.d.	N.d.	N.d.	N.d.
Er	52	59	57	55	46	40	57	36	29	30	50	46	39
Tm	6,2	6,7	6,6	6,4	5,6	4,9	6,8	4,4	3,8	4,1	5,9	5,1	4,7
Yb	34	36	36	35	32	27	37	25	21	24	33	27	25
Lu	4,5	4,7	4,6	4,4	4,3	3,5	4,5	3,5	3,6	3,6	4,6	3,3	3,7
Total	4032	4281	4308	4232	3681	3828	4189	5231	4957	5434	6282	4883	5115
$(La/Yb)_n$	14,5	12,8	13,7	13,5	15,0	19,3	12,4	32,8	44,8	43,1	28,9	24,0	31,2
$(Eu/Eu^{*})_n$	0,28	0,24	0,23	0,24	0,32	0,35	0,25	0,29	0,37	0,39	0,23	0,17	0,20

(Continued)

Table 5.2 (Continued).

<i>Boggy Plain massif, New South Wales province, Australia</i>												
[Hoskin et al., 2000], SIMS												
	16gdv-1.I	16gdv-2.I	16gdv-3.I	16gdv-5.I	16gdv-6.I	16gdv-7.I	22adv-3.I	22adv-4.I	22adv-5.I	22adv-6.I	22adv-7.I	22adv-8.I
Element	<i>Granodiorites (inner)</i>						<i>Adamellites (outer)</i>					
La	1635	1452	1132	1684	1366	1332	1208	1266	1263	1197	1167	1482
Ce	2997	2588	2028	3097	2498	2384	2818	2877	2879	2743	2763	3286
Pr	304	257	203	327	277	246	350	352	338	336	347	400
Nd	1039	839	669	1117	968	829	1336	1358	1255	1282	1337	1534
Sm	138	109	85	151	133	110	199	201	175	192	204	235
Eu	13,4	12	8,6	13,1	9,9	10,6	15	15,4	14,9	15	16	17
Gd	104	75	63	113	102	80	150	145	132	138	153	184
Tb	N.d.	N.d.	N.d.	N.d.	N.d.	N.d.	N.d.	N.d.	N.d.	N.d.	N.d.	N.d.
Dy	60	45	35	63	52	44	90	87	78	87	91	102
Ho	N.d.	N.d.	N.d.	N.d.	N.d.	N.d.	N.d.	N.d.	N.d.	N.d.	N.d.	N.d.
Er	29	23	17	29	22	20	45	42	41	44	46	46
Tm	4	2,9	2,2	3,5	2,6	2,5	5,9	5,4	5,3	6	5,9	5,8
Yb	24	19	13	22	14,3	15	36	32	33	37	36	32
Lu	3,4	2,8	2,1	3,1	2,2	2,3	5,2	4,6	4,8	5,5	5,3	4,6
Total	6351	5425	4258	6623	5447	5075	6258	6385	6219	6083	6171	7328
(La/Yb) _n	46,0	51,6	58,8	51,7	64,5	59,9	22,7	26,7	25,8	21,8	21,9	31,3
(Eu/Eu*) _n	0,33	0,38	0,34	0,29	0,25	0,33	0,26	0,26	0,29	0,27	0,27	0,24

(Continued)

Table 5.2 (Continued).

<i>Boggy Plain massif, New South Wales province, Australia</i>												
	[Hoskin et al., 2000], SIMS											
Element	II advn-1.I	II advn-2.I	II advn-3.I	II advn-4.I	II advn-5.I	II advn-6.I	II advn-7.I	II advn-8.I	42-3.I	42-6.I	42-8.I	42-10.I
Adamellites (inner)									Aplites			
La	1717	1578	1370	1135	1330	1399	1298	1807	1119	1508	1493	1292
Ce	3784	3448	3098	2680	2916	3016	2948	3759	2777	3432	3346	2771
Pr	453	411	388	335	344	349	365	415	352	403	399	332
Nd	1734	1515	1488	1251	1231	1234	1410	1429	1289	1431	1423	1183
Sm	260	216	246	192	189	197	227	185	227	224	236	231
Eu	19	18	17	17,8	15,2	15,5	17	17,8	20,4	18	18	17
Gd	191	153	185	139	136	139	170	123	184	164	175	199
Tb	N.d.	N.d.	N.d.	N.d.	N.d.	N.d.	N.d.	N.d.	N.d.	N.d.	N.d.	N.d.
Dy	130	105	128	93	102	111	127	82	178	167	171	224
Ho	N.d.	N.d.	N.d.	N.d.	N.d.	N.d.	N.d.	N.d.	N.d.	N.d.	N.d.	N.d.
Er	66	56	65	49	54	62	66	40	94	103	99	119
Tm	8,9	7,5	8,5	6,9	7,7	8,8	9,2	5,6	15,5	17,7	16,5	18
Yb	56	49	53	43	47	57	57	35	108	134	122	123
Lu	8,2	7	7,5	6,1	7,1	8,1	8,4	4,9	15,3	20	18	16,6
Total	8427	7564	7054	5948	6379	6596	6703	7903	6379	7622	7517	6526
$(\text{La/Yb})_n$	20,7	21,7	17,5	17,8	19,1	16,6	15,4	34,9	7,0	7,6	8,3	7,1
$(\text{Eu/Eu}^*)_n$	0,25	0,29	0,23	0,32	0,28	0,27	0,25	0,34	0,30	0,27	0,26	0,24

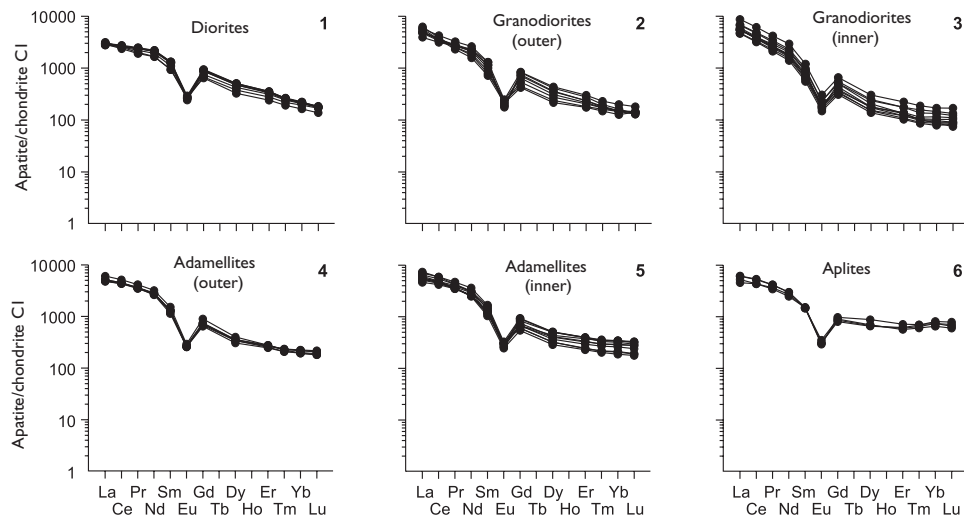


Figure 5.3 Chondrite-normalized REE patterns for apatites from diorites (1), granodiorites (2, 3), adamellites (4, 5), and aplites (6) from Boggy Plain massif (New South Wales province, Australia) (data Table 5.2).

Table 5.3 Average REE composition of apatites from diorites, granodiorites, adamellites, and aplites from Boggy Plain massif (New South Wales province, Australia) (ppm).

Element	Diorites	Granodiorites (outer)	Granodiorites (inner)	Adamellites (outer)	Adamellites (inner)	Aplites
	n = 8	n = 8	n = 10	n = 6	n = 10	n = 4
La	718	1264	1456	1264	1438	1353
Ce	1654	2305	2635	2894	3162	3082
Pr	219	259	272	354	375	372
Nd	955	998	927	1350	1370	1332
Sm	181	160	122	201	205	230
Eu	16	12	12	16	17	18
Gd	169	132	90	150	147	181
Tb	N.d.	N.d.	N.d.	N.d.	N.d.	N.d.
Dy	114	83	50	89	103	185
Ho	N.d.	N.d.	N.d.	N.d.	N.d.	N.d.
Er	53	38	24	44	54	104
Tm	6,2	4,6	3,0	5,7	7,4	16,9
Yb	34,0	25,5	18,3	34,3	46,2	122
Lu	4,4	3,7	2,7	5,0	6,7	17,5
Total	4124	5284	5613	6407	6929	7011
$(La/Yb)_n$	14,3	33,5	53,8	24,8	21,0	7,5
$(Eu/Eu^{*})_n$	0,27	0,27	0,33	0,26	0,29	0,27

Note: Data Table 5.2.

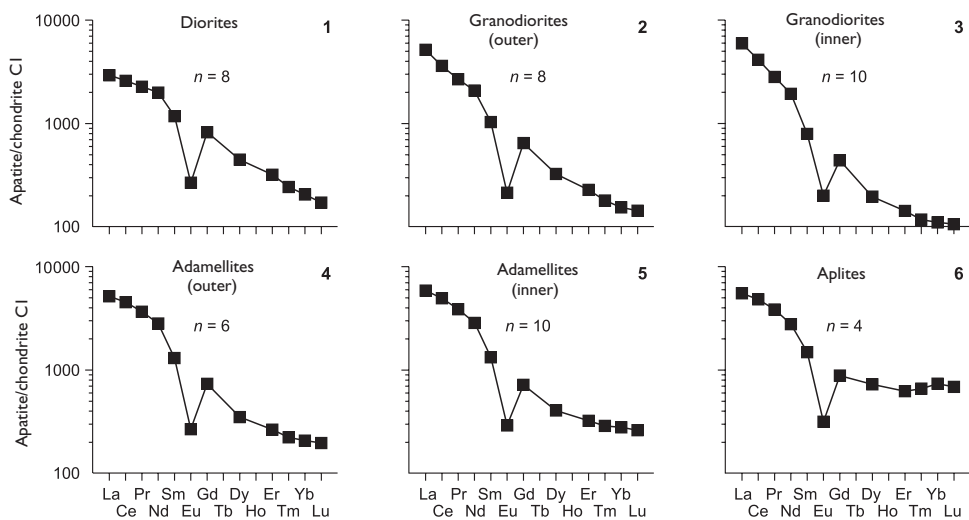


Figure 5.4 Chondrite-normalized REE patterns for average composition of apatites from diorites (1), granodiorites (2, 3), adamellites (4, 5), and aplites (6) from Boggy Plain massif (New South Wales province, Australia) (data Table 5.3).

bole, rutile, ilmenite and diopside, which by initial letters are called MARID. It was ascertained that apatites from MARID have the REE composition that is slightly unusual for this mineral. It primarily occurs in arched upwards REE patterns, which is unusual for this mineral. The researchers assumed that such REE composition of the apatites is due to mantle metasomatism, which influenced the MARID formation. Approximately the same anomalous REE distribution was observed in apatites from biotitic pyroxenites of magmatic complex (Aldan province, Russia), which were characterized by lower chondrite-normalized content of La and Ce compared with contents of Nd, Sm, Gd and Yb [Tabuns, 1996] (Table. 5.1, Figure 5.1, 2). A similar REE distribution was observed by the author in apatites from shonkinites, syenites and calciphyres of the same magmatic complex. It was assumed that the identified shortage of La and Ce in apatites from the rocks of Ukduskinsky complex was due to the mobilization and subtraction of these elements during the percolation of fluids enriched with carbon dioxide into these rocks on the latemagmatic and postmagmatic stages of mineral genesis.

A large amount of analytical data on the REE composition of apatites was obtained by Belousova *et al.*, [2002] in a study of this mineral from different types of magmatic rocks, including granites, granodiorites, tonalites, adamellites and granitic pegmatites (Australia, Norway, Ukraine), lherzolites (Australia and USA), dolerites (Ukraine), carbonatites (Norway, South Africa, Russia), larvikites and jacupirangites (Norway), as well as the rocks represented in iron-ore deposits (Mexico, Norway, Sweden) (Table 5.4, Figure 5.5). As shown in this work, the apatites from granitoids have the most volatile REE composition. The relatively low average total REE content is typical of apatites from dolerites (3130 ppm), granitic pegmatites (4130 ppm) and carbonatites (4800 ppm). This index is slightly higher for the mineral from granitoids

Table 5.4 Maximum, minimum, and average REE compositions of apatites from lherzolites, dolerites, granitoids, granite pegmatites, carbonatites, larvikites, jacupirangites, and iron ores from different manifestation (ppm).

[Belousova et al., 2002] LA ICP-MS												
	Lherzolites			Dolerites			Granitoids			Granitic pegmatites		
	n = 8			n = 11			n = 669			n = 52		
Element	Aver.	Min.	Max.	Aver.	Min.	Max.	Aver.	Min.	Max.	Aver.	Min.	Max.
La	1761	679	4457	390	288	553	704	9,9	6722	211	46	419
Ce	4620	1198	7642	1081	794	1430	2165	20	13979	751	119	1258
Pr	392	109	803	149	114	199	265	1,8	1392	129	24	213
Nd	1036	305	2618	755	599	1047	1032	7,9	5756	723	137	1367
Sm	104	26	313	202	153	248	215	1,9	972	345	69	950
Eu	32	8,7	79	21	18	25	23	1,5	240	26	6	77
Gd	60	16	192	199	158	255	208	2,6	1057	489	121	1659
Tb	N.d.	N.d.	N.d.	N.d.	N.d.	N.d.	N.d.	N.d.	N.d.	N.d.	N.d.	N.d.
Dy	N.d.	N.d.	N.d.	162	138	207	172	2,8	1483	600	121	1981
Ho	4,5	1,7	14	32	27	41	36	0,5	353	113	16	426
Er	9,9	4,5	14	78	65	99	97	1,8	1029	306	31	1185
Tm	N.d.	N.d.	N.d.	N.d.	N.d.	N.d.	14	0,6	151	46	3,8	176
Yb	6,2	3,7	8,1	51	49	66	85	2,3	1032	332	23	1244
Lu	0,86	0,51	1,0	6,6	5,4	8	13	0,4	150	58	2,7	197
Total	N.d.	N.d.	N.d.	3127	2408	4178	5029	54	34316	4129	720	11152
(La/Yb) _n	192	124	371	5,16	3,97	5,66	5,59	2,91	4,40	0,43	1,35	0,23
(Ce/Yb) _n	193	84	244	5,49	4,19	5,61	6,59	2,25	3,51	0,59	1,34	0,26
(La/Sm) _n	10,7	16,4	8,97	1,22	1,19	1,40	2,06	3,28	4,35	0,39	0,42	0,28

(Continued)

Table 5.4 (Continued).

[Belousova et al., 2002], LA ICP-MS												
	Carbonatites			Larvikites			Jacupirangites			Iron ores		
	n = 61			n = 34			n = 14			n = 35		
Element	Aver.	Min.	Max.	Aver.	Min.	Max.	Aver.	Min.	Max.	Aver.	Min.	Max.
La	959	549	3931	3423	2242	4188	2052	1452	3709	1301	161	4569
Ce	2060	1369	7728	8144	6278	9797	4585	3578	7542	2463	802	4965
Pr	261	178	920	880	672	1024	539	446	907	324	151	393
Nd	1081	741	3487	3070	2126	3665	2185	1685	3343	1140	723	1587
Sm	189	115	459	445	293	542	353	270	517	165	138	324
Eu	43	30	111	35	22	50	66	53	75	24	15	55
Gd	126	72	265	294	186	363	261	195	385	156	118	306
Tb	N.d.	N.d.	N.d.	N.d.	N.d.	N.d.	N.d.	N.d.	N.d.	N.d.	N.d.	N.d.
Dy	52	38	102	198	121	243	166	127	261	131	82	281
Ho	7,2	5,3	13	35	22	44	30	23	49	27	17	61
Er	13	8,7	24	85	50	106	70	51	115	70	41	166
Tm	N.d.	N.d.	N.d.	10	6,1	13	8,1	6	13,9	14	7,8	24
Yb	7,5	3,3	11	61	35	76	45	34	82	62	32	161
Lu	0,8	0,3	2,2	7,5	4,2	9,4	6	4,2	10,7	8,7	4,1	23
Total	4800	3110	17053	16688	12057	20120	10366	7924	17010	5886	2292	12915
(La/Yb) _n	86	112	241	38	43	37	31	29	31	14	3,40	19
(Ce/Yb) _n	71,1	107	182	34,6	46,4	33,4	26,4	27,2	23,8	10,3	6,49	7,98
(La/Sm) _n	3,19	3,01	5,39	4,84	4,82	4,86	3,66	3,39	4,52	4,96	0,73	8,88

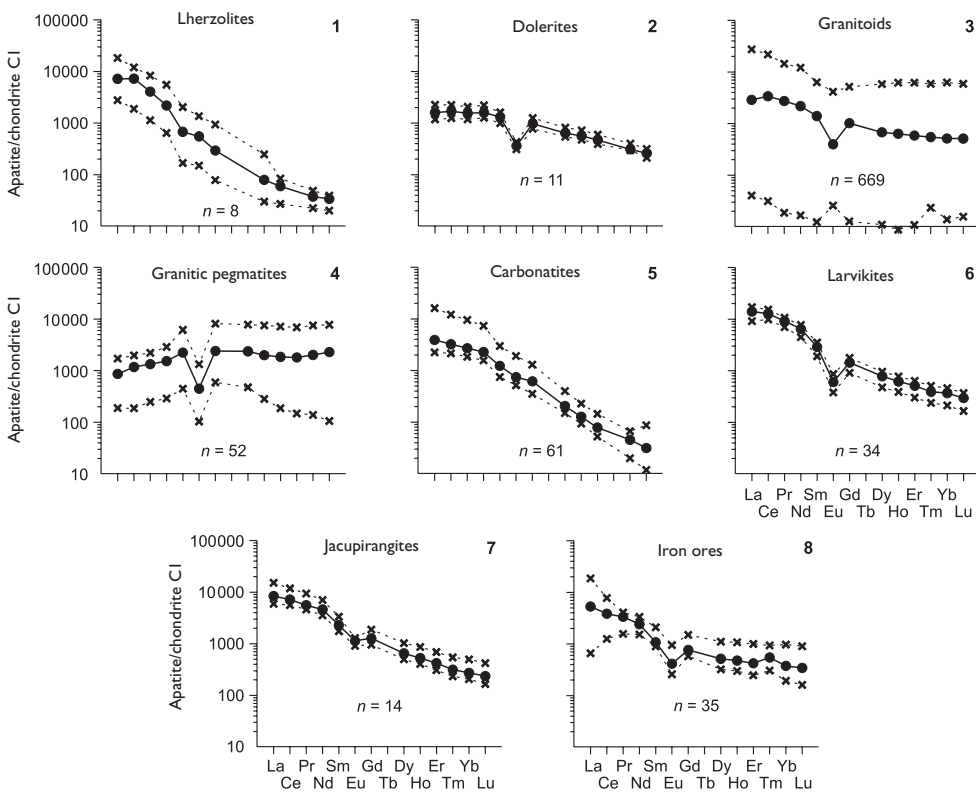


Figure 5.5 Chondrite-normalized REE patterns for average composition (solid line), as well as maximum and minimum composition (dashed lines) for apatites from lherzolites (1), dolerites (2), granitoids (3), granitic pegmatites (4), carbonatites (5), larvikites (6), jacupirangites (7), and iron ores (8) from some manifestations (data Table 5.4).

(5030 ppm), from rocks of iron-ore deposits (5890 ppm), as well as from some lherzolites (8030 ppm), jacupirangites (10370 ppm) and larvikites (16690 ppm). The vast majority of apatites from the collections studied by Belousova *et al.*, have the values of $(\text{La/Yb})_n$ and $(\text{Ce/Yb})_n$ greater than 1 and the highest values were observed in the mineral from lherzolites and carbonatites. In apatites from granitic pegmatites there was a slight excess of chondrite-normalized HREE contents over the LREE contents, which is rarely observed in this mineral. The patterns of the vast majority of apatite samples from the collection showed negative Eu anomalies of various intensity. Judging by the average estimates of $(\text{Eu/Eu}^*)_n$ parameter, the intensity of these anomalies was increasing in the following row of rocks: carbonatites (0.80) → jacupirangites (0.67) → metasomatic rocks of iron-ore deposits (0.45) → granitoids (0.33) → dolerites (0.32) → larvikites (0.28) → granitic pegmatites (0.19). For some apatites from granitoids the intensity of negative Eu anomalies was even higher – $(\text{Eu/Eu}^*)_n = 0.01 - 0.06$, while for the samples of lherzolites there were identified positive Eu anomalies: the mean value of $(\text{Eu/Eu}^*)_n = 1.14$.

Thus, the observations show that variations of the REE composition of apatites significantly correlate with petrographic belonging and formation conditions of rocks containing them. Hallmarks of the overwhelming majority of the investigated apatites are, firstly, more or less significant predominance of chondrite-normalized LREE contents over the HREE, and, secondly, the presence on their REE patterns of negative Eu anomalies of various intensity. In addition, these results suggest that in-depth study of REE distribution in apatites from rocks that form separate magmatic massifs allows using such data to specify the taxonomy of rocks within these massifs, as well as to ascertain the postmagmatic transformations of apatite-bearing rocks. Therefore, a further detailed research of REE composition of apatites from rocks of different composition and origin is an urgent task.

5.2 THE COEFFICIENTS OF REE DISTRIBUTION BETWEEN APATITE AND MELTS AS WELL AS COEXISTING PEROVSKITES

Among the first the estimates of K_d (apatite/melt) values were obtained by the example of samples from the natural system – basanites [Irving & Frey, 1984], and later on – based on the results of experimental studies of basaltic melts [Ozawa & Shimizu, 1995] (Table 5.5). These observations showed that all the REE have values of K_d (apatite/melt) > 1 . In addition, for the values of basanitic melts the values of K_d (La, Ce)

Table 5.5 The coefficients of REE distribution between apatites and basanitic, and basaltic melts.

Element	Basanitic melt		Basaltic melt
	Nature system		Experimental system
	[Irving, Frey, 1984]	[Ozawa, Shimizu, 1995]	OZ-I
La	8,8	20,0	3,3
Ce	10,0	21,0	4,0
Pr	N.d.	N.d.	N.d.
Nd	N.d.	12,0	7,7
Sm	12,0	16,0	7,7
Eu	12,0	15,0	6,4
Gd	N.d.	N.d.	N.d.
Tb	9,4	13,0	N.d.
Dy	N.d.	N.d.	7,0
Ho	N.d.	N.d.	N.d.
Er	N.d.	N.d.	10,3
Tm	N.d.	N.d.	N.d.
Yb	4,5	8,9	7,0
Lu	3,7	7,0	N.d.
K_d (La)/ K_d (Yb)	1,96	2,25	0,47

were significantly higher than the values of K_d (Lu), while for basaltic melts, on the contrary, values of K_d (La, Ce) were slightly lower than K_d (Lu). Therefore, the graphs of K_d (REE) values for basanitic melts have a steep negative slope, and for basaltic melts – a gentle positive slope (Figure 5.6).

Watson & Green [1981] performed a series of experiments with melts of different composition and at different *PT* conditions including the presence of water in order to determine the values of K_d (apatite/melt) for La, Sm, Dy and Lu. As a result of these studies the authors stated the following: 1) under all determined *PT* condi-

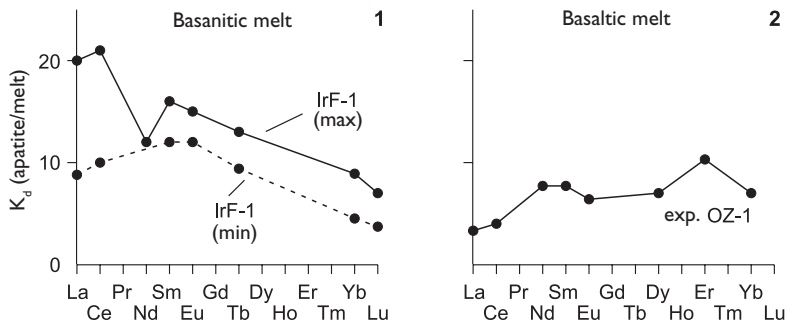


Figure 5.6 The graphs of coefficients of REE distribution between apatites, and basanitic (nature system) and basaltic (experimental system) melts (data Table 5.5).

Table 5.6 The coefficients of La, Sm, Dy, and Lu distribution between apatites and melts of different composition, and under different *PT*-conditions (experimental data).

[Watson, Green, 1981]							
No experiment	Melt composition	<i>T</i> , °C	<i>P</i> , kbar	La	Sm	Dy	Lu
804ta	ta	1120	7,5	2,5	5,6	3,7	1,9
811ta	ta	1080	4,8	2,5	5,5	4,1	2,5
812ta	ta	950	7,5	3,4	7,8	5,4	2,9
822ta	ta	1120	7,5	2,5	5,6	4,6	2,2
808a	a	950	7,5	6,4	19,1	15,2	8,1
815a	a	1080	20	4,4	9,8	8,1	4,0
811b	b	1080	8	2,6	4,7	4,2	1,8
812b	b	950	7,5	4,9	12,4	8,3	3,7
814b	b	950	7,5	4,6	9,9	7,3	3,4
815b	b	1080	20	2,8	4,5	4,2	1,8
818ba	b	1080	7,5	3,2	5,4	3,9	1,7
818bb	b	1080	7,5	3,0	5,3	3,9	1,9
818bc	b	1080	7,5	2,5	4,5	3,9	1,7
814nh	nh	950	7,5	4,9	10,5	8,9	3,8
812g	g	950	7,5	11,9	38,4	37,0	20,4
823g	g	1080	20	8,0	18,5	15,9	7,5

Note: Composition of melts: ta – tholeiite-andesitic; a – andesitic; b – basanitic; nh – nepheline-hawaiitic; g – granitic.

tions of experiments and for all studied melts the named four REE had values of K_d (apatite/melt) > 1; 2) the values of K_d (apatite/granite melt) and K_d (apatite/nepheline-hawaiite melt) in most cases were higher than the respective values of K_d (apatite/tholeiite-andesite melt); 3) in all experiments the values of K_d (La, Lu) were slightly lower than the values of K_d (Sm, Dy); 4) the values of K_d obtained in experiments with tholeiite-andesite and basanite melts at relatively low temperatures were higher than

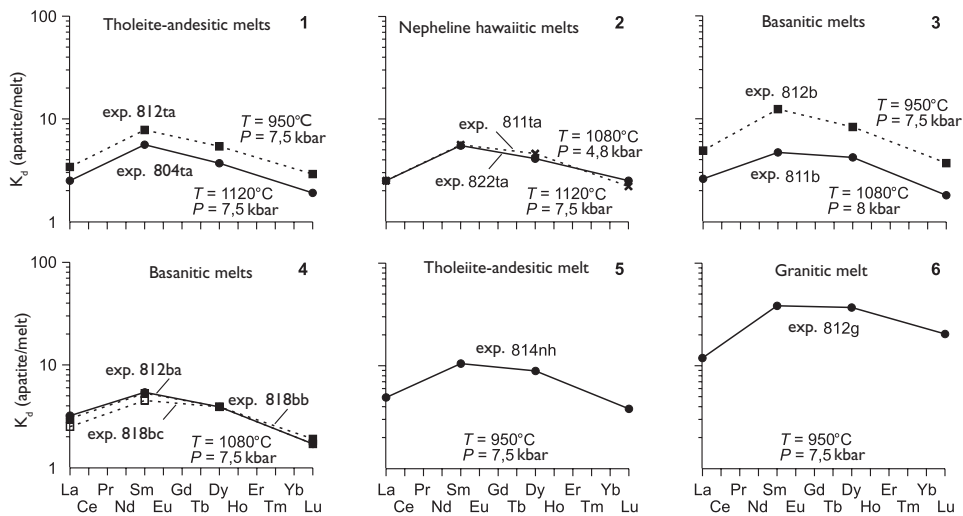


Figure 5.7 The graphs of coefficients of La, Sm, Dy, and Lu distribution between apatites and melts of different composition and under different PT-conditions (data Table 5.6).

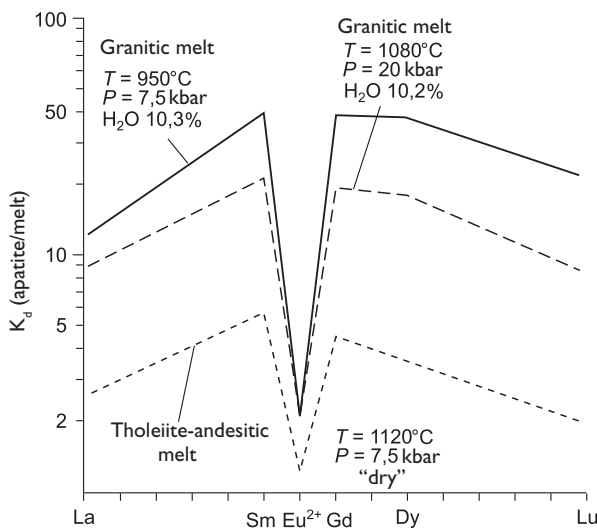


Figure 5.8 The graphs of coefficients of some REE distribution between apatites and tholeiitic, andesitic and granitic melts under different PT-conditions (experimental data [Watson & Green, 1981]).

the values of K_d obtained at higher temperatures; and 5) the results of experiments with basanitic melts at $T = 1080^\circ\text{C}$ and $P = 20$ kbar determined that the values of K_d (La, Sm) are slightly lower than those values that were obtained at the same temperature but at a lower pressure (7.5 kbar) (Table 5.6, Figure 5.7).

On the respective graphs of the K_d (apatite/melt) values for La, Sm, Gd, Dy and Lu, as well as for Eu^{2+} , which are shown in the work of Watson & Green, there have been very intense negative Eu^{2+} anomalies observed (Figure 5.8). It follows that, under the certain PT -conditions of experiments the Eu^{2+} ions were significantly less compatible with the structure of apatites in comparison with the trivalent ions of La, Sm, Gd, Dy and Lu.

There were also obtained estimates of the coefficients of REE distribution between apatites and coexisting perovskites by example of samples from jacupirangites, ijolites and nepheline syenites forming xenoliths in tuffs of Oldoinyo Lengai volcano (Tanzania) [Dawson *et al.*, 1994]. It was shown in this study that in the absence of titanites in these rocks the values of K_d (apatite/perovskite) were: La ~0.11, Ce ~0.063, Nd ~0.105, while in titanite-bearing samples of these rocks the values of K_d for these elements were slightly higher.

5.3 ON ISOMORPHISM OF REE IN APATITES

As noted above, the apatites are one of the most important minerals concentrating REE in magmatic, metasomatic and metamorphic rocks. In this regard, from theoretical and practical points of view it is interesting to study the reasons for such an intense REE accumulation in apatites and mechanisms of their isomorphous incoming into crystalline structure of apatites, as well as the reasons that cause the Eu deficiency often observed in the mineral. According to some reports, the intensity of negative Eu anomalies in the apatites increased with increasing degree of minerals fractionation in the rocks of mafic and ultramafic composition [Belousova *et al.*, 2002]. It is assumed that such dependence is due to the presence of plagioclase in these rocks, the structure of which is very favorable for the occurrence of a significant proportion of Eu in it, which was a part of crystallizing parental melt. Given the ability of Eu to change its valence state and to change from Eu^{2+} to the Eu^{3+} under oxidizing conditions, we can assume that this fact had a significant effect on the Eu accumulation in the structure of apatites, which were in parageneses with plagioclase. It is known that under oxidizing conditions the prevailing ions of Eu^{3+} have a much smaller ionic radius (0.947 \AA) compared with the Eu^{2+} ions (1.17 \AA) prevailing under reduced conditions [Shannon, 1976]. Therefore, by isomorphic substitution of Ca^{2+} ions, the radius size of which is 1.00 \AA , Eu^{3+} ions, apparently, became less compatible with the structure of apatite. Thus, these differences in ionic radii size seem to have caused the fact that for Eu^{3+} ions, which prevailed in oxidizing conditions, K_d (apatite/melt) have relatively low values, which leads to the appearance of frequently observed negative anomalies of this element on the REE patterns of apatites. In addition, the crystallization of apatites at reducing conditions was accompanied by an increase in the number of Eu^{2+} ions in the melt and increase of K_d (apatite/melt) values for Eu. Owing to this fact, the patterns of these apatites experienced decrease in intensity or complete levelling of negative Eu anomalies and sometimes appearance of positive anomalies.

For example, on the REE patterns of apatites from some lherzolites and carbonatites the negative Eu anomalies are absent (Figure 5.5, 1 and 5), which according to the model of Eu isomorphism presupposes the crystallization of apatites in relatively reducing conditions. The presence of rather intense negative Eu anomalies on the REE patterns of many apatites from granitoids (Figure 5.3) dolerites, granitic pegmatites, larvikites, jacupirangites, rocks from iron-ore deposits (Figure 5.5, 2, 4, 6, 8) and from the products of experiments with granitic and andesite-tholeiite melts (Figure 5.8) might indicate that these apatites were crystallized in a relatively oxidizing conditions. At the same time, the presence of positive Eu anomalies on the patterns of apatites from granite pegmatites from the State of South Dakota (USA) (Figure 5.1, 5, 6) also suggests their crystallization under reducing conditions.

* * *

Summarizing the above, we emphasize again that the apatites are able to concentrate in their structure very significant amounts of those REE that were present in crystallizing environments, and almost always LREE are dominating among them. Depending on the composition of melts and their crystallization conditions the total amount of REE in apatites can range from 10–100 ppm to 10000–35000 ppm. Intensive fractionation of REE, which is expressed in a rather steep negative slope of REE patterns and also corresponding high values of $(La/Yb)_{\text{m}}$, is characteristic for most of the studied apatites. Negative Eu anomalies that are commonly observed in the REE patterns of apatites are supposed to be the result of crystallization under oxidizing conditions. Negative Eu anomalies observed in the patterns of apatites from some lherzolites, kimberlites, basanites, hawaiites and other rocks are characterized by relatively low intensity and in some cases they are either absent or replaced by positive anomalies, which might indicate the crystallization of mineral in a poorly oxidizing or even reducing environment. The values of K_d (apatite/melt) for most of REE are usually greater than 1. This suggests that when isomorphic occurrence of these elements into the structure of apatites takes place, they have the properties inherent in compatible trace elements.

This page intentionally left blank

Chapter 6

Titanites

As accessory minerals, titanites are observed in many varieties of magmatic, metamorphic and some metasomatic rocks. Most often titanites are present in the granites, diorites, syenites, nepheline syenites, lamprophyres, in some volcanic rocks and rarely does it occur in the gabbros, pyroxenites and others.

This mineral is a silicate of titanium and calcium, the formula is written as CaTiSiO_5 . Titanite has been known for being one of the concentrators of heightened amounts of REE [Sahama, 1946; Sahama & Vahatalo, 1941]; at the same time the regularities of distribution of these impurities in this mineral are not well studied and among the published works the most common are the analyses of titanites from granitic pegmatites, granodiorites, dacites, trachyandesites and some metamorphic rocks [Lesnov, 2006].

Liakhovich [1967] showed that titanite presented in diverse granitoids plays the role of second-largest REE concentrator after monazite and according to him the average weight of titanite content in these rocks is about 640 ppm. According to the same data, the titanites from granitoids can concentrate up to 27% of the total REE present in them. The research of titanites from granodiorites of Peninsular Ranges batholith (South California) also showed that they contain a considerable part of the amount of REE, which is present in them [Gromet & Silver, 1983]. Titanites that were also described are present in gabbros of some mafic-ultramafic Ural massifs (Russia) [Fershtater, 2000; Shagalov, 2003] and Tuva (Russia) [Egorova, 2005].

According to Gromet & Silver [1983], the REE patterns of titanites from granodiorites of Peninsular Ranges batholith are usually negatively sloped almost straight lines, moreover, a zonal REE distribution was observed in some of their grains. Thus, the concentration of Ce_2O_3 was decreasing from the central zones of the grains (~0.5 wt%) to the periphery (~0.3 wt%). According to these authors, during the crystallization of titanites the residual melts were significantly depleted by REE.

Russell *et al.* [1994] studied the REE distribution in titanites from granitic pegmatites of Bisson Mountain (British Columbia, Canada). In addition to titanite, these rocks contain other accessory minerals enriched with REE: orthite, apatite, ilmenite, zircon and thorite. In different crystals of titanite from these granitic pegmatites the chondrite-normalized REE contents varied significantly (t.ch.): La (270–10000), Ce (4000–12000), Pr (3500–20000), Nd (5500–15000), Sm (2000–10000). In addition to this, the titanites from granitoids of Shartashsky massif (Middle Urals, Russia) have the total REE content up to 7000 ppm [Shardakova, 2001].

According to Nakada [1991], in dacites from the volcanic province in the Andes (Chile and Bolivia) the modal quantity of titanite segregations are from 0.1 to 0.4% of the rock bulk. Segregations of the mineral are presented as phenocrysts and as micro-inclusions in hornblende grains. A chemical zoning was identified in titanite phenocrysts and it reflected in the change of the contents of Ti, Ca, Al, Fe and REE. At the same time, in different zones of titanite phenocrysts the total REE contents increased with decreasing content of Ca in them, in this case dependence of REE contents from Ti contents has not been revealed. Nakada suggested that an isomorphic substitution of Ca ions by REE ions and simultaneous substitution of Ti ions by Al ions occurred in titanites structure during their crystallization.

Mulroney & Rivers [2005] studied the REE distribution in accessory titanites from some metamorphic rocks of San-Antonio complex (Newfoundland Island, Canada). In these rocks small idiomorphic and subidiomorphic titanite segregations were presented in the matrix consisting mostly of plagioclase crystals and of the subordinate amphibole and epidote segregations. The total REE content in these titanites varied in the range from 1500 to 2400 ppm (Table 6.1). On REE patterns of some of these titanites there are observed negative Eu anomalies of low intensity (Figure 6.1).

It is known that along with REE and some other isomorphic impurities the titanite can accumulate different amounts of Zr in its structure. In particular, it was found that titanite from lamprophyres commonly presented in East Germany contains 9.5 wt% of ZrO_2 [Seifert & Kramer, 2003].

As demonstrated by studying the REE distribution in titanites and trachyandesite pumices of El Chichon volcano (Mexico) containing them, K_d (titanite/trachyandesite melt) are characterized by very high values: La (46), Ce (87), Nd (152), Sm (204), Eu (181), Tb (248), Yb (104), Lu (92) [Luhr *et al.*, 1984; Key & Gordillo, 1994]. The graph of K_d is arched upwards line with a maximum for Tb (Figure 6.2).

Green [1994] summarized the data on the estimates of distribution coefficients for La, Sm, Ho and Lu between titanite and melts of different composition – basalt-andesite, andesite and rhyolite obtained in experiments at different *PT*-conditions (Figure 6.3). For example, by using products of crystallization of basalt-andesitic melt at $T = 1000^\circ C$ and $P = 0.75$ GPa the following values of K_d (titanite/melt) were obtained: La (~2), Sm (~9), Ho (~8.5), Lu (~5). Generally, the values of K_d (titanite/silicate melt) increase with increasing SiO_2 content in melts, as well as with increasing pressure and decreasing crystallization temperature.

According to the results of tests on REE from coexisting titanites, apatites and perovskites of different alkaline rocks (jacupirangites, ijolites, nepheline syenites) forming xenoliths in tuffs of Oldoinyo Lengai volcano (Tanzania), it was found that in the case of perovskite absence in these rocks the La and Nd mainly accumulated in apatites and Ce-in titanite. In addition, it was determined that for Zr the values of K_d (titanite/perovskite) in these rocks were about 15 [Dawson *et al.*, 1994].

Sahama was the first to propose a model of isomorphous occurrence of REE into titanite structure and according to it, during the crystallization the REE ions and, possibly, the ions of Na, Mn, Sr and Ba substituted Ca ions in them, while Ti ions could be substituted by ions of Al, Fe^{3+} , Fe^{2+} , Mg, Nb, Ta, V and Cr [Sahama & Vahatalo, 1941; Sahama, 1946]. Later on, this model has been upgraded and got the following form: $[Ca^{2+} + Ti^{4+}] \leftrightarrow [LREE, Y]^{3+} + [Al^{VI}, Fe^{3+}]$ [Russell *et al.*, 1994]. At present there are two more alleged models of the isomorphous occurrence of REE

Table 6.1 Average REE compositions and standard deviations of titanites from some metamorphic rocks and granodiorite (ppm).

	San-Antonio province (Newfoundland, Canada)						Peninsular Ranges, (South California, USA)		
	[Mulroney, Rivers, 2005], LA ICP-MS						[Gromet, Silver, 1983], IDMS		
	46 (3)		48 (3)		49 (2)		06 (3)		Grom-I
	Aver.	St. dev.	Aver.	St. deviation	Aver.	Stand. Deviat.	Aver.	St. dev.	
Element	Metamorphic rocks						Granodiorite		
La	134	55,35	177	47,30	68,95	44,13	207	70,56	N.d
Ce	423	129	588	76,3	268	154	785	195	3305
Pr	63,9	21,3	100	6,96	48,2	24,0	137	45,8	N.d
Nd	342	101	548	18,8	299	142,9	760	342	2680
Sm	113	27,9	172	3,89	116	52,6	251	183	655
Eu	39,7	10,4	61,5	0,71	34,8	17,6	73,8	39,6	165
Gd	152	27,6	213	8,15	160	76,6	247	222	564
Tb	26,1	4,38	34,0	1,40	26,3	12,5	34,3	30,1	N.d
Dy	183	25,2	242	9,27	196	98,0	182	171	470
Ho	37,4	4,39	47,1	1,19	38,95	19,4	23,4	19,6	N.d
Er	111	12,9	136	1,14	114	55,1	45,4	30,7	237
Tm	15,5	1,99	19,0	0,57	16,5	9,23	4,57	3,43	N.d
Yb	106	13,4	129	9,23	111	48,9	21,7	12,7	207
Lu	14,5	2,20	16,7	1,85	14,8	6,30	1,94	1,28	N.d
Total	1761	N.d.	2484	N.d.	1512	N.d.	2773	N.d.	N.d.
(La/Yb) _n	0,85	N.d.	0,92	N.d.	0,42	N.d.	6,42	N.d.	N.d.

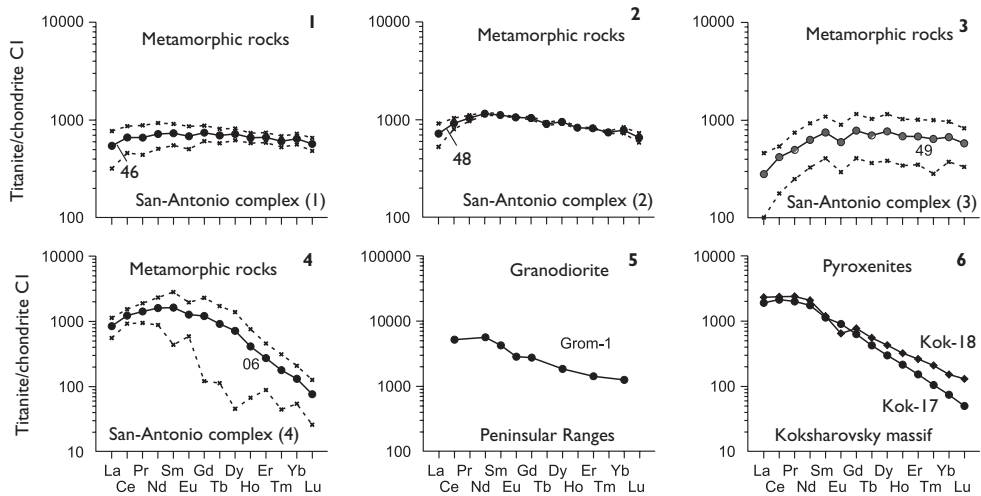


Figure 6.1 Chondrite-normalized REE patterns for titanites from pyroxenites, granodiorites, and some metamorphic rocks. Dotted lines show the patterns for maximum and minimum REE-compositions of individual grains of titanites (data Table 6.1).

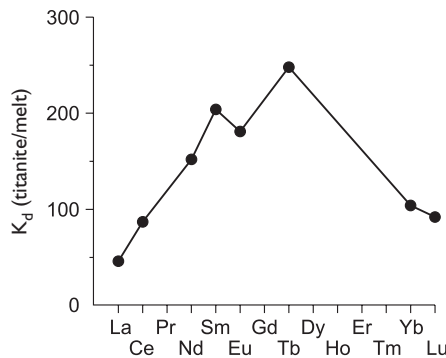


Figure 6.2 The graph of coefficients of REE distribution between titanite and trachite-andesitic melt (data [Kay & Gordillo, 1994]).

in the titanite structure [Seifert & Kramer, 2003]: 1) $\text{Ca}^{2+} + \text{Ti}^{4+} \rightarrow \text{REE}^{3+} + (\text{Al}, \text{Fe})^{3+}$; 2) $2\text{Ca}^{2+} + \text{Ti}^{4+} \rightarrow 2\text{REE}^{3+} + \text{Fe}^{2+}$.

In conclusion of this summary of the information available to date on the regularities of REE distribution in titanites, let us pay attention to one important aspect of this problem. Perkins & Pearce [1996] while considering the optimization techniques for the REE analysis in bulk samples of titanite-bearing rocks using the ICP-MS method, drew attention to the fact that the presence in these rocks of more or less significant amounts of accessory titanite should be taken into account when interpreting the results of the analysis. Their opinion is based on the grounds that titanites along with

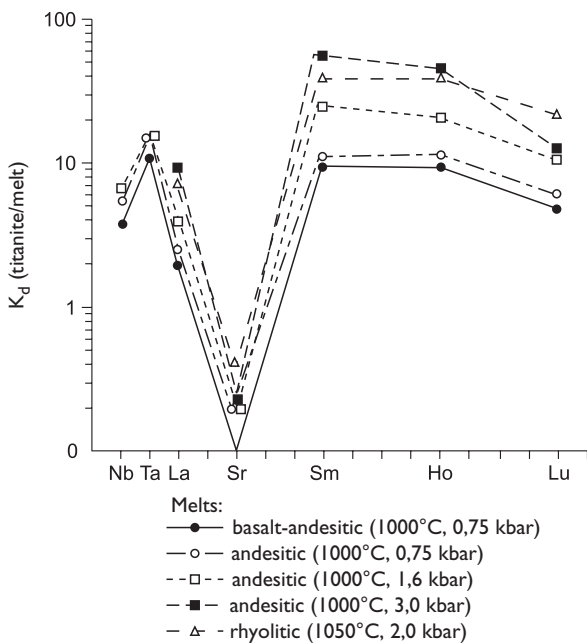


Figure 6.3 The graphs of coefficients of Nb, Ta, La, Sr, Sm, Ho and Lu distribution between titanites and basalt-andesitic, andesitic, and rhyolitic melts under different PT-conditions (experimental data [Green, 1994]).

zircons, monazites and other accessory minerals containing significant REE amounts are quite resistant to reagents used in the decomposition of the samples. Because of this, some amounts of their microparticles are often not fully decomposed, respectively, the REE they contain are not turning into the analyzed solutions and this leads to underdetermination of these elements in the analyzed rocks.

This page intentionally left blank

Chapter 7

Perovskites

Perovskites are among the relatively rare types of accessory minerals of magmatic rocks enriched with REE. Most often they are found in kimberlites, lamproites, melilitic and leucite basalts, carbonatites, jacupirangites, ijolites, nepheline syenites, olivine nephelinites, and more rarely found in rocks of titanomagnetite and chromites deposits, and also in the picrites, some contact-metasomatic formations, chlorite schist, limestone and meteorites. The CaO content in the perovskites ranges from 36.6 to 41 wt% and the TiO₂ content – from 54.5 to 59 wt%. The chemical formula of perovskite, which is usually written as CaTiO₃, is similar to the formula of ilmenite, which has almost all the Fe ions substituted by Ca ions.

In addition to REE this mineral can contain various amounts of impurities such as Fe, Mg, Cr, V, Al, Si, Na, Zr, Nb, Y, Sc. According to data obtained mainly by samples of kimberlite, the perovskite can accumulate in its structure very significant amounts of REE, mainly light elements, and the total REE content might range from 0.9 to 5.4 wt%. Below we consider some regularities of REE distribution in perovskites by the example of kimberlite samples of several provinces (Table 7.1).

Studies on perovskites from some kimberlite manifestations of Southern Africa showed that the perovskite presented in them is characterized by generally higher REE concentration in comparison with the mineral from kimberlites of South India [Jones & Wyllie, 1984]. It was also ascertained that in perovskites from Benfontein sill and Wesselton province the values of parameter $(La/Ce)_n < 1$. In mineral samples from kimberlites of Premier pipe and Dharwar craton the values of parameter $(La/Sm)_n > 1$. In all of these perovskites of the manifestations mentioned an intense REE fractionation is observed, their REE patterns tend to have a steep negative slope (Figure 7.1). The patterns of perovskites of Benfontein sill and Wesselton province have minor intensity peaks for Ce (Figure 7.2). The same peaks are present in the patterns of perovskite from kimberlites of Monastery pipe, as well as Bellsbank, De Beers, Liqhobong and Green Mountain provinces [Jones & Wyllie, 1984]. Having considered the general regularities of REE distribution in perovskites, the stated researchers paid attention to the fact that the configuration of REE patterns of this mineral in many respects is similar to the configuration of patterns of kimberlites, in which they reside.

In kimberlites and kamafugites of Alto Paranaiba province (Brazil) the REE and other impurities were identified both in perovskites and in coexisting olivines, clinopyroxenes, phlogopites and ilmenites. Total REE content in perovskites of these rocks varies in the range from 12455 to 66860 ppm, and the values for $(La/Yb)_n$ range

Table 7.1 REE compositions of perovskites from kimberlites, olivine nephelinites, kamaufugites, and carbonatites from some provinces (ppm).

Element	South Africa												South India		Meimecha-Kotuy prov. (Russia) [data Yu. Vasiliev]	
	Benfontein sill	Wesselton province	Premier pipe	[Chalapathi et al., 2004], WDS												
Bnf-1	Bnf-2	WM-3	PM-5	P3	P4	P4a	CH10	P11/2C	KK10	NP	PD/2	PD/2a	Vas-1	Vas-2		
<i>Kimberlites</i>															Olivine nephelinites	
La	8842	8024	7478	2729	9590	7360	7040	4590	5210	2600	3800	2620	3060	6100	6100	
Ce	26066	25169	24162	6805	22800	17490	19380	9170	12380	6680	7570	4050	5670	14200	14200	
Pr	2914	2803	2862	530	2820	2440	1520	2440	2850	660	440	210	620	2400	2400	
Nd	10811	10537	11077	2589	9590	6690	7110	4620	4770	2980	3090	2520	2130	6400	6400	
Sm	1207	1362	1267	345	1040	850	700	480	420	190	220	100	170	6100	6100	
Gd	650	755	729	165	60	140	650	740	60	280	530	370	260	1140	1240	
Total	49840	47895	46846	12998	45840	34830	35750	21300	25630	13110	15120	9500	11650	36340	36440	
(La/Sm) _n	4,98	5,81	5,45	6,33	6,02	7,81	8,62	10,9	16,5	11,3	4,98	5,81	5,45	0,63	0,63	
(La/Ce) _n	0,88	0,83	0,81	1,05	1,10	1,10	0,95	1,31	1,10	1,02	1,31	1,69	1,41	1,12	1,12	

(Continued)

Table 7.1 (Continued).

<i>Alto Paranaiba (Brazil)</i>										<i>Koksharovskiy (Russia)</i>	
<i>[Melluso et al., 2008], LA ICP-MS</i>										<i>Oktiabr'skiy et al., 2008 ICP-MS</i>	
Element	<i>Ind-r</i>	<i>Ind-c</i>	<i>Lim-c1</i>	<i>Lim-c2</i>	<i>Pan-c</i>	<i>Pan-r</i>	<i>SR-c1*</i>	<i>Sr-c2*</i>	<i>Mal-c1*</i>	<i>Mal-c2*</i>	<i>Kok-16</i>
<i>Kimberlites and kamacfugites</i>										<i>Carbonatite</i>	
La	6990	6990	13011	14555	10423	1771	5134	7837	3762	3030	6652
Ce	22985	20392	36067	35637	25792	2092	9017	21081	9742	6322	14022
Pr	2051	1869	4265	3279	2517	196	1009	1916	802	528	1561
Nd	7505	7204	11366	10643	8707	654	4157	6782	2723	1850	4624
Sm	922	943	1307	954	1107	121	526	903	446	307	669
Eu	209	199	236	161	202	35	125	204	114	87	188
Gd	410	408	450	314	427	101	345	400	229	186	520
Tb	32,1	34,2	31,8	22,9	32,8	11,4	40,6	38	22	19,2	62,1
Dy	114	124	93,9	85,4	116	53,2	190	155	86,5	84	282
Ho	12,2	13,9	11	9,5	14,3	8,4	29,3	18,6	10,5	11,2	39,8
Er	17,4	21,2	15	16,2	22,3	14,5	54	31,7	17	19,2	73,8
Tm	1,51	1,64	1,15	1,17	1,74	1,38	3,78	2,69	1,4	1,82	7,16
Yb	6,17	6,42	4,44	7,74	6,83	6,02	19,8	12,5	5,92	8,48	31,5
Lu	0,53	0,55	0,32	0,51	0,58	0,5	2,92	1,04	0,45	0,69	3,6
Total	41256	38207	66860	65686	49370	5065	20653	39383	17962	12455	28736
$(\text{La}/\text{Yb})_n$	765	735	1978	1269	1030	199	175	423	429	241	143

(Continued)

Table 7.1 (Continued).

	<i>Africa</i>								<i>Somerset Island (Canada)</i>	
	[Wu et al., 2010], LA ICP-MS									
	W3-680	W2-680a	W2-680b	ND#WX	BF-18b	OND1-2	TF-7	Kao-1b	JPI-102	JPI-103
<i>Element</i>	<i>Kimberlites</i>									
La	7150	7084	6754	5732	8264	2004	2619	3437	5170	4841
Ce	18764	19455	16860	13443	22421	4583	5740	7997	13242	11548
Pr	2227	2315	2002	1586	2721	548	652	983	1804	1565
Nd	8978	8979	8158	6472	10869	2295	2613	3750	6639	5875
Sm	1179	1165	1067	884	1333	372	386	481	805	711
Eu	268	266	233	204	278	97,9	96,6	108	165	157
Gd	602	622	510	446	614	233	214	278	352	331
Tb	50,2	50,5	47,6	42,1	48,9	24,4	21,8	21,2	32	31
Dy	179	177	181	159	168	98,5	89,3	84,4	122	120
Ho	20,4	20,9	20,9	18,7	18,4	12,9	11,4	9,84	15	15
Er	30,3	37,2	33,5	29,8	27,1	21,2	19,7	16,2	23	24
Tm	2,34	2,66	2,66	2,29	2,00	1,77	1,67	1,29	1,96	2,11
Yb	9,73	11,3	11,3	10,1	8,24	7,57	7,60	5,53	8,18	8,57
Lu	0,75	0,82	0,94	0,82	0,66	0,64	0,67	0,47	0,76	0,81
Total	39461	40179	35882	29030	46773	10300	12473	17173	28381	25229
(La/Yb) _n	496	460	403	383	677	179	233	420	427	381

(Continued)

Table 7.1 (Continued).

<i>Somerset Island (Canada)</i>										
	[Wu et al., 2010], LA ICP-MS									
	JPI-104	C8	PC-03	PC-04	BND2-2	Tunraq	EL-6	Ham	Amayersuk	BSD5-I
Element	Kimberlites									
La	4591	6977	7042	6970	5209	5662	6138	6734	7527	7292
Ce	10909	15810	16083	16754	11191	12499	14148	15546	17603	17320
Pr	1467	1683	2096	2184	1225	1645	1854	2005	2237	2189
Nd	5454	6352	7574	7813	4636	5999	6682	7165	8050	8111
Sm	663	695	822	844	579	726	729	809	886	933
Eu	147	149	170	171	135	158	154	172	179	191
Gd	317	301	342	339	290	338	306	347	358	397
Tb	29,1	25,8	29,5	28,8	27,0	30,6	25,5	30,1	30,5	34,1
Dy	115	94,3	110	105	103	119	95	111	112	128
Ho	14,3	10,8	13,0	12,5	12,5	14,3	11,1	13,0	12,9	15,1
Er	22,4	17,5	20,4	19,4	20,5	23,1	17,5	19,7	20,1	23,7
Tm	1,94	1,38	1,64	1,56	1,71	1,94	1,37	1,68	1,57	1,91
Yb	8,50	6,17	6,72	6,68	7,75	7,81	5,61	6,66	6,45	7,98
Lu	0,78	0,52	0,60	0,60	0,70	0,79	0,51	0,56	0,58	0,77
Total	23740	31923	34311	35250	23438	27225	30168	32961	37004	36645
(La/Yb) _n	365	763	707	704	454	489	739	682	788	617

Note: WDS – long wave dispersion spectroscopic method; c – core of grain; r – rim of grain; (*) – samples from kamafugites.

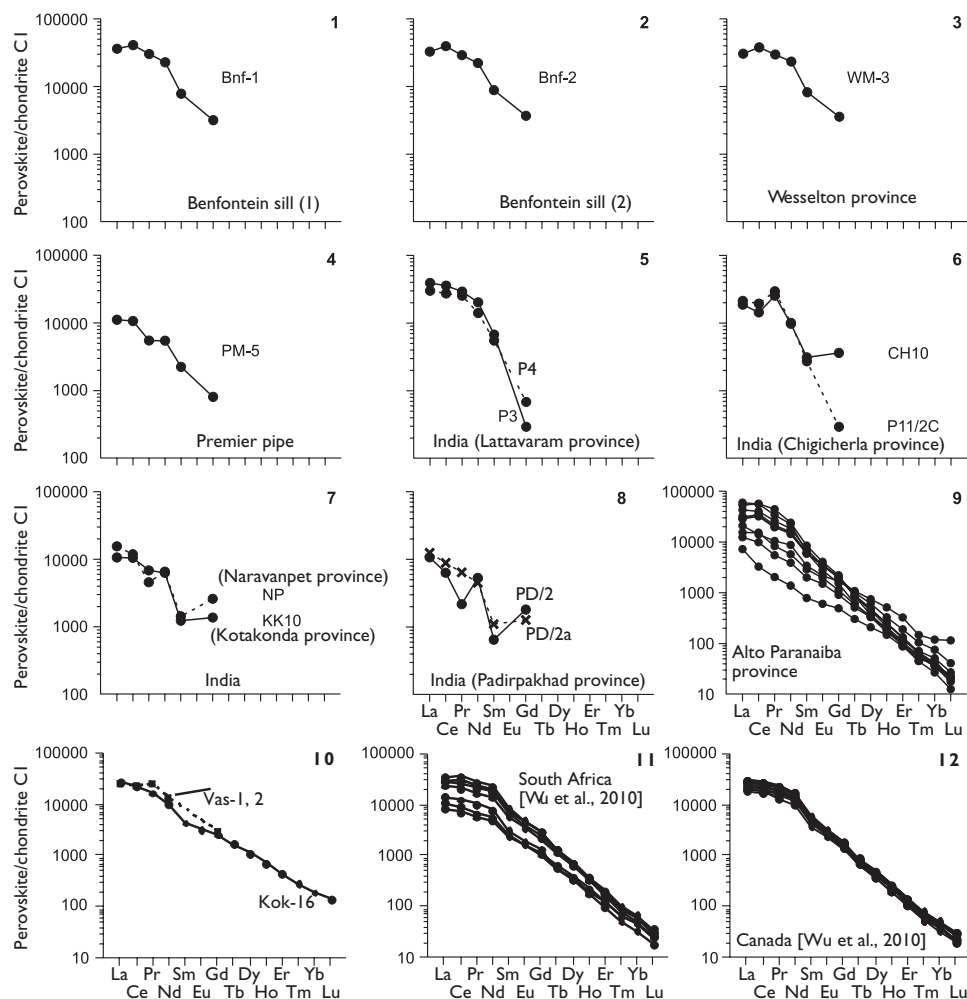


Figure 7.1 Chondrite-normalized REE patterns for perovskites (data Table 7.1).

from 175 to 1030 (Figure 7.1, 9). According to data obtained by the microprobe fluorescent technique, the contents of La, Ce, Nb, Na and Sr in the perovskites of India manifestation of the mentioned province decreased from the inner zones to the periphery of their grains. At the same time, the analyses by LA ICP-MS method that were carried out on a single grain of perovskite of the same kimberlite manifestation, have shown that in its inner zone the total REE content is slightly lower than in the outer zone (Table 7.1). In addition, the total REE content in the outer zone of the perovskite grain from kimberlites of Pantano manifestation of the same province also turned out to be significantly lower than in its inner zone (Table 7.1).

Studies on regularities of distribution of REE and other impurities in perovskites from some kimberlite manifestations of South Africa and Somerset Province (Canada),

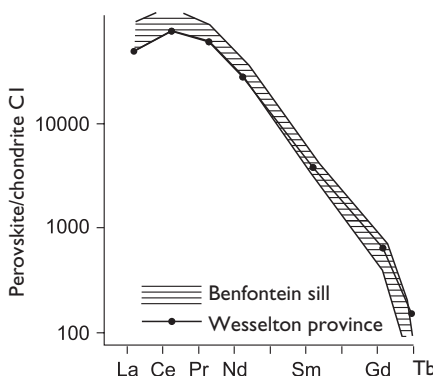


Figure 7.2 Chondrite-normalized average composition REE patterns for perovskites from kimberlites of Benfontein sill ($n = 2$) and Wesselton province ($n = 6$) (data [Jones & Wyllie, 1984]).

which were conducted by Wu *et al.* [2010], showed that the total REE compositions in the mineral samples from the manifestations of Southern Africa vary from 10300 to 46773 ppm, and the values for $(\text{La/Yb})_n$ – from 179 to 677 (Table 7.1). In perovskites of Somerset province the total REE compositions ranged from 23438 to 37004 ppm, values for $(\text{La/Yb})_n$ – from 381 to 788. The patterns of distribution of chondrite-normalized REE compositions in perovskites from kimberlites of South Africa and Somerset province are the lines with a very steep negative slope that are almost identical in configuration and location (Figure 7.1, 11, 12). By the nature of their REE patterns, the perovskites studied by Wu *et al.*, in many respects are similar to the patterns of mineral samples from Alto Paranaiba province, Benfontein sill and Wesselton province (Figure 7.2). A large concentration of REE and their slightly less intense fractionation were ascertained in perovskite from carbonatites of Koksharovsky alkaline ultramafic massif (Primorie, Russia) (Figure 7.1, 10), as well as in the samples of mineral from olivine nephelinites of Meimecha-Kotuy province (Siberian platform, Russia) (Table 7.1).

It was shown in observations that the high modal contents of perovskite in kimberlites can greatly affect the overall level of REE accumulation, as well as the configuration of the patterns of their distribution in these rocks. This conclusion follows from the identified positive correlation between REE compositions of kimberlites, on the one hand, and the contents of TiO_2 in them, on the other hand [Vasilenko *et al.*, 2003].

Estimates of the values of K_d (perovskite/silicate melt), which were obtained based on the results of experimental studies, have shown that for La, Sm, Eu and Tb the values of these coefficients are slightly greater than 1, which means that during the crystallization of perovskites the REE possessed properties of compatible elements. Contrasting to them, the values of K_d for Yb and Lu do not exceed 1, therefore these REE possessed properties of incompatible elements during their iso-morphous incoming into the structure of perovskites (Table 7.2, Figure 7.3). Some of the data on K_d (perovskite/melt) values estimates for REE were obtained by Jones & Wyllie [1984] during their studies on natural and experimental systems (Figure 7.4).

For natural systems the K_d (REE) values were determined between kimberlites and melilite-nepheline basalts, on the one hand, and the perovskites they contain, on the other hand. The following diagram shows that for the perovskite/kimberlite system the K_d values for La, Ce, Pr, Nd, Sm, Gd and Ho > 1. A similar trend is ascertained for K_d (La, Nd, Sm) in the perovskite/melilite-nepheline basalt system. For both of these systems the curves of changes in the values of K_d have a common negative slope. The curves shown in the same picture reflect the changes in the values of K_d (perovskite/kimberlite) for the natural system and for some systems studied during the experiment and also have a common negative slope, but the K_d values for the experimental systems were lower than for the natural system. In addition, in some kimberlites the accessory apatite plays the role of a concentrator of significant LREE amounts, along with the perovskite, but the modal contents of them are usually much smaller than those of perovskite.

The study of REE distribution between minerals from jacupirangites, ijolites and nepheline syenites represented as xenoliths in tuffs of Oldoinyo Lengai volcano

Table 7.2 The coefficients of REE distribution between perovskites and silicate melts (experimental data [Nagasawa et al., 1981]).

Element	Nag-1	Nag-2	Nag-3	Nag-4	Nag-5
La	2,4	2,96	2,15	2,44	3,04
Ce	N.d.	N.d.	N.d.	N.d.	N.d.
Pr	N.d.	N.d.	N.d.	N.d.	N.d.
Nd	N.d.	N.d.	N.d.	N.d.	N.d.
Sm	2,76	3,12	2,16	2,47	3,01
Eu	2,28	2,67	2,07	1,87	2,04
Gd	N.d.	N.d.	N.d.	N.d.	N.d.
Tb	1,45	1,83	1,37	1,49	1,77
Dy	N.d.	N.d.	N.d.	N.d.	N.d.
Ho	N.d.	N.d.	N.d.	N.d.	N.d.
Er	N.d.	N.d.	N.d.	N.d.	N.d.
Tm	N.d.	N.d.	N.d.	N.d.	N.d.
Yb	0,482	0,517	0,445	0,443	0,553
Lu	0,408	0,412	0,389	0,413	0,432

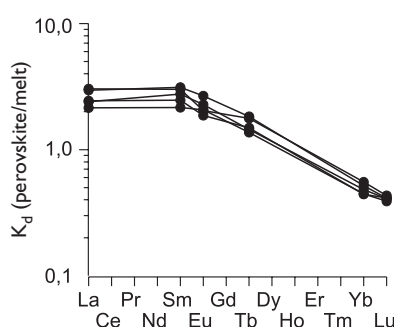


Figure 7.3 The graphs of coefficients of REE distribution between perovskites and siliceous melts (experimental data [Nagasawa et al., 1981]) (data Table 7.2).

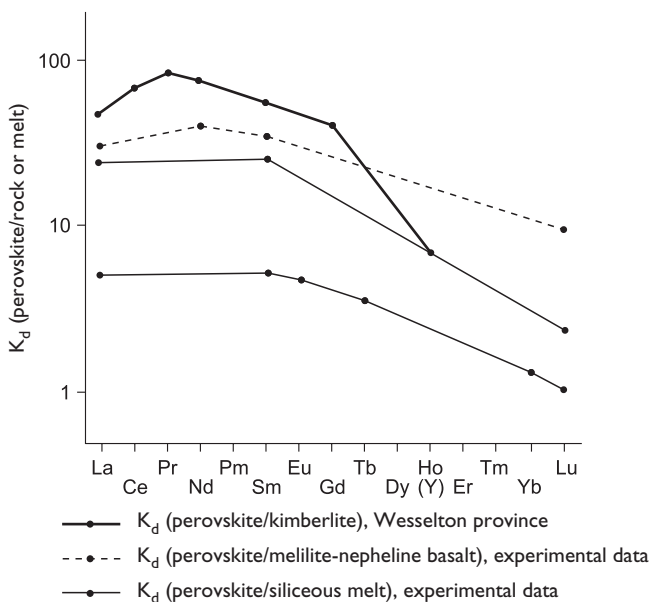


Figure 7.4. The graphs of coefficients REE distribution between perovskites and kimberlites, melilite-nepheline basalts and siliceous melts (experimental data [Jones & Wyllie, 1984]).

(Tanzania) showed that in the cases when there was absence of titanites in these rocks the values of K_d (perovskite/apatite) were: La-9, Ce-16, Nd-9,5. However, when samples of the same rocks contained titanites, the values of K_d (perovskite/apatite) for these elements were much lower [Dawson *et al.*, 1994].

Having considered very scarce data on the contents of REE in perovskites, we emphasize again that this mineral, presented as an accessory phase in some varieties of magmatic rocks, can accumulate in its structure very substantial LREE amounts and much smaller quantities of medium and heavy elements. Therefore, if there is a significant modal content of perovskite in the rocks it might have a noticeable effect on the REE distribution in these rocks, which is well illustrated by the kimberlites. The high values of LREE distribution coefficients between perovskite and its parent melts indicate that during the isomorphic incoming into its structure the LREE usually possessed properties of compatible elements.

Taking into account the ability of perovskites to accumulate in its structure very significant amounts of REE, one should pay attention to another important geochemical aspect. Thus, the estimates show that a significant portion of the Earth's mantle at depths greater than 670 km for about 70% might consist of a high-pressure perovskite-like phase [Urusov & Puscharovskii, 1999; Puscharovskii, Yu., Puscharovskii, D., 2010]. In this regard, with a considerable degree of conditionality we can assume that if the perovskite-like phase is similar to normal perovskite not only in its crystal structure but also in geochemical properties, than those REE, which are accumulated in the matter of undepleted mantle are probably concentrated in these high-pressure phases such as CaSi-perovskite and CaTi-perovskite pointed out by Garanin [2006].

This page intentionally left blank

Chapter 8

Micas

Micas are primarily presented in magmatic rocks with high content of silica, alkaline and volatile components, as well as in metamorphic and some metasomatic rocks. Less frequently micas occur as a secondary phase in some rocks of mafic and ultramafic composition and what is more, most often they are represented by phlogopite.

Chemical formula of mica group of minerals is as follows: $K(Mg, Fe)_3[Si_3AlO_{10}] \cdot [F, OH]_2$. The content of the main components of phlogopite change in the following ranges (wt%): MgO-21–29, FeO-up to 9, K₂O-7–10, H₂O-0.3–5.4. Biotites are characterized by a high content of FeO (2.7–27.6 wt%) and K₂O (6.2–11.4 wt%) and by wider variations in the content of MgO (0.28–28.3 wt%) [Betekhtin, 1956].

Analytical data on the REE composition of micas from high-magnesium rocks is now available in fairly limited amounts and characterizes the composition of this mineral not from all the varieties of these rocks but mainly from kimberlites, peridotites, wehrlites, websterites and clinopyroxenites (Table 8.1). Total REE contents in phlogopites from wehrlites and pyroxenites composing xenoliths from minettes of Bearpaw province (Montana, USA) vary from 29 to 112 ppm, while the chondrite-normalized La contents are higher (10.2–54.2 t.ch.) than Yb contents (3.6–7.2 t.ch.) [Downes *et al.*, 2004]. The REE patterns of these phlogopites have the shape of lines with a gentle negative slope and are described by the values of $(La/Yb)_n$ parameter in the range of 2.3–7.5 (Figure 8.1).

Phlogopites from ultramafic rocks that form xenoliths in alkaline basalts from Vitim province are characterized by total REE contents that are lower (1.4–20 ppm) than the previous ones [Litasov, 1998]. The REE composition, which is very close to phlogopites from Vitim province, was identified in the phlogopites from concentrate that have been isolated from kimberlite sample from Yubileynaya pipe (Yakutia), the total REE content of which is 10.8 ppm [Aschepkov *et al.*, 2004]. Phlogopites from ultramafic xenoliths of Vitim province, as well as from the kimberlites of Yubileynaya pipe, are characterized by a more intensive REE fractionation in comparison with the mineral from Bearpaw province. Thus, in phlogopites from Vitim province the values of $(La/Yb)_n$ parameter vary in the range from 14.2 to 21.8, while in the mineral from kimberlites of Yubileynaya pipe ~55. On REE patterns of phlogopites from ultramafic xenoliths of Vitim province there are negative Ce anomalies (Figure 8.1, 3), which are absent on the pattern of the mineral from kimberlites, while the latter show a weak positive Eu anomaly (Figure 8.1, 4). Mica that is presented in the olivine nephelinite from Germany and Austria is characterized by relatively low overall REE accumulation in comparison with the mineral from the manifestations mentioned above (Figure 8.1, 5).

Table 8.1 REE compositions of phlogopites, and biotites from some magmatic rocks (ppm).

	Bearpaw province (USA)			Vitim province (Russia)				Yubileynaya pipe (Yakutia, Russia)		Germany, Austria		Twin Peaks (USA)
	[Downes et al., 2004] ICP-MS			[Litasov, 1998] SIMS				[Aschepkov, 2004] ICP-MS		[Irving, Frey, 1984]		[Nash, Crecraft, 1985]
	201	237	188	V878	LF-4	V244	V439	Asch-3	RRa	32M1		N-4
Element	Wehrlite	Pyroxenites		Peridotites				Kimberlite	Nephelinite		Rhyolite	
La	2,50	4,05	13,3	0,420	0,980	4,04	0,970	2,12	0,970	0,990	81,1	
Ce	8,25	14,3	43,1	0,020	0,270	0,040	0,060	5,70	1,60	1,60	168	
Pr	1,50	2,46	6,45	N.d.	N.d.	N.d.	N.d.	0,520	0,200	N.d.	N.d.	
Nd	7,79	10,9	27,4	0,690	1,24	11,7	1,71	1,65	0,850	N.d.	61,0	
Sm	2,36	3,61	6,30	0,080	0,180	1,26	0,150	0,260	0,051	0,097	7,88	
Eu	0,69	1,14	1,45	0,030	0,060	0,430	0,060	0,113	0,051	0,097	0,400	
Gd	2,13	3,17	5,25	N.d.	N.d.	N.d.	N.d.	0,202	0,086	N.d.	N.d.	
Tb	0,29	0,470	0,750	N.d.	N.d.	N.d.	N.d.	0,020	0,012	N.d.	0,710	
Dy	1,64	2,70	3,89	0,110	0,200	1,65	0,250	0,135	0,080	N.d.	4,23	
Ho	0,290	0,480	0,700	N.d.	N.d.	N.d.	N.d.	0,015	N.d.	N.d.	N.d.	
Er	0,680	1,28	1,75	0,050	0,070	0,740	0,100	0,022	N.d.	N.d.	N.d.	
Tm	N.d.	N.d.	N.d.	N.d.	N.d.	N.d.	N.d.	0,006	0,004	N.d.	N.d.	
Yb	0,600	1,17	1,20	0,020	0,040	0,140	0,030	0,026	0,029	N.d.	2,49	
Lu	0,090	0,160	0,160	N.d.	N.d.	N.d.	N.d.	0,007	0,004	N.d.	0,370	
Total	28,8	45,9	112	N.d.	N.d.	N.d.	N.d.	10,8	3,94	N.d.	N.d.	
(La/Yb) _n	2,8	2,3	7,5	14,2	16,5	19,5	21,8	55,0	22,6	N.d.	22,0	

(Continued)

Table 8.1 (Continued).

	Twin Peaks (USA)		Kok sarovsky massif (Russia)		Alto Paranaiba province (Brazil)								
	[Nash, Crecraft, 1985], INAA		[Oktiabr'sky et al., 2008]		[Melluso et al., 2008], LA ICP-MS								
	N-8	N-20	Kok-20		Ind-c	Ind-r	Lim-c	Lim-r	Pan-c	Pan-r	Po-c	Ver-c	Mal-c
Element	Rhyolites		Nepheline syenite	Kimberlites									
La	459	41,5	0,77	0,028	0,038	0,897	2,14	0,171	10,97	0,411	5,03	0,99	
Ce	770	100	0,73	N.d.	0,051	0,662	2,22	0,292	7,12	0,108	9,6	0,44	
Pr	N.d.	N.d.	0,11	0,004	0,008	0,055	0,162	0,037	0,572	0,016	1,22	0,044	
Nd	187	39,0	0,38	N.d.	0,053	0,201	0,571	0,078	2,3	N.d.	5,84	0,12	
Sm	23,1	6,45	0,11	0,02	N.d.	0,017	0,162	N.d.	0,581	N.d.	1,01	0,049	
Eu	1,67	0,220	0,013	0,017	0,028	0,019	0,057	0,005	0,247	0,042	0,352	0,05	
Gd	N.d.	N.d.	0,05	0,022	N.d.	0,027	0,12	0,002	0,739	0,025	0,04	0,046	
Tb	2,71	0,700	0,01	0,002	N.d.	0,003	0,01	N.d.	0,108	N.d.	0,133	0,01	
Dy	16,4	4,49	0,06	0,005	0,003	0,035	0,062	N.d.	0,509	N.d.	0,58	0,046	
Ho	N.d.	N.d.	0,01	N.d.	0,001	0,005	0,008	N.d.	0,078	N.d.	0,116	0,005	
Er	N.d.	N.d.	0,02	N.d.	N.d.	0,012	0,043	0,015	0,208	0,032	0,282	N.d.	
Tm	N.d.	N.d.	N.d.	N.d.	0,003	0,004	0,007	N.d.	0,024	0,011	0,033	0,003	
Yb	12,7	2,84	0,05	0,015	N.d.	0,017	0,012	0,052	0,216	N.d.	0,193	N.d.	
Lu	2,00	0,42	0,01	N.d.	0,005	0,01	N.d.	N.d.	0,024	N.d.	0,035	0,003	
Total	N.d.	N.d.	2,32	0,11	0,19	1,96	5,57	0,65	23,7	0,65	24,5	1,81	
(La/Yb) _n	24,4	9,9	10,4	1,26	N.d.	35,6	120	2,22	34,3	N.d.	17,6	N.d.	

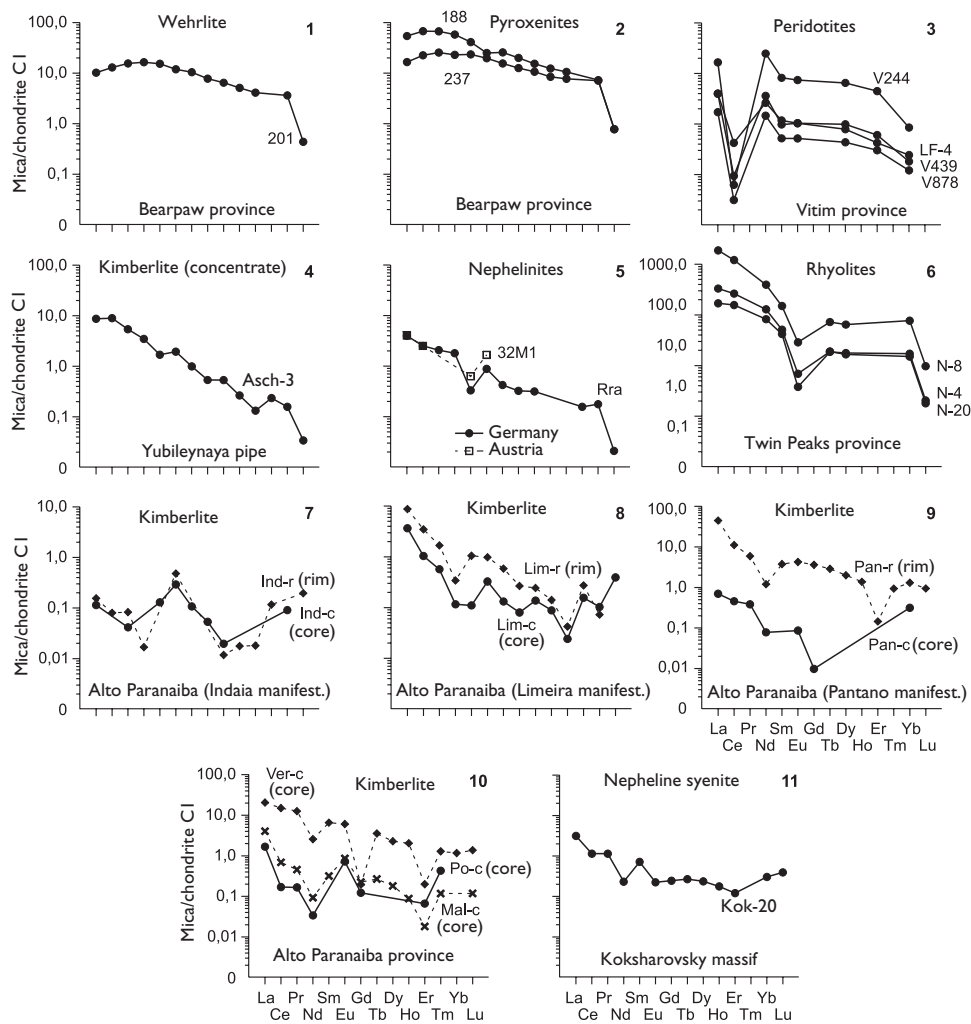


Figure 8.1 Chondrite-normalized REE patterns for biotites and phlogopites from wehrlite (1), pyroxenites (2), peridotites (3), kimberlites (4, 7–10), nephelinites (5) and nepheline syenite of some provinces and manifestations (data Table 8.1).

While studying REE composition of phlogopites from kimberlites of Alto Paranaiba province, it was determined that the total REE contents in them range from 0.11 to 24.5 ppm and that these minerals from various manifestations are markedly different in the configuration of REE patterns. On REE patterns of the central and outer zones of phlogopite grains from Indaia manifestation of this province there are intense positive Eu anomalies (Figure 8.1, 7). To add more, the inner and outer zones of grains of phlogopite from kimberlites of Limeira manifestation are characterized by significant enrichment with LREE, while positive Eu anomalies on their patterns are of lower intensity. The REE content in the outer zone of phlogopite grain is slightly higher than in its inner zone (Figure 8.1, 8).

A similar trend, but in the absence of clearly defined Eu anomalies, was observed in phlogopite from kimberlites of Pantano manifestation, but the content of almost all the REE in it was significantly higher in the outer zone than in the inner zone (Figure 8.1, 9). We should also note the increased concentration of REE in the inner zone of grain of phlogopite from kimberlites of Veridiana manifestation, as well as the presence of positive Eu anomalies in the patterns of the central zones of grains of phlogopite from other kimberlite manifestations of Alto Paranaiba province (Figure 8.1, 10).

A study of biotites from nepheline syenites forming Koksharovskiy alkaline ultramafic massif (Primorie province, Russia) showed that the overall level of REE accumulation, as well as the intensity of REE fractionation are lower than most of the above-described phlogopites from kimberlites (Figure 8.1, 11). The biotites from rhyolites of volcanic complex in Twin Peaks province (USA) have relatively high total REE contents. Their chondrite-normalized REE patterns show a predominance of LREE over HREE and a significant Eu deficit (Figure 8.1, 6).

Representative data have been published on the content of REE in biotites from gneisses, schists, metasomatites and some granites belonging to the series of metamorphic complexes [Drugova & Skublov, 2004]. These biotites are characterized by variations in total REE contents in the range of 2–29 ppm, as well as by a significant range of values of $(\text{La/Yb})_n$ parameter – from 1.7 to 105 (Table 8.2). On the

Table 8.2 REE compositions of biotites from gneisses, schists, and metasomatic rocks from some metamorphic complexes (ppm).

<i>Laplandsky complex (Baltic shield, Russia)</i>						
<i>[Drugova, Skublov, 2004] ICP-MS</i>						
	606	619	620	627g	LN-126	LN-127
<i>Element</i>	<i>Gneisses</i>					<i>Granitoid</i>
La	7,51	3,62	0,790	1,05	2,60	0,610
Ce	12,9	4,92	1,16	2,03	5,67	0,860
Pr	N.d.	N.d.	N.d.	N.d.	N.d.	N.d.
Nd	5,64	2,24	0,610	1,23	2,92	0,340
Sm	2,14	1,77	0,510	0,550	1,19	0,160
Eu	0,150	0,170	0,180	0,180	0,190	0,340
Gd	0,610	0,600	0,270	0,200	0,390	0,190
Tb	0,055	0,074	0,020	0,021	0,041	0,008
Dy	0,150	0,280	0,077	0,077	0,130	0,034
Ho	N.d.	N.d.	N.d.	N.d.	N.d.	N.d.
Er	0,066	0,125	0,043	0,036	0,059	0,023
Tm	N.d.	N.d.	N.d.	N.d.	N.d.	N.d.
Yb	0,087	0,120	0,180	0,050	0,099	0,180
Lu	0,021	0,02	0,056	0,012	0,026	0,060
Total	29,33	13,94	3,90	5,44	13,85	2,81
$(\text{La/Yb})_n$	58,27	20,36	2,96	14,17	17,73	2,29
$(\text{Eu/Eu}^*)_n$	0,31	0,41	1,34	1,36	0,68	5,95

(Continued)

Table 8.2 (Continued).

Complexes						
	Laplandsky (Baltic shield, Russia)	Belomorsky (Baltic shield, Russia)	Korva-Tundra (Russia)	Karateginsky (Tien Shan, Kyrgyzstan)		
<i>[Drugova, Skublov, 2004], ICP-MS</i>						
	LN-130	28c	633b	900	834b	1005c
Element	Schist	Metasomatic rock	Schist	Gneisses		
La	0,300	1,07	10,4	5,96	0,910	1,11
Ce	0,500	2,22	9,05	10,6	1,48	2,29
Pr	N.d.	N.d.	N.d.	N.d.	N.d.	N.d.
Nd	0,310	0,910	5,75	4,99	0,750	1,90
Sm	0,200	0,510	1,72	2,31	0,360	1,19
Eu	0,079	0,089	0,170	0,170	0,074	0,250
Gd	0,110	0,280	0,690	0,950	0,200	0,600
Tb	0,020	0,055	0,063	0,120	0,038	0,069
Dy	0,110	0,270	0,150	0,390	0,230	0,250
Ho	N.d.	N.d.	N.d.	N.d.	N.d.	N.d.
Er	0,071	0,160	0,058	0,140	0,160	0,086
Tm	N.d.	N.d.	N.d.	N.d.	N.d.	N.d.
Yb	0,120	0,210	0,067	0,130	0,220	0,083
Lu	0,026	0,038	0,015	0,023	0,037	0,018
Total	2,03	5,81	28,1	25,8	4,46	7,85
$(La/Yb)_n$	1,69	3,44	105	31,0	2,79	9,03
$(Eu/Eu^*)_n$	1,48	0,66	0,40	0,30	0,77	0,81

REE patterns of many biotites from metamorphic rocks, which often show a negative slope, there are positive Sm anomalies, as well as smooth lows in the Nd area and in the parts of the patterns between Dy and Er (Figure 8.2). The patterns of biotites from granites from Laplandsky complex in contrast to the patterns of this mineral from metamorphic rocks, as well as from rhyolites of Twin Peaks province (Figure 8.1, 6), are complicated by a very intense positive Eu anomaly (Figure 8.2, 3). According to the observations of Drugova & Skublov, the variations of the REE distribution parameters in biotites from metamorphic rocks are in one way or another predetermined by the composition of mineral parageneses of the rocks in which they reside. According to the observations of these researchers, the content of HREE in biotites decreases with increasing temperature of metamorphism of those protolite that formed biotite-bearing metamorphic rocks. However, according to Fleet [1984], who studied the REE composition of biotites from gneiss of several districts in Norway, high concentrations of La, Ce, Dy and Yb in this mineral are

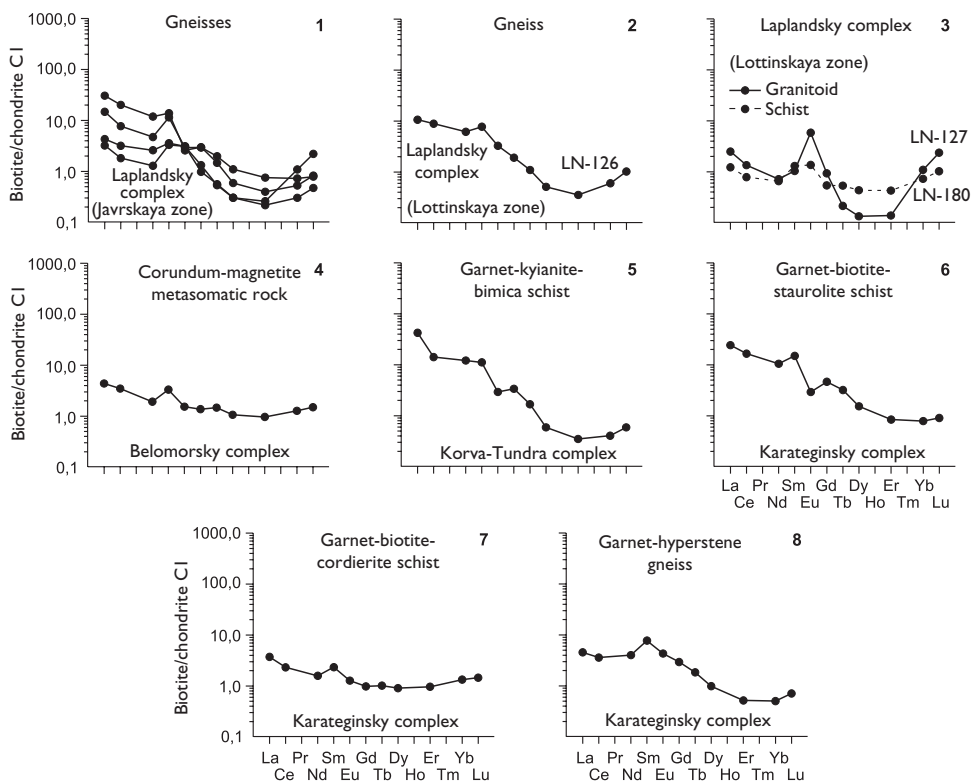


Figure 8.2 Chondrite-normalized REE patterns for biotites from different gneisses and schists of some metamorphic complexes (data Table 8.2).

often associated with epigenetic redistribution of these elements during the chemical weathering of rocks.

Studies on REE composition of individual mica samples and basanites and basalts containing them provided approximate estimates of the values of K_d (mica/melt) that appeared to be generally very low (Table 8.3). You can see that the K_d graphs have a complex configuration, which may be due to insufficiently correct determination of the contents of some elements (Figure 8.3).

Green [1994] published data on the values of K_d (phlogopite/melt) for some impurities including REE, which were obtained based on the results of physical experiments (Figure 8.4). The data imply that the K_d values for La, Sm, Ho and Lu do not exceed 1 and also that the coefficient variation curves in the segment from La to Ho has a positive slope, while in the section from Ho to Lu it acquires a negative slope.

In conclusion, we should emphasize that according to yet limited analytical data, there are more or less significant differences ascertained between micas of magmatic and metamorphic rocks, which are in the general level of REE accumulation and in

Table 8.3 The coefficients of REE distribution between micas and basanitic, and basaltic melts.

Element	Basanitic melt		Basaltic melt
	K_d (mica/matrix) (experimental data)		K_d (mica/melt) combined
	[Irving, Frey, 1984]	[Litasov, 1998]	
La	0,006	0,036	0,031
Ce	0,005	0,027	0,007
Pr	N.d.	N.d.	0,011
Nd	0,017	N.d.	0,012
Sm	0,004	0,028	0,012
Eu	0,022	0,036	0,031
Gd	0,014	N.d.	0,026
Tb	0,015	N.d.	N.d.
Dy	0,019	N.d.	0,026
Ho	N.d.	N.d.	0,03
Er	N.d.	N.d.	0,03
Tm	N.d.	N.d.	N.d.
Yb	0,02	0,041	0,03
Lu	0,018	0,031	0,04

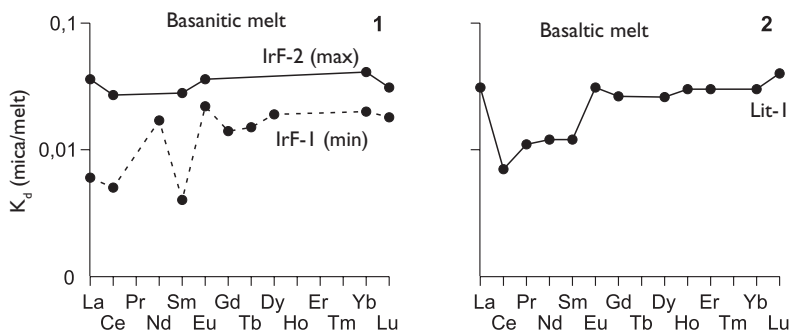


Figure 8.3 The graphs of coefficients REE distribution between phlogopites and basanitic and basaltic melts (data Table 8.3).

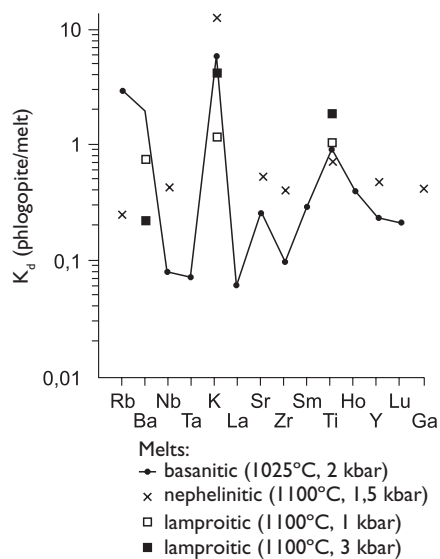


Figure 8.4 The graphs of coefficients of REE distribution between phlogopites and basanitic, nephelinitic, and lamproitic melts under different PT-conditions (experimental data [Green, 1994]).

the configuration of the patterns of their chondrite-normalized contents. Chondrite-normalized LREE contents in most of the samples of mica are slightly higher than the contents of MREE and HREE and, accordingly, their patterns have a common negative slope. It should also be emphasized that phlogopites from kimberlites, wehrlites, peridotites and pyroxenites are able to concentrate in its structure much smaller amounts of REE compared to biotites from rhyolites and metamorphic rocks.

This page intentionally left blank

Chapter 9

Some general regularities of REE distribution in the minor and accessory minerals of ultramafic, mafic and some other rocks

Mineral is a structural sieve for elements and this sieve is dirty.

D. Shaw

In recent years the development of modern microprobe methods of REE determining, and the lowering of the limits of REE detection, have expanded the study on the regularities of distribution of these impurities not only on rock-forming, but also on minor and accessory minerals of the ultramafic and mafic rocks, which include garnets, chrome-spinels, ilmenites, zircons, apatites, titanites, perovskites and micas. As it was shown in previous chapters, these minerals are significantly different from each other in the general chemical composition, crystal-chemical properties and formation conditions, have different abilities to accumulate REE and other impurities. There are reasons to believe that an appropriate use of data on the REE distribution in these minerals can help to gain additional geochemical criteria and typomorphic signs for their diagnosis, discrimination, systematization and genetic interpretation.

Geochemical studies conducted on this issue suggest that the same types of accessory minerals that are presented in ultramafic and mafic rocks of different composition and origin and in magmatic complexes composed of them, to some extent, differ in the level of REE accumulation, the degree of fractionation and in a number of other features. There are reasons to believe that these differences were due to various factors, such as an initial concentration of REE in the maternal melts of these minerals, as well as differences in temperature, pressure and redox conditions of melts generation and minerals crystallization. Along with the general level of accumulation and other parameters of REE distribution in minor and accessory minerals there is a very important characteristic of them which is the calculated on the basis of data on natural and experimental systems distribution coefficients of REE between minerals and their parent melts, as well as between coexisting mineral phases. Given the ability to concentrate in its structure one or another amount of isomorphous REE impurity, the accessory and minor minerals from the ultramafic, mafic and related rocks can be divided into the following five groups: 1) garnets and zircons that accumulate significant amounts of REE with substantial prevalence of chondrite-normalized contents of HREE; 2) apatites and perovskites that can accumulate significant amounts of REE with substantial predominance of LREE; 3) titanites that accumulate medium amounts of light and heavy REE at near their chondrite-normalized concentrations, 4) micas that accumulate medium amounts of REE with a slight predominance

of chondrite-normalized LREE contents over HREE contents; 5) ilmenites and chrome-spinels that accumulate a limited amount of REE often with HREE predominance. It is important to pay attention to the fact that along with isomorphous REE impurity that reside directly in their structure, in some cases the crystals of minor and accessory minerals may contain one or another amount of non-structural impurity of these elements, which was accumulated in microcracks and different microinclusions as a result of infiltration of the epigenetic fluids. Generalizing the information outlined in previous chapters of the book, let us pay attention to the most significant aspects of REE distribution in the accessory and minor minerals of ultramafic, mafic and other rocks of different genesis.

Garnets, which reside as an accessory phase in composition of many rocks of magmatic, metamorphic and metasomatic origin, can crystallize in a wide range of *PT*-parameters and vary considerably in the content of the main components and impurities. Therefore, the study of regularities of REE distribution in them remains one of the most important trends in mineralogy and geochemistry of the rocks in which they reside. In this regard the more detailed studies were conducted upon high-Mg garnets from peridotite xenoliths presented in kimberlites, especially upon those that reside as microinclusions directly in diamond crystals.

It is ascertained that the overall level of REE accumulation in garnets of different composition increases from their subcalcium varieties to high-calcic and high-iron varieties of eclogites, gabbros, as well as metamorphic and metasomatic formations. Generally, chondrite-normalized HREE contents in the garnets are in varying degrees higher than the content of MREE and especially LREE. The $(La/Yb)_n$ parameter for the majority of garnets have very low values, respectively, the chondrite-normalized REE patterns usually have a steep positive slope. The studies on garnets that are in paragenesis with diamonds showed that their REE patterns often have a particular sinusoidal configuration. According to the common view, the patterns with a similar configuration are inherent to pyrope garnets from ultramafic rocks, which in one way or another have undergone the so-called "mantle metasomatism" under the influence of carbonatite melts and associated fluids. Such REE patterns of garnets are usually considered one of the main criteria in the search and predictive estimates of diamondiferous kimberlite pipes.

On the REE patterns of garnets from some hybrid gabbroid rocks some Eu anomalies were found, which is not typical of this mineral, while on the patterns of some garnets from volcanic rocks of medium and acid composition some negative Eu anomalies were observed. In crystals of some garnets from eclogites along with their optical and chemical zoning a zonal REE distribution was determined, which is due to a lower concentration of HREE in the peripheral zones of their crystals compared with their inner zones.

The estimates of K_d (garnet/melt) values received to date indicate that for all REE they increase in a row from high-Mg to high-Fe melts and thus increase from LREE to HREE. Under the experimental investigations it was ascertained that K_d (garnet/melt) values are usually increasing with decreasing of the temperature of mineral crystallization. At the same time K_d values for LREE, as a rule, have values less than 1, while for HREE and sometimes for MREE their values are almost always greater than 1. These data give grounds to suggest that during isomorphous coming into the structure of the garnet HREE and partly MREE had properties of compatible impurities, while

LREE during this process had properties of incompatible impurities. In addition, the values of K_d (garnet/clinopyroxene) have been estimated for some ultramafic rocks, which can be used as indicators of the geochemical systematizations of these rocks. It is important to note that the approximate location and the same configuration of the curves of K_d (garnet/clinopyroxene) values for rock samples selected from a single manifestation may indicate that the garnets and clinopyroxenes in these rocks are in chemical equilibrium, which was not disturbed by later processes.

Based on the limited data available we can assume that REE coming into the garnet crystal structure was carried out mainly through heterovalent isomorphous substitution of Ca^{2+} ions by trivalent REE ions. The ions of elements such as Fe, Mg and Al, apparently, could perform the function of a compensating charge. The preferable accumulation of HREE in the crystal structure of garnet, apparently, was due to the fact that the trivalent ions of the REE have somewhat smaller radii compared with trivalent ions of LREE.

Chrome-spinels. There is currently very limited data on the REE contents in this mineral. Study of the distribution of isomorphous REE impurity in chrome-spinels is complicated by their very low concentrations and by a frequent presence of non-structural impurity concentrated in the microcracks and other defects of crystals. Relatively high amounts of REE with a slight predominance of chondrite-normalized LREE contents have been identified in chrome-spinels from the ore deposits of Voykar-Syn'insky massif (Urals, Russia). In addition, the chondrite-normalized REE patterns in high-Cr varieties of chrome-spinels of this massif showed Eu anomalies of low intensity. Accessory chrome-spinels from lherzolites forming xenoliths in alkaline basalts of Dreiser Weiher province (Germany) are represented by two types – greatly depleted by REE and moderately enriched with REE, while both of these types have similar in configuration chondrite-normalized patterns of these elements. In the accessory chrome-spinels from lherzolites and harzburgites forming Ergak massif (Tuva, Russia) the chondrite-normalized LREE content is usually much higher than the HREE one. In peridotites and websterites of Ronda massif (Spain) the values of K_d (chrome-spinels/clinopyroxene) are progressively decreasing in a row from La to HREE.

It is quite possible that much of the observed irregularity of REE distribution in chrome-spinels, as well as inherent to many of them more or less significant enrichment of LREE, could be due to the presence of variable amounts of non-structural impurity, which was introduced by epigenetic fluids and resides in the defects of their crystals. Obviously, for a more accurate determination of the content of isomorphous REE impurity by using LA ICP-MS method, it is reasonable to expose the grains of chrome-spinels, as well as of the other accessory minerals, to a preliminary acid leaching.

Ilmenites. The REE composition of ilmenites presented as an accessory phase in many magmatic and metamorphic rocks, as well as composing the deposits and placer deposits, has been studied mainly by the example of their samples of kimberlites and some gabbro, to a less extent – of pyroxenites and other rocks. The level of REE accumulation in the majority of analyzed ilmenites is usually inferior to their level of C1chondrite. Many of ilmenites have the chondrite-normalized HREE contents that are slightly higher than the content of LREE. The patterns of some ilmenites from gabbros showed positive Eu anomalies while the patterns of the samples from rhyolites – negative Eu anomalies. The REE distribution coefficients between ilmenites and parent melts, which were calculated according to the results of physical experiments, typically

have very low values and slightly increase in the row from LREE to HREE. Further research will enhance understanding of the regularities of REE distribution in ilmenites from the rocks of different composition and origin.

Zircon is one of the best concentrators of isomorphous REE impurity in the content of rocks of different composition and genesis, including ultramafites and gabbros. In addition to the REE they contain in their structure many other impurities including Hf, Y, Ta, U, Th, Pb, Fe, Ti and Ca, the total content of which can reach the first wt%. Chondrite-normalized HREE content in this mineral is almost always much higher than the content of MREE and particularly LREE. Published data on the geochemistry of REE in zircons characterize their samples from many petrographic rock types and the largest number of tests was performed on zircons from granites, tonalites, granodiorites, while the least data is available for the samples from kimberlites, gabbros, minettes, basanites, syenites, eclogites, charnockites, amphibolites, ultramafic rocks and other rock types. The overall level of REE accumulation in zircons increases in a row of samples from ultramafites to gabbros followed by alkaline, granitoids and other rocks. On REE patterns of almost all zircons there are Ce anomalies of varying intensity and negative Eu anomalies. For those zircons that have undergone various transformations including melting under the influence of melts the configuration of REE patterns in one way or another changes, in particular, due to the leveling of Ce and Eu anomalies. Based on the crystal-chemical assumptions, we can assume that the observed Ce and Eu anomalies in the patterns of zircon are the result of crystallization of minerals under conditions of relatively high oxygen fugacity. Based on materials of experimental studies it was established that for all REE and for all of their maternal melts the K_d (zircon/melt) values are greater than 1, and thus increase from the first units (for LREE) to many hundreds and first thousands (for HREE). There is a reason to believe that REE accumulation in zircons structure was carried out through heterovalent isomorphous substitution of tetravalent Zr ions by trivalent REE ions. Such a substitution could be carried out with the participation of Ti, Fe, Li and Mo ions, which performed the function of compensating charge. In connection with the strengthening of the isotope-geochronological studies of various magmatic including gabbro and ultramafic rocks by using the U-Pb method on zircons, obviously, more attention will be given to detailed geochemical studies of this mineral, with special emphasis on its REE composition.

Apatite as an accessory mineral is presented in so many varieties of rocks of magmatic and metasomatic origin, including gabbros and some high-Mg rocks. They are able to concentrate in its structure very significant amounts of REE, which are usually heavily fractionated with a tendency to a significant enrichment with LREE. Depending on the composition of maternal rocks and conditions of their formation the total REE content in apatites ranges from 10–100 to 10000–35000 ppm. Higher REE contents of apatite are characteristic of granite and various high-alkaline rocks, the lower contents were defined in the mineral from granitic pegmatites, gabbros, pyroxenites. In most cases, the chondrite-normalized REE patterns of apatites are close to a straight line with a steep negative slope. The values of $(La/Yb)_n$ parameter for them vary between 4 and 370. The patterns of apatites are often complicated by negative Eu anomalies. The $(Eu/Eu^*)_n$ parameter for apatites typically ranges from 0.17–0.38. The nature of Eu anomalies in apatites is supposed to be due to crystallization at high oxygen fugacity, when in an environment is dominated by Eu^{3+} ions

that are much less compatible with the structure of apatite compared to Eu²⁺ ions. In contrast to the apatite from many other rocks, in the spectra of REE patterns of the samples from some of lherzolites, kimberlites, basanites and hawaiites the negative Eu anomalies were not identified. This characteristic of patterns of apatite suggests that they crystallized in a neutral or reducing environment, when a substantial part of Eu ions was in the form of Eu²⁺ ions, which are better compatible with the crystal structure of apatite. However, the values of K_d (apatite/melt) for all REE, which were calculated based on the results of physical experiments, were usually greater than 1. This indicates that during crystallization of apatite the REE elements had the properties of the elements that are compatible with the structure of this mineral.

Titanites are among the accessory minerals that make up so many magmatic rocks, as well as some rocks of different origin. The structure of this mineral is able to concentrate a very large amount of REE. Their total content ranged from tenths fractions wt% to the first wt%. For some titanite crystals along with the zonal distribution of elements such as Ca, Ti, Al and Fe a zonal REE distribution was observed, what is more, these crystals got inversely proportional relationship between the contents of REE and Ca. The chondrite-normalized REE patterns of titanite often have a form of subhorizontal and slightly convex upward lines, indicating relatively high concentrations of MREE. Titanite got a high chemical resistance, which is why there is sometimes an incomplete decomposition during the preparation of rock samples for analysis and, therefore, under determination of REE in these samples.

Perovskites. This accessory mineral is commonly represented in kimberlites, lamproites, melilite and leucite basalts, sometimes it can be found in the rocks of titanomagnetite and chromite deposits, in chlorite schist and meteorites. Perovskites usually accumulate significant amounts of REE with substantial predominance of light elements. For example, in kimberlites from South Africa and India the total REE content ranges from 9500 to 49800 ppm. At higher modal amounts of perovskite in the rocks the vast majority of REE in their overall balance is concentrated in this mineral. The values of K_d (perovskite/silicate melt) for LREE and MREE >1. During the isomorphous incoming into the perovskite structure these REE had properties of compatible elements.

Micas. As a minor mineral, mica is presented in many magmatic and metamorphic rocks. Total REE content in them usually ranges from the first ppm to 100 ppm, more rarely it is slightly more. In the studied phlogopites from kimberlites, peridotites, pyroxenites and gabbros the total REE content is generally lower than in biotites that reside in granitoids and metamorphic rocks. Chondrite-normalized LREE contents in micas in many cases are slightly higher than the contents of MREE and HREE. The chondrite-normalized REE patterns of some of the studied micas have a common negative slope and winding configuration, which is probably due to inexact determination of some elements. The patterns of biotites from granites showed positive Eu anomalies, while the patterns of biotites from rhyolites are complicated by an intense negative Eu anomaly.

These are the most significant features of REE distribution in the accessory and minor minerals of ultramafic, mafic and some other types of rocks. It should be noted that to date the REE composition of accessory minerals from rocks of mafic-ultramafic complexes has been studied unevenly and is generally much less detailed than the composition of rock-forming minerals.

This page intentionally left blank

Geochemical relationship between REE and PGE in mafic and ultramafic rocks and their petrogenetic significance

It is known that REE began to be used as geochemical indicators for the diagnosis and classification of magmatic, metamorphic and metasomatic rocks and their minerals, as well as for reconstructions of the processes of their formation as developed the analytical methods for determining its quite low concentrations in the analyzed samples. At present, the analysis of REE in geological objects became a rather routine procedure even while studying the ultramafic and mafic rocks and minerals depleted by them. Due to this reason, the rare contemporary publications on the problems of Geochemistry, Mineralogy, Petrology of magmatic rocks and geodynamics do not use the results of REE analysis by one of the existing analytical methods. The same trend is approximately observed with respect to platinum group elements (PGE), the determination of relatively low concentrations of which became possible with the introduction of several new analytical techniques including ICP-MS method.

Zharikov & Yaroshevsky [2003] while examining the challenges and prospects for further development of the geochemical sciences, among other things, pointed at two important problems of petrology that can be solved by using geochemical methods: 1) a comprehensive study of the behavior of different groups of compatible and incompatible impurities in magmatic processes, and 2) identification of correlations between groups of impurities that are different in their geochemical properties in order to develop consistent models of dispersion and concentration during the generation, differentiation, contamination and crystallization of magmatic melts of different composition.

Barnes *et al.* [1985] while discussing some aspects of geochemistry of PGE in a variety of products of magmatic processes, came to the conclusion that the determination processes, during which the fractionation of PGE in nature occurred, were such as partial melting of mantle sources, crystallization differentiation of melts, as well as some epigenetic processes.

In recent years, some studies were executed aiming to identify relationships between REE and PGE in rocks of ultramafic and mafic composition [Lazarenkov *et al.*, 1989; Naldrett *et al.*, 1994; Roman'ko *et al.*, 1994; Shengrong *et al.*, 1994; Lesnov *et al.*, 2000, 2001, 2004b, 2005c; Pearson & Woodland, 2000; Lesnov & Oydup, 2002; Lesnov, 2003a, b; Schmidt *et al.*, 2003; Lesnov & Balykin, 2005; Zhou *et al.*, 2005; Karipi *et al.*, 2006; Day *et al.*, 2008; Lesnov, 2006, 2009; and others]. Despite the limited number of analyses performed, the results of these studies have shown that comprehensive data on the contents of REE and PGE provide an

opportunity to get some additional information that can be used in carrying out geochemical discrimination and systematization of ultramafic and mafic rocks, as well as massifs and complexes composed of them.

In this chapter, the problems of relations between REE and PGE are discussed on the basis of the results that were obtained recently on the example of some of the mafic-ultramafic massifs and complexes of various geneses that are located in Russia, Mongolia, China, Germany, Greece, Vietnam, South Africa, Canada, Australia, Colombia, and others.

10.1 MAFIC-ULTRAMAFIC MASSIFS IN TUVA (RUSSIA)

For a long time we have been studying the problems of petrology of mafic-ultramafic massifs located in the territory of Tuva, including those associated with distribution of REE and PGE impurities in their rocks. At the initial stage the determination of REE was performed by using the INAA method and the determination of PGE – by atomic absorption method [Lesnov & Tsimbalist, 1983; Lesnov *et al.*, 2000, 2001; Lesnov & Oydup, 2002; Lesnov, 2003a, c; Lesnov *et al.*, 2004c; Lesnov, 2009]. As a result, in the studied rocks we identified a trend of inverse relation between the contents of REE and PGE. Rock samples for studies were selected from the massifs located in the central (Mazhalyksky, Kalbagdagsky, Karashatsky, Maysky), eastern (Bulkinsky) and western (Khobseksky, Birdagsky, Khayalygsky) areas of the territory. These massifs are characterized by different structural-tectonic position, size, internal structure, petrographic composition and quantitative relations between ultramafic and mafic rocks composing them. In these massifs there were more or less clearly marked evidences of an earlier formation of ultramafic rocks in relation to gabbros, which allowed us to consider these massifs as polychronic and polygenic plutonic associations [Lesnov, 1986]. The model of the formation of polygenic mafic-ultramafic massifs considered in the work stated is based on numerous field and petrographic observations made on such objects. According to this model, the tectonic intrusion of ultramafic restite protrusions of various sizes, morphologies, and structural positions preceded the intrusion of gabbro intrusions that are spatially brought together with them, which occurred through the same faults. The ultramafic restites that compose these massifs are usually represented by harzburgites, lherzolites and dunites, as well as serpentinized derivatives thereof. Gabbro intrusions that are spatially brought together with the intrusions, are predominantly composed of gabbro and gabbro-norites, rarely containing olivine. Along the contacts of gabbro intrusions with protrusions of ultramafites intruded by them there are often localized contact-reaction zones of different thickness, structures and petrographic composition. The zones are composed of a various hybrid ultramafic and gabbro rocks, including plagioclase-bearing harzburgites, plagioclase-bearing lherzolites, plagioclase-bearing dunites, wehrellites, plagioclase-bearing wehrellites, clinopyroxenites and websterites, their plagioclase-bearing varieties, as well as widely ranging in quantitative-mineral composition olivine gabbro and gabbro-norites, which in many cases have a banded texture. Let us concentrate upon a brief review of geological and petrographic features of these massifs, as well as on available data on the distribution of REE and PGE in the rocks composing them, which is based not only on my own observations but

involving some of the data from previously published works [Volokhov *et al.*, 1972; Poliakov & Bognibov, 1979; Poliakov *et al.*, 1984; Mongush *et al.*, 1999; Mongush, 2000, 2002, and others].

Kalbagdagsky massif with dimensions of 1.5×6 km is exposed over an area of 9 sq · km. Its marginal zones are almost everywhere concealed beneath unconsolidated deposits, with the exception of the south-eastern flank, where the intrusive contact of the massif with the Lower Cambrian volcanic strata is uncovered. The massif is predominantly composed of olivine gabbro, to a lesser extent – of gabbro-norites and gabbro, but all of these rocks have good preservation properties. Among the gabbro there are occurring stripe-like bodies of different length, which are composed of plagioclase-bearing wehrlites, plagioclase-bearing clinopyroxenites and olivine clinopyroxenites sometimes containing orthopyroxene impurity. The massif is injected with anorthosite veins containing an impurity of clinopyroxene and olivine.

Mazhalyksky massif is exposed over an area of 1 sq · km. and the dominant part is covered by unconsolidated deposits. It occurs among the Lower Cambrian terrigenous-volcanic formations, together with which it is injected with granite dikes. Uncovered part of the massif is composed of serpentinized harzburgites, dunites, and plagioclase-bearing wehrlites with an impurity of orthopyroxene, olivine clinopyroxenites, clinopyroxenites, troctolites, subordinate amounts of olivine gabbro, gabbro, gabbro-norites, among which there are gabbro-anorthosites veins. Plagioclase-bearing wehrlites and pyroxenites contain unevenly distributed and ranging in size and shape porphyroblastic- and pocket-isolations of plagioclase. According to Borodina *et al.* [2004], the type of the massif is stratiform intrusion, which is formed as a result of intrachamber differentiation of mafic melts. However, according to unconfirmed reports, among gabbros there are occurring certain xenoliths of ultramafites, which suggests their earlier formation in relation to gabbro intrusion. Therefore, we believe that this massif is a polygenic body consisting of an ancient protrusive block of ultramafic restites, a later intrusion of gabbros and various transformation products of ultramafic restites under the influence of mafic melts. According to the analysis of amphiboles from gabbro-norites using Ar-Ar isotopic method the age of Mazhalyksky massif amounted to 484.2 ± 2.3 Ma [Borodina *et al.*, 2004]. According to the study of zircon from the gabbro-anorthosite dikes cross-cutting rocks of the massif using U-Pb isotopic method, the age of gabbro-anorthosites amounted to 478 ± 1.4 Ma [Sal'nikova *et al.*, 2004].

Karaossky massif, which is a part of Kaa-Khem ophiolite belt, is a small xenogeny block that lies among the rocks of granitoid pluton that is intruding metamorphic formations of the age ranging from the Late Proterozoic to Early Cambrian [Mongush, 2002; Rudnev *et al.*, 2006]. This massif is composed of gabbro-norites and subordinate olivine gabbro-norites, among which there are occurring isolations of websterites and wehrlites.

Maysky massif located on the right bank of Kaa-Khem river is exposing an area of about 40 sq · km. and is divided by faults into several blocks that occur among metaporphyrites and carbonate deposits [Mongush, 2002]. It is composed of leucocratic gabbro-norites, amphibole gabbros, gabbro-norites, olivine gabbros, websterites and anorthosites. Influenced by the close located Early Middle Paleozoic granitoid pluton, the rocks of the massif underwent an intensive amphibolization, potash-feldspatization, silicification, epidotization and chloritization.

Rocks from the other studied massifs located in the territory of Tuva (Bulkinsky, Irbiteysky, Karashatsky, Khobseksky, Birdagsky and Khayalygsky) are presented by plagioclase-bearing lherzolites, wehrlites, plagioclase-bearing wehrlites, plagioclase-bearing websterites, olivine clinopyroxenites, leucocratic troctolites, olivine gabbros, gabbros, gabbro-norites, gabbro-anorthosites, hornblende-bearing gabbros and hornblendites. REE content determination in them was carried out by using instrumental neutron activation method and ICP-MS method. Almost all the rocks of the studied massifs are significantly depleted by REE, except for some samples that are anomalously enriched with LREE. By the general level of REE accumulation the entire collection of analyzed rock samples can be divided into two groups: 1) depleted, and 2) moderately depleted. The first group consists of rocks from Mazhalytsky, Kalbagdagsky, Karashatsky, Khobseksky and Irbiteysky massifs, the total REE contents of which range from 1.4 to 14 ppm (Table 10.1). The second group includes rocks that compose Karaossky and Maysky massifs, their total REE contents are slightly higher – 16 to 28 ppm. For most samples of both groups the chondrite-normalized LREE contents are slightly higher than HREE contents and, respectively, their REE patterns have a flat negative slope. Among the rocks of the first group the minimum REE contents are defined in the rocks of Kalbagdagsky massif. It is assumed that those melts, from which the gabbros of Kalbagdagsky and Mazhalytsky massifs crystallized, were more depleted with respect to REE compared to the melts from which the rocks of Karaossky and Maysky massifs crystallized.

Estimations of Pd, Pt and Rh in the rocks of these massifs were originally performed using atomic absorption method (Table 10.2). For the entire studied collection the total PGE contents range from 29 to 112 ppb. Moreover, the contents of Rh are significantly lower than the contents of Pd and Pt and, in some cases, the content of this element was below the limit of detection by atomic absorption method. In the rocks of Kalbagdagsky, Karashatsky and Khobseksky massifs the contents of Pd, Pt and Rh are generally slightly higher than in rocks from the rest of the massifs studied. In the rocks of Mazhalytsky, Kalbagdagsky and Karashatsky massifs Pd/Pt parameter varies in the range from 1 to 5.6, and in the rocks of Maysky massif this value does not exceed 1.

The observed limited data on the contents of REE and PGE in the rocks of mafic-ultramafic massifs of Tuva allow us to consider as a rough approximation the question of relations between elements of these groups. As can be seen on the presented graphs, the contents of Pd, Pt and Rh in these rocks are generally increasing as the content of La and Ce is diminishing. This fact gives grounds to suggest that in these rocks there is an inverse relation between the contents of REE and PGE (Figure 10.1).

To further examine the relationship between REE and PGE in rocks of Tuva massifs, a part of the samples was studied by ICP-MS method. Development of analytical geochemistry of PGE long time hampered by a number of objective reasons including: 1) lowering the detection limits of these elements that can be achieved using the available methodology, and 2) increasing the requirements on the level of contamination associated with the use of insufficiently pure reagents, water and glassware, and 3) incomplete decomposition of microparticles of platinum minerals in sample preparation, and 4) loss of Os at the volatile phase in sample preparation, and some other reasons.

Table 10.1 REE compositions (ppm) of rocks from some mafic-ultramafic massifs from Central and West Tuva (Russia).

Sample's number	Rocks	La	Ce	Nd	Sm	Eu	Gd	Tb	Tm	Yb	Lu	Total REE	(La/Yb) _n
Mazhalysky massif													
L-106	Wehrlite	0,12	0,40	0,40	0,10	0,04	0,15	0,02	0,02	0,10	0,02	1,37	0,81
L-101a	N.d.	0,45	1,20	1,00	0,29	0,14	0,44	0,06	0,04	0,20	0,04	3,86	1,52
Mazh-35-5	N.d.	1,00	3,30	3,10	1,10	0,32	0,80	0,16	0,08	0,51	0,07	10,44	1,32
L-104A	Wehrlite Pl-bearing	0,89	3,60	3,00	1,27	0,44	1,39	0,21	0,12	0,64	0,10	11,66	0,94
Mazh-30-4	N.d.	1,30	4,20	4,10	1,31	0,48	1,60	0,20	0,12	0,68	0,10	14,09	1,29
Karaosky massif													
M-35-95	Clinopyroxenite	2,30	7,30	7,70	2,97	0,88	3,00	0,49	0,21	1,37	0,21	26,43	1,13
M-26-98	Websterite Pl-bearing	2,90	7,94	7,40	2,60	0,62	2,60	0,37	0,20	1,16	0,18	25,97	1,69
M-36-98	Gabbro-norite	1,60	5,00	4,50	1,34	0,47	1,60	0,21	0,12	0,78	0,12	15,74	1,38
M-25-97	Amphibole gabbro	3,40	7,30	6,00	2,11	1,02	2,10	0,33	0,18	1,10	0,18	23,72	2,09
Kalbagdagsky massif													
Kal-3-3	Wehrlite	0,77	2,00	1,20	0,35	0,16	1,29	0,11	0,06	0,36	0,06	6,36	1,44
Kal-6-3	N.d.	0,64	1,30	0,80	0,32	0,15	0,50	0,06	0,04	0,29	0,05	4,15	1,49
Kal-8-1	N.d.	0,97	2,20	1,90	0,49	0,22	0,61	0,13	0,08	0,56	0,09	7,25	1,17
Kal-9-2	N.d.	1,54	4,10	2,80	1,00	0,39	1,66	0,24	0,16	1,00	0,16	13,05	1,04
Kal-5-2	Wehrlite Pl-bearing	0,90	2,50	2,00	0,68	0,25	0,80	0,14	0,10	0,69	0,11	8,17	0,88
Kal-3-2	Olivine clinopyroxenite	0,70	1,90	2,10	0,82	0,31	1,10	0,17	0,11	0,70	0,10	8,01	0,67
Kal-10-3	Olivine gabbro	0,50	1,10	0,70	0,38	0,18	0,50	0,08	0,06	0,40	0,07	3,97	0,84
Kal-12-4	Gabbro-norite	0,70	1,20	0,90	0,34	0,19	0,40	0,06	0,04	0,32	0,06	4,21	1,48

(Continued)

Table 10.1 (Continued).

Sample's number	Rocks	La	Ce	Nd	Sm	Eu	Gd	Tb	Tm	Yb	Lu	Total REE	$(La/Yb)_n$
Karashatsky massif													
L-50	Websterite Amph-bearing	0,46	1,40	1,10	0,47	0,22	0,89	0,15	0,10	0,72	0,12	5,63	0,43
L-37	Websterite Pl-bearing	0,30	0,70	0,40	0,10	0,06	0,15	0,03	0,02	0,09	0,02	1,87	2,25
L-48	Clinopyroxenite Amph-bearing	0,56	1,40	1,00	0,30	0,10	0,44	0,08	0,05	0,35	0,06	4,34	1,08
L-36	Olivine gabbro	0,15	0,50	0,40	0,13	0,08	0,22	0,04	0,03	0,20	0,03	1,79	0,50
L-44	Gabbro-norite	0,30	0,90	0,60	0,25	0,24	0,43	0,08	0,08	0,51	0,10	3,50	0,39
L-45	N.d.	0,20	0,60	0,70	0,30	0,14	0,67	0,10	0,09	0,61	0,10	3,50	0,22
Khobseksky massif													
L-69	Clinopyroxenite	0,14	0,40	0,40	0,14	0,05	0,33	0,04	0,03	0,18	0,03	1,74	0,52
L-70	N.d.	0,96	2,80	2,00	0,79	0,29	0,95	0,14	0,08	0,43	0,05	8,49	1,52
L-78	N.d.	0,24	0,60	0,60	0,15	0,11	0,29	0,04	0,04	0,27	0,05	2,39	0,61
L-84	N.d.	0,24	0,40	0,20	0,09	0,04	0,33	0,02	0,02	0,09	0,02	1,45	1,74
Irbiteysky massif													
L-66	Olivine gabbro	0,98	2,50	1,90	0,67	0,32	0,91	0,16	0,09	0,58	0,09	8,20	1,14
L-68	N.d.	0,74	1,90	1,80	0,64	0,32	1,30	0,15	0,10	0,54	0,09	7,58	0,92
Maysky massif													
2530	Olivine gabbro	3,80	9,00	5,20	1,48	0,70	1,60	0,26	0,12	0,74	0,11	23,01	3,47
2150	Gabbro-norite	5,00	10,60	6,60	1,85	0,84	1,60	0,29	0,18	1,14	0,17	28,27	2,96

Note: The analyses were done in the Analytical Center of IGM SB RAS, INAA method (analyst M.S. Mel'gunov).

Table 10.2 Pt, Pd, and Rh compositions (ppb) of rocks from some mafic-ultramafic massifs from Central and West Tuva (Russia).

Sample's number	Pt	Pd	Rh	(Pt + Pd + Rh)	Pd/Pt
Mazhaliksky massif					
L-106	29	35	4	68	1,21
L-106a	25	36	4	65	1,44
L-101a	15	38	5	48	1,87
Mazh-35-5	19	21	5	43	1,11
L-104A	9	30	4	43	3,33
Mazh -30-4	23	29	5	55	1,26
Karaossky massif					
M-35-97	15	19	5	39	1,27
M-26-98	16	18	5	39	1,13
M-36-98	12	12	5	29	1,00
M-25-97	20	29	5	53	1,45
Kalbagdagsky massif					
Kal-3-3	42	40	4	86	0,95
Kal-6-3	35	40	4	79	1,14
Kal-8-1	41	52	5	98	1,27
Kal-9-2	30	44	4	78	1,47
Kal-5-2	28	54	7	89	1,93
Kal-3-2	29	61	8	98	2,10
Kal-10-3	25	80	7	112	3,20
Kal-12-4	17	23	5	44	1,35
L-31	9	28	4	41	3,11
Karashatsky massif					
L-50	48	59	6	113	1,23
L-50a	39	80	6	125	2,05
L-37	8	8	3	19	1,00
L-48	78	97	7	182	1,24
L-36	10	56	6	72	5,60
L-44	20	36	4	60	1,80
L-45	28	43	5	76	1,54
Khobseksky massif					
L-69	13	31	4	48	2,38
L-70	17	48	5	70	2,82
L-78	23	32	4	59	1,39
L-84	40	90	6	136	2,25
L-84a	36	70	6	112	2,16
Irbiteysky massif					
L-66	15	66	4	85	4,40
L-68	15	44	4	63	2,93
Maysky massif					
2530	58	17	7	82	0,29
2150	36	10	5	51	0,28
Lower detection limits	10	5	5	—	—

Note: Sample's number and rock's name correspond to Table 10.1. The analyses were done in the Analytical Center of IGM SB RAS, atom-absorption method (analyst V. Tsimbalist).

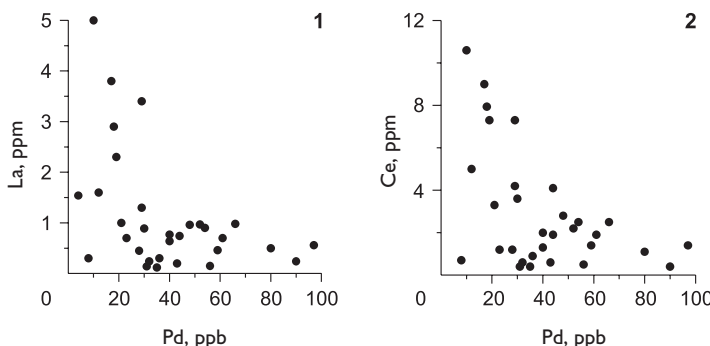


Figure 10.1 Relationships between La and Pd compositions (1), Ce and Pd compositions (2) for rocks from some mafic-ultramafic massifs of Central Tuva (Russia) (data Tables 10.1 and 10.2).

In order to overcome these difficulties that arise in PGE analysis the chemists Nikolaeva, Palesskii and Koz'menko (IGM SB RAS Analytical Center, Novosibirsk, Russia) developed an improved method of sample preparation, which made it possible to make a comprehensive analysis of REE and PGE by 'Element' mass-spectrometer (Finnigan MAT, Germany) [Lesnov *et al.*, 2005b; Palesskii, 2008]. At the same time we took into account the experience of studies on the subject gained in a number of analytical laboratories [Pearson & Woodland, 2000; Meisel & Moser, 2004; Zhou *et al.*, 2005]. The result was a method of sample preparation that allows achieving a more complete decomposition of the samples with a weighed sample ~0.2–0.4 g. The Pd, Pt, Ru, Os, Ir and Re isotope-shifted spikes were added into the weighed sample. The necessary characteristics of spikes were defined beforehand, such as isotopic composition and concentration of the corresponding element. Decomposition of samples was carried out in sealed Teflon autoclaves of MARS-5 system by using a mixture of nitric, hydrofluoric and hydrochloric acids pre-cleaned by subboiling. After achieving the complete decomposition and isotopic homogenization, the samples were transferred to a solution, which was divided into two aliquots. The first aliquot was used to measure REE contents by direct measurement using mass-spectrometer and adding in as an internal standard. The second aliquot was subjected to the enrichment and separation of PGE from the matrix by means of chromatographic columns with Dowex cation resin. Then, the PGE concentrations were measured by isotope dilution with mass-spectrometric ending.

Testing of the developed method based on the results of control experiments showed that when using the proposed complex of procedures for sample preparation the contamination introduced into the sample is insignificant compared to the content of PGE in the analyzed sample. The exception was Pt, the measurement accuracy of which was reduced due to the fact that the mass-spectrometer was simultaneously used in analyzing solutions prepared using platinum glassware. Figure 10.2 show a scheme of procedures of sample preparation and analysis of REE and PGE by ICP-MS method. Note that when testing this method the control

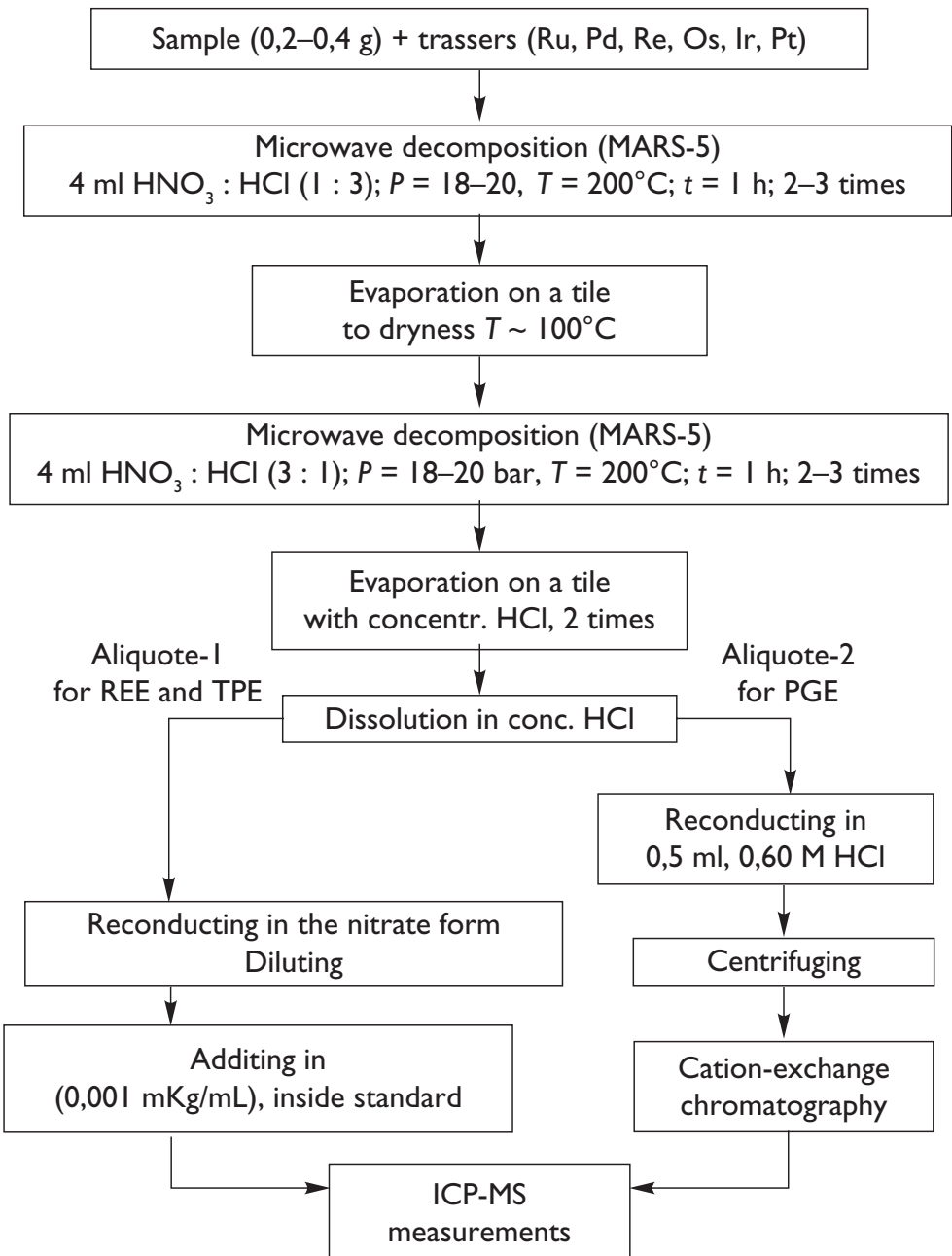


Figure 10.2 The scheme of method of chemical preparation of rock samples for REE, and platinum element group (PGE) analyses (ICP-MS) (data [Palesskii, 2008]. DME – difficult-melting elements (Zr, Nb, Ta, Hf).

test of PGE was carried out maintaining GP-13 international standard (spinel lherzolite). Comparison of results of PGE determination by this standard with its passport data [Pearson & Woodland, 2000; Meisel & Moser, 2004] showed good convergence.

In addition to the rocks of the massifs described above, determination of REE and PGE by ICP-MS method was performed on samples from Bulkinsky massif, which is located in the extreme north-eastern part of Tuva (Ergak-Targak-Tayga ridge, West Sayan) and is structurally confined to junction of Kurtushibinsky and North-Sayan ophiolite belts [Mongush *et al.*, 2005]. Its elliptical body is exposing an area of about 100 sq · km. with the long axis oriented to the submeridional direction. The massif lies among terrigenous Upper Cambrian and Ordovician deposits and is composed of gabbro-anorthosites, anorthosites, gabbros, gabbro-norites and troctolites, among which stripe-like isolations of olivinites, olivine pyroxenites and hornblendites occur. Quantitative-mineral composition of rocks from this and from other massifs, in which REE contents were determined by ICP-MS method, is shown in the Table 10.3.

Table 10.3 Modal mineral compositions of ultramafic and mafic rocks from some massifs from Central and East Tuva (Russia).

Samples	Rocks	Mineral composition, %
	Mazhaliksky massif	
30-1	Gabbro leucocratic with Hornb	Cpx (17), Pl (80), Horb (3)
30-6	Olivine gabbro	Ol (11), Cpx (45), Pl (50), Mt (4)
35-4	Wehrlite Pl-bearing with Hornb	Ol (50), Cpx (40), Pl (4), Horb (6)
	Karaossky massif	
M-27-98	Websterite Pl-bearing	Opx (36), Cpx (60), Pl (4)
M-29-98	Gabbro-norite	Opx (10), Cpx (40), Pl (50)
M-30-98	Wehrlite with Opx	Ol (85), Opx (3), Cpx (12)
	Kalbagdagsky massif	
9-3	Gabbro olivine-bearing with Hornb	Ol (20), Cpx (45), Pl (34), Horb (1)
1-2	Gabbro-norite	Cpx (35), Opx (15), Pl (50)
2-5	Clinopyroxenite olivine-bearing with Hornb	Ol (8), Cpx (80), Pl (4), Horb (8)
	Maysky massif	
2150	Gabbro-norite	Cpx (30), Opx (15), Pl (55)
2530	Gabbro olivine-bearing, leucocratic with Hornb	Ol (20), Cpx (8), Pl (70), Horb (2)
2530-I	Gabbro olivine-bearing, mesocratic with Opx	Ol (40), Opx (4), Cpx (10), Pl (45), Mt (1)
	Bulkinsky massif	
Bl-4	Gabbro olivine-bearing, leucocratic with Hornb	Ol (10), Cpx (15), Pl (70), Horb (4), Mt (1)
Bl-7	Troctolite leucocratic with Cpx, Opx, and Hornb	Ol (20), Opx (3), Cpx (1), Pl (70), Horb (5), Mt (1)
Bl-17	Gabbro-anorthosite with Ol, Cpx, Opx, and Hornb	Ol (2), Opx (2), Cpx (2), Pl (80), Horb (10), Mt (1)

Note: Ol – olivine, Opx – orthopyroxene, Cpx – clinopyroxene, Pl – plagioclase, Hornb – hornblende, Mt – magnetite.

Judging by the results of the analysis, in the rocks of the studied massifs the total REE contents ranged from 3.5 to 75 ppm (Table 10.4). And the maximum total REE contents were determined in samples from Maysky massif, the lower ones – in the rocks from Mazhalyksky, Kalbagdagsky, Karaossky and Bulkinsky massifs. The rocks of Maysky and Bulkinsky massifs are characterized by high LREE content and the resulting relatively high values of $(La/Yb)_n$ parameter (Figure 10.3). The REE distribution patterns of clinopyroxene and olivine gabbro-norite of Kalbagdagsky massif have similar configuration, which indicates their depletion by LREE and some enrichment with MREE. The REE distribution pattern of olivine gabbro of the massif also indicates its enrichment with LREE. A distinctive feature of the rocks from Kalbagdagsky massif is the lack of positive Eu anomalies in their patterns,

Table 10.4 REE (ppm), and PGE (ppb) compositions of ultramafic and mafic rocks from some massifs from Central and East Tuva (Russia), ICP-MS.

Massifs							
	Kalbagdagsky			Mazhalyksky			Karaossky
	I-2	9-3	2-5	30-1	30-6	35-4	M-29-98
Element	Gabbro-norite	Olivine gabbro	Clinopyroxenite olivine-bearing	Gabbro	Olivine gabbro	Wehrlite	Gabbro-norite
Pd	7,60	8,77	5,69	3,28	3,74	8,51	N.d.
Pt	25,4	25,7	9,27	18,4	7,52	2,65	8,39
Ru	4,23	2,09	5,03	1,74	0,75	3,76	3,95
Ir	0,097	0,046	0,067	0,29	0,029	N.d.	0,19
Total	37,3	37,0	20,1	23,7	12,0	14,9	12,5
Pt/Ir	262	558	138	63	252	N.d.	44
Pd/Ir	78,4	191	84,9	7,86	129	N.d.	N.d.
La	0,729	1,11	0,742	2,88	1,99	1,84	2,89
Ce	2,05	2,42	2,06	6,15	4,94	4,83	5,71
Pr	N.d.	N.d.	N.d.	N.d.	N.d.	N.d.	N.d.
Nd	2,05	1,81	2,07	3,89	3,98	4,24	3,62
Sm	0,772	0,581	0,737	0,900	1,16	1,19	0,872
Eu	0,312	0,244	0,305	0,463	0,430	0,415	0,448
Gd	1,07	0,724	1,06	0,984	1,21	1,34	0,872
Tb	0,195	0,143	0,196	0,168	0,207	0,236	0,143
Dy	1,32	0,941	1,31	0,979	1,30	1,47	0,863
Ho	0,276	0,198	0,270	0,195	0,254	0,288	0,172
Er	0,748	0,586	0,776	0,542	0,679	0,778	0,462
Tm	0,114	0,088	0,113	0,084	0,099	0,109	0,076
Yb	0,715	0,498	0,747	0,474	0,576	0,686	0,439
Lu	0,100	0,074	0,098	0,068	0,078	0,092	0,067
$(La/Yb)_n$	0,69	1,51	0,67	4,11	2,34	1,81	4,45
$(Eu/Eu^*)_n$	1,05	1,15	1,05	1,50	1,10	1,00	1,55

(Continued)

Table 10.4 (Continued).

Massifs								
	Karaossky		Maysky			Bulkinsky		
	M-27-98	M-30-98	2150	2530	2530-I	Bl-17	Bl-4	Bl-7
Element	Websterite	Wehrlite	Gabbro-norite	Olivine gabbro	Gabbro-anorthosite	Olivine gabbro leucocratic	Troctolite leucocratic	
Pd	0,78	1,11	1,65	N.d.	0,82	24,0	1,54	1,03
Pt	13,0	5,48	4,05	5,55	3,45	10,5	8,03	23,2
Ru	6,56	3,95	2,35	1,99	2,02	0,25	2,15	1,90
Ir	0,29	0,90	0,16	0,22	0,15	0,041	0,11	0,016
Total PGE	20,6	11,4	8,21	7,76	6,44	37,8	11,8	26,1
Pt/Ir	45	6	26	25	23	257	74	1449
Pd/Ir	2,69	1,23	10,3	N.d.	5,47	585	14,0	64,4
La	3,88	0,789	3,39	3,11	14,1	0,694	0,981	0,568
Ce	11,8	1,70	7,71	7,89	28,82	1,348	3,060	1,208
Pr	N.d.	N.d.	N.d.	N.d.	N.d.	N.d.	N.d.	N.d.
Nd	11,3	1,23	5,26	5,47	15,7	0,786	3,44	0,703
Sm	3,23	0,336	1,350	1,380	3,021	0,159	1,195	0,140
Eu	0,910	0,136	0,680	0,618	0,975	0,239	0,668	0,274
Gd	3,71	0,395	1,45	1,47	2,71	0,166	1,56	0,125
Tb	0,647	0,068	0,259	0,250	0,413	0,025	0,286	0,019
Dy	3,79	0,424	1,64	1,52	2,23	0,146	1,78	0,115
Ho	0,739	0,088	0,346	0,295	0,413	0,027	0,344	0,024
Er	2,091	0,234	1,03	0,825	1,11	0,077	0,924	0,058
Tm	0,306	0,034	0,168	0,120	0,162	0,014	0,128	0,010
Yb	1,84	0,244	1,05	0,770	0,968	0,077	0,761	0,067
Lu	0,248	0,039	0,154	0,110	0,142	0,009	0,103	0,010
(La/Yb) _n	1,42	2,19	2,18	2,73	9,85	6,05	0,87	5,69
(Eu/Eu*) _n	0,80	1,14	1,48	1,32	1,02	4,46	1,50	6,23

Note: The analyses were done in the Analytical Center of IGM SB RAS (analysts S. Palesskii, I. Nikolaeva, O. Koz'menko). Detection limits of PGE (ppb): Os – 0,07; Ir – 0,002; Ru – 0,005; Pt – 0,07; Pd – 0,09. N.d. – no data.

which indicates that during the crystallization of their parent melt, no significant fractionation of plagioclase crystals occurred (Figure 10.3, 1–3).

The REE patterns of gabbro, olivine gabbro and wehrlite of Mazhalyksky massif, that have steep negative slopes, are complicated by positive Eu anomalies due to fractionation of plagioclase (Figure 10.3, 4–6). In the rocks of Karaossky massif the lowest REE contents are observed in wehrlite, slightly higher in gabbro-norite, and much higher in websterite. The REE distribution patterns in all these rocks have a common negative slope (Figure 10.3, 7–9). It was already mentioned, that rocks of Maysky massif differ from samples of other massifs by a generally high REE content and especially LREE content. Similar configuration of REE

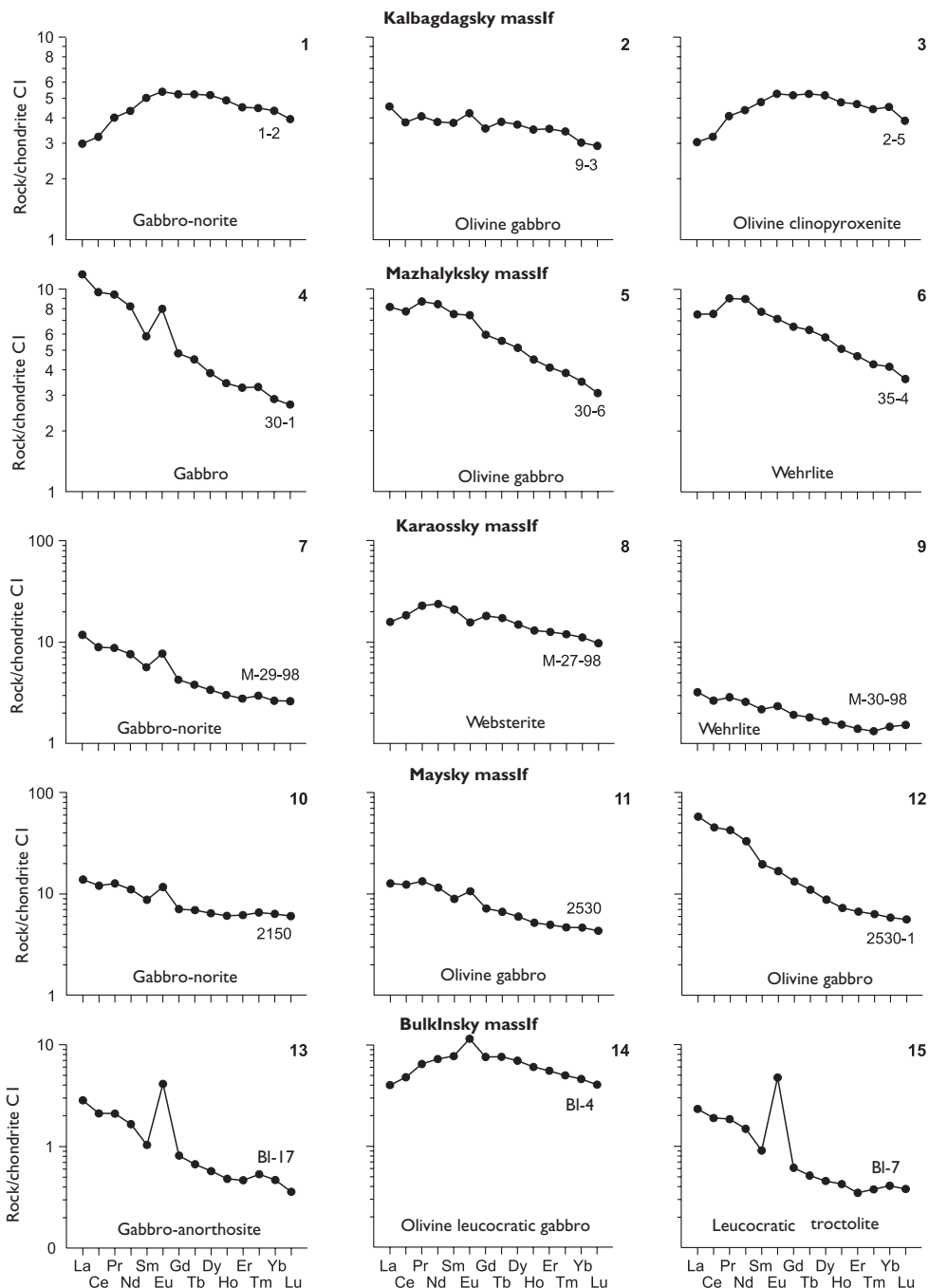


Figure 10.3 Chondrite-normalized REE patterns for rocks from Kalbagdagsky, Mazhalyksky, Karaossky, Maysky, and Bulkinsky mafic-ultramafic massifs (Tuva, Russia) (data Table 10.4).

patterns of gabbro-norite and olivine gabbro from this massif shows weak positive Eu anomalies, while the pattern of olivine gabbro from the massif that has a steep negative slope doesn't show such anomaly (Figure 10.3, 10–12). We can assume that the anomalous enrichment with LREE of the rocks from Maysky massif is due to the presence of non-structural impurity of these elements in them, which was introduced by fluids from the melts that formed the granitoids pluton located nearby.

The rocks of Bulkinsky massif are also enriched with LREE. Their distribution patterns of gabbro-anorthosite and leucocratic troctolite are complicated by positive Eu anomalies of moderate intensity. Olivine leucocratic gabbro that is significantly enriched with all REE, has a pattern complicated by especially intense positive Eu anomaly (Figure 10.3, 13–15).

The determination of Pd, Pt, Ru and Ir in rocks of the massifs located in the territory of Tuva performed by ICP-MS method showed that the total PGE content in them ranges from 6.0 to 38 ppb. Contents of certain elements vary in the following ranges (ppb): Pt (2.65–26.7); Pd (0.82–24.0); Ru (0.25–6.56); Ir (0.02–0.90). In most samples the content of Pt is higher than the content of Pd, with the exception of wehrlites of Mazhalyksky massif and gabbro – anorthosite from Bulkinsky massif. In the rocks of Kalbagdagsky and Mazhalyksky massifs the Pd content is higher than the content of Ru, but in the rocks of Karaossky, Maysky and Bulkinsky massifs, with the exception of Bl-17 sample, the content of Ru is higher than that of Pd content. In addition, the rocks of Karaossky massif are characterized by relatively high Ir content. The mentioned features of PGE geochemistry

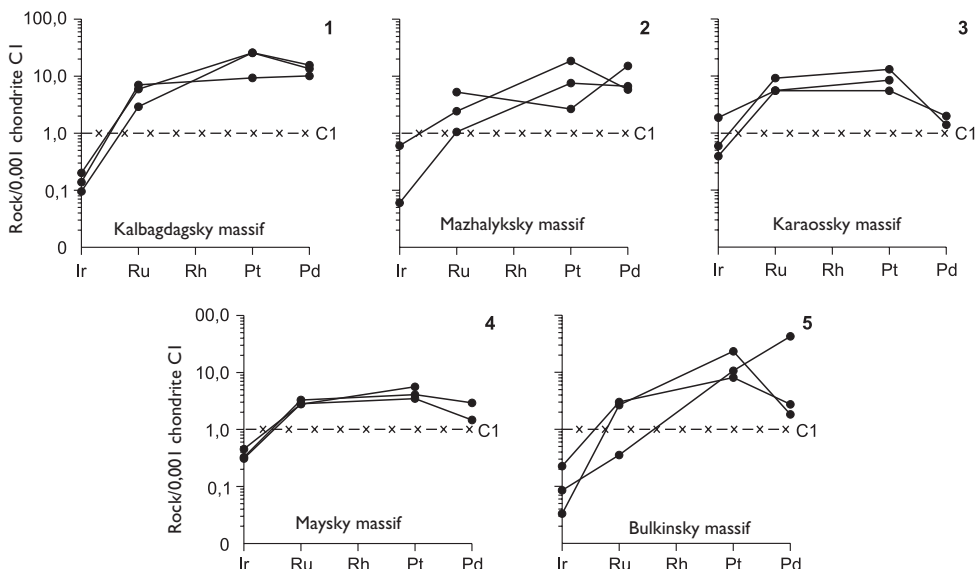


Figure 10.4 Chondrite-normalized PGE patterns for gabbro, gabbro-norite, olivine gabbro, troctolite, wehrlite, websterite and gabbro-anorthosite from Kalbagdagsky, Mazhalyksky, Karaossky, Maysky and Bulkinsky mafic-ultramafic massifs (Central and East Tuva, Russia) (data Table 10.4). Used PGE composition of chondrite C1 (ppb) [Anders & Grevesse, 1989]: Pd – 560; Pt – 990; Rh – 134; Ir – 481.

in rocks of the studied massifs are reflected in their chondrite-normalized patterns (Figure 10.4). Almost all of these patterns are arched upwards, which indicates a slight enrichment of these rocks with platinum and ruthenium relative to palladium and iridium.

The Pt/Ir parameter, as it was already mentioned, can be used as a geochemical indicator of estimating the degree of PGE fractionation during the formation of rocks containing them. In the rocks of mafic-ultramafic massifs of Tuva the values of this parameter vary in a wide range—from 6 to 1450. By using these values the massifs can be divided into two groups. The first group includes those massifs, the rocks of which have higher values of this parameter: Kalbagdagsky (138–558), Bulkinsky (74–1450) and Mazhalyksky (63–252). The second group consists of massifs of rocks that are characterized by low values of this parameter: Maysky (23–26) and Karaossky (6–45).

Data on the distribution of REE and PGE in rocks of the massifs of Tuva obtained by ICP-MS method allow reconsidering the links between these two groups of chemical elements. Using the full sample of analyses of these rocks we have calculated the coefficients of pair correlation between the contents of certain REE and PGE, which are presented in the form of the following graphs (Figure 10.5). They imply that in almost all cases the correlation coefficients between Pd and Pt, on the one hand, and certain REE, on the other hand, have negative values that vary in the range from −0.20 to −0.40. However, all these coefficients are statistically insignificant since being less than the critical value of this sample (0.48) (Figure 10.5, 1). Subhorizontal position of the graphs of changing of correlation coefficients indicates that the negative correlation between LREE and HREE, on the one hand, and Pd, on the other hand, have approximately the same intensity. Slight positive slope

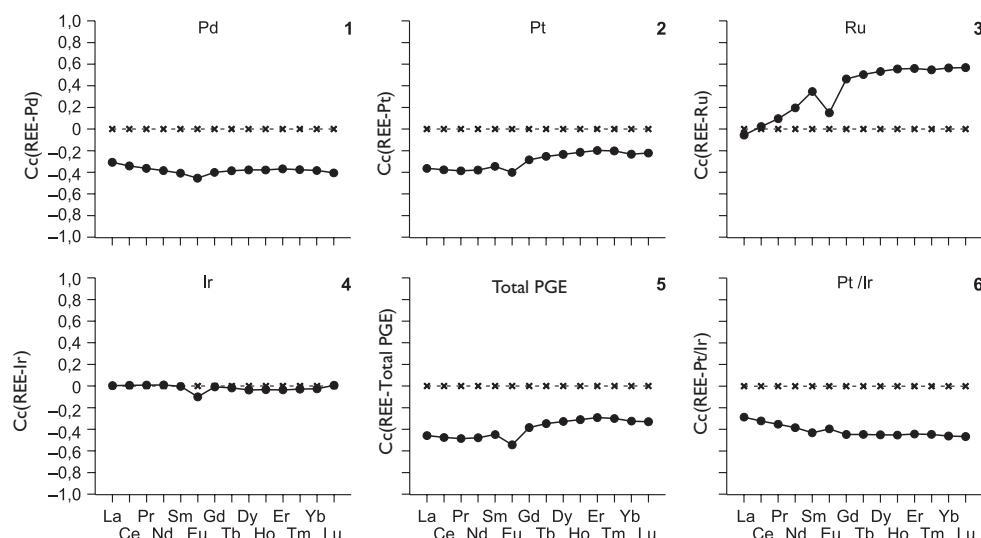


Figure 10.5 Graph of correlation coefficients (Cc) between REE and PGE compositions for rocks from some mafic-ultramafic massifs (Central and East Tuva, Russia) (data Table 10.4).

of the curve of changing of correlation coefficients between REE and Pt indicate that the latter has a slightly stronger negative correlation with LREE compared to HREE (Figure 10.5, 2). The type of the graph of changing of coefficients for Ru indicates that this element has a positive relation with all REE, except for La and Ce (Figure 10.5, 3). A relatively small number of available tests did not allow determining the nature of relationship between REE and Ir (Figure 10.5, 4). In contrast to the statistically insignificant negative correlation coefficients between total PGE contents and most of the REE, the values for Eu (-0.54) are statistically significant (Figure 10.5, 5). We can also assume a negative correlation between HREE and Pt/Ir parameter (Figure 10.5, 6). The possibility of an inverse relation between REE and PGE contents in these rocks is confirmed by the location of figurative points in Figure 10.6.

These data allow us to refer to the ratio of two indicator parameters – Pd/Ir and Pt/Ir. Thus, in the rocks of Kalbagdagsky massif both of these parameters have higher values if compared with rocks from Karaossky and Maysky massifs. Leucocratic troctolite from Bulkinsky massif has the highest value of Pt/Ir parameter (see Table 10.4). Judging by the diagrams in the coordinates (Pd/Ir-Yb) and (Pt/Ir-Yb), there can be assumed a definite relationship between these two indicators of fractionation of PGE and Yb (Figure 10.7).

Next, we consider the possible relationship between REE and PGE in rocks of two more massifs – Birdagsky and Khayalygsky. The data obtained indicate that the

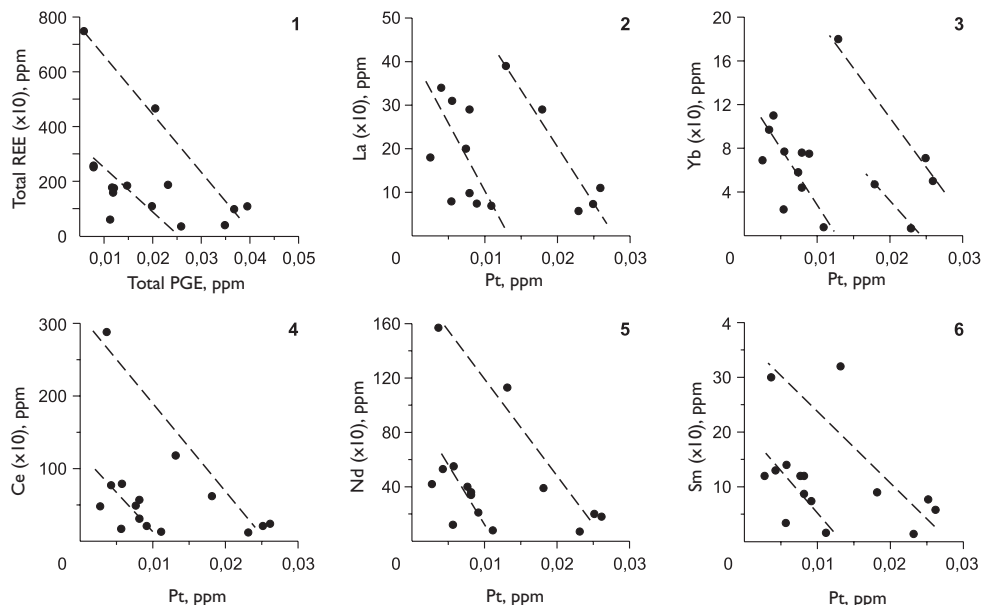


Figure 10.6 Relationship between REE and total PGE, and Pt compositions for rocks from some mafic-ultramafic massifs (Central and East Tuva, Russia) (data Table 10.4). For constructing of graphs REE contents were increased by 10 times. Here and below the dotted lines – estimated trends.

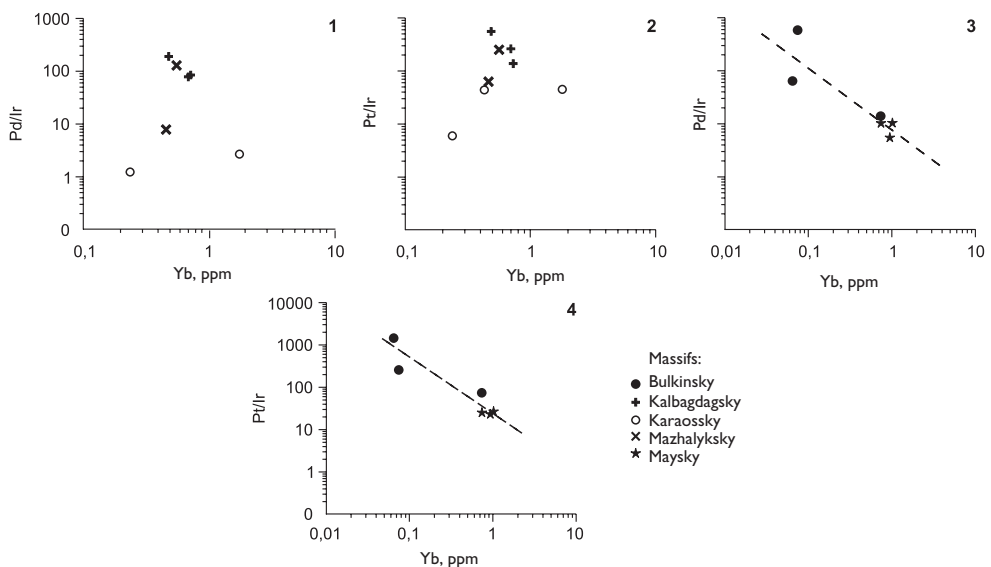


Figure 10.7 Relationship between Yb compositions and Pd/Ir parameter values (1 and 3) and Pt/Ir parameter values (2 and 4) for rocks from Kalbagdagsky, Mazhalyksky, Karaossky, Maysky and Bulkinsky massifs (Central and East Tuva, Russia) (data Table 10.4).

rocks of Birdagsky massif have lower total REE contents in comparison with the rocks of Khayalygsky massif (Table 10.5). The level of HREE and MREE accumulation in the rocks of both massifs is lower than in N-MORB basalts, while the level of LREE accumulation is higher, on the contrary. By the nature of the patterns of chondrite-normalized REE contents we can conclude that LREE contents in these rocks are slightly higher than HREE contents and that in some samples there is a slight Eu excess (Figure 10.8). By the content of REE the rocks of Birdagsky massif are divided into two types. The first is represented by hornblende-bearing gabbro containing heightened concentrations of these impurities in comparison with the rocks of the second type – plagioclase-bearing lherzolites and wehrlites. The rocks of Khayalygsky massifs can also be divided into two geochemical types: 1) hornblende-bearing gabbro with lower REE content, and 2) hornblendites that have heightened contents of them. In general, almost all samples of these two massifs have higher REE concentrations in comparison with rocks that form the massifs located in central and eastern regions of Tuva.

According to data obtained by atomic absorption method, in rocks of Birdagsky and Khayalygsky massifs the total Pt, Pd and Rh contents range from 20 to 74 ppb. At the same time, in some samples the content of Pt is higher than Pd content, while in the others – the opposite situation. According to the analysis by ICP-MS method in the rocks of both massifs the total Os, Ir, Ru, Pt and Pd contents ranged from 0.6 to 21 ppb (Table 10.5). In plagioclase-bearing lherzolites and wehrlites of Birdagsky massif, as well as in amphibole gabbro of Khayalygsky massif the level of PGE accumulation is generally higher than in the

Table 10.5 REE (ppm), PGE, and Re (ppb) compositions of ultramafic and mafic rocks from Birdagsky and Khayalygsky massifs, South-West Tuva (Russia).

[Oydup et al., 2007] ICP-MS											
Massifs											
	Birdagsky						Khayalygsky				
Element	M-42	M 42a	M-39	M-40	M-27	M-41	Mkh-5	Mkh-37	Mkh-11	Mkh-12	Mkh-2
	1	2	3	4	5	6	7	8	9	10	11
La	1,73	1,47	0,72	3,92	4,20	5,48	8,19	5,31	8,14	3,92	4,48
Ce	3,92	3,40	1,98	10,34	9,02	11,22	25,55	12,75	18,59	8,49	10,60
Pr	0,61	0,53	0,34	1,62	1,28	1,63	4,64	1,95	2,62	1,22	1,66
Nd	2,49	2,23	2,09	8,29	5,69	7,17	24,38	10,03	12,17	5,72	7,67
Sm	0,57	0,58	0,66	2,14	1,49	1,69	7,80	2,87	2,96	1,62	2,00
Eu	0,28	0,19	0,19	0,74	0,74	0,46	2,05	1,01	1,10	0,85	1,04
Gd	0,73	0,65	0,64	2,22	1,59	1,92	8,80	3,38	2,91	1,95	2,44
Tb	0,12	0,08	0,11	0,41	0,28	0,33	1,41	0,57	0,49	0,34	0,42
Dy	0,77	0,60	0,67	2,83	1,67	2,01	9,15	3,88	3,22	2,21	2,82
Ho	0,17	0,12	0,17	0,58	0,33	0,42	1,93	0,83	0,66	0,51	0,60
Er	0,43	0,34	0,42	1,91	1,00	1,34	5,12	2,31	1,90	1,45	1,71
Tm	0,07	0,06	0,07	0,32	0,17	0,22	0,76	0,33	0,30	0,23	0,26
Yb	0,51	0,43	0,34	2,00	1,08	1,34	4,62	2,23	1,82	1,45	1,71
Lu	0,07	0,06	0,06	0,30	0,16	0,19	0,66	0,32	0,25	0,20	0,25
Total REE	12,5	10,7	8,46	37,6	28,7	35,4	105	47,8	57,12	30,16	37,65
(La/Yb) _n	57,8	58,4	35,6	35,0	55,4	60,2	39,0	39,5	74,82	41,45	42,44
(Eu/Eu ³⁺) _n	1,34	0,94	0,87	1,03	1,46	0,79	0,75	0,99	1,13	1,46	1,44
Rb	4,57	3,82	1,32	58	27	5,93	6,27	37	71	34	75
Sr	62	67	35	67	323	201	99	312	379	324	438
Y	5,13	4,15	4,51	21	11,9	13,7	61	25	22	14,6	18,8
Zr	21	14,8	4,70	20	40	30	90	74	86	37	43
Nb	1,65	1,02	0,13	1,61	2,48	1,00	8,00	7,38	5,04	2,91	3,68
Cs	7,91	6,74	0,45	3,71	4,17	2,39	0,60	1,62	2,66	2,13	2,69

(Continued)

Table 10.5 (Continued).

[Oydup et al., 2007] ICP-MS											
Massifs											
	Birdagsky						Khayalygsky				
	M-42	M-42a	M-39	M-40	M-27	M-41	Mkh-5	Mkh-37	Mkh-11	Mkh-12	Mkh-2
Element	1	2	3	4	5	6	7	8	9	10	11
Ba	18,80	31	11,08	259	279	86	89	230	386	270	1219
Hf	0,50	0,33	0,16	0,65	0,89	0,82	2,95	1,94	2,02	1,00	1,25
Ta	0,19	0,28	0,05	0,091	0,18	0,18	0,46	0,45	0,36	0,19	0,37
Th	0,46	0,18	0,09	0,27	0,89	0,63	0,90	0,71	1,68	0,37	0,37
U	0,17	0,084	0,082	0,081	0,24	0,16	0,33	0,32	0,48	0,17	0,083
Sr/Ba	3,30	2,13	3,20	0,26	1,16	2,33	1,12	1,35	0,98	1,20	0,36
Sr/Rb	13,6	17,5	26,9	1,15	3,56	33,9	15,8	8,47	5,31	9,59	5,82
Zr/Hf	42,9	44,2	28,7	30,8	44,2	36,8	30,6	38,3	42,7	36,6	34,7
Zr/Y	4,17	3,56	1,04	0,97	3,33	2,20	1,49	2,99	3,96	2,50	2,31
Ta/Nb	0,11	0,28	0,40	0,06	0,07	0,18	0,06	0,06	0,07	0,06	0,05
U/Th	0,36	0,46	0,91	0,30	0,27	0,26	0,36	0,46	0,29	0,46	0,23
Os	0,08	0,03	0,62	0,02	0,02	N.d.	0,03	0,43	0,17	0,51	0,07
Ir	0,06	0,07	0,16	0,04	0,02	0,01	0,02	0,05	0,10	0,09	0,02
Ru	0,62	0,60	0,55	0,51	0,12	0,47	0,09	0,91	1,78	0,55	0,58
Pt	5,28	3,33	19,0	0,93	0,09	0,60	0,10	0,91	3,77	1,12	0,34
Pd	4,96	5,34	0,70	0,80	0,36	1,04	0,32	1,54	4,43	2,68	0,98
Total PGE	11,00	9,37	21,03	2,30	0,61	2,12	0,56	3,84	10,25	4,95	1,99
Re	0,36	0,36	0,16	0,08	0,17	0,26	0,21	0,12	0,48	0,41	0,19
Pd/Pt	0,94	1,60	0,04	0,86	4,00	1,73	3,20	1,69	1,18	2,39	2,88
Pd/Ir	82,7	76,3	4,4	20,0	18,0	104	16,0	30,8	44,3	29,8	49,0
Pt/Ir	88,0	47,6	119	23,3	4,5	60,0	5,00	18,2	37,7	12,4	17,0
Ru/Ir	10,3	8,57	3,44	12,8	6,00	47,0	4,50	18,2	17,8	6,11	29,0

Note: 1, 2 – Iherzolites Pl-bearing, serpentinized; 3 – olivine clinopyroxenites (wehrlite); 4 – hornblendite Pl-bearing; 5 – hornblende gabbro; 6 – olivine gabbro-norite with hornblende, melanocratic; 7 – hornblende Pl-bearing, coarse-grained; 8 – hornblende gabbro, melanocratic; 9 – hornblende gabbro, coarse-grained; 10 – hornblende gabbro; 11 – hornblende gabbro with phlogopite. The analyses were done in the Analytical Center of IGM SB RAS (analysts S.V. Palesskii, I.V. Nikolaeva, O.A. Koz'menko). Detection limits of PGE (ppb): Os – 0,07; Ir – 0,002; Ru – 0,005; Pt – 0,07; Pd – 0,09. N.d. – no data.

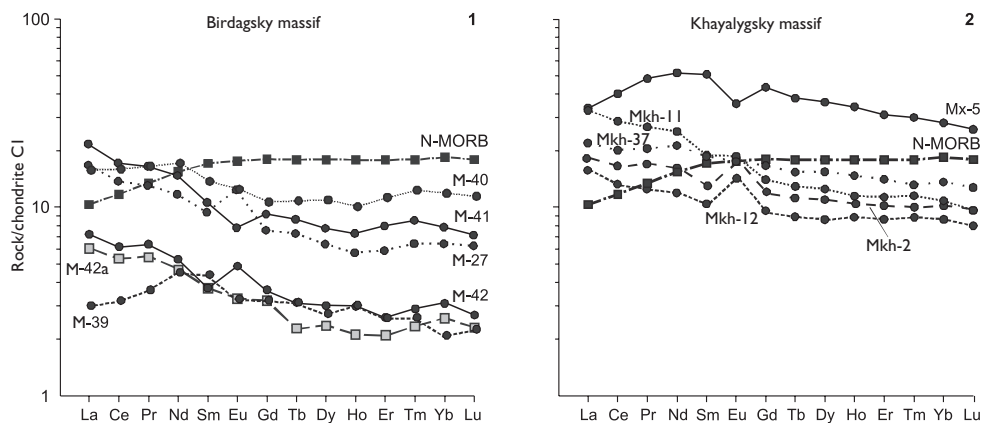


Figure 10.8 Chondrite-normalized REE patterns for some rocks from Birdagsky (1) and Khayalygsky (2) massifs (West Tuva, Russia) (data Table 10.5).

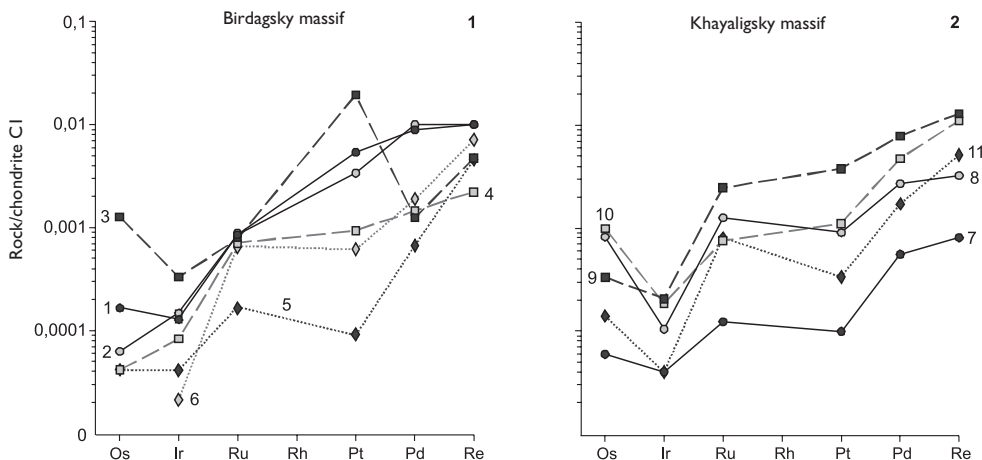


Figure 10.9 Chondrite-normalized PGE patterns for some rocks from Birdagsky (1) and Hayaligsky (2) massifs (West Tuva, Russia) (data Table 10.5). Pattern's numbers are corresponded to the ordinal numbers of analyses in Table 10.5.

rest of samples. Total Pt and Pd contents in all rocks of both massifs exceed the total contents of Os, Ir and Ru. In all rocks of Khayalygsky massif and some samples from Birdagsky massif the content of Pd is higher than Pt content, in the rest of the rocks from Birdagsky massif the reaction between these elements is inverse. Plagioclase-bearing lherzolites of Birdagsky massif and also some hornblende-bearing gabbro from Khayalygsky massif are characterized by slightly heightened Re concentrations.

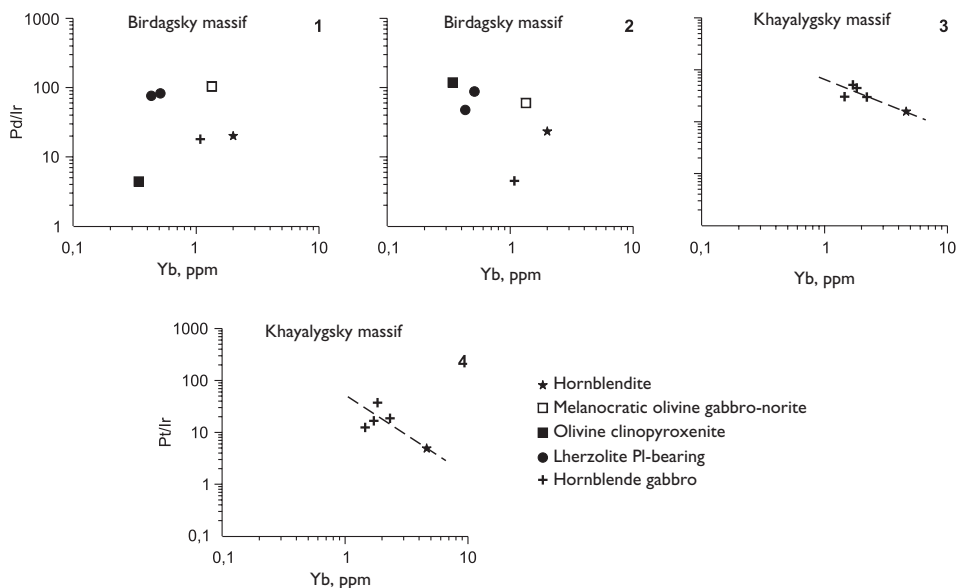


Figure 10.10 Relationships between Yb compositions and Pd/Ir (1 and 3) and Pt/Ir (2 and 4) parameters values for Pl-bearing lherzolite, olivine clinopyroxenite, melanocratic olivine gabbro-norite, hornblende gabbro and hornblendite from Birdagsky (1, 2) and Khayalygsky (3, 4) massifs (West Tuva, Russia) (data Table 10.5).

The chondrite-normalized patterns of PGE and Re contents in the rocks of Birdagsky and Khayalygsky massifs are similar in configuration and have a common positive slope (Figure 10.9). At the same time some of the patterns are complicated by minima for Ir and Pt, and minima for Ir in the patterns of rocks from Khayalygsky massifs have a slightly greater intensity than in the other cases. The values of Pd/Pt parameter in rocks from both of these massifs vary in a narrow range compared with the values of Pd/Ir and Pt/Ir parameters. In the rocks of Birdagsky massif the relationship between the values of Pd/Ir and Pt/Ir parameters, on the one hand, and Yb contents, on the other hand, has not been ascertained, while in the rocks of Khayalygsky massif an inverse relationship between these characteristics should not be excluded (Figure 10.10).

Based on data on the relations between REE and PGE in rocks, the mafic-ultramafic massifs of Tuva can be divided into three types: 1) massifs of rocks that are relatively enriched with REE, but significantly depleted by PGE; 2) massifs of rocks that are relatively depleted by REE and relatively enriched with PGE; 3) massifs of rocks that are characterized by low concentrations of both REE and PGE. An inverse relationship between the contents of REE and PGE occurs primarily in the rocks of the first two types of massifs.

The above material on geochemistry of REE and PGE in rocks of mafic-ultramafic massifs located in the territory of Tuva, with some exceptions, generally does not contradict the assumption of the existence of a sort of antagonism between these two groups of elements in different products of mafic-ultramafic magmatism.

10.2 NARANSKY MASSIF (WEST MONGOLIA)

This chromite-bearing massif located 15 km south-east of the Gobi Altai city is one of the largest mafic-ultramafic massifs in the territory of West Mongolia. It is a part of Dzabkhan ophiolite belt that traces the zone of abyssal fracture. The massif is extended to the west-northwest direction at 38 km at a width of 0.5–10 km. Its structural position, internal structure, petrographic, mineralogical, petrochemical, geochemical and metallogenetic features were discussed in many publications [Pinus *et al.*, 1976, 1984; Lesnov, 1979, 1981, 1982; Lesnov & Simonov, 1989; Dmitrenko *et al.*, 1991]. Below, we discuss the previously obtained data on the distribution of REE and PGE in rocks of the massif [Lesnov & Tsimbalist, 1983; Lesnov *et al.*, 1990; Lesnov *et al.*, 1993], as well as new materials related to this issue.

Naransky massif is a complex plutonic body, the structure of which contains three main elements [Lesnov, 1982]: 1) the large steeply dipping ultramafic restite protrusion, and 2) intruding through this protrusion along its southern tectonic contact, much inferior to it in size and also steeply dipping gabbro intrusion of elongated form, and 3) the contact-reaction zone localized along the boundaries of ultramafic protrusion and gabbro intrusion, which is composed of hybrid rocks of ultramafic and mafic composition. To the south of the massif, among the host strata there are several small tectonic blocks of ultramafic restites and gabbro stocks intruding through them and the host strata. The host strata is represented by metamorphosed terrigenic-volcanic and carbonate rocks of the Vendian-Cambrian age. Naransky massif and its host strata are transgressive overlain by horizons of volcanites of average composition and conglomerates of Devonian age. The later formation of gabbro intrusion in relation to ultramafic protrusion is confirmed by the contact-reaction zone located along their borders, xenoliths of ultramafic restites in the composition of gabbro intrusion found in several places, as well as their veined bodies of gabbro and pyroxenites injecting them. Ultramafic restites are represented by harzburgites and by less common lherzolites and dunites, stripe-like bodies of which alternate with harzburgites. All these rocks are serpentized and dinamometamorphosed on different levels, especially when close to the faults. Gabbro intrusion and its stock-like satellites are composed of gabbro-norites and gabbro, as well as olivine-bearing varieties of them. The structure of the contact-reaction zone involves websterites that alternate with lenticular and stripe-like isolations of wehrellites and olivine gabbro of variable quantitative-mineral composition. Among the ultramafic restites many diluvial-eluvial and as well as some indigenous manifestations of ore chromitites there were found. In websterites of the contact-reaction zone there was scattered sulphide mineralization identified, which contains microparticles of copper-bearing minerals of Pd and Pt. In many schlich samples from the alluvium and proluvium of temporary channels draining the massif there were grains of PGE minerals of various composition, as well as Au were found [Lesnov, 1982; Dmitrenko *et al.*, 1991, Lesnov *et al.*, in print].

The distribution of REE, PGE and Au in rocks of Naransky massif has been studied using atomic absorption method, as well as RNAA and ICP-MS methods (Table 10.6, 10.7). According to the available analyses, the lowest total REE contents are characteristic of dunites (0.18 ppm). Note that approximately the same average total REE content (0.20 ppm) was determined in dunites from the Twin Sisters massif (USA) [Frey *et al.*, 1971], as well as in the international geochemical standard of

Table 10.6 REE (ppm), PGE, and Re (ppb) compositions of dunite, harzburgite, websterite, and gabbro-norite from Naransky massif (West Mongolia).

	L-204	L-205	L-104	L-209	266	269	278
<i>Methods</i>							
	ICP-MS				RNAA		
Element	Dunite	Harzburgite	Websterite	Gabbro-norite	Websterite	Gabbro-norite	Primitive mantle**
La	0,034*	0,10	0,38	0,47	0,250	N.d.	0,48
Ce	0,087*	0,23	1,04	N.d.	0,330	0,42	0,6
Pr	0,008*	0,016*	0,18	0,075	N.d.	N.d.	N.d.
Nd	0,026*	0,082	1,16	0,31	0,230	0,28	0,3
Sm	0,002*	0,011*	0,51	0,079	0,064	0,1	0,13
Eu	0,0009*	0,004*	0,18	0,042	0,027	0,1	0,1
Gd	0,003*	0,017	0,66	0,12	0,120	0,24	0,27
Tb	0,0009*	0,002*	0,13	0,021	0,023	0,042	0,05
Dy	0,006*	0,017	0,89	0,17	N.d.	N.d.	N.d.
Ho	0,002*	0,004*	0,19	0,038	N.d.	N.d.	N.d.
Er	0,005*	0,014	0,59	0,11	N.d.	N.d.	N.d.
Tm	0,0009*	0,002*	0,086	0,024	0,027	0,039	0,046
Yb	0,006*	0,020	0,58	0,18	0,150	0,25	0,29
Lu	0,0009*	0,003*	0,091	0,025	0,025	0,037	0,045
Total REE	0,18	0,53	6,66	4,57	1,25	1,51	2,31
(La/Yb) _n	3,69	3,52	0,44	1,82	1,1	N.d.	1,12
(Eu/Eu*) _n	1,07	0,88	0,97	1,30	N.d.	N.d.	N.d.
Rb	0,21*	0,36	1,11	0,77	N.d.	N.d.	N.d.
Sr	0,33*	0,97	38	35	N.d.	N.d.	N.d.
Y	0,051*	0,16	5,9	1,44	N.d.	N.d.	N.d.
Zr	35	47	78	97	N.d.	N.d.	N.d.
Nb	0,039*	0,14	0,10	0,032*	N.d.	N.d.	N.d.
Ba	0,23	0,97	16,7	22	N.d.	N.d.	N.d.
Hf	0,79	0,92	3,4	2,1	N.d.	N.d.	N.d.
Th	0,028*	0,051	0,076	0,035*	N.d.	N.d.	N.d.
U	0,010*	0,011*	0,036*	0,030*	N.d.	N.d.	N.d.
Os	0,50	0,70	0,06	0,16	N.d.	N.d.	N.d.
Ir	0,10	0,49	0,023	0,04	N.d.	N.d.	N.d.
Ru	0,64	0,57	0,09	0,15	N.d.	N.d.	N.d.
Pt	4,96	0,14	2,89	10,52	N.d.	N.d.	N.d.
Pd	0,21	0,46	18,5	26,4	N.d.	N.d.	N.d.
Total PGE	6,41	2,36	21,6	37,2	N.d.	N.d.	N.d.
Re	0,004*	0,006*	0,006*	0,015	N.d.	N.d.	N.d.
Pd/Ir	2,1	0,94	804	660	N.d.	N.d.	N.d.
Pt/Ir	49,6	0,29	126	263	N.d.	N.d.	1,94

Note: The analyses were done in the Analytical Center of IGM SB RAS, ICP-MS method (analysts S. Palesskii, I. Nikolaeva, O. Koz'menko). *Element compositions are lower than the detection limits. **REE composition of primitive mantle [Sun, McDonough, 1989]; PGE composition of primitive mantle [Rollinson, 1993].

Table 10.7 Average PGE and Au compositions (ppb) of rocks from Naransky massif (West Mongolia).

Rocks	Pd	Pt	Rh	Au	Number of definitions
Dunites serpentinized	7,3	8,9	N.d.	14,7	6
Serpentinites (apodunite)	8,6	4,5	N.d.	11,5	4
N.d.	8,1	7,5	N.d.	18,1	10
Wehrlites	10,0 (4)	15,7 (4)	1,5 (1)	—	—
Websterites	12,4 (21)	12,9 (21)	1,7 (5)	22,0 (6)	—
Websterites Pl-bearing	21,8 (7)	14,0 (7)	N.d.	59,7 (5)	—
Gabbro-norites	24,0	8,7	N.d.	77,6	5
Chromitites	10,7 (38)	22,0 (32)	8,2 (37)	—	—
N.d.	Os – 58,3 (1); Ir – 123 (1); Ru – 84,3 (1).		—	—	—

Note: The analyses were done in the Analytical Center of IGM SB RAS, atom-absorption method (analyst V. Tsimbalist). In brackets – number of definitions.

DTS-1 dunite (0.17 ppm) [Gladney *et al.*, 1991]. The higher total REE content is defined in harzburgites from this massif – 0.53 ppm. To add more, an approximately same level of total REE content was determined in harzburgites of Ronda massif (Spain) – from 0.34 to 1.08 ppm [Van der Wal & Bodinier, 1996]. In websterites of Naransky massif the total REE contents are much higher (6.66 ppm) than in dunites and harzburgites, but lower than in websterites of Balmuccia massif (Italy) [Rivalenti *et al.*, 1995].

It should be emphasized that, despite the overall depletion by REE the analyzed ultramafites of this massif are anomalously enriched with LREE (Figure 10.11). This kind of anomalous enrichment of ultramafic restites with LREE, according to our observations, is due to the presence of not only structural (isomorphic) impurity of these elements, but also of variable amounts of unstructured impurity in intragranular and intergranular microcracks. Total REE content in the gabbro-norite of the massif (4.57 ppm) yields to its content in rocks from many other mafic-ultramafic massifs [Lesnov, 2010]. Possibly, the gabbro-norites from the considered massif crystallized from the melt, which emerged during the partial melting of pre-depleted mantle source.

According to the determinations made by ICP-MS method, the total contents of Os, Ir, Ru, Pt and Pd in dunite and harzburgite are inferior to their total content in websterite and gabbro-norite. The content of Ir in the harzburgite was higher than in dunite. The content of Re in all these rocks is very low (Table 10.6). The results of PGE determination in rocks of the massif made by atomic absorption method are in good accordance with their estimations by ICP-MS method on Pt – in dunite and gabbro-norite, as well as on Pd – in websterite and gabbro-norite (Table 10.7). The chondrite-normalized patterns of distribution of the primitive mantle of contents of PGE and Re in websterite and gabbro-norite that were obtained by ICP-MS method are very similar by their configuration. Judging by them, in both of these rocks there

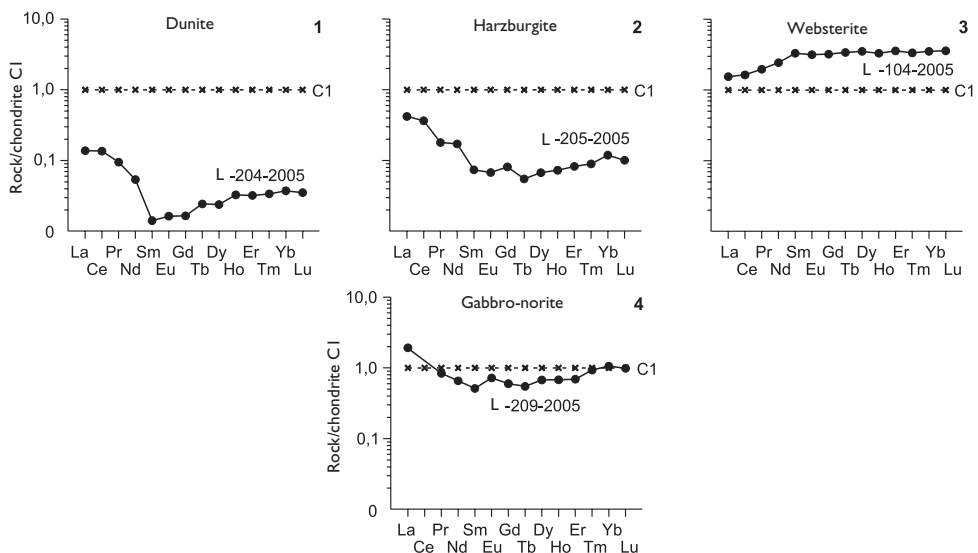


Figure 10.11 Chondrite-normalized REE patterns for dunite (1), harzburgite (2), websterite (3) and gabbro-norite (4) from Naransky massif (West Mongolia) (data Table 10.6).

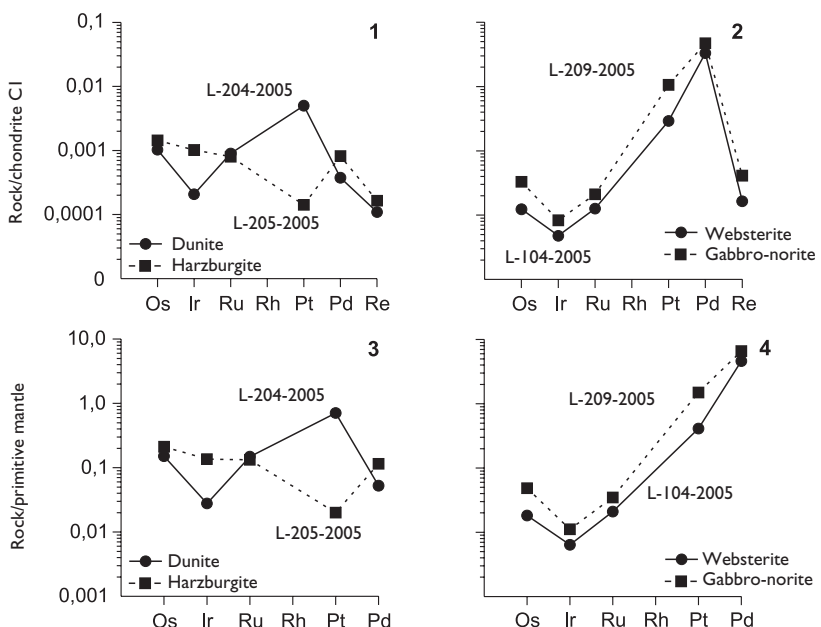


Figure 10.12 Chondrite-normalized (1, 2) and primitive mantle-normalized (3, 4) PGE and Re patterns for dunite, harzburgite, websterite and gabbro-norite from Naransky massif (West Mongolia) (data Table 10.6).

is an insignificant Ir deficit, as well as some Pd excess (Figure 10.12). Studied rocks of this massif, particularly harzburgite, are characterized by low values of Ru/Ir parameter. The values of Pd/Ir parameter in websterite and gabbro-norite are two orders of magnitude higher than in the dunite and harzburgite.

The diagrams in the coordinates of total REE – total PGE and total REE – Pd/Pt the figurative points of dunite and harzburgite are located apart from the points of websterites and gabbro-norites (Figure 10.13, 1). On these diagrams, just like

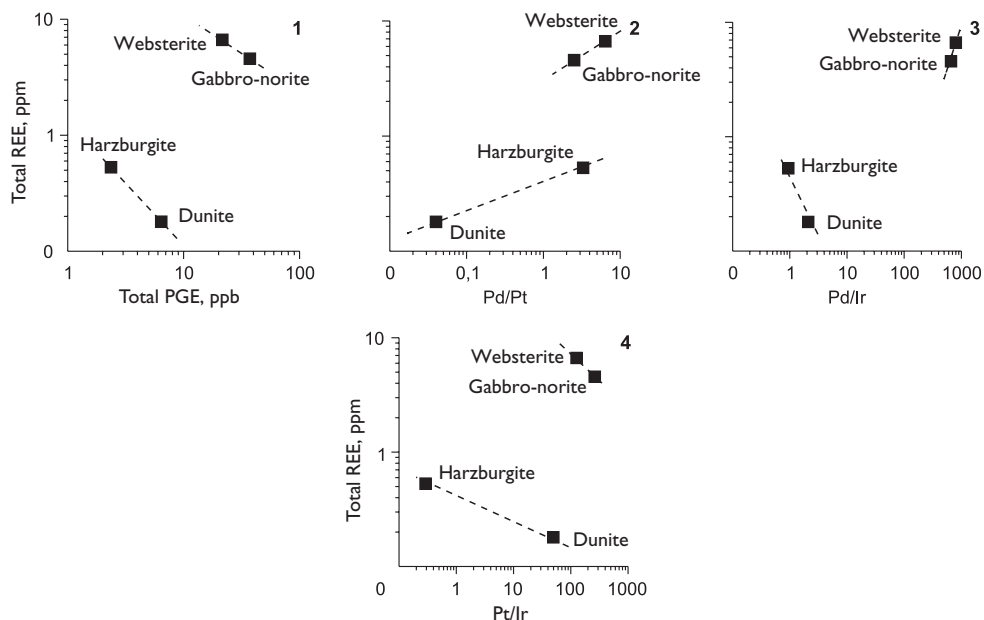


Figure 10.13 Relationship between total REE compositions, and total PGE compositions (1), as well as Pd/Pt (2), Pd/Ir (3) and Pt/Ir (4) parameters values for dunite, harzburgite, websterite and gabbro-norite from Naransky massif (West Mongolia) (data Table 10.6).

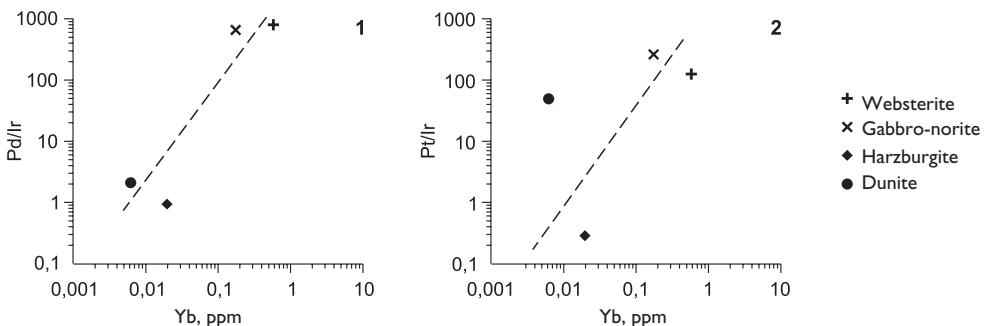


Figure 10.14 Relationship between Yb compositions and Pd/Ir (1) and Pt/Ir (2) parameters values for dunite, harzburgite, websterite and gabbro-norite from Naransky massif (West Mongolia) (data Table 10.6).

the diagram in the coordinates (total REE – Pd/Pt) we can assume the existence of two separate trends (Figure 10.13, 2–4). The position of figurative points in the diagrams in the coordinates (Yb – Pd/Ir) and (Yb – Pt/Ir) assumes discontinuity of geochemical characteristics of the ultramafites and gabbro. In these rocks with increasing contents of less refractory Pd and Pt against more refractory Ir contents, the contents of Yb are increasing (Figure 10.14). In general, these data do not contradict the assumption that during the formation of ultramafic restites and gabbros composing this massif, a multidirectional fractionation of REE and PGE occurred.

10.3 KOKPEKTINSKY MASSIF (SOUTH URALS, KAZAKHSTAN)

Kokpektinsky massif is located in the basin of the Kokpeky River (South Urals) and structurally confined to the area of Main Urals deep-seated fault [Petrology, ..., 1991; Fershtater & Bea, 1996; Fershtater, 2004]. It is exposed over an area of 70 sq · km. and has a form that is elongated to north-eastern direction. This massif is considerably gabbro and is directly connected with the large Kempirsaysky ultramafic protrusion located to the east of it; they both comprise the Kempirsay ophiolite association. The structure of Kokpektinsky massif includes troctolites, olivine gabbro and gabbro, and also the located among them isolations of serpentized dunites and wehrlites of various size. The rocks of the massif are cut by dikes of pegmatite gabbro and anorthosites. Among the gabbros of Kokpektinsky massif close to the contact with Kempirsaysky ultramafic protrusion there were xenoliths of ultramafites forming this protrusion found. The xenoliths size varies from a few centimeters to hundreds of meters, the shape – from angular to rounded and the contacts with others gabbros – from sharp to gradual. According to our observations, the Kokpektinsky massif has intruded after the formation of Kempirsaysky ultramafic protrusion [Petrology, ..., 1991], which gives grounds to consider it as a polygenic ultramafic-mafic body. It is assumed that whole variety of rock types that compose the massif was formed as a result of crystallization of primary mantle, as well as contaminated mafic melts that appeared under the active collaboration of primary melts with ultramafic restite substance. According to the results of dating by different isotopic methods (Rb-Sr, Sm-Nd, U-Pb, Ar-Ar) it was ascertained that Kempirsay ophiolite association was formed in the range from 420 to 396 Ma [Edwards & Wasserburg, 1985; Sharma & Wasserburg, 1996; Sharma *et al.*, 1995; Melcher *et al.*, 1999].

Judging by the data obtained by ICP-MS method, the rocks of Kokpektinsky massif are largely depleted by REE, the chondrite-normalized contents of which are generally lower than in N-MORB basalts (Table 10.8, Figure 10.15). As we can see by the level of REE accumulation, the wehrlites and anorthosite are inferior to non-olivine and olivine gabbro, while the chondrite-normalized Yb contents in them are slightly higher than La contents. Note that in a sample of anorthosite there is no significant excess of chondrite-normalized LREE contents over HREE observed, as typical of many samples enriched with plagioclase. In addition, in the rocks of this massif, especially in the olivine gabbro and troctolites, there is a slight Eu excess, and the lowest values of $(\text{Eu}/\text{Eu}^*)_n$ parameter were identified in wehrlites, while the highest – in the

Table 10.8 REE (ppm), PGE and Re (ppb) compositions of wehrlites, olivine gabbros, anorthosites and altered gabbros from Kokpektynsky massif (South Urals, Kazakhstan).

[Lesnov et al., 2007] ICP-MS												
	L-53	L-54	B4445	B5605	B5518	B5508	B5517	B5468	B5603	B4499	B5579	B5602
	Wehrlites		Olivine gabbros						Troctolite leucocratic	Anorthosite	Gabbros altered	
Element	1	2	3	4	5	6	7	8	9	10	11	12
La	0,24	0,14	0,32	0,48	0,26	0,25	0,24	0,55	0,24	0,14	0,16	0,53
Ce	0,41	0,33	0,99	1,37	0,63	0,59	0,74	1,81	0,68	0,37	0,52	1,78
Pr	0,057	0,051	0,21	0,25	0,096	0,11	0,12	0,40	0,12	0,052	0,11	0,39
Nd	0,35	0,27	1,39	1,39	0,46	0,48	0,76	2,6	0,74	0,28	0,85	2,5
Sm	0,17	0,076	0,61	0,53	0,14	0,11	0,28	1,15	0,24	0,098	0,43	1,12
Eu	0,075	0,085	0,41	0,37	0,21	0,18	0,28	0,54	0,29	0,11	0,28	0,71
Gd	0,29	0,14	1,01	0,72	0,17	0,13	0,50	1,88	0,33	0,12	0,67	1,70
Tb	0,057	0,028	0,19	0,13	0,033	0,016	0,098	0,36	0,061	0,023	0,12	0,33
Dy	0,40	0,19	1,29	0,86	0,22	0,11	0,67	2,3	0,39	0,16	0,93	2,2
Ho	0,084	0,039	0,27	0,18	0,044	0,025	0,14	0,51	0,10	0,033	0,20	0,52
Er	0,26	0,12	0,81	0,53	0,14	0,076	0,40	1,54	0,25	0,10	0,57	1,51
Tm	0,043	0,021	0,13	0,090	0,024	0,016	0,060	0,24	0,042	0,016	0,096	0,24
Yb	0,27	0,13	0,76	0,55	0,13	0,11	0,41	1,42	0,26	0,094	0,53	1,53
Lu	0,040	0,018	0,11	0,070	0,020	0,016	0,055	0,18	0,035	0,013	0,073	0,20
Total REE	2,75	1,65	8,51	7,52	2,57	2,22	4,76	15,5	3,79	1,60	5,53	15,4
(La/Yb) _n	0,60	0,73	0,28	0,59	1,38	1,52	0,39	0,26	0,62	0,98	0,20	0,23

(Eu/Eu*) _n	1,01	2,45	1,57	1,80	4,02	4,42	2,28	11,1	3,13	3,18	1,62	1,57
Rb	0,33	0,58	0,59	0,75	0,78	0,83	0,93	0,74	0,26	0,55	1,73	1,38
Ba	2,4	20,3	3,3	5,4	5,1	15,3	2,2	4,3	5,3	3,2	14,0	9,2
Sr	24	59	145	176	182	109	127	145	162	115	113	122
Th	0,010	0,025	0,009	0,046	0,014	0,013	0,007	0,021	0,010	0,017	0,011	0,015
U	0,032	0,028	0,027	0,026	0,037	0,084	0,016	0,026	0,013	0,032	0,024	0,058
Nb	0,080	0,095	0,083	0,23	0,087	0,069	0,11	0,21	0,051	0,099	0,22	0,10
Zr	55	68	171	194	179	96	293	409	159	173	172	158
Hf	2,5	3,1	7,5	8,5	7,7	3,3	12,9	17,9	7,4	7,4	7,8	7,3
Y	2,6	1,28	8,6	6,2	1,94	0,72	4,7	16,8	2,6	1,16	6,1	14,8
Os	N.d.	N.d.	N.d.	0,13	0,1	N.d.	0,07	0,13	0,06	0,15	0,12	0,05
Ir	0,05	0,06	0,03	0,11	0,06	0,06	0,11	0,05	0,05	0,04	0,11	0,02
Ru	0,16	0,28	0,01	0,23	0,01	N.d.	N.d.	0,01	0,02	N.d.	0,06	0,11
Pt	0,36	0,23	0,33	2,89	2,68	1,96	1,02	1,68	1,97	0,12	9,06	0,3
Pd	0,85	0,71	0,36	3,19	2,31	2,58	0,47	2,84	0,76	0,29	9,18	0,44
Total PGE	1,42	1,28	0,73	6,55	5,16	5,60	1,67	4,71	2,86	0,60	18,53	0,92
Re	0,08	0,35	0,24	0,89	0,35	0,16	0,26	0,05	0,38	0,02	0,13	0,21
Pd/Pt	2,4	3,1	1,1	1,1	0,86	1,3	0,46	1,7	0,39	2,4	1,0	1,5
Pd/Ir	17,0	11,8	12,0	29,0	38,5	43,0	4,3	56,8	15,2	7,3	83,5	22,0
Pt/Ir	7,2	3,8	11,0	26,3	44,7	32,7	9,3	33,6	39,4	3,0	82,4	15,0
Ru/Ir	3,2	4,7	0,33	2,1	0,17	N.d.	N.d.	0,20	0,40	N.d.	0,55	5,5

Note: The analyses were done in the Analytical Center of IGM SB RAS (analysts S., Palesskii, I., Nikolaeva, O., Koz'menko).

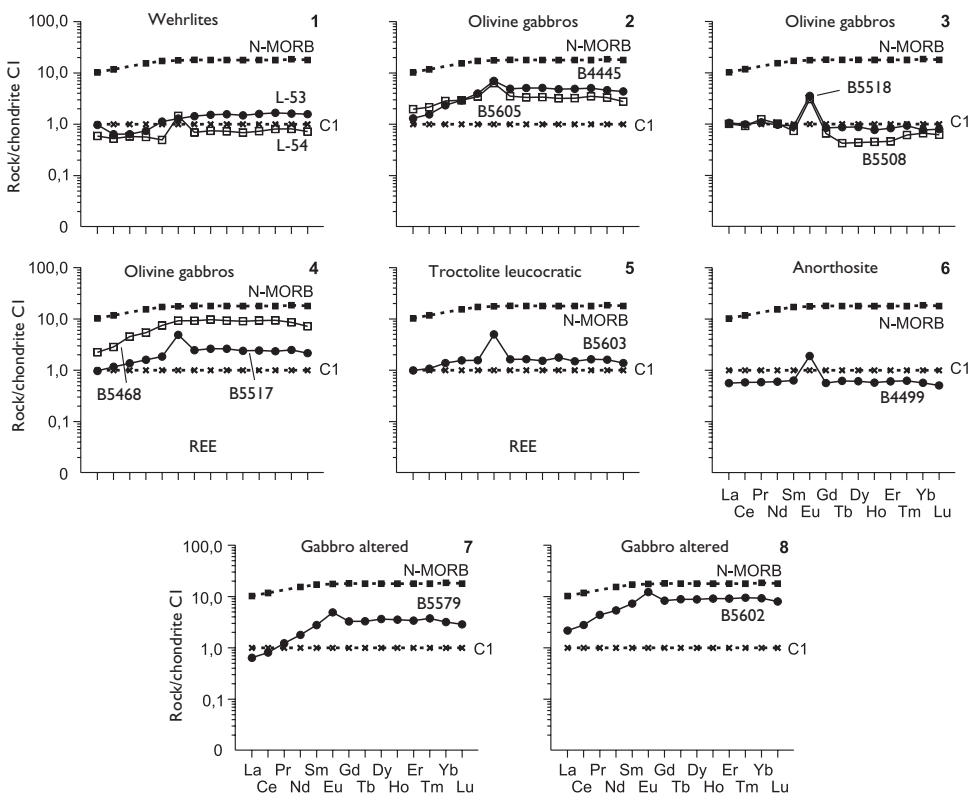


Figure 10.15 Chondrite-normalized REE patterns for wehrlites (1), olivine gabbros (2–4), leucocromatic troctolite (5), anorthosite (6) and altered gabbros (7, 8) from Kokpektinsky massif (South Urals, Kazakhstan) (data Table 10.8). N-MORB—(data [Sun, McDonough, 1989].

olivine gabbro. By the level of REE accumulation, as well as by the configuration of their distribution patterns the rocks of Kokpektinsky massif are in many respects comparable to the same samples from Samail massif composing the ophiolite association of Oman [Pallister & Knight, 1981].

In the rocks of Kokpektinsky massif analyzed by ICP-MS, the total Os, Ir, Ru, Pt and Pd contents range from 0.6 to 18.5 ppb, the highest total PGE content was determined for one of the gabbro samples that was subjected to epigenetic changes (Table 10.8). Values of Pd/Pt parameter in rocks of the massif range in between 0.39–3.09. Almost all of the rocks from the massif are depleted by Re. All the rocks of the massif, excepting anorthosite sample, have the patterns of the distribution of PGE and Re with a steep positive slope and some of them are complicated by a minimum of Ru (Figure 10.16). Figurative points of the composition of the rocks from the massif in the diagrams in the coordinates of (Pt-Ir) and (Pd-Ir) form two distinct aggregates, corresponding to two types of them – more depleted and less depleted with respect to Pt and Pd. The second type includes mainly olivine gabbro. In the diagram in the coordinates of $Pd/Ir \cdot (La/Yb)_n < 1$ the points corresponding to the composition of gabbro,

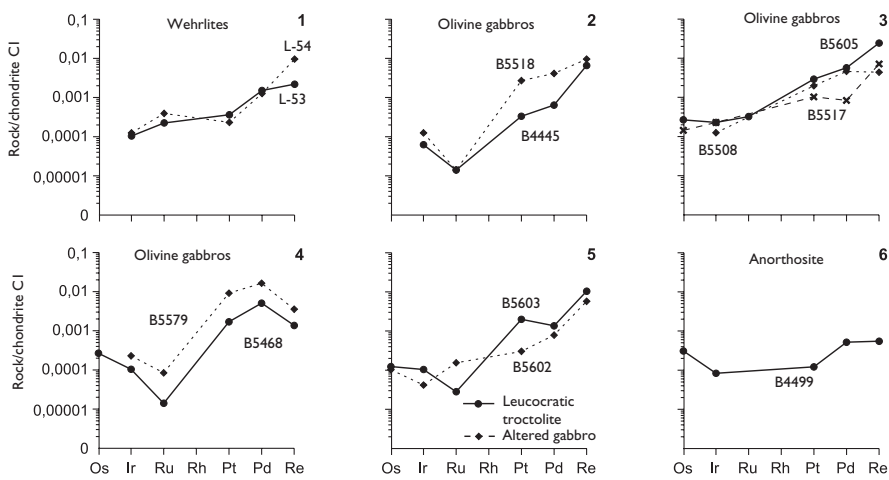


Figure 10.16 Chondrite-normalized PGE and Re patterns for wehrellites (1), olivine gabbros (2–4), leucocratic troctolite and altered gabbro (5), and anorthosite (6) from Kokpektinsky massif (South Urals, Kazakhstan) (data Table 10.8).

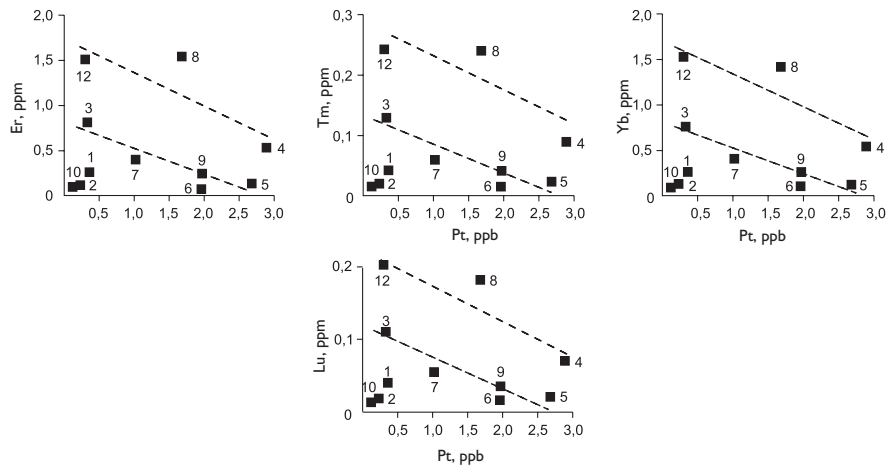


Figure 10.17 Relationship between Pt compositions and heavy REE compositions for anorthosite, wehrlite, altered gabbros, olivine gabbros and leucocratic troctolite from Kokpektinsky massif (South Urals, Kazakhstan). Numbers of points correspond to the numbers of analyses in the Table 10.8.

part of olivine gabbro samples, of troctolites, anorthosites and wehrllites, are located along two weakly manifested trends with negative slopes; another trend is formed by the points of olivine gabbro samples that have the values of parameter $(La/Yb)_n > 1$. In addition, figurative points of the massif rocks form two poorly defined trends with a negative slope in the diagram in the coordinates (Pt-HREE), while the points

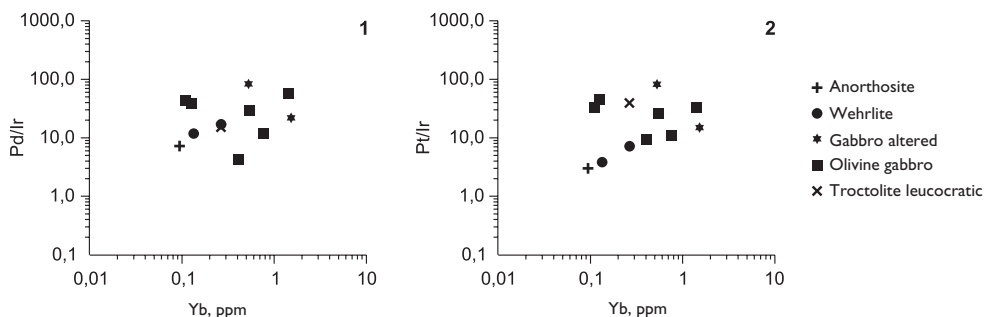


Figure 10.18 Relationship between Yb composition and Pd/Ir (1) and Pt/Ir (2) parameters values for anorthositic, wehrelite, altered gabbros, olivine gabbros and leucocratic troctolite from Kokpektinsky massif (South Urals, Kazakhstan) (data Table 10.8).

corresponding to the composition of wehrellites and anorthosites are away from these trends (Figure 10.17). The values of Pd/Ir and Pt/Ir parameters, as well as the content of Yb in these rocks are subject to considerable variation, but no relationship between these characteristics was detected (Table 10.8, Figure 10.18).

Thus, the data on the geochemistry of REE and PGE suggests that in the rocks from Kokpektinsky massif there is an inverse relationship between the contents of elements of these two groups. It is not excluded, however, that in those rocks that presumably occurred during the crystallization of mantle mafic melts contaminated by a substance of older ultramafic restites, i.e., have a hybrid nature (olivine gabbro, troctolites, wehrellites), the originally existed inverse relationship between the contents of REE and PGE could be disturbed.

10.4 ULTRAMAFIC XENOLITHS IN ALKALINE BASALTS FROM EIFEL AND VOGELSBERG PROVINCES (GERMANY)

The contents of REE and PGE were determined in non-amphibole and amphibole harzburgites, lherzolites and pyroxenites, which composed xenoliths in alkaline basalts from these provinces [Schmidt *et al.*, 2003]. It was ascertained that in most cases the contents of LREE, as well as total REE contents, in non-amphibole samples of peridotites are lower than their contents in the amphibole samples (Table 10.9). Total PGE and Au contents in non-amphibole peridotites were also slightly lower than in their amphibole samples. In addition, it was determined that the REE content in pyroxenites is higher, while PGE content is lower than in harzburgites and lherzolites. In the diagrams in the coordinates (La-PGE) and (Sm-PGE) the figurative points corresponding to the composition of harzburgites and lherzolites form positively sloped trends, while in the diagrams in the coordinates (Yb-PGE) correlation between these characteristics is not observed (Figure 10.19).

These data suggest that in the rocks from these xenoliths the La and other LREE, as well as some PGE, had undergone a redistribution of different intensity and trend

Table 10.9 REE (ppm), PGE and Au (ppb) compositions of harzburgites, lherzolites, and pyroxenites from xenoliths in Eifel and Vogelsberg alkaline-basalt provinces (Germany).

	[Schmidt et al., 2003] INAA									
Element	194*	826	832	589*	1343*	1342	211*	229*	1317*	
	Harzburgites									Lherzolite
La	0,92	0,30	0,42	1,68	1,86	0,38	3,30	2,07	2,51	
Ce	2,40	0,41	0,58	5,00	7,00	0,87	10,20	5,30	9,20	
Nd	0,90	N.d.	0,37	N.d.	3,30	N.d.	3,80	3,00	2,70	
Sm	0,25	0,07	0,10	0,51	0,62	0,10	0,82	0,43	0,63	
Eu	0,07	0,02	0,03	0,15	0,17	0,03	0,22	0,13	0,18	
Tb	0,03	0,03	0,03	0,05	0,06	N.d.	0,07	0,06	0,08	
Yb	0,07	0,04	0,06	0,11	0,12	0,05	0,15	0,12	0,20	
Lu	0,01	0,01	0,02	0,02	0,02	0,01	0,02	0,02	0,04	
Total REE	4,65	N.d.	1,60	N.d.	13,15	N.d.	18,59	11,12	15,54	
(La/Yb) _n	9,27	5,06	4,80	10,3	10,5	5,61	14,7	11,6	8,51	
Os	0,28	1,30	0,18	4,24	4,55	1,34	6,47	1,37	3,37	
Ir	0,36	2,19	0,58	7,06	5,46	1,06	9,07	1,91	3,36	
Ru	1,70	2,82	2,74	14,48	8,22	1,62	15,98	2,93	7,16	
Rh	0,47	0,43	0,41	1,48	2,94	0,73	3,23	1,01	1,69	
Pt	1,83	2,80	1,80	13,51	12,40	1,65	18,00	4,55	12,17	
Pd	1,22	1,11	1,41	7,30	5,74	0,41	8,42	1,98	0,42	
Au	0,18	0,43	0,50	0,66	0,79	0,25	0,10	0,35	0,12	
Total PGE + Au	6,04	11,08	7,62	48,73	40,10	7,06	61,27	14,10	28,29	
Pd/Ir	3,39	0,51	2,43	1,03	1,05	0,39	0,93	1,04	0,13	
Pt/Ir	5,08	1,28	3,10	1,91	2,27	1,56	1,98	2,38	3,62	

(Continued)

Table 10.9 (Continued).

	[Schmidt et al., 2003] INAA								
	848*	210*	788*	599	214	1182	196	909	906
Element	Lherzolites							Pyroxenites	
La	1,54	1,46	2,44	0,60	0,60	0,66	0,54	3,25	4,18
Ce	3,50	N.d.	5,80	1,20	1,30	1,32	N.d.	12,00	15,00
Nd	N.d.	N.d.	2,10	0,54	N.d.	1,00	N.d.	5,00	8,00
Sm	0,10	0,14	0,34	0,20	0,30	0,33	0,37	1,70	2,52
Eu	0,03	0,04	0,09	0,07	0,11	0,13	0,16	0,51	0,81
Tb	0,03	0,04	0,07	0,05	0,49	0,09	0,09	0,27	0,30
Yb	0,11	0,12	0,15	0,25	0,29	0,35	0,43	0,44	0,55
Lu	0,02	0,02	0,02	0,04	0,04	0,07	0,07	0,06	0,08
Total REE	N.d.	N.d.	11,01	2,95	N.d.	3,94	N.d.	23,23	31,44
(La/Yb) _n	9,45	8,08	11,0	1,62	1,40	1,28	0,85	4,99	5,13
Os	0,17	1,59	2,69	1,43	2,89	2,75	0,19	0,08	0,16
Ir	0,47	2,51	3,01	2,30	3,07	2,18	3,00	4,30	0,23
Ru	0,89	3,88	2,58	3,43	8,52	8,31	3,80	1,67	0,93
Rh	0,39	1,17	0,86	1,21	2,38	0,94	0,72	3,27	0,35
Pt	0,78	8,80	5,10	6,91	5,18	10,30	5,10	25,76	0,72
Pd	1,20	7,57	2,75	3,28	5,54	4,60	2,25	17,66	1,10
Au	0,15	0,99	N.d.	0,79	1,71	1,14	1,11	0,92	0,32
Total PGE + Au	4,05	26,51	N.d.	19,35	29,29	30,22	16,17	53,66	3,81
Pd/Ir	2,55	3,02	0,91	1,43	1,80	2,11	0,75	4,11	4,78
Pt/Ir	1,66	3,51	1,69	3,00	1,69	4,72	1,70	5,99	3,13

Note: (*) Amphibole-bearing samples, others – without amphibole samples.

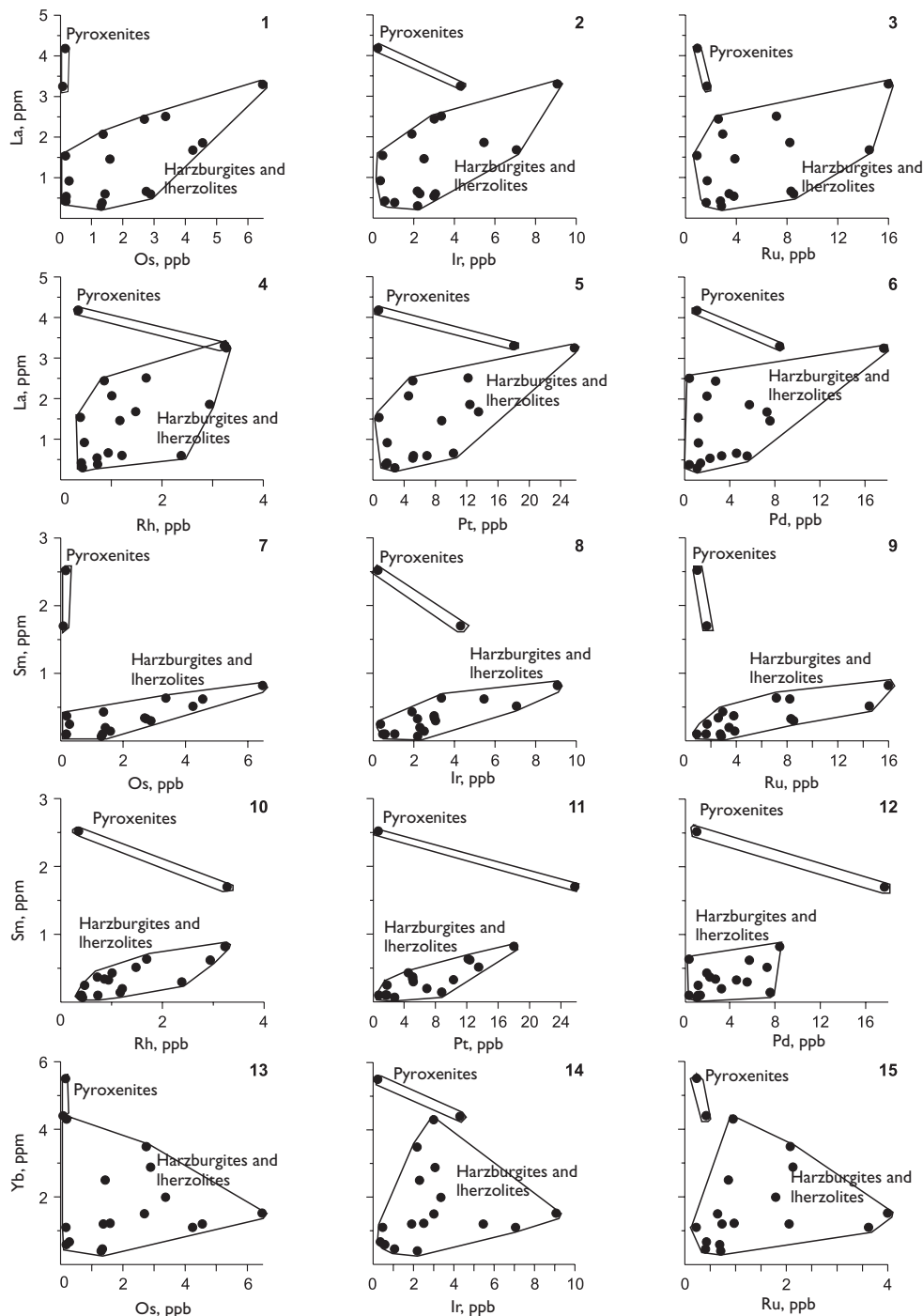


Figure 10.19 (Continued).

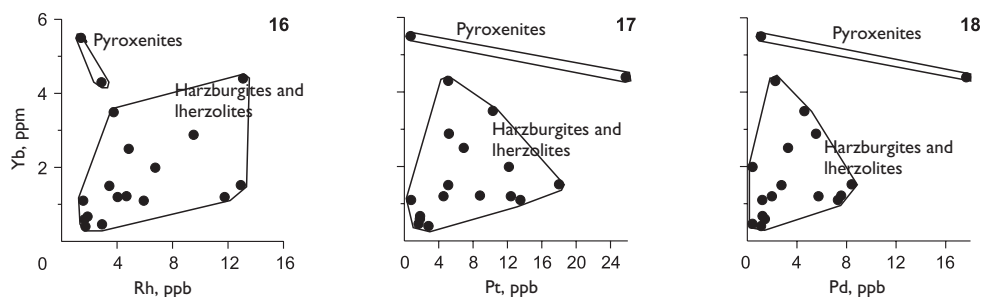


Figure 10.19 Relationship between PGE compositions and La (1–6), Sm (7–12), Yb (13–18) compositions for harzburgites, lherzolites and pyroxenites from xenoliths in alkaline basalts from Eifel and Vogelsberg provinces (Germany) (data Table 10.9).

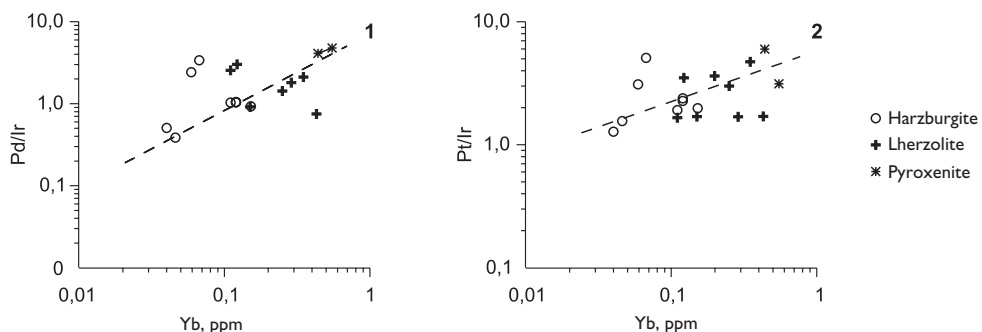


Figure 10.20 Relationship between Yb compositions and Pd/Ir (1) and Pt/Ir (2) parameters values for harzburgites, lherzolites and pyroxenites from xenoliths in alkaline basalts from Eifel and Vogelsberg provinces (Germany) (data Table 10.9).

that occurred during the infiltration of fluid components coming from alkaline basalts relocating them. Apparently, the less mobile HREE in contrast to the highly mobile LREE were subject to such redistribution to a lesser extent. In addition, it is likely that those amphiboles that occur in these ultramafites could be formed under the influence of the same fluids. Judging by the location of the figurative points in the diagrams in the coordinates (Yb-Pd/Ir) and (Yb-Pt/Ir) in the row from harzburgites to lherzolites and pyroxenites, the values of these three characteristics are increasing (Figure 10.20). Thus, we believe that under the influence of fluids coming from basaltic melts into the xenoliths of ultramafites, not only LREE, but also Pd and Pt could change to a relatively mobile state. If this assumption is confirmed on the basis of representative analytical data, it will serve as a convincing argument in favor of the view that the results of REE and PGE analyses in ultramafites from upper mantle xenoliths in most cases do not correspond to those contents of these elements, which originally characterized them; that is, till the moment when these ultramafites came into direct contact with the basaltic melts carrying them. At the same time, these observations give grounds to believe that the infiltration of basalt fluids has been able to more or less disturb the original inverse relationship between the contents of REE and PGE in the ultramafic restites.

10.5 LUOBUSA MASSIF (SOUTHERN TIBET, CHINA)

Luobusa ultramafic massif that is a part of ophiolite association of Southern Tibet is a steeply dipping lenticular body having a length of 20 km and a width of 4 km. The massif is composed of harzburgites and subordinate dunites [Zhou *et al.*, 2005]. Dunites form a large separate body lying along a tectonic contact of the massif with host rocks, as well as several small lenticular isolations occurring among harzburgites. In addition, the dunites are composing narrow zones around the bodies of ore chromitites localized among harzburgites.

As follows from the analysis, the content of REE in harzburgites is usually slightly higher than in dunites, with the exception of those types of dunites that form isolations among harzburgites (Table 10.10). Total REE contents in the dunites from their large body range from 17 to 75 ppm and in those samples that compose small isolations among harzburgites, it is higher and the average is 114 ppm. In harzburgites the total REE content ranges from 280 to 1250 ppm. Both among the dunites and harzburgites there are some samples with abnormally high LREE content.

Total Ir, Ru, Rh, Pt and Pd contents in ultramafites of this massif range from 16 to 29 ppb, while the configuration of patterns of PGE distribution show some Pt deficiency in dunites. The presented graphs indicate that dunites have an inverse relationship between total Pd, Pt and Rh contents on the one hand, and the contents of REE on the other hand (Figure 10.21). One can also assume that in the dunites and harzburgites from the massif there is an inverse relationship between Yb contents and the values of Pd/Ir and Pt/Ir parameters (Figure 10.22). In general, data on the distribution of REE and PGE in dunites and harzburgites from Luobusa ultramafic massif do not contradict the model of their formation that occurred during the partial melting of mantle source.

10.6 ITI AND KALLIDROMON MASSIFS (GREECE)

These two massifs that are composed of lherzolites and subordinate harzburgites are a part of the ophiolite association of Central Greece [Karipi *et al.*, 2006]. In lherzolites from both massifs the total REE content ranges from 0.83 to 1.81 ppm, in harzburgites – from 0.47 to 0.57 ppm (Table 10.11). Total PGE content in lherzolites ranges from 15.1 to 38.8 ppb, which is slightly higher than in harzburgites (9.6–18.1 ppb). By the position of figurative points on the graphs we can assume that in these ultramafites the contents of Sm, Eu and Gd are inversely related to the contents of Os and that for some reason there is a direct relation between REE and Ir (Figure 10.23). There is also an inverse relation between Yb content and the values of Pd/Ir and Pt/Ir parameters (Figure 10.24).

10.7 KOMATIITE-BASALT COMPLEX OF NORTH-WEST VIETNAM

During the petrological and geochemical studies of the Permian-Triassic volcanic complex of North-West Vietnam in the composition of the residing komatiites,

Table 10.10 REE (ppm), and PGE (ppb) compositions of dunites, and harzburgites from Luobusa massif, South Tibet (China).

[Zhou et al., 2005] ICP-MS												
	D0	D5	D10	D15	D20	D25	D30	D55	D65	D70	D75	D80
Element	Dunites											
La	9,88	5,70	7,94	6,49	9,91	9,76	2,13	1,89	2,61	2,21	3,62	7,82
Ce	18,0	10,4	14,5	17,8	15,8	15,6	3,17	2,90	3,84	35,7	5,44	13,3
Pr	2,13	1,18	1,28	1,33	2,10	17,6	0,41	0,33	0,46	0,44	0,58	1,35
Nd	8,10	4,79	3,38	2,46	5,87	4,64	1,28	1,16	1,41	1,26	1,76	4,12
Sm	1,60	0,85	0,94	0,27	1,28	1,23	0,26	0,23	0,20	0,20	0,34	0,69
Eu	0,41	0,28	0,20	0,20	0,21	0,18	0,15	0,15	0,17	0,13	0,24	0,35
Gd	1,39	1,10	1,54	0,61	1,93	1,44	0,38	0,42	0,51	0,28	0,42	1,30
Tb	0,27	0,23	0,44	0,11	0,38	0,29	0,08	0,01	0,13	0,06	0,14	0,31
Dy	2,07	2,09	3,46	1,00	2,97	2,49	0,88	0,91	1,48	0,42	1,55	3,08
Ho	0,68	0,72	1,25	0,33	0,95	0,75	0,32	0,44	0,63	0,22	0,57	1,00
Er	2,86	2,99	4,76	1,76	3,58	3,32	1,64	1,87	3,25	1,09	3,13	4,24
Tm	0,72	0,70	1,00	0,43	0,78	0,78	0,41	0,53	0,80	0,38	0,70	0,98
Yb	6,58	6,55	9,21	4,49	7,30	6,66	4,40	5,41	7,60	4,83	7,33	8,62
Lu	1,41	1,43	1,84	1,09	1,47	1,49	1,03	1,14	1,73	1,34	1,67	1,91
Total REE	56,09	39,02	51,74	38,41	54,55	66,22	16,54	17,39	24,82	48,56	27,49	49,07
(La/Yb) _n	1,01	0,59	0,58	0,98	0,92	0,99	0,33	0,24	0,23	0,31	0,33	0,61
Ir	5,72	6,16	5,13	6,32	5,11	5,33	4,54	5,24	4,17	5,01	5,77	4,63
Ru	10,8	7,72	8,41	10,7	7,12	10,3	10,0	9,8	7,41	8,26	8,92	8,62
Rh	0,75	0,64	1,57	1,06	0,52	0,42	0,73	1,09	0,52	0,79	0,59	1,42
Pt	2,02	1,61	9,67	3,17	1,18	1,61	1,84	3,99	2,10	1,91	1,95	9,02
Pd	3,23	3,57	4,93	3,04	1,68	1,99	2,97	3,06	2,40	1,92	1,73	5,13
Total PGE	22,52	19,7	29,71	24,29	15,61	19,67	20,12	23,18	16,6	17,89	18,96	28,82
Rh + Pt + Pd	6,00	5,82	16,2	7,27	3,38	4,02	5,54	8,14	5,02	4,62	4,27	15,57
Pd/Ir	0,56	0,58	0,96	0,48	0,33	0,37	0,65	0,58	0,58	0,38	0,30	1,1
Pt/Ir	0,35	0,26	1,88	0,50	0,23	0,30	0,41	0,76	0,50	0,38	0,34	2,0

(Continued)

Table 10.10 (Continued).

[Zhou et al., 2005], ICP-MS											
	D85	D140	D145	D150	L16*	L18*	L6	L17	LH5	L22	L12
Element	Dunites						Harzburgites clinopyroxene-bearing			Harzburgites	
La	2,16	6,34	15,5	2,17	4,85	21,4	8,88	5,70	3,69	244	91,6
Ce	3,26	9,48	30,0	3,45	7,76	36,4	8,63	9,16	5,39	498	158
Pr	0,39	1,15	2,63	0,47	0,86	4,30	1,44	1,24	0,73	56,0	18,0
Nd	1,37	4,00	8,20	1,75	2,80	14,7	5,93	7,83	6,07	208	62,5
Sm	0,19	1,18	2,69	0,46	0,99	3,05	5,20	12,6	10,4	39,6	13,3
Eu	0,15	0,18	0,30	0,16	0,21	1,21	3,18	6,12	4,97	8,53	3,57
Gd	0,40	0,94	1,56	0,52	0,66	3,98	19,8	34,2	24,9	43,1	17,4
Tb	0,09	0,18	0,24	0,18	0,08	0,80	0,23	1,00	0,70	0,71	0,38
Dy	0,75	1,80	2,38	1,59	0,62	5,57	64,0	91,7	63,5	45,7	29,7
Ho	0,31	0,57	0,68	0,55	0,25	1,52	17,5	22,9	16,6	11,1	8,13
Er	1,75	2,51	3,05	3,68	0,95	6,18	63,7	78,0	56,1	35,4	29,4
Tm	0,46	0,57	0,66	0,64	0,22	1,24	11,4	13,1	9,07	6,11	5,57
Yb	5,46	5,62	6,00	5,93	2,74	11,0	90,1	94,7	67,5	43,4	42,9
Lu	1,44	1,22	1,32	1,40	0,73	2,29	15,1	15,6	11,5	7,98	7,85
Total REE	18,18	35,74	75,19	22,95	23,72	114	315	394	281	1248	488
(La/Yb) _n	0,27	0,76	1,74	0,25	1,19	1,31	0,07	0,04	0,04	3,79	1,44
Ir	6,01	5,74	5,44	4,14	6,53	5,75	5,72	1,68	N.d.	5,56	6,01
Ru	8,92	11,37	12,62	7,43	N.d.	N.d.	N.d.	N.d.	N.d.	N.d.	8,92
Rh	1,35	0,58	0,66	0,52	1,51	0,68	1,59	1,28	N.d.	2,06	1,35
Pt	8,78	1,44	2,47	2,06	6,55	1,60	8,18	7,16	N.d.	8,44	8,78
Pd	4,19	2,81	2,00	3,03	3,34	0,90	7,60	7,87	N.d.	4,86	4,19
Total PGE	29,25	21,94	23,19	17,18	N.d.	N.d.	N.d.	N.d.	N.d.	20,92	29,25
Rh + Pt + Pd	14,32	4,83	5,13	5,61	11,40	3,18	17,37	16,31	N.d.	15,36	6,39
Pd/Ir	0,70	0,49	0,37	0,73	0,51	0,16	1,3	1,8	N.d.	0,87	0,70
Pt/Ir	1,5	0,25	0,45	0,50	1,0	0,28	1,4	4,3	N.d.	1,5	1,5

Note: (*) Dunite samples from lens-similar bodies which are disposed among harzburgites.

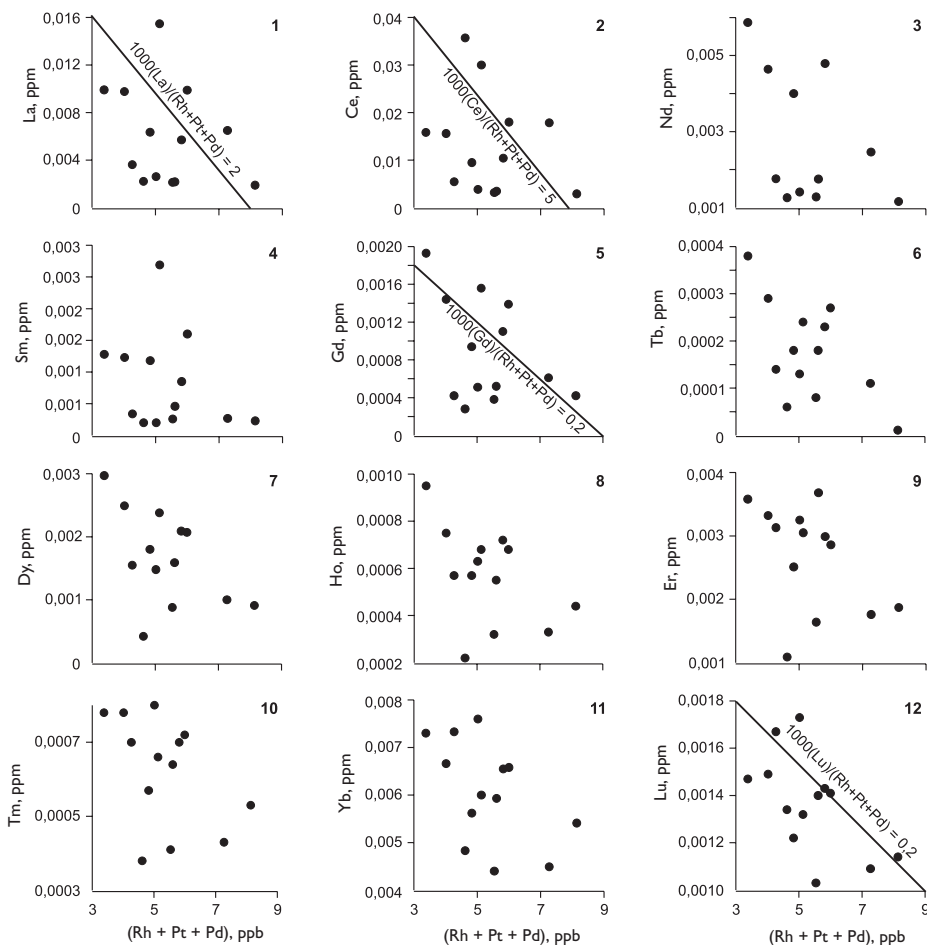


Figure 10.21 Relationship between REE compositions and Rh, Pt and Pd total compositions for dunites and harzburgites from Luobusa massif, Tibet (China) (data Table 10.10).

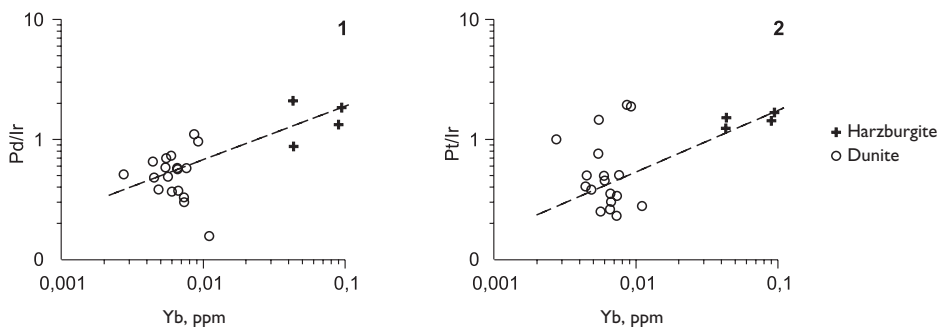


Figure 10.22 Relationships between Yb compositions and Pd/Ir (1) and Pt/Ir (2) parameters values for dunites and harzburgites from Luobusa massif, Tibet (China) (data Table 10.10).

Table 10.11 REE (ppm), PGE, and Au (ppb) compositions of lherzolites, and harzburgites from Iti and Kallidromon massifs (Greece).

[Karipi et al., 2006] INNA										
Element	Iti				Kallidromon				Iti	
	I-126	I-130	I-617	I-290	K-119	K-124a	K-144	K-124	I-189	I-317
<i>Lherzolites</i>										
La	N.d.	0,06	N.d.	N.d.	N.d.	N.d.	N.d.	N.d.	0,25	0,28
Ce	N.d.	0,08	N.d.	0,05	N.d.	0,07	0,06	0,12	0,22	0,29
Pr	0,02	N.d.	0,01	N.d.	N.d.	0,02	0,02	0,01	0,04	0,04
Nd	0,18	0,07	0,09	0,06	0,16	0,12	0,14	N.d.	0,1	0,12
Sm	0,13	0,09	0,05	0,05	0,07	0,05	0,06	0,05	0,03	0,03
Eu	0,06	0,05	0,03	0,03	0,03	0,02	0,03	0,02	0,01	0,01
Gd	0,24	0,20	0,11	0,09	0,12	0,1	0,12	0,1	0,02	0,02
Tb	0,05	0,05	0,03	N.d.	0,03	0,02	0,03	N.d.	N.d.	N.d.
Dy	0,37	0,31	0,22	0,20	0,21	0,19	0,21	0,19	0,02	0,03
Ho	0,09	0,07	0,05	0,05	0,05	0,05	0,05	0,05	N.d.	N.d.
Er	0,27	0,20	0,17	0,18	0,16	0,16	0,17	0,16	0,03	0,04
Tm	0,05	0,03	0,03	0,03	0,03	0,03	0,03	0,03	0,01	0,01
Yb	0,3	0,18	0,18	0,17	0,18	0,19	0,19	0,19	0,16	0,20
Lu	0,05	0,03	0,03	0,04	0,03	0,03	0,03	0,03	0,05	0,07
Total REE	1,81	1,28	1,00	0,90	1,07	0,98	1,08	0,83	0,47	0,57
Os	2,0	2,0	2,0	2,0	2,3	2,0	1,9	2,5	3,0	2,0
Ir	3,3	2,2	2,3	1,5	3,3	2,8	2,7	3,2	1,9	0,2
Ru	6,5	6,2	5,3	N.d.	10,6	7,5	8,6	6,2	N.d.	N.d.
Rh	1,6	1,3	1,4	0,6	2,7	1,4	1,7	1,5	0,7	N.d.
Pt	6,5	4,8	6,3	7,0	14,7	6,7	N.d.	7,6	N.d.	0,3
Pd	4,0	3,4	4,0	4,0	5,2	5,9	6,0	3,2	4,0	15,6
Total PGE	23,9	19,9	21,3	15,1	38,8	26,3	N.d.	24,2	N.d.	N.d.
Au	3,2	2,7	4,6	1,0	7,3	1,9	9,7	2,5	1,2	3,5
Pd/Ir	1,2	1,6	1,7	2,7	1,6	2,1	2,2	1,0	2,1	77
Pt/Ir	2,0	2,2	2,7	4,7	4,5	2,4	N.d.	2,4	N.d.	1,5

komatiitic and normal basalts the contents were determined for REE and among PGE – only for Os [Hanski et al., 2004; Lesnov & Balykin, 2005] (Table 10.12). Komatiites and komatiitic basalts have higher contents of MgO and Cr, higher contents of Os, as well as lower total REE contents compared to normal basalts. As can be seen in the diagrams, between the contents of MgO and Cr, as well as between MgO and Os, there is an evident direct relationship (Figure 10.25). Based on these data, we can assume that in the volcanic rocks of this complex, the parent melts of which were, obviously, formed at different degrees of partial melting of mantle sources, there is an inverse relation between REE contents and contents of all PGE.

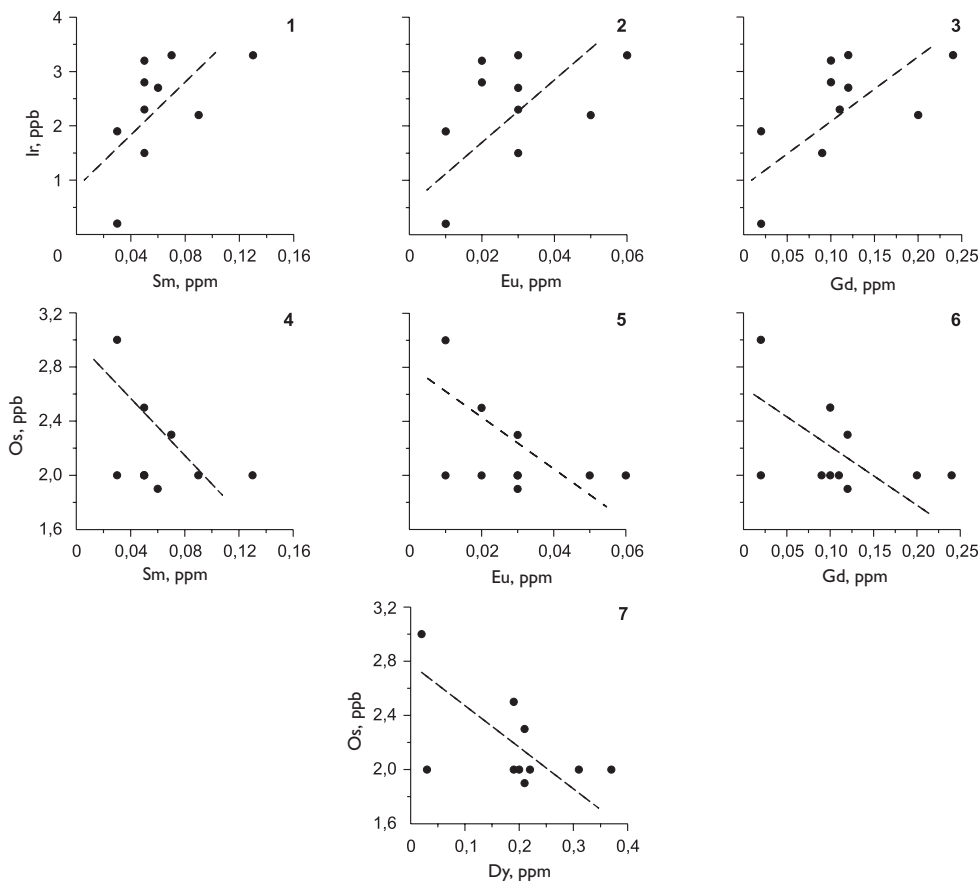


Figure 10.23 Relationship between Ir compositions and Sm, Eu, Gd compositions (1–3), as well as between Os compositions and Sm, Eu, Gd, Dy compositions (4–7) for Iherzolites and harzburgites from Kallidromon and Iti massifs (Greece) (data Table 10.11).

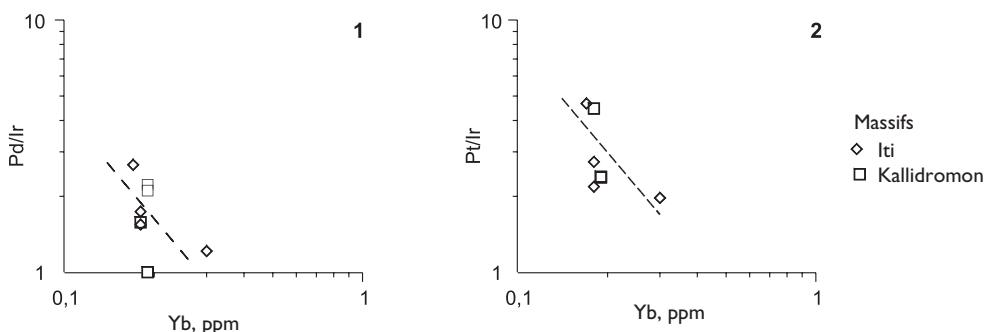


Figure 10.24 Relationship between Yb composition and Pd/Ir (1) and Pt/Ir (2) parameters values for Iherzolites from Kallidromon and Iti massifs (Greece) (data Table 10.11).

10.8 KOMATIITE-BASALT COMPLEXES OF GORGONA ISLAND (COLOMBIA), ALEXO (ONTARIO, CANADA), ONVERWACHT, BARBERTON, PERSEVERANCE (AFRICA) AND KAMBALDA (WEST AUSTRALIA) PROVINCES

Based on the analytical data obtained by geochemical studies of several komatiitic provinces, we can conclude that in these rocks between the contents of Os, Ir and Ru, on the one hand, and MgO contents, on the other hand, there is a direct relation, while between the contents of Rh, Pt and Pd and MgO contents – is an inverse relation [Brugmann *et al.*, 1987]. At the same time, the position of figurative points on the presented diagrams shows that between MgO contents and contents of Dy and Yb there is an inverse relation (Figure 10.26). Thus, these facts also suggest, albeit indirectly, that in komatiites there is an inverse relation between REE and PGE contents.

10.9 BUSHVELD MASSIF (SOUTH AFRICA)

In the area of this massif there are widely-spread fields of picrites as well as of high-magnesian and tholeiitic basalts, for which PGE, Au and La contents were

Table 10.12 REE (ppm), Os (ppb), and MgO (wt%) compositions of komatiites, basaltic komatiites, and tholeiitic basalts from volcanogenic complex from North-West Vietnam.

[Hanski <i>et al.</i> , 2004; Balykin <i>et al.</i> , 2004] ICP-MS								
	VB6892	VB6889	G1448	VB6891	V8/86	VB6865	V9/86	G1456
Element	Komatiites							
La	0,68	0,64	0,91	1,24	0,66	0,36	1,00	0,70
Ce	2,03	2,05	2,90	3,20	2,05	1,18	2,39	2,08
Pr	0,38	0,39	N.d.	0,50	0,40	0,22	0,35	0,33
Nd	2,34	2,37	2,80	2,70	2,45	1,36	1,82	2,25
Sm	1,07	1,11	1,10	1,08	1,01	0,35	0,71	0,99
Eu	0,45	0,48	0,47	0,47	0,49	0,30	0,33	0,38
Gd	1,93	1,84	1,70	1,79	1,74	1,12	1,25	1,78
Tb	0,36	0,36	0,30	0,33	0,32	0,23	0,24	0,31
Dy	2,35	2,33	N.d.	2,23	2,17	1,58	1,67	2,39
Ho	0,51	0,53	N.d.	0,51	0,45	0,37	0,37	0,49
Er	1,50	1,55	N.d.	1,44	1,29	1,14	1,01	1,48
Tm	0,22	0,22	N.d.	0,19	0,19	0,17	0,16	0,2
Yb	1,42	1,41	1,31	1,36	1,23	1,07	1,02	1,43
Lu	0,20	0,21	0,20	0,19	0,19	0,17	0,16	0,23
Total	15,4	15,5	N.d.	17,2	14,6	9,62	12,5	15,0
REE								
(La/Yb) _n	0,32	0,31	0,47	0,62	0,36	0,23	0,66	0,33
Cr	1844	1930	2300	1763	1804	2519	2575	2034
Os	3,915	2,841	2,626	2,529	2,511	2,082	1,874	1,625
MgO	22,37	22,08	20,53	21,05	22,13	22,6	24,85	20,78

(Continued)

Table 10.12 (Continued).

[Hanski et al., 2004; Balykin et al., 2004] ICP-MS							
	P46/89	VII/86	VB6887	VI2/86	P73/89	G1436	G1436a
Element	Komatiites		Basaltic komatiites		Basalts		
Os	1,366	6,995	4,075	1,238	0,1166	0,0338	0,033
La	0,89	N.d.	N.d.	0,76	11,20	2,91	N.d.
Ce	2,00	N.d.	N.d.	1,57	22,00	6,51	N.d.
Pr	0,31	N.d.	N.d.	0,27	N.d.	0,82	N.d.
Nd	1,69	N.d.	N.d.	1,61	12,00	4,00	N.d.
Sm	0,72	N.d.	N.d.	0,71	3,00	1,22	N.d.
Eu	0,32	N.d.	N.d.	0,32	0,60	0,51	N.d.
Gd	1,46	N.d.	N.d.	1,32	3,90	1,90	N.d.
Tb	0,24	N.d.	N.d.	0,25	0,70	0,36	N.d.
Dy	1,79	N.d.	N.d.	1,77	N.d.	2,47	N.d.
Ho	0,40	N.d.	N.d.	0,41	N.d.	0,58	N.d.
Er	1,30	N.d.	N.d.	1,27	N.d.	1,90	N.d.
Tm	0,19	N.d.	N.d.	0,19	N.d.	0,28	N.d.
Yb	1,26	N.d.	N.d.	1,38	2,20	1,76	N.d.
Lu	0,21	N.d.	N.d.	0,21	0,32	0,27	N.d.
Total	12,8	N.d.	N.d.	12,0	N.d.	25,5	N.d.
(La/Yb) _n	0,48	N.d.	N.d.	0,37	3,44	1,12	N.d.
Cr	2072	N.d.	N.d.	3687	530	316	N.d.
MgO	21,64	29,76	30,94	11,39	8,93	8,20	8,20

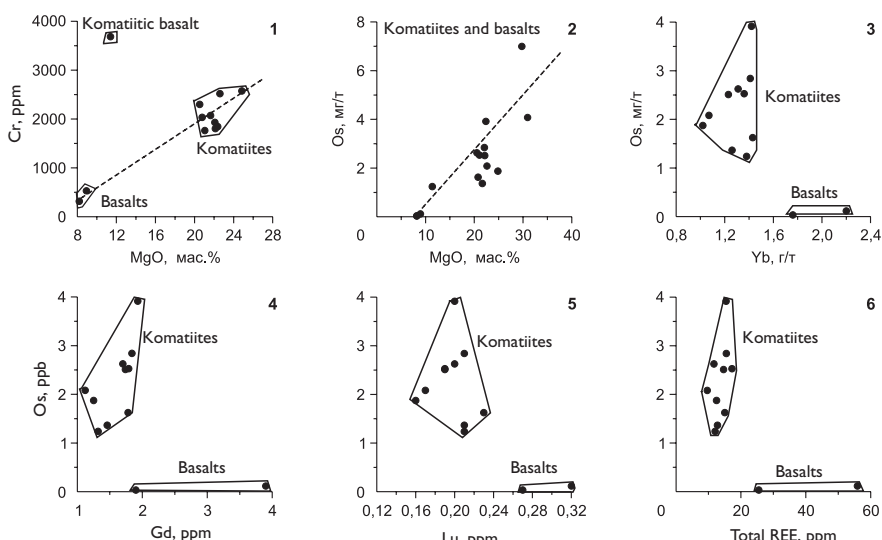


Figure 10.25 Relationship between Os compositions and MgO (1), Cr (2), Yb (3), Gd (4), Lu (5), and total REE (6) compositions for komatiites, komatiitic basalts and tholeiitic basalts from volcanogenic complex of North-West Vietnam (data Table 10.12).

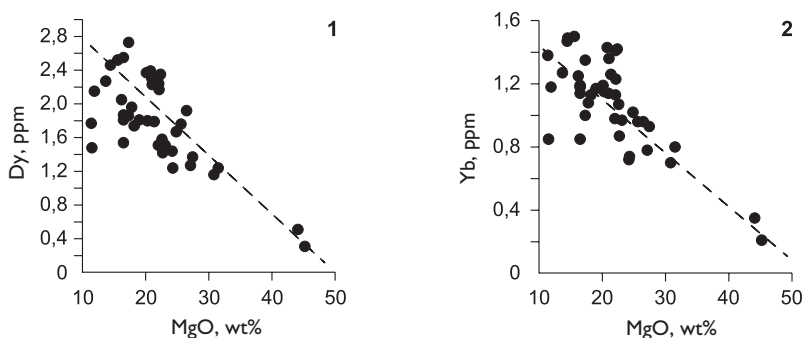


Figure 10.26 Relationships between MgO compositions, and Dy (1) and Yb (2) compositions for komatiites from Gorgona (data [Revillon et al., 2000]), Onwervah (data [Jahn et al., 1982]), Barberton (data [Sun & Nesbit, 1978]) and Kambalda (data [Lesher & Arndt, 1995]) and Perseverance provinces (data [Barnes et al., 1995]).

determined [Davies & Tredoux, 1985]. The average La contents increase in the row from picrites (5.2 ppm) to magnesium basalts (24.8 ppm) and tholeiitic basalts (30.4 ppm). Average total Pd, Pt, Rh, Ru and Ir contents, on the contrary, decrease from picrites (45.2 ppb) to magnesium basalts (33.8 ppb) and tholeiitic basalts (19.0 ppb) (Table 10.13). The results of these analyses and their graphical interpretation (Figures 10.27, 10.28) allow us to conclude that between the contents of La, as of the other REE, and PGE contents in these volcanic rocks, there is an inverse relation. Moreover, as La contents are increasing in the same row of rocks the values of Pd/Ir parameter are also increasing (Figure 10.29). The observed correlations between REE and PGE in volcanic rocks of this area, as it can be assumed, were the result of differences in the degree of partial melting of mantle sources during the generation of parent melts.

10.10 MUSKOX MASSIF (CANADA)

While studying this mafic-ultramafic massif located in the northwestern part of the Canadian Shield, there were data on the distribution of REE and PGE obtained for the rocks composing it: dunites, peridotites, websterites, olivine clinopyroxenites, gabbros, gabbro-norites and chromitites (Table 10.14). Almost all the rocks of this massif, including dunites, were relatively enriched with LREE (Figure 10.30). It should be noted that by an increased level of REE accumulation and its distribution patterns the dunites of the Musko massif are comparable to the samples that are dredged in the area of Romanish fault (Atlantic ocean) [Nikol'skaya & Kogarko, 1995]. At the same time, the rocks of the massif show a higher PGE concentration in comparison with rocks from most of the mafic-ultramafic massifs and complexes discussed above and the highest total PGE contents are characteristic for dunites and websterites. The chondrite-normalized contents of Os, Ir and Ru in all the rocks of the massif are inferior to the contents of Rh, Pt and Pd. In RGE distribution patterns of dunites, peridotites and websterites the maxima are observed for Pt and

Table 10.13 La (ppm), and platinum group elements (ppb) compositions of picrites, high-Mg basalts and tholeiitic basalts from the region of Bushveld pluton (South Africa).

[Davies, Tredoux, 1985] NAA										
	PEU1	PEU2	PEU3	Average	PES1	PEQ1	PEQ2	PEQ3	PEM1	EB13
Element	Picrites				High-Mg basalts					
La	8,00	4,70	2,80	5,20	25,1	22,0	24,3	35,6	32,5	1,70
Ir	1,88	1,48	2,91	2,09	0,59	0,26	0,25	0,22	0,11	1,90
Ru	8,00	5,00	6,00	6,00	2,00	2,00	N.d.	2,00	N.d.	4,00
Rh	4,80	2,80	7,70	5,10	2,40	0,70	1,70	0,70	0,30	4,30
Pt	20,0	18,0	29,0	22,0	15,0	21,0	21,0	18,0	8,00	24,0
Pd	8,00	12,0	11,0	10,0	8,00	12,0	17,0	10,0	6,00	16,0
Total PGE	42,7	39,3	56,6	45,2	28,0	36,0	40,0	30,9	14,4	50,2
Pd/Ir	4,26	8,11	3,78	4,78	13,6	46,15	68,0	45,5	54,6	8,42
Pt/Ir	10,6	12,2	9,97	10,5	25,4	80,8	84,0	81,8	72,7	12,6

(Continued)

Table 10.13 (Continued).

[Davies, Tredoux, 1985] NAA										
	PWS1	PWS2	PWS4	Average	PWM3	PWM4	PEM2	PEM3	PEM4	Average
Element	High-Mg basalts				Tholeiitic basalts					
La	17,8	23,6	18,0	24,8	24,7	66,6	33,1	13,0	14,6	30,40
Ir	0,05	0,07	0,63	0,35	0,03	0,01	0,15	0,10	0,14	0,09
Ru	N.d.	5,00	2,00	3,00	N.d.	N.d.	N.d.	1,20	1,80	1,50
Rh	1,10	0,60	0,80	1,40	0,20	0,30	0,40	0,60	0,50	0,40
Pt	13,0	17,0	13,0	17,0	9,00	5,00	17,0	12,0	10,0	11,0
Pd	25,0	7,00	8,00	12,0	N.d.	N.d.	14,0	8,00	N.d.	6,00
Total PGE	39,2	29,7	24,4	33,8	9,23	5,31	31,6	21,9	12,4	19,0
Pd/Ir	500	100	12,7	34,3	N.d.	N.d.	93,3	80,0	N.d.	66,7
Pt/Ir	260	243	20,6	48,6	300	500	113	120	71,4	122

in the patterns of olivine clinopyroxenites and gabbros the maxima are observed for Pd. (Figure 10.31). The rocks of the massif, regardless of petrographic origin, slightly differ by the values of Pd/Ir parameter that range in dunites – 0.28–85, in peridotites – 1.6–23, in websterites – 0.52–50, in clinopyroxenites and gabbros – 0.48–37. Variations of the values of Pd/Ir are due to both Pd dispersion and Ir dispersion.

The following diagrams show the correlations between the contents of REE and PGE in rocks of Muskox massif (Figure 10.32). Judging by the location of figurative points in them, we can assume quite certainly that the rocks of the

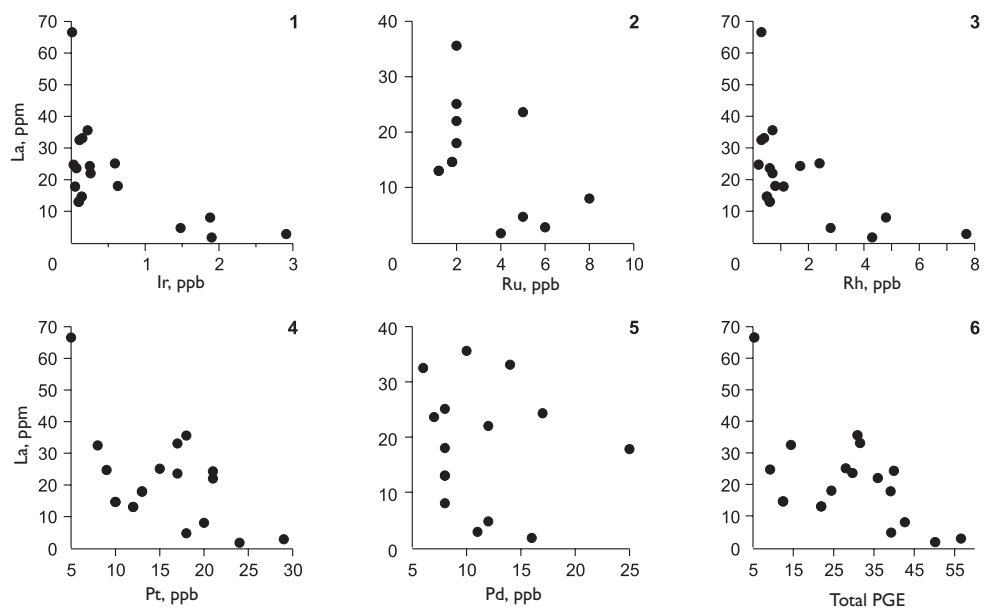


Figure 10.27 Relationship between La compositions, and Ir, Ru, Rh, Pt, Pd and total PGE compositions for picrites, high-Mg and tholeiitic basalts from Bushveld pluton's region (South Africa) (data Table 10.13).

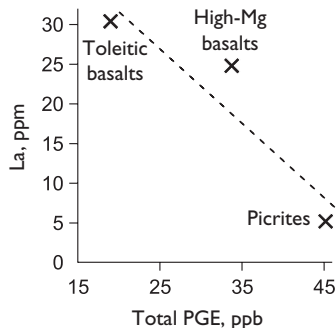


Figure 10.28 Relationship between average La compositions and average total PGE compositions for picrites, high-Mg and tholeiitic basalts from region of Bushveld pluton (South Africa) (data Table 10.13).

massif have a more or less distinctly marked inverse relation between contents of elements from these groups. In turn, the location of points in the diagrams illustrating the correlation between the contents of Yb and the values of Pd/Ir and Pt/Ir parameters shows that at comparatively limited variations of REE contents the values of Pd/Ir and Pt/Ir vary in rather wide ranges, which is most clearly illustrated by the example of points corresponding to the dunites composition (Figure 10.33).

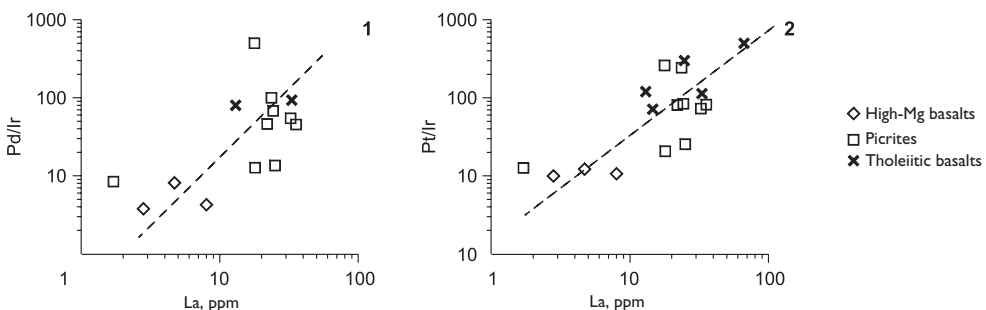


Figure 10.29 Relationship between La compositions and Pd/Ir (1) and Pt/Ir (2) parameters values for picrites, high-Mg and tholeiitic basalts from region of Bushveld pluton (South Africa) (data Table 10.13).

10.11 GALMOENAN MASSIF (KORYAK HIGHLAND, RUSSIA)

Galmoenan massif is located in the Koryak highland (Kamchatka). Detailed petrological and geochemical studies on the massif were performed in the course of exploration and exploitation of closely located and genetically associated large placer deposit of platinum group metals [Koryak-Kamchatka region, ..., 2002]. Body of the massif elongated in the submeridional direction, has a length of about 16 km and a width of 2–4 km, and is exposed on an area of approximately 48 sq · km. It is composed of dunites that make up its interior part, less commonly of olivine-, plagioclase-bearing and magnetite clinopyroxenites that compose a 200–700 m wide zone surrounding the dunite body, while among the pyroxenites some xenogeny isolations of wehrlites and serpentinites occur. Along the contacts of pyroxenite zone with terrigenic-volcanic formations that are framing the massif there is a gabbro intrusion fragmentarily uncovered by erosion.

Based on the results of comprehensive research, including numerical modeling, Batanova *et al.* [2011] concluded that the diversity of ultramafic and mafic rocks that form the massif arose from an intrachamber differentiation of single upper mantle mafic melt. However, our observations and, in particular, the presence of xenogeny isolations of wehrlites and serpentinites among pyroxenites do not allow to exclude the possibility of existence of an alternative model of the genesis of this massif, which is based on an idea of polygenic formation of complex mafic-ultramafic massifs [Lesnov, 1981, 1982, 1986]. According to the model, the dunite body of the considered massif is an earlier protrusive block of upper mantle restites. In its peripheral part the dunites were transformed into clinopyroxenites as a result of exposure to later mantle mafic melts and their fluids. Mafic melts intruded along tectonic contacts of dunite protrusion with the framing rocks and then formed gabbro intrusion that is unevenly uncovered on the perimeter of this complex massif. However, the applicability of this alternative model of formation to this mafic-ultramafic massif requires further studies.

Published data on the contents of REE and PGE in dunites from Galmoenan massif (Table 10.15), as well as diagrams based on them (Figure 10.34) give ground

Table 10.14 REE (ppm), platinum group elements, and Re (ppb) compositions of dunites, peridotites, websterites, olivine clinopyroxenites, gabbro-norites, gabbro, and chromitites from Muskox massif (Canada).

	[Day et al., 2008], ICP-MS								
	N-75	N-115	N-129	S-44	S-51	S-60	S-102	S-110	S-128
Element	Dunites								
La	0,22	0,87	0,05	0,26	0,74	0,06	1,24	1,34	0,99
Ce	0,56	2,1	0,33	0,58	1,81	0,15	2,79	3,03	2,36
Pr	0,09	0,31	0,02	0,08	0,27	0,03	0,39	0,44	0,3
Nd	0,43	1,45	0,33	0,34	1,24	0,17	1,71	1,93	1,53
Sm	0,12	0,37	0,09	0,08	0,33	0,04	0,42	0,48	0,37
Eu	0,05	0,11	0,02	0,02	0,08	0,01	0,1	0,14	0,11
Gd	0,14	0,43	0,13	0,09	0,37	0,05	0,44	0,53	0,38
Tb	0,02	0,07	0,02	0,01	0,06	0,01	0,07	0,08	0,06
Dy	0,15	0,41	0,15	0,09	0,39	0,05	0,41	0,48	0,36
Ho	0,03	0,08	0,03	0,02	0,08	0,01	0,08	0,09	0,07
Er	0,11	0,22	0,1	0,06	0,21	0,04	0,21	0,25	0,19
Tm	0,02	0,03	0,02	0,01	0,03	0,01	0,03	0,04	0,03
Yb	0,15	0,22	0,12	0,07	0,2	0,07	0,21	0,24	0,18
Lu	0,03	0,03	0,02	0,01	0,03	0,01	0,04	0,04	0,03
Total REE	2,12	6,70	1,43	1,72	5,84	0,71	8,14	9,11	6,96
(La/Yb) _n	0,99	2,67	0,28	2,51	2,50	0,58	3,99	3,77	3,71
Os	77,4	1,62	19,3	7,74	5,71	0,956	2,04	3,89	6,25
Ir	50,2	1,49	11,4	9,77	3,04	0,575	1,31	2,93	5,50
Ru	49,7	8,14	78,9	17,2	9,11	2,16	11,0	7,60	15,6
Pt	36,9	25,6	48,1	8,60	38,0	99,8	17,5	29,1	115
Pd	21,6	37,6	201	2,67	26,4	80,9	14,6	28,5	20,6
Total PGE	236	74	358	46	82	184	46	72	163
Re	0,312	0,509	2,70	0,022	0,105	0,035	0,103	0,079	0,105
Pd/Ir	0,43	25,2	17,6	0,27	8,70	141	11,2	9,73	3,75
Pt/Ir	0,73	17,2	4,24	0,88	12,5	174	13,4	9,95	20,9

(Continued)

Table 10.14 (Continued).

	[Day et al., 2008], ICP-MS								
	S-133	S-144	S-151	S-154	N-59	N-104	S-171	N-35	N-46
Element	Dunites				Peridotites			Websterites	
La	1,22	1,01	2,19	2,23	0,74	0,7	4,09	5,75	2,89
Ce	2,97	2,56	4,94	5,13	1,76	1,73	9,24	13	6,66
Pr	0,39	0,38	0,7	0,74	0,27	0,28	1,24	1,87	1,01
Nd	1,93	1,87	3,08	3,27	1,31	1,44	5,75	8,74	4,83
Sm	0,46	0,49	0,72	0,77	0,38	0,45	1,33	2,23	1,35
Eu	0,14	0,12	0,21	0,22	0,15	0,15	0,44	0,77	0,52
Gd	0,48	0,53	0,75	0,81	0,49	0,58	1,45	2,66	1,67
Tb	0,08	0,09	0,12	0,13	0,08	0,1	0,23	0,43	0,27
Dy	0,48	0,5	0,69	0,74	0,48	0,6	1,31	2,45	1,58
Ho	0,09	0,1	0,14	0,15	0,1	0,12	0,26	0,47	0,31
Er	0,24	0,26	0,35	0,38	0,25	0,33	0,68	1,22	0,79
Tm	0,04	0,04	0,05	0,06	0,04	0,06	0,11	0,19	0,12
Yb	0,23	0,25	0,33	0,37	0,25	0,31	0,65	1,1	0,72
Lu	0,04	0,04	0,06	0,06	0,04	0,05	0,11	0,18	0,11
Total REE	8,79	8,24	14,3	15,1	6,34	6,90	26,9	41,1	22,8
(La/Yb) _n	3,58	2,73	4,48	4,07	2,00	1,52	4,25	3,53	2,71
Os	5,35	6,55	5,99	6,55	0,693	4,26	3,98	1,83	2,92
Ir	4,46	6,23	6,10	6,61	0,546	1,66	3,28	1,48	1,80
Ru	12,5	15,8	18,9	15,9	8,12	19,2	6,85	5,24	8,10
Pt	51,2	31,1	48,2	68,9	11,2	10,1	11,6	19,4	68,3
Pd	9,26	13,7	104	153	8,85	6,76	49,7	83,1	147
PGE	83	73	183	251	29	42	75	111	228
Re	0,072	0,141	0,234	0,198	0,095	0,135	0,348	1,67	0,119
Pd/Ir	2,08	2,19	17,0	23,2	16,2	4,07	15,2	56,0	81,4
Pt/Ir	11,5	4,99	7,90	10,4	20,5	6,08	3,55	13,1	37,9

(Continued)

Table 10.14 (Continued).

[Day et al., 2008], ICP-MS										
	N-55	N-56	N-100	S-123	N-27	MU-21	MU-76	MX-04a	MX-26a	MX-40a
Element	Websterites		Olivine clinopyroxenites		Gabbro	Gabbro-norites		Chromitites		
La	3,84	2,73	0,27	0,85	5,33	3,53	3,08	1,75	2,02	1,47
Ce	9,06	6,6	0,95	2,16	11,9	8,0	7,0	4,32	4,74	3,36
Pr	1,33	1,02	0,2	0,3	1,7	1,12	1,0	0,66	0,68	0,50
Nd	6,6	5,16	1,29	1,62	7,72	5,16	4,63	3,38	3,23	2,45
Sm	1,84	1,53	0,51	0,46	1,89	1,31	1,17	0,96	0,87	0,68
Eu	0,59	0,5	0,17	0,14	0,66	0,45	0,43	0,31	0,31	0,31
Gd	2,28	1,93	0,8	0,52	2,12	1,54	1,38	1,20	1,03	0,83
Tb	0,38	0,31	0,14	0,09	0,33	0,24	0,23	0,19	0,16	0,13
Dy	2,16	1,85	0,84	0,53	1,93	1,46	1,35	1,12	0,97	0,8
Ho	0,43	0,37	0,17	0,1	0,39	0,2	0,28	0,21	0,19	0,16
Er	1,09	0,95	0,44	0,28	0,99	0,81	0,74	0,56	0,52	0,41
Tm	0,17	0,15	0,07	0,04	0,15	0,12	0,11	0,08	0,08	0,06
Yb	0,98	0,86	0,39	0,28	0,93	0,79	0,72	0,50	0,49	0,38
Lu	0,15	0,13	0,06	0,05	0,15	0,12	0,12	0,07	0,08	0,06
Total REE	30,90	24,09	6,30	7,42	36,19	24,85	22,24	15,31	15,37	11,60
(La/Yb) _n	2,64	2,14	0,47	2,05	3,87	3,02	2,89	2,36	2,78	2,61
Os	1,58	1,47	0,597	1,85	0,197	2,20	1,94	39,9	56,8	201
Ir	1,06	0,927	0,855	0,928	0,131	1,75	1,58	N.d.	N.d.	N.d.
Ru	1,80	1,72	3,08	8,71	0,470	7,03	6,16	N.d.	N.d.	N.d.
Pt	0,388	0,851	26,3	83,2	0,893	14,6	10,2	N.d.	N.d.	N.d.
Pd	0,819	2,84	1,61	4,66	7,21	1,07	2,46	N.d.	N.d.	N.d.
Total PGE	5,65	7,81	32,4	99,3	8,90	26,6	22,3	N.d.	N.d.	N.d.
Re	0,194	0,146	0,018	0,029	0,347	0,33	0,398	0,771	1,75	0,656
Pd/Ir	0,77	3,06	1,88	5,02	55,0	0,61	1,56	N.d.	N.d.	N.d.
Pt/Ir	0,37	0,92	30,8	89,7	6,82	8,34	6,46	N.d.	N.d.	N.d.

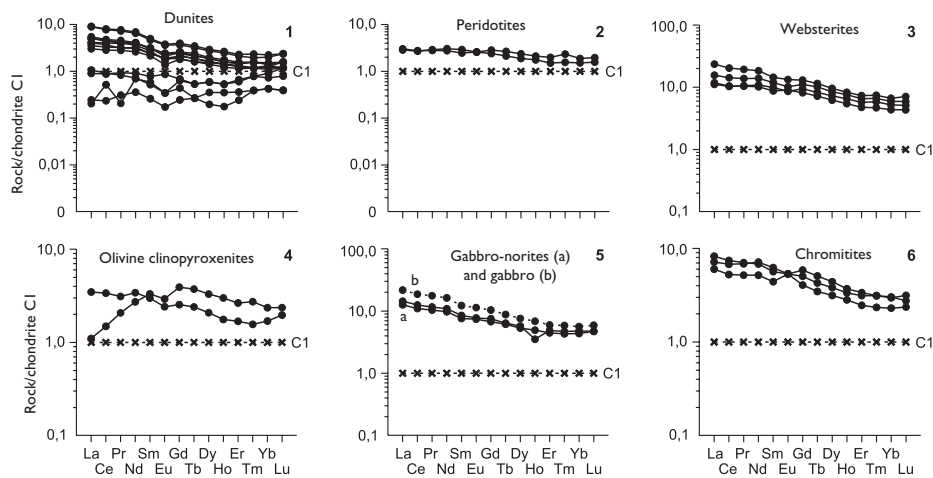


Figure 10.30 Chondrite-normalized REE patterns for dunites (1), peridotites (2), websterites (3), olivine clinopyroxenites (4), gabbro-norites and gabbro (5), and chromitites (6) from Muskox massif (Canada) (data Table 10.14).

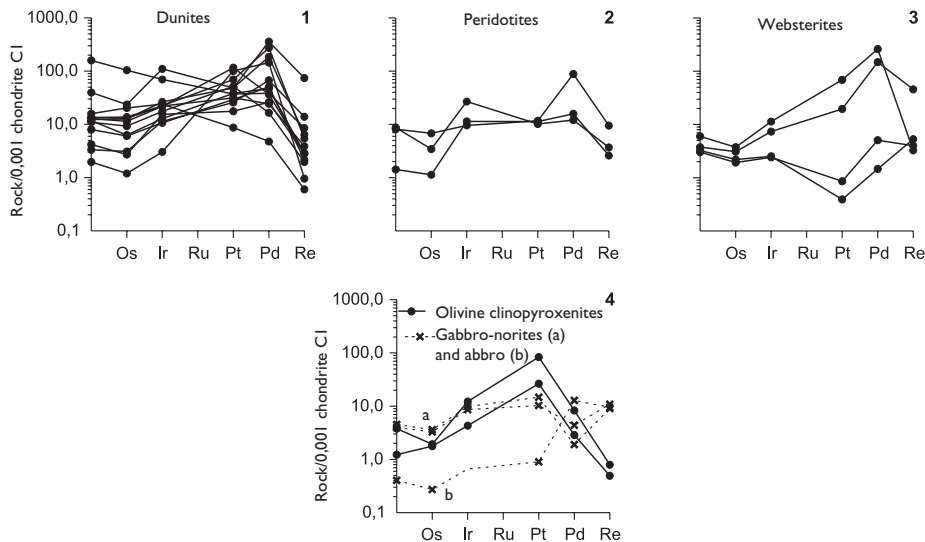


Figure 10.31 Chondrite-normalized PGE patterns for dunites (1), peridotites (2), websterites (3), olivine clinopyroxenites, gabbro-norites and gabbro (4) from Muskox massif (Canada) (data Table 10.14).

to assume that in this case there is an inverse relation between the contents of the elements of these two groups.

Based on the synthesis of available analytical data on PGE contents in different types of ultramafic and mafic rocks Barnes *et al.* [1985] proposed to single out three following mechanisms of fractionation of these elements, which were implemented

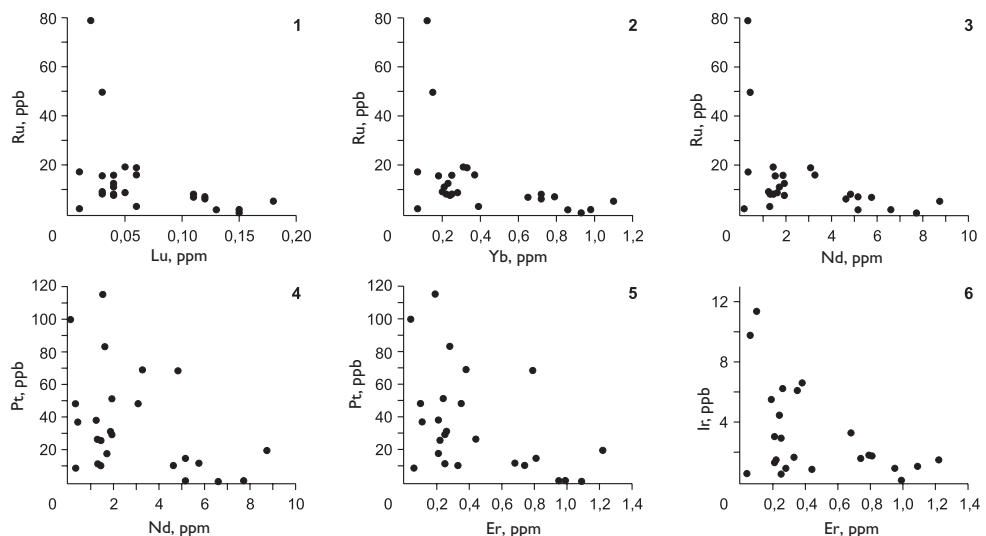


Figure 10.32 Relationship between some REE compositions and some PGE compositions for dunites, peridotites, websterites, olivine clinopyroxenites, gabbro-norites, gabbro and chromitites from Muskox massif (Canada) (data Table 10.14).

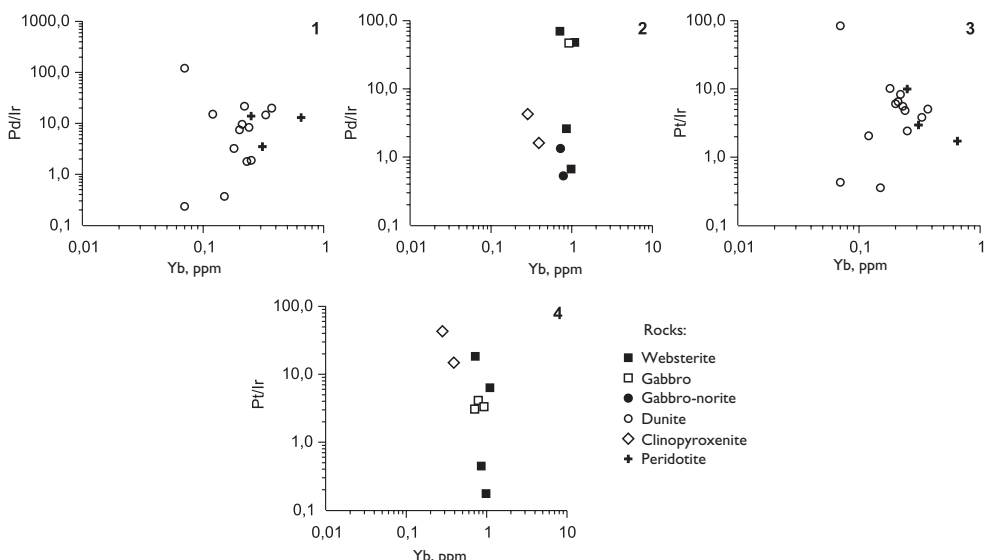


Figure 10.33 Relationship between Yb compositions and Pd/Ir and Pt/Ir parameters values for dunites, peridotites, websterites, olivine clinopyroxenites, gabbro-norites and gabbro from Muskox massif (Canada) (data Table 10.14).

Table 10.15 REE, platinum group elements, Au, and Re (ppm) compositions of dunites from Galmoenan massif (Koryak highland, Kamchatka, Russia).

[Koryak-Kamchatka region., ..., 2002] ICP-MS											
	Dunites										
Element	Gal-2	Gal-7	Gal-9	Gal-11	Gal-12	Gal-13	Gal-15	Gal-16	Gal-17	Gal-18	Gal-19
La	0,099	0,02	0,035	0,02	0,02	0,02	0,324	0,099	0,035	0,098	0,113
Ce	0,132	0,02	0,166	0,02	0,021	0,02	0,406	0,187	0,147	0,177	0,137
Pr	0,011	0,01	0,01	0,01	0,01	0,01	0,033	0,013	0,01	0,017	0,01
Nd	0,034	0,02	0,022	0,044	0,015	0,02	0,02	0,048	0,029	0,128	0,02
Sm	0,02	0,02	0,02	0,02	0,02	0,032	0,02	0,02	0,031	0,033	0,015
Eu	0,02	0,02	0,02	0,02	0,02	0,02	0,02	0,02	0,02	0,02	0,02
Gd	0,02	0,02	0,02	0,02	0,02	0,02	0,02	0,02	0,02	0,029	0,017
Tb	0,01	0,01	0,01	0,01	0,01	0,01	0,01	0,01	0,01	0,01	0,01
Dy	0,02	0,02	0,02	0,015	0,02	0,02	0,02	0,02	0,019	0,02	0,036
Ho	0,01	0,01	0,01	0,01	0,01	0,01	0,01	0,01	0,01	0,01	0,01
Er	0,02	0,02	0,015	0,018	0,02	0,016	0,015	0,02	0,014	0,017	0,038
Tm	0,01	0,01	0,01	0,01	0,01	0,01	0,01	0,01	0,01	0,01	0,01
Yb	0,02	0,027	0,029	0,02	0,02	0,02	0,02	0,02	0,019	0,014	0,04
Lu	0,01	0,01	0,01	0,01	0,01	0,01	0,01	0,01	0,01	0,01	0,01
Total REE	0,44	0,24	0,40	0,25	0,23	0,24	0,94	0,51	0,38	0,59	0,49
Os	0,02	0,038	0,055	0,02	0,024	0,02	0,02	0,022	0,02	0,02	0,02
Ir	0,01	0,01	0,01	0,015	0,01	0,082	0,01	0,01	0,01	0,01	0,01
Ru	0,037	0,02	0,02	0,02	0,025	0,02	0,02	0,02	0,02	0,019	0,02
Rh	0,013	0,016	0,1	0,034	0,01	0,05	0,01	0,01	0,01	0,01	0,01
Pt	0,035	0,367	0,115	0,291	0,097	0,492	0,022	0,083	0,02	0,11	0,021
Pd	0,11	0,489	0,311	0,093	0,17	0,02	0,034	0,09	0,043	0,087	0,02
Total PGE	0,23	0,94	0,61	0,47	0,34	0,68	0,12	0,24	0,12	0,26	0,10
Re	1,497	0,01	0,01	0,01	0,01	0,01	0,045	0,01	0,01	0,496	0,01
Au	0,02	0,02	0,047	0,02	0,063	0,02	0,02	0,02	0,02	0,02	0,02

(Continued)

Table 10.15 (Continued).

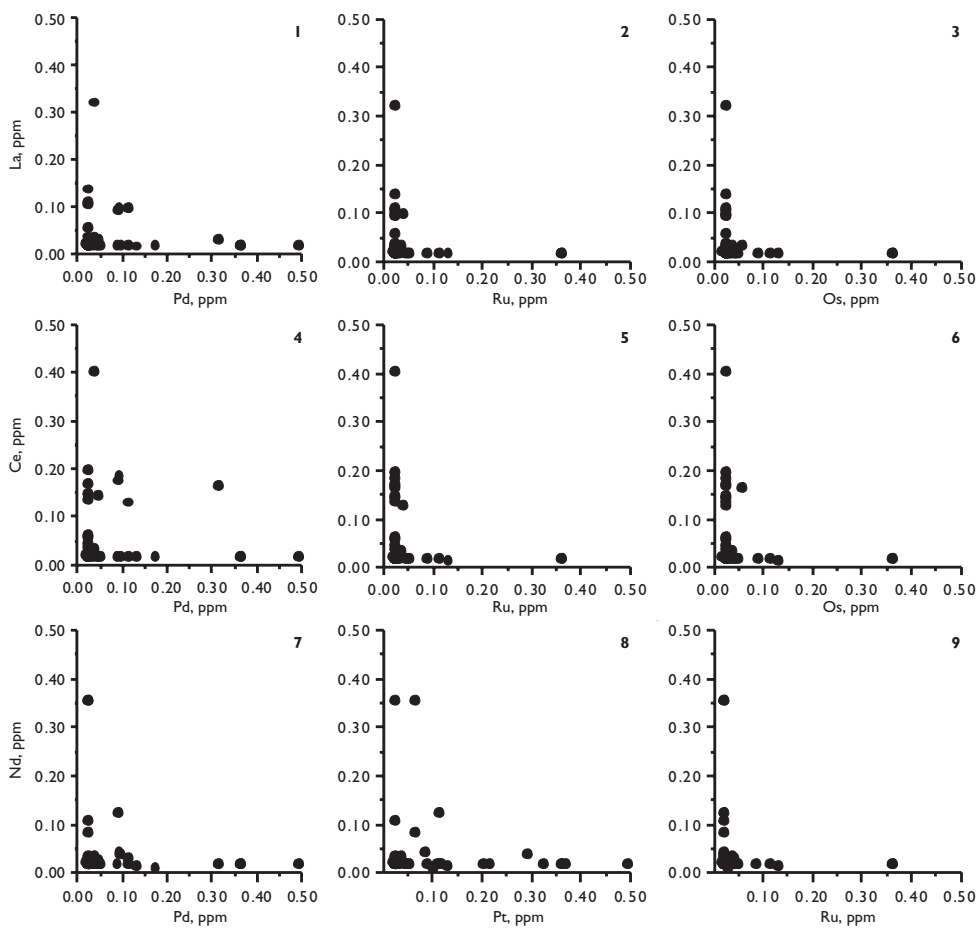


Figure 10.34 Relationship between some REE compositions and some PGE compositions for dunites from Galmoenan massif (Koryak highland, Kamchatka, Russia) (data Table 10.15).

at different magmatic processes: 1) partial melting of mantle sources, 2) crystallization fractionation of magmatic melts, and 3) reallocation at late-magmatic and post-magmatic transformations of rocks. These researchers believed that PGE can not be in the form of isomorphous impurity in the structure of minerals such as olivine and chromite. A similar point of view was later expressed by Borisov [2005], who believed that all PGE are incompatible with the structure of major silicate phases composing the upper mantle – olivine, orthopyroxene, clinopyroxene and garnet. According to Borisov, the values of K_d (silicate mineral/melt) for all PGE are less than 1. He also suggested that, when the degree of partial melting of mantle sources is 20%, an almost full transition into melt of all those phases that originally contained PGE occurs.

Calculations made by McDonough & Sun [1995] showed that the average PGE contents in non-depleted upper mantle are (ppb): Os – 3.4; Ir – 3.2; Ru – 5; Pt – 7.1; Pd – 3.9. Similar estimates for primitive mantle were previously given by Rollinson [1993] (ppb): Os – 3.3; Ir – 3.6; Ru – 4.3; Pt – 7. McDonough & Sun noted that in

basaltic smelting formed during partial melting of non-depleted upper mantle the overall balance of PGE should grow by about half-order compared to the original mantle source, thus to be (ppb): Os – 17; Ir – 16; Ru – 25; Pt – 35; Pd – 20. When extrapolating these values to a lower degree of partial melting of the mantle source, for example, to 10%, the PGE contents in basaltic smelting, obviously, will be (ppb): Os – 8.5; Ir – 8; Ru – 12.5; Pt – 17.5; Pd – 10. To add more, Barnes *et al.* [1985] proposed to divide the PGE group into two subgroups 1) subgroup of iridium (Os, Ir, Ru), and 2) subgroup of palladium (Rh, Pt, Pd); however, as they emphasized, such division should not be considered as an analogy for the separation of REE group into subgroups of LREE and HREE. These researchers also pointed at the possibility of using Pd/Ir parameter as one of the geochemical indicators for discrimination and classification of rocks of ultramafic and mafic composition. They estimated the average values of this parameter and found it increasing from peridotite komatiites (10) to pyroxenite komatiites (30) and further to the basalts of continents and ocean floor (100). Note that in plutonic varieties of ultramafic and mafic rocks the values of this parameter vary over a wider range, for example, in some varieties of samples from mafic-ultramafic Stillwater massif (Montana, USA) the value of Pd/Ir reached 865, while in ore chromitites of ophiolite associations it is close to 0.1.

Taking into account the data mentioned above on the distribution of REE and PGE in ultramafic and mafic rocks, as well as on correlations between the contents of the elements of these two groups, one can assume that in the mantle basaltic smelting that is formed when the degree of partial melting was 20%, the concentration of REE, which are elements that are relatively easy to transform into melt, should be lower than their concentration in basaltic smelting, which arose at about 10% degree of partial melting of a similar in composition mantle source. It is obvious that the increase of degree of partial melting of mantle source was accompanied by a decrease in REE contents of each subsequent portion of melt and simultaneous relative enrichment of this portion with platinum group elements. However, as can be seen from the analytical data mentioned above in this chapter, even at the highest degrees of partial melting and resulting intense depletion of the mantle source by fusible components the ultramafic restites formed as a result of that process were not fully sterilized with respect to REE.

Summarizing the considered materials on REE and PGE relations in different types of rocks and mafic-ultramafic associations, we can conclude that partial melting of non-depleted upper mantle, resulted in the formation of ultramafic restites and basaltic melts complementary to them, in fact was the earliest stage of a multi-stage fractionation and redistribution of PGE and REE within the mantle-crust system. At the same time with increasing of degrees of partial melting of mantle sources in the forming ultramafic restites, as well as in complementary mafic smelting, and then – also in the products of their crystallization, an increase in PGE concentrations was accompanied by a decrease in REE concentrations. As a result, in these rocks we can observe an inverse relation between the contents of the elements from these two groups contrasting in their properties. Apparently, the same type of mechanism could provide a described by some specific examples ‘phenomenon’ of geochemical antagonism between REE and PGE. However, such interpretation of the relations between these elements in ultramafic and mafic rocks can be considered only as a first approximation to the forthcoming solution of these complex petrological and geochemical problems.

This page intentionally left blank

Conclusion

The materials considered in this book on the basic regularities of REE distribution in minor and accessory minerals of ultramafic, mafic and some other types of rocks give grounds to conclude that these minerals are so far an insufficiently studied and, therefore, rarely used additional source of information about the features of their trace element composition and typomorphism that can be used to solve various petrological and geochemical problems. On the basis of the existing materials on the subject we can formulate some relevant, from the author's viewpoint, problems to be solved within this subject matter in the near future.

- A more in-depth study of the basic laws of REE distribution in all varieties of minor and accessory minerals from rocks of ultramafic and mafic composition by using more representative collections of minerals from the reference mafic-ultramafic massifs.
- The implementation of detailed geochemical systematization of minor and accessory minerals from the rocks of ultramafic and mafic composition based on an expanded analytical data on REE distribution in them and the use of multi-parameter computer methods of discrimination.
- To gain more representative and statistically valid estimates of REE distribution coefficients between minor and accessory minerals of ultramafic and mafic rocks and their parent melts, as well as between the accessory and rock-forming minerals on the basis of the results of the study of various experimental systems.
- To continue the studies on crystal-chemical aspects of REE isomorphism in minor and accessory minerals of ultramafic and mafic rocks by using different experimental techniques.
- A more detailed study of REE distribution in the zoned crystals of minor and accessory minerals of the ultramafic and mafic rocks.
- More detail study of forms of finding the chemical and phase composition and the mechanisms of accumulation of nonstructural (isomorphic) REE impurity in the minor and accessory minerals of ultramafic and mafic rocks in order to determine the complex of procedures of sample preparation that can minimize the error of analyses caused by the presence of such unstructured impurity in the mineral samples analyzed.

This page intentionally left blank

References

- Anders, E. & Grevesse, N. (1989) Abundances of the elements: meteoritic and solar. *Geochim. Cosmochim. Acta*, 53, 197–214.
- Ariasova, O.V. & Khasan, Ya.M. (2007) Large scale fractionation of rare earth elements in mantle of cratons. *Reports of the Ukrainian National Academy of Science*, 8, 110–115 (in Ukr.)
- Asavin, A.M. (1994) Distribution Zr, Hf, Nb, Ta, Th, U in equilibriums of mineral – melt (revive). *Gekhimiya*. 10, 1398–1417.
- Aschepkov, I.V., Vladykin, N.V., Nikolaeva, I.V. et al. (2004) About mineralogy and geochemistry of mantle inclusions and structure of mantle columns kimberlite pipe Yubileynaya, the Alakitsky field, Yakutia. *Doklady of the Russian Academy of Sciences*, 395 (4), 1–7 (in Rus.).
- Ashcepov, I.V., Vladykin, N.V., Pokhilenko, N.P., Logvinova, A.M., Afanasiev, V.P., Kostrovitskii, S.I., Alyanova, N.V., Stegnitsky, Yu.B., Khemel'nikova, O.S. & Rotman, A.Y. (2007) Variations of ilmenite compositions from Yakutian Kimberlites and problems of their origin. Napolj-Irkutsk. 2007. Irkutsk: Publishing House of the Institute of geography of Siberian branch of Russian Academy of Sciences, 71–90.
- Avsiuk, Yu.N. (2002) The preface. *Disputable aspects of tectonics of plates and possible alternatives*. M: Publishing House of Institute of Physics of the Earth of Russian Academy of Sciences, 3–4 (in Rus.).
- Bakirov, A.B. (1964) Some questions of a metamorphism of the Atbashinsky ridge. *Questions Precambrian stratigraphy and the lower Palaeozoic of Kirghizia*. Frunze: Publishing House of Academy of Sciences of the Kirghiz Soviet Socialist Republic, 54–64 (in Rus.).
- Balykin, P.A., Krivenko, A.P., Konnikov, E.G., Lesnov, F.P. et al. (1991) Petrology of post-harzburgite intrusions of Kempirsay-Hkabarninsky ophiolitic association (South Urals). Sverdlovsk: Publishing House of Institute of Institute of Geology and Geochemistry of Ural Branch of Academy of Sciences of USSR, 160 p. (in Rus.).
- Balykin, P.A., Polyakov, G.V., Hanski, E. et al. (2004) The Late Permian komatiite-basalt complex in the Song Da Rift, North-Western Vietnam. *J. Geology. Series B*, 23, 52–64.
- Barnes, S.-J., Naldrett, A.J. & Gorton, M.P. (1985) The origin of fractionation of platinum-group elements in terrestrial magmas. *Chemical Geology*, 53, 303–323.
- Barnes, S.-J., Lesher, C.M. & Keays, R.R. (1995) Geochemistry of mineralized and barren komatiites from the Perseverance nickel deposit, Western Australia. *Lithos*, 34, 209–234.
- Barth, M.G., Rudnick, R.L., Horn, I. et al. (2002) Geochemistry of xenolithic eclogites from Western Africa. Part 2: Origins of high MgO eclogites. *Geochim. Cosmochim. Acta*, 66, 4325–4345.
- Batanova, V.G., Pertsev, A.N., Kamenetsky, V.S., Ariskin, A.A., Mochalov, A.G. & Sobolev, A.V. (2011) Crustal evolution of island-arc ultramafic magma: Galmoenan pyroxenites-dunite plutonic complex, Koryak highland (Far East Russia). *J. Petrology*, 46 (7), 1345–1366.

- Baumgartner, L.P. & Skora, S. (2006) Modeling diffusion limited uptake of trace elements by eclogites garnets. *ICP Inf. Newslet.*, 32 (1), 36.
- Bea, F., Montero, P. & Ortega, M.A. (2006) LA-ICP-MS evaluation of Zr reservoirs in common crustal rocks: implications for Zr and Hf geochemistry, and zircon-forming processes. *Canadian Mineralogist*, 44, 693–714.
- Beattie, P. (1993) On the occurrence of apparent non-Henry's law in experimental partitioning studies. *Geochim. Cosmochim. Acta*, 57 (1), 47–55.
- Belousova, E.A., Griffin, W.L. & O'Reilly, S.Y. (1998) Trace element composition and catodoluminescence properties of kimberlite zircons. *Proc. 7th International Kimberlite Conference. Extended Abstracts*. Cape Town, 67–69.
- Belousova, E.A., Griffin, W.L., O'Reilly, S.Y. & Fisher, N.I. (2002) Apatite as indicator mineral for mineral exploration: trace element compositions and their relationship to host rock type. *J. Geochemical Exploration*, 76, 45–69.
- Berryman, A.K., Stienhofer, J., Shee, S.R. et al. (1999) The discovery and geology of the Timber Creek kimberlites, northern territory, Australia. *Proc. 7th Intern. Kimberlite Conf. Extended Abstracts*. Cope Town, 30–39.
- Betekhtin, A.G. (1956) Mineralogy course. Moscow: Publishing House of literature on geology and protection of bowels. 1956. 558 p. (in Rus.).
- Bingen, B., Austrheim, H., Whitehouse, M.J. & Davis, W.J. (2004) Trace element signature and U-Pb geochronology of eclogites-facies zircon, Berge Arcs, Caledonides of Western Norway. *Contrib. Mineral. Petrol.*, 147, 671–683.
- Blundy, J.D., Robinson, J.A.C. & Wood, B.J. (1998) Heavy REE are competitive in clinopyroxene on the spinel lherzolite solidus. *Earth Planet. Sci. Lett.* 160, 493–504.
- Bocchio, R., DeCapitani, L., Ottolini, L. & Cella, F. (2000) Trace element distribution in eclogites and their clinopyroxene/garnet pair: a case study from Soazza (Switzerland). *Europ. J. Miner.* 12 (Iss. 1), 147–161.
- Bodinier, J.-L., Guiraud, M., Fabries, J. et al. (1987) Petrogenesis of layered pyroxenites from the Lherz, Freychinéde and Prades ultramafic bodies (Ariège, French Pyrenees). *Geochim. Cosmochim. Acta* 51 (2), 279–291.
- Borisenko, L.F. & Liapunov, S.M. (1980) About distribution La, Ce, Sm, Eu, Tb, Yb and Lu in an ilmenite of various magmatic formations. *Doklady of Academy of Sciences of USSR*. 253 (2), 454–457 (in Rus.).
- Borisov, A.A. (2005) Crystallization and stability of alloys of precious metals in magmatic process. *Geology of ore deposits*, 47 (6), 516–523 (in Rus.).
- Borodina, E.V., Egorova, V.V. & Izokh, A.E. (2004) Petrology of Ordovician collisional aperidotite-gabbro of files. *Geologia i geofizika*, 45 (9), 1074–1091 (in Rus.).
- Brugmann, G.E., Arndt, N.T., Hofmann, A.W. & Tobischall, H.J. (1987) Noble metal abundances in komatiite suites from Alexo, Ontario and Gorgona Island, Columbia. *Geochim. Cosmochim. Acta*, 51, 2159–2169.
- Burgess, S.R. & Harte, B. (1998) Tracing lithosphere evolution through the analysis of heterogeneous G9/G10 garnets in peridotite xenoliths. *Proc. 7th International Kimberlite Conference. Extended Abstracts*. Cape Town, 122–126.
- Caporuscio, F.A. & Smith, J.R. (1990) Trace element crystal chemistry of mantle eclogites. *Contrib. Miner. Petrol.*, 105 (5), 550–561.
- Cesbron, F., Onenstetter, D., Blanc, P. & Roner, O. (1993) Incorporation de terres rares dans des zircons de synthèse: Etude par catodoluminescence. *C. R. Acad. Sci. Ser. 2*, 316 (9) 1231–1238.
- Chalapathi, Rao, N.V., Gibson, S.A., Pyle, D.M. & Dicken, A.P. (2004) Petrogenesis of proterozoic lamproites and kimberlites from Cuddapah Basin and Dharwar craton, Southern India. *J. Petrol.*, 45 (5), 907–948.

- Cherniak, D.J. (1998) Rare earth element and gallium diffusion in yttrium garnet. *Phys. Chem. Miner.*, 26, 156–163.
- Cherniak, D.J., Hanchar, J.M. & Watson, E.B. (1997) Rare-earth diffusion in zircon. *Chemical Geology*, 134, 289–301.
- Cox, K.G., Bell, J.D. & Pankhurst, R.J. (1982) The interpretation of igneous rocks. Moscow: Publishing House Mir. 416 p. (in Rus.).
- Davies, G. & Tredoux, M. (1985) The platinum-group element and gold contents of the marginal rocks and sills of Bushveld complex. *Economic Geology*, 80, 838–848.
- Dawson, J.B. (1983) Kimberlites and xenoliths in them. Moscow: Publishing House Mir, 400 p. (in Rus.).
- Dawson, J.B., Smith, J.V. & Steele, I.M. (1994) Trace-element distribution between coexisting perovskite, apatite and titanites from Oldoinyo Lengai, Tanzania. *Chem. Geol.* 117 (Iss. 1–4), 285–290.
- Day, J.M.D., Pearson, D.G. & Hulbert, L.J. (2008) Rhenium-osmium isotope and platinum-group element constraints on the origin and evolution of 1,27 Ga Muskox layered intrusion. *J. Petrol.*, 49 (7), 1255–1295.
- Demaiffe, D., El Fadili, S. & Andre, L. (1998) Geochemical and isotopic (Sr, Nd) study of eclogite nodules from the Mbuji Mayi kimberlite, Kasai, Congo. *Proc. 7th International Kimberlite Conference. Extended Abstracts*. Cape Town, 190–192.
- Dmitrenko, G.G., Lesnov, F.P., Makhorkina, T.I. et al. (1991) The platinum minerals in chromitites from Naransky massif (Western Mongolia). *Doklady of Academy of Sciences of USSR*, 317 (5), 1220–1222 (in Rus.).
- Downes, H., McDonald, R., Upton, B.G.J. et al. (2004) Ultramafic xenoliths in the Bearpaw Mountains, Montana, USA: Evidence for multiple metasomatic events in lithospheric mantle beneath the Wyoming craton. *J. Petrol.* 45 (8), 1631–1662.
- Drugova, G.M. & Skublov, S.G. (2004) Distribution of rare earth elements in garnets, clinopyroxenes, amphiboles and biotites of metamorphic rocks. *Proceedings of the All-Russian Society mineralogy Society*, 133 (2), 47–58 (in Rus.).
- Edwards, R.L. & Wasserburg, G.J. (1985) The age and emplacement of obducted oceanic crust in the Urals from Sm-Nd and Rb-Sr systematics. *Earth Planet. Sci. Lett.*, 72, 389–404.
- Egging, S.M., Rudnick, R.L. & McDonough, W.F. (1998) The composition of peridotites and their minerals: a laser-ablation ICP-MS study. *Earth Planet. Sci. Lett.*, 154, 53–71.
- Egorova, V.V. (2005) Basic melt crystallization in deep magma chambers as an example gabbroic xenoliths and intrusions of the West Sangilen. *Abstract of Dissertation. PhD geology and mineralogy*. Novosibirsk: Publishing House of Institute geology and mineralogy Siberian branch of Russian Academy of Sciences. 22 p. (in Rus.).
- Evensen, N.M., Hamilton, P.J. & O'Nions, R.K. (1978) Rare earth abundances in chondritic meteorites. *Geochim. Cosmochim. Acta*, 42, 1199–1212.
- Exley, R.A. & Smith, J.V. (1982) The role of apatite in mantle enrichment processes and in the petrogenesis of some alkali basalt suites. *Geochim. Cosmochim. Acta*, 46 (8), 1375–1384.
- Fershtater, G.B. & Bea, F. (1996) Geochemical typing of Uralian ophiolite. *Geochemistry*, 3, 195–218 (in Rus.).
- Fedorovich, J.S., Jain, J.C. & Kerrich, R. (1995) Trace element analysis of garnet by laser-ablation microprobe ICP-MS. *Canadian Mineralogist*, 33, 469–480.
- Fedotova, A., Bibikova, E.V. & Simakin, S.G. (2008) Geochemistry of zircons (microprobe data) as indicators of mineral genesis at geochronological researches//*Geokhimya*, 9, 980–997 (in Rus.).
- Fershtater, G.B. (2000) Anatetic granites and the composition of the crust of the Ural Paleozoic orogen. *Petrography at XXI Century frontier: Results and Prospects*, 2. Syktyvkar: Publishing House Geoprint, 345–348 (in Rus.).

- Fershtater, G.B. (2004) On the nature of the Silurian-Early Devonian mafic-ultramafic intrusions associated with the ophiolite of the Southern Urals. *Lithosphere*, 4, 3–29 (in Rus.).
- Fleet, A.J. (1984) Aqueous and sedimentary geochemistry of the rare earth elements. *Rare earth element geochemistry* (Ed. P. Henderson). Amsterdam: Publishing House Elsevier, 343–373.
- Frantsesson, E.V. (1968) Petrology of kimberlite. Moscow: Publishing House Nedra, 150 p. (in Rus.).
- Frey, F.A., Haskin, L.A. & Haskin, M.A. (1971) Rare earth abundances in some ultramafic rocks. *J. Geophys. Res.*, 76 (8), 2057–2070.
- Garanin, V.K. (2006) Mineralogy of kimberlites and related rocks from diamondiferous provinces of Russia in relation to their genesis and searches. Moscow: Moscow State University. Department of Mineralogy. 36 p. (in Rus.).
- Garrido, C.J. & Bodinier, J.-L. (1999) Distribution of trace elements in minerals from anhydrous spinel peridotites and websterites from the Ronda peridotite: implications for the nature of LIL, REE and HFSE reservoirs in the subcontinental lithosphere mantle. *Mineralogical Magazine*. 62 A, 498–499.
- Gaspar, M., Knaak, C., Meinert, L.D. & Moretti, R. (2008) REE in skarn systems: A LA-ICP-MS study of garnets from the Crown Jewel gold deposit. *Geochim. Cosmochim. Acta*, 72, 185–205.
- Gladney, E.S., Jones, E.A., Nickell, E.J. & Roelandts, I. (1991) 1988 Compilation of Elemental Concentration Data for USGS DTS-1, G-1, PCC-1 and W-1. *Geostandards Newsletter*, 15, 199–396.
- Golubeva, I.I., Afon'kin, M.M. & Makhlaev, L.V. (2007) Metamorfogenic ilmenite in parashists of Harbeysky complex (Polar Ural Mountains). *Mineralogy of Ural -2007*. Miass: Publishing House of Institute mineralogy of Ural branch of the Russian Academy of Sciences, 156–160 (in Rus.).
- Green, T.H. (1994) Experimental studies of trace-element partitioning applicable to igneous petrogenesis – Sedona 16 years later. *Chem. Geol.*, 117, 1–36.
- Green, T.H. & Pearson, N.J. (1987) An experimental study Nb and Ta partitioning between Ti-rich minerals and silicate liquids at high pressure and temperature. *Geochim. Cosmochim. Acta*, 51, 55–62.
- Grieco, G., Ferrario, A., Von Quadt, A. et al. (2001) Zircon-bearing chromitites of the phlogopite peridotite of Finero (Ivrea zone, Southern Alps): Evidence and geochronology of metasomatized mantle slab. *J. Petrol.*, 42, 89–101.
- Griffin, W.L. & Brueckner, H.K. (1985) REE and Rb-Sr and Sm-Nd studies of Norwegian eclogites. *Chem. Geol.*, 52 (2), 249–271.
- Gromet, L.P. & Silver, L.T. (1983) Rare earth element distributions among minerals in a granodiorite and their petrogenetic implications. *Geochim. Cosmochim. Acta*, 47 (5), 925–939.
- Hamilton, M.A., Pearson, D.G., Stern, R.A. & Boyd, F.R. (1998) Constraints on MARID petrogenesis: SHRIMP II U-Pb zircon evidence for pre-eruption metasomatism at Kampfersdam. *Proc. 7th International Kimberlite Conference. Extended Abstracts*. Cape Town, 296–298.
- Hanchar, J.M., Finch, R.J., Hoskin, P.W.O. et al. (2001) Rare earth elements in synthetic zircon. Part 1: Synthesis and rare earth element and phosphorus doping. *American Mineralogist*, 86 (5–6), 667–680.
- Hanski, E., Walker, R.J., Huhma, H. et al. (2004) Origin of Permian-Triassic komatiites, north-western Vietnam. *Contrib. Mineral. Petrol.*, 147, 453–469.
- Harris, J.W., Stachel, T., Leost, J. & Brey, G.P. (2004) Peridotitic diamonds from Namibia: constraints on the composition and evolution of their mantle source. *Lithos*, 77 (1–4), 209–223.
- Harrison, W.J. (1981) Partitioning of REE between minerals and coexisting melts during partial melting of a garnet lherzolite. *American Mineralogist*, 66, 242–259.

- Harte, B. & Kirkley, M.B. (1997) Partitioning of trace elements between clinopyroxene and garnet: data from mantle eclogites. *Chem. Geol.*, 136, 1–24.
- Haskin, L.A. & Frey, F.A. (1966) Dispersed and not-so-rare earths. *Science*, 152, 299. (cit.: [Masuda, 1967]).
- Hauri, E.H., Wagner, T.P. & Grove, T.L. (1994) Experimental and natural partitioning of Th, U, Pb and other trace elements between garnet, clinopyroxenes and basaltic melts. *Chem. Geol.*, 117, 149–166.
- Hickmott, D.D. & Shimizu, N. (1990) Trace element zoning in garnet from the Kwoiek Area, British Columbia: disequilibrium partitioning during garnet growth? *Contrib. Mineral. Petrol.*, 104 (6), 619–930.
- Hinton, R.W. & Upton, G.J. (1991) The chemistry of zircon: variation within and between large crystals from syenite and alkali basalt xenoliths. *Geochim. Cosmochim. Acta*, 55 (11), 3287–3302.
- Hirose, K. & Kawamoto, T. (1995) Hydrous partial melting of lherzolite at 1 GPa: The effect of H₂O on the genesis of basaltic magmas. *Earth Planet. Sci. Lett.*, 133, 463–473.
- Hoal, K.E.O., Hoal, B.G., Erlank, A.J. & Simizu, N. (1994) Metasomatism of the mantle lithosphere recorded by rare earth elements in garnets. *Earth Planet. Sci. Lett.*, 126, 303–313.
- Hoskin, P.W.O. & Ireland, T.R. (2000) Rare element chemistry of zircon and its use as provenance indicator. *Geology*, 28, 627–630.
- Hoskin, P.W.O., Kinny, P.D., Wyborn, D. & Chappell, B.W. (2000) Identifying accessory mineral saturation during differentiation in granitoid magmas: an integrated approach. *J. Petrol.*, 41 (9), 1365–1396.
- Inoue, T., Rapp, R., Zhang, J. et al. (2000) Garnet fractionation in a hydrous magma ocean and the origin of Al-depleted komatiites: melting experiments of hydrous pyrolite with REEs at high pressure. *Earth Planet. Sci. Lett.*, 177, 81–87.
- Ionov, D.A., Ashchepkov, I.V., Stosch, H.-G. et al. (1993) Garnet peridotite xenoliths from the Vitim field, Baikal region: the nature of the garnet-spinel peridotite transition zone in the continental mantle. *J. Petrol.*, 34 (6), 1141–1175.
- Irving, A.J. & Frey, F.A. (1978) Distribution of trace elements between garnet megacrysts and host volcanic liquids of kimberlitic to rhyolitic compositon. *Geochim. Cosmochim. Acta*, 42, 771–787.
- Irving, A.J. & Frey, F.A. (1984) Trace element abundances in megacrysts and their host basalts: Constraints on partition coefficients and megacrysts genesis. *Geochim. Cosmochim. Acta*, 48, 1202–1221.
- Izokh, A.E., Smirnov, S.Z., Egorova, V.V., Chang, Tuan Anh, Kovayzin, S.V., Ngo, Thi Phuong & Kalinina, V.V. (2010) The condition of formation of sapphire and zircon in the areas of alkali-basalt volcanism in Central Vietnam//Geologia i Geofizika, 51 (7), 925–943 (in Rus.).
- Jacob, D.E. & Foley, S.F. (1998) Evidence for Archean ocean crust with island arc signature from diamondiferous eclogites xenoliths. *Proc. 7th International Kimberlite Conf. Extended Abstracts*. Cape Town, 358–360.
- Jacob, D.E. & Mattey, D.P. (1998) Geochemistry of layered kyanite-bearing eclogites from the Roberts Victor Mine, South Africa. *Proc. 7th International Kimberlite Conference Extended Abstracts*. Cape Town, 364–365.
- Jacob, D.E., Kjarsgaard, B. & Horn, I. (1998) Trace element concentrations laser ablation ICP-MS in subcalcic garnets from Saskatchewan and Somerset island, Canada. *Proc. 7th International Kimberlite Conference Extended Abstracts*. Cape Town, 361–363.
- Jahn, B., Gruau, G. & Glikson, A.Y. (1982) Komatiites of the Onverwacht group, South Africa: REE geochemistry, Sm/Nd age and mantle evolution. *Contrib. Mineral. Petrol.*, 80, 25–40.
- Jang, Y.D. & Naslund, H.R. (2002) Major and trace element variation in ilmenite in the Skaergaard intrusion: petrologic implication. *Chem. Geol.*, 193, 109–125.

- Johnson, K.T.M. (1998) Experimental cpx/and garnet/melt partitioning of REE and other trace elements at high pressures: petrogenetic implications. *Mineralogical Magazine*, 58 A, 454–455.
- Jolliff, B.L., Papike, J.J. & Shearer, C.K. (1989) Inter and intra-crystal REE variation in apatite from the Bob Ingersoll pegmatite, Black Hill, South Dakota. *Geochim. Cosmochim. Acta*, 53, 429–441.
- Jones, R.A. (1987) Strontium and neodimium isotopic and rare earth element evidence for the genesis of megacrysts in kimberlites of Southern Africa (Ed. P.H. Nixon). *Mantle xenoliths*, Wiley, Chechester, 711–724.
- Jones, A.P. & Wyllie, P.J. (1984) Minor elements in perovskite from kimberlites and distribution of the rare elements: an electron probe study. *Earth Planet. Sci. Lett.*, 69, 128–140.
- Karipi, S., Tsikouras, B. & Hatzipanagiotou, K. (2006) The petrogenesis and tectonic setting of ultramafic rocks from Iti and Kallidromon mountains, continental central Greece: vestiges of the Pindos ocean. *Canadian Mineralogist*, 44 (Part 1), 267–287.
- Kaulina, T.V. (2010) Formation and transformation of zircon in polymetamorphic complexes. Apatity: Publishing House of Geological Institute of Kola Science Centre of the Russian Academy of Sciences. 145 p. (in Rus.).
- Kay, S.M. & Gordillo, C.E. (1994) Pocho volcanic rocks and the melting of depleted continental lithosphere above a shallowly dipping subduction zone in the central Andes. *Contrib. Mineral. Petrol.*, 117 (10), 25–44.
- Khazan, Ya.M. & Ariasova, O.V. (2007) Spatial fractionation of REE in the carton's mantle: analysis of observes, model and connection with kimberlite forming. *Geofizicheskiy zhurnal*, 29 (6), 45–63 (in Rus.).
- Koryak-Kamchatka region – New platinumiferous province of Russia (2002) (Sci. Eds. V.P. Zaytsev, A.F. Litvinov, E.A. Landa). Sanct-Peterburg. Publishing House “Kartfabrika VSEGEI”. 383 p. (in Rus.).
- Krasnobaev, A.A., Bea, F. & Fershtater, G.B. (2004) Age, morphology and geochemical characteristics of zircons from mafic rocks of the Urals (ophiolites and Platinum-bearing belt) and the associated acid rocks. *Geology and metallogeny of ultramafic-mafic and granitoid intrusive associations of folded regions*. Ekaterinburg: Publishing House of Institute Geological and Geochemistry of Ural branch of the Russian Academy of Sciences, 211–216 (in Rus.).
- Krivenko, A.P., Podlipskii, M.Yu. & Agafonov, L.V. (2004) Petrology and mineralogy of the ultramafic rocks from Ergak massif. *The status and exploration of natural resources of Tuva and adjacent regions of Central Asia. Geoeocology of the environment and society*. Kyzyly: Publishing House of Tuvian Institute of for exploration of natural resources of Siberian branch of the Russian Academy of Sciences, 61–77 (in Rus.).
- Lazarenkov, V.G., Balmasova, E.A., Vaganov, P.A. & Onischina, N.M. (1989) The distribution of precious metals and rare earth elements in the ore chromitite from Burakovo-Aganozersky massif. *Newsletter of Leningradsky State University. Series 7, Issue 4*, 68–70 (in Rus.).
- Lehtonen, M. (2005) Rare earth characteristics of pyrope garnets from the Kaavi-Kuopio kimberlites – implications for mantle metasomatism//*Bull. Geol. Soc. Finl.* 77 (1), 31–47.
- Lesher, C.M. & Arndt, N.T. (1995) REE and Nd isotope geochemistry, petrogenesis and volcanic evolution of contaminated komatiites at Kambalda, Western Australia. *Lithos*, 34 (3–4), 127–157.
- Lesnov, F.P. (1979) On the mafic-ultramafic associations of Mongolia. *Geology and Magmatism of Mongolia*. Moscow: Publishing House Nauka, 156–157 (in Rus.).
- Lesnov, F.P. (1981) Structural and genetic relationships ultramafic rocks and gabbroid in the ophiolite belts of Mongolia. *Questions of magmatism and metallogeny of the Mongolian People's Republic*. Novosibirsk: Publishing House Nauka, Siberian branch, 62–71 (in Rus.).
- Lesnov, F.P. (1982) Naransky polygenic mafic-ultramafic pluton (Western Mongolia). *Ultramafic association of folded regions. Issue 1*. Novosibirsk: Publishing House of Institute geology and geophysics of Academy of Sciences of USSR, 58–95 (in Rus.).

- Lesnov, F.P. (1986) Petrochemistry of polygenic mafic-ultramafic plutons of folded regions. Novosibirsk: Publishing House Nauka. Siberian branch, 136 p. (in Rus.).
- Lesnov, F.P. (1993) Regularities in the distribution of platinum group elements in the Naran polygenic mafic-ultramafic pluton (Western Mongolia). *Ultramafic association of folded regions. Issue 7.* Novosibirsk: Publishing House of Institute geology and geophysics of Academy of Sciences of USSR, 6–35 (in Rus.).
- Lesnov, F.P. (2001) On the trend of the distribution coefficients of rare earth elements between garnet and melt. *Petrology of igneous and metamorphic complexes*, Vol. 2. Tomsk: Publishing House of Tomsk State University, 65–70 (in Rus.).
- Lesnov, F.P. (2002) State and problems of research in the field of geochemistry of rare earth elements in kimberlites. *Petrology of igneous and metamorphic complexes*. Tomsk: Publishing House of Tomsk State University, 126–133 (in Rus.).
- Lesnov, F.P. (2003a) Role of rare earth and platinum group elements in the problem of typing ultramafic-mafic formations. *Modern Problems formation analysis, petrology and igneous rocks of the ore.* Novosibirsk: Publishing House “Geo”, Siberian Branch. 195–196 (in Rus.).
- Lesnov, F.P. (2003b) Role of rare earth elements in studying the genesis of kimberlite. *New Ideas in Earth Sciences: Proceedings of the 6-th International Conference*, Vol. 2. Moscow: Publishing House of MGGRU, 32 (in Rus.).
- Lesnov, F.P. (2003c) The correlation between platinum and rare earth elements in mafic-ultramafic rocks as a possible criterion for their typing. *Geochemistry of igneous rocks. Proceedings of the 21-th All-Russian Seminar-School “Alkaline Magmatism of the Earth”.* Apatity: Publishing House of Geological Institute of Kola Science Centre of the Russian Academy of Sciences, 101–102 (in Rus.).
- Lesnov, F.P. (2005) Regularities in the distribution of rare earth elements in zircons (review). *Petrology of igneous and metamorphic complexes*. Tomsk: Publishing House of Tomsk State University, 105–111 (in Rus.).
- Lesnov, F.P. (2006) On the distribution of rare earth elements in titanites (short review). *Metallogenesis of ancient and modern ocean-2006. Formation and development of deposits in uneven ocean margins.* Miass: Publishing House of Institute of mineralogy of Ural branch of Russian Academy of Sciences, 291–295 (in Rus.).
- Lesnov, F.P. (2007) Rare Earth Elements in ultramafic and Mafic Rocks and their minerals. Main types rocks. Rock-forming minerals. Novosibirsk: Publishing House “Geo”, 404 p. (in Rus.).
- Lesnov, F.P. (2010) Rare Earth Elements in ultramafic and mafic rocks and their minerals. Main types rocks. Rock-forming minerals. Leiden: Publishing House CRC. Taylor & Francis Group, 580 p.
- Lesnov, F.P. (2006) The correlation between rare earth and platinum group elements as reflection of partial melting process of mantle resource at forming of mafic and ultramafic rocks. *Ophiolite: geology, petrology, metallogenesis, geodynamics. Proceedings of the International Scientific Conference.* Yekaterinburg. Publishing House of Institute geology and geochemistry. Ural branch of Russian Academy of Sciences, 209–213 (in Rus.).
- Lesnov, F.P. (2009) Contrast fractionation of rare earth and platinum group elements at partial melting and depletion of upper mantle. *Geology and mineral resources of European North-East of Russia*, Vol. 2. Syktyvkar: Publishing House of Institute geology. Komi Science Center. Ural branch of Russian Academy of Sciences, 345–347 (in Rus.).
- Lesnov, F.P. (2011) The isomorphism of rare earth elements in zircons and conditions of their crystallization. *Mineralogical perspectives-2011.* Syktyvkar: Publishing House of Institute of Geology of Komi Science center of Russian Academy of Sciences, 92–94.
- Lesnov, F.P. & Balykin, P.A. (2005) On the additional evidences of “antagonism” of platinum and rare earth elements in igneous rocks. *Precious and Rare Metals of Siberia and the*

- Far East. Irkutsk: Publishing House of Institute of geochemistry of Siberian branch of Russian Academy of Sciences, 17–19 (in Rus.).
- Lesnov, F.P. & Balykin, P.A. (2007) Distribution of rare earth and platinum group elements in rocks of Kokpektinsky dunite-troctolite-gabbro massif (Southern Urals). *Ultrabasite-mafic complexes of folded regions: Proceedings of the International conference*. Irkutsk: Publishing house of Irkutsk State technical University, 192–196 (in Rus.).
- Lesnov, F.P. & Gora, M.P. (1993) On the chemical composition of chrome spinels from Dovrensky mafic-ultramafic pluton (Northern Baikal region). *Ultramafic association of folded regions. Issue 7*. Novosibirsk: Publishing House of United Institute of geology, mineralogy and geophysics of Siberian branch of the Russian Academy of Sciences, 86–100 (in Rus.).
- Lesnov, F.P. & Gora, M.P. (1998) Geochemistry of rare earth elements in coexisting pyroxenes of different types of mafic-ultramafic rocks. *Geokhimiya*, 9, 899–918 (in Rus.).
- Lesnov, F.P. & Oydup, Ch.K. (2002) On the “antagonism” of palladium and platinum with rare earth elements in rocks of ultramafic-mafic massifs. *Geology, genesis and questions of development of complex deposits of precious metal. Proceedings of the All-Russian Symposium*. Moscow: Publishing House of IGEM of Russian Academy of Sciences, 48–52 (in Rus.).
- Lesnov, F.P. & Simonov, V.A. (1989) Chromitites of Naransky mafic-ultramafic massif in Western Mongolia (chemical composition and gas components). *Ultramafic association of folded regions. Issue 5*. Novosibirsk: Publishing House of Institute of geology and geophysics of Siberian branch of Academy of Sciences of USSR, 65–85 (in Rus.).
- Lesnov, F.P. & Tsimbalist, V.G. (1983) Distribution of platinum group elements and gold in mafic-ultramafic associations of Mongolia. *Ultramafic association of folded regions. Issue 2*. Novosibirsk: Publishing House of Institute of geology and geophysics of Siberian branch of Academy of Sciences of USSR, 66–71 (in Rus.).
- Lesnov, F.P., Bobrov, V.A. & Palesskii, S.V. (2004a) On the rare-earth composition of the ilmenites from rocks of Tigrovyy mafic-ultramafic massif (Sikhote-Alin' ridge). *Petrology of igneous and metamorphic complexes*. Tomsk: Publishing House of Tomsk State University, 51–58 (in Rus.).
- Lesnov, F.P., Lomonosova, E.I., Goncharenko, A.I. et al. (1995) Distribution of rare earth elements in olivines from ophiolite associations. *Geologiya i Geofizika*, 36 (2), 50–60 (in Rus.).
- Lesnov, F.P., Mongush, A.A. & Mel'gunov, M.S. (2004c) On some features of the geochemistry of platinum group elements and rare earth elements in rocks from the ultramafic-mafic massifs (Tuva). *The state and exploration of natural resources of Tuva and adjacent regions of Central Asia. Geoecology of the environment and society*. Kyzyl: Publishing House of Tuvinian Institute for exploration of natural resources of Siberian branch of the Russian Academy of Sciences, 54–60 (in Rus.).
- Lesnov, F.P., Mongush, A.A. & Oydup, Ch.K. (2001) Geochemical communication of platinum elements and rare earth elements in mafic-ultramafic rocks of Tuva (first data). Platinum in geological formations of Siberia. Abstracts. All-Russian Seminar. Krasnoyarsk: Publishing House of KNIIGiMS, 107–110 (in Rus.).
- Lesnov, F.P., Mongush, A.A. & Tsimbalist, V.G. (2000) On some features of the geochemistry of platinum group elements in rocks from massifs of mazhalyksky mafic-ultramafic complex (Tuva Republic). *Geology and mineral resources of Central Siberia*. Krasnoyarsk: Publishing House of KNIIGiMS, 164–166 (in Rus.).
- Lesnov, F.P., Razin, L.V., Kiseliova, O.N. & Khazina, I.V. (2012, in press) Noble metal mineralization associated with chromites-bearing Naran polygenetic mafic-ultramafic massif (Western Mongolia)//*Russian Geology and Geophysics*.
- Lesnov, F.P., Simonov, V.A., Simonova, V.I. & Gora, M.P. (1990) Geochemical features of ophiolite association of the Naransky massif (Western Mongolia). *Geodynamic conditions of formation, geochemical aspects of the genesis of mafic and ultramafic rocks*. Irkutsk

- Publishing House of Institute of geochemistry of Siberian branch of Academy of Sciences of USSR, 109–113 (in Rus.).
- Lesnov, F.P., Kuchkin, A.M., Palesskii, S.V. & Volkova, N.I. (2005a) Rare earth elements in garnets from eclogites of Atbashi metamorphic complex (Southern Tien Shan, Kyrgyzstan). *Metallogenesis of ancient and modern ocean-2005. Formation and development of deposits in island arc systems*. Miass: Publishing House of the Institute of mineralogy of Ural branch of the Russian Academy of Sciences, 63–67 (in Rus.).
- Lesnov, F.P., Mongush, A.A., Anoshin, G.N. et al. (2005b) Investigating the distribution of rare earth and platinum group elements in rocks from the mafic-ultramafic massifs of Tuva by ICP-MS method (first data). *Petrology of igneous and metamorphic complexes*. Tomsk: Publishing House of Tomsk State University, 268–277 (in Rus.).
- Lesnov, F.P., Mongush, A.A. & Palesskii, S.V. (2005c) The correlation between platinum and rare earth elements in some rocks, mafic-ultramafic massifs of Tuva (according to ICP-MS method). *Precious and Rare Metals of Siberia and the Far East: the ore-forming system of integrated and non-traditional fields of ore types*. Irkutsk: Publishing House of Institute of geochemistry of Siberian branch of the Russian Academy of Sciences, 19–22 (in Rus.).
- Lesnov, F.P., Oydup, Ch.K., Palesskii, S.V. et al. (2007) The first data on the geochemistry of zircons from gabbro in Hayalygsky mafic-ultramafic massif (South-Western Tuva). *State and development of natural resources of Tuva and adjacent regions of Central Asia. Geoecology of the environment and society. Issue 9*. Kyzyl: Publishing House of Tuvinian Institute for exploration of natural resources of Siberian branch of the Russian Academy of Sciences, 83–90 (in Rus.).
- Lesnov, F.P., Podlipskii, M.Yu. & Palesskii, S.V. (2008a) The first data on rare earth elements composition of the accessory chrome-spinels from rock of Ergaksky ultramafic massif (Western Sayan), *The Structure and diversity of the mineral world*. Syktyvkar: Publishing House of Institute of geology of Komi Scientific Center of Ural branch of the Russian Academy of Sciences, 79–81 (in Rus.).
- Lesnov, F.P., Podlipskii, M.Yu., Poliakov, G.V. & Palesskii, S.V. (2008b) Geochemistry of accessory chrome-spinels from ultramafic rocks of Ergaksky chromites-bearing massif and the conditions of its formation (West Sayan). *Doklady of the Russian Academy of Sciences*, 422 (5), 660–664 (in Rus.).
- Lesnov, F.P., Volkova, N.I., Bakirov, A.B. et al. (2004b) New data on the composition of minerals and the conditions of formation of eclogites from Atbashi ridge (Southern Tien Shan). *Petrology of igneous and metamorphic complexes*. Tomsk: Publishing House of Tomsk State University, 255–263 (in Rus.).
- Lesnov, F.P., Palesskii, S.V., Nikolaeva, I.V. et al. (2009) Detailed mineralogical-geochemical study of large spinel lherzolith in alkali basalt of Shavaryn Tsaram Paleovolcano, Mongolia. *Geochem. Int.*, 47 (1), 18–40.
- Li, X.-P., Zhang, L.-F., Wilde, S.A., Song, B. & Liu, X.-M. (2010) Zircons from rodingites in the Western Tianshan serpentinite complex: Mineral chemistry and U-Pb ages define nature and timing of rodingitization. *Lithos*, 118, 17–34.
- Liakhovich, V.V. (1967) Features of the distribution of rare earth elements in accessory minerals of granites. *Geokhimiya*, 7, 828–832 (in Rus.).
- Liati, A. & Froitzheim, N. (2006) Assessing the Valais ocean, Western Alps: U-Pb SHRIMP zircon geochronology of eclogites in the Balma unit, on top of the Monte Rosa nappe. *Eur. J. Mineral.*, 18, 299–308.
- Liati, A., Franz, L., Gebauer, D. & Fanning, C.K. (2004) The timing of mantle and crustal events in South Namibia, as defined by SHRIMP-dating of zircon domains from a garnet peridotite xenolith of the Gibeon kimberlite province. *J. Afr. Earth Sci.*, 39, 147–157.

- Liberi, F., Piluso, E. & Langone, A. (2011) Permo-Triassic thermal events in the lower Variscan continental crust section of the Northern Calabrian Arc, Southern Italy: Insights from petrological data and in situ U-Pb zircon geochronology on gabbros. *Lithos.*, 124 (3–4), 291–307.
- Litasov, K.D. (1998) Geochemical models of mantle magma systems according to the study of deep xenoliths from Vitim and Udokan volcanic fields (Eastern Transbaikalia). *Abstract of Dissertation. PhD geology and mineralogy*. Novosibirsk: Publishing House of Institute geology and mineralogy Siberian branch of Russian Academy of Sciences, 22 p. (in Rus.).
- Loock, G., Stosch, H.-G. & Seck, H.A. (1990) Granulite facies lower crustal xenoliths from Eifel, West Germany: petrological and geochemical aspects. *Contrib. Mineral. Petrol.*, 105 (1), 25–41.
- Luhr, J.F., Carmichael, I.S.E. & Varekamp, J.C. (1984) The 1982 eruptions El Chichon Volcano, Chiapas, Mexico: mineralogy and petrology of the anhydrite-bearing pumices. *J. Volc. Geotherm. Res.*, 23, 69–108.
- Makeev, A.B. (1992) Mineralogy of alpine ultramafic rocks of the Urals. Sankt-Peterburg: Publishing House Nauka, 200 p. (in Rus.).
- Makeev, A.B., Perevozchikov, B.V. & Afanasiev, A.K. (1985) Chromite-bearing of the Polar Urals. Syktyvkar: Publishing House of Institute of Geology. Komi branch of Academy of Sciences of USSR, 152 p. (in Rus.).
- Malakhov, I.A. (2002) The calculation of formulas of minerals and their use their typochemism to identify the genetic nature and the formational affiliation of rocks. Ekaterinburg: Publishing House of UGGGA of Ministry of Education of Russia, 230 p. (in Rus.).
- Malich, K.N., Efimov, A.A. & Ronkin, Yu.L. (2009) Archean U-Pb zircon age of from dunites of Lower-Tagilsky massif (Platinum-bearing belt of the Urals). *Doklady of the Russian Academy of Sciences*, 427 (1), 101–105 (in Rus.).
- Masuda, A. (1967) Lanthanide concentration ratios between pyroxene and garnet. *Earth Planet. Sci. Lett.*, 3, 25–28.
- Mazzucchelli, M., Rivalenti, G., Vannucci, R. et al. (1992) Trace element distribution between clinopyroxene and garnet in gabbroic rocks of the deep crust: An ion microprobe study. *Geochim. Cosmochim. Acta.*, 56, 2371–2385.
- McCallum, M.T. & Charette, M.P. (1978) Zr and Nb partition coefficients: Implications for the genesis of mare basalts, KREEP, and sea from basalts. *Geochim. Cosmochim. Acta*, 42, 859–869.
- McDonough, W.F. & Sun, S.-S. (1995) The composition of the Earth. *Chem. Geol.*, 120, 223–253.
- McDonough, W.F., Stosch, H.-G. & Ware, N.G. (1992) Distribution of titanium and rare earth elements between peridotite minerals. *Contrib. Mineral. Petrol.*, 110, 321–328.
- McKay, G., Wagstaff, J. & Yang, S.-R. (1986) Zr, Hf, and REE partition coefficients for ilmenite and other minerals in nigh Ti lunar mare basalts: An experimental study. *Proc. 16th Lunar Plan. Sci. Conference*, 229–237.
- Meisel, T. & Moser, J. (2004) Reference materials for geochemical PGE analysis: new analytical data for Ru, Rh, Pd, Os, Ir, Pt and Re by isotope dilution ICP-MS in 11 geological reference materials. *Chem. Geol.*, 208 (1–4), 87–107.
- Melcher, F., Grun, W., Thalhammer, T.V. & Thalhammer, O.A.R. (1999) The giant chromites deposits at Kempirsai, Urals: constraints from trace element (PGE, REE) and isotope data. *Mineralium Deposita*, 34, 250–272.
- Mel'gunov, M.S. & Lesnov, F.P. (2003) On the rare-earth composition of picrolilmenite from kimberlite pipe Mir (Yakutia). *Metallogeny of ancient and modern ocean-2003. Formation and development of deposits in island arc systems*. Miass: Publishing House of the Institute of Mineralogy of Ural branch of the Russian Academy of Sciences, 294–295 (in Rus.).

- Melluso, L., Lustrino, M., Ruberti, E. *et al.* (2008) Major and trace-element composition of olivine, perovskite, clinopyroxene, Cr-Fe-Ti oxides, phlogopite and host kamafugites and kimberlites, Alto Paranaiba, Brazil. *Canadian Mineralogist*, 46, 1–19.
- Mongush, A.A. (2000) Massifs of mazhalyksky complex in Kaakhemsky rift and Tannuolskoy zones of Tyva (geological position, and composition of minerals). *Petrology of igneous and metamorphic complexes*. Tomsk: Publishing House of Tomsk State University, 50–54 (in Rus.).
- Mongush, A.A. (2002) Petrography and mineralogy of the Early Paleozoic ultramafic-mafic massifs of East Tuva. *Abstract of Dissertation. PhD geology and mineralogy*. Novosibirsk: Publishing House of UIGGM of Siberian branch of Russian Academy of Sciences, 16 p. (in Rus.).
- Mongush, A.A., Oydup, Ch.K., Agafonov, L.V. & Lesnov, F.P. (1999) Geological position and platinum-bearing of Lower Cambrian mafic-ultramafic massifs of mazhalyksky complex (Tuva). *Geology and Mineral Resources of the Krasnoyarsk Territory*. Krasnoyarsk: Publishing House of KNIIGiMS, 183–188 (in Rus.).
- Mongush, A.A., Lesnov, F.P., Oydup, Ch.K. & Popov, V.A. (2004) On mineralogy of olivines, serpentines and chromites from rocks of the southern part of Ergaksky ultramafic massif (Kurtushibinsky ophiolite belt). *State and development of natural resources of Tuva and adjacent regions of Central Asia. Geoecology of the environment and society*. Kyzyl: Publishing House of Tuvinian Institute for exploration of natural resources of Siberian branch of the Russian Academy of Sciences, 78–82 (in Rus.).
- Mongush, A.A., Agafonov, L.V. & Tunay, G.O. (2005) Mineralogy of the upper part of the fiber Bulkinsky gabbroic massif (Western Sayan). *Ultramafic-mafic complexes of folded regions of the Precambrian*. Ulan-Ude: Publishing House of Buriat Science Centre of Siberian branch of the Russian Academy of Sciences, 62–64 (in Rus.).
- Mori, Y., Orihashi, Y., Miyamoto, T., Shimada, K., Shigeno, M. & Nishiyama, T. (2011) Origin of zircon in jadeite from the Nishisonogi metamorphic rocks, Kyushu, Japan. *Journal of Metamorphic Geology*, 29, 673–684.
- Morisset, C.-E. & Scoates, J.S. (2008) Origin of zircon rims around ilmenite in mafic plutonic rocks of Proterozoic anorthosite suites. *Canadian Mineralogist*, 46 (Part 2), 289–304.
- Mulroney, D. & Rivers, T. (2005) Redistribution of the rare-earth elements among coexisting minerals in metamorphic rocks across the epidote-out isograd: an example from the St. Anthony complex, Northern Newfoundland, Canada. *Canadian Mineralogist*, 263–294.
- Murali, A.V., Parthasarthy, R., Mahadevan, T.M. & Das, M.S. (1983) Trace element characteristics, REE patterns and partition coefficients of zircons from different geological environments: A case study on Indian zircons. *Geochim. Cosmochim. Acta*, 47 (11), 2047–2052.
- Mysen, O.B. (1978) Experimental determination of rare earth element partitioning between hydrous silicate melt, melt, amphibole and garnet peridotite minerals at upper mantle pressure and temperatures. *Geochim. Cosmochim. Acta*, 42, 1253–1263.
- Naldrett, A.J., Fedorenko, V.A., Latfut, P.K. *et al.* (1994) Deposits of Ni-Cu-PGE of Norilsk area, Siberia: their formation in the feeding channels of plateau basaltic volcanism. *7-th International Platinum Symposium: Abstracts*. Moscow: Publishing House Moscow contact, 78 (in Rus.).
- Nagasawa, H. (1970) Rare earth concentrations in zircons and apatites and their host dacites and granites. *Earth. Planet. Sci. Lett.*, 9, 359–364.
- Nagasawa, H., Shreiber, H.D. & Morris, R.V. (1981) Experimental mineral/liquid partition coefficients of the rare earth elements (REE), Sc and Sr for perovskite, spinel and melilite. *Earth Planet. Sci. Lett.*, 46, 431–437.
- Nakada, S. (1991) Magmatic processes in titanites-bearing dacites, central Andes of Chile and Bolivia. *American Mineralogist*, 76, 548–560.

- Nakamura, N. (1974) Determination of REE, Ba, Fe, Mg, Na and K in carbonaceous and ordinary chondrites. *Geochim. Cosmochim. Acta*, 38, 757–775.
- Nakamura, Y., Fujimaki, H., Nakamura, N. & Tatsumoto, M. (1986) Hf, Zr, and REE partition coefficients between ilmenite and liquid: Implication for lunar petrogenesis. *Proc. 16th Lun. Plan. Conf.*, D239–D250.
- Nash, W.P. & Crecraft, H.R. (1985) Partition coefficients for trace elements in silica magmas. *Geochim. Cosmochim. Acta*, 49 (11), 2309–2322.
- Nicholls, I.A. & Harris, K.L. (1980) Experimental rare earth partition coefficients for garnet, clinopyroxene and amphibole coexisting with andesitic and basaltic liquids. *Geochim. Cosmochim. Acta*, 44, 287–308.
- Nicolescu, S., Cornell, D.H., Sodervall, U. & Odelius, H. (1998) Secondary ion mass spectrometry analysis of rare earth elements in grandite garnets and other skarn related silicates. *Eur. J. Mineral.*, 10, 251–259.
- Nikol'skaya, N.E. & Kogarko, L.N. (1995) Geochemical features of ultramafic rocks from Romanche fault (Equatorial Atlantic). *Geokhimiya*, 9, 1280–1295 (in Rus.).
- Nielsen, R.G., Gallahan, W.E. & Newberger, F. (1992) Experimentally determined mineral-melt partition coefficients for Sc, Y, REE, for olivine, orthopyroxene, pigeonite, magnetite and ilmenite. *Contrib. Mineral. Petrol.*, 140 (4), 488–499.
- Nixon, P.H., van Calstern, P.W., Boyd, F.R. & Hawkesworth, C.J. (1987) Harzburgites with garnets of diamond facies from Southern African kimberlites. *Mantle xenoliths* (Ed. P.H. Nixon. N.Y.): Publishing House J. Wiley & Sons, 523–533.
- Nowell, G.M., Pearson, D.G., Kempton, P.D. et al. (1999) Origins of kimberlites: A Hf isotope perspective. *Proc. 7th Intern. Kimberlite Conference*, Vol. 2, Cape Town, 616–624.
- Oktiabr'sky, R.A., Vrzhosek, A.A., Lennikov A.M. et al. (2008) Geochemistry of igneous rocks of Koksharovsky alkaline-ultramafic massif (Primorie) and the results of trace element modeling. *Pacific geology*, 27 (4), 50–62 (in Rus.).
- Osipenko, A.B., Sidorov, E.G., Shevchenko, S.S. et al. (2007) Geochemistry and U-Pb geochronology of zircons from the garnet amphibolite peninsula of Kamchatka Cape (Eastern Kamchatka). *Geochemistry*, 3, 259–268 (in Rus.).
- Oydup, Ch.K., Lesnov, F.P., Kozakov, I.K. et al. (2006) The first data on isotopic age of mafic-ultramafic complex in South-Western Tuva (U-Pb method on zircon). *Geodynamic evolution of lithosphere of the Central Asian mobile belt (from ocean to continent)*, Vol. 2. Irkutsk: Publishing House of Institute of geochemistry of Siberian branch of the Russian Academy of Sciences, 69–72 (in Rus.).
- Oydup, Ch.K., Lesnov, F.P., Palesskii, S.V. et al. (2007) Distribution of rare earth, platinum and other trace elements in rocks from the mafic-ultramafic massifs of ophiolite association in South-Western Tuva (according to the method of ICP-MS). *Status and development of natural resources of Tuva and adjacent regions of Central Asia. Geoeconomy of the environment and society*, Vol. 9. Kyzyl: Publishing House of Tuvanian Institute for exploration of natural resources of Siberian branch of the Russian Academy of Sciences, 116–128 (in Rus.).
- Oydup, Ch.K., Lesnov, F.P., Yarmoliuk, V.V., Lebedev, V.I. & Sal'nikova, E.B. (2011) Ultramafic-mafic magmatism in southwestern Tuva. *Russian Geology and Geophysics*, 52 (3), 354–372 (in Rus.).
- Osawa, K. & Shimizu, N. (1995) Open-system melting in the upper mantle: Constraints from the Hayachine-Miyamori ophiolite, northeastern Japan. *J. Geophys. Res.*, 100 (10), 22315–22335.
- Page, P., Bedard, J.H., Schroetter, J.-M. & Tremblay, A. (2008) Mantle petrology and mineralogy of Thetford Mines ophiolite complex. *Lithos*, 100, 255–292.
- Palesskii, S.V. (2008) Determination of rare and trace elements by mass-spectrometry inductively coupled plasma method. *Abstract of Dissertation. PhD. Chemical sciences*. Novosibirsk:

- Publishing House of Institute of Inorganic Chemistry of Siberian branch of Russian Academy of Sciences, 18 p. (in Rus.).
- Pallister, J.S. & Knight, R.J. (1981) Rare-earth element geochemistry of the Samail ophiolite near Ibrea, Oman. *J. Geoph. Res.*, 86 (B4), 2673–2697.
- Paster, T.P., Schauwecker, D.S. & Haskin, L.A. (1974) The behavior of some trace elements during solidification of the Skaergaard layered series. *Geochim. Cosmochim. Acta*, 38 (10), 1549–1579.
- Pearce, N.J.G. (1990) Zirconium and niobium-bearing ilmenites from the Igalic dyke swarm, South Greenland. *Mineralogical Magazine*, 54, 585–588.
- Pearson, D.G., Davies, G.R. & Nixon, P.H. (1993) Geochemical constraints on the petrogenesis of diamond facies pyroxenites from the Beni Bousera peridotite massif, North Morocco. *J. Petrol.*, 34 (Part 1), 125–172.
- Pearson, D.G. & Milledge, H.J. (1998) Diamond growth conditions and preservation: inferences from trace elements in a large garnet inclusion in Siberian diamond. *Proc. 7th Intern. Kimberlite Conf. Extended Abstracts*, Cape Town, 667–669.
- Pearson, D.G. & Woodland, S.J. (2000) Solvent extraction/anion exchange separation and determination of PGEs (Os, Ir, Pt, Pd, Ru) and Re-Os isotopes in geological samples by isotope dilution ICP-MS. *Chem. Geol.*, 165, 87–107.
- Pearson, D.G., Griffin, W.L., Kaminsky, F.V. et al. (1998) Trace element discrimination of garnet from diamondiferous kimberlites and lamproites. *Proc. 7th Intern. Kimberlite Conf. Extended Abstracts*. Cape Town, 673–675.
- Perkins, W.T. & Pearce, N.J.G. (1996) Problems and progress in the determination of trace and ultra trace elements by ICP-MS and application to petrogenetic studies of igneous rocks. *J. Conf. Abstract*, 1, 459.
- Petrology of postharzburgite intrusives of Kempirsay-Khabarninsky ophiolite association (South Urals)/P. Balykin et al. Sverdlovsk: Publishing House IGG, Ural Branch of AS USSR. 1991. 160 p. (in Rus.).
- Philpotts, J.A., Schnetzler, C.C. & Thomas, H.H. (1972) Petrogenetic implications of some new geochemical data on eclogitic and ultrabasic inclusions. *Geochim. Cosmochim. Acta*, 36, 1131–1166.
- Piatenko, Yu.A. & Ugriumova, N.G. (1988) Mineralogical Crystal Chemistry of rare earth elements. *Izvestia Academy of Sciences USSR. Geology Series*, 11, 75–86 (in Rus.).
- Pinus, G.V., Velinskii, V.V. & Lesnov, F.P. (1976) Ultramafic belts of Central Asia, and some general questions of petrology of ultramafic rocks. *Problems of petrology*. Moscow: Publishing House Nauka, 94–104 (in Rus.).
- Pinus, G.V., Agafonov, L.V. & Lesnov, F.P. (1984) Alpine ultramafic rocks of Mongolia. Moscow: Publishing House Nauka, 200 p. (in Rus.).
- Plaksenko, A.N. (1989) The typomorphism of accessory chromites from ultramafic-mafic igneous formations. Voronezh: Publishing House of Voronezh State University, 224 p. (in Rus.).
- Poitrasson, F., Hancher, J.M. & Scheltegger, U. (2002) The current state and future of accessory mineral research. *Chem. Geol.*, 200, 3–24.
- Pokhilenko, N.P., Sobolev, N.V., Boyd, F.R. et al. (1993) The megacrystalline pyrope peridotites in the lithosphere of the Siberian platform: mineralogy, geochemistry and problem of origin. *Russian Geology and Geophysics*, 34 (1), 71–84 (in Rus.).
- Pokhilenko, N.P., McDonald, J.A., Melnyk, W. et al. (1998) Kimberlites of Camsell Lake field and some features of convection, and composition of lithosphere roots south-eastern part of Slave Craton, Canada. *Proc. 7th Intern. Kimberlite Conf. Extended Abstracts*, Cape Town, 699–701.
- Poliakov, G.V. & Bognibov, V.I. (1979) Early Paleozoic peridotite-pyroxenite-gabbro-norite complex of Salairide of Eastern Tuva. *Mafic and ultramafic complexes of Siberia*. Novosibirsk: Siberian branch of Publishing House Nauka, 118–126 (in Rus.).

- Poliakov, G.V., Bognibov, V.I., Izokh, A.E. *et al.* (1984) Peridotite-pyroxenite-gabbro-norite formation of East Tuva and North-Western Mongolia. *Plutonic formations of Tuva and their ore-bearing*. Novosibirsk: Siberian branch of Publishing House Nauka, 3–57 (in Rus.).
- Poliakov, G.V., Balykin, P.A., Glotov, A.I. *et al.* (1991) Permo-Triassic association of Shongda high-Mg volcanic zone. *Russian Geology and Geophysics*, 9, 3–15 (in Rus.).
- Pride, C. & Muecke, G.K. (1981) Rare earth element distributions among coexisting granulite facies minerals, Scourian complex, NW Scotland. *Contrib. Mineral. Petrol.*, 76 (4), 463–471.
- Promprated, P., Taylor, L.A., Anand, M. *et al.* (2004) Multiple-mineral inclusions in diamonds from Snap Lake-King Lake kimberlite dike, Slave craton, Canada: a trace-element perspective. *Lithos*, 77 (1–4), 69–81.
- Puscharovskii, Yu. & Puscharovskii, D. (2010) Geology of the Earth's mantle. M.: Publishing House GEOS. 140 p. (in Rus.).
- Quartieri, S., Chaboy, J., Antonioli, G. & Geiger, C.A. (1999) XAFS characterization on the structural site of Yb in synthetic pirope and grossular garnets. *Phys. Chem. Miner.*, 27, 88–94.
- Rikhvanov, L.P., Kropanin, S.S., Babenko, S.A. *et al.* (2001) Zircon-ilmenite placer deposits as a potential source of development of West-Siberian region. Kemerovo: Publishing House of Tomsk Polytechnic University. 200 p. (in Rus.).
- Roman'ko, A., Kuznetsov, G., Savicheva, A. *et al.* (1994) Early Proterozoic magmatism in the Eastern Baltic shield and metallogeny of the peculiarities of the PGE. *7-th International Platinum Symposium: Abstracts*. Moscow: Publishing House Moscow Contact, 78 (in Rus.).
- Ronkin, Yu.L. & Nesbitt, R.W. (1997) REE geochemistry of single crystals of zircon from Berdyushsky massif, Southern Urals. *The structure and evolution of the mineral world: Proceedings of the International Seminar*. Syktyvkar: Publishing House Geoprint, 131–132 (in Rus.).
- Revillon, S., Arndt, N.T., Chauvel, C. & Hallot, E. (2000) Geochemical study ultramafic volcanic and plutonic rocks from Gorgona Island, Colombia: the plumbing system of an oceanic plateau. *J. Petrol.*, 41 (7), 1127–1153.
- Rivalenti, G., Mazzucchelli, M., Vannucci, R. *et al.* (1995) The relationship between websterite and peridotite in the Balmuccia peridotite massif (NW Italy) as revealed by trace element variations in clinopyroxene. *Contrib. Mineral. Petrol.*, 121 (3), 275–288.
- Rollinson, H.R. (1993) Using Geochemical Data: Evaluation, Presentation, Interpretation. Publishing House Longman Group, UK, 152 p.
- Root, D.B., Hacker, B.R., Mattinson, J.M. & Wooden, J.L. (2004) Zircon geochronology and ca. 400 Ma exhumations of Norwegian ultrahigh-pressure rocks: an ion microprobe and chemical abrasion study. *Earth Planet. Sci. Lett.*, 228, 325–341.
- Rubatto, D. (2002) Zircon trace element geochemistry: partitioning with garnet and the link between U-Pb ages and metamorphism. *Chemical Geology*, 184, 123–138.
- Rudnev, S.N., Vladimirov, A.G., Ponomarchuk, V.A. *et al.* (2006) Kaakhemsky polychronal batholith (West Tuva): composition, age, sources and geodynamic position. *Litosfera*, (2), 3–33. (In Rus.).
- Russell, J.K., Groat, L.A. & Halleran, A.A.D. (1994) LREE-rich niobian titanite from mount Bisson, British Columbia: chemistry and exchange mechanisms. *Canadian Mineralogist*, 32 (Part 3), 575–587.
- Sahama, Th.G. (1946) On the chemistry of the mineral titanites. *Bull. Geol. Comm. Finlande*, 24 (138), 88.
- Sahama, Th.G. & Vahatalo, V. (1941) X-ray spectrographic study of the rare earths in some Finnish eruptive rocks and minerals. *Bull. Geol. Comm. Finlande*, 126, 50.
- Salters, V.J.M. & Longhi, J. (1999) Trace element partitioning during the initial stages of melting beneath mid-ocean ridges. *Earth Planet. Sci. Lett.*, 166, 15–30.
- Sakiev, K.S. (2002) Conditions of metamorphism of ophiolite of the Tien Shan. *Abstract of Doctoral dissertation. Geology and mineralogy science. ertation*. Bishkek: Publishing House of Institute of Geology of Kirgizian National Academy of Sciences. 32 p. (in Rus.).

- Saltykova, A.K., Nikitina, L.P. & Matukov, D.I. (2008) U-Pb age of zircons from the mantle peridotite xenoliths in Cenozoic alkali basalts from Vitim plateau (Transbaikalia). *Reports of Russian Mineralogy Society*, 3, 1–22 (in Rus.).
- Sal'nikova, E.B., Kovach, V., Kozakov, I.K. et al. (2004) Age and geodynamic position of peridotite-pyroxenite-gabbro-anartosite mazhalyksky complex, Eastern Tuva. *Petrologiya*, 12 (6), 656–662 (in Rus.).
- Savel'eva, G.N., Shishkin, M.A., Larionov, A.N. et al. (2006) Tectono-magmatic events of late Vendian in mantle ophiolite complexes of the Polar Urals: U-Pb data of zircon from chromitites. *Ophiolites: Geology, petrology, metallogeny and geodynamics*. Ekaterinburg: Publishing House of Institute of Geology and Geochemistry of Ural Branch of Russian Academy of Sciences, 160–164 (in Rus.).
- Savel'eva, G.N., Suslov, P.V. & Larionov, A.N. (2007) Vendian tectono-magmatic events in mantle ophiolite complexes of the Polar Urals: the data U-Pb dating of zircon from chromitites. *Geotektonika*, 2, 23–33 (in Rus.).
- Scheka, S.A., Oktiabr'skii, R.A., Vrzhosek, A.A. & Starkov, G.N. (1973) Main regularity of evolution of mafic-ultramafic magmatism in the Primorie. *Igneous rocks of the Far East*. Vladivostok: Publishing House of Far East Science Centre of Academy of Sciences of USSR, 9–61 (in Rus.).
- Scheka, S.A., Vrzhosek, A.A. & Vysotskii, S.V. (2003) Jurassic meymechite-picrite complexes of Primorie, Russia: comparative study with komatiite and Japanese picrites suites. *Plume and problems of deep sources of alkaline magmatism. Proc. Int. Conf.* Khabarovsk, 184–200. (In Rus.).
- Schmidt, G., Witt-Eickschen, G., Palme, H. et al. (2003) Highly siderophile elements (PGE, Re and Au) in mantle xenoliths from the West Eifel volcanic field (Germany). *Chem. Geol.*, 196, 77–105.
- Schnetzler, C.C. & Philpotts, J.A. (1970) Partition coefficients of rare earth elements between igneous matrix and rock-forming mineral phenocrysts-II. *Geochim. Cosmochim. Acta*, 34, 331–340.
- Schwandt, C.S., Papike, J.J., Sheare, C.K. & Brearle, A.J. (1993) A SIMS investigation of REE chemistry of garnet in garnetite associated with Broken Hill Pb-Zn-Ag orebodies, Australia. *Canadian Mineralogist*, 31 (2), 371–379.
- Seifert, W. & Kramer, W. (2003) Accessory titanites: an important carrier of zirconium in lamprophyres. *Lithos*, 71, 81–98.
- Shagalov, E.S. (2003) Gabbroids from Syrostansky massif as a possible representative of sub-alkaline interplate magmatism in the Urals. *Geochemistry of igneous rocks: Proceedings of the 21st All-Russia Seminar and schools "Alkaline magmatism of the Earth"*. Apatity: Publishing House Kola Science Centre of Russian Academy of Sciences, 169–170 (in Rus.).
- Shannon, R.D. (1976) Reversed effective ionic radii and systematic studies of interatomic distances in halides and chalcogenides. *Acta Crystallographica*, A32, 751–767.
- Shardakova, G.Yu. (2001) REE in minerals from Shartashsky granitic massif (Middle Urals). *Young Scientists of the Volga-Ural region at Centuries frontier*. Ufa: Publishing House of Bashkir State University, 56–57 (in Rus.).
- Sharma, M. & Wasserburg, G.J. (1996) The neodymium isotopic compositions and rare earth patterns in highly depleted ultramafic rocks. *Geochim. Cosmochim. Acta*, 60, 4537–4550.
- Sharma, M., Wasserburg, G.J., Papanastassiou, D.A. et al. (1995) High $^{143}\text{Nd}/^{144}\text{Nd}$ in extremely depleted mantle rocks. *Earth Planet. Sci. Lett.*, 135, 101–114.
- Shatskii, V.S. (1990) High-pressure mineral assemblages of eclogites-bearing complexes of the Urals-Mongolian folded belt. *Abstract of Doctoral dissertation. Geology and mineralogy science*. Novosibirsk: Publishing House of Institute of Geology and Geophysics of Siberian branch of Academy of Sciences of USSR, 24 p. (in Rus.).
- Shengrong, L., Tsennmin, G. & Nansheng, Ch. (1994) Platinum group elements – a possible diagnostic and metallogeny indicator. *7-th International Platinum symposium. Abstracts*. Moscow: Publishing House Moscow Contact, 61–62 (in Rus.).

- Shimizu, H. (1980) Experimental study on rare earth element partitioning in minerals formed at 20 and 30 kb for basaltic systems. *Geochim. Journ.*, 14, 185–202.
- Shimizu, N. (1975) Rare earth elements in garnets and clinopyroxenes from garnet lherzolite nodules in kimberlites. *Earth Planet. Sci. Lett.*, 25, 26–32.
- Shimizu, N. & Kushiro, L. (1975) The partitioning of rare earth elements between garnet and liquid at high pressure: preliminary experiments. *Geophys. Res. Lett.*, 3, 413–416.
- Shimizu, N. & Richardson, S.H. (1987) Trace element abundance patterns of garnet inclusions in peridotite-suite diamonds. *Geochim. Cosmochim. Acta*, 51, 755–758.
- Shimizu, N. & Sobolev, N.V. (1995) Young peridotite diamonds from the Mir kimberlite pipe. *Nature*, 375, 394–397.
- Shimizu, N., Boyd, F.R., Sobolev, N.V. & Pokhilenko, N.P. (1994) Chemical zoning of garnets in peridotites and diamonds. V.M. Goldschmidt conference. Edinburg: *Pabl. Miner. Mag.*, 831–832.
- Shimizu, N., Pokhilenko, N.P., Boyd, F.R. & Pearson, D.G. (1997a) Geochemical characteristics of mantle xenoliths from kimberlite pipe Udachnaya. *Geologia i Geofisika*, 38 (1), 194–205 (in Rus.).
- Shimizu, N., Sobolev, N.V. & Efimova, E.S. (1997b) Chemical heterogeneity of garnet inclusions and juvenile in peridotitic diamonds from Siberia. *Geologia i Geofisika*, 38 (2), 337–352. (in Rus.).
- Show, D.M. (1969) Geochemistry of trace elements of crystalline rocks. Leningrad: Publishing House Nedra, 208 p. (in Rus.).
- Sibilev, A.K. (1980) Petrology and asbestos-bearing ophiolite. Novosibirsk: Siberian branch of Publishing House Nauka, 213 p. (in Rus.).
- Skublov, S.G. & Drugova, G.M. (2004) Rare earth elements in zoned metamorphic minerals. *Geochemiya*, 3, 288–301 (in Rus.).
- Skublov, S.G. & Terekhov, E.N. (2009) High pressure granulites from Kandalaksha massif: geochemistry of minerals and condition of metamorphism. *Doklady of Russian Academy of Sciences*, 425 (3), 384–390 (in Rus.).
- Sobolev, N.V. (1964) Paragenetic types of garnets. Moscow: Publishing House Nauka, 218. (in Rus.).
- Sobolev, N.V., Lavrent'ev, Y.G., Pokhilenko, N.P. & Usova, L.V. (1973) Chrome-rich garnets from the kimberlites of Yakutia and their paragenesis. *Contrib. Mineral. Petrol.*, 40, 39–52.
- Song, S.G., Zhang L.F., Niu, Y.N. et al. (2005) Geochronology of diamond-bearing zircons from garnet peridotite in the North Quidam UHPM belt, Northern Tibetan Plateau: a record of complex histories from oceanic lithosphere subduction to continental collision. *Earth Planet. Sci. Lett.*, 234, 99–118.
- Spera, F.J., Bohrson, W.A., Till, C.B. & Ghiorso, M.S. (2007) Partitioning of trace elements among coexisting crystals, melt, and supercritical fluid during isobaric crystallization and melting. *Amer. Mineral.*, 92 (Iss. 11–12), 1881–1896.
- Spetsius, Z.V. & Griffin, W.L. (1998) Trace element composition of garnet kelyphites in xenoliths from Udachnaya as evidence of their origin. *Proc. 7th International Kimberlite Conference. Extended Abstracts*. Cape Town, 853–856.
- Spetsius, Z.V., Taylor, W.R. & Griffin, W.L. (1998) Major and trace element partitioning between mineral phases in diamondiferous and non-diamondiferous eclogites from the Udachnaya kimberlite pipe, Yakutia. *Proc. 7th International Kimberlite Conference. Extended Abstracts*. Cape Town, 856–858.
- Stachel, T., Viljoen, K.S., Brey, G. & Harris, J.W. (1998) Metasomatic processes in lherzolitic and harzburgitic domains of diamondiferous lithospheric mantle: REE in garnets from xenoliths and inclusions in diamonds. *Earth Planet. Sci. Lett.*, 159, 1–12.
- Stachel, T., Aulbach, S., Brey, G.P. et al. (2004) The trace element composition of silicate inclusions in diamonds: review. *Lithos*, 77 (1–4), 1–19.

- Stosch, H.-G. (1982) Rare earth partitioning between minerals from anhydrous peridotite xenoliths. *Geochim. Cosmochim. Acta*, 46, 793–811.
- Stosch, H.-G. & Seck, H.A. (1980) Geochemistry and mineralogy of two spinel peridotite suites from Dreiser Weiher, West Germany. *Geochim. Cosmochim. Acta*, 44, 457–470.
- Sun, S.-S. & McDonough, W.F. (1989) Chemical and isotopic systematics of oceanic basalt: implications for mantle composition and processes. *Magmatism in ocean basins* (Eds. A.D. Saunders., M.J. Norry). *Geological Society Special Publication*, 42, 313–345.
- Sun, S.-S. & Nesbitt, R.W. (1978) Petrogenesis of Archaean ultrabasic and basic volcanics: evidence from rare earth elements. *Contrib. Mineral. Petrol.*, 65 (5), 301–325.
- Sweeney, R.J., Prozesky, V. & Przybilowicz, W. (1995) Selected trace and minor element partitioning between peridotite minerals and carbonatite melts at 18–46 kb pressure. *Geochim. Cosmochim. Acta*, 59, 3671–3683.
- Tabuns, E.V. (1996) Distribution of REE in apatites of MARID type in Ukduskinsky complex. Regularity of evolution of the Earth's crust: *Proceedings of the International conference*, Vol. 2. Sankt-Petersburg: Publishing House of Sankt-Petersburg State University, 121 (in Rus.).
- Thomas, J.B., Bodnar, R.J., Shimizu, N. & Sinha, A.K. (2002) Determination of zircon/melt trace element partition coefficient from SIMS analysis of melt inclusions in zircon. *Geochim. Cosmochim. Acta*, 66 (16), 2887–2901.
- Turkina, O.M., Urmantseva, L.N., Berezhnaya, N.G. & Skublov, S.G. (2011) Formation and metamorphism of Middle Archaea hypersthene gneisses in Irkutny granulites-gneisses block. *Geologia i Geophysika*, 52 (1), 122–137 (in Rus.).
- Urusov, V.S. & Puscharovsky, D.Yu. (1999) Recent advances and new horizons of structural mineralogy and crystal chemistry of minerals, *Newsletter of Moscow State University, Series 4, Geology*, 3–14 (in Rus.).
- Van Achterbergh, E., Griffin, W.L., Shee, L. et al. (1998) Natural trace element distribution coefficients for garnet, clino – and orthopyroxene: variations with temperature and pressure. *Proc. 7th Intern. Kimberlite Conf. Extended Abstracts*, Cape Town, 934–936.
- Van der Wal, D. & Bodinier, J.-L. (1996) Origin of the recrystallisation front in the Ronda peridotite by km-scale pervasive porous melt flow. *Contrib. Mineral. Petrol.*, 122, 387–405.
- Vannucci, R., Shimizu, N., Piccardo, G.B. & Bottazzi, P. (1993) Distribution of trace elements during breakdown of mantle garnet: an example from Zabargad. *Contrib. Mineral. Petrol.*, 114 (1), 437–449.
- Vakhrusheva, N.V., Ivanov, K.S., Erokhin, Yu.V. & Ronkin, Yu.L. (2006) Distribution of REE in ultramafic rocks and ore-forming chromic soinels of Voykar-Syn'insky massif. *Ophiolite: geology, petrology, metallogeny and geodynamics*. Ekaterinburg: Publishing House of Institute of geology and geochemistry. Ural branch of Russian Academy of Sciences, 92–95 (in Rus.).
- Vasilenko, V.B., Lesnov, F.P., Zinchuk, N.N. et al. (2003) About an associativity of distributions of rare-earth elements and rock-forming oxides in the rocks of kimberlite formations. *Problems of forecasting, searches and studying of mineral deposits on a XXI-st century threshold*. ALROSA Company, TSNIGRI. Voronezh: Publishing House of Voronezh state university, 33–38 (in Rus.).
- Volokhov, I.M., Ivanov, V.M., Arnautov, N.V. et al. (1970) Mazhalyksky gabbro-pyroxenites-peridotite pluton (East Tannu-Ola, Tuva). *Problems of a petrology of the ultramafic and the mafic basic rocks*. Novosibirsk: Publishing House Nauka, Siberian branch, 130–145 (in Rus.).
- Voytkevich, G.V., Miroshnikov, F.E., Povarenikh, A.S. & Prokhorov, V.G. (1970) *Short reference book on geochemistry*. Moscow: M: Publishing House Nedra. 280 p. (in Rus.).
- Watson, E.B. (1980) Some experimentally determined zircon/liquid partition coefficients for the rare earth elements. *Geochim. Cosmochim. Acta*, 44, 895–897.

- Watson, E.B. & Green, T.H. (1981) Apatite/liquid partition coefficients for the rare earth elements and strontium. *Earth Planet. Sci. Lett.*, 56, 405–421.
- Wim van Westrenen, Blundy, J. & Wood, B. (1999) Crystal-chemical controls on trace element partitioning between garnets and anhydrous silicate melt. *American Mineralogist*, 84 (5–6), 838–847.
- Wu, F.-Y., Yang, Y.-H., Mitchel, R.H., Li, Q.-L., Yang, J.-H. & Zhang, Y.-B. (2010) In situ U-Pb age determination and Nd isotopic analysis of perovskites from kimberlites in southern Africa and Somerset Island, Canada. *Lithos*, 115, 205–222.
- Yatsenko, G.M., Panov, B.S., Belousova, E.A., Lesnov, F.P. et al. (2000) Distribution of rare earth elements in zircons from minettes in Kirovograd block (Ukraine). *Doklady of Russian Academy of Sciences*, 370 (4), 524–528 (in Rus.).
- Zack, T. & Brumm, R. (1998) Ilmenite/liquid partition coefficients of 26 trace elements determined through ilmenite/clinopyroxene partitioning in garnet pyroxenites. *Proc. 7th International Kimberlite Conference. Extended Abstracts*. Cape Town, 986–987.
- Zhang, R.Y., Yang, J.S., Wooden, J.L. et al. (2005) U-Pb SHRIMP geochronology of zircon in garnet peridotite from the Sulu UHP terrane, China: implications for mantle metasomatism and subduction-zone UHP metamorphism. *Earth Planet. Sci. Lett.*, 237, 729–743.
- Zharikov, V.A. & Yaroshevsky, A.A. (2003) Geochemistry and its problems. *Newsletter of Moscow State University. Geology series*, 4 (in Rus.).
- Zheng, J., Griffin, W.L., O'Reilly, S.Y. et al. (2006a) Zircons in mantle xenoliths the Triassic Yangtze-North China continental collision. *Earth Planet. Sci. Lett.*, 247, 130–142.
- Zheng, J., Griffin, W.L. & O'Reilly, S.Y. (2006b) Mineral chemistry of peridotites from Paleozoic, Mesozoic and Cenozoic Lithosphere: constrains on mantle evolution beneath Eastern China. *Journal of Petrology*, 47 (11), 2233–2256.
- Zhou, M.F., Robinson, P.T., Malpas, J. et al. (2005) REE and PGE geochemical constraints on the formation of dunites in the Luobusa ophiolite, Southern Tibet. *J. Petrol.* 46 (3), 615–639.
- Zinger, T.F., Bortnikov, N.S., Sharkov, E.V., Borisovsky, S.E. & Antonov, A.V. (2010) Effect of plastic deformation in zircon on its chemical composition (for example, the gabbro from zone of the spreading of the Mid-Atlantic Ridge, depression Markov, 6°N). *Doklady of the Russian Academy of Sciences*, 433 (6), 785–791 (in Rus.).
- Zircon. Reviews in Mineralogy and Geochemistry. Vol. 53. Ed. J.M. Hancher, P.W.O. Hoskin. Washington: DC, 2003. 500 p.

This book presents an extensive overview of literature published globally in the last decades on REE distribution in minor and accessory minerals from various types of ultramafic, mafic and other plutonic rocks. It is a continuation of the author's work published in 2010: **"Rare Earth Elements in Ultramafic and Mafic Rocks and their minerals. Main types of rocks. Rock-forming minerals."** The analytical database created includes over 900 analyses of minerals, including garnets (341), chrome-spinels (38), ilmenites (160), zircons (210), apatites (62), titanites (51), perovskites (46) and micas (35). The book offers a brief historical background on REE distribution for each of the minerals and analytical methods for their determination; further, the main features of concentration of these impurities in the samples of different rocks and their manifestations are described and the regularities of REE distribution between coexisting phases, including parent melts, systematized available estimates of distribution coefficients are considered. REE isomorphism in these minerals is discussed as well as the possibilities of using data on REE distribution as typomorphic signs of determining the crystallization conditions of minerals. The numerous analyses of REE presented in this book can be used as reference data. Finally, there is an additional chapter on a new problem: the study of geochemical relations between REE and platinum group elements.

As an overview of modern data on the geochemistry of REE in minor and accessory minerals from rocks of mafic-ultramafic complexes and as a reference book, this work will be of interest to a wide range of specialists studying petrology and geochemistry of products of ultramafic and mafic magmatism, including ore mineralization, as well as for graduate and undergraduate university students in geology departments.



Felix P. Lesnov is Senior Research Fellow, Laboratory of Geodynamics and Magmatism, V. Sobolev Institute of Geology and Mineralogy, Siberian Branch, Russian Academy of Sciences, Member of Russian Academy of Natural Sciences. He specializes in research on mafic-ultramafic magmatism of folded regions (geology, petrology, petrochemistry, mineralogy, geochemistry, metallogenesis), and he has (co-)authored more than 290 papers and nine monographs.



CRC Press
Taylor & Francis Group
an **informa** business
www.crcpress.com

6000 Broken Sound Parkway, NW
Suite 300, Boca Raton, FL 33487
Schipholweg 107C
2316 XC Leiden, NL
2 Park Square, Milton Park
Abingdon, Oxon OX14 4RN, UK



an **informa** business